Universitat Autònoma de Barcelona

Development and application of modern pure shift NMR techniques and improved HSQC/HSQMBC experiments

Laura Castañar Acedo

Doctoral Thesis
Ph.D. in Chemistry

Chemistry Department
Faculty of Sciences

2015

Supervisors:
Teodor Parella Coll
Albert Virgili Moya

Universitat Autònoma de Barcelona

Chemistry Department
Faculty of Sciences

Memòria presentada per aspirar al Grau de Doctor per Laura Castañar Acedo

Vist i plau,

Dr. Teodor Parella Coll **Dr. Albert Virgili Moya** **Laura Castañar Acedo**

Bellaterra, 21 de Mayo de 2015

TABLE OF CONTENTS

ACKNOWLEDGMENTS

I would like to thank the financial support for this research provided by the following institutions:

- Universitat Autònoma de Barcelona and Chemistry Department for giving me a PIF (Personal Investigador en Formació) grand to carry out this doctoral thesis.

- Project: “Nuevas metodologías en Resonancia Magnética Nuclear (part IV)” CTQ2012-32436. MINECO, IP: Dr. Teodor Parella Coll

I would also like to thanks for all the grants received from GERMN (*Grupo Especializado de Resonancia Magnética Nuclear*) to attend to different scientific meetings and courses along this doctoral thesis.

En primer lugar quiero dar las gracias a mis directores de tesis, Albert y Teo. Muchas gracias por la confianza depositada, por vuestra ayuda, consejos, entrega y dedicación. No me puedo sentir más afortunada. Recuerdo perfectamente el día que vine a hacer la entrevista. Llegué nerviosa, asustada y con mil preguntas en mi cabeza pero tenía una cosa clara: quería aprender RMN. Tras casi cuatro años con vosotros estoy convencida de que aquel día tomé una de las mejores decisiones de mi vida. He tenido la gran suerte de aprender de los mejores, de empaparme no sólo de vuestros conocimientos científicos sino también de vuestra manera de hacer las cosas, de trabajar y de organizaros en el día a día. Todo el trabajo realizado habría sido imposible sin vosotros y por eso todos los reconocimientos recibidos en los últimos meses no son míos, son nuestros. Albert, gracias por tantos buenos momentos, por esas increíbles paellas de grupo (a las que sin duda me seguiré apuntando cuando me haya ido), por los abrazos y achuchones recibidos y por ayudarme cuando lo he necesitado. Teo, gracias por esas interminables y divertidas conversaciones de la vida, la ciencia, la RMN, el futbol, la política y la "historia natural". Gracias por todos los buenos momentos vividos, los consejos dados y las risas compartidas.

En segundo lugar he de hacer una mención especial a una persona que ha sido indispensable para mí en estos cuatro años: Miquel. Sin él mi nivel de desesperación con todo lo que tiene que ver con la electrónica y la tecnología habría sido increíble. Seguramente habría "quemado" la sonda, "apaleado" la IPSO o "tirado" el ordenador por la ventana. Pero no, porque ahí está Miquel siempre para ayudarme. Mil millones de gracias Miquel por toda la ayuda, por todo el tiempo dedicado y la paciencia invertida. Y como no mencionar a alguien realmente importante para mí durante todo este tiempo…Pau. Tú fuiste la persona con la que di mis primeros pasos en este mundo de la RMN, la que me enseñó cómo funcionaba todo y como arreglarlo cuando no funcionaba. Me has ayudado con cada problema, me has respondido a cada una de las mil preguntas hechas y hasta hemos aprendido juntos! Pero nuestra relación ha ido más allá de los imanes, te has convertido en un gran amigo que espero que forme parte siempre de mi vida.

Muchas gracias también a todos los compañeros del Servei y del laboratorio: Eva, Silvia, Miriam, Josep, Albert, Eduard, Nuria, André, Ana, Marta y Josep. Gracias a todos por haberme recibido con los brazos abiertos, por vuestra ayuda y por hacer que el día a día sea más ameno. Muchos de vosotros os habéis convertido en algo más que compañeros de trabajo y sé que aquí tendré unos amigos para toda la vida. También me gustaría dar las gracias a todos los doctorandos del Departament con los que he compartido grandes momentos, fiestas, viernes de birras, calçotadas y barbacoas varias. Gracias Joseju, Silvia, Cris, Marc, Carme, Sergio, Asli, Rubén, Roser, Mery, Marc, Julen. Y como no, he de hacer una mención especial a todos aquellos con los que he compartido mi vida en estos últimos cuatro años: Laurita, Pau, Joseju, Josep, Carol, Alba, Albert, Couso, Silvia, Katia y Alba. Mil gracias por haber hecho que me sienta en Barcelona como en casa, os habéis convertido en mi pequeña familia catalana!

Y a ti, Diego, mi inseparable compañero de aventuras, mi otra mitad. Mil millones de gracias por tu apoyo incondicional, por tu cariño, por tu paciencia y comprensión. Mil gracias por embarcarte conmigo en esta aventura y en las que vendrán para que pueda cumplir una parte de mis sueños. Sin ti nada de esto habría sido posible, sin ti nada de esto tendría sentido. Mil millones de gracias mon amour!

Finalmente me gustaría darle las gracias a las personas más importantes de mi vida: mis abuelos, mis padres y mi hermana. En los últimos años cientos de kilómetros me separan de vosotros, pero a pesar de la distancia siempre habéis estado a mi lado y siempre me habéis apoyado en todos mis proyectos e ilusiones. Por eso, todos los éxitos que tenga en la vida sin duda serán también vuestros porque sin vosotros habrían sido imposibles!

LIST OF ACRONYMS

AP	**A**nti-**P**hase
ASAP	**A**cceleration by **S**haring **A**djacent **P**olarization
BASHD	**BA**nd-**S**elective **H**omonuclear **D**ecoupling
BIRD	**BI**linear **R**otation **D**ecoupling
CLAP	**CL**ean **A**nti-**P**hase
CLIP	**CL**ean **I**n-**P**hase
COSY	**CO**rrelation **S**pectroscop**Y**
CPD	**C**omposite **P**ulses **D**ecoupling
CPMG	**C**arr-**P**urcell-**M**aiboom-**G**ill pulse sequence
CSAs	**C**hiral **S**olvating **A**gents
CTP	**C**oherence **T**ransfer **P**athway
DIPSI	**D**ecoupling **I**n **P**resence of **S**calar **I**nteractions
DOSY	**D**iffusion-**O**rdered **S**pectroscop**Y**
DQ	**D**ouble **Q**uantum
DQC	**D**ouble **Q**uantum **C**oherence
E/A	**E**cho/**A**nti-echo
FID	**F**ree **I**nduction **D**ecay
HMBC	**H**eteronuclear **M**ultiple **B**ond **C**orrelation
HMQC	**H**eteronuclear **M**ultiple **Q**uantum **C**orrelation
HOBB	**HO**modecoupled **B**road**B**and
HOBS	**HO**modecoupled **B**and-**S**elective
HSQC	**H**eteronuclear **S**ingle **Q**uantum **C**orrelation
HSQMBC	**H**eteronuclear **S**ingle **Q**uantum **M**ultiple-**B**ond **C**orrelation
INEPT	**I**nsensitive **N**uclei **E**nhanced by **P**olarization **T**ransfer
IP	**I**n-**P**hase
IPAP	**I**n-**P**hase **A**nti-**P**hase
IR	**I**nversion **R**ecovery
ME	**M**ultiplicity-**E**dited

MQ	**M**ultiple **Q**uantum
MQC	**M**ultiple **Q**uantum **C**oherence
MRI	**M**agnetic **R**esonance **I**maging
NMR	**N**uclear **M**agnetic **R**esonance
NOESY	**N**uclear **O**verhauser **E**ffect **S**pectroscopy
NUS	**N**on-**U**niform **S**ampling
PEP	**P**reservation of **E**quivalent **P**athways
PFG	**P**ulse **F**ield **G**radient
PO	**P**roduct **O**perators
PROJECT	**P**eriodic **R**efocusing **O**f **J** **E**volution by **C**oherence **T**ransfer
PS	**P**ure **S**hift
PSYCHE	**P**ure **S**hift **Y**ielded **b**y **CH**irp **E**xcitation
RE-BURP	**RE**focusing **B**and-selective **U**niform-**R**esponse **P**ure-phase
RESET	**R**educing nucl**E**ar **S**pin multipliciti**E**s to singule**T**s
RDC	**R**esidual **D**ipolar **C**oupling
ROESY	**R**otating-frame **O**verhauser **E**ffect **S**pectroscop**Y**
SA	**S**pectral **A**liasing
SAPS	**S**pectral **A**liased **P**ure **S**hift
SNR	**S**ignal to **N**oise **R**atio
SPFGE	**S**ingle **P**ulsed **F**ield **G**radient **E**cho
SQ	**S**ingle **Q**uantum
SQC	**S**ingle **Q**uantum **C**oherence
SS	**S**lice **S**elective
TOCSY	**TO**tal **C**orrelation **S**pectroscop**Y**
ZQ	**Z**ero **Q**uantum
ZQC	**Z**ero **Q**uantum **C**oherence
ZQF	**Z**ero **Q**uantum **F**ilter
ZS	**Z**angger-**S**terk

THESIS OUTLINE

This thesis is presented as a compendium of publications. All the results here exposed have already been evaluated and analyzed by expert researchers in the fields of the *Nuclear Magnetic Resonance* (NMR) spectroscopy and Chemistry, and published in prestigious peer-reviewed international scientific journals. The complete list is:

1. Title: Simultaneous multi-slice excitation in spatially encoded NMR experiments.
   Authors: L. Castañar, P. Nolis, A. Virgili and T. Parella.
   Reference: *Chem. Eur. J.,* **2013**, *19,* 15472-15475.
   DOI: 10.1002/chem.201303272

2. Title: Full sensitivity and enhanced resolution in homodecoupled band-selective NMR experiments.
   Authors: L. Castañar, P. Nolis, A. Virgili and T. Parella.
   Reference: *Chem. Eur. J.,* **2013**, *19*, 17283-17286.
   DOI: 10.1002/chem.201303235

3. Title: Measurement of T_1/T_2 relaxation times in overlapped regions from homodecoupled ^{1}H singlet signals.
   Authors: L. Castañar, P. Nolis, A. Virgili and T. Parella.
   Reference: *J. Magn. Reson.,* **2014**, *244,* 30-35.
   DOI: 10.1016/j.jmr.2014.04.003

4. Title: Enantiodifferentiation through frequency-selective pure-shift ^{1}H Nuclear Magnetic Resonance spectroscopy.
   Authors: L. Castañar, M. Pérez-Trujillo, P. Nolis, E. Monteagudo, A. Virgili and T. Parella.
   Reference: *ChemPhysChem.,* **2014**, *15,* 854-857.
   DOI: 10.1002/cphc.201301130

5. Title: Simultaneous ^{1}H and ^{13}C NMR enantiodifferentiation from highly-resolved pure shift HSQC spectra.
   Authors: M. Pérez-Trujillo, L. Castañar, E. Monteagudo, L. T. Kuhn, P. Nolis, A. Virgili, R. T. Williamson and T. Parella.
   Reference: *Chem. Comm.,* **2014**, *50,* 10214-10217.
   DOI: 10.1039/C4CC04077E

6. Title: Implementing homo- and heterodecoupling in region-selective HSQMBC experiments.
   Authors: L. Castañar, J. Saurí, P. Nolis, A. Virgili and T. Parella.
   Reference: *J. Magn. Reson.,* **2014**, *238,* 63-69.
   DOI: 10.1016/j.jmr.2013.10.022

7. Title: Disentangling complex mixtures of compounds with near-identical ^{1}H and ^{13}C NMR spectra using pure shift NMR spectroscopy.
   Authors: L. Castañar, R. Roldán, P. Clapés, A. Virgili and T. Parella.
   Reference: *Chem. Eur. J*., **2015**, *21*, 7682-7685.
   DOI: 10.1002/chem.201500521

8. Title: Pure in-phase heteronuclear correlation NMR experiments.
   Authors: L. Castañar, J. Saurí, R. T. Williamson, A. Virgili and T. Parella.
   Reference: *Angew. Chem. Intl. Ed.,* **2014**, *53,* 8379-8382.
   DOI: 10.1002/anie.201404136

9. Title: Suppression of phase and amplitude J_{HH} modulations in HSQC experiments.
   Authors: L. Castañar, E. Sistaré, A. Virgili, R. T. Williamson and T. Parella.
   Reference: *Magn. Reson. Chem*., **2015**, 53, 115-119.
   DOI: 10.1002/mrc.4149

10. Title: Recent advances in small molecule NMR: Improved HSQC and HSQMBC experiments.
    Authors: L. Castañar and T. Parella.
    Reference: *Annu. Rep. NMR Spectrosc.,* **2015***, 84,* 163-232.
    DOI: 10.1016/bs.arnmr.2014.10.004

The research work carried out during this doctorate (October 2012 – May 2015) is framed within the NMR field, more specifically in the design of new NMR methodologies. The starting point was the prior knowledge and experience of our research group in the development of modern NMR methodologies, with special emphasis in methods to measure homo- and heteronuclear coupling constant through HSQC and HSQMBC-type experiments. One of the two parts of the present thesis is framed in this line of research and the other part is centered on the design and application of new pure shift NMR methodologies, which is a new research topic started in our group during this Ph.D.

This thesis has been organized in five sections:

1. **Introduction**. This section contains a brief general explanation of the most important NMR concepts needed to understand the work carried out.

2. **Objectives**. Here the main specific goals that led to the development of this thesis are described.

3. **Results and Discussion**. This section is the main part of the thesis. Here, all the new developed NMR methods and their applications are presented as Original Research Papers (Publications). Since every published paper has gone through a peer-review process by NMR experts, not much attention is devoted to the discussion of the results beyond discussed in each publication. Nevertheless, a little introduction is presented for each one of published papers.

4. **Summary and Conclusions**. Finally, a brief summary with the main conclusions extracted from the experimental results is exposed.

5. **Appendix**. Additionally, some results obtained during this doctoral thesis which have not could be used as Publication are included in this last section.

1. INTRODUCTION

1.1. Pure shift NMR spectroscopy[1]

Nuclear Magnetic Resonance (NMR) spectroscopy is one of the most powerful tools for determining structural, dynamics, chemical and physical properties of small and medium-size molecules under a great variety of sample conditions. The most significant aspects that determine the quality of NMR spectra are sensitivity and spectral resolution. Advances in sensitivity have been occurring over the years by a multitude of different techniques intended to improve NMR data acquisition and processing. The development and the improvements in NMR instrumentation have also played a key role to enhance sensitivity, with a particular emphasis in the technical design of cryogenically cooled probes or higher magnetic fields. On the other hand, spectral resolution is also improved inherently in higher magnetic fields, which disperse the chemical shifts over a wider frequency range, although the effects of signal overlap can still be a limiting factor when analyzing complex NMR spectra. The continuous development of new pulse sequences and the improvement of the existing ones have been another very important factor to understand the enormous potential of the NMR spectroscopy. Additionally, the incorporation of multiple-frequency dimensions achieves a tremendous qualitative and quantitative leap, particularly when it comes to improving signal dispersion.

The associated benefits of decoupling through-bond interactions for the apparent simplification of scalar coupling constant splittings are easily understood when analysing a typical ^{13}C spectrum, which is routinely recorded under broadband heteronuclear ^{1}H decoupling during data acquisition.[2] In a standard 1D $^{13}C\{^{1}H\}$ spectrum, all signals appear as singlet lines providing excellent signal dispersion, allowing the knowledge of the number of signals that are present and also measuring accurate chemical shift values in a very straightforward way. In contrast, despite using high magnetic fields, 1D ^{1}H NMR spectra often suffer of low signal resolution and severe signal overlap due to the limited range of ^{1}H chemical shifts (~10-15 ppm) and also to the additional proton-proton scalar coupling (J_{HH}) splittings observed in each proton resonance. The analysis of the fine multiplet structure contains valuable structural information such as the number and the

[1] Introduction about pure shift NMR spectroscopy has been adapted from the recently published review: L. Castañar, T. Parella, *Mag. Reson. Chem.,* **2015**, *53,* 399.

[2] a) M. H. Levitt, R. Freeman, T. Frenkiel, *J. Magn. Reson.,* **1982**, *47*, 328. b) A. J. Shaka, J. Keeler, T. Frenkiel, R. Freeman, *J. Magn. Reson.,* **1983**, *52*, 335. c) A. J. Shaka, P. B. Barker, R. Freeman, *J. Magn. Reson.,* **1985**, *64*, 547. d) E. Kupče, R. Freeman, *J. Magn. Reson.,* **1995**, *115*, 273. e) R. Fu, G. Bodenhausen, *Chem. Phys. Lett.,* **1995**, *245*, 415.

nature of neighbouring spins or dihedral angle constraints. However, in many cases, signal overlap hampers a definitive multiplet analysis or the accurate extraction of chemical shifts, which are also fundamentals in the analysis and interpretation of NMR spectra. On the other hand, scalar coupling constant (*J)* information can become redundant when multidimensional NMR spectra are analyzed, because only the correlation between chemical shifts is usually of interest for assignment purposes.

Signal resolution in ^{1}H NMR spectra could be significantly enhanced if all signals could be converted into singlets. This is the aim of broadband homodecoupled NMR techniques, also referred to as "pure shift NMR spectroscopy". The advantages of obtaining pure shift ^{1}H NMR spectra have been extensively recognized for years, although there is no easy and general solution to achieve this goal. Only as an example of the potential of this approach, Figure 1 shows how the simplified *J* multiplet structures achieved for all resonances in a small molecule like progesterone is a clear proof of the excellent complementarity between the homodecoupled and the standard 1D ^{1}H spectra. The absence of coupling splittings improves signal dispersion, facilitates and accelerates chemical shift recognition, and simplifies the analysis and assignment of complex regions, as observed for the overlap signals resonating around 1.6 and 2.0 ppm.

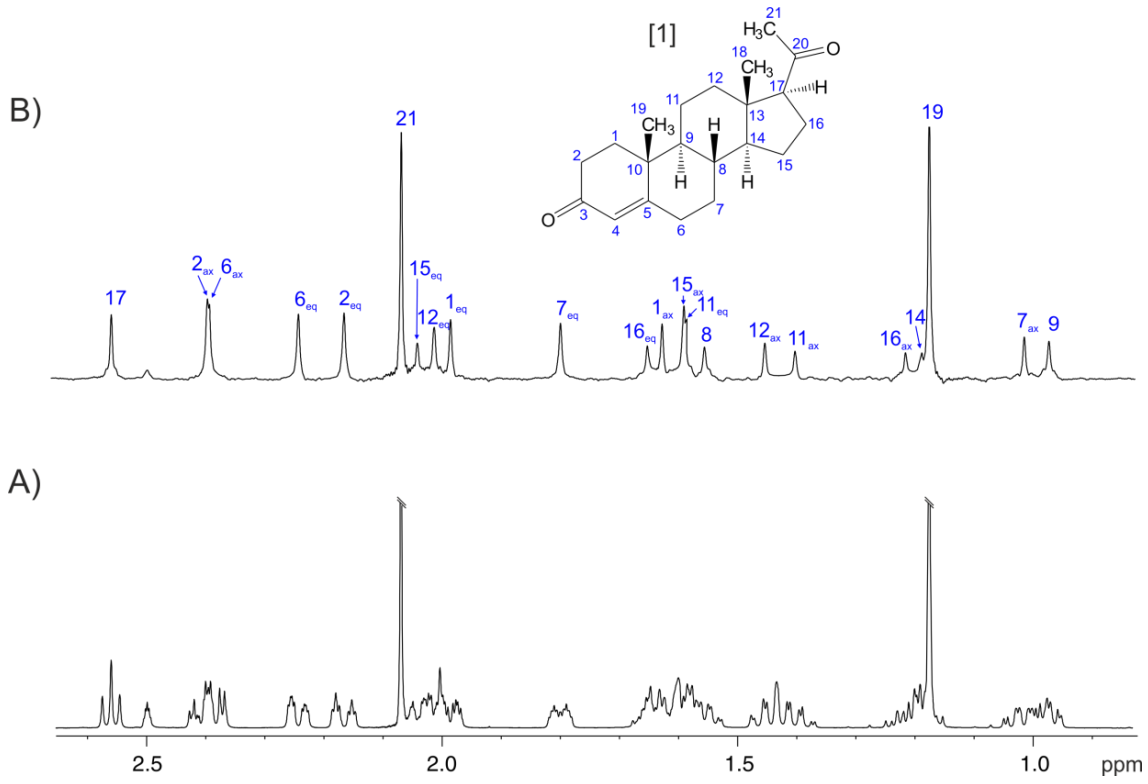

Figure 1: 600 MHz A) conventional and B) broadband homodecoupled 1D ^{1}H NMR spectra of the steroid progesterone [1] in DMSO-d_6. Note how all simplified singlet resonances at their chemical shift frequencies can be distinguished in the pure shift spectrum.

In the last few years, there has been a revival in the development of pure shift NMR techniques. Several strategies have been suggested being the experiments based on the original *Zangger-Sterk* (ZS) methodology[3] the most widely used. This introduction aims to describe the fundamental key points for understanding the principles of modern broadband homodecoupled ^{1}H NMR experiements.

1.1.1. Homodecoupling NMR building blocks

The development and implementation of new homodecoupling building blocks into specific pulse schemes is nowadays an expanding area of research. Efforts are mainly concentrated in the design of methodologies that guarantee a routine use involving a simple and non-extended acquisition set-up, a standard and non-sophisticated data processing procedure, and a general applicability on a wide range of NMR experiments.

The most widely used pure shift experiments are based on the refocusing of the homonuclear coupling evolution. To achieve it, several *J*-refocused pulse sequence elements can be used in the middle of a given evolution time. These elements divide the available spins into two subsets: (i) active spins, which provide the final detected signal, and (ii) passive spins, which are decoupled but not observed. Figure 2 illustrates a general *J*-refocused building block to achieve broadband homodecoupling by combining the effects of a pair of NMR elements: a non-selective 180^{o} pulse and a selective inversion element that affects only the active spins. Some basic selective elements that perform such specific perturbation have been proposed: (i) a ^{12}C/^{13}C isotopic *BIlinear Rotational Decoupling* (BIRD)[4] module (Figure 2A), (ii) frequency- or region-selective 180^{o} pulses (Figure 2B-D), and (iii) spatially-resolved elements consisting of a frequency- or region-selective or adiabatic 180^{o} pulse applied simultaneously to a weak *Pulsed Field Gradient* (PFG) (Figure 2E-H). In all these cases, the passive spins experience a 180^{o} pulse whereas the active spins are unperturbed because they undergo an overall rotation of 360^{o}. In practical terms, this means that chemical shift of active nuclei will not be affected and therefore it will evolve, while all homonuclear $J_{\mathrm{H_{passive}\text{-}H_{active}}}$ couplings will be efficiently refocused.

[3] K. Zangger, H. Sterk, *J. Magn. Reson.,* **1997**, *124,* 486.

[4] a) J. P. Garbow, D. P. Weitekamp, A. Pines, *Chem. Phys. Lett,.* **1982**, *93,* 504. b) D. Uhrín, T. Liptaj, K. E. Kövér, *J. Magn. Reson.,* **1993**, *101*, 41.

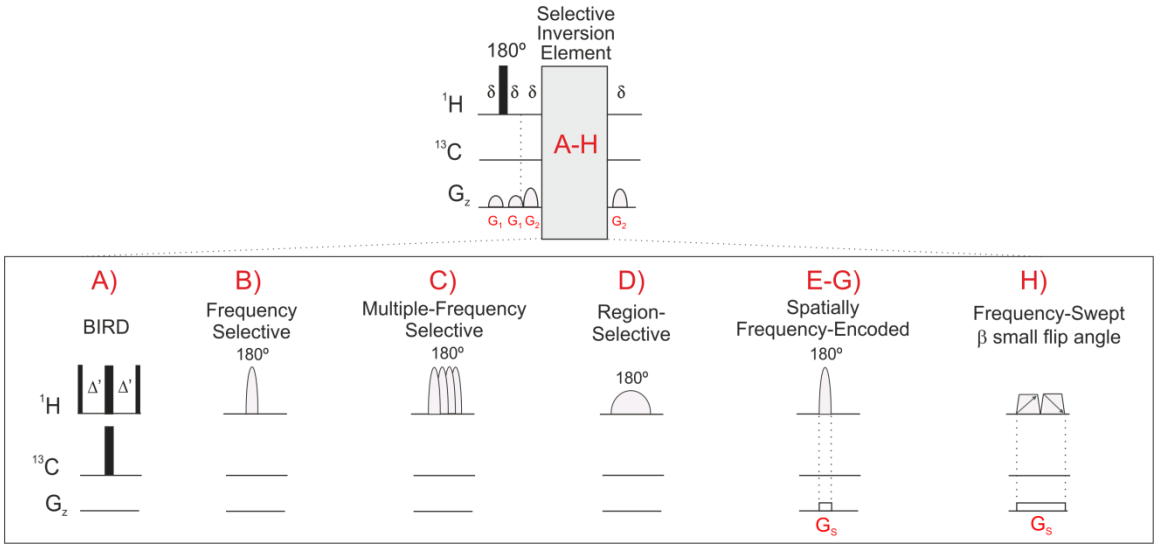

Figure 2: Basic NMR building blocks to perform homonuclear decoupling, consisting of a non-selective 180° pulse and a selective inversion element: A) BIRD[x] cluster to selectively invert ^{1}H-^{13}C *vs* ^{1}H-^{12}C protons; B-D) frequency-selective 180° pulses designed to invert/refocus a single or specific groups of signals; E-G) slice-selective element to achieve spatial frequency-encoding along the *z*-axis thanks to the simultaneously application of an encoding G_s gradient and a single-, multiple- or region-selective 180° pulse; H) spatially-selective element using a pair of small flip angle frequency-swept adiabatic pulses jointly with an encoding G_s gradient. The use of gradients G_1 and G_2 flanking each inversion element can be optionally applied to remove improper refocusing/inversion.

This double effect on active and passive spins can be analyzed using the *Product Operator* (PO) formalism[5]. Consider the simplest situation:

- A weakly coupled spin system comprising an active spin (I_a) and a passive spin (I_p) with $J_{I_aI_p}$.
- A NMR building block consisting of "τ_1 – hard 180° – selective 180° – τ_1" element, where a selective 180° pulse (Figure 2B) is applied on I_a.

Initially, the active spins arrive as *In-Phase* (IP) magnetization, $-I_{ay}$, prior to τ_1. During the first delay (τ_1), the magnetization evolves freely under the effects of the chemical shift (Ω_a) and the homonuclear coupling with the passive spin ($J_{I_aI_p}$):

$$-I_{ay} \xrightarrow{\Omega_a\tau_1} -I_{ay}\cos(\Omega_a\tau_1) + I_{ax}\sin(\Omega_a\tau_1) \xrightarrow{\pi J_{I_aI_p}\tau_1} \begin{aligned} &-I_{ay}\cos(\Omega_a\tau_1)\cos(\pi J_{I_aI_p}\tau_1) \\ &+2I_{ax}I_{pz}\cos(\Omega_a\tau_1)\sin(\pi J_{I_aI_p}\tau_1) \\ &+I_{ax}\sin(\Omega_a\tau_1)\cos(\pi J_{I_aI_p}\tau_1) \\ &+2I_{ay}I_{pz}\sin(\Omega_a\tau_1)\sin(\pi J_{I_aI_p}\tau_1) \end{aligned}$$

Eq.1.1

[5] O. W. Sørensen, G. W. Eich, M. H. Levitt, G. Bodenhausen, R. R. Ernst. *Prog. Nucl. Magn. Reson. Spectrosc.*, **1983**, *16*, 163.

Next, a broadband 180° pulse is applied followed by a selective 180° pulse on active spins:

$$\xrightarrow{180^{o}(I_x)}\begin{matrix}+I_{ay}\cos(\Omega_a\tau_1)\cos(\pi J_{I_aI_p}\tau_1)\\ -2I_{ax}I_{pz}\cos(\Omega_a\tau_1)\sin(\pi J_{I_aI_p}\tau_1)\\ +I_{ax}\sin(\Omega_a\tau_1)\cos(\pi J_{I_aI_p}\tau_1)\\ +2I_{ay}I_{pz}\sin(\Omega_a\tau_1)\sin(\pi J_{I_aI_p}\tau_1)\end{matrix}\xrightarrow{180^{o}(I_{ax})}\begin{matrix}-I_{ay}\cos(\Omega_a\tau_1)\cos(\pi J_{I_aI_p}\tau_1)\\ -2I_{ax}I_{pz}\cos(\Omega_a\tau_1)\sin(\pi J_{I_aI_p}\tau_1)\\ +I_{ax}\sin(\Omega_a\tau_1)\cos(\pi J_{I_aI_p}\tau_1)\\ -2I_{ay}I_{pz}\sin(\Omega_a\tau_1)\sin(\pi J_{I_aI_p}\tau_1)\end{matrix}$$

Eq.1.2

Finally, the system evolves again for a time τ_1 under both $\Omega_a$and $J_{I_aI_p}$ effects:

$$\xrightarrow{\Omega_a\tau_1}\begin{matrix}-I_{ay}\cos^2(\Omega_a\tau_1)\cos(\pi J_{I_aI_p}\tau_1)\\ +I_{ax}\cos(\Omega_a\tau_1)\sin(\Omega_a\tau_1)\cos(\pi J_{I_aI_p}\tau_1)\\ -2I_{ax}I_{pz}\cos^2(\Omega_a\tau_1)\sin(\pi J_{I_aI_p}\tau_1)\\ -2I_{ay}I_{pz}\cos(\Omega_a\Omega\tau_1)\sin(\Omega_a\tau_1)\sin(\pi J_{I_aI_p}\tau_1)\\ +I_{ax}\sin(\Omega_a\tau_1)\cos(\Omega_a\tau_1)\cos(\pi J_{I_aI_p}\tau_1)\\ +I_{ay}\sin^2(\Omega_a\tau_1)\cos(\pi J_{I_aI_p}\tau_1)\\ -2I_{ay}I_{pz}\sin(\Omega_a\tau_1)\cos(\Omega_a\tau_1)\sin(\pi J_{I_aI_p}\tau_1)\\ +2I_{ax}I_{pz}\sin^2(\Omega_a\tau_1)\sin(\pi J_{I_aI_p}\tau_1)\end{matrix}\xrightarrow{\pi J_{I_aI_p}\tau_1}\begin{matrix}-I_{ay}\cos^2(\Omega_a\tau_1)\cos^2(\pi J_{I_aI_p}\tau_1)\\ +2I_{ax}I_{pz}\cos^2(\Omega\tau_1)\cos(\pi J_{I_aI_p}\tau_1)\sin(\pi J_{I_aI_p}\tau_1)\\ +I_{ax}\cos(\Omega_a\tau_1)\sin(\Omega_a\tau_1)\cos^2(\pi J_{I_aI_p}\tau_1)\\ +2I_{ay}I_{pz}\cos(\Omega_a\tau_1)\sin(\Omega_a\tau_1)\cos(\pi J_{I_aI_p}\tau_1)\sin(\pi J_{I_aI_p}\tau_1)\\ -2I_{ax}I_{pz}\cos^2(\Omega_a\tau_1)\sin(\pi J_{I_aI_p}\tau_1)\cos(\pi J_{I_aI_p}\tau_1)\\ -I_{ay}\cos^2(\Omega_a\tau_1)\sin^2(\pi J_{I_aI_p}\tau_1)\\ -2I_{ay}I_{pz}\cos(\Omega_a\tau_1)\sin(\Omega_a\tau_1)\sin(\pi J_{I_aI_p}\tau_1)\cos(\pi J_{I_aI_p}\tau_1)\\ +I_{ax}\cos(\Omega_a\tau_1)\sin(\Omega_a\tau_1)\sin^2(\pi J_{I_aI_p}\tau_1)\\ +I_{ax}\sin(\Omega_a\tau_1)\cos(\Omega_a\tau_1)\cos^2(\pi J_{I_aI_p}\tau_1)\\ +2I_{ay}I_{pz}\sin(\Omega_a\tau_1)\cos(\Omega_a\tau_1)\cos(\pi J_{I_aI_p}\tau_1)\sin(\pi J_{I_aI_p}\tau_1)\\ +I_{ay}\sin^2(\Omega_a\tau_1)\cos^2(\pi J_{I_aI_p}\tau_1)\\ -2I_{ax}I_{pz}\sin^2(\Omega_a\tau_1)\cos(\pi J_{I_aI_p}\tau_1)\sin(\pi J_{I_aI_p}\tau_1)\\ -2I_{ay}I_{pz}\sin(\Omega_a\tau_1)\cos(\Omega_a\tau_1)\sin(\pi J_{I_aI_p}\tau_1)\cos(\pi J_{I_aI_p}\tau_1)\\ +I_{ax}\sin(\Omega_a\tau_1)\cos(\Omega_a\tau_1)\sin^2(\pi J_{I_aI_p}\tau_1)\\ +2I_{ax}I_{pz}\sin^2(\Omega_a\tau_1)\sin(\pi J_{I_aI_p}\tau_1)\cos(\pi J_{I_aI_p}\tau_1)\\ +I_{ay}\sin^2(\Omega_a\tau_1)\sin^2(\pi J_{I_aI_p}\tau_1)\end{matrix}$$

Eq.1.3

Regrouping the terms according some basic trigonometric identities, the magnetization components are reduced to:

$$-I_{ay}\cos^2(\Omega_a\tau_1)\left[\cos^2\left(\pi J_{I_aI_p}\tau_1\right)+\sin^2(\pi J_{I_aI_p}\tau_1)\right]$$

$$+I_{ay}\sin^2(\Omega_a\tau_1)\left[\cos^2\left(\pi J_{I_aI_p}\tau_1\right)+\sin^2(\pi J_{I_aI_p}\tau_1)\right]$$

$$+I_{ax}\,2\cos(\Omega_a\tau_1)\sin(\Omega\tau_1)\left[\cos^2(\pi J_{I_aI_p}\tau_1)+\sin^2(\pi J_{I_aI_p}\tau_1)\right]$$

$$\downarrow \quad \cos^2\theta+\sin^2\theta=1$$

$$-I_{ay}\left[\cos^2(\Omega_a\tau_1)-\sin^2(\Omega_a\tau_1)\right]+I_{ax}\,2\cos(\Omega_a\tau_1)\sin(\Omega_a\tau_1)$$

$$\downarrow \quad \cos^2\theta-\sin^2\theta=\cos 2\theta$$

$$\downarrow \quad 2\cos\theta\sin\theta=\sin 2\theta$$

$$\boldsymbol{-I_{ay}\cos(2\Omega_a\tau_1)+I_{ax}\sin(2\Omega_a\tau_1)}$$

Eq.1.4

These results demonstrate that with this building block Ω_a evolves during the period $2\tau_1$ while $J_{I_aI_p}$ is fully refocused.

The choice of the selective inversion element is dependent on the sample analyzed and on the information required. Importantly, the amount of active spins being inverted is typically much smaller than the passive spins, entailing some cost in sensitivity that must be carefully evaluated in each case.

1.1.1.1 BIRD-based elements

A simple way to perform homonuclear decoupling in heteronuclear spin systems is using the BIRD module,[4b] which is based on a different isotopic $^{12}C/^{13}C$ behavior. Mainly, two different BIRD blocks are available: $BIRD^x$ and $BIRD^y$ (Figure 3):

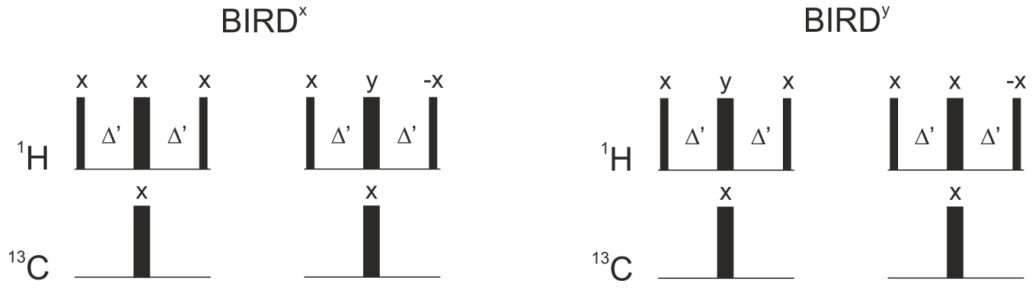

Figure 3: Different implementations of the $BIRD^x$ (left) and $BIRD^y$ (right) NMR building blocks. Δ' is adjusted according to $1/(2^1J_{CH})$.

The BIRD^{y} block inverts ^{12}C-bound protons while keep the magnetization of protons bound to ^{13}C unchanged (Figure 4). Starting with 90^{o} ^{1}H excitation, the magnetization of ^{13}C-bound protons evolves under the effect of the one-bond coupling to the directly-attached carbon ($^{1}J_{CH}$) during the Δ' periods (where Δ' is adjusted to $1/(2^{1}J_{CH})$). ^{1}H chemical shift evolutions for both ^{1}H-^{13}C and ^{1}H-^{12}C components are not considered because all they will be refocused by the central 180^{o} ^{1}H pulse (spin-echo). The final 90^{o} pulse rotates the magnetization of ^{13}C-bound protons onto the +*z*-axis and ^{12}C-bound protons onto –*z*-axis producing the desired selective inversion of the ^{1}H–^{12}C resonances. The BIRD^{x} block works in the reverse mode.

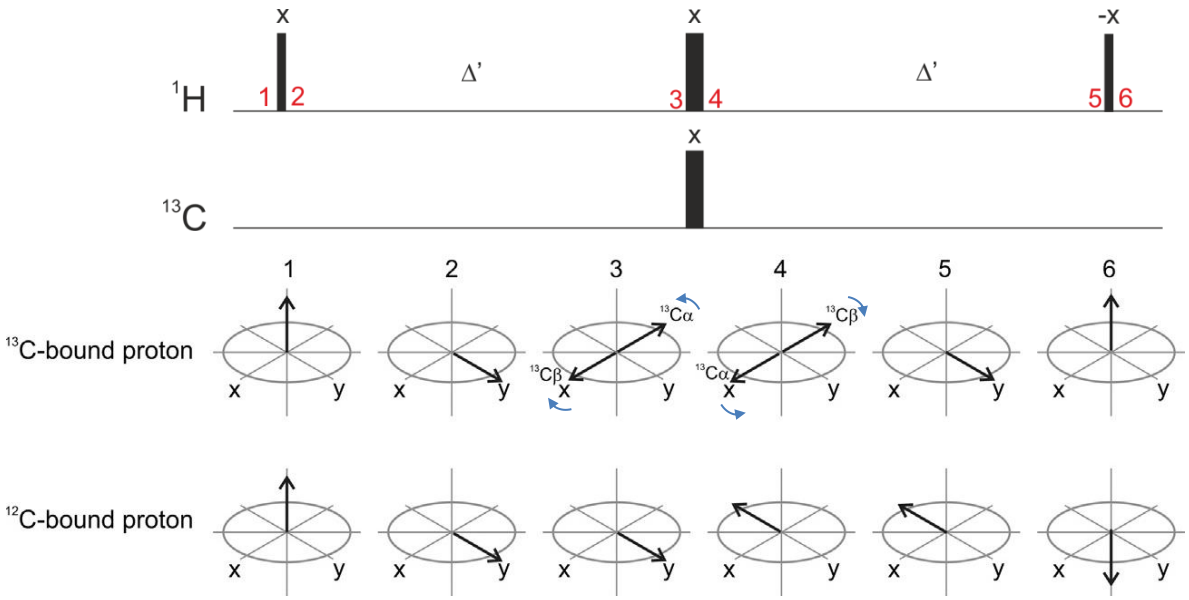

Figure 4: Pulse sequence of the BIRD^{y} element used to invert the magnetization of ^{12}C-bound protons while leaving the magnetization of ^{13}C-bound protons essentially unaffected. The fates of the ^{13}C- and ^{12}C-bound protons magnetizations are shown in the vector representation. The spin state of the bound ^{13}C nucleus is also indicated.

BIRD-based homodecoupling was introduced by Garbow and coworkers more than thirty years ago.[4a] The basic homodecoupling block consists of the combination of a hard 180^{o} ^{1}H pulse followed by a BIRD^{x} element (Figure 2A), and the net effect is therefore a 360^{o} rotation of protons directly ^{13}C bounded and a 180^{o} rotation of the protons attached to ^{12}C. The main features of the success use of BIRD homodecoupling are as follows:

i. Problems associated to strong J_{HH} coupling effects are minimized.

ii. The geminal $^{2}J_{HH}$ interaction between diastereotopic protons is retained because the BIRD element cannot distinguish between protons directly bound to the same ^{13}C nucleus. As a practical consequence, BIRD-based pure shift spectra will show doublets for non-equivalent methylene protons. Recently, novel concepts based on

constant-time BIRD[6] or perfect BIRD[7] elements have been proposed to remove such $^2J_{HH}$ effects.

iii. The ideal behavior expected for spins during the BIRD block can be compromised in real situations because of the single delay Δ' (optimized to $1/(2^1J_{CH})$) that may not simultaneously satisfy the heteronuclear couplings arising for different spins of the molecule and because of imperfect inversions for ^{13}C sites spanning up to 200 ppm in their chemical shift ranges. Either of these two deviations can affect the behaviour expected for the ^{13}C-bonded protons, leading to artefacts. In practice, a suitable compromise value of Δ' can be found to minimize the J_{CH}-derived artefacts whereas the use of adiabatic-shaped 180^o ^{13}C pulses eliminates off-resonance effects.[8]

iv. The price to pay for applying BIRD-based homodecoupling is sensitivity. Natural abundance of ^{13}C is approximately 1,1%, and therefore, an unavoidable sensitivity loss of about 99% is obtained after using a BIRD filter. This sensitivity penalty is avoided in experiments that preselect ^1H-^{13}C magnetization, as carried out in pure shift HSQC experiments.[9]

v. BIRD fails for fully ^{13}C-labeled compounds because of J_{CC} evolution.

The BIRD-based homodecoupling method has been further refined and adapted for pure shift 1D[8,10] and 2D HSQC experiments,[9,11] and recently applied in a variety of structural problems.[6,12]

1.1.1.2 Frequency-selective pulses

The use of a frequency-selective 180^o pulse is a simple option to achieve selective inversion on a single or multiple ^1H signals (Figure 2B-D). The performance is under the

[6] T. Reinsperger, B. Luy, *J. Magn. Reson.,* **2014**, *239*, 110.

[7] L. Kaltschnee, A. Kolmer, I. Timári, V. Schmidts, R. W. Adams, M. Nilsson, K. E. Kövér, G. A. Morris, C. M. Thiele, *Chem. Commun.,* **2014**, *50*, 15702.

[8] A. Lupulescu, G. L. Olsen, L. Frydman, *J. Magn. Reson.,* **2012**, *218*, 141.

[9] L. Paudel, R. W. Adams, P. Király, J. A. Aguilar, M. Foroozandeh, M. J. Cliff, M. Nilsson, P. Sándor, J. P. Waltho, G. A. Morris, *Angew. Chem. Int. Ed.,* **2013**, *52*, 11616.

[10] J. A. Aguilar, M. Nilsson, G. A. Morris, *Angew. Chem. Int. Ed.,* **2011**, *50*, 9716.

[11] P. Sakhaii, B. Haase, W. Bermel, *J. Magn. Reson.*, **2009**, *199*, 192.

[12] a) I. Timári, L. Kaltschnee, A. Kolmer, R. W. Adams, M. Nilsson, C. M. Thiele, G. A. Morris, K. E. Kövér, *J. Magn. Reson.,* **2014**, *239*, 130. b) Y. Liu, M. D. Green, R. Marques, T. Pereira, R. Helmy, R. T. Williamson, W. Bermel, G. E. Martin, *Tetrahedron Lett.,* **2014**, *55*, 5450. c) J. A. Aguilar, G. A. Morris, A. M. Kenwright, *RSC Adv.,* **2014**, *4*, 8278. d) K. J. Donovan, L. Frydman, *Angew. Chem. Int. Ed.,* **2014**, *54*, 594.

control of the NMR user by an appropriate choice of the duration and shape of the selected 180^{o} pulse that defines the effective bandwidth of the selective excitation. Several options are feasible, including single frequency (Figure 2B), multiple-frequency (Figure 2C) or band-selective (Figure 2D) excitation covering a specific region of the proton spectrum. The only requirement for a proper homodecoupling is that this selective pulse must not affect to mutually *J* coupled protons to avoid the evolution of this mutual coupling.

These building blocks were initially used to significantly increase the spectral resolution in the indirect F1 dimension of 2D experiments, by collapsing J_{HH} multiplets to singlets by *BAnd-Selective Homonuclear Decoupling* (BASHD) techniques.[13] This strategy can be combined with other homodecoupling techniques along the detected F2 dimension in order to obtain ultra-high resolution in both dimensions of fully homodecoupled 2D spectra.

1.1.1.3 Spatial encoding

Conventional NMR experiments involve the nonspecific excitation and detection of the NMR signal in the entire detector coil (Figure 5A). The incorporation of the spatial encoding concept, traditionally used in *Magnetic Resonance Imaging* (MRI) applications, into high-resolution NMR spectroscopic techniques is attracting an increasingly larger interest. Several strategies have been developed to perform spatial encoding into an NMR tube:

i. Data collection is focused on a specific *z*-slice along the NMR sample (Figure 5B). Spatially resolved NMR applications have been reported for the analysis and characterization of heterogeneous samples, for instance, to study biphasic systems,[14] to detect and quantify sample inhomogeneities and spatial distribution in different alignment media such as gels or liquid crystals,[15] to investigate solvation and diffusion of CO_2 in ionic liquids,[16] to perform fast titrations and *in situ* reaction monitoring for obtaining information about reaction mechanisms and detecting

[13] a) R. Brüschweiler, C. Griesinger, O. W. Sørensen, R. R. Ernst, *J. Magn. Reson.,* **1988**, *78*, 178. b) V. V. Krishnamurthy, *Magn. Reson. Chem.,* **1997**, *35*, 9.

[14] a) W. Kozminski, *Pol. J. Chem.,* **2000**, *1189*, 1185. b) B. T. Martin, G. C. Chingas, O. M. McDougal, *J. Magn. Reson.,* **2012**, *218*, 147. c) C. Mantel, P. A. Bayle, S. Hediger, C. Berthon, M. Bardet, *Magn. Reson. Chem.,* **2010**, *48*, 600.

[15] a) P. Trigo-Mouriño, C. Merle, M. R. M. Koos, B. Luy, R. R. Gil, *Chem. Eur. J.,* **2013**, *19*, 7013. b) A. C. Pöppler, S. Frischkorn, D. Stalke, M. John, *Chemphyschem,* **2013**, *14*, 3103.

[16] J. Allen, K. Damodaran, *Magn. Reson. Chem.,* **2015**, *53*, 200.

intermediates[17] or to avoid *z*-gradient imperfections in diffusion NMR experiments.[18]

ii. Achievement of a selective and simultaneous signal perturbation, where each proton frequency is excited at different *z* positions (Figure 5C). This is the basis of the original ZS experiment,[3] and it has also been applied in single-scan T_1 relaxation time measurements,[19] to measure coupling constants,[20] or for the efficient diagonal peak suppression in 2D experiments.[21]

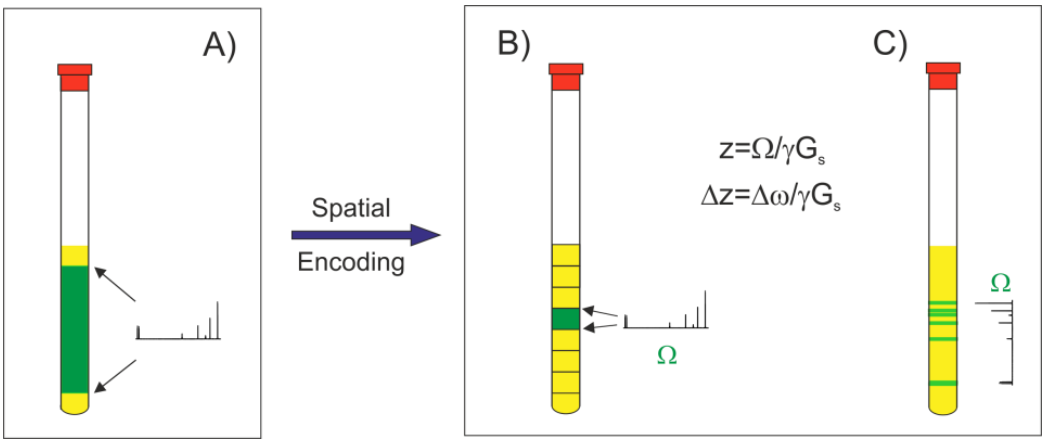

Figure 5: Different strategies to induce spatial selection along the *z*-axis of a NMR tube: A) standard excitation/detection over the entire coil; B) single-slice selection; C) frequency-selective spatial selection.

Most of the reported slice-selective applications have been implemented in conventional liquid-state NMR spectrometers equipped with a basic hardware configuration; this is a direct or indirect detection probe incorporating a gradient coil that can delivers maximum gradient strengths around 50-60 G/cm along the *z*-axis. Experimentally, spatial frequency encoding is achieved by simultaneous application of a frequency-selective 90° or 180° pulses and a weak spatial-encoding PFG (G_s) both with the same duration (Figure 2E-G).

When a PFG is applied along the *z*-axis, the B_0 field is made spatially inhomogeneous by varying linearly along the applied dimension. Thus, during the application of a PFG, different parts of the sample experience a different magnetic field strength depending of their *z*-position, leading to a spatial-dependent frequency shift across the sample volume. Figure 6 compares the effects to apply a hard 90° pulse, a frequency-selective 90° pulse

[17] T. Niklas, D. Stalke, M. John, *Chem. Commun.*, **2014**, *51*, 1275.

[18] a) B. Antalek, *Concepts Magn. Reson.*, **2002**, *14*, 225. b) K. D. Park, Y. J. Lee, *Magn. Reson. Chem.*, **2006**, *44*, 887.

[19] N. M. Loening, M. J. Thrippleton, J. Keeler, R. G. Griffin, *J. Magn. Reson.*, **2003**, *164*, 321.

[20] a) N. Giraud, L. Béguin, J. Courtieu, D. Merlet, *Angew. Chem. Int. Ed.*, **2010**, *49*, 3481. b) M. E. Di Pietro, C. Aroulanda, D. Merlet, *J. Magn. Reson.*, **2013**, *234*, 101.

[21] S. Glanzer, E. Schrank, K. Zangger, *J. Magn. Reson.*, **2013**, *232*, 1.

and a simultaneous frequency-selective 90° pulse/gradient element. In the conventional ^{1}H spectrum, all signals from any part of the NMR tube into the active detector coil contribute to the observed signal (Figure 6A). In the selective experiment, only those signals experiencing the selective pulse contribute to the detected data; although the maximum sensitivity for these signals is retained (Figure 6B). In the slice-selective experiment, a complete ^{1}H spectrum can be obtained using optimized pulses and gradients, but each individual signal exclusively comes from a different part of the tube along the *z*-dimension (Figure 6C). As an obvious consequence, a decrease of overall sensitivity is always associated with any slice-selective experiment, which is proportional to the number of generated *z*-slices.

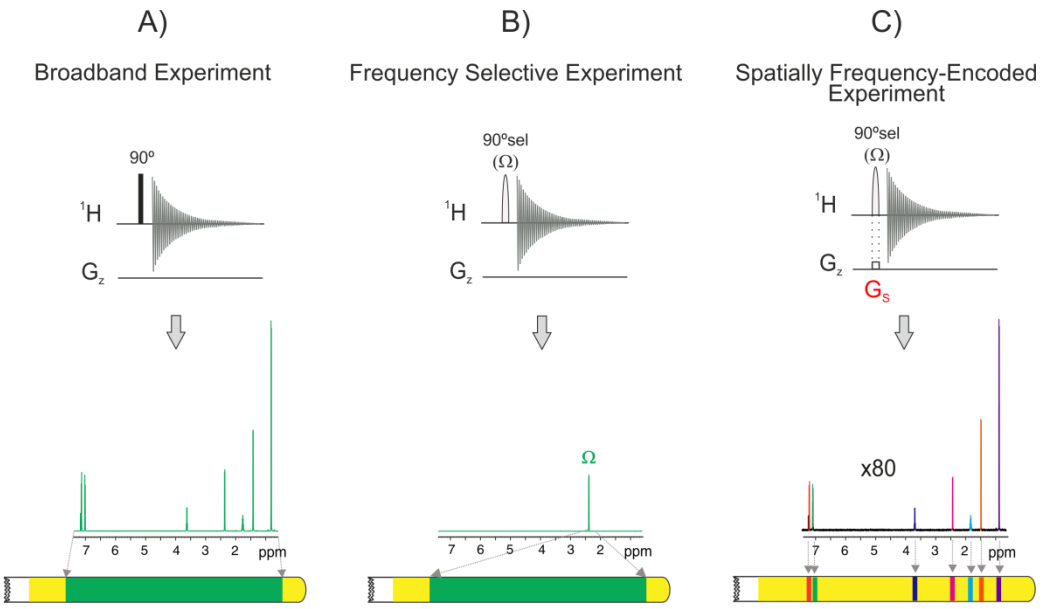

Figure 6: General illustration to understand slice-selective excitation: A) conventional acquisition scheme to obtain a ^{1}H spectrum; B) selective excitation using a frequency-selective 90° pulse; C) slice selection consisting of the simultaneous application of a 90° frequency-selective pulse and a weak encoding gradient (G_s). In the latter case, the full spectrum is obtained thanks to the spatial-dependent *z*-position of each individual resonance along the NMR tube.

Experimentally, the range of sampled frequencies (SW_G) which include the entire chemical shift of interest is defined by the strength of G_S according to:

$$SW_G = \gamma L G_S \qquad \text{Eq.1.5}$$

where γ is the gyromagnetic ratio of the spatially-encoded nucleus and L is the active volume coil length.

On the other hand, the carrier frequency (Ω) and the selective pulse bandwidth ($\Delta\omega$) determine the *z*-position of each nuclear spin (z) and the slice thickness (Δz) according to these two expressions, respectively:

$$z = \Omega/ (\gamma G_S) \quad \text{Eq. 1.6}$$

$$\Delta z = \Delta\omega/ (\gamma G_S) \quad \text{Eq. 1.7}$$

The *Signal to Noise Ratio* (SNR) in slice-selective experiments depends on the active slice thickness because the detected signal only comes from a selected *z*-slice. As shown, Δz depends both on the strength of G_S (which is proportional to SW_G) and on the selectivity of the pulse (which should not exceed the smallest chemical shift difference expected between any coupled proton pairs). For instance, a typical 20 ms Gaussian shaped 180° pulse (bandwidth of 60.7 Hz) applied simultaneous with a gradient G_S of 0.74 G/cm splits the sample height (L=1.8 cm) into around 94 slices along the *z* axis, defining a Δz of about 0.019 cm and covering an SW_G of 5694 Hz (9.5 ppm in a 600 MHz spectrometer). Thus, under these general conditions, the single-slice selection procedure would afford only about 1% of the sensitivity of a conventional ^{1}H spectrum.

Another fundamental aspect when optimizing and applying slice-selection in homodecoupling experiments it is the presence of strong couplings. Slice selection works well for weakly coupled spin systems, but it can fail for strongly coupled signals. If the chemical shift difference ($\Delta\delta$) of coupled spins is less than the selective pulse bandwidth

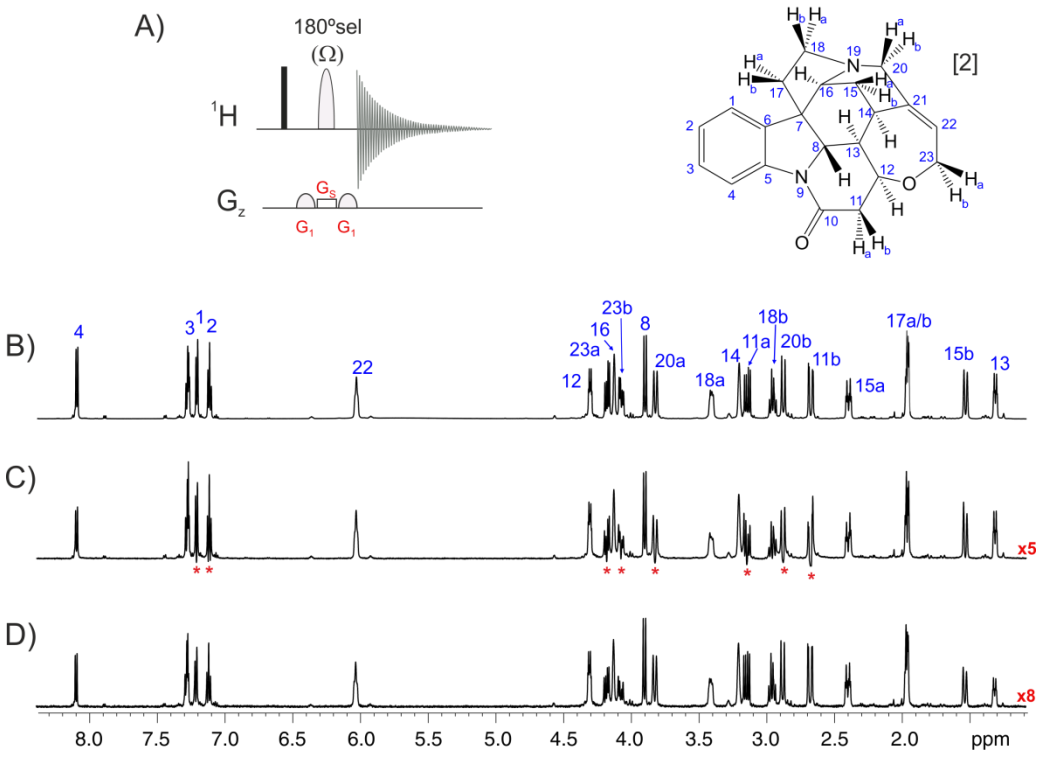

Figure 7: A) Pulse scheme of the ss-SPFGE experiment. B) 600 MHz ^{1}H NMR spectrum of strychnine [2] in $CDCl_3$; C,D) ss-SPFGE spectra acquired with an encoding strength of 1.1 G/cm and with a selective 180° ^{1}H gaussian-shaped pulse of C) 20 and D) 30 ms, respectively. In C) phase distorted multiplets are observed due to the excitation of two *J*-coupled protons into the same slice. Also note the different SNR observed in C and D in function of the selective 180° ^{1}H pulse applied.

($\Delta\omega$) but they are not very strongly coupled ($\Delta\omega > \Delta\delta > J$), couplings within $\Delta\omega$ become active, but the effects of couplings to other spins remain suppressed, retaining much of the resolution advantage. Where spins are fairly strongly coupled ($\Delta\omega > \Delta\delta \approx J$), weak extra signals appear at intermediate frequencies, and if they are very strongly coupled ($\Delta\omega > J > \Delta\delta$), it will typically yields distorted signals. The optimum selective 180^{o} pulse and the encoding G_s gradient strength can be calibrated using a *Slice-Selective Single Pulsed Field Gradient Echo* (ss-SPFGE) experiment (Figure 7A). The excitation of two *J*-coupled protons into the same slice can be observed as phase distorted multiplets (*Anti-Phase* (AP) contributions) in the corresponding 1D ss-SPFGE spectrum (Figure 7C).

1.1.2. Homodecoupling acquisition modes

1.1.2.1. Historical review

Each signal in a ^{1}H NMR spectrum exhibits a particular multiplet J_{HH} pattern as a result of its through-bond interactions with their neighboring protons. Thus, experimental issues such as signal dispersion, spectral resolution or signal overlap become very relevant to identify and assign each individual signal, in particular when a large number of resonances are present in a narrow range of frequencies. The use of NMR methods affording simplified multiplet structures are of interest because they can facilitate the analysis and the interpretation of the corresponding spectra. The traditional way to achieve such simplification is by frequency-selective continuous-wave irradiation on a single-target signal during the acquisition period.[22] The method has been improved by multiple irradiation of different signals using multiple-frequency homodecoupling,[23] polychromatic pulses[24] or irradiating a group of signals resonating into the same region,[25] among others,[26] being one of the most reported applications the band-selective homodecoupling of the well-defined NH or H_α regions in peptides and proteins.[27] All

[22] W. A. Anderson, R. Freeman, *J. Chem. Phys.,* **1962**, *37*, 85.

[23] A. P. D. M. Espindola, R. Crouch, J. R. DeBergh, J. M. Ready, J. B. MacMillan, *J. Am. Chem. Soc.,* **2009**, *131*, 15994.

[24] D. Carnevale, T. F. Segawa, G. Bodenhausen, *Chem. Eur. J.,* **2012**, *18*, 11573.

[25] a) C. W. Vander Kooi, E. Kupče, E. R. P. Zuiderweg, M. Pellecchia, *J. Biomol. NMR,* **1999**, *15*, 335. b) A. Hammarström, G. Otting, *J. Am. Chem. Soc.,* **1994**, *116*, 8847. c) E. Kupče, R. Freeman, *J. Magn. Reson. Ser. A*, **1993**, *102*, 364. d) J. P. Jesson, P. Meakin, G. Kneissel, *J. Am. Chem. Soc.,* **1973**, *95*, 618. E) J. Weigelt, A. Hammarström, W. Bermel, G. Otting, *J. Magn. Reson.,* **1996**, *110*, 219.

[26] V. D. M. Koroleva, N. Khaneja, *J. Chem. Phys.,* **2012**, *137*, 094103.

[27] a) E. Kupče, H. Matsuo, G. Wagner, "*Biological Magnetic Resonance: Modern Techniques in Protein NMR*", Springer,(Eds: N. R. Krishna, L. J. Berliner), **1999**, *16*, 149. b) E. Kupče, G. Wagner, *J. Magn. Reson.,* **1995**, *109*, 329. c) E. Kupče, G. Wagner, *J. Magn. Reson.,* **1996**, *110*, 309. d) B. Vögeli, H. Kovacs, K. Pervushin, *J. Biomol. NMR,* **2005**, *31*, 1.

these approaches do not provide broadband homodecoupling in the entire spectrum, so only multiplet patterns of some signals are partially simplified according to the irradiated signals, and therefore, success is limited to specific and well-isolated spin systems.

A simple and classical approach to achieve a broadband homodecoupled ^{1}H spectrum is the 1D projection extracted from the detected dimension of a tilted homonuclear 2D *J*-resolved experiment.[28] The standard experiment suffers of poor phase-twist lineshapes and alternatives to obtain absorptive homonuclear spectra, such as the incorporation of spatial-selective encoding at expense of important sensitivity losses[28k] or using a *z*-filter combined with a post-processing pattern recognition algorithm[28l] have been proposed. Another drawback that has been recognized and evaluated in detail is the presence of extra peak artifacts due to strong coupling effects.[28j] The use of appropriate data processing in *J*-resolved experiments has also been an interesting topic to enhance sensitivity.[29] The *J*-resolved module has been appended as an NMR building block to standard 2D experiments, such as reported for homodecoupled versions of DOSY[30] and HMBC experiments,[28o] although that the resulting experiments become more time-consuming than the original ones. The *J*-resolved experiment has also been successfully used in the determination of small chemical shifts differences in complex mixtures, such as metabonomics[31] or enantiodiferentation[28n] studies, among others.

Separation of chemical shifts and *J* couplings while retaining absorption-mode lineshapes can also be obtained from the diagonal projected spectrum of a modified anti *z*-COSY experiment.[32] Another group of NMR experiments performs broadband homonuclear decoupling in the indirectly detected dimension of multi-dimensional experiments using time reversal,[33] constant-time evolution,[34] or BIRD editing in the case of heteronuclear experiments.[35]

---

[28] a) W. P. Aue, J. Karhan, R. R. Ernst, *J. Chem. Phys.,* **1976**, *64*, 4226. b) A. Bax, R. Freeman, G. A. Morris, *J. Magn. Reson.,* **1981**, *43*, 333. c) A. J. Shaka, J. Keeler, R. Freeman, *J. Magn. Reson.*,**1984**, *56*, 294. d) M. Woodley, R. Freeman, *J. Magn. Reson. Ser. A,* **1994**, *109*, 103. e) M. Woodley, R. Freeman, *J. Magn. Reson. Ser. A,* **1994**, *111*, 225. f) J. M. Nuzillard, *J. Magn. Reson.,* **1996**, *118*, 132. g) S. Simova, H. Sengstschmidt, R. Freeman, *J. Magn. Reson.,* **1997**, *124*, 104. h) V. Mandelshtam, H. Taylor, A. J. Shaka, *J. Magn. Reson.,* **1998**, *133*, 304. i) P. Mutzenhardt, F. Guenneau, D. Canet, *J. Magn. Reson.,* **1999**, *141*, 312. j) M. J. Thrippleton, R. A. E. Edden, J. Keeler, *J. Magn. Reson.,* **2005**, *174*, 97. k) A. J. Pell, J. Keeler, *J. Magn. Reson.,* **2007**, *189*, 293. l) B. Luy, *J. Magn. Reson.,* **2009**, *201*, 18. m) U. R. Prabhu, S. R. Chaudhari, N. Suryaprakash, *Chem. Phys. Lett.,* **2010**, *500*, 334. n) S. R. Chaudhari, N. Suryaprakash, *Chem. Phys. Lett.,* **2013**, *555*, 286. o) P. Sakhaii, B. Haase, W. Bermel, *J. Magn. Reson.,* **2013**, *228*, 125.

[29] P. Sakhaii, W. Bermel, *J. Magn. Reson.,* **2014**, *242*, 220.

[30] a) J. C. Cobas, M. Martín-Pastor, *J. Magn. Reson.,* **2004**, *171*, 20. b) L. H. Lucas, W. H. Otto, C. K. Larive, *J. Magn. Reson,*. **2002**, *156*, 138.

[31] C. Ludwig, M. R. Viant, *Phytochem. Anal.,* **2010**, *21*, 22.

[32] A. J. Pell, R. A. E. Edden, J. Keeler, *Magn. Reson. Chem.,* **2007**, *45*, 296.

[33] O. W. Sørensen, C. Griesinger, R. R. Ernst, *J. Am. Chem. Soc.,* **1985**, *107*, 7778.

Actually, the homonuclear decoupling in most of current pure shift experiments is carried out in the direct dimension (so-called "proton dimension" or "acquisition dimension"). There are two different schemes available to achieve broadband homodecoupling in the acquisition dimension: (i) a pseudo-2D acquisition mode where a 1D homodecoupled *Free Induction Decay* (FID) is reconstructed by concatenating data chunks extracted from individual time domain datasets of a 2D experiment[3] and (ii) a real-time acquisition mode that provides directly the homodecoupled 1D FID.[8,36]

1.1.2.2. Pseudo-2D Zangger-Sterk experiment

The original *Zangger-Sterk* (ZS) experiment, reported in 1997,[3] uses a slice-selective 2D pulse timing where a variable delay is incremented stepwise as usual (Figure 8A). The homodecoupling block (see several options in Figure 2) is applied in the middle of this incremented delay to refocus any J_{HH} evolution. A special post-processing is needed, where the first data chunks of each FID are assembling to create a new reconstructed 1D FID that is processed and transformed by ordinary procedures to lead a homodecoupled ^{1}H NMR spectrum. Later, a more robust ZS pulse scheme version was proposed where the timing of the decoupling element was carefully designed to provide homodecoupling in the middle of each data chunk, whereas PFGs were also applied to afford better spectral quality by suppressing strong signals from passive spins.[37]

Experimentally, the evolution time (t_1) in the ZS experiment is incremented according to $1/SW_1$, where SW_1 is the defined spectral width in the indirect dimension (typically SW_1=60-100 Hz), and the first 10-20 ms of each individual FID are selected and concatenated for a further FID reconstruction. In case of large scalar coupling constants, the increments must be set to smaller values in order to avoid scalar coupling evolution. The residual effect is a slight decrease in signal intensity either side of the time at which *J* is refocused so that in each chunk the signal intensity is slightly less at the edges than in the center. Fourier transformation converts this periodic decrease in intensity into small

[34] a) M. E. Girvin, *J. Magn. Reson. Ser. A,* **1994**, *108*, 99. b) F. J. M. van de Ven, M. E. P. Philippens, *J. Magn. Reson.,* **1992**, *97*, 637. c) Y. Xia, G. Legge, K. Y. Jun, Y. Qi, H. Lee, X. Gao, *Magn. Reson. Chem.,* **2005**, *43*, 372. d) M. Rance, G. Wagner, O. W. Sørensen, K. Wüthrich, R. R. Ernst, *J. Magn. Reson.,* **1984**, *59*, 250. e) A. Bax, R. Freeman, *J. Magn. Reson.,* **1981**, *44*, 542. f) A. G. Palmer, W. J. Fairbrother, J. Cavanagh, P. E. Wright, M. Rance, *J. Biomol. NMR,* **1992**, *2*, 103. g) A. Bax, A. F. Mehlkopf, J. Smidt, *J. Magn. Reson.,* **1979**, *35*, 167. h) B. T. Farmer, L. R. J. Brown, *J. Magn. Reson.,* **1987**, *71*, 365. i) J. A. Aguilar, A. A. Colbourne, J. Cassani, M. Nilsson, G. A. Morris, *Angew. Chem. Int. Ed.,* **2012**, *51*, 6460.

[35] A. Bax, *J. Magn. Reson.,* **1983**, *53*, 517.

[36] N. H. Meyer, K. Zangger, *Angew. Chem. Int. Ed.,* **2013**, *52*, 7143.

[37] J. A. Aguilar, S. Faulkner, M. Nilsson, G. A. Morris, *Angew. Chem. Int. Ed.,* **2010**, *49*, 3901.

artifacts, typically in the form of weak sidebands at multiples of SW_1, around each decoupled signal. The intensity of the sidebands is proportional to the square of J/SW_1, and it decays rapidly either side of the decoupled signal. In typical SW_1 condition used in these experiments the sidebands are of comparable intensity to that of the ^{13}C satellites. On the other hand, the resolution of the signals is directly related with the number of increments in the indirect dimension. Normally 16-32 increments are enough to obtain a high-quality 1D homodecoupled spectrum with optimum resolution and narrow line widths. Only as a reference, typical standard parameters to afford a nice 1D homodecoupled spectrum in ~5-10 minutes for a sample concentration about 10 mM would involve Gaussian or rSNOB shaped 180^o ^1H pulses with a duration of 40-60 ms and an encoding G_s gradient around 0.5-1 G/cm. Under these general conditions, the pseudo-2D ZS method would afford only ~1-5% of the sensitivity of a conventional ^1H spectrum. SNR could be improved by using shorter and less selective pulses and/or less intense encoding gradients but always with an increased probability of accidental excitation of two coupled protons within the same *z*-slice. The original ZS experiment was based on slice-selection[3] and a BIRD-based ZS experiment has also been reported,[10] but in both cases the sensitivity is still far from that obtained in conventional ^1H NMR spectra.

In a recent improvement, referred to as *Pure Shift Yielded by Chirp Excitation* (PSYCHE) experiment,[38] a pair of low flip angle swept-frequency pulses applied during a weak PFG are used as a selective inversion element (Figure 2H). By adjusting the pulse flip angle of the adiabatic pulse, it is possible to balance optimum sensitivity and full broadband homodecoupling for all signals in a given sample. PSYCHE can offer sensitivity improvements of almost one order of magnitude over conventional ZS methods performed by slice-selection or BIRD pulses.

The pseudo-2D ZS experiment has been recently applied to measure homonuclear[39] and heteronuclear coupling constants,[12c,40] and successfully implemented into a number of 2D experiments, as reported for pure shift DOSY,[37,41] TOCSY,[42] NOESY,[34i] HSQC[6,11,12a]

[38] M. Foroozandeh, R. W. Adams, N. J. Meharry, D. Jeannerat, M. Nilsson, G. A. Morris, *Angew. Chem. Int. Ed.,* **2014**, *53*, 6990.

[39] S. R. Chaudhari, N. Suryaprakash, *ChemPhysChem,* **2015**, *16*, 1079.

[40] a) S. R. Chaudhari, N. Suryaprakash, *RSC Adv.,* **2014**, *4*, 15018. b) I. Timári, T. Z. Illyés, R. W. Adams, M. Nilsson, L. Szilágyi, G. A. Morris, K. E. Kövér, *Chem. Eur. J.,* **2015**, *21*, 3472.

[41] a) M. Nilsson, G. A Morris, *Chem. Commun.,* **2007**, 933. b) S. Islam, J. A. Aguilar, M. W. Powner, M. Nilsson, G. A. Morris, J. D. Sutherland, *Chem. Eur. J.,* **2013**, *19*, 4586.

[42] a) G. A. Morris, J. A. Aguilar, R. Evans, S. Haiber, M. Nilsson, *J. Am. Chem. Soc.,* **2010**, *132*, 12770. b) J. J. Koivisto, *Chem. Commun.,* **2013**, *49*, 96. C) M. Foroozandeh, R. W. Adams, M. Nilsson, G. A. Morris, *J. Am. Chem. Soc.,* **2014**, *136*, 11867.

and HSQMBC.[40b] The main drawback of these resulting pseudo-3D experiments is that their overall acquisition times can become extremely long for routine use.

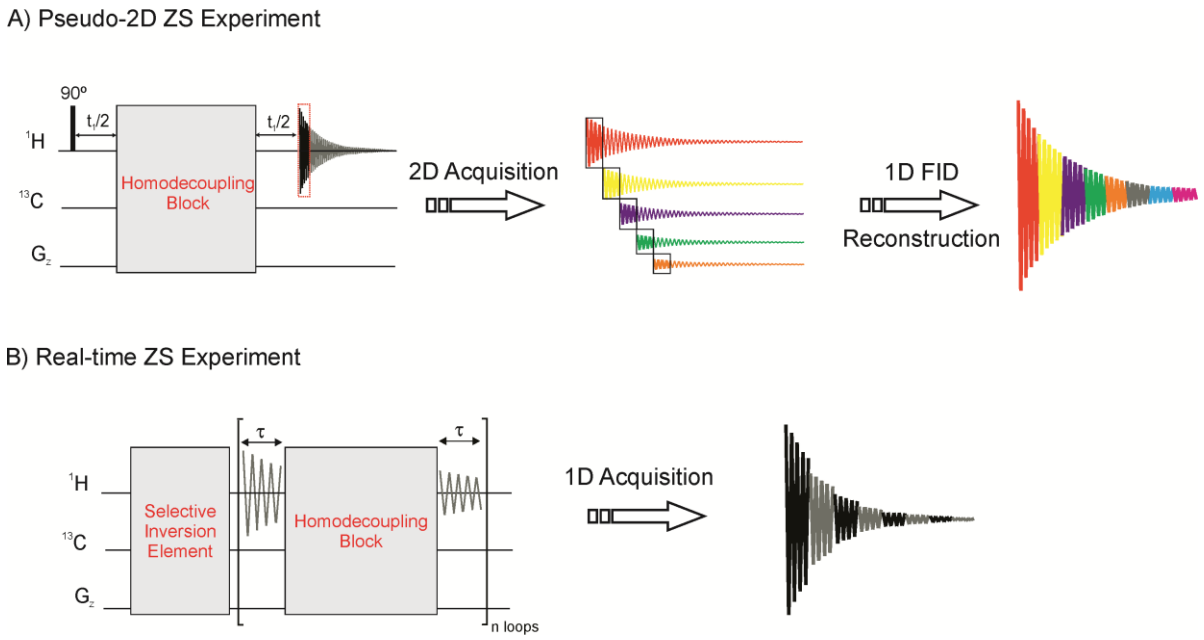

Figure 8: General schemes leading to 1D broadband homodecoupled ^{1}H NMR spectra: A) the original ZS method is based on a 2D acquisition mode followed by an FID reconstruction from the initial data chunks of each increment; B) the real-time ZS experiment incorporates periodically the homodecoupling block in the middle of the FID acquisition. The homodecoupling block in both approaches can be any option described in Figure 2.

1.1.2.3. Real-time ZS experiment

Real-time broadband homodecoupling was initially proposed using the BIRD element as homodecoupling block during data acquisition,[8] and shortly after, a slice selective version was also reported[36] using the general scheme of Figure 8B. This new acquisition technique, referred to as real-time ZS or *HOmodecoupled BroadBand* (HOBB), directly generates a single 1D FID that after standard processing can lead to a broadband homodecoupled 1D ^{1}H NMR spectrum. This method offers instant and speed-up data acquisition and an improved SNR per time unit compared to the original ZS experiment, although the attainable sensitivity is still far from a regular ^{1}H spectrum because of the involved ^{13}C editing or slice selection procedures.

In the real-time ZS method, instead of recording each fraction of the FID in a series of individual experiments, the FID is collected directly in a single scan. The acquisition is interrupted after every τ period to perform either slice-selective or BIRD-based

homodecoupling, as shown in Figure 9A. Note, that the first fraction of acquisition is only half as long as the subsequent ones. Thereby, full scalar decoupling is achieved in the middle of each fraction of the FID. These acquisition segments are assembled consecutively in a conventional FID which can be treated like a regular 1D NMR experiment. The τ period is defined as AQ/2*n* where AQ is the acquisition time and *n* the number of loops. As long as $\tau << 1/J_{HH}$, homonuclear *J* modulations occurring during these acquisition segments can be disregarded with no compromise in the final spectral resolution, leading to the potential collapse of all J_{HH} splittings. As in the pseudo-2D acquisition mode, deviations from this condition lead to incomplete homodecoupling and the appearance of distinct decoupling sidebands flanking each purely shifted resonance at spacing multiples of 2*n*/AQ. Moreover, while the acquisition is interrupted for decoupling, the magnetization is relaxing, and therefore, it is critical to keep the interruptions as short as possible, especially for larger molecules that have shorter T_2 relaxation times. As longer time interruptions, there are more differences in intensity between previous and next acquired FID. Fourier transform converts this periodic FID discontinuity in sidebands at multiples of 2n/AQ, around each decoupled signal. The intensity of these sidebands is greater the larger is the FID discontinuity. On the other hand, it is also important to keep the interruptions as short as possible because the signals are slightly broadened due to the extra T_2 relaxation during this refocusing time. If a BIRD-based homodecoupling block is used, the FID is interrupted about 6-8 ms (to $^1J_{CH}$ between 120-160 Hz). In the case of use a selective 180^o pulse, a compromise duration of 5-10 ms balances between an optimum slice selection and an effective homodecoupling of nearby signals, while minimizes the T_2 relaxation effects.

In practice, real-time ZS acquisition reduces the overall experimental time and improving SNR per time unit but at some cost in spectral quality and the achievement of wider line widths. As an example, the HOBB spectrum of cyclosporine, quickly acquired in a single scan, shows full homodecoupling for most of the signals (except in some aliphatic CH_2 resonances) thanks to the well dispersed spin systems (Figure 9C). Importantly, the SNR of the HOBB experiment also suffers of the unavoidable losses due to slice selection (~8% of the maximum theoretical signal).

The real-time ZS acquisition mode becomes an attractive NMR building block for the design of pure shift methods and, as a major advantage, it can be incorporated as a detection scheme in standard multidimensional experiments without increase their original dimensionalities and continuing to use the same data-processing protocols. This represents a boost in SNR per time unit when compared to the pseudo-2D ZS experiment,

as reported recently for HOBB-DOSY,[43] HOBB-TOCSY,[36] HOBB-ROESY,[44] and HOBB-HSQC[9,12b,45] experiments. From a strategic point of view, it is advisable to optimize first a 1D HOBB experiment in order to determine the best homodecoupling conditions for the sample under study. The signal simplification observed in the resulting 2D HOBB spectra will be the same obtained in a 1D HOBB spectrum recorded under the same conditions.

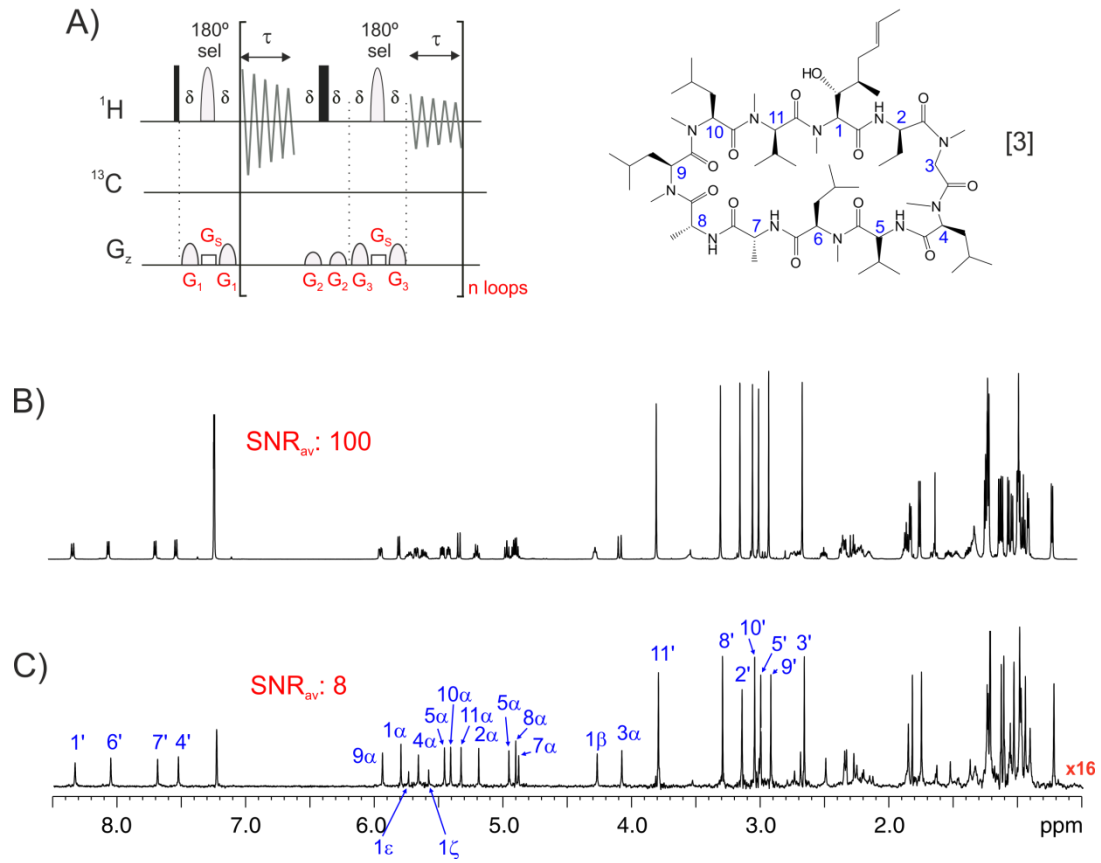

Figure 9: A) General pulse scheme of the real-time 1D HOBB experiment; B) 600 MHz conventional ^{1}H spectrum of cyclosporine [3]; C) 1D HOBB spectrum acquired with a RE-BURP pulse of 5 ms for both excitation and decoupling and G_s=1.1 G/cm. For an objective comparison of real sensitivities, the experimental averaged SNR is indicated for each 1D dataset. For a real comparison, both spectra have been recorded and processed in the same way: with the same receiver gain, using a single scan, processed with a Fourier transformation without any additional window function and plotted with the same absolute vertical scaling factor.

[43] S. Glanzer, K. Zangger, *Chem. Eur. J.,* **2014**, *20*, 11171.

[44] V. M. R. Kakita, J. Bharatam, *Magn. Reson. Chem.,* **2014**, *52*, 389.

[45] N. H. Meyer, K. Zangger, *Chem. Commun.,* **2014**, *50*, 1488.

1.1.3. Homodecoupled experiments and applications

Recently, all of the aforementioned ZS methodologies, using BIRD or slice-selective homodecoupling and pseudo-2D or real-time acquisition modes, have been implemented in different 1D and 2D NMR experiments (Table 1). It is important to note that a requirement for a success implementation of any ZS module is to have *In-Phase* (IP) proton-proton magnetization because experiments involving AP signals, like those found in conventional COSY or HMBC, cancel out under homodecoupling conditions.

Pure shift NMR spectra have a wide range of potential uses, as demonstrated for the analysis of complex mixtures,[37] to carry out structural elucidation studies,[9,11,12b,34i,36,42a,42b,44,45] to analyze diffusion data[43]and to measure homonuclear[39] and heteronuclear coupling constants.[6,11,12c,40] A more exhaustive description of the different applications can be found in a recent review work publish by us.[1] As a complement to this introduction, two excellent and very comprehensive revision works about broadband homodecoupling methods, including detailed description of all indirect methods, have been also reported recently.[46]

Table 1: Summary of reported broadband homodecoupled 1D and 2D ^{1}H NMR experiments.

		Homodecoupling		Acquisition mode		
NMR Experiment		**BIRD**	**Slice selection**	**Pseudo-2D**	**Real-time**	**References**
1D	^{1}H NMR	✓		✓		[10][12c]
			✓	✓		[3][37][38][40a][47][48]
		✓			✓	[8][12d]
			✓		✓	[36]
	Quick-Serf		✓		✓	[49][50]
2D	TOCSY		✓	✓		[42]
			✓		✓	[36]
	DOSY		✓	✓		[37][41]
			✓		✓	[43]
	NOESY		✓	✓		[34i]
	ROESY		✓		✓	[44]
	HSQC/HSQCed		✓		✓	[45]
		✓		✓		[6][7][11][12a]
		✓			✓	[9]
	HSQMBC		✓	✓		[40b]

[46] a) N. H. Meyer, K. Zangger, *ChemPhysChem,* **2014**, *15*, 49. b) R. W. Adams, eMagRes, **2014**, *3*, 295.

[47] P. Sakhaii, B. Haase, W. Bermel, R. Kerssebaum, G. E. Wagner, K. Zangger, *J. Magn. Reson.,* **2013**, 233, 92.

[48] N. Lokesh, N. Suryaprakash, *Chem. Commun.,* **2014**, *50*, 8550.

[49] N. Gubensäk, W. M. F. Fabian, K. Zangger, *Chem. Commun.,* **2014**, *50*, 12254.

[50] N. Lokesh, S. R. Chaudhari, N. Suryaprakash, *Chem. Commun.,* **2014**, *50*, 15597.

1.2. 2D HSQC and HSQMBC NMR experiments[51]

Proton-detected heteronuclear 2D NMR experiments, essentially based on two different pulse schemes referred to as *Heteronuclear Single Quantum Correlation* (HSQC)[52] and *Heteronuclear Multiple Quantum Correlation* (HMQC),[53] have been key NMR tools during many years for chemists and biochemists to provide valuable structural information on ^{1}H-^{13}C (and ^{1}H-^{15}N) chemical bonds. These experiments provide information about structure, conformation and dynamics of rigid and flexible molecules in solution, as well as they can serve for many other interests such as structural validation methods, determine intermolecular interactions or to measure *Residual Dipolar Couplings* (RDCs) in molecules dissolved in weakly aligned media. Nowadays, these experiments are usually performed in a complete automation mode in both data acquisition and processing steps, practically without any need for direct user intervention. The resulting 2D maps are very simple to analyze and to interpret, even for non-experienced NMR users, typically displaying well dispersed cross-peaks that correlate ^{1}H (direct F2 dimension) and ^{13}C (indirect F1 dimension) chemical shifts between directly attached ^{1}H-^{13}C groups, through the $^{1}J_{CH}$ transfer mechanism (Figure 10A,B).

The HMQC scheme is simpler in terms of the number of pulses, but its major complication relies on that proton magnetization is located in the transverse plane during the entire pulse sequence. Additionally, proton-proton coupling constants (J_{HH}) also evolve during the variable t_1 period and, as a result, cross peaks present strongly distorted twist-phased patterns along the detected F2 dimension and a characteristic skew shape along the indirect F1 dimension of the 2D map. On the other hand, the HSQC experiment uses *Insensitive Nuclei Enhanced by Polarization Transfer* (INEPT) blocks for heteronuclear magnetization transfer, and the evolution during the t_1 period is not affected by $J_{HH.}$ However, the influence of J_{HH} coupling evolution during the INEPT period on the phase and amplitude signal modulation must be considered when a detailed analysis is required.

To better understand the improved HSQC-related experiments described in the "Results and Discussion" section, this introduction aims to explain the fundamental key points of HSQC-type experiments. Special focus will be made on the effects of the intensity and phase signal modulation dependence with respect to J_{CH} and $J_{HH.}$ A recommendable work describing the different features, options and practical details of

[51] Part of this introduction has been adapted from: L. Castañar, T. Parella, *Annu. Rep. NMR Spectrosc.,* **2015**, *84*, 163.

[52] G. Bodenhausen, D. J. Ruben, *Chem. Phys. Lett.,* **1980**, *69*, 185.

[53] A. Bax, R. Griffey, B. Hawkins, *J. Mag. Reson.,* **1983,** *55*, 301.

both HMQC and HSQC experiments is available as a complementary reading to this introduction.[54]

1.2.1. The HSQC experiment

Since its introduction, the HSQC experiment has been modified in so many different ways in order to improve important experimental aspects (such as sensitivity, resolution, efficiency, robustness and performance) and to provide additional and complementary information from a single NMR experiment. All these modifications have been done changing and/or introducing some elements or building blocks in the pulse scheme, therefore a detailed study of the basic HSQC pulse sequence is advisable for a better understanding of the further improvements.

1.2.1.1. Basic HSQC pulse scheme

Figure 10C shows the five basic independent steps that can be identified in a standard 2D gradient-selected HSQC pulse scheme:

1- The pre-scan period is usually defined by a long recycle delay (some seconds of duration, accordingly to the existing $T_1(^1H)$ relaxation times) to allow the recovery of the ^1H magnetization to a pre-equilibrium state just before to start the sequence.

2- After the initial ^1H excitation, heteronuclear transfer takes place using an INEPT block optimized to single $^1J_{CH}$ value, accordingly to $\Delta=1/(2^1J_{CH})$.

3- AP ^{13}C *Single Quantum Coherences* (SQCs) evolve during a variable t_1 period under the effect of ^{13}C chemical shift whereas the evolution of $^1J_{CH}$ is refocused by the central 180^o ^1H pulse.

4- During the refocused INEPT element, ^{13}C magnetization is reconverted to AP ^1H magnetization followed by the subsequent $^1J_{CH}$ evolution to generate IP magnetization prior to acquisition.

5- The sequence finishes with a ^1H detection period under optional broadband heteronuclear decoupling.

[54] P. K. Mandal, A. Majumdar, *Conc. Magn. Reson.*, **2004**, *20A*, 1.

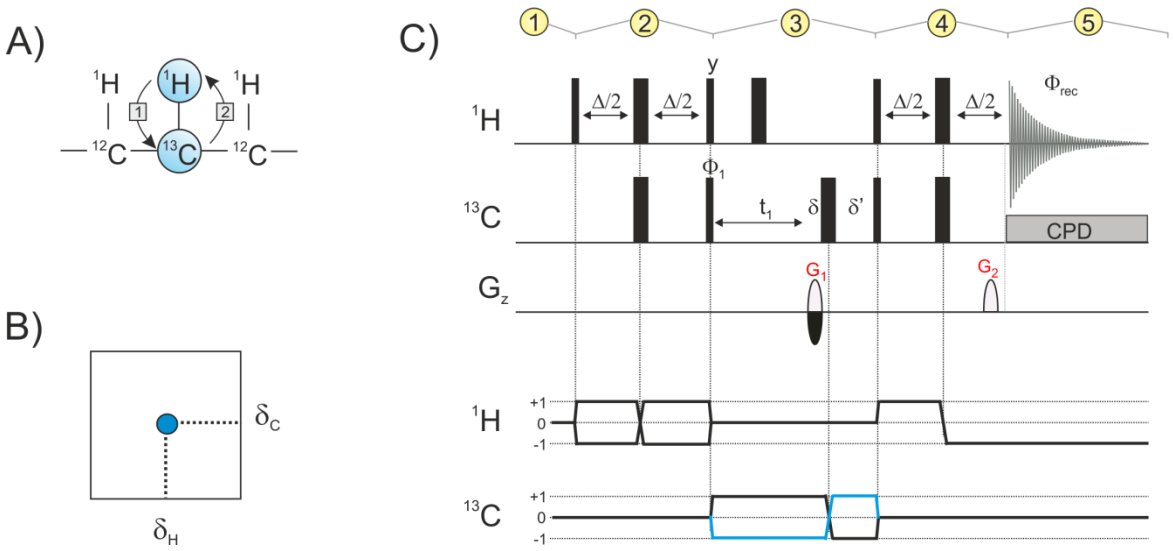

Figure 10: Schematic representation of the A) molecular transfer mechanism; B) cross-peak pattern and C) pulse sequence of a standard 2D ^{1}H-^{13}C HSQC experiment. Thin and thick vertical rectangles represent 90° and 180° hard pulses, respectively. The delay Δ should be set to $1/(2^{1}J_{CH})$ and δ represents the duration of the PFG and its recovery delay. Coherence selection is performed by the gradient pair G_1:G_2 (±80:20.1) using the echo-antiecho protocol. A basic two-step phase cycling is executed with Φ_1= x,-x and Φ_{rec}= x,-x. Below, the corresponding coherence transfer pathway diagram is shown: blue line stands for N-type magnetization (echo dataset), while black line stands for P-type magnetization (anti-echo dataset).

Historically, a major development in HSQC pulse sequence was the incorporation of PFGs for *Coherence Transfer Pathway* (CTP) selection. PFGs allow a clear distinction between ^{1}H-^{12}C *vs* ^{1}H-^{13}C magnetization, which results in the collection of high-quality HSQC spectra under standard routine conditions.[55] One of the most widely protocols used to achieve coherence selection using PGFs is the *Echo/Anti-echo* (E/A) method.[54,56] For a successful implementation of such methodology, two different PFGs must be properly inserted into the HSQC pulse sequence (Figure 10C): the encoding G_1 gradient will select CTPs in which only ^{13}C SQCs are in the transverse plane during the evolution t_1 period, and the decoding G_2 gradient will select CTPs in which only ^{1}H magnetization is in the transverse plane during the detection t_2 period.

An important aspect when applying PFGs during t_1 is that the signal obtained is not sine/cosine amplitude-modulated but phase modulated, which means that is modulated according to the rotation sense of the magnetization (S^{+}, echo; or S^{-}, anti-echo). This results in P-type data selection (anti-echo), in which the sense of the frequency modulation is the same in t_1 and t_2, and in N-type data selection (echo), in which the sense is the opposite:

[55] a) T. Parella, *Magn. Reson. Chem.,* **1998**, *36*, 467. b) W. Willker, D. Leibfritz, R. Kerssebaum, W. Bermel, *Magn. Reson. Chem,* **1993**, *31*, 287.

[56] J. Keeler, "*Understanding NMR spectroscopy*", John Wiley and Sons, Ltd, England, **2007**.

$$S(t_1, t_2)_{anti-echo} = \gamma . e^{i\Omega_S t_1} . e^{i\Omega_S t_2} \quad \text{Eq. 1.8}$$

$$S(t_1, t_2)_{echo} = \gamma . e^{-i\Omega_S t_1} . e^{i\Omega_S t_2} \quad \text{Eq. 1.9}$$

That signal phase encoding makes the gradient only able to select one of the two desired CTPs in each scan. Therefore, the spectrum will present cross peaks with undesirable phase-twisted lineshapes. To solve that problem the acquisition of the E/A pathways has to be done in alternate acquisitions and then combined in a proper way during the processing step to provide amplitude-modulated signals, so that phase-sensitive spectra can be obtained.

For data coherence selection, the gradient strengths have to be adjusted to:

$$\frac{G_1}{G_2} = \frac{\gamma_I}{\gamma_S} \quad \text{Eq. 1.10}$$

where γ_I and γ_S are the gyromagnetic ratio of sensitive (*I*) and insensitive (*S*) nuclei, respectively. In the case of ^{1}H-^{13}C correlation experiments such ratio is $\gamma_H/\gamma_C \approx 4$. N-type coherence (blue line in Figure 10C) is selected using G_1:G_2=4 (typical experimental ratio of 80:20.1 in percentage), while P-type coherence (black line in Figure 10C) is selected by G_1:G_2=-4 (typical experimental ratio of -80:20.1 in percentage).

In terms of sensitivity, the use of PFGs during t_1 produces a SNR decrease by a factor of $\sqrt{2}$ with respect to the original experiment because only one CTP can be selected. Nonetheless, the main advantages are that higher quality spectra are obtained, strong solvent signals (typically water) are efficiently suppressed, t_1 noise is better cleaned, and a considerable decrease in the overall acquisition time is achieved if the use of an extended phase cycle is avoided.

The signal intensity and phase dependences generated during the INEPT periods can be easily analyzed by the PO formalism.[5] To carry out this analysis, a weakly coupled $I_1 I_2 S$ spin system has been defined with a heteronuclear coupling constant ($^{1}J_{IS}$) and a homonuclear coupling constant ($^{n}J_{I1I2}$).

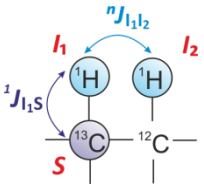

At the beginning of the sequence (step 1 in Figure 10C), the initial magnetization ($+I_{1z}$) is rotated to the *y*-axis ($-I_{1y}$). During the Δ delay (step 2 in Figure 10C), the magnetization evolves simultaneously under the effects of chemical shift (Ω) and coupling constants (*J*). In weakly coupled spin systems, these effects commute and they can be analyzed in

cascade.[57] In the following analysis, each effect is separately analyzed for a better compression.

- *Effect of chemical shift (Ω_I) evolution during the INEPT block*

  The magnetization evolves during the first $\Delta/2$ delay and then, the 180^o (I_x) inverts the I_1 magnetization along the *x*-axis:

$$-I_{1y} \xrightarrow{\Omega_I\,\Delta/2} -I_{1y}\cos\left(\Omega_{I_1}\,\Delta/2\right) + I_{1x}\sin\left(\Omega_{I_1}\,\Delta/2\right) \xrightarrow{180^o\,(I_x)} +I_{1y}\cos\left(\Omega_{I_1}\,\Delta/2\right) + I_{1x}\sin\left(\Omega_{I_1}\,\Delta/2\right)$$

Eq. 1.11

  During the second $\Delta/2$ delay, all components evolve again under the chemical shift effect:

$$\begin{aligned} Eq.\,1.11 \xrightarrow{\Omega_I\,\Delta/2} \; & +I_{1y}\cos\left(\Omega_{I_1}\,\Delta/2\right)\cos\left(\Omega_{I_1}\,\Delta/2\right) - I_{1x}\cos\left(\Omega_{I_1}\,\Delta/2\right)\sin\left(\Omega_{I_1}\,\Delta/2\right) \\ & +I_{1x}\sin\left(\Omega_{I_1}\,\Delta/2\right)\cos\left(\Omega_{I_1}\,\Delta/2\right) + I_{1y}\sin\left(\Omega_{I_1}\,\Delta/2\right)\sin\left(\Omega_{I_1}\,\Delta/2\right) \end{aligned}$$

Eq. 1.12

  Regrouping the terms and applying trigonometric identities:

$$+I_{1y}\left[\cos^2\left(\Omega_{I_1}\,\Delta/2\right) + \sin^2\left(\Omega_{I_1}\,\Delta/2\right)\right] \xRightarrow{\cos^2\theta+\sin^2\theta\,=\,1} +I_{1y}$$

Eq. 1.13

  It can be stated that, during the INEPT block, the magnetization does not evolve under the effect of Ω_I and therefore the I magnetization is refocused to its original position.

- *Effect of heteronuclear coupling constant ($^1J_{I1S}$) evolution during the INEPT block*

  The magnetization evolves during the first $\Delta/2$ delay under the effect of $^1J_{IS}$, the $180°$ (I_x) pulse inverts the I_1 magnetization along the *x*-axis and the $180°$ (S_x) pulse inverts the α/β-labels of the doublet I component:

$$-I_{1y} \xrightarrow{\pi\,J_{IS}\,\Delta/2} \begin{matrix} -I_{1y}\cos\left(\pi J_{I_1S}\Delta/2\right) \\ +2I_{1x}S_z\sin\left(\pi J_{I_1S}\Delta/2\right) \end{matrix} \xrightarrow[180°\,(S_x)]{180^o\,(I_x)} \begin{matrix} +I_{1y}\cos\left(\pi J_{I_1S}\Delta/2\right) \\ -2I_{1x}S_z\sin\left(\pi J_{I_1S}\Delta/2\right) \end{matrix}$$

Eq. 1.14

[57] G. Bodenhausen, R. Freeman, J. *Magn. Reson.,* **1979**, *36*, 221.

During the second $\Delta/2$ delay, both components evolve again under the $^1J_{IS}$ effect:

$$Eq.1.14 \xrightarrow{\pi J_{IS}\Delta/2} \begin{aligned} &+I_{1y}\cos(\pi J_{I_1S}\Delta/2)\cos(\pi J_{I_1S}\Delta/2) \\ &-2I_{1x}S_z\cos(\pi J_{I_1S}\Delta/2)\sin(\pi J_{I_1S}\Delta/2) \\ &-2I_{1x}S_z\sin(\pi J_{I_1S}\Delta/2)\cos(\pi J_{I_1S}\Delta/2) \\ &-I_{1y}\sin(\pi J_{I_1S}\Delta/2)\sin(\pi J_{I_1S}\Delta/2) \end{aligned}$$

Eq. 1.15

Regrouping the terms and applying basic trigonometric identities:

$$\begin{aligned} &+I_{1y}[\cos^2(\pi J_{I_1S}\Delta/2)-\sin^2(\pi J_{I_1S}\Delta/2)] \\ &-2I_{1x}S_z[2\cos(\pi J_{I_1S}\Delta/2)\sin(\pi J_{I_1S}\Delta/2)] \end{aligned} \xrightarrow[2\cos\theta\sin\theta=\sin 2\theta]{\cos^2\theta-\sin^2\theta=\cos 2\theta} \begin{aligned} &I_{1y}\cos(\pi J_{I_1S}\Delta) \\ &-2I_{1x}S_z\sin(\pi J_{I_1S}\Delta) \end{aligned}$$

Eq. 1.16

Now, if the effect of homonuclear J_{I1I2} coupling is not considered, a $90°\,(I_y)$ pulse generates *zz*-magnetization in the form of $2I_{1z}S_z$ and a $90°\,(S_x)$ pulse returns the magnetization to the *xy*-plane but now converted into AP magnetization of the nucleus S:

$$Eq.1.16 \xrightarrow{90°\,(I_y)} +I_{1y}\cos(\pi J_{I_1S}\Delta)+2I_{1z}S_z\sin(\pi J_{I_1S}\Delta) \xrightarrow{90°\,(S_x)} +I_{1y}\cos(\pi J_{I_1S}\Delta)-2I_{1z}S_y\sin(\pi J_{I_1S}\Delta)$$

Eq. 1.17

In summary, during the INEPT block the initial IP $-I_{1y}$ magnetization has been transferred to the S nucleus in the form of AP $2I_{1z}S_y$ magnetization. This coherent heteronuclear magnetization transfer process is the key in most modern multidimensional NMR experiments.

- *Effect of homonuclear coupling constant (J_{I1I2}) evolution during INEPT block*

In conventional HSQC experiments, the effects of the homonuclear $J_{I_1I_2}$ evolution during the INEPT blocks are usually neglected because the contribution of the resulting components is considered low. However, a detailed analysis, as described from Eq. 1.14-1.17, leads to the following four terms at the end of the first INEPT period:

$$-I_{1y} \xrightarrow{INEPT} \begin{aligned} &+I_{1y}\cos(\pi J_{I_1I_2}\Delta)\cos(\pi J_{I_1S}\Delta)-2I_{1z}S_y\cos(\pi J_{I_1I_2}\Delta)\sin(\pi J_{I_1S}\Delta) \\ &+2I_{1z}I_{2x}\sin(\pi J_{I_1I_2}\Delta)\cos(\pi J_{I_1S}\Delta)+4\,I_{1z}I_{2x}S_y\sin(\pi J_{I_1I_2}\Delta)\sin(\pi J_{I_1S}\Delta) \end{aligned}$$

Eq. 1.18

Thus, the initial $-I_{1y}$ magnetization has been converted to four different terms: i) an IP term (I_{1y}), ii) an AP heteronuclear SQC term ($2I_{1z}S_y$), iii) an AP homonuclear SQC term ($2I_{1z}I_{2x}$), and iv) an heteronuclear *Multiple Quantum Coherence* (MQC) term ($4I_{1z}I_{2x}S_y$). Only the second term will be selected by the encoding PGF (G_1 in Figure 10C), which evolves during the t_1 period (step 3 in Figure 10C) according to the heteronuclear chemical shift (Ω_S). By applying an $180°\ (I_x)$ pulse at the middle of the t_1 period, the evolution of the heteronuclear coupling constant is refocused. Hence at the end of this increment t_1 delay, two different components remain:

$$Eq.\,1.18 \xrightarrow{t_1} \begin{matrix} +2I_{1z}S_y \cos(\Omega_S t_1)\cos(\pi J_{I_1I_2}\Delta)\sin(\pi J_{I_1S}\Delta) \\ -2I_{1z}S_x \sin(\Omega_S t_1)\cos(\pi J_{I_1I_2}\Delta)\sin(\pi J_{I_1S}\Delta) \end{matrix}$$

Eq. 1.19A

In terms of shift operators[58] the Eq. 19A can be described as:

$$\begin{matrix} +\frac{1}{i}I_{1z}(S^+ + S^-)\cos(\Omega_S t_1)\cos(\pi J_{I_1I_2}\Delta)\sin(\pi J_{I_1S}\Delta) \\ -I_{1z}(S^+ + S^-)\sin(\Omega_S t_1)\cos(\pi J_{I_1I_2}\Delta)\sin(\pi J_{I_1S}\Delta) \end{matrix}$$

Eq. 1.19B

As it is described in Eq.1.10, G_1 and G_2 gradients select the E/A pathways in alternate acquisitions to obtain the N-type (S^+, echo) and P-type (S^-, antiecho).

Then, two simultaneous $90°\ (I_x)$ and $90°\ (S_x)$ pulses are applied:

$$Eq.\,1.19A \xrightarrow[90°\ (S_x)]{90°\ (I_x)} \begin{matrix} -2I_{1y}S_z \cos(\Omega_S t_1)\cos(\pi J_{I_1I_2}\Delta)\sin(\pi J_{I_1S}\Delta) \\ +2I_{1y}S_x \sin(\Omega_S t_1)\cos(\pi J_{I_1I_2}\Delta)\sin(\pi J_{I_1S}\Delta) \end{matrix}$$

Eq. 1.20

Finally, these two components evolve again under chemical shift, homonuclear and heteronuclear coupling constant effects during the Δ delay of the refocused ^{13}C-to-^{1}H

[58] To describe the effects of PFGs, it is convenient to convert the Cartesian operators I_x and I_y in terms of raising and lowering operators I^+ and I^-:

$$I^+ = I_x + iI_y \qquad I_x = \frac{1}{2}(I^+ + I^-)$$

$$I^- = I_x - iI_y \qquad I_y = \frac{1}{2i}(I^+ + I^-)$$

INEPT block (step 4 in Figure 10C). A decoding PGF (G_2 in Figure 10C) is applied prior to acquisition, which only will select those CTPs involving SQCs of the I spin. The observable magnetization for the heteronuclear three spin system can be described as a mixture of IP and AP components as follows:

$$
\begin{aligned}
&+ I_{1x}\cos^2\left(\pi J_{I_1I_2}\Delta\right)\sin^2\left(\pi J_{I_1S}\Delta\right) && \text{Term I}\\
&- 2I_{1y}S_z\cos^2\left(\pi J_{I_1I_2}\Delta\right)\sin\left(\pi J_{I_1S}\Delta\right)\cos\left(\pi J_{I_1S}\Delta\right) && \text{Term II}\\
&+ 2I_{1y}I_{2z}\cos\left(\pi J_{I_1I_2}\Delta\right)\sin\left(\pi J_{I_1I_2}\Delta\right)\sin^2\left(\pi J_{I_1S}\Delta\right) && \text{Term III}\\
&+4I_{1y}I_{2z}S_z\cos\left(\pi J_{I_1I_2}\Delta\right)\sin\left(\pi J_{I_1I_2}\Delta\right)\cos\left(\pi J_{I_1S}\Delta\right)\sin\left(\pi J_{I_1S}\Delta\right) && \text{Term IV}
\end{aligned}
$$

Eq. 1.21

The IP term I is the more relevant in HSQC spectra, showing an amplitude signal dependence to a $\cos^2\left(\pi J_{I_1I_2}\Delta\right)\sin^2\left(\pi J_{I_1S}\Delta\right)$ function.

2D HSQC cross-peaks can show strongly distorted twist-phased patterns along the detected F2 dimension due to these unwanted AP components (terms II, III and IV). These terms arise from two main factors:

- The mismatch between the experimental value of Δ delay (ideally optimized to single *J* value, accordingly to Δ=1/(2$^1J_{CH}$) and the magnitude of the different $^1J_{CH}$, because Δ may not simultaneously satisfy the heteronuclear coupling arising for different spins of the molecule. This affects all terms having AP heteronuclear components (term II and IV).
- The evolution under the homonuclear coupling constants during the INEPT and refocused INEPT periods. This affects terms having AP homonuclear components (term III and IV).

In practice, the magnitudes of $^1J_{CH}$ (120–250 Hz) are generally more than one order of magnitude larger than J_{HH} (0–15 Hz) therefore, the deleterious effects of J_{HH} on the detected signal have usually been neglected in HSQC experiments. Table 2 shows the theoretical contribution of each term of Eq. 1.21 to the final detected signal in a conventional HSQC experiment assuming J_{H1H2}= 10 Hz and 30 Hz.

Table 2: Effect of J_{HH} on the different magnetization components to the detected signal in a conventional HSQC experiment ($^1J_{CH1}$=145 Hz; Δ=3.6 ms).

Term	Contribution (%)	
	J_{HH} =10 Hz	J_{HH} =30 Hz
I	85.1	70.1
II	4.8	3.9
III	9.6	24.5
IV	0.5	1.4

Phase distortions in 2D cross peaks are a huge source of error when a precise and accurate measurement of homo- and heteronuclear coupling constants or volume integrations are carried out. On the other hand, the complex signal intensity dependence also hinders any attempt for the quantitative analysis of HSQC datasets. Therefore, to solve or minimize these problems the design of more robust and improved J_{HH} and J_{CH}-compensated HSQC sequences are strongly required.

The application of broadband heteronuclear decoupling during the acquisition in HSQC experiments presents several advantages: (i) substantial spectral simplification due to the heteronuclear *J* splitting is removed, (ii) improved SNR due to the collapse of the multiplets, and (iii) the phase distortion problems due to AP contributions of J_{CH} are removed. As it was mentioned before, a mixture of IP and AP components are available just prior to the acquisition (see Eq.1.21). Under heterodecoupling conditions, terms II and IV in Eq. 1.21 are converted to non-observable MQCs. Therefore, only two terms will contribute to the final signal detected:

$$+ I_{1x}\cos^2(\pi J_{I_1I_2}\Delta)\sin^2(\pi J_{I_1S}\Delta) \quad \text{Term I}$$
$$+ 2I_{1y}I_{2z}\cos(\pi J_{I_1I_2}\Delta)\sin(\pi J_{I_1I_2}\Delta)\sin^2(\pi J_{I_1S}\Delta) \quad \text{Term III}$$

Eq. 1.22

1.2.1.2. HSQC with PEP: improved sensitivity

The *Preservation of Equivalent Pathways* (PEP) methodology[59] is based on the implementation of a second refocused INEPT (90° shifted in relation to the first refocused INEPT) into the regular HSQC pulse sequence (Figure 11), which allows to obtain a maximum sensitivity enhancement by a factor of $\sqrt{2}$ for *IS* spin systems.

[59] L. E. Kay, P. Keifer, T. Saarinen, *J. Am. Chem. Soc.*, **1992**, *114*, 10663.

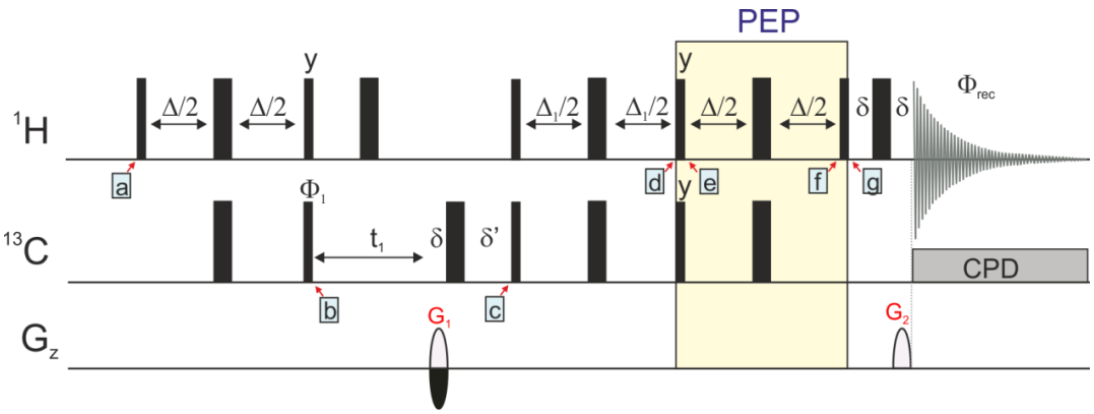

Figure 11: ^{1}H-^{13}C HSQC-PEP pulse sequence using the E/A method. Δ=1/(2$^1J_{CH}$), $Δ_1$= Δ for CH multiplicities, $Δ_1$=1/(4$^1J_{CH}$) for all multiplicities. A basic two-step phase cycling is executed with $Φ_1$= x,-x and $Φ_{rec}$= x,-x. Coherence selection is performed by the gradient pair G_1:G_2 (±80:20.1) using the E/A protocol.

For a simple *IS* spin system, the most important magnetization components at different points of the HSQC-PEP sequence are:

Point a	**Point b**	**Point c**
$+I_z$	$+ I_y \cos(\pi J_{IS}\Delta)$	$-2I_zS_y \cos(\Omega_S t_1)\sin(\pi J_{IS}\Delta)$
	$-2I_zS_y \sin(\pi J_{IS}\Delta)$	$+2I_zS_x \sin(\Omega_S t_1)\sin(\pi J_{IS}\Delta)$

Eq. 1.23

In the original HSQC experiment, the conventional refocused INEPT converts the AP term $2I_zS_y$ into detectable IP proton magnetization (I_x) while the AP $2I_zS_x$ term is converted into non-observable $2I_yS_x$ MQCs (point d). At this point, a second refocusing INEPT is added in the HSQC-PEP version to recover this MQC. The strategy is based on keeping momentarily the observable magnetization I_x along to the *z*-axis (I_z), whereas the $2I_yS_x$ term is converted into AP $2I_yS_z$ magnetization (point e):

$$\text{Eq.1.23} \xrightarrow{r\ INEPT} \begin{matrix} +I_x \cos(\Omega_S t_1)\sin(\pi J_{IS}\Delta)\sin(\pi J_{IS}\Delta_1) \\ +2I_yS_x \sin(\Omega_S t_1)\sin(\pi J_{IS}\Delta) \end{matrix} \xrightarrow[90°\ (S_y)]{90°\ (I_y)} \begin{matrix} +I_z \cos(\Omega_S t_1)\sin(\pi J_{IS}\Delta)\sin(\pi J_{IS}\Delta_1) \\ +2I_yS_z \sin(\Omega_S t_1)\sin(\pi J_{IS}\Delta) \end{matrix}$$

Point d **Point e**

Eq. 1.24

After the second refocused INEPT (point f), the $2I_yS_z$ term evolves to IP magnetization in the form of I_x, while the I_z term is still kept along the *z*-axis. Finally, a $90°\ (I_x)$ converts the I_z term to I_y magnetization whereas the other I_x term is not affected (point g):

$$\text{Eq. 1.24} \xrightarrow{r\ INEPT} \begin{matrix} +I_z \cos(\Omega_S t_1) \sin(\pi J_{IS}\Delta) \sin(\pi J_{IS}\Delta_1) \\ +I_x \sin(\Omega_S t_1) \sin^2(\pi J_{IS}\Delta) \end{matrix} \xrightarrow{90°\ (I_x)} \begin{matrix} -I_y \cos(\Omega_S t_1) \sin(\pi J_{IS}\Delta) \sin(\pi J_{IS}\Delta_1 \\ +I_x \sin(\Omega_S t_1) \sin^2(\pi J_{IS}\Delta) \end{matrix}$$

Point f **Point g**

Eq. 1.25

Because two orthogonal magnetization terms with sine and cosine modulation are retained in each acquisition, the detected signal is sine/cosine phase-modulated and therefore, a sensitivity enhancement of $\sqrt{2}$ is obtained when compared with the conventional HSQC pulse sequence. Very importantly, such gain is retained even by the use the E/A method because the experiment is fully compatible with the phase-modulated nature of the signals. Nevertheless, it is not possible to completely refocus both magnetization terms for all multiplicities[60] so that the Δ_1 delay must be adjusted accordingly to the maximum sensitivity enhancement that can be reached for a given spin system. When only *IS* pairs are to be observed, the INEPT delays should be optimized to $\Delta = \Delta_1 = 1/(2J_{IS})$, whereas for the detection of all multiplicities (*IS*, I_2S and I_3S) the Δ_1 period should be reduced to an average $1/(4J_{IS})$ value.

1.2.1.3. Measurement of heteronuclear $^1J_{CH}/^1T_{CH}$ coupling constants

Heteronuclear one-bond ($^1J_{CH}$) and long-range coupling constants ($^nJ_{CH}$; n>1) are important parameters in the structural, stereochemical, and conformational analysis of small- medium-sized organic compounds, natural products and biomolecules. $^1J_{CH}$ are related to the *s*-character of the CH bond and, for instance, can be key tools for the rapid characterization of anomeric centers in carbohydrates or to identify acetylenic functional groups, among others.[61,62] Two-bond coupling constants ($^2J_{CH}$) can be experimentally correlated with substitution patterns and bond orientations in ^{1}H-C-^{13}C-X spin systems.

[60] J. Schleucher, M. Schwendinger, M. Satller, P. Schmidt, O. Schedletzky, S. J. Glaser, O. W. Sørensen, C. Griesinger, *J. Biomol. NMR*, **1994**, *4*, 301.

[61] R. H. Contreras, J. E. Peralta, *Prog. Nucl. Magn. Reson. Spectrosc*., **2000**, *37*, 321.

[62] a) I. Tvaroska, F. R. Taravel, *Carbohydr. Res.*, **1991**, *221*, 83. b) S. Uhrinova, D. Uhrin, T. Liptaj, J. Bella, J. Hirsch, *Magn. Reson. Chem*., **1991,** *29*, 912. c) I. Tvaroska, F. R. Taravel, *J. Biomol. NMR,* **1992***, 2*, 421. d) N. C. Maiti, Y. P. Zhu, I. Carmichael, V. E. Anderson, *J. Org. Chem*., **2006**, *71*, 2878.

On the other hand, three-bond coupling constants ($^3J_{CH}$) can be correlated with dihedral angles in ^{1}H-C-C-^{13}C spin systems following classical Karplus-type relationships.[63]

In recent years, it has appeared an enormous interest for the measurement of *Residual Dipolar Coupling* (RDC) constants, especially one-bond proton–carbon RDC constants ($^1D_{CH}$) in small molecules dissolved in weakly aligned anisotropic media.[64] RDCs are anisotropic NMR parameters, which become observable if the compound in question is (marginally) oriented with respect to the magnetic field. If the degree of order is very small, the dipolar coupling interaction *D* is scaled down by the same factor affording a residual dipolar coupling value. In these cases RDCs are obtained from the difference in multiplet splitting between anisotropic ($T = J + D$) and isotropic samples (J). As they are calculated from the difference of two coupling constants it is of prime importance to measure *J* and *T* with high accuracy and precision. Due to their global orientation information content, RDCs have shown significant impact on the structure determination of large label biomolecular[65] and natural abundance organic compounds.[64]

The HSQC experiment has been largely used for the sensitive measurement of $^1J_{CH}$ /$^1T_{CH}$ coupling constants in solution and anisotropic media, respectively. $^1J_{CH}$ values are large in magnitude (in the range of 120–250 Hz) and positive in sign, and they can be quickly measured for the large doublet observed in F1- or F2-heterocoupled HSQC spectra. In the case of $^nJ_{CH}$, their values are in the same range as J_{HH}, typically between 0 and 15 Hz, and they are more complicated to measure. Nowadays, both $^1J_{CH}$ and $^nJ_{CH}$ coupling constants can be efficiently measured by modern NMR methods based on HSQC- and HMBC/HSQMBC-related methods.

The nature of a cross-peak coupling pattern obtained from a particular NMR experiment is an important factor that must be taken into account when measuring quantitatively $^1J_{CH}$ or $^nJ_{CH}$. Different methodologies to extract coupling constants values according to their coupling pattern can be devised, as illustrated in Figure 12.

[63] R. Aydin, H. Günther, *Magn. Reson. Chem.*, **1990**, *28*, 448.

[64] a) S. Uhrinova, D. Uhrin, T. Liptaj, J. Bella, J. Hirsch, *Magn. Reson. Chem*., **1991**, *29*, 912. b) C. M. Thiele, *Concepts Magn. Reson. Part A*, **2007**, *30*, 65. c) C. M. Thiele, *Eur. J. Org. Chem.,* **2008**, *34*, 5673. d) G. Kummerlowe, B. Luy, *Trends Anal. Chem.*, **2009**, *28*, 483. e) G. Kummerlowe, B. Luy, *Annu. Rep. NMR Spectrosc*., **2009**, *68*, 193. f) R. R. Gil, *Angew. Chem. Int. Ed*., **2011**, *50*, 7222.

[65] a) N. Tjandra, A. Bax, *Science*, **1997**, *278*, 1111. b) M. Blackledge, *Prog. Nucl. Magn. Reson. Spectrosc.*, **2005**, *46*, 23. c) J. R. Tolman, K. Ruan, *Chem. Rev*., **2006**, *106*, 1720. d) A. Annila, P. Permi, *Concepts Magn. Reson*., **2004**, *23A*, 22. e) M. Ottiger, F. Delaglio, A. Bax, *J. Magn. Reson*., **1998**, *131*, 373. f) M. H. Lerche, A. Meissner, F. M. Poulsen, O. W. Sørensen, *J. Magn. Reson.*, **1999**, *140*, 259. g) L. S. Yao, J. F. Ying, A. Bax, *J. Biomol. NMR*, **2009**, *43*, 161.

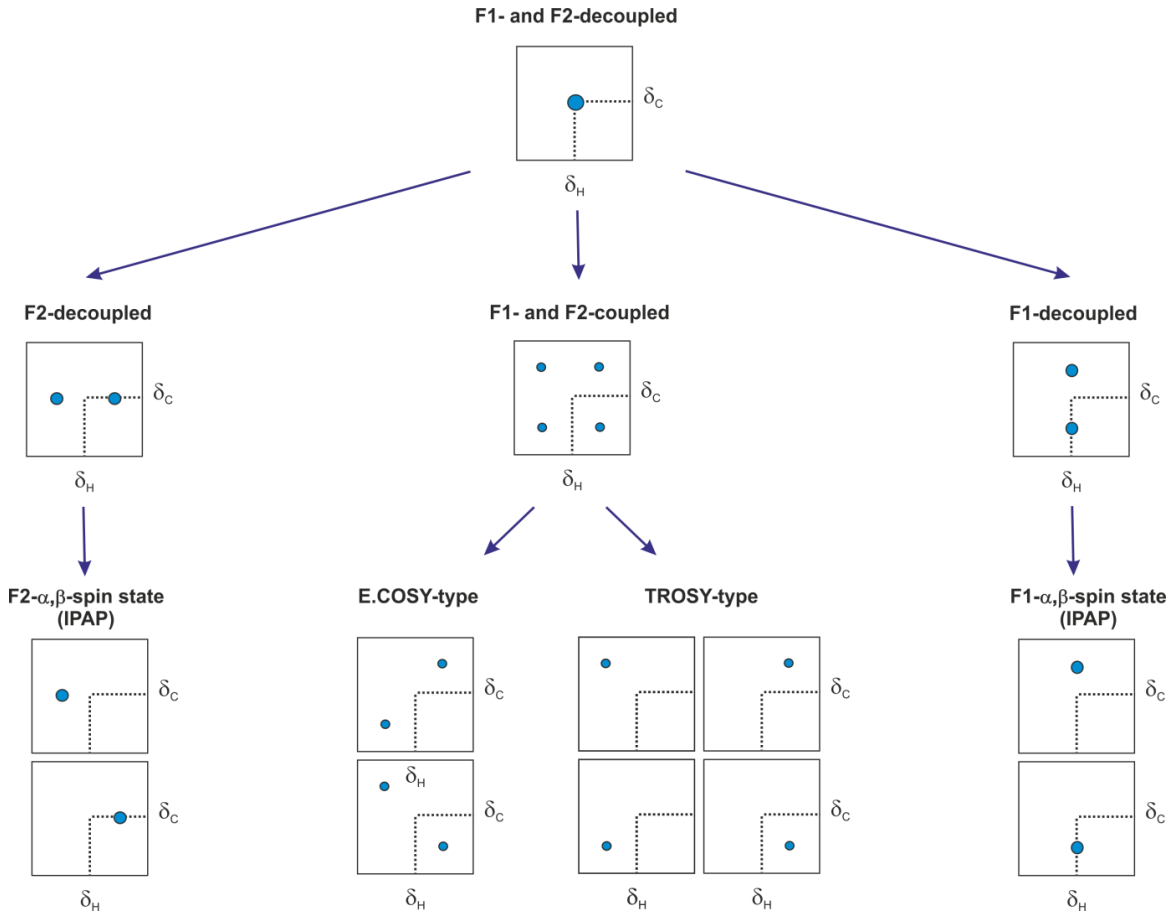

Figure 12: Coupling patterns obtained for a CH cross-peak in different 2D HSQC-type spectra.

HSQC-based pulse schemes have been generally chosen for measuring $^{1}J_{CH}/^{1}T_{CH}$ but the accuracy and the simplicity on these experimental determinations are subjects of discussion. Some topics of recent interest have been:

i. The design of general and robust NMR methods that works efficiently for all multiplicities.

ii. The discussion about whether the $^{1}J_{CH}/^{1}T_{CH}$ splitting should be measured from the direct F2 (^{1}H) or the indirect F1 (^{13}C) dimension of a coupled 2D HSQC spectrum.

iii. The optimum measurement when large variations of $^{1}J_{CH}/^{1}T_{CH}$ values are present.

iv. The accurate measurement of $^{1}J_{CH}/^{1}T_{CH}$ for individual protons in diastereotopic CH_2 or NH_2 groups.

v. The simultaneous determination of additional coupling constants from the analysis of the same cross-peak, being the maximum interest the sign-sensitive determination of geminal $^{2}J_{HH}/^{2}T_{HH}$ values.

vi. The detection and recognition of the presence of undesired strong coupling effects and evaluation of their influence on the accuracy of the measurement.

- **CLIP-HSQC: Measurement of $^1J_{CH}$ along the detected F2 dimension**

The easier method to measure $^1J_{CH}/^1T_{CH}$ is from the detected dimension of a conventional HSQC experiment recorded without heteronuclear decoupling during proton acquisition, referred to as F2-coupled HSQC experiment (Figure 13A). The main advantages of such an approach are (i) its easy and direct measurement due to the presence of large doublets (Figure 13C), (ii) the high levels of digital resolution readily available in the proton dimension, and (iii) different peaks belonging to diastereotopic CH_2 groups can be individually analyzed. The main drawback is that signals exhibit the typical J_{HH}/T_{HH} multiplet pattern structure along F2 dimension, which can hamper the accurate $^1J_{CH}/^1T_{CH}$ measurement. In addition, broad signals and/or the large contributions of RDCs can generate poorly defined multiplets that make even more difficult accurate measurements.

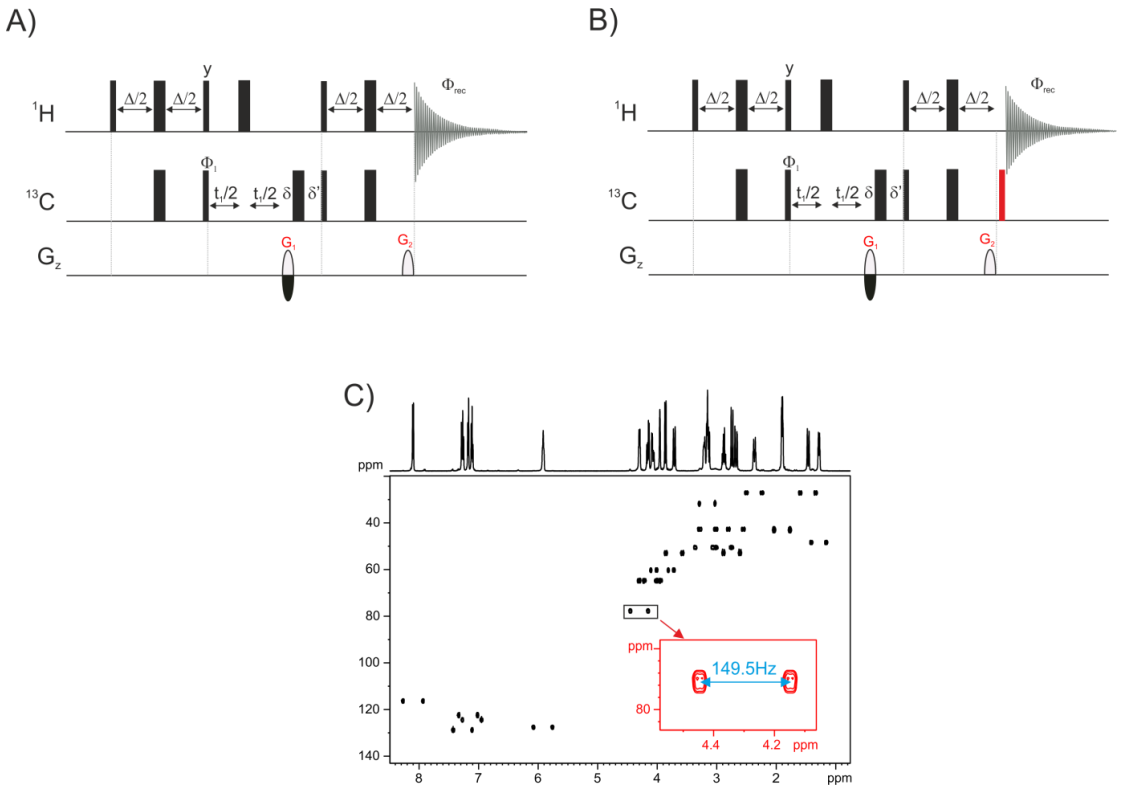

Figure 13: A) F2-coupled HSQC and B) CLIP-HSQC pulse schemes for the measurement of $^1J_{CH}$ along the direct F2 dimension. The interpulse delay Δ is set to $1/(2^1J_{CH})$ and a basic two-step phase cycling is executed with Φ_1= x,-x and Φ_{rec}= x,-x. Gradients for coherence selection using the E/A protocol are represented by G_1 and G_2 (G_1:G_2=±80:20.1) and δ stands for the duration and the gradient and its recovery delay. The final 90° (^{13}C) stands for the so-called CLIP pulse to remove heteronuclear AP contributions. C) F2-coupled CLIP-HSQC spectrum of strychnine [2] recorded in a 500 MHz spectrometer. The magnitude of $^1J_{CH}$ can be easily measured from the large clean IP doublet observed along the detected dimension, as shown in the inset.

The effects on the phase and the intensity observed in different HSQC cross-peaks as a function of the magnitudes of J_{HH}, $^1J_{CH}$, and the delay Δ optimization for several

F2-heterocoupled HSQC schemes can be monitored from 1D spectral simulations. Thus, the phase anomalies observed in conventional F2-heterocoupled HSQC cross-peaks (Figure 14A) result from the mismatch between the optimized Δ delay and the active $^{1}J_{CH}$ value (terms II and IV derived in Eq. 1.21), and from the evolution of J_{HH} during the INEPT periods (term III and IV in Eq. 1.21). Such distortions limit any attempt to realize an accurate analysis in terms of signal quantification via peak integration or direct measurement of $^{1}J_{CH}$ and J_{HH} magnitudes.

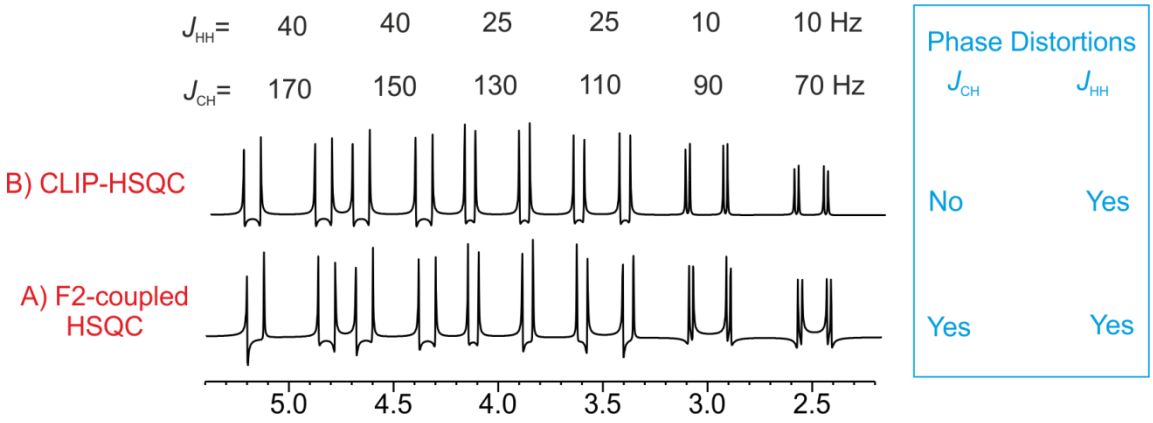

Figure 14: Simulated 1D spectra showing the phase peak distortion effects in 140-Hz optimized A) F2-heterocoupled HSQC and B) CLIP-HSQC spectra. Six protons belonging to three different diastereotopic CH_2 groups have been simulated with a wide range of J_{HH} and $^{1}J_{CH}$ values, as shown in the upper part.

A simple solution to partially solve these phase distortions was proposed with the *CLean In-Phase* HSQC (CLIP-HSQC) experiment[66] which applies a 90° ^{13}C pulse (from *x*-axis) just prior the acquisition (Figure 13B). In this way, the AP contributions due to $^{1}J_{CH}$ are converted to MQCs (terms IIa and IVa) and, apparently, clean IP patterns should be obtained in the absence of any J_{HH} coupling (term IIIa).

$$Eq.\,1.21$$

$$\downarrow \; 90°\,(C_x)$$

$$+ H_{1x}\cos^2(\pi J_{H_1H_2}\Delta)\sin^2(\pi J_{H_1C}\Delta) \quad \text{Term Ia}$$
$$+ 2H_{1y}C_y\cos^2(\pi J_{H_1H_2}\Delta)\sin(\pi J_{H_1C}\Delta)\cos(\pi J_{H_1C}\Delta) \quad \text{Term IIa}$$
$$- 2H_{1y}H_{2z}\cos(\pi J_{H_1H_2}\Delta)\sin(\pi J_{H_1H_2}\Delta)\sin^2(\pi J_{H_1C}\Delta) \quad \text{Term IIIa}$$
$$- 4H_{1y}H_{2z}C_y\cos(\pi J_{H_1H_2}\Delta)\sin(\pi J_{H_1H_2}\Delta)\cos(\pi J_{H_1C}\Delta)\sin(\pi J_{H_1C}\Delta) \quad \text{Term IVa}$$

Eq. 1.26

[66] A. Enthart, J. C. Freudenberger, J. Furrer, H. Kessler, B. Luy, *J. Magn. Reson.*, **2008**, *192*, 314.

However, in the presence of J_{HH}, a mixture of observable IP (term Ia) and AP components (term IIIa) are still active, as shown in the simulated spectrum of Figure 14B. In practice, due to the large difference of magnitudes between $^1J_{CH}$ and J_{HH}, these unwanted contributions are small and they have been traditionally omitted in cross-peak analysis in CLIP-HSQC or F2-heterodecoupled HSQC experiments. A simple calculation shows that these effects may become important. For instance, the relative percentage of the term IIIa with respect to term Ia in a 140-Hz optimized CLIP-HSQC experiment is of 5.6% and 17% for J_{HH} values of 5 and 15 Hz, respectively. Such percentages can be more pronounced when measuring RDCs in anisotropic media, where higher J_{HH} values are usually involved.

The CLIP-HSQC experiment (Figure 13B) proves to be an efficient tool to determine the $^1J_{CH}/^1T_{CH}$ value from the resulting clean in-phase doublets.[66] However, strong J_{HH} coupling effects can generate a high degree of asymmetry between the high- and low-field multiplet lines in F2-coupled HSQC spectra, which can preclude reliable determination of $^1J_{CH}/^1T_{CH}$ coupling constants values. This drawback has already been described, particularly for CH spin systems in carbohydrates or in the typical strong geminal interaction found in diastereotopic CH_2 spin systems, and some practical solutions have been proposed.[67]

- **BIRD-HSQC: Measurement of $^1J_{CH}$ along the indirect F1 dimension**

The measurement of $^1J_{CH}/^1T_{CH}$ exclusively along the indirect F1 dimension of a HSQC spectrum is recommended to avoid the interferences of J_{HH}/T_{HH} splittings, but a major inconvenient arises for the need of a large number of t_1 increments, and therefore longer acquisition times. The successful use of *Non-Uniform Sample* (NUS) techniques,[68] *J* scaling factors or spectral folding/aliasing can speed up data acquisition and/or increase the digital resolution in the F1 dimension. Several F1-coupled HSQC pulse schemes have been compared and evaluated by Thiele and Bermel.[69] The most simple approach results from the removing of the central 180^o ^{1}H pulse placed in the middle of the t_1 evolution period in the conventional HSQC experiment, referred to as F1-coupled HSQC experiment

[67] a) C. M. Thiele, *J.Org. Chem*., **2004**, *69*, 7403. b) B. W. Yu, H. van Ingen, S. Vivekanandan, C. Rademacher, S. E. Norris, D. I. Freedberg, *J. Magn. Reson*., **2012**, *215*, 10. c) B. W. Yu, H. van Ingen, D. I. Freedberg, *J. Magn. Reson.*, **2013**, *228*, 159. d) P. Tzvetkova, S. Simova, B. Luy, *J. Magn. Reson*., **2007**, *186*, 193. e) K. Fehér, S. Berger, K. E. Kövér, *J. Magn. Reson*., **2003,** *163*, 340.

[68] a) K. Kazimierczuk, V. Y. Orekhov, *Angew. Chem. Int. Ed.*, **2011**, *50*, 5556. b) K. Kazimierczuk, W. Kozminski, I. Zhukov, *J. Magn. Reson.*, **2006**, *179*, 323.

[69] C. M. Thiele, W. Bermel, *J. Magn. Reson.,* **2012***, 216*, 134.

(Figure 15A). A more convenient method incorporates a G-BIRD^{x} module (Figure 15B) to allow the simultaneous evolution of both $^{1}J_{CH}/^{1}T_{CH}$ (with optional *k* scaling factor) and ^{13}C chemical shift evolution while contributions from $^{n}J_{CH}/^{n}T_{CH}$ are efficiently refocused.[69e] The better line shapes along the indirect dimension allow the determination of $^{1}J_{CH}/^{1}T_{CH}$ by simply measuring the frequency difference between the peak maxima of singlets instead of the centers of complex multiplets.

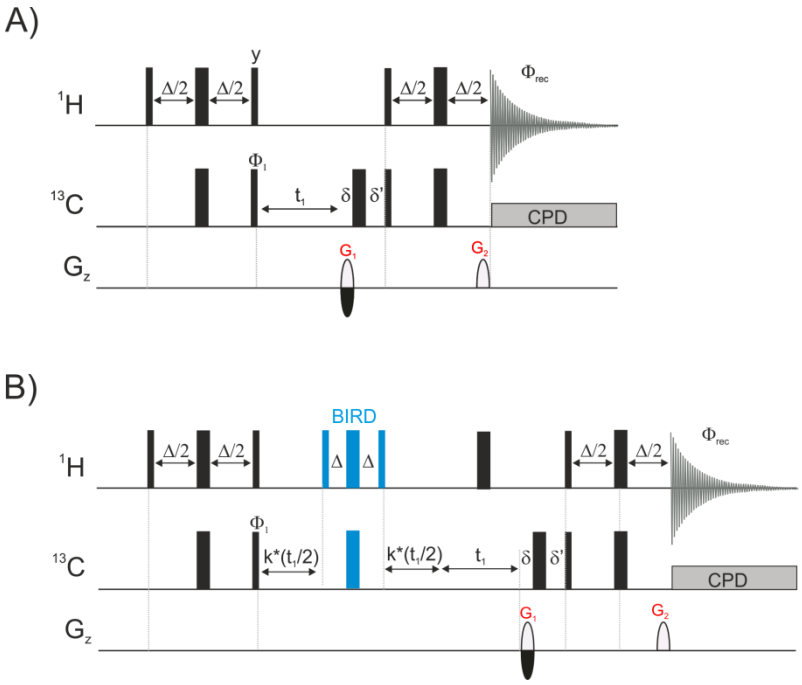

Figure 15: Several pulse schemes to achieve F1-heterocoupled HSQC spectra: A) F1-coupled HSQC, and B) F1-coupled BIRD-HSQC. The interpulse delay in INEPT and BIRD elements are optimized according to $\Delta=1/(2^{1}J_{CH})$. A minimum two-step phase cycling is executed with Φ_1=x,-x and Φ_{rec}= x,-x, all other unlabeled pulses are from the *x*-axis. Gradients G_1 and G_2 are used for coherence selection using E/A (G_1:G_2=±80:20.1).

The accurate measurement of the two $^{1}J_{CH}/^{1}T_{CH}$ values and particularly the geminal $^{2}J_{HH}/^{2}T_{HH}$ coupling in diastereotopic C_{HAHB} groups has always been a challenging task, particularly for F1-coupled HSQC experiments. Several methods have been proposed for measuring them either from the F1 or from the F2 dimension, but they all present some drawbacks that have prevented their general use. For instance, the passive $^{1}J_{CHB}/^{1}T_{CHB}$ value can be separately measured into the active H_A cross-peak, and vice versa, along the F1 dimension of a *J*-resolved HMQC experiment.[70] In addition, the large doublet is further split by the $^{2}J_{HAHB}/^{2}T_{HAHB}$ coupling yielding a doublet of doublets. The disadvantage is that additional experiments can be required to measure $^{1}J_{CH}/^{1}T_{CH}$ for CH or CH_3 spin systems, and significant distortions on the cross-peaks (banana shape peaks) are frequently observed in the spectra of complex small molecules. Another important group of NMR experiments are those based on spin-state selection specifically designed for methylene

[70] K. E. Kövér, K. Fehér, *J. Magn. Reson.*, **2004**, *168*, 307.

groups that yield simplified coupling patterns, and where the sign and the magnitude of the geminal $^2J_{HH}$/$^2T_{HH}$ can sometimes be additionally extracted.[71]

1.2.2. The HSQMBC experiment

The *Heteronuclear Multiple Bond Correlation* (HMBC)[72] and the *Heteronuclear Single Quantum Multiple-Bond Correlation* (HSQMBC) experiment[73] are the long-range optimized versions of the HMQC and HSQC experiment, respectively. They provide heteronuclear correlations between protons and both protonated and non-protonated carbon atoms separated by more than one bond (usually two- and three-bond correlations). Long-range proton-carbon correlations routinely extracted from HMBC and HSQMBC spectra are key elements in the structural characterization of small and medium-sized molecules in solution.[74] The HMBC experiment usually gives better sensitivity ratios but, in many cases, the equivalent HSQMBC is the preferred technique because it generally affords a better performance in terms of simplicity, peak phase behavior and pulse sequence analysis.

Additionally, the measurement of $^nJ_{CH}$ (n>1) has been another hot topic of interest in small molecule NMR.[75] Typically, the $^nJ_{CH}$ values cover a range from 0 to 15 Hz and that makes that HMBC and HSQMBC experiments present some additional problems compared to their analogs HMQC and HSQC experiments, respectively:

i. HMBC/HSQMBC experiments are usually optimized to 5-8 Hz, which means that the inter-pulse delay lasts about 50-70 ms, whereas in HSQC/HMQC pulse sequences such delay is about 3.5 ms (usually optimized to $^1J_{CH}$ =140 Hz). For that reason, the pulse sequences can become too long and relaxation losses are more severe, especially for molecules with short T_2 relaxation times. To reduce the duration of the

[71] a) M. Ottiger, F. Delaglio, J. L. Marquardt, N. Tjandra, A. Bax, *J. Magn. Reson*., **1998**, *124*, 365. b) P. Nolis, T. Parella, *Curr. Anal. Chem*., **2007**, *3*, 47. c) T. N. Pham, T. Liptaj, K. Bromek, D. Uhrin, *J. Magn. Reson.*, **2002**, *157*, 200. d) T. Carlomagno, W. Peti, C. Griesinger, *J. Biomol. NMR,* **2000**, *17*, 99. e) P. Permi, *J. Biomol. NMR*, **2002**, *22*, 27. f) E. Miclet, D. C. Williams Jr., G. M. Clore, D. L. Bryce, J. Boisbouvier, A. Bax, *J. Am. Chem. Soc*., **2004**, *126*, 10560. g) G. Guichard, A. Violette, G. Chassaing, E. Miclet, *Magn.Reson. Chem.*, **2008**, *46*, 918. h) T. Parella, M. Gairí, *J. Am. Chem. Soc.*, **2004**, *126*, 9821. i) P. Permi, *J. Magn. Reson*., **2001**, *153*, 267. j) E. Miclet, E. O'Neil-Cabello, E. P. Nikonowicz, D. Live, A. Bax, *J. Am. Chem. Soc.,* **2003,** *125*, 15740. k) P. Nolis, J. F. Espinosa, T. Parella, *J. Magn. Reson*., **2006**, *180*, 39.

[72] A. Bax, M. Summers. *J. Am. Chem. Soc*., **1986**, *108*, 2093.

[73] a) R. Marek, L. Kralik, V. Sklenar. *Tetrahedron Lett.,* **1997**, *38*, 665. b) R. T. Williamson, B. L. Márquez, W. H. Gerwick, K. E. Kover, *Magn. Reson. Chem.,* **2000**, *38*, 265.

[74] R. C. Breton, W. F. Reynolds, *Nat. Prod. Rep*., **2013**, *30*, 501.

[75] a) B. L. Márquez, W. H. Gerwick, R. T. Williamson, *Magn. Reson. Chem*., **2001**, *39*, 499. b) T. Parella, J. F. Espinosa, *Prog. Nucl. Magn. Reson. Spectrosc*., **2013**, *73*, 17.

sequence as much as possible, these experiments are usually recorded under non-refocusing conditions and the resulting cross-peaks present AP multiplet pattern with respect to the active $^{n}J_{CH}$.[73b]

ii. Since J_{HH} and $^{n}J_{CH}$ values have similar sizes, simultaneous evolutions of J_{HH} and $^{n}J_{CH}$ during the inter-pulse delays generate mixtures of IP and AP magnetization components. This results in highly phase-distorted and complex cross-peaks and can produce important reduction of signal intensities due to signal cancellation, which can lead to difficult data analysis.

1.2.2.1. Basic HSQMBC pulse scheme

Similarly to HSQC, the HSQMBC experiment is based on the heteronuclear polarization INEPT transfer through $^{n}J_{CH}$, via the selection of SQCs during the t_1 period. The transfer mechanism allows to obtain long-range heteronuclear correlations between protons and both protonated and non-protonated carbon atoms (Figure 16). Experimentally, the only requirement is the re-optimization of the inter-pulse Δ delay to a small coupling value, about typically 5–8 Hz (Figure 16C). Under these conditions, the undesired effects of J_{HH} evolution during the long INEPT periods become very important.

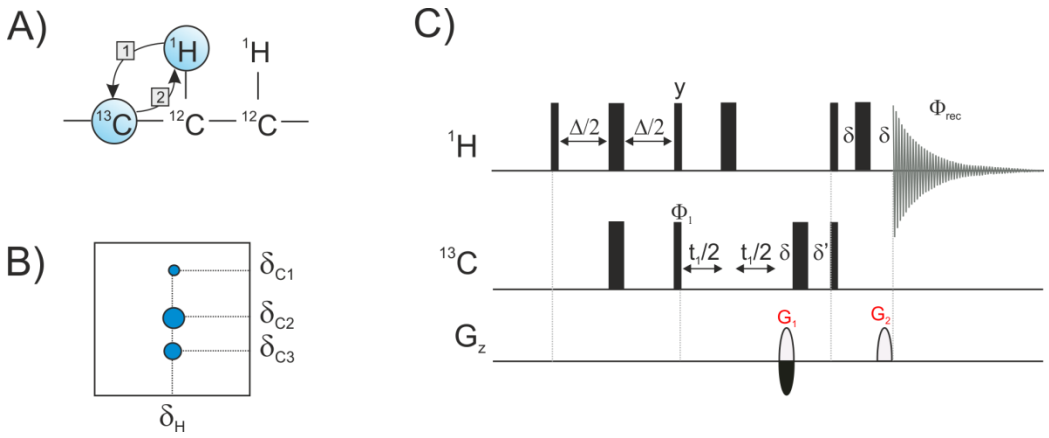

Figure 16: Schematic representation of the A) transfer mechanism; B) cross-peak pattern and C) pulse sequence of the standard non-refocused HSQMBC experiment. Thin and thick vertical rectangles represent 90° and 180° hard pulses, respectively. The delay Δ should be set to $1/(2^{n}J_{CH})$ and δ represents the duration of the PFG and its recovery delay. Coherence selection is performed by the gradient pair G_1/G_2 using the E/A protocol (G_1:G_2=±80:20.1). A basic two-step phase cycling is executed with Φ_1= x,-x and Φ_{rec}= x,-x.

HSQMBC has a great advantage with respect to the HMBC experiment because J_{HH} evolution is not present during the t_1 period. In addition, data can be presented in a phase sensitive mode with pure absorption lineshapes which means that is perfectly suitable for easy measurement of ${}^{n}J_{CH}$.

The PO analysis of the HSQMBC pulse sequence is exactly like HSQC (see section 1.2.1.1.), the only change is that the interpulse Δ delay of the INEPT block is adjusted to ${}^{n}J_{CH}$ instead of ${}^{1}J_{CH}$ and the refocused INEPT period is not applied. So that, if a weakly coupled H_1H_2C spin system is considered, the observable magnetization just before acquisition can be described as:

$$-2H_{1y}C_z \cos\left(\pi J_{H_1H_2}\Delta\right)\sin\left(\pi^n J_{H_1C}\Delta\right) \qquad \text{Eq. 1.27}$$

In the case of a refocused HSQMBC, the detected signal is described as shown in Eq. 1.21. As a result, the cross peaks of the 2D ${}^{1}H$-${}^{13}C$ HSQMBC spectrum appear phase distorted because of the AP character with respect to ${}^{n}J_{CH}$ (term II and IV) and J_{HH} (term III and IV) modulations during the long INEPT period. Table 3 shows the contribution of each term to the final detected signal in a refocused HSQMBC experiment:

Table 3: Contribution of each magnetization to the final detected signal in a conventional HSQMBC experiment (${}^{n}J_{CH1}$= 6 Hz, J_{H1H2}= 10 Hz, Δ= 62.5 ms)

Term	Contribution (%)
I	20.7
II	8.6
III	50.0
IV	20.7

In addition, cross-peak intensities in HSQMBC strongly depend on the mismatch between Δ optimization and the corresponding ${}^{n}J_{CH}$ values and also on the potential losses by T_2 relaxation. The hard analysis of these complex multiplets has prevented its general use as a routine task.

1.2.2.2. Improvements in HSQMBC experiments

Due to the above mentioned problems associated to the simultaneous evolution of J_{HH} and $^{n}J_{CH}$ coupling constants during the INEPT blocks, several improvements have been proposed, specially focused on the easy measurement of $^{n}J_{CH}$, without need of sophisticated and time-consuming post-processing tasks. Some of these new HSQMBC experiments are described below.

- **Implementing BIRD block: BIRD-HSQMBC**

The BIRD[4b] element is generally used for two main purposes: (i) to selectively observe protons bound to ^{13}C and suppress those bound to ^{12}C (see section 1.1.1.1.), and (ii) to differentiate direct from long-range heteronuclear correlations thanks to the large difference in their values. As an application of the BIRD^{y} module, Figure 17B shows the pulse scheme for the HSQMBC-BIRD experiment.[75a] It is a non-refocused HSQMBC experiment where the BIRD block is introduce in the middle of the INEPT element to minimize direct $^{1}J_{CH}$ responses. In addition, J_{HH} are partially refocused (except for $^{2}J_{HH}$) reducing phase distortions and additional J_{HH} signal modulation in the resulting cross-peaks.

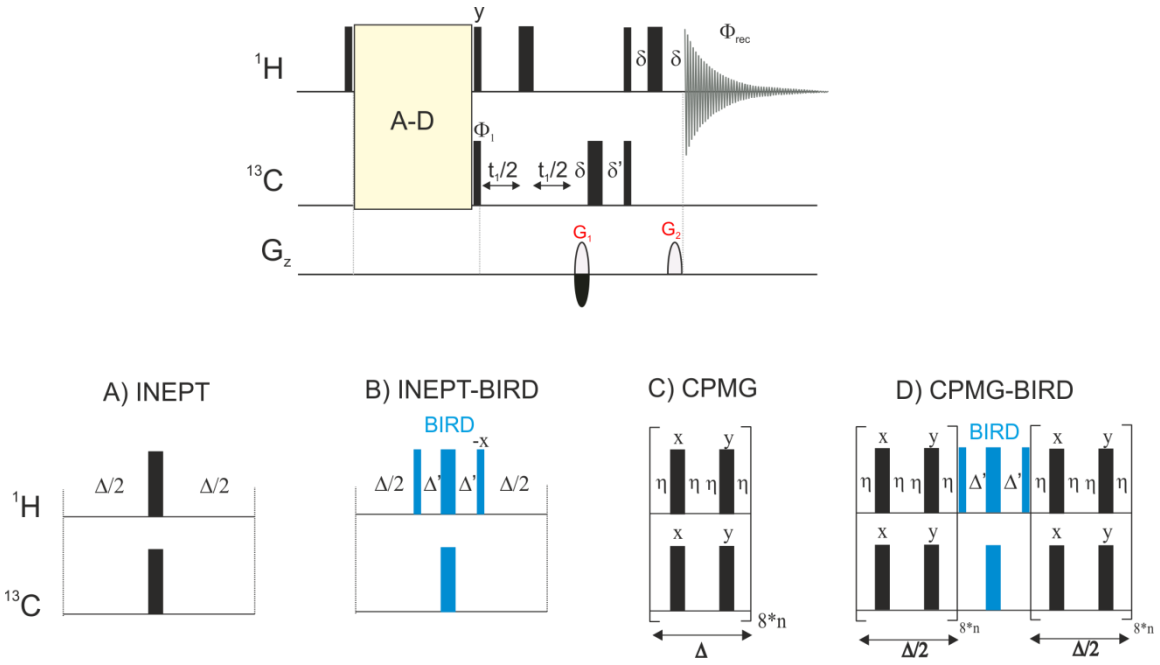

Figure 17: Several 2D non-refocused HSQMBC pulse schemes to obtain heteronuclear long-range correlation spectra ($\Delta=1/(2^{n}J_{CH})$). The initial transfer step is: A) a basic INEPT, B) an INEPT-BIRD block ($\Delta'=1/(2^{1}J_{CH})$); C) a CPMG XY-16 super cycle consisting of simultaneous ^{1}H and ^{13}C pulses applied at intervals 2η; D) a CPMG-BIRD element combining the features described in B and C.

- **Implementing CPMG pulse train: CPMG-HSQMBC**

It has been also reported that by applying a *Carr-Purcell-Maiboom-Gill* (CPMG) pulse train during the INEPT period[76] (Figure 17C), the J_{HH} evolution can be minimized if the interpulse delay between the π pulses is shortening than $1/2\sqrt{J^2 + \Delta\nu^2}$. In case of weak coupling the condition can be approximated as $1/2\Delta\nu_{max}$, where $\Delta\nu_{max}$ is the larger chemical shift difference between the weakly coupled proton partners.

Thus, with the use of the CPMG element the effect of undesired homonuclear J_{HH} modulation from HSQMBC-like sequences could be minimized. However, it has been accepted that J_{HH} coupling constants cannot be completely removed for all spin systems using CPMG due to the need to use a very short delays between pulses ($2\eta < 100$ μs). Importantly, the use of very short inter-pulse delays can put in serious troubles the limits of the probehead due to sample heating effects. In addition, it is important to note that homonuclear TOCSY transfer can be also effective during the CPMG period.

In general, the proposed CPMG-HSQMBC experiment performs better than the original HSQMBC sequence and it has been demonstrated that an efficient measurement of $^{n}J_{CH}$ can be carried out. Williamson and co-workers published the BIRD-CPMG-HSQMBC experiment[77] where the concepts of BIRD and CPMG were implemented into the same pulse sequence (Figure 17D) obtaining spectra with minimum distortions.

- **Implementing frequency-selective 180° ^{1}H pulses: selHSQMBC**

Despite the fact that BIRD-HSQMBC and CPMG-HSQMBC experiments have proved efficient for the measurement of $^{n}J_{CH}$ in both protonated and non-protonated carbon atoms, the modulation of the intensity by the homonuclear J_{HH} couplings still remain as the most important drawback to overcome. A very simple solution to avoid such J_{HH} interferences in HSQMBC pulse schemes was proposed by our research group.[78] The central 180° ^{1}H pulse into the INEPT periods can be replaced by a frequency-selective 180° ^{1}H pulse (Figure 18A) to prevent the undesired J_{HH} coupling evolution, whereas selective heteronuclear polarization transfer for the selected proton is still achieved. The proposed selective experiment has been implementing in the refocused HSQMBC version

[76] K. E. Kövér, G. Batta, K. Fehér, *J. Magn. Reson*., **2006**, *181*, 89.

[77] L. Valdemar Jr, V. Gil, M. G. Constantino, C. F. Tormena, R. T. Williamson, B. Marquez, *Magn. Reson. Chem.,* **2006**, *44*, 95.

[78] S. Gil, J. F. Espinosa, T. Parella, *J. Magn. Reson*., **2011**, *213*, 145.

to obtain cross peaks displaying IP coupling pattern with respect to $^{n}J_{CH}$. Although that idea can be implemented in the original non-refocused HSQMBC experiment where the resulting cross peaks would present AP coupling pattern with respect to the active $^{n}J_{CH}$, accidental line cancelation and/or complex analysis of AP multiplets could still remain, meaning that tedious and time-consuming fitting procedures would be required.

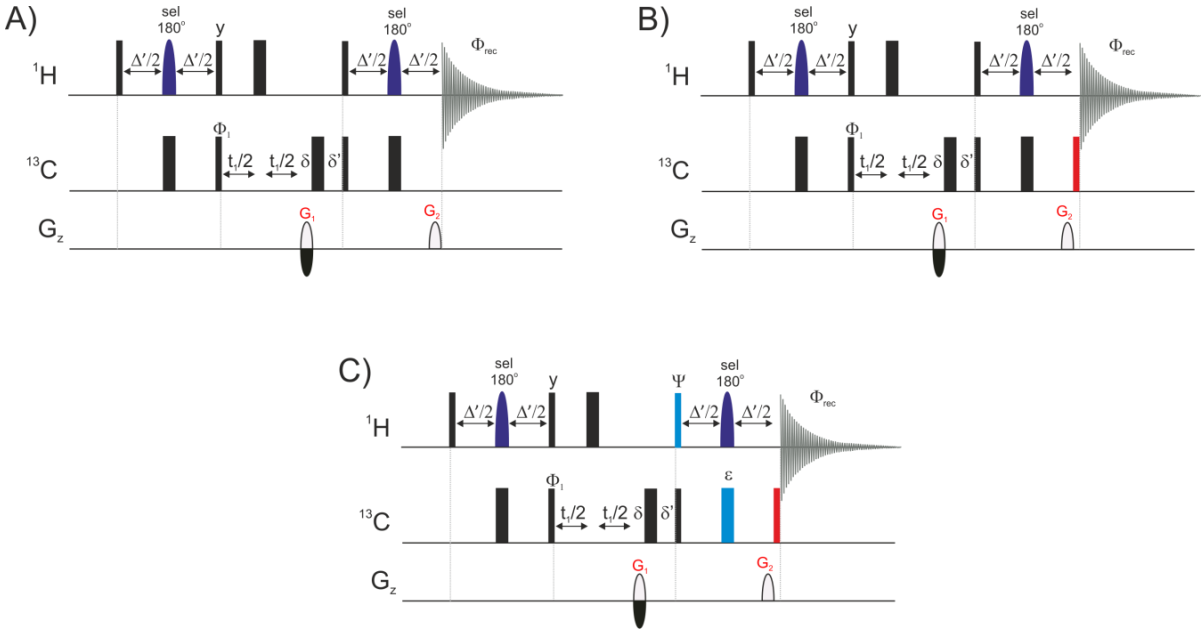

Figure 18: Several ^{1}H-selective 2D HSQMBC schemes designed to measure long-range proton-carbon coupling constants: A) selHSQMBC; B) CLIP-selHSQMBC; C) CLIP-HSQMBC IPAP. Frequency-selective 180° ^{1}H pulses represented as shaped pulses are applied in the middle of the INEPT blocks (Δ=1/(2$^{n}J_{CH}$)= Δ'+p180 where p180 is the duration of the selective 180° ^{1}H pulse that must be set accordingly to the required selectivity in each case). ^{1}H data are acquired without ^{13}C decoupling. In C) the IPAP methodology is applied: two independent IP and AP data are separately collected as a function of the pulses marked with ε: IP (Ψ=y and ε=on) and AP (Ψ=x and ε=off). α/β data are obtained after time-domain addition/subtraction data (AP±IP). A minimum two-step phase cycling is executed with Φ_1= x,-x and Φ_{rec}= x,-x. All other unlabeled pulses are from the *x*-axis. Gradients G_1 and G_2 are used for coherence selection using E/A (G_1:G_2=±80:20.1).

As it has been shown before, in conventional HSQMBC experiment the observable magnetization just before acquisition can be described as a mixture of IP and AP components (Eq. 1.21). In selHSQMBC experiments the evolution under the J_{HH} is prevented, such that the final magnetization can be described as:

$$+ H_{1x}\sin^2(\pi^n J_{H_1C}\Delta) \qquad \text{IP Term}$$
$$- 2H_{1y}C_z\sin(\pi^n J_{H_1C}\Delta)\cos(\pi^n J_{H_1C}\Delta) \qquad \text{AP Term}$$

Eq. 1.28

As a result, selHSQMBC cross-peaks show AP contribution which distorts the signal phases along the detected F2 dimension. The application of the CLIP technique has been proposed to solve that problem.[79] The CLIP-HSQMBC experiment yields undistorted IP ^{1}H multiplets with pure absorptive line shapes along the detected dimension from which the easy, direct, and accurate measurement of $^{n}J_{CH}$ can be performed. As discussed before for other CLIP experiments, the key point of this sequence is the 90^{o} ^{13}C pulse applied just prior to acquisition (Figure 18B), which efficiently converts the existing dispersive AP contribution to non-observable MQCs. The resulting cross-peaks show an additional splitting compared to the conventional ^{1}H multiplet (Figure 19A) arising from the active proton–carbon coupling because proton acquisition is performed without heteronuclear decoupling. The magnitude of $^{n}J_{CH}$ can be extracted directly by analyzing peak frequency separation as usually made for conventional ^{1}H multiplets. The phase properties of the multiplet and therefore the accurate extraction of $^{n}J_{CH}$ are independent of experiment optimization, with a small uncertainty of 0.1-0.2 Hz, but important errors of 20-30% should be easily introduced when omitting the CLIP pulse (Figure 19B). In practice, a perfect match between $^{n}J_{CH}$ and the experiment optimization is not critical, cross-peaks show a clear dependence with the $\sin^2(\pi^n J_{H_1C}\Delta)$ function, and $^{n}J_{CH}$ values in the range 3-10 Hz can be measured in a 4–8 Hz optimized selHSQMBC experiment (Figure 19B).

For more complex multiplets, the separation of the outer peaks of the multiplet can be compared to that in the ^{1}H spectrum to extract indirectly the additional splitting. Alternatively, a simple fitting procedure taking the internal satellite $^{1}J_{CH}$ component as decoupled reference multiplet can be applied. On the other hand, a double-selective 1D version of a refocused HSQMBC experiment has been also proposed for the fast and accurate measurement of specific $^{n}J_{CH}$ values from pure IP 1D multiplets.[80]

[79] J. Saurí, T. Parella, J. F. Espinosa, *Org. Biomol. Chem*., **2013**, *11*, 4473.

[80] J. F. Espinosa, P. Vidal, T. Parella, S. Gil, *Magn. Reson. Chem*., **2011**, *49*, 502.

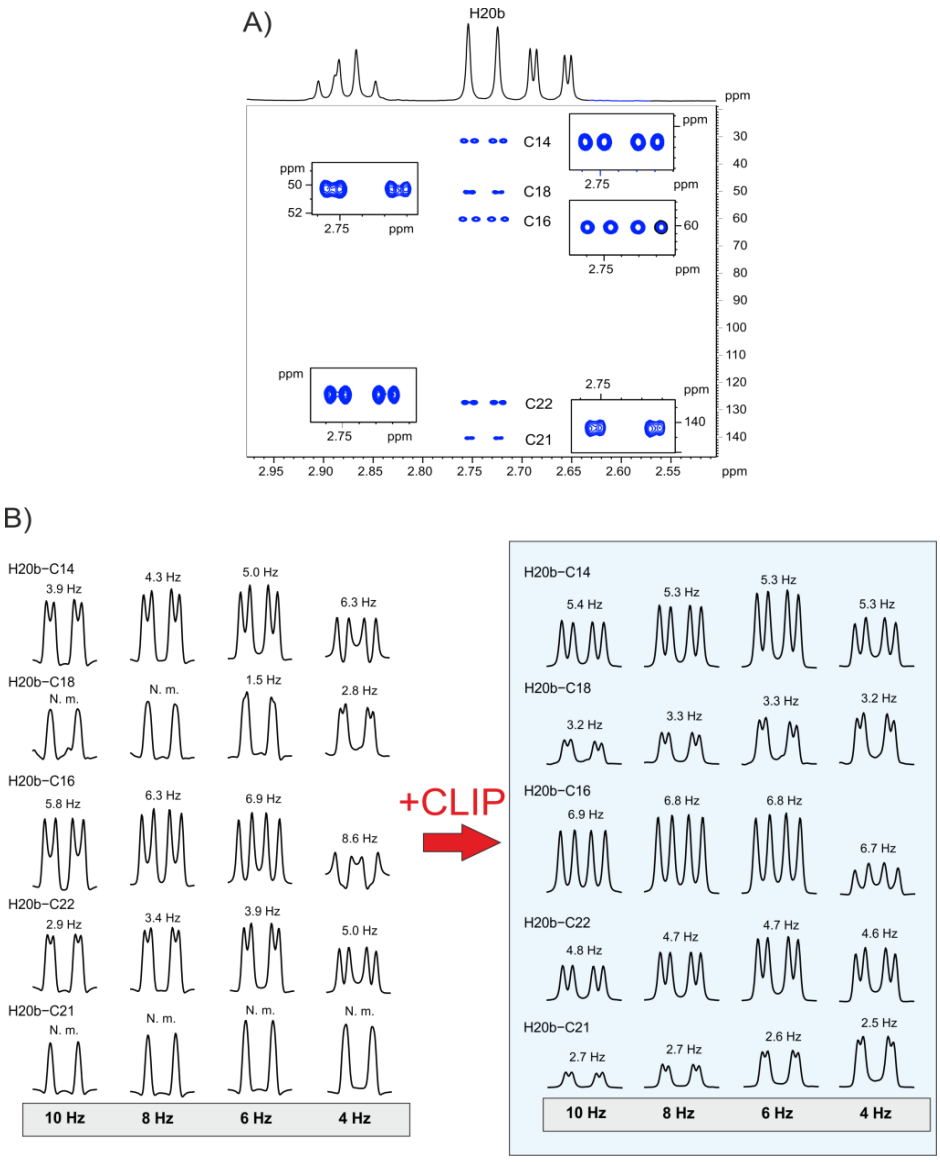

Figure 19: A) 2D CLIP-selHSQMBC spectrum of strychnine [2] after pulsing on H20b with a 20 ms Gaussian-shaped 180° ^{1}H pulse. The inter-pulse delay Δ was optimized to 62.5 ms (corresponding to $^{n}J_{CH} = 8$ Hz). B) Direct extraction of $^{n}J_{CH}$ can be made from pure in-phase cross-peaks, independent of experiment optimization (from 4 to 10 Hz).

A powerful alternative for the simple and direct determination of $^{n}J_{CH}$ in broad, unresolved, or highly complex selHSQMBC multiplets is based on the incorporation of the IPAP principle that relies on the separate acquisition of complementary IP and AP datasets[78] (left part of Figure 20). The IP data are generated applying the initial hard 90° ^{1}H pulse of the refocused INEPT (mark in blue) from *y*-axis (Ψ=y) and the hard 180° ^{13}C pulse (ε=on), whereas the AP data are obtained using the same scheme with Ψ=x and omitting the last 180° and 90° ^{13}C pulses to avoid $^{n}J_{CH}$ refocusing (ε=off). Time-domain data combination (IP±AP) affords two separate pure-phase α- and β-selHSQMBC subspectra where the $^{n}J_{CH}$ value can be extracted by direct analysis of the relative

frequency displacement between these α/β cross-peaks along the highly resolved F2 dimension (right part of Figure 20). In this manner, accurate $^{n}J_{CH}$ values can be easily extracted, irrespective of the multiplet complexity and avoiding the typical overestimation associated to the direct analysis of AP signals or the lack of multiplet definition in IP signals. The success of the IPAP technique relies on the complementarity between the IP and AP data, and the percentage of undesired cross-talk generated during IP±AP data combination will be proportional to a $\sin^2(\pi^n J_{H_1C}\Delta)$-$\sin(\pi^n J_{H_1C}\Delta)$ factor. The use of individualized scaling factor (AP±*k**IP) factors can compensate unbalanced IPAP cross-peaks. As a bonus, the IPAP methodology offers additional controls to confirm the accuracy of the measurement or the presence of cross-talking. Three different multiplets (IP, AP, and α/β) are available for independent measurements and proper data comparison and validation.

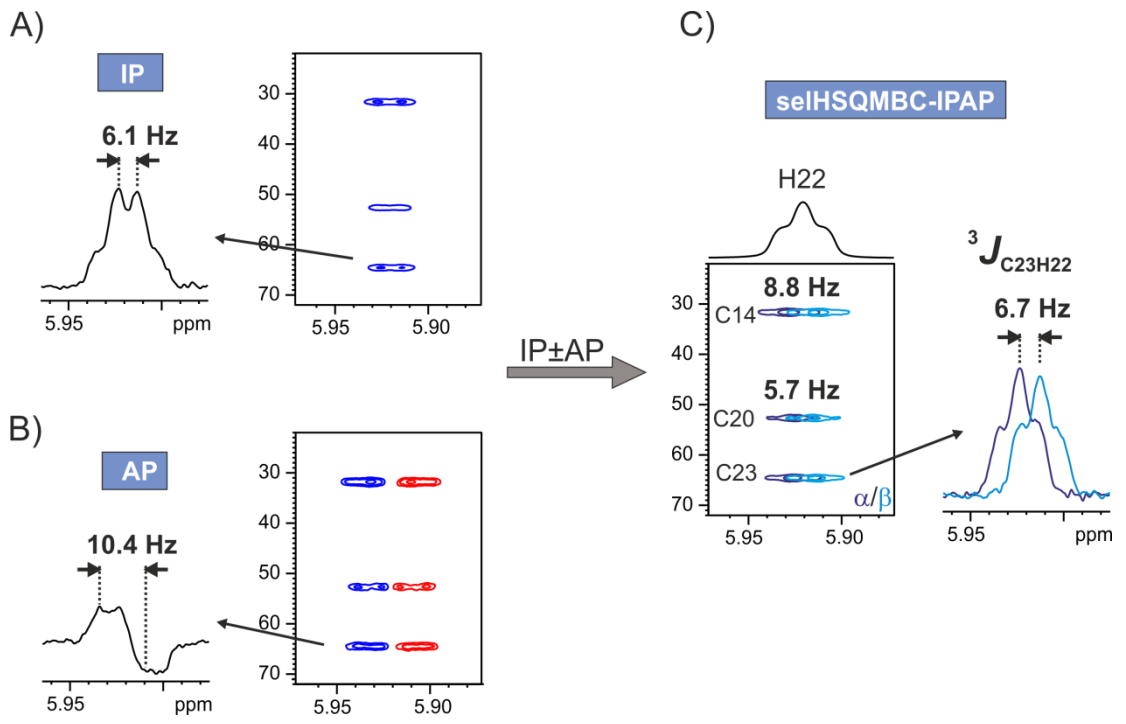

Figure 20: selHSQMBC-IPAP experiments after selective excitation of the olefinic H22 proton in strychnine [2]. The acquired A) IP and B) AP datasets are added/subtracted to provide C) separate α/β subspectra. The relative displacement between α/β cross-peaks along the F2 dimension provides a direct measurement of $^{n}J_{CH}$ without any posterior analysis.

The main limitation of these experiments relies on the selective concept because not all protons can be simultaneously excited/observed at the same time and several experiments may be needed to measure all the targeted couplings. However, multiple protons can be simultaneously studied in a single experiment using region-selective or

multiple frequency-selective pulses, provided that all excited protons are not mutually *J*-coupled.

As it was mention before, in the case of $^{n}J_{CH}/^{n}T_{CH}$ the values are in the same range as J_{HH}/T_{HH} and they are more complicated to measure. Most of these available long-range methods rely on the basic HMQC and HSQMBC pulse schemes, or on related hybrid HSQC-TOCSY experiments[81] with a limited application to protonated carbons. Figure 21 shows different topologies defining the transfer mechanism followed in HSQC/HSQMBC-based experiments designed to measure J_{CH}. In the last few years, several modified selHSQMBC methods (c.a. selHSQMBC-TOCSY[82] and selHSQMBC-COSY[83]) have been developed for the measurement of the sing and the magnitude of $^{n}J_{CH}$.

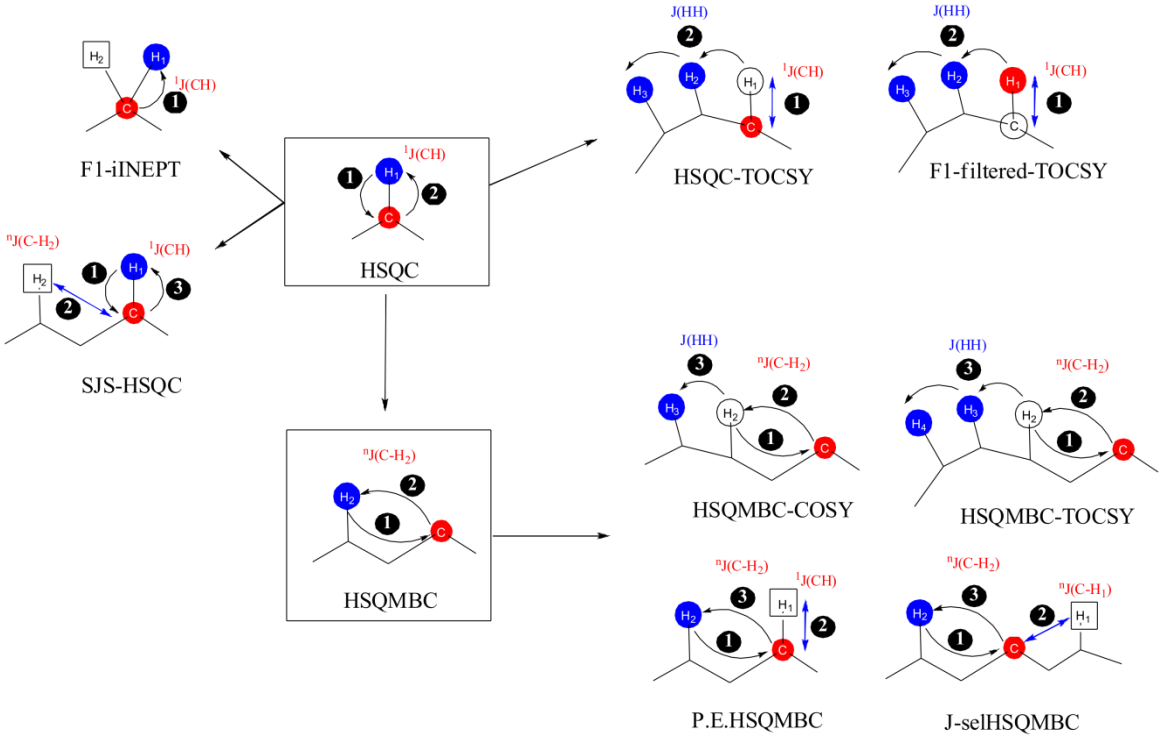

Figure 21: Schematic representation of several spin systems that can be studied by HSQC and HSQMBC type experiments

[81] W. Kozminski, *J. Magn. Reson.*, **1999**, *137*, 408.

[82] J. Saurí, J. F. Espinosa, T. Parella, *Angew. Chem. Int. Ed.*, **2012**, *51*, 3919.

[83] J. Saurí, T. Parella, *Magn. Reson. Chem.*, **2012**, *50*, 717.

2. OBJECTIVES

The general and specific aims of this doctoral thesis are briefly described below:

- Learn the main theoretical, technical and practical aspects of the NMR spectroscopy and acquire experience working on different spectrometers, in the implementation and set-up of NMR experiments and in pulse programming skills. All these knowledge are essential to be able to carry out the rest of the proposed objectives.

- Know, evaluate and compare the existing NMR methods related with the field we wanted to study, in order to better understand the advantages/drawbacks of each methodology.

- Design of new NMR methods to overcome the different drawbacks/limitations observed in the existing ones and its application to solve real chemical problems. As a starting point, a main objective was especially focused on the development of improved HSQC and HSQMBC experiments to measure coupling constants, with special interest in the determination of small coupling values, their positive/negative sign, and the implementation of fast and accurate methods to extract *J* values from the direct analysis of multiplets.

- Explore the possibilities of modern NMR methodologies, with special interest in broadband homodecoupled techniques. Analysis of pros and cons, and evaluation of their potential to solve real chemical problems, such as the eternal problem of NMR signal overlap.

- Develop new NMR experiments that offer the following basic features:
  - Easy implementation with emphasis to achieve the maximum level of automation.
  - Simple in terms of data acquisition and without extensive and sophisticated set-up and post-processing tasks.
  - General applicability covering a wide range of sample and NMR experimental conditions.
  - Optimal spectral quality in terms of resolution and sensitivity.

3. RESULTS AND DISCUSSION

This section is centered on the experimental results obtained during this doctoral thesis in relation to the development and application of modern pure shift NMR methodologies and improved HSQC and HSQMBC experiments. The results have been published in different scientific journals as ten original research papers. Below, a brief description of each publication is presented:

- In **Publication 1** an improved sensitivity-improved slice-selective NMR method based on a multiple-slice excitation concept is proposed. The success of the method is demonstrated by enhancing SNR by more than one order of magnitude in ZS experiments.

- In **Publication 2** a new, fast and full-sensitive pure shift NMR technique, referred to as *HOmodecoupled Band-Selective* (HOBS), is presented. HOBS experiments yields broadband homodecoupled spectra in particular areas of the ^{1}H spectrum where do not appear mutually *J*-coupled protons. Implementation on 2D experiments is also illustrated with practical examples.

- Practical applications of the HOBS methodology have been published to differentiate signals with small chemical shift differences, such as shown in the analysis of individual signal intensity decays for measuring T_1 and T_2 relaxation times in overlapped regions (**Publication 3**), in enantiodifferentiation studies by using chiral solvating agents (**Publication 4**) and in the measurement of long-range heteronuclear coupling constants or the design of pure shift selHSQMBC experiments (**Publication 6**).

- Introduction to the concept of ultra-high-resolution NMR spectroscopy. It is shown that pure shift HSQC experiments incorporating broadband homonuclear decoupling along the acquisition F2 dimension combined with other resolution-enhanced NMR techniques, such as spectral aliasing or NUS along the indirect F1 dimension improve key NMR features, such as spectral resolution and digital resolution, using standard spectrometer configurations. These new highly-resolved experiments have been applied to determine very small chemical shift differences simultaneously for ^{13}C and ^{1}H in enantiodifferentiation studies (**Publication 5**) and to analyze highly complex mixtures of very similar stereoisomers exhibiting near-identical ^{1}H and ^{13}C NMR spectra. (**Publication 7**).

- In **Publication 8,** a new *Pure In-Phase* (PIP) heteronuclear correlation NMR experiment (referred to as PIP-HSQC and PIP-HSQMBC) is proposed as a method to avoid complex data analysis. In these new experiments, all the undesired AP contributions present in conventional HSQC and HSQMBC experiments are efficiently suppressed, obtaining spectra where all the cross-peaks display perfect IP multiple patterns which are suitable for an accurate extraction of scalar *J* couplings and RDCs.

- In **publication 9,** an improved HSQC experiment (referred to as perfect-HSQC) is proposed for the efficient suppression of phase and amplitude J_{HH} modulations. The features of the obtained spectrum allow carrying out an accurate measurement of homo- and heteronuclear scalar and dipolar coupling constants. In addition, guidelines are provided for the future use of HSQC datasets as a quantitative NMR tools by peak volume integration.

- In **Publication 10,** a compilation and discussion of the different improvements reported for HSQC and HSQMBC experiments in the last years is presented. Some of the new experiments exposed along this doctoral thesis are also included and exemplified with practical examples.

Since every published paper has gone through a review process by chemists and NMR experts, not much attention is devoted to the discussion of the results beyond what is discussed into each original publication. Nevertheless, a little introduction is presented for each one of the published papers.

PUBLICATION 1

Simultaneous multi-slice excitation in spatially encoded NMR experiments

Laura Castañar, Pau Nolis, Albert Virgili and Teodor Parella.
Chem. Eur. J., **2013**, *19*, 15472-15475.

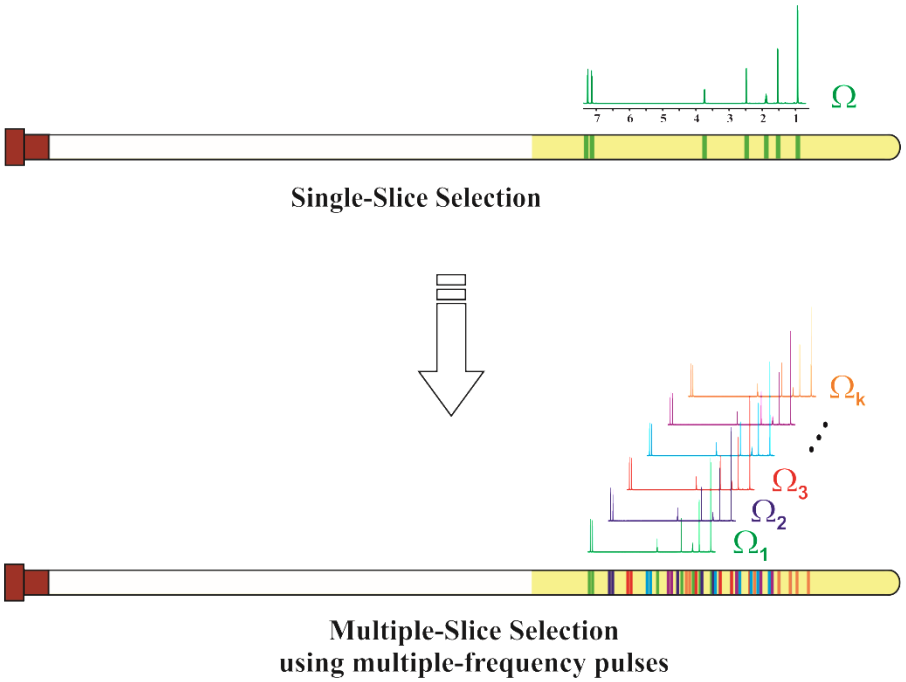

Introduction

The most serious drawback of spatially encoded NMR experiments is their reduced SNR because the observed signal only arises from a discrete slice of the sample. Therefore, novel approaches are required to improve the inherent low SNR of slice-selective NMR experiments and make them of practical and general use with moderately concentrated samples.

In the last few years, several approaches have been reported to enhance SNR per time unit in slice-selective experiments:

i. Sequential slice excitation with the aim of reducing the long recycle delay and shortening the overall acquisition time in 1D and 2D experiments[47,84] or performing continuous data acquisition, as described in fast monitoring reaction studies.[85] This strategy uses a fast pulsing approach with around 100 ms of recycle delay, and after each scan, the offset of the selective shaped pulse is changed to access fresh equilibrium magnetization from adjacent frequency/spatial regions. Sakhaii *et al*. reported how an optimized division of the NMR tube in eight slices by changing the offset accordingly affords an experiment increment by a $\sqrt{8}$ factor in the original ZS experiment.[47] Similarly, spatially selective HMQC spectra have been rapidly recorded within 45-90 s dividing the NMR tube of protein samples in four *z*-slices.[84b]

ii. It has been reported that the use of the so-called through-polarization sharing can afford an average enhancement by a factor of two.[48] This approach is based on the original *Acceleration by Sharing Adjacent Polarization* (ASAP) technique that uses a short recycle delay consisting of a 40 ms isotropic DIPSI-2 pulse train flanked by two gradients.[86] The method presents some limitations because sensitivity enhancement is not uniform for all signals and strongly dependent of the different relaxation properties of the excited protons while other spins remain unperturbed, preventing any attempt of quantification.

In this article a novel strategy to enhance the experimental sensitivity in spatially encoded NMR experiments applying a multiple-frequency modulated pulse to simultaneously excite different slices in a single NMR experiment is proposed. The

[84] a) M. Vega-Vazquez, J. C. Cobas, M. Martin-Pastor, *Magn. Reson. Chem.,* **2010**, *48*, 749. b) B. Sathyamoorthy, D. M. Parish, G. T. Montelione, R. Xiao, T. Szyperski, *Chemphyschem,* **2014**, *15*, 1872.

[85] G. E. Wagner, P. Sakhaii, W. Bermel, K. Zangger, *Chem. Commun.,* **2013**, *49*, 3155.

[86] R. Freeman, E. Kupče, *Magn. Reson. Chem.,* **2007**, *45*, 2.

increased sensitivity observed in the ^{1}H spectrum is proportional to number of offsets applied. The proposal is based on the careful setting of multiple offsets to avoid the excitation of mutually *J*-coupled protons within the same slice which would result in distorted multiplets due to J_{HH} evolution. As a proof of the method, we have applied it on a sample of the anti-inflammatory drug ibuprofen, that contains a relative simple ^{1}H spectrum, and on a sample of cyclosporine, which presents a more complex ^{1}H spectrum. In both cases, the sensitivity of slice-selective experiments has been substantcially improved compared with the conventional experiments.

One of the advantages of this proposal is the easy implementation of multi-frequency pulses without the need to modify existing pulse sequences, having a considerable impact on the success of a wide variety of NMR applications. As predicted theoretically, the SNR in pure shift ^{1}H NMR spectra of the cyclopeptide cyclosporine recorded with the pseudo-2D ZS and real-time techniques is enhanced by an average experimental factor of ~7 when an 8-site multiple-frequency 180^{o} pulse is applied instead of a conventional single-frequency pulse.

CHEMISTRY
A EUROPEAN JOURNAL

ChemPubSoc
Europe

DOI: 10.1002/chem.201303272

Simultaneous Multi-Slice Excitation in Spatially Encoded NMR Experiments

Laura Castañar, Pau Nolis, Albert Virgili, and Teodor Parella*[a]

Recently, there has been a growing interest in spatially localized NMR spectroscopic techniques based on the incorporation of the traditional slice selection concept implemented in magnetic resonance imaging (MRI) applications. Several high-resolution NMR methods applying spatial frequency encoded excitation along an NMR tube have been suggested as means of obtaining specific information from a particular slice. For instance, selective spin-lattice T_1 relaxation times[1] and all proton–proton coupling constants for a selected proton resonance from a slice-selective *J*-resolved (G-SERF) experiment have been measured,[2] broadband homodecoupled ^{1}H spectra with the Zangger-Sterk (ZS) method have been obtained,[3–5] slice-selective diffusion experiments have been carried out[6] and diagonal-suppressed 2D experiments are also possible.[7] Sequential multi-slice selection has been exploited for cases in which nuclear spins in different parts of the NMR tube are exclusively excited during subsequent transients by changing the offset frequency while the previously used spins have time to relax towards equilibrium before being excited again, resulting in significantly shorter overall acquisition times. Examples have been utilized to accelerate data acquisition in multidimensional NMR experiments,[8] to improve the signal-to-noise ratio (SNR) per time unit in the ZS method[9] or to study the kinetics of a reaction on the ms time scale.[10] The use of multiple-frequency pulses[11] has been recently suggested as a method of effective broadband ^{13}C homodecoupling in slice-selected HSQC experiments for highly-enriched ^{13}C samples.[12]

Experimentally, spatial frequency encoding is achieved easily by simultaneous application of a frequency-selective 90° or 180° ^{1}H pulse and a spatial-encoding gradient, G_s. The range of sampled frequencies (SW_G) is defined by the strength of G_s according to $SW_G = \gamma L G_S$, in which γ is the gyromagnetic ratio of the spatially encoded nucleus and L is the active volume coil length. On the other hand, the carrier frequency (Ω) and the selective pulse bandwidth ($\Delta\omega$) determine the z-position of each nuclear spin ($z = \Omega/(\gamma G_s)$) and the slice thickness ($\Delta z = \Delta\omega/(\gamma G_s)$), respectively. Thus, the overall SNR of a slice-selective experiment will depend both on the strength of the encoding gradient and on the selectivity of the pulse. For instance, a typical 20 ms Gaussian-shaped 180° pulse (bandwidth of 60.7 Hz) applied simultaneous with a gradient of 0.743 G cm^{-1} (this is 1.39% of the maximum gradient strength of 53.5 G cm^{-1} delivered by our gradient unit) splits the sample height (L = 1.8 cm) into around 94 slices along the z axis, defining a slice thickness of about 0.019 cm and covering a SW_G of 5694 Hz (9.47 ppm in a 600 MHz spectrometer). Thus, under these general conditions, the single-slice selection procedure would afford only about 1% of the sensitivity of a conventional ^{1}H spectrum. This low SNR could be improved by using shorter and less selective pulses and/or less intense encoding gradients but always with an increase in the probability of accidental excitation of two coupled spins within the same slice.

As mentioned, the most serious drawback of spatially encoded NMR experiments is their reduced sensitivity because the observed signal only arises from a discrete slice of the sample. Therefore, novel approaches are required to improve the low SNR and to make these types of experiments practical for use with moderately concentrated samples. Herein, we exploit the sensitivity benefits of applying a multiple-frequency modulated pulse to simultaneously excite different slices in a single NMR experiment. Our proposal is based on the careful setting of multiple offsets to avoid the excitation of mutually *J*-coupled protons within the same slice (Figure 1) which would result in distorted multiplets due to J_{H-H} evolution.

We have used two basic experiments to evaluate the effectiveness of multiple-frequency pulses in slice-selective experiments. The 1D z-profile image of the sample can be obtained with the conventional echo gradient pulse sequence including an initial selective 180° pulse and a simultaneous encoding gradient to visualize the frequency excitation achieved in the z direction (Figure 2A). The experimental effects on the NMR spectrum can be quickly monitored by recording spatially encoded single pulsed-field gradient echo (se-SPFGE) experiments (Figure 2B). This sequence consists of a selective gradient echo in which a slice-selection gradient (G_S) is switched on in conjunction with the central refocusing 180° ^{1}H pulse. When G_S is not applied, this is the conventional SPFGE pulse sequence used for frequency-selective excitation, in which the G_1 gradients act as defocusing/refocusing coherence elements.

Figures 2C–H show 1D z-profile images of a D_2O sample as a function of the number of offsets defined by the shape

[a] L. Castañar, Dr. P. Nolis, Prof. A. Virgili, Dr. T. Parella
Servei Ressonància Magnètica Nuclear and Departament de Química
Universitat Autònoma de Barcelona
08193 Bellaterra, Barcelona (Spain)
E-mail: teodor.parella@uab.cat

Supporting information for this article is available on the WWW under http://dx.doi.org/10.1002/chem.201303272.

CHEMISTRY
A EUROPEAN JOURNAL

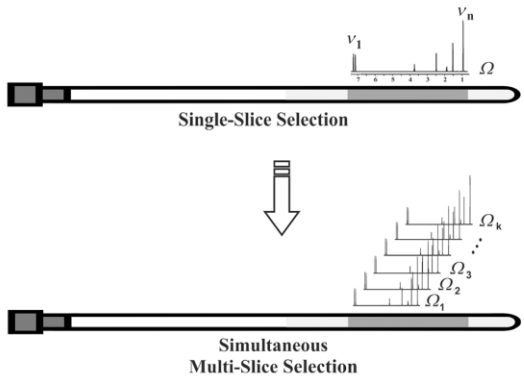

Figure 1. Schematic representation of a conventional single-slice pulse sequence compared to simultaneous multi-slice selection by a multiple-frequency pulse modulated according to different offset frequencies (Ω_1 … Ω_k). A methodology is described that avoids the simultaneous excitation of mutually J-coupled spins within the same z slice.

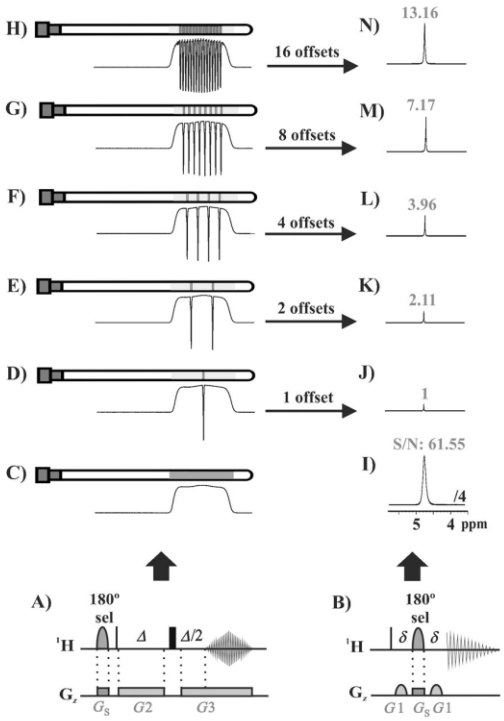

Figure 2. Pulse schemes for the A) 1D z-profile image and B) se- SPFGE experiments. C–H) Schematic z-profile of a 99.96% D_2O sample (obtained with the pulse sequence shown in A) with a multiple-frequency pulse with 0 (G_s=off), 1, 2, 4, 8 and 16 different offsets, respectively; J–N) se-SPFGE spectra (obtained with the pulse sequence shown in B) with a multiple-frequency pulse with 1, 2, 4, 8 and 16 different offsets and with the experimental signal-to-noise ratio related to the conventional ^{1}H NMR spectra (I). In all experiments, a 20 ms Gaussian-shaped 180° ^{1}H pulse was simultaneous applied with an encoding gradient G_s= 0.865 G cm^{-1}.

of the selective pulse, in which the exact z-position of each selected slice along the NMR tube is evident. The relative SNR of the corresponding se-SPFGE spectra follow a clear dependence on the number of offsets applied (Figure 2 I–N). As expected, whereas a 1.6% of the maximum attainable sensitivity is reached in the single-slice experiment, a substantial signal increase by a factor of 13 is achieved with a 16-site multiple-frequency pulse generated with a linear increment of 300 Hz. The small deviation with respect to the theoretical gain can be related to the imperfect top hat profile of the Gaussian-shaped selective pulse and the decreased sensitivity obtained at both edges of the coil due to the non-uniformity of the gradients. The use of a reduced and centered volume for which uniformity is better and/or the use of other pulse shapes offering a better inversion profile at the expense of longer durations is advisable in some cases.

The situation becomes more complex in real samples because multiple signals with different frequencies are present and, in addition, each of them is individually localized at different z positions as a function of the applied offset. The probability that two J-coupled protons are excited within the same slice is increased and, therefore, a procedure for the calculation of a set of offsets to avoid this must be designed. Let us assume we have a conventional ^{1}H NMR spectrum containing n different signals with frequencies ν_1, ν_2… ν_n, being ν_1 and ν_n the lowest (upfield) and the highest (downfield) frequencies, respectively. The complete spectral width to be excited will be defined by $SW_G = \nu_n - \nu_1$ and the center position by $\Omega = (\nu_1 + \nu_n)/2$. As an initial recommendation, we propose the use of a spectral width amplification factor k (kSW; in which $k > 1$) to increase the offset range that will not cause the signals from the edges of the spectrum to appear beyond the coil position. In this case, the required encoding gradient will be redefined by $G_s = k SW_G/(\gamma L)$. In a second step, a complete set of offset values is calculated to excite different parts of the sample with the restriction that two or more mutually J-coupled protons are not perturbed within the same slice, especially those which are strongly coupled. The interval of possible offsets to be used will be a range between two values, Ω_1 and Ω_k, representing offsets for which the ν_1 and ν_n frequencies appear at the top and bottom of the active volume coil, respectively [Eq. (1) and (2)].

$$\Omega_1 = (L \gamma G_s)/2 + \nu_1 \quad (1)$$

$$\Omega_k = -(L \gamma G_s)/2 + \nu_n \quad (2)$$

For each selected offset (Ω_p; $1 < p < k$), the z position of each individual resonance ($z(i,\Omega_p)$) may be theoretically known from the relationship given in Equation (3):

$$z(i,\Omega_p) = (\Omega_p - \nu_i)/(\gamma G_s) \quad (3)$$

Therefore, taking the frequencies of each resonance extracted from the ^{1}H spectrum as input values, a complete

CHEMISTRY
A EUROPEAN JOURNAL

position-dependent calculation can be created for a set of offset values which must be incremented in a stepwise fashion as a function of the resulting slice thickness ($\Delta\Omega > \Delta z$).

Successful application of the multi-slice selection concept to an unknown sample containing many different resonances will depend of the complexity of its ^{1}H spectrum. The se-SPFGE pulse sequence is an effective and rapid tool to check the viability of the multi-slice selection process as a function of the spectral width to be excited, the number of resonances contained into it and also the probability of two coupled protons in close proximity. Experimentally, the unwanted excitation of different *J*-coupled protons within the same slice would be quickly observed by the anti-phase contributions in the corresponding *J* multiplet structure. As a proof of the method, we have applied it to a sample of ibuprofen which has a relatively simple ^{1}H spectrum (Figure 3A). The single-slice experiment recorded with a normalization factor of $k=1$ (Figure 3C) suffers from the poor gradient homogeneity at the ends of the coil. This is evidenced by the decreased SNR observed for the outer signals with respect to the central ones. More uniform response can be obtained with a factor of $k=2$ because data is collected in the central part of the coil but with some sensitivity penalty due to the thinner slice thickness (Figure 3D). Very interestingly, an average SNR improvement factor of 13.5 is obtained when applying a 15-site multiple-frequency pulse versus its conventional single-slice counterpart (Figure 3E). In other words, increases of up to 22% of the maximum attainable signal are fully recovered taking individual SPFGE signals as a reference (see Figure 3B) and without observing phase distortions due to J_{H-H} evolution.

An additional signal enhancement at the risk of non-uniform excitation can be achieved by moving the spectrum partially out of the limits of the active coil. This increases the potential number of offsets to be used although some signals do not contribute equally to the data collected. For a more complex spectrum, such as those of the alkaloid strychnine, the use of a 11-site excitation affords an averaged SNR enhancement of 9.2% with respect to the ^{1}H spectrum if the selection is restricted to the $\pm L/2$ area, whereas a further improvement up to 12.8% is achieved with a 16-site multiple-frequency pulse when unrestricted offsets are allowed in the calculation (see Supporting information). The latter approach could be useful in situations for which quantitative analysis is not necessary.

The advantage of the easy implementation of multi-frequency pulses without the need to modify existing pulse sequences can have a considerable impact on the success of a wide variety of NMR applications. As an example, Figure 4 shows how the SNR in a broadband homodecoupled ^{1}H NMR spectrum of the cyclopeptide cyclosporine recorded with the pure-shift pseudo-2D ZS technique[3,15] is enhanced by an average experimental factor of 6.7 when an 8-site multiple-frequency 180° pulse is applied instead of a conventional single-frequency pulse (Figure 4B vs. 4C). Similar sensitivity gains can also be achieved with the recently proposed instant pure-shift ZS technique (see the Supporting Information),[5] and probably such enhancements could offer important SNR benefits in more time-consuming multidimensional slice-selective NMR experiments.[13–15]

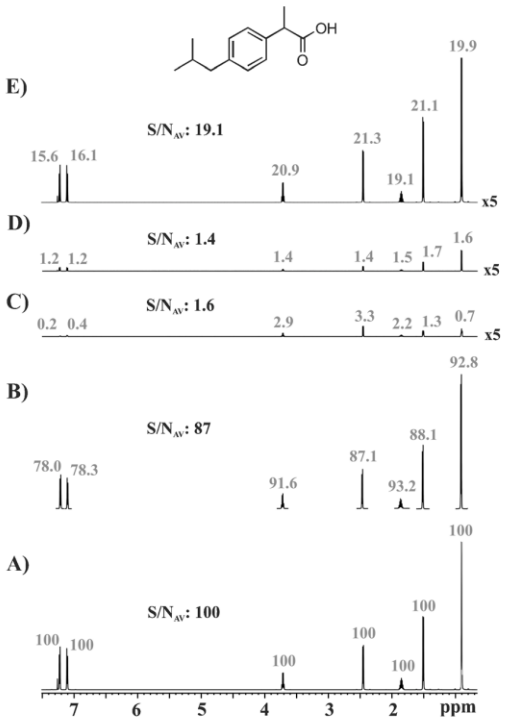

Figure 3. A) Conventional ^{1}H NMR spectra of ibuprofen in $CDCl_3$. The experimental signal-to-noise ratio in the ^{1}H NMR spectra has been normalized for each individual signal. B) Signals arising of individual SPFGE experiments ($G_s=0$) to account for T_2 relaxation losses during the echo; C and D) single-slice se-SPFGE spectra with a normalized scaling *k* factor of 1 and 2, respectively; E) Multi-slice se-SPFGE spectrum with 15 different offsets to avoid the simultaneous excitation of different coupled protons into the same slice. A single scan and a 20 ms Gaussian-shaped pulse were used in all experiments. Spectrum C was recorded with an amplification *k* factor of 1 ($SW_G=3793$ Hz), a square-shaped encoding gradient (G_S) of 0.495 G cm^{-1}. Spectra D and E were recorded with an amplification *k* factor of 2 ($SW_G=7586$ Hz), a square-shaped encoding gradient of 0.99 G cm^{-1}.

In conclusion, an improved data collection technique with simultaneous multi-slice data acquisition has been presented. The sensitivity of slice-selective NMR experiments can be substantially improved by simultaneously applying a multiple-frequency pulse and spatial encoding gradient. The experimental procedure to fulfill the sampled frequency requirement is simple and the results can be inmediately adapted to a wide range of applications. Further investigations are in progress to develop novel applications and other new and/or complementary strategies to further improve the sensitivity and the performance of spatially encoded NMR experiments.

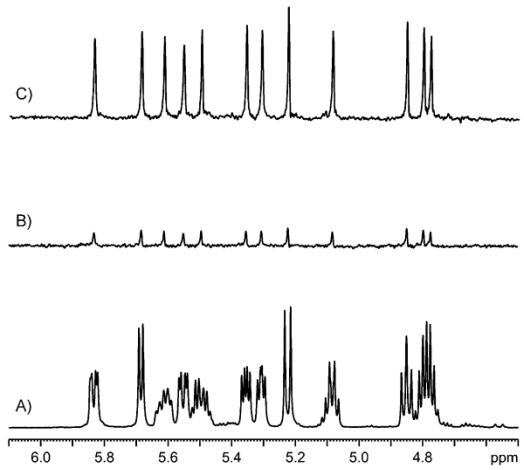

Figure 4. Sensitivity-enhanced broadband-homodecoupled ^{1}H NMR spectra of cyclosporine with the pure-shift pseudo-2D technique.[3,15] Expanded H_α region from the A) conventional; B and C) single-slice and 8-site multi-slice pure-shift ^{1}H spectra, respectively. The 8 offsets were limited to the sample coil and the experimental sensitivity enhancement was around 6.7%. All experimental details remain the same for spectra B and C: an amplification k factor of 2 ($SW_G = 9140$ Hz), a square-shaped encoding gradient of 1.13 G cm^{-1} and a 80 ms Rsnob 180° ^{1}H pulse to achieve a perfect homodecoupling for the strong coupled AB proton spin system resonating at 5.50 and 5.61 ppm. 4 transients were collected for each one of the 32 t_1 increments in an experimental time of ≈4 min. More details can be found in the supporting information.

Experimental Section

All NMR Experiments were performed in a 600 MHz BRUKER Avance-III spectrometer equipped with a TXI probe and a gradient unit delivering 53.5 G cm^{-1}. The samples used were 99.96% D_2O, 100 mM of ibuprofen in $CDCl_3$, and 25 mM cyclosporine in [D_6]benzene. Additional details about experimental NMR conditions and offsets calculation can be found in the Supporting Information.

Acknowledgements

Financial support for this research provided by MICINN (project CTQ2012–32436) and Bruker Española S.A. is gratefully acknowledged. We thank to the Servei de Ressonància Magnètica Nuclear, Universitat Autònoma de Barcelona, for allocating instrument time to this project. The authors also thank Prof. K. Zangger for providing experimental details and the pulse program code for the original instant experiment.

Keywords: multiple-frequency pulses · multi-slice selection · NMR spectroscopy · pure-shift NMR · spatial encoding

[1] N. M. Loening, M. J. Thrippleton, J. Keeler, R. G. Griffin, *J. Magn. Reson.* **2003**, *164*, 321–328.
[2] N. Giraud, L. Béguin, J. Courtieu, D. Merlet, *Angew. Chem.* **2010**, *122*, 3559–3562; *Angew. Chem. Int. Ed.* **2010**, *49*, 3481–3484.
[3] K. Zangger, H. Sterk, *J. Magn. Reson.* **1997**, *124*, 486–489.
[4] N. Giraud, M. Joos, J. Courtieu, D. Merlet, *Magn. Reson. Chem.* **2009**, *47*, 300–306.
[5] N. H. Meyer, K. Zangger, *Angew. Chem.* **2013**, *125*, 7283–7286; *Angew. Chem. Int. Ed.* **2013**, *52*, 7143–7146.
[6] a) B. Antalek, *Concepts Magn. Reson.* **2002**, *14*, 225–258; b) K. D. Park, Y. J. Lee, *Magn. Reson. Chem.* **2006**, *44*, 887–891.
[7] S. Glanzer, E. Schrank, K. Zangger, *J. Magn. Reson.* **2013**, *232*, 1–6.
[8] M. Vega-Vázquez, J. C. Cobas, M. Martin-Pastor, *Magn. Reson. Chem.* **2010**, *48*, 749–752.
[9] P. Sakhaii, B. Haase, W. Bermel, R. Kerssebaum, G. E. Wagner, K. Zangger, *J. Magn. Reson.* **2013**, *233*, 92–95.
[10] G. E. Wagner, P. Sakhaii, W. Bermel, K. Zangger, *Chem. Commun.* **2013**, *49*, 3155–3157.
[11] S. L. Patt, *J. Magn. Reson.* **1992**, *96*, 94–102.
[12] M. Foroozandeh, P. Giraudeau, D. Jeannerat, *ChemPhysChem* **2011**, *12*, 2409–2411.
[13] a) G. A. Morris, J. A. Aguilar, R. Evans, S. Haiber, M. Nilsson, *J. Am. Chem. Soc.* **2010**, *132*, 12770–12772; b) J. J. Koivisto, *Chem. Commun.* **2013**, *49*, 96–98.
[14] J. A. Aguilar, A. A. Colbourne, J. Cassani, M. Nilsson, G. A. Morris, *Angew. Chem.* **2012**, *124*, 6566–6569; *Angew. Chem. Int. Ed.* **2012**, *51*, 6460–6463.
[15] a) M. Nilsson, G. A. Morris, *Chem. Commun.* **2007**, 933–935; b) J. A. Aguilar, S. Faulkner, M. Nilsson, G. A. Morris, *Angew. Chem.* **2010**, *122*, 3993–3995; *Angew. Chem. Int. Ed.* **2010**, *49*, 3901–3903.

Received: August 20, 2013
Published online: October 7, 2013

CHEMISTRY
A EUROPEAN JOURNAL

Supporting Information

Simultaneous Multi-Slice Excitation in Spatially Encoded NMR Experiments

Laura Castañar, Pau Nolis, Albert Virgili, and Teodor Parella*[a]

chem_201303272_sm_miscellaneous_information.pdf

Contents

Experimental Section

All the NMR experiments were carried out on a 14.1T (600MHz) Bruker AVANCE III spectrometer equipped with a 5mm TXI probe and with a z field gradient unit of maximum strength of 53.5 G cm^{-1}. The probe temperature was set to 298 K. The four samples used in this work were 99.96% D_2O, 0.1M ibuprofen (in $CDCl_3$), 0.1M strychnine (in $CDCl_3$) and 25mM cyclosporine (in Benzene-d6).

1D image experiments (Figures 2C-2H)

Imaging profiles of the 99.96% D_2O sample in Fig. 2C-H were obtained with the pulse sequence of Fig. 2A. All the experiments were recorded using a single scan (without dummy scans), and the inter-pulse Δ delay and the acquisition time (3K data points) were both set to 10 ms. Square-shape gradients of 5.35 G cm^{-1} were used and applied during 10 ms (G2) and 15 ms (G3). In Fig. 2C, the selective 180º pulse and the encoding gradient (G_S) were not applied. In Fig. 2D-2H, a 20 ms Gaussian-shaped 180º pulse (bandwidth of 60.74 Hz) was applied simultaneous with a square-shaped encoding gradient (G_S) of 0.865 G/cm. The number to offsets used in each experiment and its values are: D) 1 offset (5 ppm); E) 2 offsets (7 and 3 ppm); F) 4 offsets (8, 6, 4 and 2 ppm); G) 8 offsets (1.5, 2.5, 3.5, 4.5, 5.5, 6.5, 7.5 and 8.5 ppm) and H) 16 offsets (1.25, 1.75, 2.25, 2.75, 3.25, 3.75, 4.25, 4.75, 5.25, 5.75, 6.25, 6.75, 7.25, 7.75, 8.25 and 8.75 ppm). Data were processed using a Gaussian window function (LB=-20 and GB=0.5) and zero filling to 32K prior to Fourier Transformation.

Conventional and se-SPFGE ^{1}H NMR experiments recorded on 99.96% D_2O sample (Figures 2I-2N)

Conventional ^{1}H NMR spectrum (Fig. 2I) was recorded using 1 scan (without dummy scans) and an acquisition time of about 3 s (32K data points). Fig. 2J-2N show several se-SPFGE spectra obtained with the pulse sequence of Fig. 2B using 1 scan (without dummy scans), an acquisition time of 2.73 s (32K data points), a gradient (G1) with a duration of 1 ms and a strength of 8.03 G cm^{-1} with a smoothed squared shape (SMSQ10.100 in BRUKER nomenclature), a 20 ms Gaussian-shaped 180º pulse (bandwidth of 60.74 Hz) and an square-shaped encoding gradient (G_S) of 0.865 G cm^{-1}. The number of offsets used in each experiment (and values in ppm) were set to: J) 1 offset (5 ppm); K) 2 offsets (7 and 3 ppm); L) 4 offsets (8, 6, 4 and 2 ppm); M) 8 offsets (1.5, 2.5, 3.5, 4.5, 5.5, 6.5, 7.5 and 8.5 ppm) and N) 16 offsets (1.25, 1.75, 2.25, 2.75, 3.25, 3.75, 4.25, 4.75, 5.25, 5.75, 6.25, 6.75, 7.25, 7.75, 8.25 and 8.75 ppm). Data were processed using a conventional Fourier Transformation.

se-SPFGE ^{1}H NMR experiments recorded on ibuprofen (Figure 3)

Conventional ^{1}H NMR spectrum of ibuprofen (Fig. 3A) was recorded using 1 scan (without dummy scans) and an acquisition time of 3 s (32K data point). The experimental signal-to-noise ratio in the ^{1}H NMR spectra was normalized to 100 for each individual signal. In order to take in account T2

relaxation signal lost, several ^{1}H-frequency-selective SPFGE spectra of ibuprofen (Fig. 3B) were acquired with the pulse sequence of Fig. 2B but without applying the encoding gradient in order to know signal losses associated to the T2 relaxation. All experiments were recorded using 1 scan (without dummy scans), an acquisition time of 3s, a 1ms shaped SMSQ10.100 gradient (G1) of 8.03 G cm^{-1} and a 20 ms Gaussian-shaped 180º pulse (bandwidth of 60.74 Hz). se-SPFGE spectra (Fig. 3C-E) were recorded using 1 scan (without dummy scans), an acquisition time of 3s, a 1ms shaped SMSQ10.100 gradient (G1) of 8.03 G cm^{-1} and a 20 ms Gaussian-shaped 180º pulse (bandwidth of 60.74 Hz). Experiment 3C was recorded using an amplification k factor of 1 (SW_G=3793 Hz), a square-share encoding gradient (G_S) of 0.495 G cm^{-1} and a single-frequency selective pulse (2454 Hz). Experiment 3D and 3E were recorded using a amplification k factor of 2 (SW_G=7586 Hz), a square-shaped encoding gradient of 0.99 G/cm and a selective pulse with 1 (2454 Hz) and 15 offsets, respectively, automatically calculated using the java script *calcoff* (4259, 4035, 3534, 3236, 3042, 2784, 2557, 2291, 2063, 1832, 1561, 1378, 1086, 901 and 638 Hz) respectively. Data were processed using a conventional Fourier Transformation.

Pure-shift 1D experiment (Figure 4)

Pure shift spectra of Fig. 4B and 4C were acquired with the original pseudo-2D ZS pulse sequence described in ref 15b.

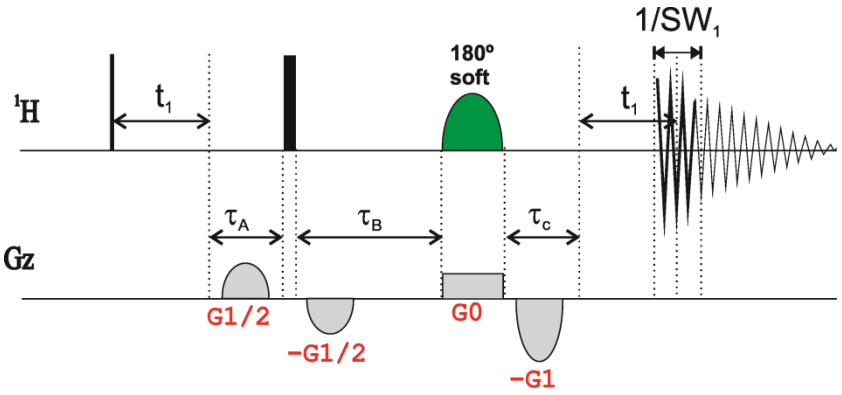

The pulse program named *push1dzs* obtained from Manchester NMR methodology group website (http://nmr.chemistry.manchester.ac.uk) was used for data acquisition. The experiments were recorded using an amplification k factor of 2 (SW_G=7586 Hz), a square-shaped encoding gradient of 0.99 G cm^{-1} and a 20 ms Gaussian-shaped 180º pulse (bandwidth of 60.74 Hz); 8 transients were collected for each one of the 32 t_1 increments of 0.68 s each were acquired with $1/SW_1$= 10 ms and a relaxation delay of 1 s, in total time of 8 min. Coherence transfer selection gradient pulses were smoothed squared shaped (SMSQ10.100) with a duration of 1 ms and amplitude G1= 13.4 G cm^{-1} (25%); the delays τ_a, τ_b and τ_c are automatically calculated so that $\tau_a + \tau_c = \tau_b$; $\tau_a = \tau_c$; $\tau_a = 1/4*SW_1$. The pulse offset (o1) and the

spectral width (SW_2) were set to 2454.5 Hz and 10.0 ppm, respectively. Spectrum of Fig. 4C used exactly the same set up as described in Fig 4B but using a 8 multi-frequency shaped pulse irradiating simultaneously at frequencies: 3534, 3236, 3042, 2784, 2557, 2291, 2063 and 1832 Hz (automatically calculated using the home made calcoff java script). The power level of the shaped pulse was decreased 18 dB compared to those of Fig. 4B. Data was processed automatically with the AU program named *pshift* provided at Manchester NMR methodology group website http://nmr.chemistry.manchester.ac.uk. This AU program converts the raw data to a new experiment that contains the pure shift FID, which is Fourier transformed with a 0.3 line broadening.

Automatic calculation of offsets: calcoff

A calculation script written in java language is available from the authors on request. Basically, the script searches a set of offsets that avoid accidental overlap of mutually coupled protons into the same z-slice. The program needs some input parameters: coil length, probe gradient strength, bandwidth and shape of the selective pulse, a frequency list from a .txt file, the amplification k factor and how many offsets wants to calculate. After some calculation iterations, the script returns a list of calculated offsets with a z-position matrix for all available frequencies. Some examples are provided at the end of this supplementary information.

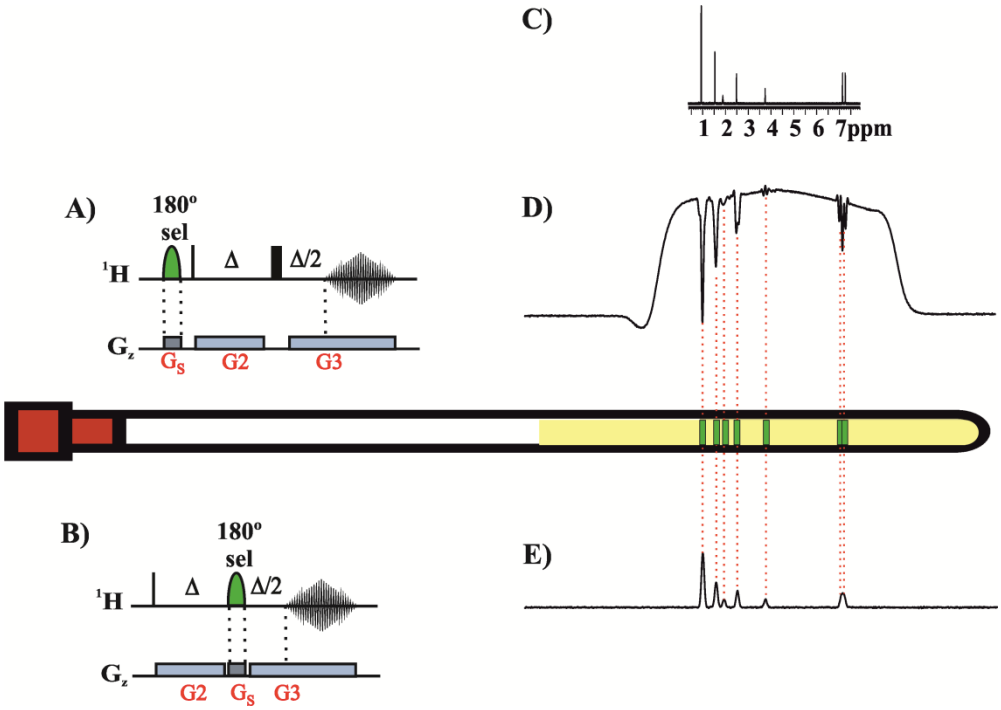

Figure S1: Schematic illustration of the single-offset slice selection. A,B) Pulse schemes used to obtain 1D z-profile images. C) Conventional ^{1}H NMR spectra of ibuprofen. D) 1D z-profile image experiment obtained with the pulse sequence A. E) 1D z-profile image experiment obtained with the pulse sequence B. A selective 20 ms Gaussian-shaped 180º pulse was applied simultaneous with a square-shaped encoding gradient (G_S) of 0.742 G cm^{-1} to obtain an image profile using a single offset (2454 Hz). All other experimental parameters as described in Fig. 2.

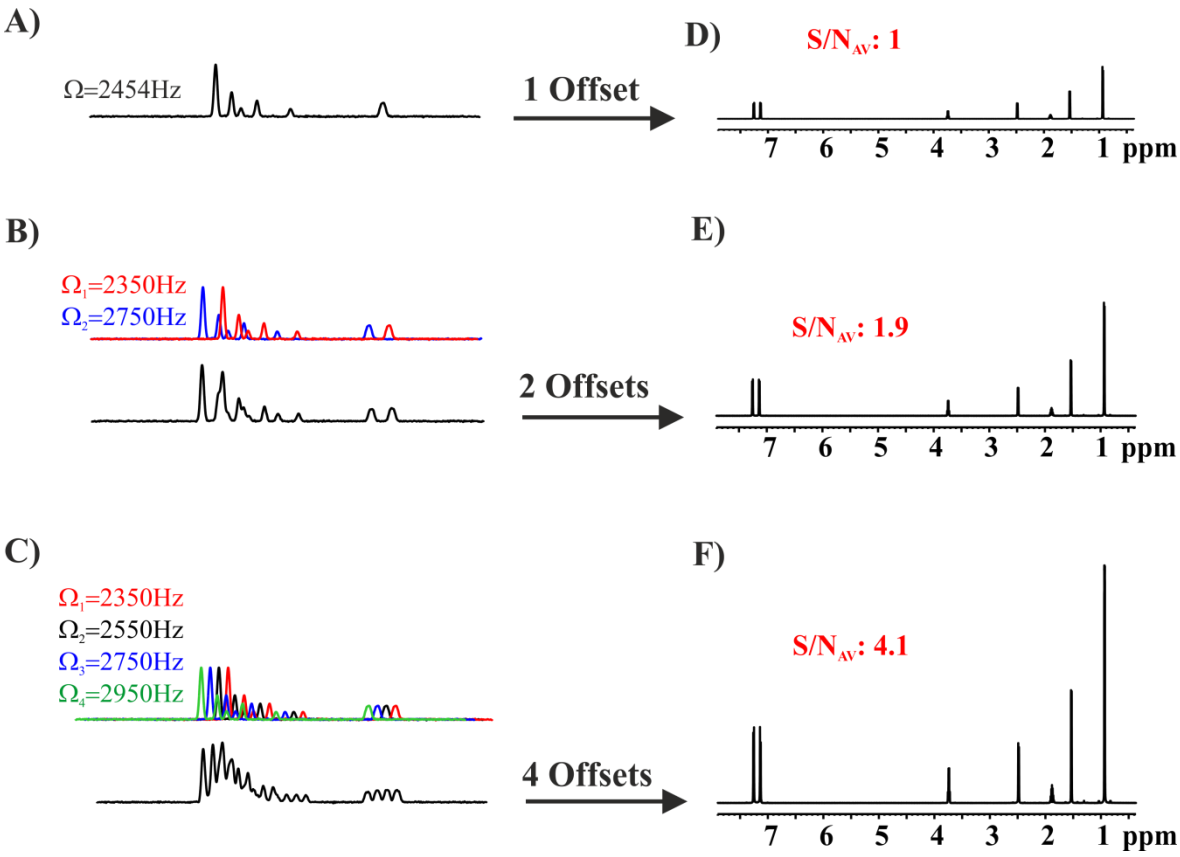

Figure S2: Schematic illustration of the multiple-offset slice selection. A-C) 1D z-profile image experiments of ibuprofen obtained with the pulse sequence of Fig. S1B. D-F) Slice selective SPFGE spectra obtained with the pulse sequence of Fig. 2B. In all experiments a 20 ms Gaussian-shaped 180º selective pulse was applied simultaneous with a square-shape encoding gradient (G_S) of 0.742 G cm^{-1}. A-C) The experiments were recorded using 1 scan (without dummy scans), Δ=10ms, an acquisition time of 10 ms, and a selective pulse with 1, 2 and 4 offsets respectively. Square-shaped gradients of 5.35G/cm were used and applied during 10ms (G2) and 15 ms (G3). D-F) All spectra were recorded using 1 scan (without dummy scans), an acquisition time of 3s, a 1ms shaped SMSQ10.100 gradient (G1) of 8.03 G cm^{-1} and a selective pulse with 1, 2 and 4 offsets respectively. In each spectrum, the averaged signal-to-noise ratio (S/N_{AV}) is reported for comparison.

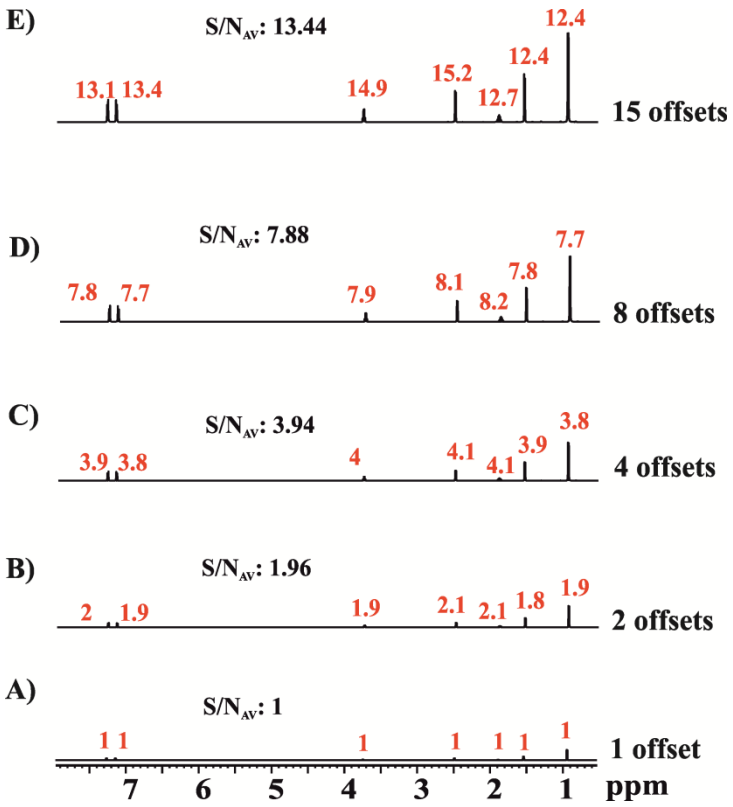

Figure S3: Multiple-frequency se-SPFGE spectra of ibuprofen. All experiments were recorded with the pulse sequence of Fig. 2B using 1 scan, an acquisition time of 3 s, a 1 ms SMSQ10.100 shape refocused gradient (G1) of 8.03 G cm^{-1}, an amplification k factor of 2 (SW_G=7586 Hz), a square-shaped encoding gradient of 0.99 G cm^{-1} and a 20 ms Gaussian-shaped 180^o pulse (bandwidth of 60.74 Hz). The number to offsets used in each experiment (and its values in Hz) are: A) 1 offset (2454 Hz); B) 2 offsets (2557 and 2291 Hz); C) 4 offsets (2784, 2557, 2291 and 2063 Hz); D) 8 offsets (3534, 3236, 3042, 2784, 2557, 2291, 2063, 1832 Hz) and E) 15 offsets (4259, 4035, 3534, 3236, 3042, 2784, 2557, 2291, 2063, 1832, 1561, 1378, 1086, 901 and 638 Hz ppm). In each spectrum, the averaged signal-to-noise ratio (S/N_{AV}) is reported for comparison.

Constant Parameters	Gyromagnetic Ratio of ^{1}H (γ_{1H})	4257,8 Hz/G
Probe parameters	Length of the active volume coil (L)	1.8 cm
	Maximum gradient strength (G_z)	53,5 G/cm
180º selective pulse parameter	Shape	Gaussian
	Duration (p12)	20 ms
	Bandwidth half height ($\Delta\omega_{1/2}$)	60,74 Hz
	Bandwidth in the base ($\Delta\omega$)	183 Hz
Parameters calculated	Spectral width (SW_G)	3793Hz
	Amplification factor (k)	2
	Spectral width and amplification factor (SW_G*k)	7586 Hz
	Center of the spectrum (o1)	2454 Hz
	Spatial-encoding gradient (G_S)	0,99 G/cm
	Offset limits	558-4351 Hz

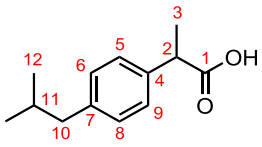

	Signal position [cm]						
Offsets[Hz]	**z (H_{12})**	**z (H_3)**	**z (H_{11})**	**z (H_{10})**	**z (H_2)**	**z (H_6)**	**z (H_5)**
638	0,019	-0,066	-0,116	-0,201	-0,380	-0,864	-0,881
901	0,081	-0,004	-0,053	-0,139	-0,318	-0,801	-0,819
1086	0,125	0,040	-0,009	-0,095	-0,274	-0,757	-0,775
1378	0,195	0,109	0,060	-0,026	-0,205	-0,688	-0,705
1561	0,238	0,153	0,103	0,018	-0,161	-0,645	-0,662
1832	0,302	0,217	0,168	0,082	-0,097	-0,580	-0,598
2063	0,357	0,272	0,222	0,137	-0,042	-0,526	-0,543
2291	0,411	0,326	0,276	0,191	0,012	-0,471	-0,489
2557	0,474	0,389	0,340	0,254	0,075	-0,408	-0,426
2784	0,528	0,443	0,393	0,308	0,129	-0,354	-0,372
3042	0,589	0,504	0,455	0,369	0,190	-0,293	-0,311
3236	0,635	0,550	0,501	0,415	0,236	-0,247	-0,265
3534	0,706	0,621	0,571	0,486	0,307	-0,177	-0,194
4035	0,825	0,740	0,690	0,605	0,426	-0,058	-0,075
4259	0,878	0,793	0,743	0,658	0,479	-0,005	-0,022

Figure S4: Calculated z-positions of all signals in ibuprofen as a function of spatial encoded NMR parameters.

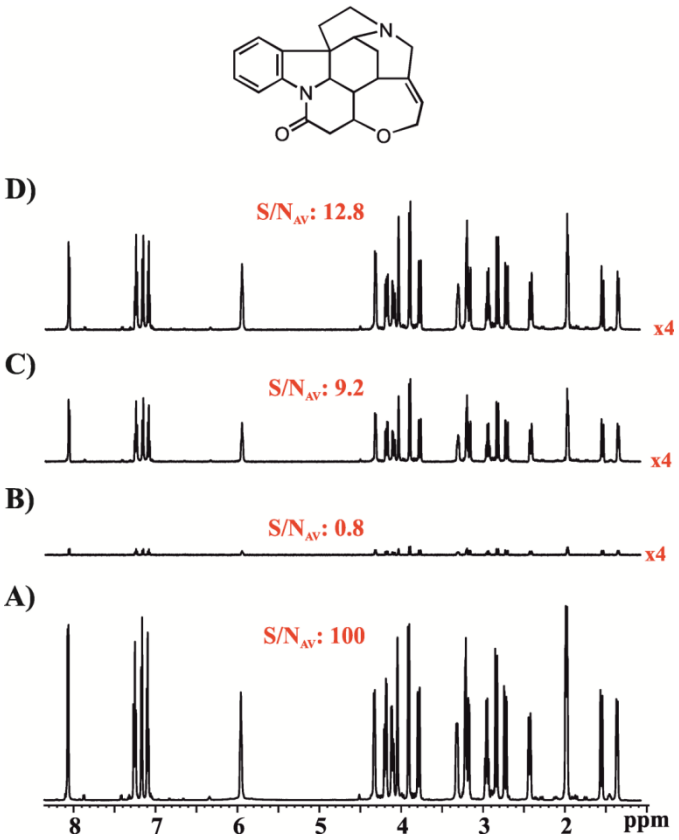

Figure S5: A) ^{1}H NMR spectrum of strychnine in $CDCl_3$; B) Single-slice se-SPFGE spectrum after using a selective gaussian-shaped pulse of 30ms and an encoding gradient strength of G_s=1.068 G/cm; C) Multiple-slice se-SPFGE experiment acquired as B) but using a 11-site multiple-frequency pulse and using the restricted condition that only offsets that contain all signals into the volume coil are used; D) The same as C) but using a 16-site multiple-frequency pulse that include offsets that include some protons out of the limits of the coil. The averaged signal-to-noise ratio percentage (S/N_{av}) is shown in each spectrum. As a reference, the S/N_{av} values of individual SPFGE experiments (Gs=0) is about 81% of the levels achieved in the conventional ^{1}H spectrum (data not shown). Spectra B-D were collected with the pulse sequence of Fig. 2B using 1 scan (without dummy scans), an acquisition time of 3 s, a 1 ms SMSQ10.100 gradient (G1) of 8.03 G cm^{-1}, an amplification k factor of 2 (SW_G=8188 Hz), a square-shaped encoding gradient (G_S) of 1.068 G cm^{-1} and a 30 ms Gaussian-shaped 180º pulse (bandwidth of 40.49 Hz). B and C was recorded using a selective pulse with 1 (2801 Hz) and 11 offsets (4760, 4360, 3960, 3560, 3160, 2760, 2360, 1960, 1560, 1160 and 760 Hz) respectively. In the later experiment, the offsets used were restricted so that all the signals were excited inside the active coil region. In the spectrum D, an additional signal enhancement was obtained using a selective pulse with 16 offsets (5960, 5560, 5160, 4760, 4360, 3960, 3560, 3160, 2760, 2360, 1960, 1560, 1160, 760, 360 and -160 Hz) where a non-uniform excitation was obtained because for higher and lower offsets a small portion of the signals from the edges of the spectrum appear beyond of the limits of the active coil (as can be seen in the z-position matrix). Data were processed using a conventional Fourier Transformation.

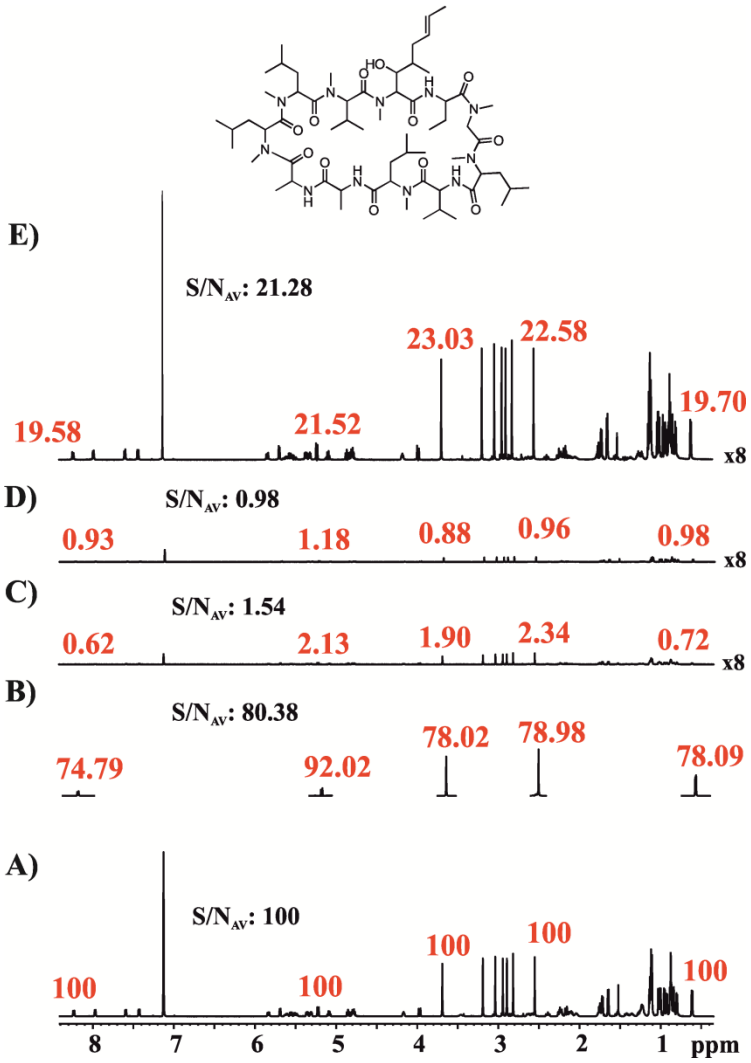

Figure S6: Multiple-frequency se-SPFGE spectra of cyclosporine. It was recorded using 1 scan (without dummy scans) and an acquisition time of 3s**.** The experimental signal-to-noise ratio in the ^{1}H NMR spectrum (A) was normalized to 100 for each individual signal. B) Signal arising of conventional SPFGE (G_s=0) to take into account for T_2 relaxation signal lost during the selective echo. C,D) single-slice se-SPFGE spectra using normalized scaling k factor of 1 and 2 respectively; E) Multi-frequency se-SPFGE were collected with the pulse sequence of Fig. 2B using 1 scan (without dummy scans), an acquisition time of 3s, a 1 ms SMSQ10.100 shape refocused gradient (G1) of 8.03 Gcm^{-1}, an amplification k factor of 2 (SW_G=9168 Hz), a square-shaped encoding gradient (G_S) of 1.196 G cm^{-1} and a 20 ms Gaussian-shaped 180º pulse with 22 offsets (4861, 4661, 4441, 4241, 4041, 3841, 3621, 3421, 3221, 3021, 2801, 2601, 2401, 2201, 1981, 1781, 1581, 1381, 1161, 961, 761 and 551Hz). In each spectrum, the averaged signal-to-noise ratio (S/N_{AV}) is reported for comparison.

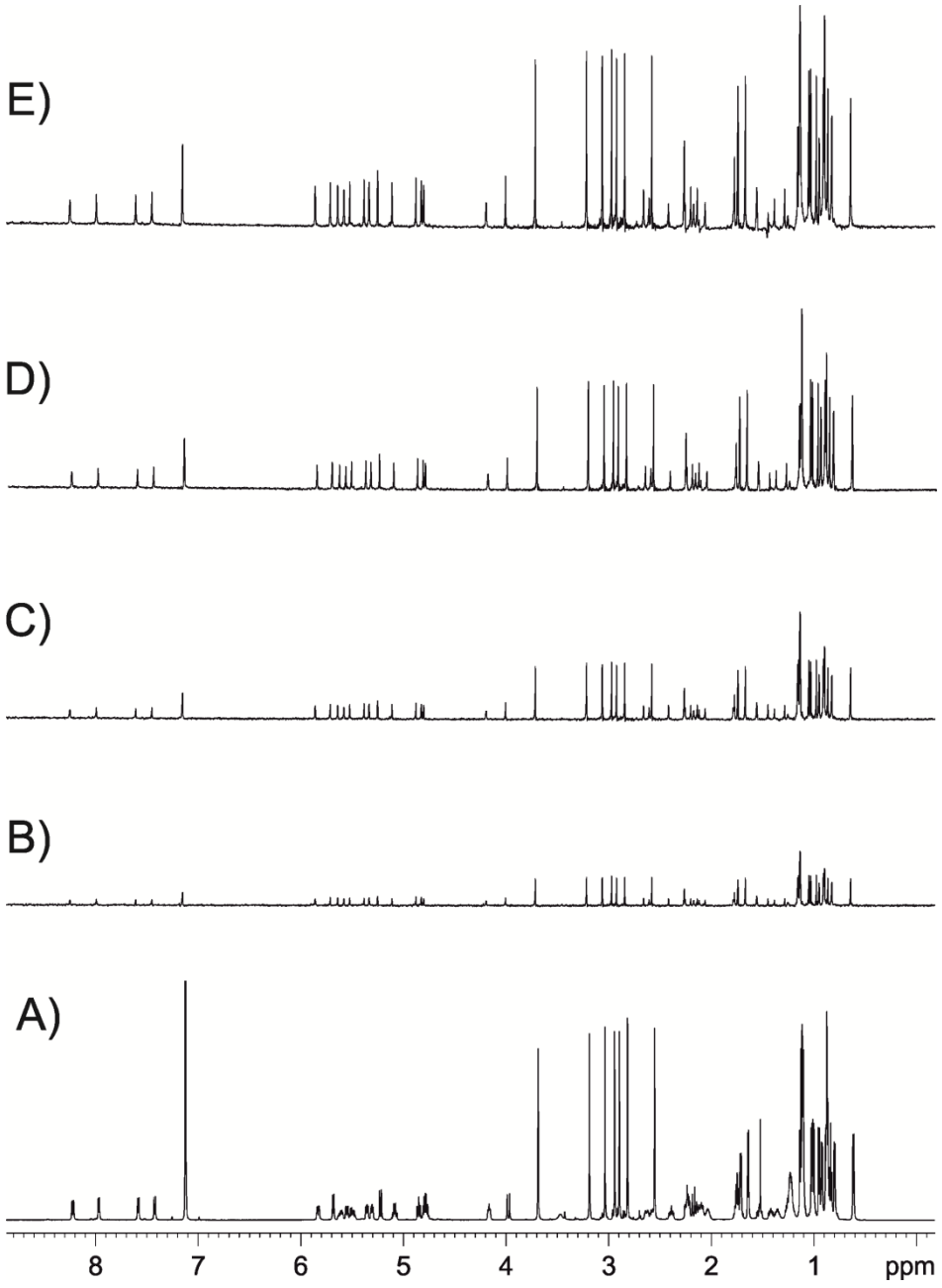

Figure S7: A) ^{1}H NMR spectrum of 25 mM cyclosporine in d-benzene (600 MHz). B) Single-slice (offset set to 2507 Hz) and C-E) multi-slice broadband homonuclear ZS spectra recorded with 2, 4 and 8 offsets, respectively, using the pseudo-2D pulse sequence described previously in the experimental section.[15b] The 8 offsets used in spectrum E were set to 3200, 3000, 2800, 2600, 2400, 2200, 2000 and 1800 Hz, and the average sensitivity gain with respect to spectrum B is 6.7. All other experimental details as described in Fig. 4 which shows an expanded area covering signals resonating between 4.5 and 6ppm.

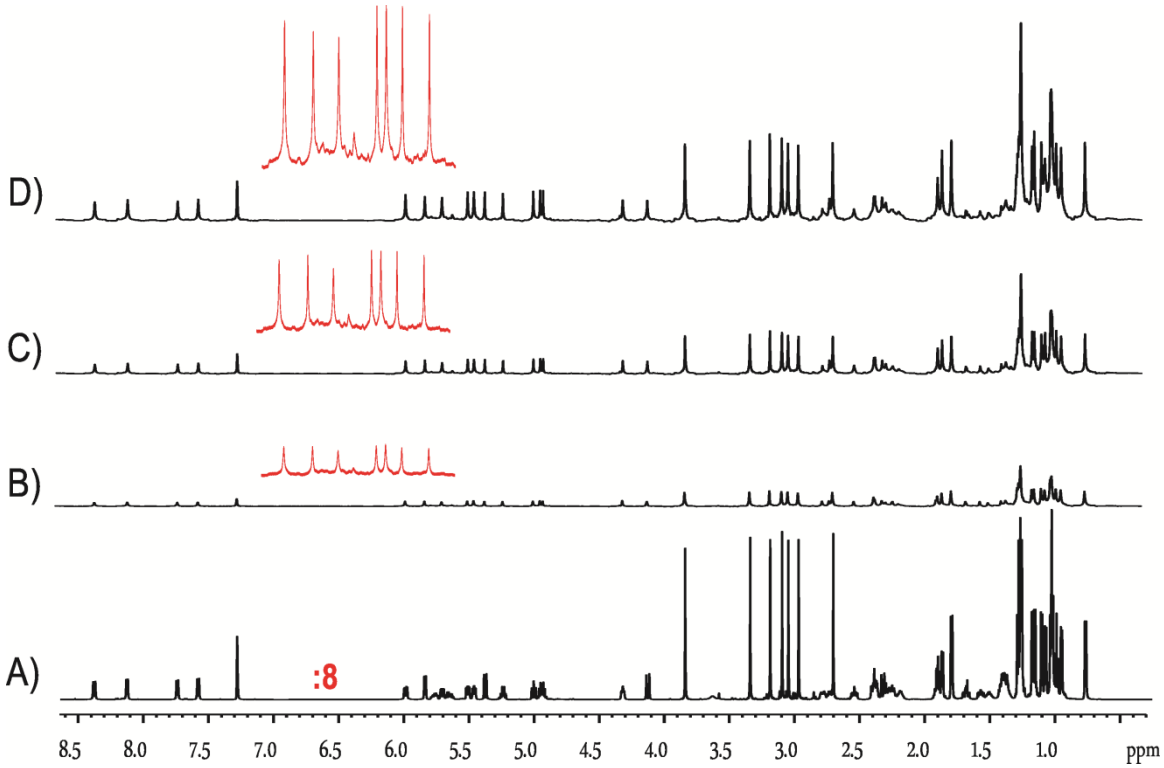

Figure S8: Effect of the use of multiple-frequency pulses into the Instant broadband-homodecoupled ^{1}H NMR spectra of a sample 25mM cyclosporine in benzene-d6 acquired with the sequence reported in ref. 5. 8 scans were collected for each 1D dataset using a 10 ms Gaussian shaped selective 180 ^{1}H pulse and an encoding gradient of 1.06 G cm^{-1}. 30 loops were used, with a recycle delay of 1 second. This selective pulse was frequency modulated with B) single (2700Hz), C) two (2800 and 2400Hz) and D) four (3200, 2800, 2400 and 2000Hz) different offsets. The experimental sensitivity gains are proportional to the number of applied offsets.

Short description of Java script for multi offset calculation

The script asks some parameters about user and also about frequencies and couplings of a given molecule or spin system. The user may introduce a shaped-pulse band width, a security amplification k factor (read the article for more information) and how many offsets want to search for. Then the script searches for a solution. If any solution is found after 50000 iterations then it decrease the number of offsets by one, and start the calculation again.

Experimental considerations:

The script asks you which protons are coupled. If you don't know you can perform the calculation just by inserting the restriction that frequencies don't match each other (like if everything was coupled), but this is a very restrictive way of working that usually give you few offsets compared to what you can really use. Our experience says us that it is better to work the other way around. So, start like if the system is not coupled, and if some distortions in a pair of signal are seen in the spectrum, just introduce that coupled pair in the calculation as a restriction.

To execute the java script download the given multi_offset.jar file and save it in C:\ directory (or whatever), then open the Windows command Prompt and once being situated in the C:\

Type: C:\java –jar multi_offset.jar

And the java script will launch.

Examples

In order to show how the java script works we present 4 examples concerning ibuprofen sample in different situations.
In the first example, we don't consider any coupling and we observe 16 offsets are found in just a single iteration.
In example the restriction of the strong aromatic coupling2 is introduced. The script takes longer time to find the solution of 16 offsets. In that case 642 iterations were needed.
In a third example, we introduce the whole coupling network. It is seen that there is no possible solution that avoids completely any random overlapping using 16 offsets, and the solution given is 10 offsets after 45185 iterations.
Then a fourth example analogous to third but reducing pulse band width half shows that 14 offset can be used. Notice, that one have to take into account that the slice thickness now is reduced half and is important to realize that third example setup will give higher SNR although less offsets are found.

Java script multi offset calculation example 1:

Sample: ibuprofen
Coupling spin system taken into account: NO
Band Width = 60 Hz
Security facotr K = 2
16 offsets as insert (16 obtained)

SCREEN CAPTURES OF THE INPUT FILE

```
//USER INSERT PARAMETERS//
-------------------------

Insert coil length in cm?: 1.8
Insert gradient strength in G/cm?: 53.5
Insert pulse band width in Hz?: 60
How many peaks to introduce?: 7
Insert peaks in ascending order:
Insert peak in Hz: 542
Insert peak in Hz: 903
Insert peak in Hz: 1110
Insert peak in Hz: 1471
Insert peak in Hz: 2228
Insert peak in Hz: 4264
Insert peak in Hz: 4336
Does frequence 542 couple to 903 (y/n): n
Does frequence 542 couple to 1110 (y/n): n
Does frequence 542 couple to 1471 (y/n): n
Does frequence 542 couple to 2228 (y/n): n
Does frequence 542 couple to 4264 (y/n): n
Does frequence 542 couple to 4336 (y/n): n
Does frequence 903 couple to 1110 (y/n): n
Does frequence 903 couple to 1471 (y/n): n
Does frequence 903 couple to 2228 (y/n): n
Does frequence 903 couple to 4264 (y/n): n
Does frequence 903 couple to 4336 (y/n): n
Does frequence 1110 couple to 1471 (y/n): n
Does frequence 1110 couple to 2228 (y/n): n
Does frequence 1110 couple to 4264 (y/n): n
Does frequence 1110 couple to 4336 (y/n): n
Does frequence 1471 couple to 2228 (y/n): n
Does frequence 1471 couple to 4264 (y/n): n
Does frequence 1471 couple to 4336 (y/n): n
Does frequence 2228 couple to 4264 (y/n): n
Does frequence 2228 couple to 4336 (y/n): n
Does frequence 4264 couple to 4336 (y/n): n
Insert k factor for not being out of tube pulsing: 2
How many offset do you want to generate? 16
```

SCREEN CAPTURES OF THE OUPUT RESULT

```
//CHECK IF YOUR INSERT VALUES ARE CORRECT//

Coupling matrix is:
-------------------

         542 Hz  903 Hz  1110 Hz 1471 Hz 2228 Hz 4264 Hz 4336 Hz
542 Hz |    1       0       0       0       0       0       0|
903 Hz |    0       1       0       0       0       0       0|
1110 Hz |    0       0       1       0       0       0       0|
1471 Hz |    0       0       0       1       0       0       0|
2228 Hz |    0       0       0       0       1       0       0|
4264 Hz |    0       0       0       0       0       1       0|
4336 Hz |    0       0       0       0       0       0       1|

0 = not coupled protons
1 = coupled protons and diagonal

Spectral width is (higher freq - lower freq) = 3794.0 Hz
Spectral width with security factor (2) is: 7588.0 Hz
Pulse Bandwith was set to 60
Coil length was set to 1.8 cm
Probe gradient strength was set to 53.5 G/cm

//CALCULATION RETURN//
----------------------
Solution found after 1 iterations
```

```
Offset set to be used for multifrequence shaped pulse is: 16
855 Hz
1003 Hz
1418 Hz
1802 Hz
1889 Hz
2052 Hz
2192 Hz
2573 Hz
2699 Hz
3113 Hz
3428 Hz
3664 Hz
3824 Hz
4028 Hz
4117 Hz
4266 Hz

Set G0 to 1,85%
```

```
Z-position matrix (cm)
----------------------

        542 Hz  903 Hz  1110 Hz 1471 Hz 2228 Hz 4264 Hz 4336 Hz
855 Hz |0,074   -0,011  -0,060  -0,146  -0,326  -0,809  -0,826|
1003 Hz |0,109  0,024   -0,025  -0,111  -0,291  -0,774  -0,791|
1418 Hz |0,208  0,122   0,073   -0,013  -0,192  -0,675  -0,692|
1802 Hz |0,299  0,213   0,164   0,079   -0,101  -0,584  -0,601|
1889 Hz |0,320  0,234   0,185   0,099   -0,080  -0,563  -0,580|
2052 Hz |0,358  0,273   0,223   0,138   -0,042  -0,525  -0,542|
2192 Hz |0,391  0,306   0,257   0,171   -0,009  -0,492  -0,509|
2573 Hz |0,482  0,396   0,347   0,261   0,082   -0,401  -0,418|
2699 Hz |0,512  0,426   0,377   0,291   0,112   -0,371  -0,388|
3113 Hz |0,610  0,524   0,475   0,390   0,210   -0,273  -0,290|
3428 Hz |0,685  0,599   0,550   0,464   0,285   -0,198  -0,215|
3664 Hz |0,741  0,655   0,606   0,520   0,341   -0,142  -0,159|
3824 Hz |0,779  0,693   0,644   0,558   0,379   -0,104  -0,121|
4028 Hz |0,827  0,741   0,692   0,607   0,427   -0,056  -0,073|
4117 Hz |0,848  0,762   0,713   0,628   0,448   -0,035  -0,052|
4266 Hz |0,883  0,798   0,749   0,663   0,483   0,000   -0,017|

rows = generated offset frequencies for shaped pulse
columns = input frequencies from user
-------------------------------------------------
NMR tube is divided into 126 slices
Slice thickness is: 0,014 cm
Experimental sensitivity respect to 1H spectrum should be around 12,7
which is given by the ratio: number_of_offsets/number_of_slices
```

Java script multi offset calculation example 2:

Sample: ibuprofen
Coupling spin system taken into account: Only aromatic strong coupling
Band Width = 60 Hz
Security facotr K = 2
16 offsets as insert (16 obtained)

SCREEN CAPTURES OF THE INPUT FILE

```
//USER INSERT PARAMETERS//
-------------------------

Insert coil length in cm?: 1.8
Insert gradient strength in G/cm?: 53.5
Insert pulse band width in Hz?: 60
How many peaks to introduce?: 7
Insert peaks in ascending order:
Insert peak in Hz: 542
Insert peak in Hz: 903
Insert peak in Hz: 1110
Insert peak in Hz: 1471
Insert peak in Hz: 2228
Insert peak in Hz: 4264
Insert peak in Hz: 4336
Does frequence 542 couple to 903 (y/n): n
Does frequence 542 couple to 1110 (y/n): n
Does frequence 542 couple to 1471 (y/n): n
Does frequence 542 couple to 2228 (y/n): n
Does frequence 542 couple to 4264 (y/n): n
Does frequence 542 couple to 4336 (y/n): n
Does frequence 903 couple to 1110 (y/n): n
Does frequence 903 couple to 1471 (y/n): n
Does frequence 903 couple to 2228 (y/n): n
Does frequence 903 couple to 4264 (y/n): n
Does frequence 903 couple to 4336 (y/n): n
Does frequence 1110 couple to 1471 (y/n): n
Does frequence 1110 couple to 2228 (y/n): n
Does frequence 1110 couple to 4264 (y/n): n
Does frequence 1110 couple to 4336 (y/n): n
Does frequence 1471 couple to 2228 (y/n): n
Does frequence 1471 couple to 4264 (y/n): n
Does frequence 1471 couple to 4336 (y/n): n
Does frequence 2228 couple to 4264 (y/n): n
Does frequence 2228 couple to 4336 (y/n): n
Does frequence 4264 couple to 4336 (y/n): y
Insert k factor for not being out of tube pulsing: 2
How many offset do you want to generate? 16
```

SCREEN CAPTURES OF THE OUPUT RESULT

```
//CHECK IF YOUR INSERT VALUES ARE CORRECT//

Coupling matrix is:
--------------------

        542 Hz  903 Hz  1110 Hz 1471 Hz 2228 Hz 4264 Hz 4336 Hz
542 Hz |   1       0       0       0       0       0       0|
903 Hz |   0       1       0       0       0       0       0|
1110 Hz |   0      0       1       0       0       0       0|
1471 Hz |   0      0       0       1       0       0       0|
2228 Hz |   0      0       0       0       1       0       0|
4264 Hz |   0      0       0       0       0       1       1|
4336 Hz |   0      0       0       0       0       1       1|

0 = not coupled protons
1 = coupled protons and diagonal

Spectral width is (higher freq - lower freq) = 3794.0 Hz
Spectral width with security factor (2) is: 7588.0 Hz
Pulse Bandwith was set to 60
Coil length was set to 1.8 cm
Probe gradient strength was set to 53.5 G/cm

//CALCULATION RETURN//
----------------------
Solution found after 643 iterations
```

```
Offset set to be used for multifrequence shaped pulse is: 16
602 Hz
929 Hz
1123 Hz
1329 Hz
1465 Hz
1639 Hz
1917 Hz
2141 Hz
2848 Hz
3012 Hz
3371 Hz
3528 Hz
3677 Hz
3895 Hz
4114 Hz
4299 Hz

Set G0 to 1,85%
```

```
Z-position matrix (cm)
----------------------

        542 Hz  903 Hz  1110 Hz 1471 Hz 2228 Hz 4264 Hz 4336 Hz
602 Hz |0,014   -0,071  -0,121  -0,206  -0,386  -0,869  -0,886|
929 Hz |0,092   0,006   -0,043  -0,129  -0,308  -0,791  -0,808|
1123 Hz |0,138  0,052   0,003   -0,083  -0,262  -0,745  -0,762|
1329 Hz |0,187  0,101   0,052   -0,034  -0,213  -0,696  -0,713|
1465 Hz |0,219  0,133   0,084   -0,001  -0,181  -0,664  -0,681|
1639 Hz |0,260  0,175   0,125   0,040   -0,140  -0,623  -0,640|
1917 Hz |0,326  0,241   0,191   0,106   -0,074  -0,557  -0,574|
2141 Hz |0,379  0,294   0,245   0,159   -0,021  -0,504  -0,521|
2848 Hz |0,547  0,461   0,412   0,327   0,147   -0,336  -0,353|
3012 Hz |0,586  0,500   0,451   0,366   0,186   -0,297  -0,314|
3371 Hz |0,671  0,585   0,536   0,451   0,271   -0,212  -0,229|
3528 Hz |0,708  0,623   0,574   0,488   0,308   -0,175  -0,192|
3677 Hz |0,744  0,658   0,609   0,523   0,344   -0,139  -0,156|
3895 Hz |0,795  0,710   0,661   0,575   0,395   -0,088  -0,105|
4114 Hz |0,847  0,762   0,713   0,627   0,447   -0,036  -0,053|
4299 Hz |0,891  0,806   0,756   0,671   0,491   0,008   -0,009|

rows = generated offset frequencies for shaped pulse
columns = input frequencies from user
-------------------------------------------------
NMR tube is divided into 126 slices
Slice thickness is: 0,014 cm
Experimental sensitivity respect to 1H spectrum should be around 12,7
which is given by the ratio: number_of_offsets/number_of_slices
```

Java script multi offset calculation example 3:

Sample: ibuprofen
Coupling spin system taken into account: all
Band Width = 60 Hz
Security facotr K = 2
16 offsets as insert (10 obtained)

SCREEN CAPTURES OF THE INPUT FILE

```
//USER INSERT PARAMETERS//
--------------------------

Insert coil length in cm?: 1.8
Insert gradient strength in G/cm?: 53.5
Insert pulse band width in Hz?: 60
How many peaks to introduce?: 7
Insert peaks in ascending order:
Insert peak in Hz: 542
Insert peak in Hz: 903
Insert peak in Hz: 1110
Insert peak in Hz: 1471
Insert peak in Hz: 2228
Insert peak in Hz: 4264
Insert peak in Hz: 4336
Does frequence 542 couple to 903 (y/n): n
Does frequence 542 couple to 1110 (y/n): y
Does frequence 542 couple to 1471 (y/n): n
Does frequence 542 couple to 2228 (y/n): n
Does frequence 542 couple to 4264 (y/n): n
Does frequence 542 couple to 4336 (y/n): n
Does frequence 903 couple to 1110 (y/n): n
Does frequence 903 couple to 1471 (y/n): n
Does frequence 903 couple to 2228 (y/n): y
Does frequence 903 couple to 4264 (y/n): n
Does frequence 903 couple to 4336 (y/n): n
Does frequence 1110 couple to 1471 (y/n): y
Does frequence 1110 couple to 2228 (y/n): n
Does frequence 1110 couple to 4264 (y/n): n
Does frequence 1110 couple to 4336 (y/n): n
Does frequence 1471 couple to 2228 (y/n): n
Does frequence 1471 couple to 4264 (y/n): n
Does frequence 1471 couple to 4336 (y/n): n
Does frequence 2228 couple to 4264 (y/n): n
Does frequence 2228 couple to 4336 (y/n): n
Does frequence 4264 couple to 4336 (y/n): y
Insert k factor for not being out of tube pulsing: 2
How many offset do you want to generate? 16
```

SCREEN CAPTURES OF THE OUPUT RESULT

```
//CHECK IF YOUR INSERT VALUES ARE CORRECT//

Coupling matrix is:
-------------------

         542 Hz  903 Hz  1110 Hz 1471 Hz 2228 Hz 4264 Hz 4336 Hz
542 Hz |   1       0       1       0       0       0       0|
903 Hz |   0       1       0       0       1       0       0|
1110 Hz |   1      0       1       1       0       0       0|
1471 Hz |   0      0       1       1       0       0       0|
2228 Hz |   0      1       0       0       1       0       0|
4264 Hz |   0      0       0       0       0       1       1|
4336 Hz |   0      0       0       0       0       1       1|

0 = not coupled protons
1 = coupled protons and diagonal

Spectral width is (higher freq - lower freq) = 3794.0 Hz
Spectral width with security factor (2) is: 7588.0 Hz
Pulse Bandwith was set to 60
Coil length was set to 1.8 cm
Probe gradient strength was set to 53.5 G/cm

//CALCULATION RETURN//
----------------------
Solution found after 45185 iterations


Offset set to be used for multifrequence shaped pulse is: 10
975 Hz
1172 Hz
1458 Hz
1458 Hz
1959 Hz
2153 Hz
2419 Hz
2616 Hz
2894 Hz
3843 Hz

Set G0 to 1,85%
```

```
Z-position matrix (cm)
----------------------

        542 Hz  903 Hz  1110 Hz 1471 Hz 2228 Hz 4264 Hz 4336 Hz
975 Hz |0,103   0,017   -0,032  -0,118  -0,297  -0,780  -0,797|
1172 Hz |0,149  0,064   0,015   -0,071  -0,251  -0,733  -0,751|
1458 Hz |0,217  0,132   0,083   -0,003  -0,183  -0,666  -0,683|
1959 Hz |0,336  0,251   0,201   0,116   -0,064  -0,547  -0,564|
2153 Hz |0,382  0,297   0,247   0,162   -0,018  -0,501  -0,518|
2419 Hz |0,445  0,360   0,311   0,225   0,045   -0,438  -0,455|
2616 Hz |0,492  0,406   0,357   0,272   0,092   -0,391  -0,408|
2894 Hz |0,558  0,472   0,423   0,338   0,158   -0,325  -0,342|
3843 Hz |0,783  0,697   0,648   0,563   0,383   -0,100  -0,117|
4322 Hz |0,897  0,811   0,762   0,676   0,497   0,014   -0,003|

rows = generated offset frequencies for shaped pulse
columns = input frequencies from user
-------------------------------------------------
NMR tube is divided into 126 slices
Slice thickness is: 0,014 cm
Experimental sensitivity respect to 1H spectrum should be around 7,9
which is given by the ratio: number_of_offsets/number_of_slices
```

Java script multi offset calculation example 4:

Sample: ibuprofen
Coupling spin system taken into account: all
Band Width = 30 Hz
Security facotr K = 2
16 offsets as insert (14 obtained)

SCREEN CAPTURES OF THE INPUT FILE

```
//USER INSERT PARAMETERS//
--------------------------

Insert coil length in cm?: 1.8
Insert gradient strength in G/cm?: 53.5
Insert pulse band width in Hz?: 30
How many peaks to introduce?: 7
Insert peaks in ascending order:
Insert peak in Hz: 542
Insert peak in Hz: 903
Insert peak in Hz: 1110
Insert peak in Hz: 1471
Insert peak in Hz: 2228
Insert peak in Hz: 4264
Insert peak in Hz: 4336
Does frequence 542 couple to 903 (y/n): n
Does frequence 542 couple to 1110 (y/n): y
Does frequence 542 couple to 1471 (y/n): n
Does frequence 542 couple to 2228 (y/n): n
Does frequence 542 couple to 4264 (y/n): n
Does frequence 542 couple to 4336 (y/n): n
Does frequence 903 couple to 1110 (y/n): n
Does frequence 903 couple to 1471 (y/n): n
Does frequence 903 couple to 2228 (y/n): y
Does frequence 903 couple to 4264 (y/n): n
Does frequence 903 couple to 4336 (y/n): n
Does frequence 1110 couple to 1471 (y/n): y
Does frequence 1110 couple to 2228 (y/n): n
Does frequence 1110 couple to 4264 (y/n): n
Does frequence 1110 couple to 4336 (y/n): n
Does frequence 1471 couple to 2228 (y/n): n
Does frequence 1471 couple to 4264 (y/n): n
Does frequence 1471 couple to 4336 (y/n): n
Does frequence 2228 couple to 4264 (y/n): n
Does frequence 2228 couple to 4336 (y/n): n
Does frequence 4264 couple to 4336 (y/n): y
Insert k factor for not being out of tube pulsing: 2
How many offset do you want to generate? 16
```

SCREEN CAPTURES OF THE OUPUT RESULT

```
//CHECK IF YOUR INSERT VALUES ARE CORRECT//

Coupling matrix is:
-------------------

         542 Hz  903 Hz  1110 Hz 1471 Hz 2228 Hz 4264 Hz 4336 Hz
542 Hz |    1       0       1       0       0       0       0|
903 Hz |    0       1       0       0       1       0       0|
1110 Hz |   1       0       1       1       0       0       0|
1471 Hz |   0       0       1       1       0       0       0|
2228 Hz |   0       1       0       0       1       0       0|
4264 Hz |   0       0       0       0       0       1       1|
4336 Hz |   0       0       0       0       0       1       1|

0 = not coupled protons
1 = coupled protons and diagonal

Spectral width is (higher freq - lower freq) = 3794.0 Hz
Spectral width with security factor (2) is: 7588.0 Hz
Pulse Bandwith was set to 30
Coil length was set to 1.8 cm
Probe gradient strength was set to 53.5 G/cm

//CALCULATION RETURN//
----------------------
Solution found after 8057 iterations


Offset set to be used for multifrequence shaped pulse is: 14
584 Hz
795 Hz
828 Hz
998 Hz
1524 Hz
1795 Hz
2009 Hz
2207 Hz
2490 Hz
3000 Hz
3627 Hz
3766 Hz
4022 Hz
4249 Hz
```

```
Z-position matrix (cm)
----------------------

         542 Hz   903 Hz   1110 Hz 1471 Hz 2228 Hz 4264 Hz 4336 Hz
584 Hz  |0,010    -0,076   -0,125  -0,210  -0,390  -0,873  -0,890|
795 Hz  |0,060    -0,026   -0,075  -0,160  -0,340  -0,823  -0,840|
828 Hz  |0,068    -0,018   -0,067  -0,153  -0,332  -0,815  -0,832|
998 Hz  |0,108    0,023    -0,027  -0,112  -0,292  -0,775  -0,792|
1524 Hz |0,233    0,147    0,098   0,013   -0,167  -0,650  -0,667|
1795 Hz |0,297    0,212    0,162   0,077   -0,103  -0,586  -0,603|
2009 Hz |0,348    0,262    0,213   0,128   -0,052  -0,535  -0,552|
2207 Hz |0,395    0,309    0,260   0,175   -0,005  -0,488  -0,505|
2490 Hz |0,462    0,376    0,327   0,242   0,062   -0,421  -0,438|
3000 Hz |0,583    0,497    0,448   0,363   0,183   -0,300  -0,317|
3627 Hz |0,732    0,646    0,597   0,511   0,332   -0,151  -0,168|
3766 Hz |0,765    0,679    0,630   0,544   0,365   -0,118  -0,135|
4022 Hz |0,826    0,740    0,691   0,605   0,426   -0,057  -0,074|
4249 Hz |0,879    0,794    0,745   0,659   0,479   -0,004  -0,021|

rows = generated offset frequencies for shaped pulse
columns = input frequencies from user
-------------------------------------------------
NMR tube is divided into 253 slices
Slice thickness is: 0,007 cm
Experimental sensitivity respect to 1H spectrum should be around 5,5
which is given by the ratio: number_of_offsets/number_of_slices
```

PUBLICATION 2

Full sensitivity and enhanced resolution in homodecoupled band-selective NMR experiments

Laura Castañar, Pau Nolis, Albert Virgili and Teodor Parella.
Chem. Eur. J., **2013**, *19*, 17283-17286.

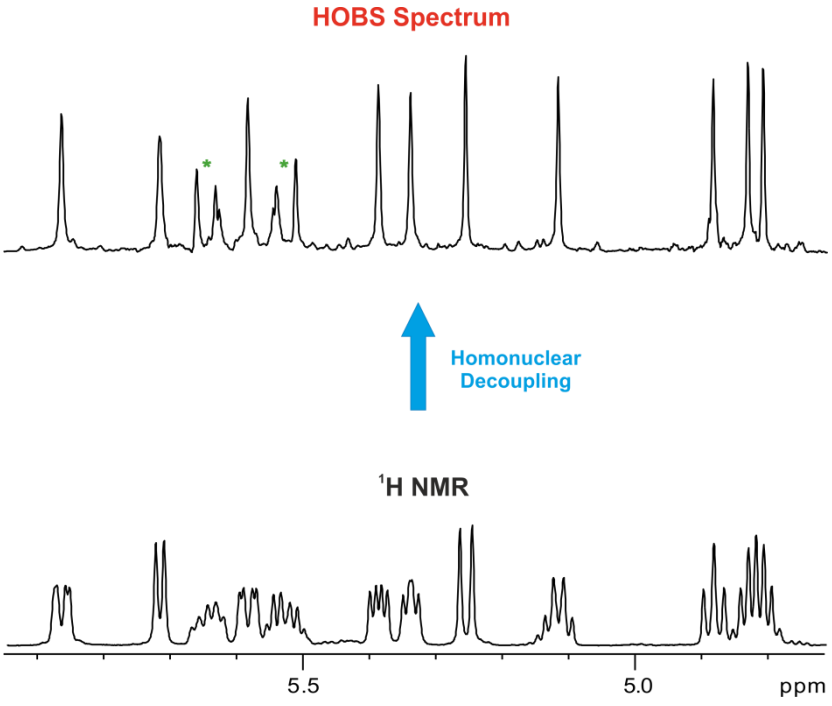

Introduction

Chemical shifts and coupling constants are fundamental parameters in the analysis and interpretation of NMR spectra. Multiplicity information can be extracted from the analysis of the fine multiplet structure and it can be related to structural parameters such as dihedral angles or the number of neighboring nuclei. The signal resolution in ^{1}H NMR spectra is rather poor, owing to the narrow proton chemical shift range and to the signal splitting by homonuclear coupling. As it has been show in Introduction, over recent years a high interest has emerged to develop broadband homodecoupled ^{1}H NMR techniques that offer increased resolution by simplifying the typical J_{HH} multiplet pattern to singlet lines, and therefore reducing signal overlapping. Most of the pure shift NMR experiments recently published are based on the *Zangger-Sterk* (ZS) method[3], which uses the spatial encoding concept along the *z*-dimension to obtain ^{1}H fully homodecoupled spectra. The main drawback of ZS methods is their very low sensitivities because signal only comes from selected *z*-slices. Thus the main challenge in this field is to design experiments which improve sensitivity.

In this publication a simple modification of the slice-selective 1D HOBB experiment[36] allows the collection of broadband homodecoupled spectra of specific regions of the ^{1}H spectrum without sacrificing sensitivity. As a major feature, this *HOmodecoupled Band-Selective* (HOBS) NMR method does not use the spatial encoding gradient G_s applied simultaneously with the selective pulses, and therefore, pure shift 1D spectra can be quickly recorded without the sensitivity losses characteristic of the slice selection process. The main limitation of this frequency-selective experiment is that only a particular part of the ^{1}H spectrum is monitored in a single-NMR spectrum. However, HOBS promises to have a potential use in spectra presenting a set of equivalent spin systems in well-separated and defined regions, such as the typical NH or H_α protons in peptides and proteins or those found in nucleic acids.

CHEMISTRY
A EUROPEAN JOURNAL

COMMUNICATION

DOI: 10.1002/chem.201303235

Full Sensitivity and Enhanced Resolution in Homodecoupled Band-Selective NMR Experiments

Laura Castañar,[a, b] Pau Nolis,[a] Albert Virgili,[b] and Teodor Parella*[a]

Chemical shifts and coupling constants (J) are fundamentals in the analysis and interpretation of NMR spectra. Multiplicity information and J values can be extracted from the analysis of the fine multiplet structure, and they can be related to structural parameters, such as the number of neighbouring spins, the trace of trough-bond connectivities or dihedral angle constraints. Over recent years, a significant interest has emerged to develop homodecoupled ^{1}H NMR spectroscopy techniques that offer increased resolution by simplifying the homonuclear splitting pattern, and therefore reducing signal overlapping.

The simplest approach for homodecoupling is the use of semiselective shaped pulse decoupling during signal detection, where the receiver and the decoupling are alternatively activated.[1] If the semiselective pulse is applied in a region A of the spectrum, the multiplet structure of J coupled signals resonating in a different region B appear simplified while they are detected. However, this is not a broadband method because protons from a third region C would not be decoupled, and therefore the corresponding coupling splittings will remain in the partially decoupled spectrum. Although the use of sophisticated multiple-region decoupling using different and simultaneous decoupling waveforms could be applied, it is difficult to achieve a perfect decoupling for all resonances and, moreover, without the interference of undesired decoupling sidebands.[2] Alternatively, the internal projection in the chemical shift dimension of J-resolved experiments[3] or the diagonal signals in anti-z-COSY experiments[4] have been also proposed to obtain broadband homodecoupled NMR spectra. They require the collection of more time consuming 2D/3D data and post-processing tasks can be further required. Some years ago, the so-called Zangger–Sterk (ZS) method based on the implementation of the spatially encoded concept along the z-dimension was also proposed.[5] The ZS method has been further refined and several applications have been reported to obtain high-resolved pure-shift multidimensional NMR spectra.[6–8] The main drawbacks of ZS methods are their low sensitivities because signal only comes from selected z slices and, on the other hand, the need for an FID reconstruction method by means of a time-consuming 2D/3D mode acquisition. Very recently, a new NMR detection scheme has been proposed for the instant and speed-up acquisition of ZS-decoupled spectra in a one-shot single-scan experiment.[9] The instant technique greatly improves the sensitivity per time unit ratio although the attainable sensitivity is still far from a regular ^{1}H spectrum. Analogous ZS methods incorporating isotopic ^{13}C editing by using BIRD elements have been also reported to efficiently minimise the effects of strong coupling, but an important penalty in sensitivity remains due to the low natural abundance of ^{13}C (1.1 %).[10]

Based on the instant ZS experiment, a novel NMR spectroscopy method for the fast acquisition of full-sensitive, homodecoupled band-selective (HOBS) NMR spectra is proposed here. It is noteworthy that the spatial encoding gradients applied simultaneously with the selective pulses in the original instant scheme are here omitted, avoiding sensitivity losses due to spatial slice selection. In addition, the HOBS method incorporates a number of advantages, such as: 1) an effective homodecoupling NMR block consisting of a pair of hard/selective 180° pulses flanked by pulsed field gradients (Figure 1), 2) an excellent spectral quality related to the use of selective gradient echoes, 3) real-time data collection without need of additional reconstruction methods that also allows conventional FID data processing, and 4) an easy implementation in multidimensional experiments. In our hands, the best results in terms of selectivity and optimum

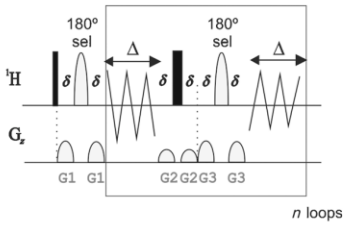

Figure 1. Schematic representation of the 1D homodecoupling band-selective (HOBS) experiment. Homodecoupling during detection is achieved by applying a pair of hard/semiselective 180° ^{1}H pulses (represented as solid and shaded shapes) at the middle of $2\Delta = AQ/n$ periods, in which AQ is the acquisition time and n the number of concatenated loops; δ is the duration of gradients and the recovery delay.

[a] L. Castañar, Dr. P. Nolis, Dr. T. Parella
Servei Ressonància Magnètica Nuclear
Universitat Autònoma de Barcelona
08193 Bellaterra, Barcelona (Spain)
E-mail: teodor.parella@uab.cat

[b] L. Castañar, Prof. A. Virgili
Departament de Química, Universitat Autònoma de Barcelona
08193 Bellaterra, Barcelona (Spain)

Supporting information for this article is available on the WWW under http://dx.doi.org/10.1002/chem.201303235.

CHEMISTRY
A EUROPEAN JOURNAL
ChemPubSoc Europe

relaxation are obtained using 180° REBURP semiselective pulses of 5–10 ms for both region-selective excitation and decoupling as a function of the selected region, and applied at intervals of $2\Delta = 10$–15 ms.[11]

Peptides and proteins are good targets for evaluating the efficiency of band-selective NMR spectroscopy experiments because a set of equivalent spins (amide NH, H_α or aliphatic side-chain protons) appear in well-separated regions. We chose the cyclic peptide cyclosporine (**1**) to verify the selectivity and sensitivity aspects of the proposed HOBS experiment. Figure 2B and C compare the individual single-scan 1D HOBS spectra obtained after selection of the H_α and NH region, respectively, with the ^{1}H spectrum acquired with the regular 90° pulse-acquisition method (Figure 2A). Clearly, all H_α or NH signals are fully homodecoupled, independent of their coupling pattern and also independent of the rest of the spectrum. It is very important to highlight that clean spectra are achieved, with minimum set-up and, in contrast to slice-selective ZS experiments, the same sensitivity levels as the conventional ^{1}H spectrum are retained.

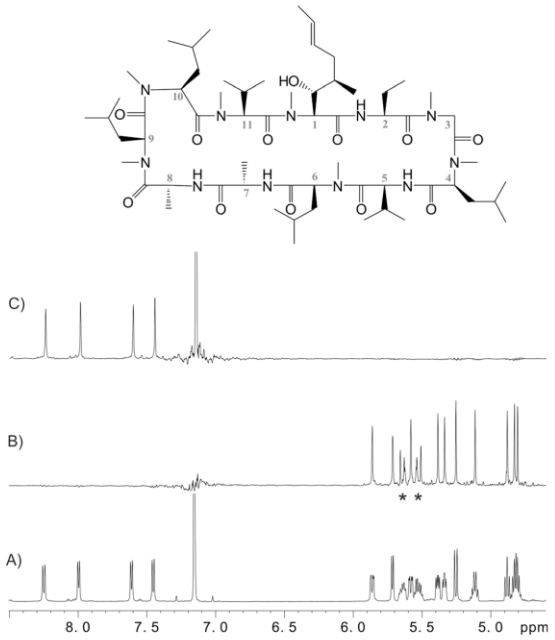

Figure 2. A) Regular pulse-acquisition, and B), C) HOBS ^{1}H NMR spectra of cyclosporine (**1**) after selection of H_α and NH regions, respectively. All spectra were recorded with the same receiver gain, with a single scan and processed with a Fourier transformation without any additional window function. All spectra are plotted with the same absolute vertical scaling factor for a comparison of their real sensitivity. HOBS spectra were recorded by applying 5 ms 180° REBURP pulses (about 1200 Hz of bandwith) for both excitation and decoupling in the region of interest. The 8 K data points were acquired using an acquisition time (*AQ*) of 576 ms (40 loops (*n*) were used with $\Delta = 7.2$ ms) and a recycle delay of 1 s. Gradients G1:G2:G3 with a duration of 500 μs were set to 23, 41 and 63% of the maximum attainable strength (53.5 G cm^{-1}). The asterisks marked in (B) stand for unavoidable non-decoupled effects of an AB two-spin system.

The H_α region (Figure 2B) additionally contains an AB two-spin system corresponding to the side-chain olefinic system of the residue 1, which can be used to evaluate the effects of mutual coupling in HOBS experiments as a function of the pulse selectivity. Sensitivity and selectivity always present opposite and conflicting points in all homodecoupling experiments. It can be shown that these protons are not fully decoupled and display their mutual coupling, because both experience the effects of the semiselective REBURP pulse. This unwanted *J* effect is not exclusive for the HOBS method, it is also present in the original instant and pseudo-2D ZS experiments recorded with the same selectivity conditions. Even the use of more selective pulses in the instant experiment (for instance, a Gaussian-shaped 180° pulse of 10 ms with an effective bandwidth of 121 Hz) does not provide complete decoupling for this spin system. Whereas the pseudo-2D ZS method can efficiently collapse these multiplets using a high-selective 60 ms Rsnob-shaped 180° pulse (effective bandwidth of 39 Hz), but at the expense of a dramatic sensitivity penalty, the instant and HOBS experiments completely fail under these conditions by severe relaxation due to the long pulse duration.

When trying to incorporate the pseudo-2D ZS method into multidimensional experiments, the overall acquisition time becomes extremely long because of the need for a 3D acquisition mode and for its reduced sensitivity. An important feature of the proposed HOBS detection scheme is its easy implementation as a powerful and general building block in existing multidimensional NMR spectroscopy experiments, with the same selectivity conditions as reproduced with the 1D version and retaining the maximum sensitivity levels of the original experiments. As an example, Figure 3 compares the conventional TOCSY versus the HOBS-TOCSY spectra of **1** acquired with the same experimental conditions and time. The 1D row analysis reveals a much better resolution in the direct dimension without affecting sensitivity, spectral quality and performance. Note that strong coupling effects remain exactly as observed in the 1D version. Other attempts to obtain pure-shift TOCSY spectra require a more extensive experimental time.[5,7]

Similarly, the non-refocused version of a F2-coupled ^{1}H-^{13}C HOBS-HSQC spectrum shows collapsed signals with improved resolution and even better sensitivity, making it highly suitable for the reliable measurement of one-bond proton–carbon coupling constants from simplified singlet lines, and demonstrating its potential for measuring accurate residual dipolar couplings (RDCs) in anisotropic media under high-sensitivity conditions (Figure 4).[12] The HOBS scheme is also fully compatible with simultaneous broadband heteronuclear decoupling during acquisition. Details of the pulse timing on the simultaneous homo- and heteronuclear decoupling and its implementation into the conventional HSQC spectrum are available in the Supporting Information.

In summary, a new band-selective detection scheme has been proposed to collect homodecoupled NMR spectra of specific regions without sacrificing sensitivity. The imple-

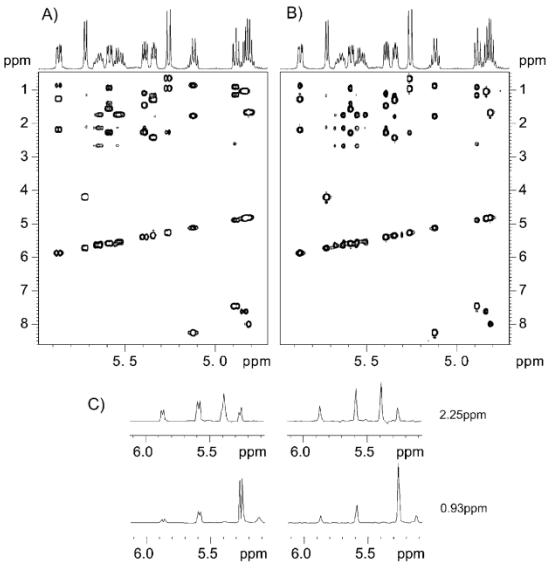

Figure 3. H_α-region selective: A) regular TOCSY, and B) HOBS-TOCSY spectra of **1** (mixing time of 60 ms); C) 1D slices taken at two different frequencies to compare the relative sensitivity and resolution levels. Four scans were collected for each 128 t_1 increments of 2 K complex points, giving an experimental time of 13 min for each 2D spectrum. Homodecoupling was achieved using 20 loops and $\Delta = 4.3$ ms ($AQ = 170$ ms) whereas all other experimental parameters were as described in the legend of Figure 2.

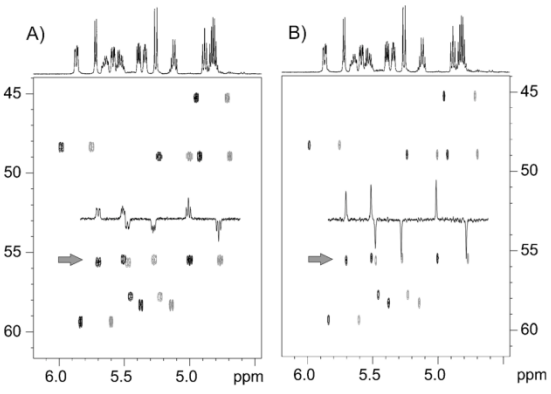

Figure 4. A) Regular, and B) HOBS spectra of the non-refocused F2 coupled ^1H-^{13}C HSQC experiment of **1**. The interpulse delays were optimised to 145 Hz. Two scans were collected for each one of the 64 t_1 increments of 2 K complex data points. Homodecoupling was achieved using $n = 50$, $\Delta = 5.7$ ms, $AQ = 570$ ms, $sw = 1800$ Hz and a REBURP 180° pulse of 5 ms. The experimental time for each 2D spectrum was of 5 min.

mentation of the HOBS approach becomes easy and reliable for a large number of multidimensional applications and guarantees rapid data acquisition even for samples at low concentrations. In particular, it can become very attractive for biomolecular NMR spectroscopy applications, particularly if combined with the gains in sensitivity and resolution offered by cryogenic probes and high magnetic fields. For instance, it could be used to remove contributions to line broadening due to residual HH dipolar couplings when working with partially oriented proteins in anisotropic media[13] or to improve the sensitivity and resolution of band-selective ^{13}C-detected NMR experiments with active J(CC) coupling constants, such as those applied on ^{13}C-labeled proteins.[14] HOBS methodology is also fully compatible with other homodecoupling methods applied in the indirect dimension of multidimensional NMR experiments[15] and many aspects are currently being explored to demonstrate the power of these pure-shift NMR solutions.

Experimental Section

All NMR spectroscopy experiments were performed in a 600 MHz Bruker Avance-III spectrometer equipped with a TXI probe and a gradient unit delivering 53.5 G cm^{-1}. The sample used was 25 mM cyclosporine in [D_6]benzene. More experimental details and pulse sequence diagram of 2D HOBS versions of the refocused HSQC-CLIP and fully homo- and heteronuclear decoupled HSQC experiments can be found in the Supporting Information.

Acknowledgements

Financial support for this research provided by MICINN (project CTQ2012-32436) and Bruker Española S.A. are gratefully acknowledged. We also thank to the Servei de Ressonància Magnètica Nuclear, Universitat Autònoma de Barcelona, for allocating instrument time to this project. The authors also thank Prof. K. Zangger for providing experimental details and the pulse program code of the original instant experiment.

Keywords: band selective · homodecoupling · NMR spectroscopy · sensitivity enhancement · structure elucidation

[1] a) J. P. Jesson, P. Meakin, G. Kneissel, *J. Am. Chem. Soc.* **1973**, *95*, 618–620; b) A. Hammarström, G. Otting, *J. Am. Chem. Soc.* **1994**, *116*, 8847–8848; c) J. Weigelt, A. Hammarström, W. Bermel, G. Otting, *J. Magn. Reson. Ser. B* **1996**, *110*, 219–224.

[2] a) E. Kupče, G. Wagner, *J. Magn. Reson. Ser. B* **1995**, *109*, 329–333; b) E. Kupče, G. Wagner, *J. Magn. Reson. Ser. B* **1996**, *110*, 309–312; c) E. Kupče, H. Matsuo, G. Wagner, in *Biological Magnetic Resonance Modern Techniques in Protein NMR, Vol. 16* (Eds.: N. R. Krishna, L. J. Berliner), Springer, Heidelberg, **1999**, 16, pp. 149–193; d) B. Vögeli, H. Kovacs, K. Pervushin, *J. Biomol. NMR* **2005**, *31*, 1–9.

[3] a) A. J. Pell, J. Keeler, *J. Magn. Reson.* **2007**, *189*, 293–299; b) B. Luy, *J. Magn. Reson.* **2009**, *201*, 18–24; c) P. Sakhaii, B. Haase, W. Bermel, *J. Magn. Reson.* **2013**, *228*, 125–129.

[4] A. J. Pell, R. A. Edden, J. Keeler, *Magn. Reson. Chem.* **2007**, *45*, 296–316.

[5] K. Zangger, H. Sterk, *J. Magn. Reson.* **1997**, *124*, 486–489.

[6] a) M. Nilsson, G. A. Morris, *Chem. Commun.* **2007**, 933–935; b) J. A. Aguilar, S. Faulkner, M. Nilsson, G. A. Morris, *Angew. Chem.* **2010**, *122*, 3993–3995; *Angew. Chem. Int. Ed.* **2010**, *49*, 3901–3903.

[7] a) G. A. Morris, J. A. Aguilar, R. Evans, S. Haiber, M. Nilsson, *J. Am. Chem. Soc.* **2010**, *132*, 12770–12772; b) J. J. Koivisto, *Chem. Commun.* **2013**, *49*, 96–98.
[8] J. A. Aguilar, A. A. Colbourne, J. Cassani, M. Nilsson, G. A. Morris, *Angew. Chem.* **2012**, *124*, 6566–6569; *Angew. Chem. Int. Ed.* **2012**, *51*, 6460–6463.
[9] N. H. Meyer, K. Zangger, *Angew. Chem.* **2013**, *125*, 7283–7286; *Angew. Chem. Int. Ed.* **2013**, *52*, 7143–7146.
[10] a) A. Lupulescu, G. L. Olson, L. Frydman, *J. Magn. Reson.* **2012**, *218*, 141–146; b) J. A. Aguilar, M. Nilsson, G. A. Morris, *Angew. Chem.* **2011**, *123*, 9890–9891; *Angew. Chem. Int. Ed.* **2011**, *50*, 9716–9717.c) P. Sakhaii, B. Haase, W. Bermel, *J. Magn. Reson.* **2009**, *199*, 192–198.
[11] H. Geen, R. Freeman, *J. Magn. Reson.* **1991**, *93*, 93–141.
[12] A. Enthart, J. C. Freudenberger, J. Furrer, H. Kessler, B. Luy, *J. Magn. Reson.* **2008**, *192*, 314–322.
[13] C. W. Vander Kooi, E. Kupče, R. P. Zuiderweg, M. Pellecchia, *J. Biomol. NMR* **1999**, *15*, 335–338.
[14] a) I. Bertini, I. C. Felli, R. Kümmerle, D. Moskau, R. Pierattelli, *J. Am. Chem. Soc.* **2004**, *126*, 464–465; b) W. Bermel, I. Bertini, L. Duma, I. C. Felli, L. Emsley, R. Pieratelli, P. R. Vasos, *Angew. Chem.* **2005**, *117*, 3149–3152; *Angew. Chem. Int. Ed.* **2005**, *44*, 3089–3092.
[15] V. V. Krishnamurthy, *J. Magn. Reson. A* **1996**, *113*, 46–52; b) V. V. Krishnamurthy, *Magn. Reson. Chem.* **1997**, *35*, 9–12.

Received: August 16, 2013
Published online: November 11, 2013

CHEMISTRY
A EUROPEAN JOURNAL

Supporting Information

Full Sensitivity and Enhanced Resolution in Homodecoupled Band-Selective NMR Experiments

Laura Castañar,[a, b] Pau Nolis,[a] Albert Virgili,[b] and Teodor Parella*[a]

chem_201303235_sm_miscellaneous_information.pdf

Experimental Section

All experiments were acquired on a Bruker AVANCE spectrometer (Bruker BioSpin, Rheinstetten, Germany) operating at 600.13 MHz proton frequency, equipped with a 5 mm triple resonance inverse probe and a z-axis pulsed field gradient accessory (maximum strength of 53.5 G/cm). The spectra were collected on a 25 mM sample of the cyclic peptide cyclosporine dissolved in benzene-d6 at a temperature T = 298 K, and processed with the software TOPSPIN 2.1.

The non-selective ^{1}H 180 pulses were of 8.0 μs duration. For all 1D and 2D HOBS experiments, a 180º band-selective REBURP shaped pulse of 5.0 ms was used for both excitation and homodecoupling. It was generated using the *stdisp* pulse shaping program available in Topspin NMR software. The setting of this pulse was initially tested and optimized using a single-scan SPFGE experiment (as Fig.1 with a conventional detection period), as shown in Fig. S1B. The strengths of the G1, G2 and G3 gradients were set to 12.3, 21.9 and 33.7 G/cm, respectively, with durations of 500 μs followed by a recovery delay of 20 μs.

1D HOBS spectra of Fig. 2B and 2C were recorded using a single scan and 1 s of recycle delay. The spectral width was 7200 Hz, and 8K complex points were recorded during an acquisition time of 576 ms. 40 loops (n) were concatenated with Δ=AQ/2n=7.2ms. The 1D time-domain data were directly transformed without any sensitivity or resolution enhancement.

The regular 2D TOCSY spectrum (Fig. 3A) was acquired using the *dipsi2ph* pulse program, using a z-filtered DIPSI-2 spinlock of ca. 8 kHz effective field strength was used with a mixing time of 60ms. The HOBS-TOCSY spectrum (Fig. 3B) was acquired using the pulse sequence displayed in Fig. S4A, with the same parameters described for the regular TOCSY and 1D HOBS experiments. Two scans of 2048 complex points were collected over an observed spectral width of 6000 Hz for each of the 128 t_1 values. Experimental parameters: AQ=170ms, n=20, Δ=4.3ms, and recycle delay of 1s. Data were transformed with a shifted sine window function along both the F1 and F2 dimensions and with a zero–filling to 1K in F1. The total experimental time was about 13 minutes for each 2D spectrum.

The non-refocused version of the 2D ^{1}H-^{13}C HSQC spectrum (Fig. 4A) was optimized to $1/(2*J_{CH})$=145Hz. Two scans of 1024 complex points were collected over an observed spectral width of 1800 Hz for each of the 128 t_1 values. Data were transformed with a shifted sine window function along both the F1 and F2 dimensions and with a zero-filling to 1K in F1. The corresponding HOBS-HSQC spectrum (Fig. 4B) was acquired using the pulse sequence displayed in Fig. S4B, with the same parameters described for the regular HSQC and 1D HOBS experiments. The 90º and 180º band-selective pulses were EBURP-2 of 3.5 ms and REBURP of 5.0 ms, respectively. The total experimental time was about 5 minutes for each 2D spectrum. The above conditions were also applied for the HOBS-HSQC-CLIP (see the pulse scheme in Fig. S4C and the corresponding spectrum in Fig. S5B) and fully-decoupled HOBS-HSQC experiments (see the pulse scheme in Fig. S6B and the corresponding spectrum in Fig. S7B). To achieve heteronuclear decoupling during the HOBS detection scheme, the pulse timing described in Fig. S7A was applied.

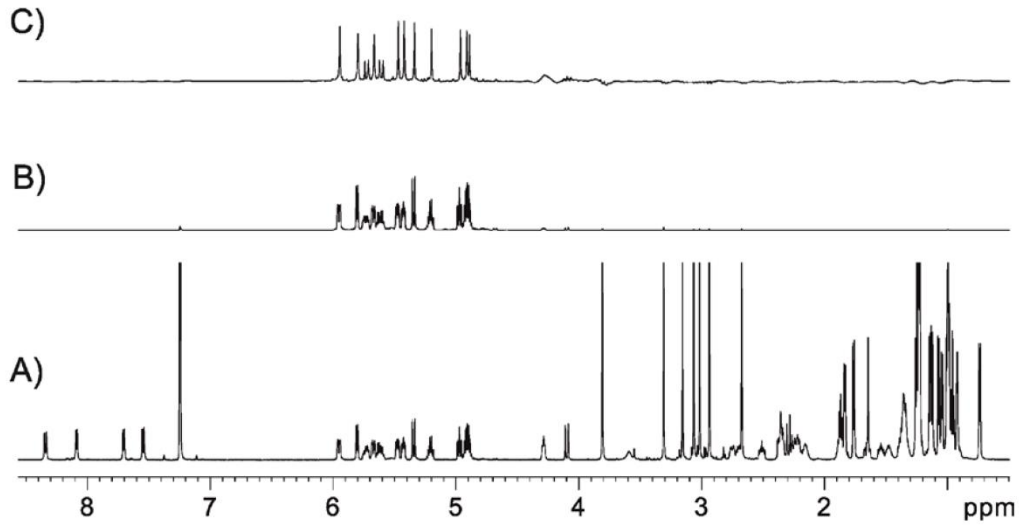

Figure S1: (A) ^{1}H spectrum of cyclosporine; B) Band-selective spectrum acquired with the single-pulsed-field gradient echo (SPFGE) sequence using a semiselective RE-BURP-shaped 180º ^{1}H pulse of 5 ms; and C) 1D HOBS spectra acquired with the pulse sequence of Fig. 1 using a 5ms REBURP-shaped pulse.

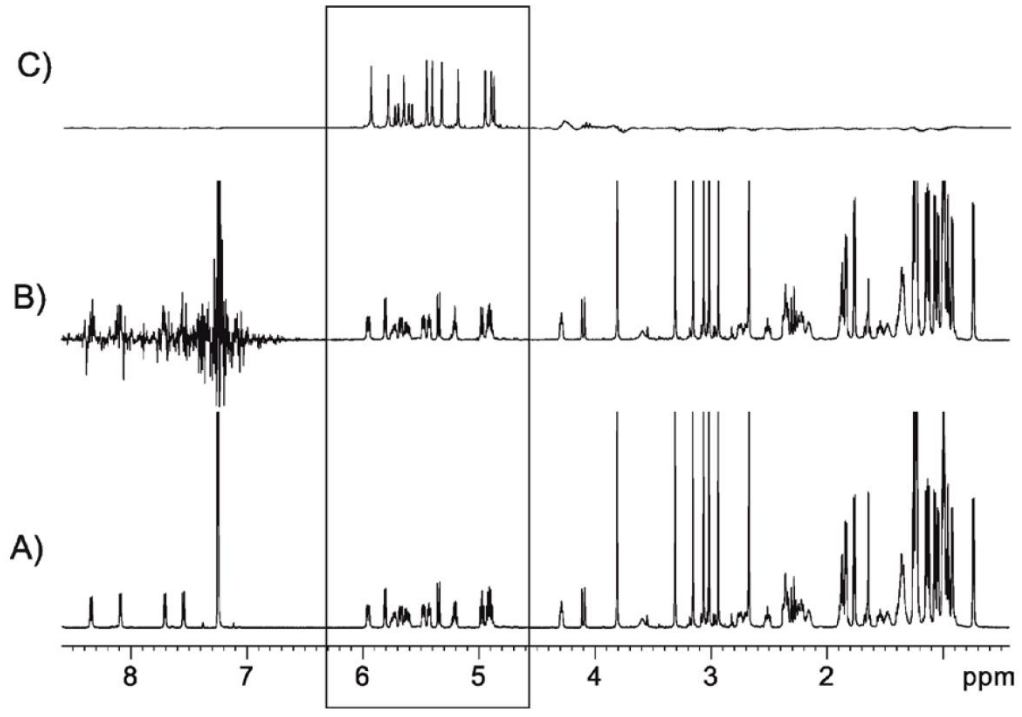

Figure S2: Comparison between the A) standard ^{1}H spectrum; B) ^{1}H spectrum (acquired with 4 scans) after SESAM decoupling of the NH region during acquisition using a *mlevsp180* pulse train with a 5 ms REBURP shaped pulse as inversion element (pulse program called zghc.3); C) Clean 1D HOBS spectra acquired with the pulse sequence of Fig. 1 using a 5ms REBURP-shaped 180º ^{1}H pulses. See Fig. S3 for a better visualization of the expanded H_{α} region.

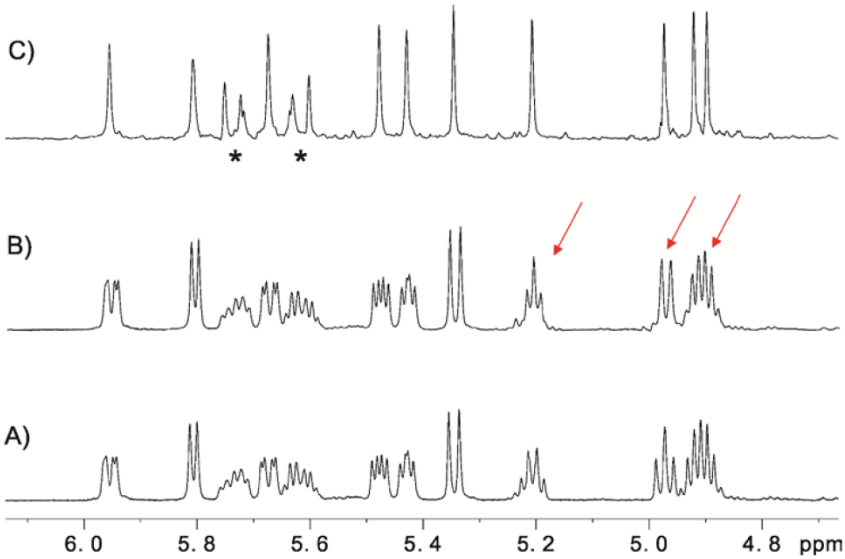

Figure S3: Expanded H_α region corresponding to the spectra of Fig. S2. The selective decoupling of the NH region in B only simplifies the H_α protons with a resolved J(NH- H_α) coupling (see arrows). Note that other couplings between H_α and other side-chain H_β protons are not affected. In C) all couplings are collapsed except the active J(HH) of the olefinic AB spin system (marked with asterisks).

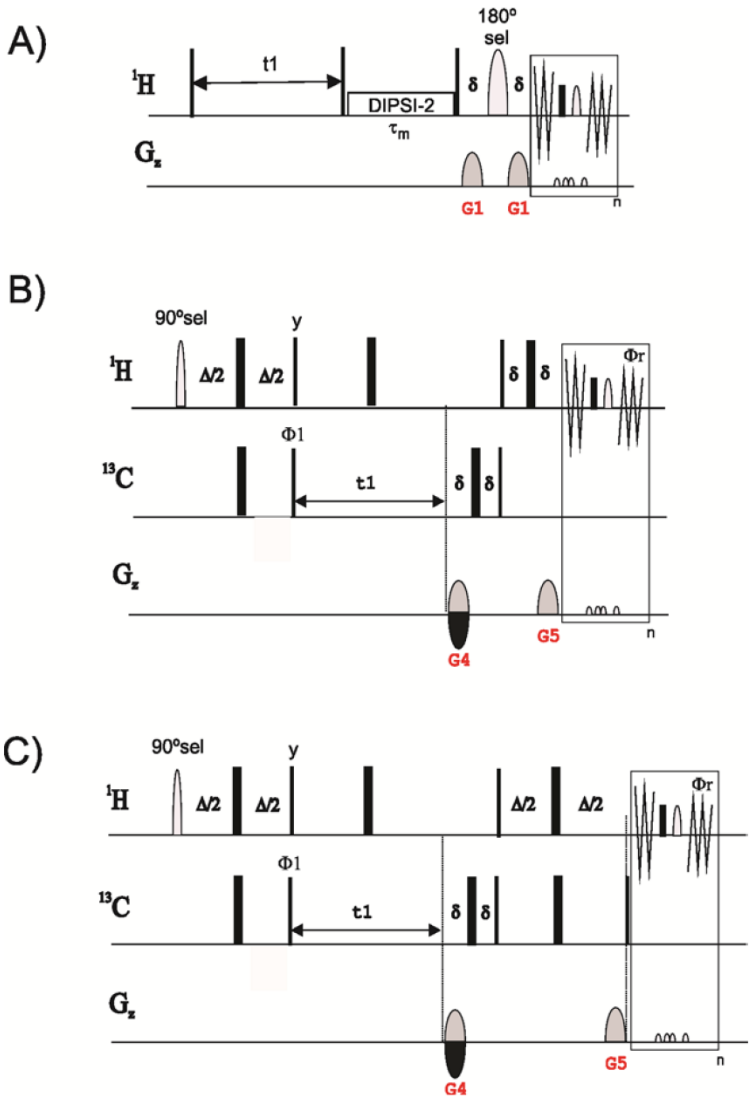

Figure S4: Basic illustration of the incorporation of the HOBS technique in conventional 2D homo- and heteronuclear NMR experiments. General pulse schemes for the A) HOBS-TOCSY, B) non-refocused HOBS-HSQC, and C) refocused HOBS-HSQC-CLIP experiments. Basically, all these experiments have been easily adapted from conventional sequences by substituting an appropriate hard 90º pulse by a selective 90º or a 90º-δ-180sel- δ SPFGE block, and changing the conventional detectino period by the HOBS scheme, as reported in Fig.1 of the manuscript. The parameters working in the 1D HOBS sequence can be directly implemented in these 2D versions without any additional calibration. All pulse powers and durations, delays, gradient strengths and phase cycles are exactly the same as set in the conventional 2D experiments. The hard and semi-selective 180 pulses in the HOBS scheme are applied from the x axis, without any further phase cycling.

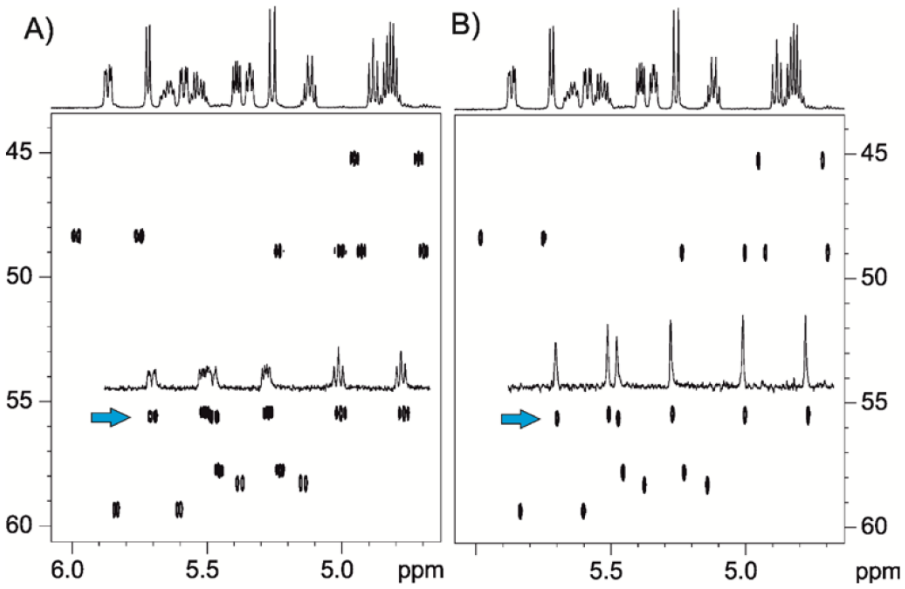

Figure S5: A) Conventional and B) HOBS versions of the F2-coupled HSQC-CLIP spectra of cyclosporine obtained using the non-refocused version of Fig. S4B with the same experimental conditions as described in Fig. 4. More details can be found in the experimental section.

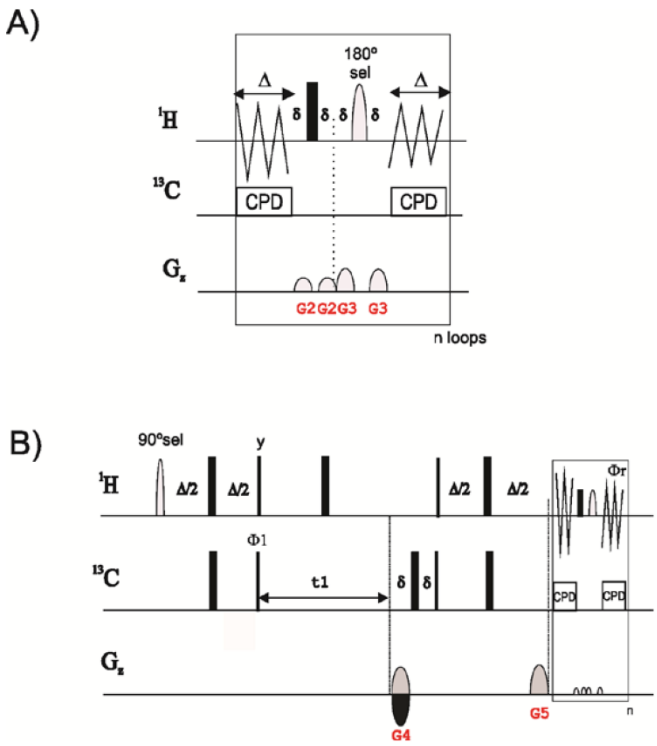

Figure S6: A) 1D HOBS detection scheme to perform simultaneous broadband homo- and heteronuclear decoupling. Heteronuclear Decoupling (CPD) is only applied during data writing and it is switch off during the application of the gradient-based inversion elements; B) Pulse scheme of the fully homo- and heteronuclear decoupled HOBS-HSQC experiment.

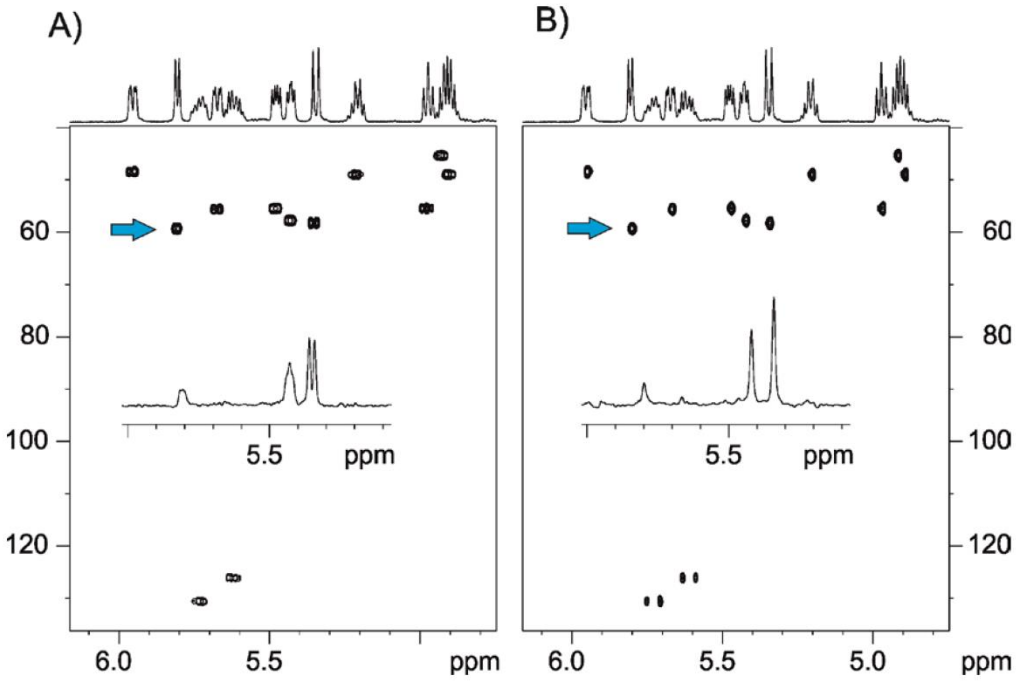

Figure S7: A) Conventional and B) fully homo- and heteronuclear decoupled HOBS-HSQC spectra of cyclosporine obtained using the non-refocused version of Fig. S6B with the same experimental conditions as described in Fig. 4. Note the J(HH) doublet splitting of the two olefinic AB protons. More details can be found in the experimental section.

PUBLICATION 3

Measurement of T_1/T_2 relaxation times in overlapped regions from homodecoupled ^1H singlet signals

Laura Castañar, Pau Nolis, Albert Virgili and Teodor Parella.
J. Magn. Reson., **2014**, *244*, 30-35.

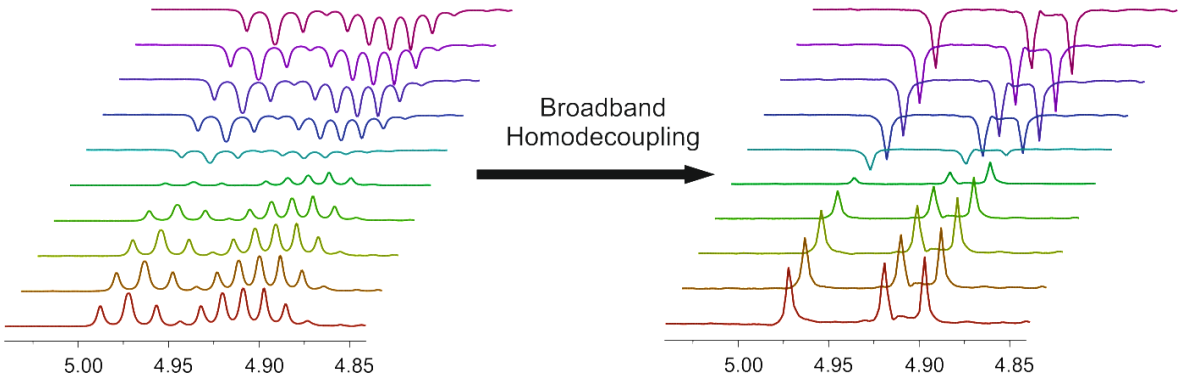

Introduction

The measurement of relaxation rates by NMR spectroscopy provides important insights into the dynamics of molecules in solution. Longitudinal spin-lattice T_1 relaxation times are usually determined from *Inversion Recovery* (IR) experiment[87] whereas transverse spin–spin T_2 relaxation times are measured from *Carr–Purcell–Meiboom–Gill* (CPMG) sequences.[88] One drawback of CPMG pulse trains is the presence of multiplet distortions due to J_{HH} evolution that can affect the accuracy of the measurement. An improved perfect CPMG sequence that achieves *Periodic Refocusing Of J Evolution by Coherence Transfer* (referred to as PROJECT) has been proposed recently to minimize the effects of *J* evolution during the echo periods, obtaining pure in-phase signals.[89]

On other hand, T_1 and T_2 values are usually extracted from the analysis of mono-exponential signal decays monitored in a series of 1D spectra. However, signal overlap hampers a simple data analysis due to the superposition of several individual decays. In these cases, the use of more sophisticated methods, such as deconvolution, line fitting techniques or the analysis of multiple-exponential decay can be required to obtain correct values for each individual signal.

In this article, the implementation of the HOBS technique (see **Publication 2**) in standard IR and PROJECT experiments is proposed to solve overlapping problems. The new homodecoupled 1D HOBS-IR and HOBS-PROJECT experiments allows the accurate measure of T_1 and T_2 relaxation times from the resulting singlet lines using conventional mono-exponential curve-fitting methods. These experiments have been tested on crowded areas of cyclosporine and progesterone samples. The experimental T_1 and T_2 data obtained from HOBS versions agree with data extracted from conventional IR and PROJECT experiments.

[87] a) P. B. Kingsley, *Concepts Magn. Reson.,* **1999**, *11*, 29. b) P. B. Kingsley, *Concepts Magn. Reson.,* **1999**, *11*, 243.
[88] a) H. Y. Carr, E. M. Purcell, *Phys. Rev.,* **1954**, *274*, 630. b) S. Meiboom, D. Gill, *Rev. Sci. Instrum.,* **1958**, *29*, 688.
[89] J. A. Aguilar, M. Nilsson, G. Bodenhausen, G. A. Morris, *Chem. Commun.,* **2012**, *48*, 811.

Journal of Magnetic Resonance 244 (2014) 30–35

Contents lists available at ScienceDirect

Journal of Magnetic Resonance

journal homepage: www.elsevier.com/locate/jmr

Measurement of T_1/T_2 relaxation times in overlapped regions from homodecoupled ^{1}H singlet signals

Laura Castañar, Pau Nolis, Albert Virgili, Teodor Parella *

Servei de Ressonància Magnètica Nuclear and Departament de Química, Universitat Autònoma de Barcelona, E-08193 Bellaterra, Catalonia, Spain

ARTICLE INFO

Article history:
Received 26 February 2014
Revised 2 April 2014
Available online 24 April 2014

Keywords:
Pure-shift NMR
Relaxation times
T_1
T_2
Inversion-Recovery
CPMG
PROJECT
HOBS

ABSTRACT

The implementation of the HOmodecoupled Band-Selective (HOBS) technique in the conventional Inversion-Recovery and CPMG-based PROJECT experiments is described. The achievement of fully homodecoupled signals allows the distinction of overlapped ^{1}H resonances with small chemical shift differences. It is shown that the corresponding T_1 and T_2 relaxation times can be individually measured from the resulting singlet lines using conventional exponential curve-fitting methods.

1. Introduction

The measurement of relaxation rates by Nuclear Magnetic Resonance (NMR) spectroscopy can provide important insights into the dynamics of molecules in solution [1]. Longitudinal spin–lattice T_1 relaxation times are usually determined from the Inversion-Recovery (IR) experiments [2,3] whereas transverse spin–spin T_2 relaxation times are measured from Carr–Purcell–Meiboom–Gill (CPMG) sequences [4,5]. Recently, an improved compensated CPMG sequence that achieves Periodic Refocusing Of J Evolution by Coherence Transfer (PROJECT) has been proposed to minimize the effects of J evolution during the echo periods, allowing a more accurate extraction of T_2 values by fitting the experimental data to a clean exponential decay of pure-phase, non-J-modulated signals [6,7]. A common feature of all these experiments is that measurements are based on exponential signal decays that can be described by first-order differential equations. In spectral regions with well resolved peaks the corresponding time constants are easily determined from nonlinear least-squares fits of each decaying signal to a separate mono-exponential function. However, simple data analysis are hampered in spectral regions with significant peak overlap, where the observed signal decays may be the result of superposition of several individual decays which are difficult to distinguish and require the use of sophisticated fitting methods [8–10]. Several NMR approaches have been proposed to avoid signal overlapping in relaxation experiments, such as the initial use of selective coherence by TOCSY transfer from an isolated signal [11], although the improved signal dispersion achieved in 2D/3D NMR experiments has become the common technique to study the conformational and dynamics aspects of biomolecules in solution [12].

On the other hand, a number of broadband homodecoupled NMR methods have been reported to obtain simplified ^{1}H singlet signals without the typical fine J(HH) multiplet structure [13–24], and recently an excellent overview of the homodecoupling techniques and applications has been reviewed [18]. The most recent applications, that have been encompassed under the term "pure-shift NMR", are based on the original Zangger–Sterk (ZS) experiment [14]. Basically exists two different acquisition protocols: (i) a time-consuming pseudo-2D acquisition mode based on adding the first part of different interferograms [14,15], and (ii) a real-time one-shot mode that reduce the experimental time and do not need for sophisticated processing tools [17]. Most of them use spatial encoded techniques, and therefore pronounced sensitivity losses due to slice selection are unavoidable that requires long acquisition times. Other homodecoupling methods using the BIRD module [19] do not suffer of sensitivity penalties but their applications are limited to heteronuclear correlation experiments [24]. Alternatively, a novel HOmodecoupled Band-Selective (HOBS)

* Corresponding author.
E-mail address: teodor.parella@uab.cat (T. Parella).

http://dx.doi.org/10.1016/j.jmr.2014.04.003
1090-7807/

approach [25,26], closely related to the instant ZS experiment [17] has been proposed. The HOBS technique is not a broadband homodecoupling method that covers all the spectral width, rather it is a frequency-selective inverse homodecoupled method. However, it has been shown to be a sensitive and valuable practical tool when focusing specifically on a narrow part of the whole spectrum and applications have been provided for enantiodifferentiation studies [27], discrimination of diastereoisomers [28] or the measurement of heteronuclear coupling constants [29]. The main drawback is that it is a frequency-selective experiment and only a particular part of the ^{1}H spectrum can be monitored in a single experiment. As a major advantage, the HOBS method omits the spatial encoding gradient applied simultaneously with the selective pulses in the original instant scheme, avoiding any sensitivity loss and allowing its performance with reasonable experimental times. This communication reports the straightforward implementation of the HOBS technique in standard IR and PROJECT experiments (Fig. 1) with the aim to resolve overlapped ^{1}H resonances with small chemical shift differences. Thus, T_1 and T_2 relaxation times can be accurately measured from the resulting singlet lines using conventional exponential curve-fitting methods, without need for additional data analysis based on deconvolution or line fitting techniques [30,31].

2. Results and discussion

The major novelty with respect to the original experiments is the incorporation of the homodecoupled element during the detection period that consists of a pair of hard/selective 180° ^{1}H pulses (represented as solid and shaded shapes) at the middle of $2\Delta = AQ/n$ periods, where AQ is the acquisition time and n the number of concatenated loops [25,26]. In addition, a ^{1}H-selective gradient echo has been inserted prior to acquisition to select the area of interest, where the involved selective 180° ^{1}H pulse is the same as used for homodecoupling. For a perfect broadband homodecoupling, these experiments should be applied to particular areas of the ^{1}H spectrum where appear overlapped protons that are not mutually J coupled.

HOBS experiments can use the same automated data acquisition, processing and fitting analysis subroutines as the original experiments. A series of 1D ^{1}H spectra are sequentially recorded as a function of the recovery delay (τ) or the total echo time ($\tau_e = 4m\tau'$) in IR (Fig. 1A) and PROJECT (Fig. 1B) experiments, respectively. Fig. 2 compares the experimental results obtained for the IR and HOBS-IR experiments applied to the H_α proton region in the peptide cyclosporine. Good agreement is observed between the T_1 measured for all isolated signals with both methods demonstrating that the incorporation of homodecoupling does not distort the measurement (Table 1). The excellence of the method is illustrated by distinguishing the individual decays of the overlapped H_7 and H_8 resonances at 4.78–4.80 ppm. Clearly, the successful analysis of the two resolved singlets (separated by 13 Hz) allows an accurate determination of each distinct T_1 value without resorting to more complex data analysis. The same strategy can be applied for T_2 measurements. The simplicity and the accuracy of the measurements is demonstrated when comparing the equivalent CPMG, PROJECT and HOBS-PROJECT spectra, all of which acquired with a total echo time of 156 ms (Fig. 3B–D). Whereas the standard CPMG spectrum shows strong multiplet distortions due to the unavoidable J_{HH} evolution, perfect in-phase multiplets are obtained from both PROJECT spectra.

Clearly, the in-phase properties are fully retained in the HOBS-PROJECT spectra (Fig. 3D), where improved sensitivity and resolution are obtained due to the efficient multiplet collapsing. The method works equally well for mutually J-coupled protons that experience the effect of the selective 180° pulse, and therefore they are not fully homodecoupled. T_2 measurements on the partially decoupled olefinic $H1_\varepsilon$ and $H1_\zeta$ protons (asterisks in Fig. 3D) can be also monitored efficiently from the simplified doublet patterns.

The HOBS methods can be very useful to simplify highly congested areas, such as those found in the aliphatic region of the steroid progesterone (Fig. 4). Three resonances with complex multiplet patterns appear completely overlapped at 2.0 ppm. The simplified HOBS spectrum shows clean singlets for each of these signals, with small chemical differences of 14–18 Hz. Note the equivalence between IR and HOBS-IR data by observing the same exact null point for the strong methyl signal (see experimental details and experimental T_1/T_2 values in the supporting information).

Experimentally, the HOBS technique requires a very simple and fast implementation. Only two parameters need to be defined in a

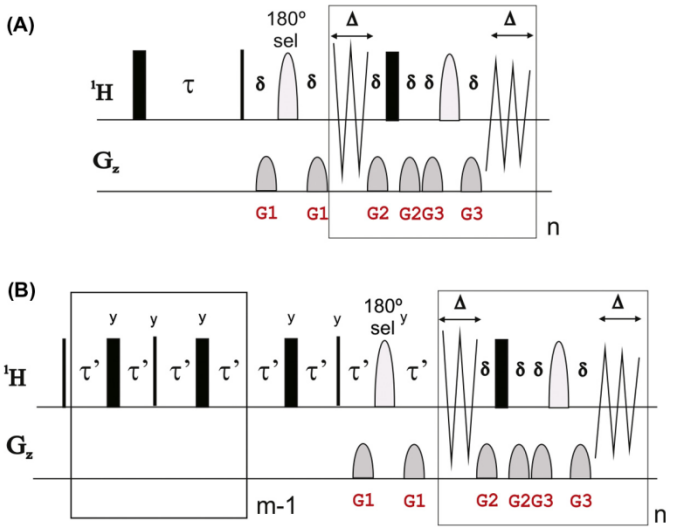

Fig. 1. NMR pulse schemes of the HOBS-IR and HOBS-PROJECT experiments used to measure T_1 and T_2 relaxation times, respectively, in overlapped proton signals.

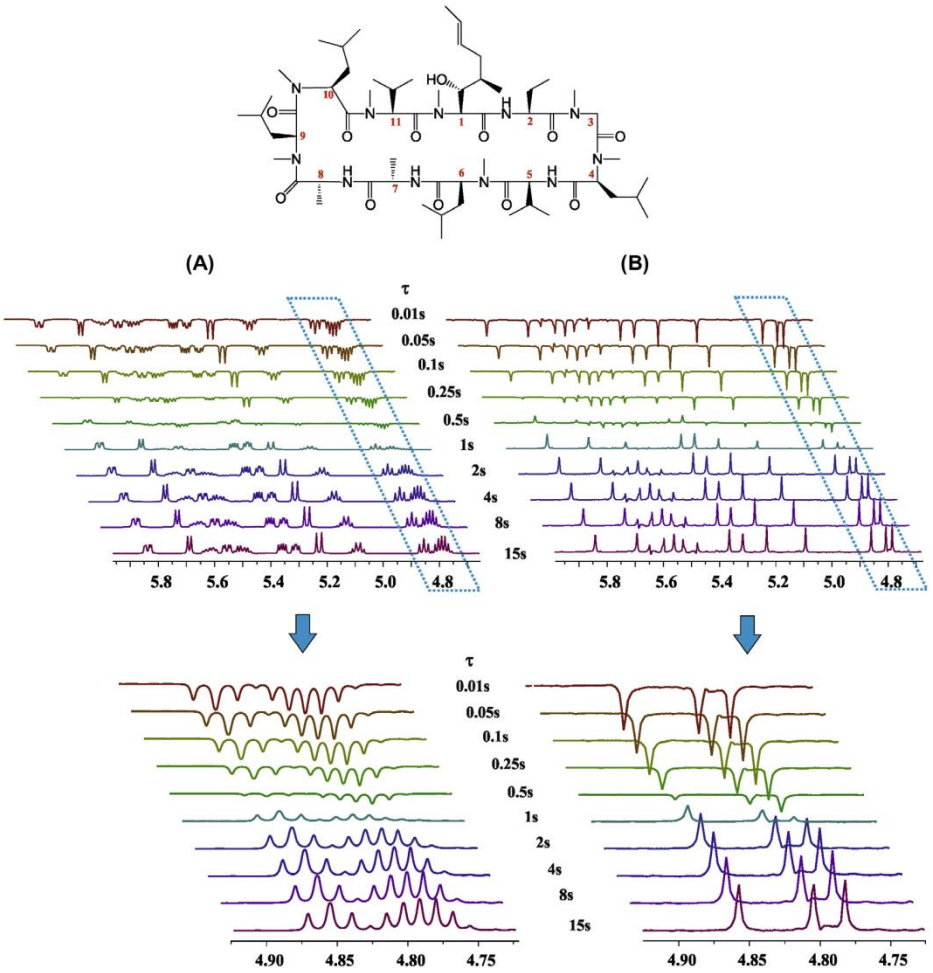

Fig. 2. 600 MHz ^{1}H NMR spectra obtained from the (A) conventional IR and (B) HOBS-IR experiments to determine T_1 values for all H_α protons on 25 mM cyclosporine in benzene-d_6. At the bottom, the clean differentiation between the overlapped H7 and H8 protons is shown. All spectra were collected under the same experimental conditions and plotted at the same absolute vertical scale. Homodecoupling was achieved using the detection scheme described in Fig. 1A with a 5 ms REBURP 180° pulse, Δ = 8.9 ms, AQ = 569 ms and n = 32.

Table 1
Experimental T_1 and T_2 values obtained from IR, HOBS-IR, PROJECT and HOBS-PROJECT experiments for H_α and olefinic protons in cyclosporine, calculated using a simple mono-exponential decay.

Proton	δ (ppm)	T_1 measurement (s)		T_2 measurement (s)	
		IR	HOBS-IR	PROJECT	HOBS-PROJECT
H9	5.83	0.41 ± 0.01	0.43 ± 0.01	0.37 ± 0.01	0.36 ± 0.01
H1	5.69	0.60 ± 0.01	0.60 ± 0.01	0.29 ± 0.02	0.33 ± 0.01
H4	5.55	0.89 ± 0.01	0.88 ± 0.01	0.32 ± 0.01	0.34 ± 0.01
H6	5.36	0.55 ± 0.01	0.57 ± 0.01	0.33 ± 0.01	0.33 ± 0.01
H10	5.31	0.41 ± 0.01	0.42 ± 0.01	0.27 ± 0.01	0.30 ± 0.02
H11	5.23	0.81 ± 0.02	0.85 ± 0.01	0.41 ± 0.03	0.35 ± 0.04
H2	5.09	0.94 ± 0.01	0.92 ± 0.01	0.35 ± 0.02	0.32 ± 0.01
H5	4.85	0.88 ± 0.02	0.88 ± 0.01	0.41 ± 0.01	0.38 ± 0.02
H8	4.80	1.14 ± 0.01	0.98 ± 0.02	0.48 ± 0.01	0.47 ± 0.01
H7	4.78		1.22 ± 0.01		0.50 ± 0.01
H1ε	5.61	1.41 ± 0.01	1.39 ± 0.02	0.57 ± 0.01	0.56 ± 0.01
H1ζ	5.50	1.27 ± 0.01	1.29 ± 0.01	0.56 ± 0.01	0.55 ± 0.02

single-scan 1D acquisition mode: the offset and the selectivity of the 180° ^{1}H pulse as a function of the crowded area to be analyzed. It is also worth to mention that maximum sensitivity is retained, although multiple experiments would be required to monitor different overlapped areas. This fact no means a severe impediment to the method as proton relaxation times do not consume large amounts of spectrometer time. Alternatively, broadband homodecoupled for all signals present in the ^{1}H spectrum should be feasible using the instant ZS experiment [17], simply applying a gradient during the selective 180° pulses in schemes of Fig. 1, but high levels of sensitivity would be lost due to spatial encoding selection. Moreover, we can anticipate that the HOBS technique could be successfully implemented to improve the analysis in other related relaxation methods [32–34], including the measurement of selective T_1 relaxation times (T_{1sel}) [35,36] or spin–lattice relaxation times in the rotating frame (T_{1rho}) [11]. Other potential applications should be the study of reaction kinetics in complex areas or the determination of individual diffusion coefficients in

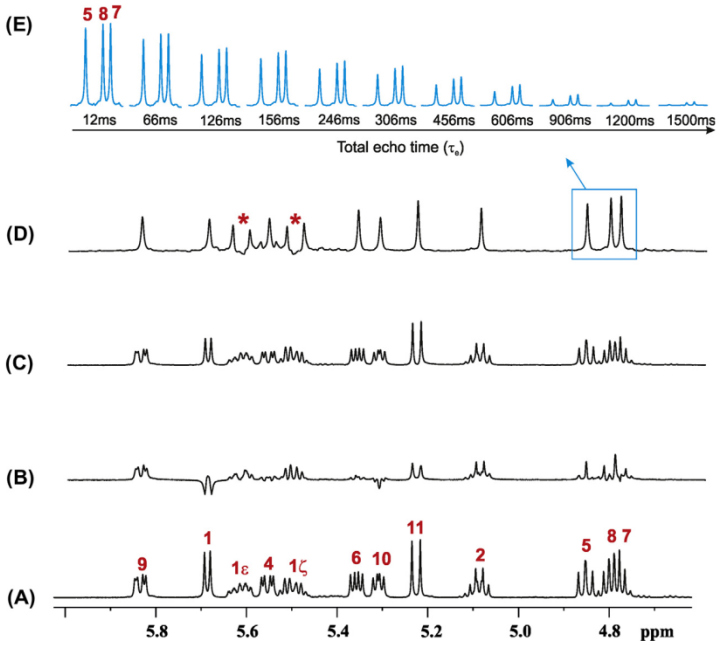

Fig. 3. Comparison of 1D (A) conventional ^{1}H, (B) CPMG, (C) PROJECT, and (D) HOBS-PROJECT spectra of cyclosporine acquired with a total echo time of τ_e = 156 ms (m = 26 and τ' = 1.5 ms). All spectra were collected under the same experimental conditions as described in Fig. 2 and are plotted at the same absolute vertical scale. (E) Signal T_2 decays for the H5, H8 and H7 protons in the HOBS-PROJECT experiment.

multi-component systems as similarly reported for analogous pure-shift DOSY experiments [15,16].

3. Conclusions

In summary, homodecoupling can improve the appearance of crowded areas of the ^{1}H spectrum by collapsing multiplet structure to singlet lines. The implementation of the HOBS technique in standard IR and PROJECT experiments can enhance the simplicity and accuracy by which T_1 and T_2 relaxation times are measured from overlapped resonances, while the sensitivity of the original experiments are retained. It has been shown that in absence of signal overlapping, individual mono-exponential decays from simplified singlet signals can be easily monitored using standard fitting procedures.

4. Methods and materials

All NMR experiments were collected at 298 K on a Bruker AVANCE spectrometer (Bruker BioSpin, Rheinstetten, Germany) operating at 600.13 MHz proton frequency, equipped with a 5 mm triple resonance inverse probe and a z-axis pulsed field gradient accessory (maximum strength of 53.5 G/cm) acquired and processed using the software TOPSPIN 3.1 (Bruker BioSpin, Rheinstetten, Germany).

The two samples used in this work were 25 mM cyclosporine (in benzene-d6) and 100 mM progesterone (in DMSO-d6). Hard 90° ^{1}H pulses of duration 7.8 μs (for cyclosporine) and 8.3 μs (for progesterone) were used in each sample. A 180° band-selective REBURP shaped pulse of 5.0 ms (for cyclosporine) and 20 ms (for progesterone) was used for both excitation and homodecoupling in HOBS experiments. The strengths of the G1, G2 and G3 gradients were set to 9.1, 21.9 and 33.7 G/cm, respectively, with durations of 500 μs followed by a recovery delay of 20 μs (δ = 520 μs). The ^{1}H spectral width was set to 7200 Hz and 8 K complex points were recorded during an acquisition time of 569 ms. 32 (for cyclosporine) and 23 (for progesterone) loops (n) were concatenated with Δ periods of 8.9 and 12.37 ms, respectively ($\Delta = AQ/2n$). The first and the last chunks are half size ($AQ/2n$) relative to the rest of chunks (AQ/n).

10 experiments with different values of recovery delay τ(0.01, 0.05, 0.1, 0.25, 0.5, 1, 2, 4, 8 and 15 s) were acquired for each IR and HOBS-IR experiment, using 8 scans and 15 s of recycle delay. 12 experiments with different number of echoes ($m - 1$ = 1, 5, 10, 20, 25, 40, 50, 75, 100, 150, 200 and 250) and a relaxation delay τ' of 1.5 ms were acquired for each PROJECT and HOBS-PROJECT experiments, using a single scan and 10 s of recycle delay. 1D time-domain data were transformed without any sensitivity or resolution enhancement, and the same phase and baseline corrections were applied for all resulting 1D spectra.

The standard IR and CPMG experiments were recorded using the *t1ir* and *cpmg1d* pulse programs that are available in the Bruker library. Pulse programs codes for Bruker spectrometers are available in our blog (http://sermn.uab.cat).

The calculation of longitudinal T_1 relaxation times was carried out with the subroutine t1guide included into the TOPSPIN3.1 software package. A set of 1D spectra recorded with different recovery delays τ were stored in a 2D data set and T_1 values were extracted by fitting the data to the equation:

$$\frac{A}{A_0} = 1 - 2e^{\left(-\frac{\tau}{T_1}\right)} \quad (1)$$

where A is the integrated area of the peak in the spectrum and A_0 is the area when $\tau \to \infty$.

The transversal T_2 relaxation times values were extracted from fitting the integrated area of a given signal as a function of total echo time τ_e assuming single exponential decay process. This natural exponential function can be rewritten in natural logarithmic

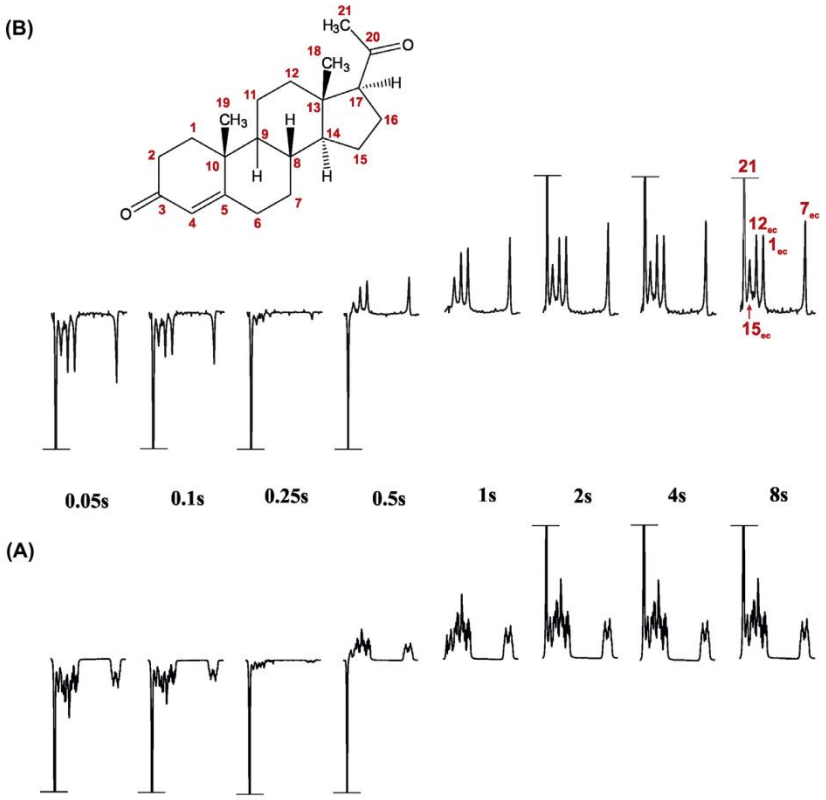

Fig. 4. Experimental decays in (A) IR and (B) HOBS-IR experiments of all protons resonating in the region 1.8–2.1 ppm in progesterone. All spectra are plotted in the same absolute vertical scale. Homodeocupling was achieved using the detection scheme described in Fig. 1A with a 20 ms REBURP 180° pulse, Δ = 12.37 ms, AQ = 569 ms and n = 23.

form where A and τ_e present a linear dependence and T_2 can be extracted from the slope:

$$A = A_0 \cdot e^{\left(-\frac{\tau_e}{T_2}\right)} \ln A = \ln A_0 - \frac{1}{T_2}\tau_e \quad (2)$$

where τ_e is calculated as $\tau_e = 4m\tau'$.

Acknowledgments

Financial support for this research provided by the spanish MINECO (project CTQ2012-32436) is gratefully acknowledged. We also thank the Servei de Ressonància Magnètica Nuclear, Universitat Autònoma de Barcelona, for allocating instrument time to this project.

Appendix A. Supplementary material

Supplementary data associated with this article can be found, in the online version, at http://dx.doi.org/10.1016/j.jmr.2014.04.003.

References

[1] V.I. Bakhmutov, Practical NMR Relaxation for Chemists, John Wiley & Sons, Chichester, 2005.
[2] P.B. Kingsley, Signal intensities and T_1 calculations in multiple-echo sequences with imperfect pulses, Conc. Magn. Reson. 11 (1999) 29–49.
[3] P.B. Kingsley, Methods of measuring spin–lattice (T_1) relaxation times: an annotated bibliography, Conc. Magn. Reson. 11 (1999) 243–276.
[4] H.Y. Carr, E.M. Purcell, Effects of diffusion and free precession in nuclear magnetic resonance experiments, Phys. Rev. 94 (1954) 630–638.
[5] S. Meiboom, D. Gill, Modified spin-echo method for measuring nuclear relaxation times, Rev. Sci. Instrum. 29 (1958) 688–691.
[6] J.A. Aguilar, M. Nilsson, G. Bodenhausen, G.A. Morris, Spin-echo NMR spectra without J modulation, Chem. Commun. 48 (2012) 811–813.
[7] T.F. Segawa, G. Bodenhausen, Determination of transverse relaxation rates in systems with scalar-coupled spins: the role of antiphase coherences, J. Magn. Reson. 237 (2013) 139–146.
[8] A.A. Istratov, O.F. Vyvenk, Exponential analysis in physical phenomena, Rev. Sci. Instrum. 70 (1999) 1233–1257.
[9] K. Holmström, J. Petersson, A review of the parameter estimation problem of fitting positive exponential sums to empirical data, Appl. Math. Comput. 126 (2002) 31–61.
[10] G.L. Bretthorst, W.C. Hutton, J.R. Garbow, J.J.H. Ackerman, Exponential parameter estimation (in NMR) using Bayesian probability theory, Conc. Magn. Reson. Part A 27 (2005) 55–63.
[11] B. Boulat, R. Konrat, I. Burghardt, G. Bodenhausen, Measurement of relaxation rates in crowded NMR spectra by selective coherence transfer, J. Am. Chem. Soc. 114 (1992) 5412–5414.
[12] L.E. Kay, D.A. Torchia, A. Bax, Backbone dynamics of proteins as studied by ^{15}N inverse detected heteronuclear NMR spectroscopy: application to staphylococcal nuclease, Biochemistry 28 (1989) 8972–8979.
[13] S. Simova, H. Sengstschmid, R. Freeman, Proton chemical-shift spectra, J. Magn. Reson. 124 (1997) 104–121.
[14] K. Zangger, H. Sterk, Homonuclear broadband-decoupled NMR spectra, J. Magn. Reson. 124 (1997) 486–489.
[15] J.A. Aguilar, S. Faulkner, M. Nilsson, G.A. Morris, Pure shift ^{1}H NMR: a resolution of the resolution problem?, Angew Chem. Int. Ed. 49 (2010) 3901–3903.
[16] M. Nilsson, G.A. Morris, Pure shift proton DOSY: diffusion-ordered ^{1}H spectra without multiplet structure, Chem. Commun. 9 (2007) 933–935.
[17] N.H. Meyer, K. Zangger, Simplifying proton NMR spectra by instant homonuclear broadband decoupling, Angew. Chem. Int. Ed. 52 (2013) 7143–7146.
[18] N.H. Meyer, K. Zangger, Boosting the resolution of ^{1}H NMR spectra by homonuclear broadband decoupling, ChemPhysChem 15 (2014) 49–55.
[19] J.R. Garbow, D.P. Weitekamp, A. Pines, Bilinear rotation decoupling of homonuclear scalar interactions, Chem. Phys. Lett. 93 (1982) 504–509.

[20] P. Sakhaii, B. Haase, W. Bermel, Experimental access to HSQC spectra decoupled in all frequency dimensions, J. Magn. Reson. 199 (2009) 192–198.
[21] A. Lupulescu, G.L. Olsen, L. Frydman, Toward single-shot pure-shift solution ^{1}H NMR by trains of BIRD-based homonuclear decoupling, J. Magn. Reson. 218 (2012) 141–146.
[22] P. Sakhaii, B. Haase, W. Bermel, R. Kerssebaum, G.E. Wagner, K. Zangger, Broadband homodecoupled NMR spectroscopy with enhanced sensitivity, J. Magn. Reson. 233 (2013) 92–95.
[23] T. Reinsperger, B. Luy, Homonuclear BIRD-decoupled spectra for measuring one-bond couplings with highest resolution: CLIP/CLAP-RESET and constant-time-CLIP/CLAP-RESET, J. Magn. Reson. 239 (2014) 110–120.
[24] I. Timári, L. Kaltschnee, A. Kolmer, R.W. Adams, M. Nilsson, C.M. Thiele, G.A. Morris, K.E. Kövér, Accurate determination of one-bond heteronuclear coupling constants with "pure shift" broadband proton-decoupled CLIP/CLAP-HSQC experiments, J. Magn. Reson. 239 (2014) 130–138.
[25] L. Castañar, P. Nolis, A. Virgili, T. Parella, Full sensitivity and enhanced resolution in homodecoupled band-selective NMR experiments, Chem. Eur. J. 19 (2013) 17283–17286.
[26] J. Ying, J. Roche, A. Bax, Homonuclear decoupling for enhancing resolution and sensitivity in NOE and RDC measurements of peptides and proteins, J. Magn. Reson. 241 (2014) 97–102.
[27] L. Castañar, M. Pérez-Trujillo, P. Nolis, E. Monteagudo, A. Virgili, T. Parella, Enantiodifferentiation through frequency-selective pure-shift ^{1}H nuclear magnetic resonance spectroscopy, ChemPhysChem 15 (2014) 854–857.
[28] R.W. Adams, L. Byrne, P. Király, M. Foroozandeh, L. Paudel, M. Nilsson, J. Clayden, G.A. Morris, Diastereomeric ratio determination by high sensitivity band-selective pure shift NMR spectroscopy, Chem. Commun. 50 (2014) 2512–2514.
[29] L. Castañar, J. Saurí, P. Nolis, A. Virgili, T. Parella, Implementing homo- and heterodecoupling in region-selective HSQMBC experiments, J. Magn. Reson. 238 (2014) 63–69.
[30] G.A. Morris, H. Barjat, T.J. Horne, Reference deconvolution methods, Prog. NMR Spectrosc. 31 (1997) 197–257.
[31] M. Geppi, C. Forte, The SPORT-NMR software: a tool for determining relaxation times in unresolved NMR spectra, J. Magn. Reson. 137 (1999) 177–185.
[32] N.M. Loening, M.J. Thrippleton, J. Keeler, R.G. Griffin, Single-scan longitudinal relaxation measurements in high-resolution NMR spectroscopy, J. Magn. Reson. 164 (2003) 321–328.
[33] R. Bhattacharyy, A. Kumar, A fast method for the measurement of long spin–lattice relaxation times by single scan inversion recovery experiment, Chem. Phys. Lett. 383 (2004) 99–103.
[34] P.E.S. Smith, K.J. Donovan, O. Szekely, M. Baias, L. Frydman, Ultrafast NMR T1 relaxation measurements: probing molecular properties in real time, ChemPhysChem 13 (2013) 3138–3145.
[35] F.W. Dahlquist, K.J. Longmur, R.B. Du Vernet, Direct observation of chemical exchange by a selective pulse NMR technique, J. Magn. Reson. 17 (1975) 406–410.
[36] D.A. Leigh, A. Murphy, J.P. Smart, M.S. Deleuze, F. Zerbetto, Controlling the frequency of macrocyclic ring rotation in benzylic amide [2]catenanes, J. Am. Chem. Soc. 120 (1998) 6458–6467.

Supporting Information

Measurement of T_1/T_2 relaxation times in overlapped regions from homodecoupled ^{1}H singlet signals

Laura Castañar, Pau Nolis, Albert Virgili and Teodor Parella*

Contents

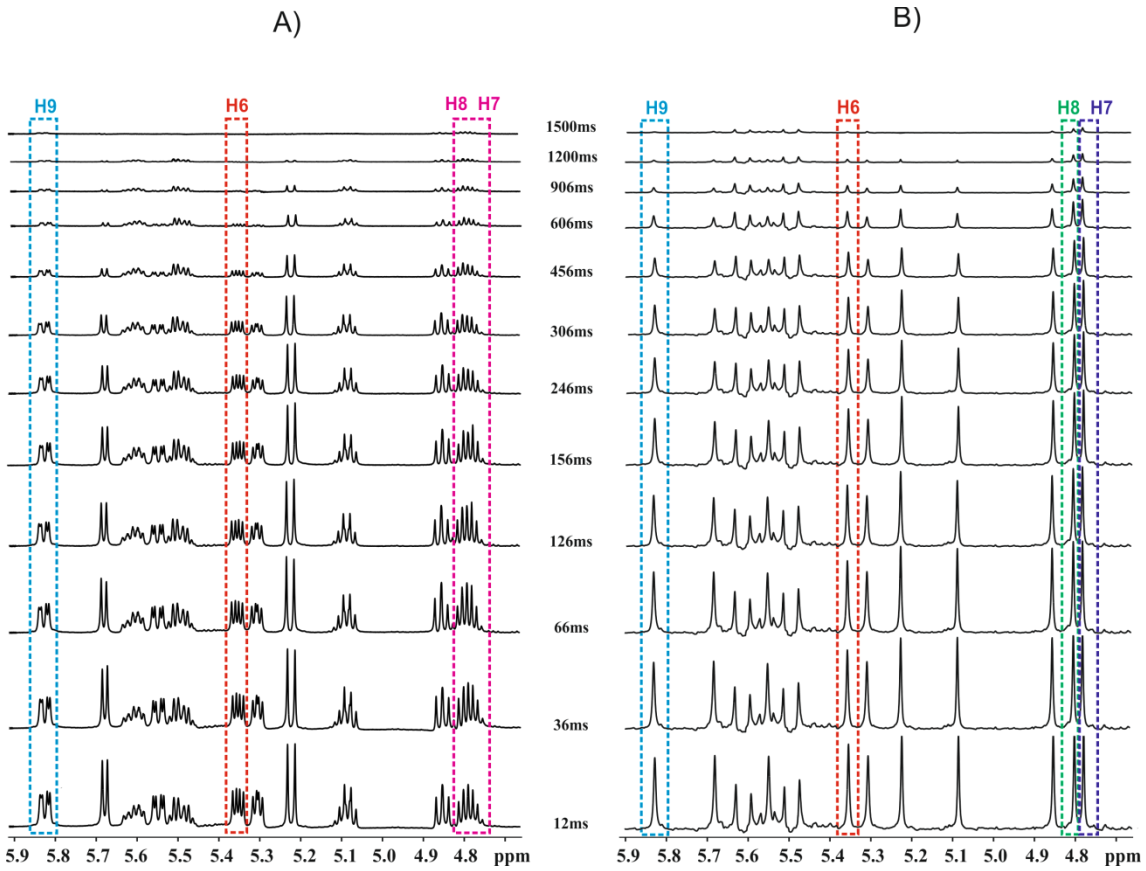

Figure S1: Stacked plot of the A) PROJECT and B) HOBS-PROJECT spectra corresponding to the H_α region of cyclosporine (see Fig. 1B of the manuscript), using the conditions described in the experimental section. The Fig. 3E in the manuscript shows an expanded area of the spectra B covering signals resonating between 4.76 and 4.90 ppm.

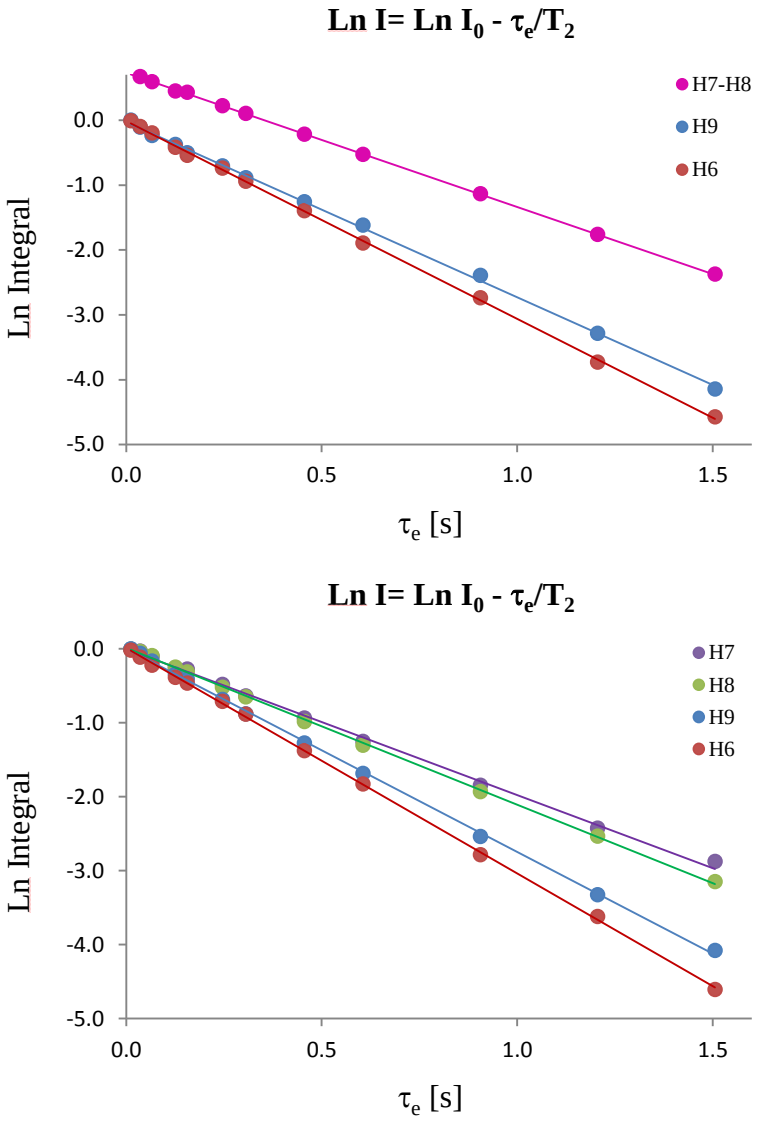

Figure S2: Comparison of the experimental mono-exponential T_2 signal decays for the isolated H6 and H9 protons and also for the overlapped H7 and H8 protons of cyclosporine in (top) PROJECT vs (bottom) HOBS-PROJECT experiments. See experimental values in Table 1.

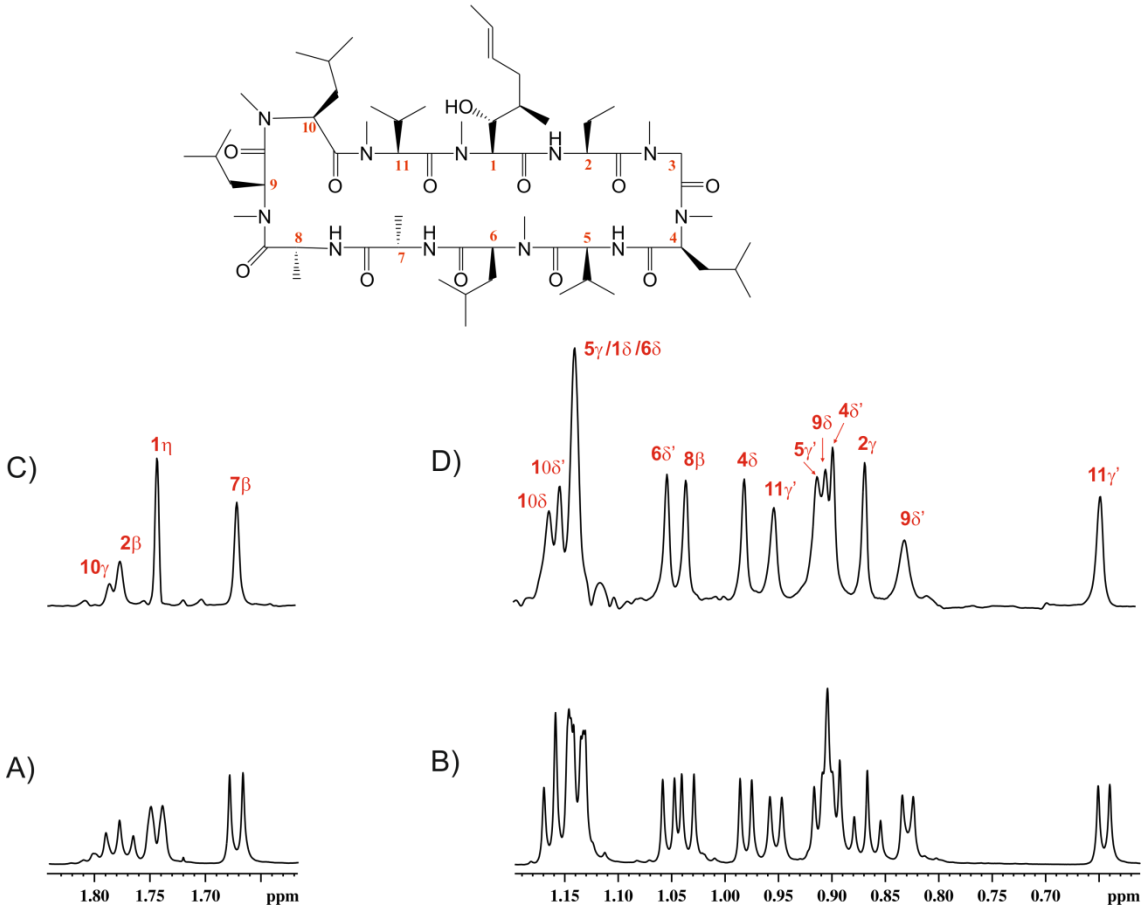

Figure S3: 600MHz 1D ^{1}H A-B) conventional and C-D) HOBS spectrum of cyclosporine after selective excitation and homodecoupling of two different aliphatic regions (Reburp 180º ^{1}H pulse of 20 ms in C and 10 ms in D, Δ=8.1 ms, AQ=569 ms and n=35 as a homodecoupling conditions). These same conditions have been used in the HOBS-IR experiment shown in Fig. S4. Both spectra are plotted in the same absolute vertical scale to compare absolute sensitivities after signal collapsing.

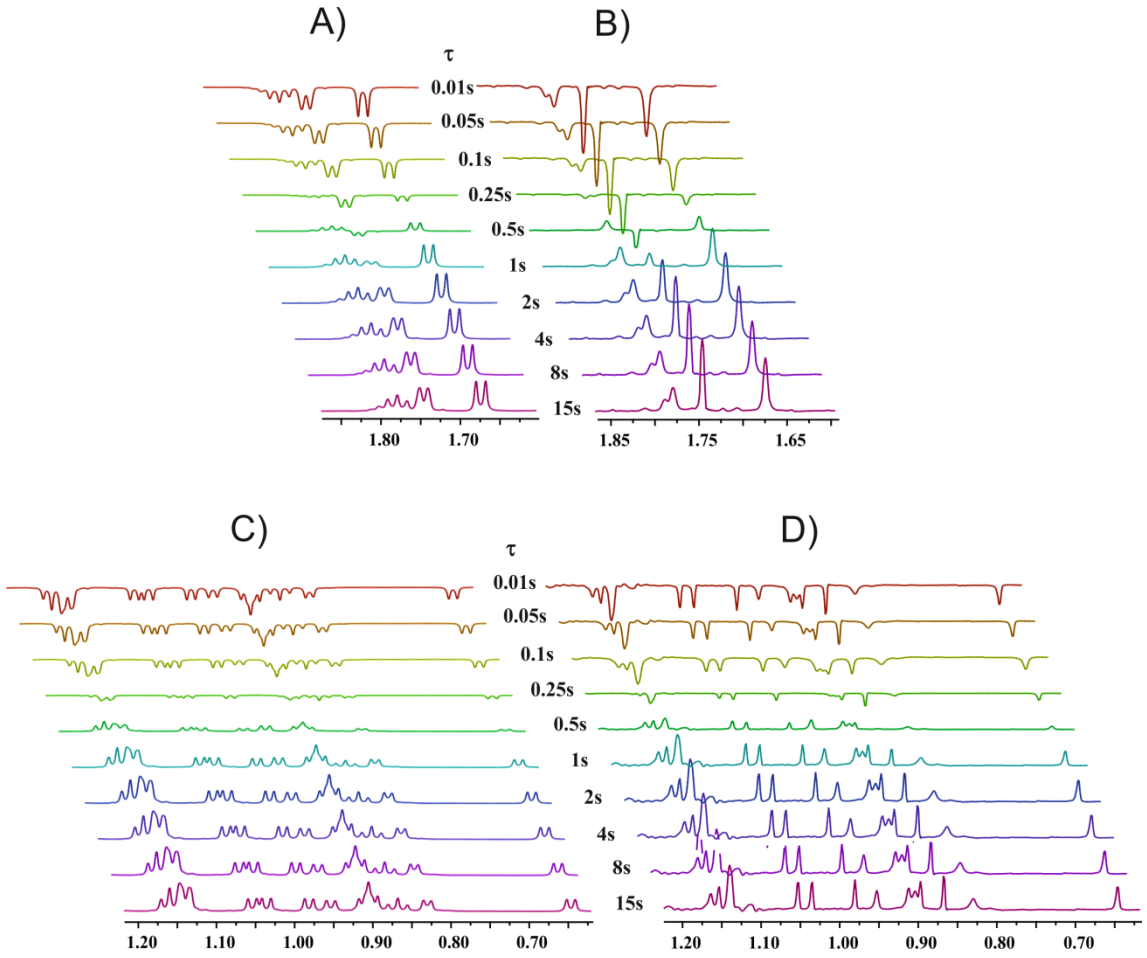

Figure S4: IR and HOBS-IR experiments of the selected aliphatic areas described in Fig. S3. The homodecoupling conditions in B and D were the same as described in Fig. S3 and the experimental T_1 values are shown in Table S1.

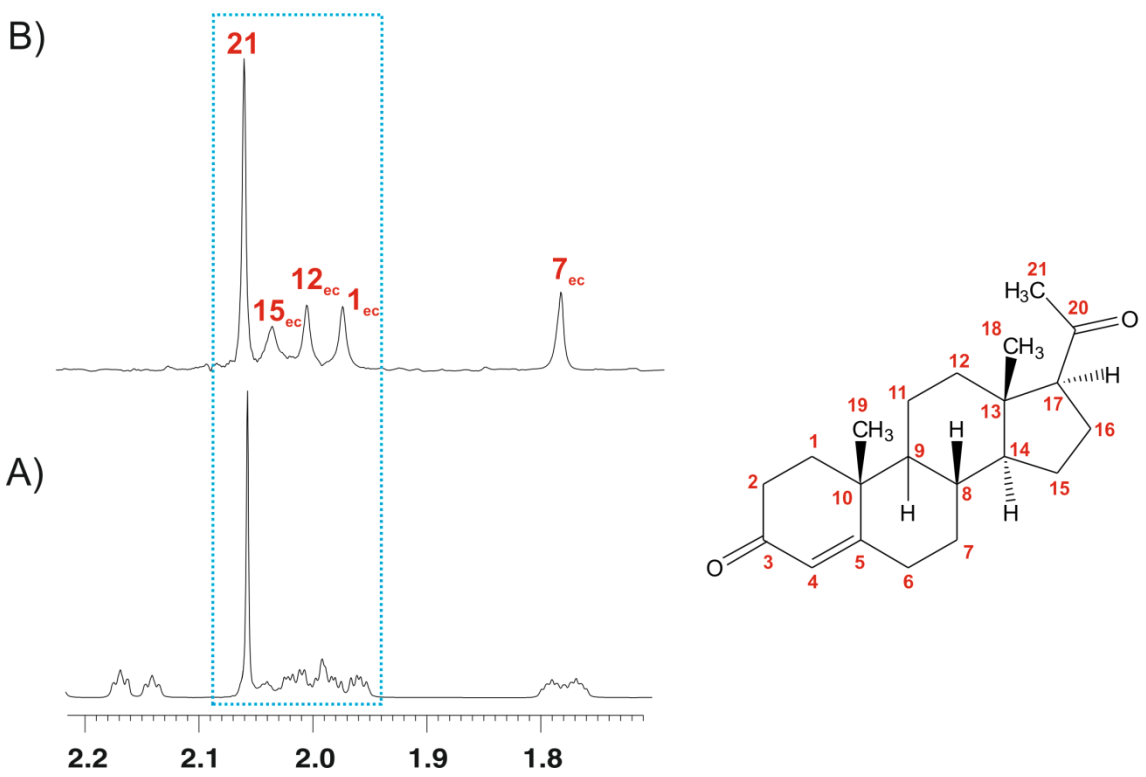

Figure S5: 600MHz 1D ^{1}H A) conventional and B) HOBS spectrum after selective excitation and homodecoupling at 2.0 ppm in progesterone (Reburp 180º ^{1}H pulse of 20ms, Δ=12.37 ms, AQ=569 ms and n=23 as a homodecoupling conditions). These same conditions have been used in the HOBS-IR experiment shown in Fig. 4 of the manuscript and in the HOBS-PROJECT shown in the next Fig. S6. A single scan was collected and both spectra are plotted in the same absolute vertical scale to compare absolute sensitivities after signal collapsing.

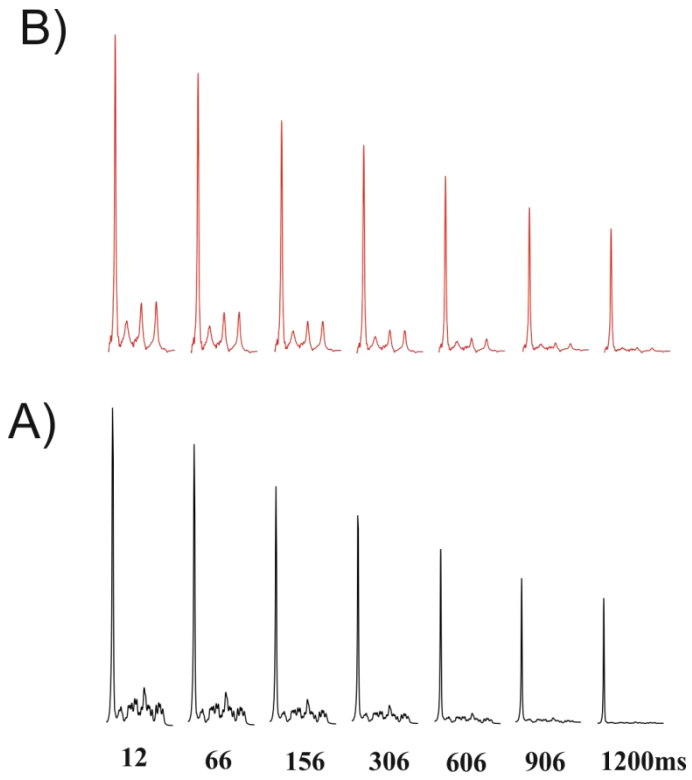

Figure S6: Stacked plot of the 600 MHz 1D spectra of progesterone acquired with the A) PROJECT and B) HOBS-PROJECT experiments using the conditions described in experimental section and Fig. S5. The individual T_2 values can be found in Table S2.

		T_1 measurement [s]	
Proton	δ [ppm]	IR	HOBS-IR
H10γ	1.79	0.53 ± 0.01	0.58 ± 0.01
H2β	1.78		0.51 ± 0.01
H1η	1.74	1.00 ± 0.02	1.02 ± 0.02
H7β	1.67	0.52 ± 0.01	0.50 ± 0.02
H10δ	1.16	0.48± 0.01	0.41 ± 0.02
H10δ'	1.15		0.44 ± 0.01
H5γ			
H1δ	1.14		0.52 ± 0.01
H6δ			
H6δ'	1.06	0.49 ± 0.01	0.48 ± 0.01
H8β	1.03		0.50 ± 0.01
H4δ	0.98	0.52 ± 0.01	0.53 ± 0.01
H11γ	0.95	0.38 ± 0.01	0.40 ± 0.02
H5γ'	0.91	0.48 ± 0.01	0.50 ± 0.02
H9δ	0.90		0.48 ± 0,02
H4δ'	0.89		0.48 ± 0,02
H2γ	0.86	0.65 ± 0.01	0.62 ± 0,03
H9δ	0.83	0.52 ± 0.01	0.52 ± 0.01
H11γ'	0.65	0.58 ± 0.01	0.59 ± 0.01

The error is given by the error of the exponential fit.

Table S1: Experimental T_1 values obtained from IR and HOBS-IR experiments for the proton signals displayed in the aliphatic areas of cyclosporine represented in Fig. S4.

		T_1 measurement [s]		T_2 measurement [s]	
H signal	δ [ppm]	IR	HOBS-IR	PROJECT	HOBS-PROJECT
H_{21}	2.07	1.38 ± 0.02	1.36 ± 0.02	1.35 ± 0.01	1.36 ± 0.01
$H15_{eq}$	2.05		0.55 ± 0.01		0.56 ± 0.01
$H12_{eq}$	2.02	0.46 ± 0.01	0.46 ± 0.01	0.50 ± 0.01	0.51 ± 0.01
$H1_{eq}$	1.99		0.41 ± 0.01		0.44 ± 0.01
$H7_{eq}$	1.80	0.40 ± 0.01	0.42 ± 0.01	0.51 ± 0.01	0.50 ± 0.01

The error is given by the error of the exponential fit

Table S2: Experimental T_1 and T_2 values obtained from IR, HOBS-IR, PROJECT and HOBS-PROJECT experiments for the five different proton signals resonating at the region 1.8-2.1 ppm in progesterone.

Pulse Program Code for Bruker: HOBS-IR

```
;HOmodecoupled Band-Selective Inversion Recovery NMR experiment (HOBS-IR)
;T1 measurement using inversion recovery
;1D Experiment
;Avance III version (17/07/2013)
;Topspin3.1

#include <Avance.incl>
#include <Grad.incl>
#include <Delay.incl>
#include <De.incl>

dwellmode explicit

"p2=p1*2"
"d2=aq/l0"
"d3=d2/2"
"l1=l0-1"
"acqt0=-p1*2/3.1416"

1 ze
2 d1  pl1:f1
  50u UNBLKGRAD
  p2 ph1
  d7 pl1:f1
  p1 ph2
  d16 pl0:f1
  p16:gp1
  (p12:sp2 ph3)
  p16:gp1
  d16
                                          ;starts HOBS
  ACQ_START(ph30,ph31)
  0.05u setrtp1|0
  0.1u setrtp1|5
  d3:r
  0.1u setrtp1^5
  0.05u setrtp1^0

  p16:gp2
  d16 pl1:f1
  p2 ph4
  p16:gp2
  d16

  p16:gp3
  d16 pl0:f1
  (p12:sp2 ph3)
  p16:gp3
  d16
```

```
3 0.05u setrtp1|0
  0.1u setrtp1|5
  d2:r
  0.1u setrtp1^5
  0.05u setrtp1^0

  p16:gp2
  d16 pl1:f1
  p2 ph4
  p16:gp2
  d16

  p16:gp3
 d16 pl0:f1
 (p12:sp2 ph3)
 p16:gp3
 d16
lo to 3 times l1

 0.05u setrtp1|0
 0.1u setrtp1|5
 d3
 5m
 0.1u setrtp1^5
 0.05u setrtp1^0

rcyc=2
wr #0
exit

ph1=0
ph2=0
ph3=0
ph30=0
ph31=0

;pl1 : f1 channel - power level for pulse (default)
;p1 : f1 channel -  90 degree high power pulse
;p2 : f1 channel - 180 degree high power pulse
;p12 : f1 channel - 180 degree band-selective pulse [ms]
;p16: homospoil/gradient pulse [500 us]
;sp2: f1 channel - shaped pulse power level for band-selective excitation
;spnam2: shaped pulse for selective excitation [REBURP]
;d1 :relaxation delay; 1-5 * T1
;d7 : delay for inversion recovery
;NS : 1 * n, total number of scans: NS * TD0
;DS: 0
;l1: number of concatenated loops

;use gradient files:
;gpnam1: SMSQ10.100
;gpnam2: SMSQ10.100
;gpnam3: SMSQ10.100
```

Pulse Program Code for Bruker: HOBS-PROJECT

```
;use gradient files:
;gpnam1: SMSQ10.100
;HOmodecoupled Band-Selective Periodic Refocusing of J Evolution
; by Coherence Transfer NMR experiment (HOBS-PROJECT)
;T2 measurement
;1D Experiment
;Avance III version (13/07/2013)
;Topspin3.1

#include <Avance.incl>
#include <Grad.incl>
#include <Delay.incl>
#include <De.incl>

"p2=p1*2"
"d12=20u"
"DELTA1=d20-p1*2/3.1416"
"DELTA2=d20-p16-d16-de"
"DELTA3=d20-p16-d16"
"acqt0=0"

dwellmode explicit

"d2=aq/l0"
"d3=d2/2"
"l1=l0-1"

1 ze
2 30m
  d1
  50u UNBLKGRAD
  d12 pl1:f1
  p1 ph1
  DELTA1
  p2 ph2
  d20

3 d20
  p2 ph2
  d20
  p1 ph2
  d20
  p2 ph2
  d20
  lo to 3 times l4

  DELTA3 pl0:f1
  p16:gp1
  d16
  p12:sp2:f1 ph2
  p16:gp1
```

```
  d16
  DELTA2
                                    ;starts HOBS
ACQ_START(ph30,ph31)

  0.05u setrtp1|0
  0.1u setrtp1|5
  d3:r
  0.1u setrtp1^5
  0.05u setrtp1^0

  p16:gp2
  d16 pl1:f1
  p2 ph4
  p16:gp2
  d16

  p16:gp3
  d16 pl0:f1
  (p12:sp2 ph3)
  p16:gp3
  d16

4 0.05u setrtp1|0
  0.1u setrtp1|5
  d2:r
  0.1u setrtp1^5
  0.05u setrtp1^0

  p16:gp2
  d16 pl1:f1
  p2 ph4
  p16:gp2
  d16

  p16:gp3
  d16 pl0:f1
  (p12:sp2 ph3)
  p16:gp3
  d16
lo to 4 times l1

 0.05u setrtp1|0
 0.1u setrtp1|5
 d3
 5m
 0.1u setrtp1^5
 0.05u setrtp1^0

rcyc=2
wr #0

exit
```

```
ph1=0
ph2=1
ph4=0
ph3=0
ph30=0
ph31=0



;pl1 : f1 channel - power level for pulse (default)
;p1 : f1 channel -  90 degree high power pulse
;p2 : f1 channel - 180 degree high power pulse
;p12 : f1 channel - 180 degree band-selective pulse [ms]
;sp2: f1 channel - shaped pulse power level for band-selective excitation
;spnam2: shaped pulse for selective excitation [REBURP]
;d1 : relaxation delay; 1-5 * T1
;d12: delay for power switching                  [20 usec]
;p16: homospoil/gradient pulse                  [500 us]
;d20: fixed echo time to allow elimination of J-mod. effects
;l1: number of concatenated loops for homodecoupling
;l4: loop for T2 filter                         [4 - 20]
;NS: 1 * n, total number of scans: NS * TD0
;DS: 0

;use gradient files:
;gpnam1: SMSQ10.100
;gpnam2: SMSQ10.100
;gpnam3: SMSQ10.100
```

PUBLICATION 4

Enantiodifferentiation through frequency-selective pure shift ^{1}H nuclear magnetic resonance spectroscopy

Laura Castañar, Miriam Pérez-Trujillo, Pau Nolis, Eva Monteagudo, Albert Virgili and Teodor Parella.

ChemPhysChem, **2014**, *15*, 854-857.

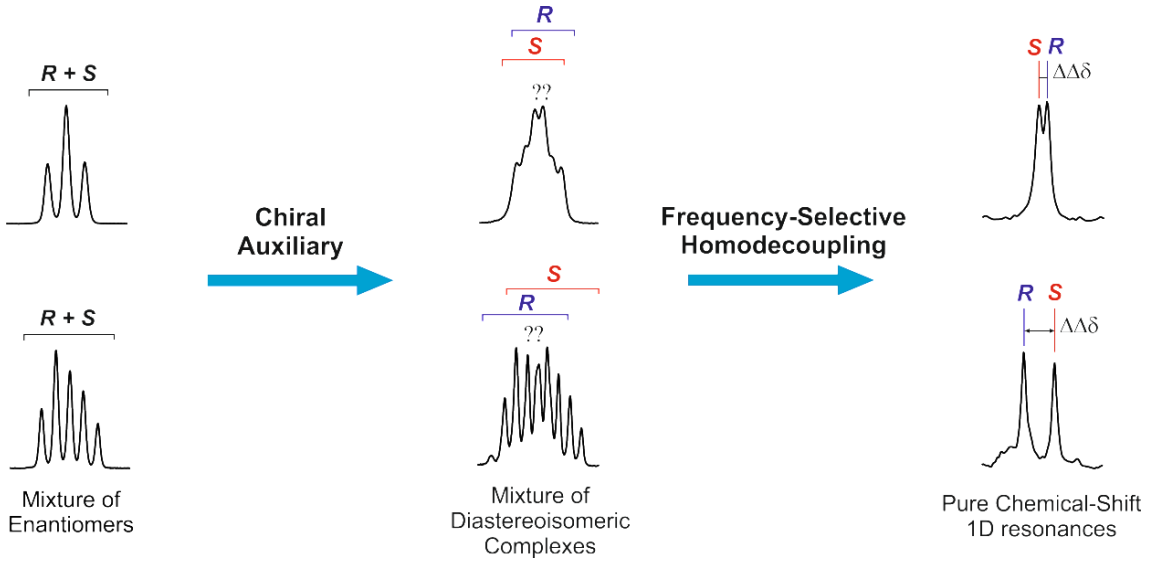

Introduction

NMR spectroscopy has proved to be a valuable technique to determine enantiomeric purity using a great variety of auxiliary chiral sources, as for example *Chiral Solvating Agents* (CSAs).[90] In the case of using CSAs, the initial indistinguishable mixture of enantiomers is converted into a chemical-shift δ-resolved mixture of complementary diastereomeric complexes. As soon as there is enough chemical shift difference to achieve resolution between the signals of analogous nuclei in these diastereomeric complexes, the measure of enantiomeric purity can be carried out by direct signal integration. However, J_{HH} broaden ^{1}H NMR resonances and accurate enantiomeric excess quantification is often hampered because of partial signal overlapping.

The features of pure shift experiments provide a great tool to avoid these overlapping problems. In this article, the HOBS methodology (see **Publication 2**) is proposed for the fast and efficient determination of very small chemical-shift differences between overlapped resonances. It is demonstrated that the frequency-selective homodecoupled method is a robust and sensitive analytical NMR spectroscopy tool for the fast and simple enantiodifferentiation and determination of the enantiomeric excess of organic molecules using CSAs. Its major advantage lies in the single-scan and 1D real-time acquisition modes, as the resulting simplified singlet signals facilitate a better analysis. Additionally, it has been shown that homodecoupled signals can also be retrieved for resonances obscured by other more intense signals or in overcrowded regions by using a preparatory TOCSY editing.

[90] a) S. R. Chaudhari, S. N, Suryaprakash, *J. Indian Inst. Sci.,* **2014**, *94*, 485. b) W. H. Pirkle, D. J. Hoover, *NMR Chiral Solvating Agents*, **2007**, vol. 13 of Topics in Stereochemistry, Wiley, Hoboken.

CHEMPHYSCHEM
COMMUNICATIONS

ChemPubSoc Europe

DOI: 10.1002/cphc.201301130

Enantiodifferentiation through Frequency-Selective Pure-Shift ^{1}H Nuclear Magnetic Resonance Spectroscopy

Laura Castañar, Míriam Pérez-Trujillo, Pau Nolis, Eva Monteagudo, Albert Virgili, and Teodor Parella*[a]

A frequency-selective 1D ^{1}H nuclear magnetic resonance (NMR) experiment for the fast and sensitive determination of chemical-shift differences between overlapped resonances is proposed. The resulting fully homodecoupled ^{1}H NMR resonances appear as resolved 1D singlets without their typical *J*(HH) coupling constant multiplet structures. The high signal dispersion that is achieved is then exploited in enantiodiscrimination studies by using chiral solvating agents.

Nuclear magnetic resonance (NMR) spectroscopy in the presence of chiral auxiliaries is a particularly well-adapted technique for determining the enantiomeric purity and, in some cases, the absolute configuration of chiral molecules.[1] Different approaches are available to accomplish enantiodifferentiation, including chemical derivatization,[2] chiral solvating agents (CSAs),[3] and the use of chiral liquid crystals.[4] In the case of CSAs, the NMR method simply requires the use of a suitable chiral derivative that converts the initial indistinguishable mixture of enantiomers into a chemical-shift (δ)-resolved mixture of complementary diastereomeric complexes. As soon as there is a large enough δ nonequivalence to achieve resolution between the signals ($\Delta\Delta\delta$) of analogous nuclei in these diastereomeric complexes, integration can enable the direct measurement of enantiomeric purity. However, homonuclear scalar couplings (J(HH)) broaden ^{1}H NMR resonances, and accurate enantiomeric excess (*ee*) quantification by optimum signal discrimination is often hampered because of partial signal overlapping and low chemical-shift dispersion ($\Delta\Delta\delta \ll \Delta\omega$, where $\Delta\omega$ is the overall width of the multiplet). The use of selective homonuclear decoupling to simplify the multiplet structure is insufficient to completely resolve overlapping.[5] However, the analysis of better-resolved fully decoupled singlet resonances in heteronuclear-decoupled ^{13}C NMR spectra is an alternative, which avoids signal overlapping, but its low sensitivity remains a limiting factor for practical use.[6] Recently, several NMR methods have been proposed to obtain pure chemical-shift ^{1}H NMR spectra.[7–11] Based on a recent instant broadband homodecoupled experiment,[10] an analogous region-selective version that does not suffer sensitivity loss but maintains the benefits of obtaining simplified singlet resonances has been reported.[11] We evaluate here the potential of this strategy for the fast and efficient enantiodifferentiation of organic molecules using CSAs.

The proposed NMR experiment (Figure 1) can be understood as a homodecoupled version of the regular 1D single pulsed-field-gradient echo (SPFGE) scheme, in which a frequency-selective 180° pulse is applied to ^{1}H NMR resonances of interest; the novelty lies in the incorporation of a broadband homodecoupling element into the acquisition period.[11] The resulting 1D ^{1}H NMR spectrum only shows the selected resonances as collapsed singlet lines, without their typical *J*(HH) multiplet structure, and from which accurate chemical-shift values can be determined, even for overlapped resonances. As the sensitivity is fully retained, data acquisition can be performed quickly with the same spectrometer time required for a conventional ^{1}H NMR spectrum. Experimentally, only a single selective 180° pulse needs to be setup, as a function of its excitation offset and the required selectivity for both excitation/homodecoupling purposes. We found that Gaussian-shaped pulses with a duration of around 10–20 ms provide good results, in terms of resolution, without a considerable decrease in the signal-to-noise ratio (SNR), owing to transverse relaxation during acquisition. Average line widths at half height of the singlets ($\nu_{1/2}$) of about 3.5–4.0 Hz are achieved by using homodecoupling settings of $\Delta = 15$–25 ms, $n = 11$–20, and $AQ = 600$ ms (where *AQ* is the acquisition time and *n* the number of concatenated loops), whereas $\nu_{1/2} = 2.3$–2.7 Hz values are generally found in

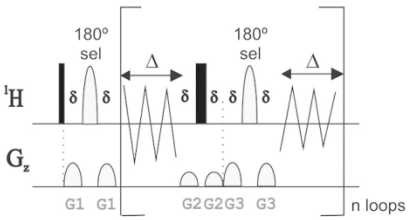

Figure 1. Pulse sequence for obtaining fully homodecoupled singlet resonances in a selected narrow part of the ^{1}H NMR spectrum. Broadband homodecoupling during detection was achieved by applying a pair of hard/selective 180° pulses (represented as solid and shaded shapes) at the middle of $2\Delta = AQ/n$ periods. Gradients G1, G2, and G3 flanking the refocusing pulses are individually optimized to provide a clean spectrum. δ represents the duration of a pulsed field gradient and its recovery delay.

[a] *L. Castañar, Dr. M. Pérez-Trujillo, Dr. P. Nolis, Dr. E. Monteagudo, Prof. A. Virgili, Dr. T. Parella*
Servei de Ressonància Magnètica Nuclear and Departament de Química
Universitat Autònoma de Barcelona, 08193 Bellaterra (Spain)
Tel: (+34) 935812291
E-mail: teodor.parella@uab.cat

Supporting Information for this article is available on the WWW under http://dx.doi.org/10.1002/cphc.201301130.

CHEMPHYSCHEM
COMMUNICATIONS
www.chemphyschem.org

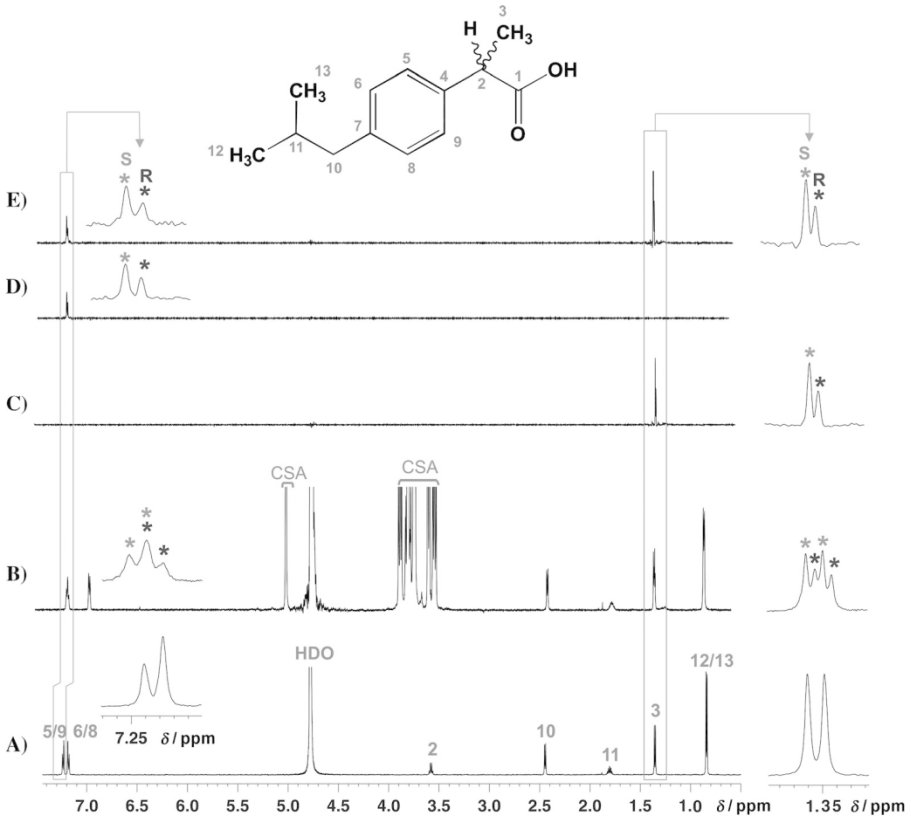

Figure 2. 600 MHz ^{1}H NMR spectra of 2.8 mM (*R*,*S*)-ibuprofen (35:65 proportion) in D_2O: A) before and B) after the addition of 3.6 equivalents of β-CD as the CSA. Selective pure-shift ^{1}H NMR spectra acquired according to Figure 1 after selection of the C) H3, D) H5, and E) both H3 and H5 protons with a Gaussian-shaped 180° pulse of 20 ms ($\Delta = 25.8$ ms, $AQ = 568$ ms, and $n = 11$). For comparison, all spectra were acquired and processed under the same conditions (a single scan for each individual 1D spectrum has been recorded with the same receiver gain) and plotted in the same vertical scale to visualize real absolute sensitivities.

the regular ^{1}H NMR spectrum (see Figure S1 in the Supporting Information).

As a proof of principle, the practicality of the method is demonstrated in the study of an (*R*,*S*) mixture of ibuprofen in the presence of β-cyclodextrin (β-CD) as the CSA (Figure 2).[3d] Whereas the conventional ^{1}H NMR spectrum shows poor signal separation between equivalent diastereomeric protons (Figure 2B), the clean homodecoupled 1D spectra simplifies the appearance of complex peaks and shows separated singlet resonances, which facilitates a better analysis and quantification (Figure 2C,D). It is worth noting that the sensitivity for each individual selective homodecoupled 1D spectrum is keep at a similar level to the conventional ^{1}H NMR spectrum, and, therefore, each one of these spectra can be obtained by using a single scan within few seconds and without any extra data processing requirement.

Figure 3 shows another example of the fast and sensitive discrimination of several ^{1}H NMR resonances belonging to a racemic mixture of (*R*,*S*)-1-aminoindan in the presence of Pirkle alcohol as the CSA.[3c] A straightforward comparison between the conventional (Figure 3B) and the fully homodecoupled multiplets (Figure 3C) shows that a simpler and more reliable determination of the chemical-shift differences and *R*/*S* molar ratios is possible, considering the highly dispersed singlets that are independent of the original multiplet complexity. In terms of quantification, it is important to note that deviations of the homodecoupling conditions ($\Delta \ll 1/J_{HH}$)[10] can lead to sidebands flanking each pure-shifted resonance at a spacing of $2n/AQ$ (see Tables S1 and S2 in the Supporting Information).

Although one limitation of the method could be its frequency-selective nature, it is not restricted to a single resonance for each individual experiment, because multiple signals can be simultaneously monitored by using band-selective[11] or multiple-frequency pulses,[12] as long as the excited protons are not mutually *J*-coupled (Figure 2E). The proposed method surpasses some other NMR approaches to discriminate enantiomers because it avoids time-consuming 2D acquisitions and/or measurements made from the unresolved indirect dimension.[13] However, homodecoupled ^{1}H NMR signals for all available resonances in the spectrum can be obtained by using other broadband pure chemical-shift NMR methods[7,11–13] although they can suffer significant decreases in sensitivity. The

CHEMPHYSCHEM
COMMUNICATIONS
www.chemphyschem.org

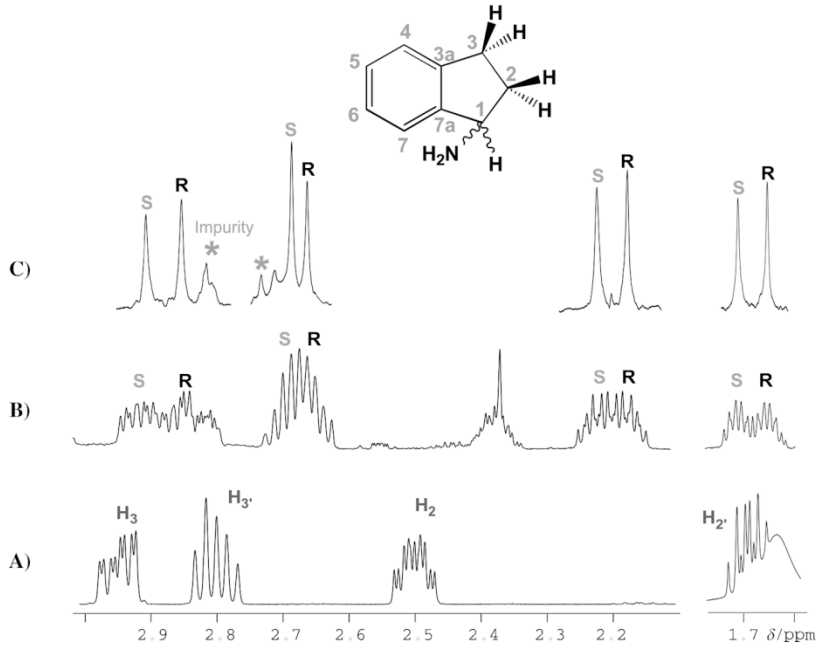

Figure 3. 600 MHz ^{1}H NMR spectra of 50 mM (*R,S*)-1-aminoindan (1:1 proportion) in $CDCl_3$: A) before and B) after the addition of 4.5 equivalents of (*R*)-(−)-1-(9-anthryl)-2,2,2-trifluoroethanol (Pirkle alcohol) as the CSA. C) Expanded multiplets extracted from individual selective 1D homodecoupled experiments acquired according to Figure 1 by using a Gaussian-shaped 180° pulse of 20 ms ($\Delta = 18.93$ ms, $AQ = 2.27$ s, and $n = 60$). For comparison, all spectra were acquired and processed under the same conditions (a single scan for each individual 1D spectrum has been recorded with the same receiver gain) and plotted in the same vertical scale to visualize real absolute sensitivities.

projection along the detected dimension of a *J*-resolved experiment requires a 2D-acquisition mode, and, therefore, the SNR reduction is proportional to the number of acquired increments.[7] Otherwise, the original Zangger–Sterk (ZS) method shows better line widths, but it requires a pseudo-2D data-collection process and presents severe sensitivity losses, owing to spatial frequency encoding.[8] Recently, single-shot ZS methods have been proposed for the fast acquisition of broadband homodecoupled 1D ^{1}H NMR spectra, but they also experience considerable sensitivity losses because of ^{13}C editing[9] or spatial selection.[10] The use of multiple slice selection through sequential or simultaneous slice excitation[14] can improve the relative SNR, but the sensitivity levels are still far from those obtained in the conventional ^{1}H NMR spectra. In terms of SNR per time unit, a single selective method is more than one order of magnitude more sensitive than the aforementioned pure-shift methods, which ensures that, for small molecules, recording series of individual selective 1D experiments can be faster and more effective than running a broadband experiment. As an example, the experimental SNR of each selective experiment is about 20 times higher than the real-time instant ZS experiment.[10] A comparison on the relative SNR for several pure-shifts methods can be found in Figure S2 (see the Supporting Information).

Interestingly, the proposed homodecoupled 1D method can be extended for the rapid visualization of singlet signals for those resonances that appear in highly overcrowded areas and that, in many cases, cannot be directly observed. This is the case for the H2 proton of ibuprofen, which resonates just below the large signals belonging to the CSA in the conventional ^{1}H NMR spectrum (Figure 4B). This hidden signal can quickly become observable by using a sensitive total correlation spectroscopy (TOCSY) transfer from another isolated proton resonance (Figure 4C).[15] Thus, a homodecoupled version of the selective TOCSY experiment can be designed by incorporating the detection period, described in Figure 1, into the conventional experiment (see Figure S3 in the Supporting Information). The two simplified singlets, corresponding to the H2 proton in *R* and *S* derivatives, can rapidly be distinguished, resolved, and quantified ($\Delta\Delta\delta = 10.44$ Hz) with enhanced sensitivity and without CSA signal interference (Figure 4C, D).

In summary, we have demonstrated that the homodecoupled SPFGE method is a robust and sensitive analytical NMR spectroscopy tool for the fast and simple discrimination of chemical-shift differences in overlapped signals and for the determination of the *ee* in the presence of CSAs. Its major advantage lies in the single-scan and 1D acquisition modes, as the resulting simplified singlet signals facilitate a better analysis. It has been shown that homodecoupled signals can also be retrieved for resonances obscured by other more intense signals or in overcrowded regions by using a preparatory TOCSY editing. Much work is in progress to use these powerful pure-shift methodologies for solving other common problems caused by NMR signal overlapping.

Experimental Section

All NMR experiments were performed by using a 600 MHz BRUKER Avance-III spectrometer equipped with a TXI probe. Complete experimental details, a comparison of the experimental sensitivity of several pure-shift NMR experiments, a description of the homodecoupled selective TOCSY pulse scheme, and a table showing the measured $\Delta\Delta\delta$ and *R/S* molar ratio values measured by signal integration and line fitting can be found in the Supporting Information.

CHEMPHYSCHEM
COMMUNICATIONS
www.chemphyschem.org

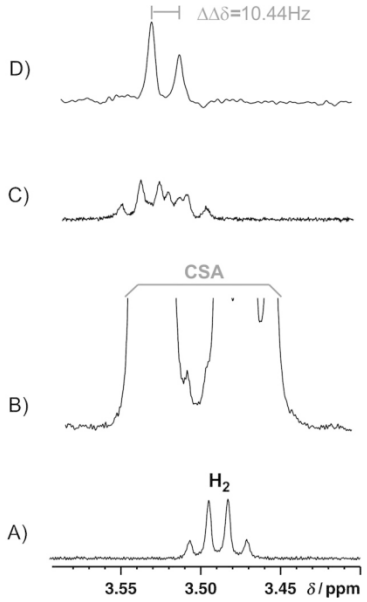

Figure 4. A, B) Expanded region corresponding to the ^{1}H NMR spectra of Figure 2A and 2B, respectively. C) Conventional and D) homodecoupled 1D TOCSY spectra showing the H2 proton after initial selective excitation of the H3 proton followed by a 60 ms TOCSY transfer. Gaussian-shaped 180° pulses of 20 ms were used for both excitation (on H3 protons at $\delta = 1.35$ ppm) and homodecoupling (on H2 protons). Spectra B–D) were acquired (four scans each one, with the same receiver gain), processed and plotted under the same conditions (see the Supporting Information) to visualize real absolute sensitivities.

Acknowledgements

Financial support for this research provided by MINECO (project CTQ2012-32436) is gratefully acknowledged. We also thank the Servei de Ressonància Magnètica Nuclear, Universitat Autònoma de Barcelona, for allocating instrument time to this project.

Keywords: chemical shift · homodecoupling · enantioselectivity · nmr spectroscopy · single pulsed-field-gradient echo

[1] a) T. J. Wenzel, *Discrimination of Chiral Compounds Using NMR Spectroscopy*; Wiley-VCH, Weinheim, **2007**; b) T. J. Wenzel, C. D. Chischolm, *Prog. Nucl. Magn. Reson. Spectrosc.* **2011**, *59*, 1 – 63.
[2] J. M. Seco, E. Quiñoá, R. Riguera, *Chem. Rev.* **2004**, *104*, 17 – 117.
[3] a) W. H. Pirkle, D. J. Hoover, *NMR Chiral Solvating Agents, Vol. 13 of Topics in Stereochemistry* (Eds.: N. L. Allinger, E. L. Eliel, S. H. Wilen), Wiley, Hoboken, **2007**; b) M. Pomares, F. Sánchez-Ferrando, A. Virgili, A. Alvarez-Larena, J. F. Piniella, *J. Org. Chem.* **2002**, *67*, 753 – 758; c) C. Estivill, M. Pomares, M. Kotev, P. Ivanov, A. Virgili, *Tetrahedron: Asymmetry* **2005**, *16*, 2993 – 2997; d) C. J. Núñez-Agüero, C. M. Escobar-Llanos, D. Díaz, C. Jaime, R. Garduño-Juárez, *Tetrahedron* **2006**, *62*, 4162 – 4172.
[4] a) M. Sarfati, P. Lesot, D. Merlet, J. Courtieu, *Chem. Commun.* **2000**, 2069 – 2081; b) J. Farjon, D. Merlet, *J. Magn. Reson.* **2011**, *210*, 24 – 30; c) K. Kobzar, H. Kessler, B. Luy, *Angew. Chem.* **2005**, *117*, 3205 – 3207; *Angew. Chem. Int. Ed.* **2005**, *44*, 3145 – 3147.
[5] a) J. P. Jesson, P. Meakin, G. J. Kneissel, *J. Am. Chem. Soc.* **1973**, *95*, 618 – 620; b) A. P. D. M. Espindola, R. Crouch, J. R. Debergh, J. M. Ready, J. B. MacMillan, *J. Am. Chem. Soc.* **2009**, *131*, 15994 – 15995.
[6] a) V. Marathias, P. A. Tate, N. Papaioannou, W. Massefski, *Chirality* **2010**, *22*, 838 – 843; b) M. Pérez-Trujillo, E. Monteagudo, T. Parella, *Anal. Chem.* **2013**, *85*, 10887 – 10894; c) T. J. Wenzel, J. D. Wilcox, *Chirality* **2003**, *15*, 256 – 270; d) A. Meddour, P. Berdague, A. Hedli, J. Courtieu, P. Lesot, *J. Am. Chem. Soc.* **1997**, *119*, 4502 – 4508; e) M. Rivard, F. Gullien, J. C. Fiaud, C. Aroulanda, P. Lesot, *Tetrahedron: Asymmetry* **2003**, *14*, 1141 – 1152; f) M. Sugiura, A. Kimura, H. Fujiwara, *Magn. Reson. Chem.* **2006**, *44*, 121 – 126.
[7] a) A. J. Pell, J. Keeler, *J. Magn. Reson.* **2007**, *189*, 293 – 299; b) B. Luy, *J. Magn. Reson.* **2009**, *201*, 18 – 24; c) S. R. Chaudhari, N. Suryaprakash, *Chem. Phys. Lett.* **2013**, *555*, 286 – 290; d) M. Pérez-Trujillo, J. C. Lindon, T. Parella, J. K. Nicholson, H. C. Keun, T. J. Athersuck, *Anal. Chem.* **2012**, *84*, 2868 – 2874.
[8] a) K. Zangger, H. Sterk, *J. Magn. Reson.* **1997**, *124*, 486 – 489; b) J. A. Aguilar, S. Faulkner, M. Nilsson, G. A. Morris, *Angew. Chem.* **2010**, *122*, 3993 – 3995; *Angew. Chem. Int. Ed.* **2010**, *49*, 3901 – 3903; c) G. A. Morris, J. A. Aguilar, R. Evans, S. Haiber, M. Nilsson, *J. Am. Chem. Soc.* **2010**, *132*, 12770 – 12772; d) J. A. Aguilar, A. A. Calbourne, J. Cassani, M. Nilsson, G. A. Morris, *Angew. Chem.* **2012**, *124*, 6566 – 6569; *Angew. Chem. Int. Ed.* **2012**, *51*, 6460 – 6463.
[9] a) A. Lupulescu, G. L. Olson, L. Frydman, *J. Magn. Reson.* **2012**, *218*, 141 – 146; b) J. A. Aguilar, M. Nilsson, G. A. Morris, *Angew. Chem.* **2011**, *123*, 9890 – 9891; *Angew. Chem. Int. Ed.* **2011**, *50*, 9716 – 9717.
[10] N. H. Meyer, K. Zangger, *Angew. Chem.* **2013**, *125*, 7283 – 7286; *Angew. Chem. Int. Ed.* **2013**, *52*, 7143 – 7146.
[11] L. Castañar, P. Nolis, A. Virgili, T. Parella, *Chem. Eur. J.* **2013**, *19*, 17283 – 17286.
[12] S. L. Patt, *J. Magn. Reson.* **1992**, *96*, 94 – 102.
[13] a) N. Giraud, M. Joos, J. Courtieu, D. Merlet, *Magn. Reson. Chem.* **2009**, *47*, 300 – 306; b) N. Nath, D. Kumari, N. Suryaprakash, *Chem. Phys. Lett.* **2011**, *508*, 149 – 154; c) R. P. Uday, N. Suryaprakash, *J. Phys. Chem. A* **2010**, *114*, 5551 – 5557.
[14] a) P. Sakhaii, B. Haase, W. Bermel, *J. Magn. Reson.* **2013**, *228*, 125 – 129; b) L. Castañar, P. Nolis, A. Virgili, T. Parella, *Chem. Eur. J.* **2013**, *19*, 15472 – 15475.
[15] F. Fernández-Trillo, E. Fernandez-Megia, R. Riguera, *J. Org. Chem.* **2010**, *75*, 3878 – 3881.

Received: November 28, 2013
Revised: January 2, 2014
Published online on February 20, 2014

CHEMPHYSCHEM

Supporting Information

Enantiodifferentiation through Frequency-Selective Pure-Shift ^{1}H Nuclear Magnetic Resonance Spectroscopy

Laura Castañar, Míriam Pérez-Trujillo, Pau Nolis, Eva Monteagudo, Albert Virgili, and Teodor Parella*[a]

cphc_201301130_sm_miscellaneous_information.pdf

Supporting Information

Experimental Section

All experiments were carried out at T=298 K on a Bruker AVANCE spectrometer (Bruker BioSpin, Rheinstetten, Germany) operating at 600.13 MHz proton frequency, equipped with a 5 mm triple resonance inverse probe and a z-axis pulsed field gradient accessory (maximum strength of 53.5 G/cm). Data were collected and processed using the software TOPSPIN 3.1 (Bruker BioSpin, Rheinstetten, Germany).

1D homodecoupled SPFGE spectra of Fig. 2B-E were recorded using a single scan, the same receiver gain and 1 s of recycle delay. The spectral width was 7200 Hz, and 8K complex points were recorded during an acquisition time of 567.98 ms. 11 loops (n) were concatenated with Δ=AQ/2n=25.81 ms and the selective 180º ^{1}H pulse had a Gaussian shape and a duration of 20 ms. A Gaussian-window function (LB=-3, GB=0.5) was applied before Fourier transformation.

All 1D spectra of Fig. 3 were recorded using a single scan, the same receiver gain and 1 s of recycle delay for comparison purposes. The spectral width was 7200 Hz, and 32K complex points were recorded during an acquisition time of 2,273 s. In homodecoupled experiments, 60 loops (n) were concatenated with Δ=AQ/2n=18,93 ms and the selective 180º ^{1}H pulse had a Gaussian shape and a duration of 20 ms. The 1D time-domain data was directly transformed without any sensitivity or resolution enhancement.

Although the homodecoupled SPFGE experiment (Fig. 1) has been executed in a single-scan to demonstrate the power of the method, a minimum four-step cycle is recommended in which the initial selective 180º pulse and the receiver are cycled using an EXORCYCLE scheme: Φ(180º)=x,y,-x,-y and Φ(receiver)=x,-x. The strengths of the G1, G2 and G3 gradients were set to 40.7, 21.9 and 33.7 G/cm, respectively, with durations of 500 μs followed by a recovery delay of 20 μs.

The samples used were the same used and described in a prior article published by us (Pérez-Trujillo et al. Analytical Chemistry **2013**, *85*, 10887-10894, reference 6b of the main manuscript). In the case of ibuprofen samples the preparation was as follows. 600 μL of a 2.2 mM solution of racemic ibuprofen was prepared mixing 100 μl of a 13.2 mM stock solution of (*RS*)-ibuprofen and 500 μL of D_2O, for the sample without CSA, and with 500 μL of a 12.1 mM β-CD solution in D_2O, for the sample with CSA. After that, both solutions were spiked with 70 μL of a 8.0 mM *S*-ibuprofen solution, resulting in a 2.8 mM solution of (*R,S*)-ibuprofen (35:65) in D_2O and in a second solution analogous to the former but containing 3.6 equivalents of β-CD. In the case of the racemic 1-aminoindan samples, (*RS*)-1-aminoindan was dissolved in $CDCl_3$ (50 mM) and after that 4.5 equivalents of *R*-(−)-1-(9-anthryl)-2,2,2-trifluoroethanol (Pirkle alcohol, PA) were added to the sample.

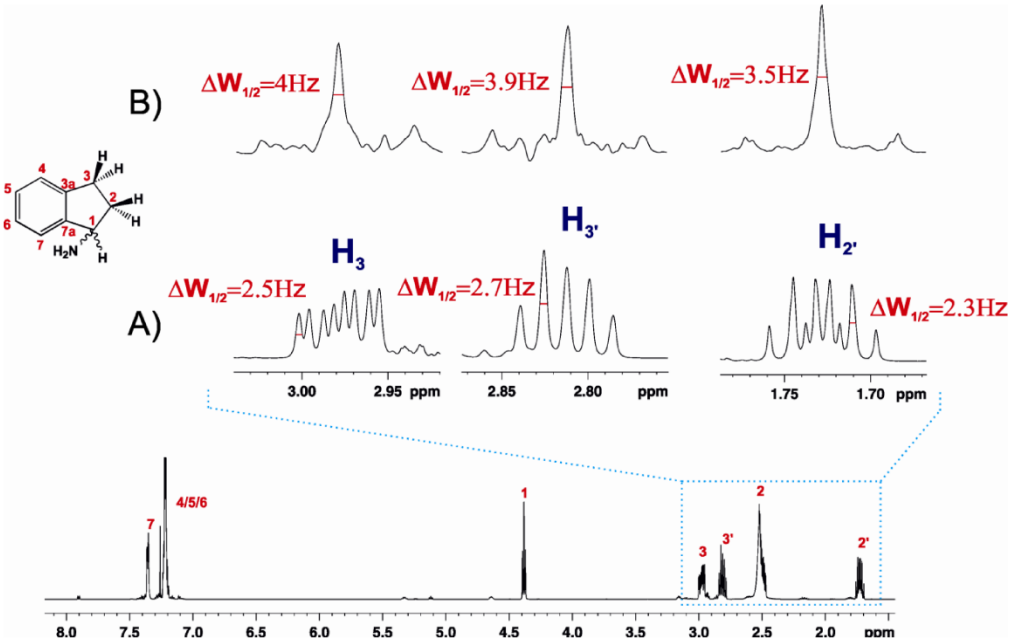

Figure S1: Experimental linewidths measured a 50mM (*RS*)-aminoindan sample dissolved in $CDCl_3$: A) conventional ^1H and B) homodecoupled ^1H SPFGE spectra after individual selection of each proton. All data were processed without any window function. The homodeocupling conditions in B) were: a 20 ms Gaussian shaped 180º ^1H pulse, Δ=19 ms, n=15 and AQ=568 ms.

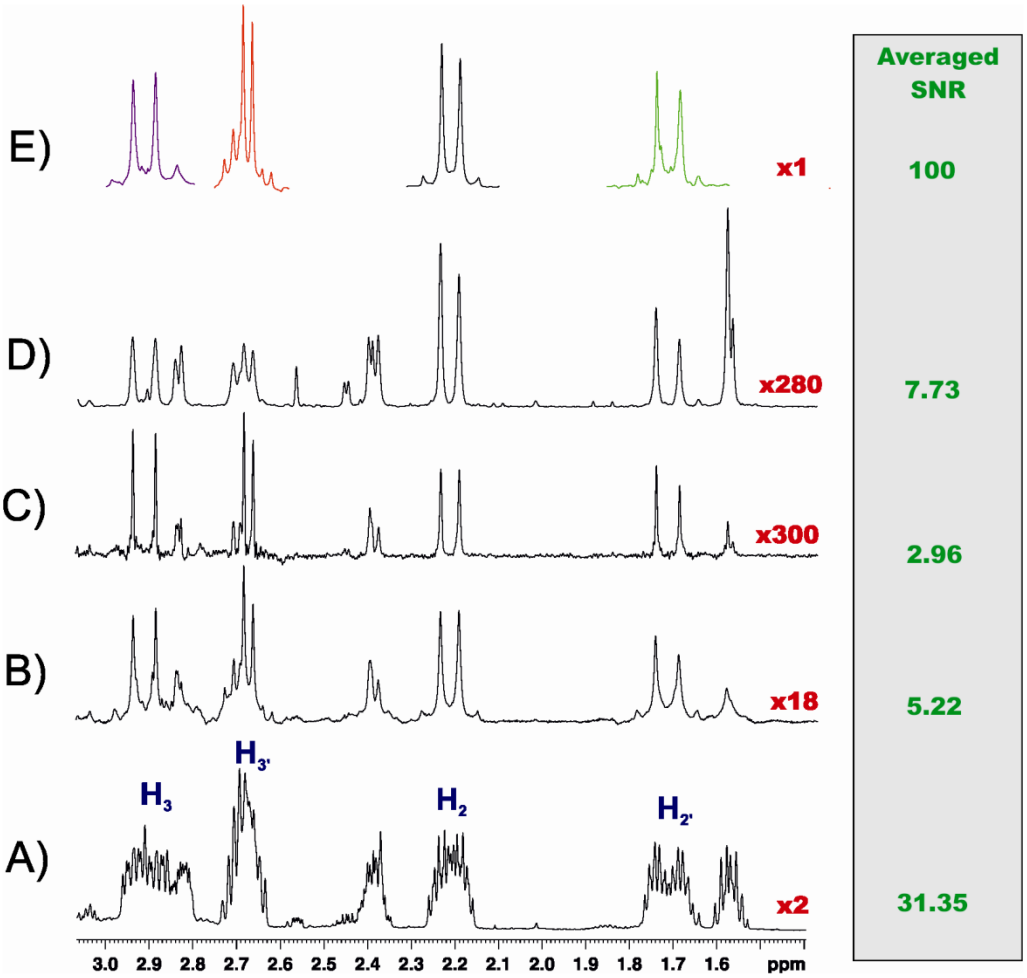

Figure S2. Comparison of the experimental SNR per time unit obtained for several pure chemical-shift NMR experiments using a sample of 50mM (*RS*)-1-aminoindan with 4.5 equivalents of (*R*)-(−)-1-(9-anthryl)-2,2,2-trifluoroethanol (Pirkle alcohol) in $CDCl_3$. A) Conventional ^1H spectrum; B) real-time instant 1D ZS spectrum (ref. 7); C) pseudo-2D ZS spectrum (ref. 12); D) Internal projection extracted along the detected dimension of a conventional 2D J-resolved after a tilting process; and E) selective homodecoupled 1D SPFGE spectra (using the scheme of Fig. 1, this work) after individual selection of each selected resonance. For an accurate SNR per time unit comparison, each experiment was recorded in equivalent conditions, using a 1.5s of recycle delay, the same receiver gain value and a total spectrometer time about 5 min. All spectra has been plotted using the selective SPFGE as a normalized intensity reference (see scaling factor) and with the averaged experimental SNR (green value) calculated from the selected four resonances in each experiment. The non-selective 90º ^1H pulse was of 7.3 μs. A) Conventional ^1H NMR spectrum was recorded using 76 scans. The spectral width was 7200 Hz, and 32K complex points were recorded during an acquisition time of 2.27s. Experiments B) and E) were recorded using 123 scans, spectral width of 7200 Hz, 8K complex points were collected during an acquisition time of 567.98 ms and 15 loops (n) were concatenated with Δ=AQ/2n=18.93 ms. The strengths of the G1, G2 and G3 gradients (smoothed squared shaped; SMSQ10.100 in Bruker format) were set to 40.7 (76%), 21.9 (41%) and 33.7 G/cm (63%), respectively, with durations of 500 μs followed by a

recovery delay of 20 μs. A 180º frequency-selective Gaussian-shaped ^{1}H pulse of 20 ms was used for both excitation and homodecoupling in spectra B, C and E. B) and C) experiments used a square-shaped encoding gradient of 0.2 G cm^{-1} (0.4%) for spatial frequency encoding. C) The pseudo-2D ZS spectrum was recorded using 4 transients for each one of the 32 t_1 increments and gradient pulses were smoothed squared shaped with a duration of 1 ms and amplitude G1= 26.8 G cm^{-1} (50%). All 1D time-domain data were directly transformed without any sensitivity or resolution enhancement. D) In the J-resolved spectrum 4 transients were collected for each one of the 32 t_1 increments. The spectral width was 7200 Hz, and 8K complex points were recorded during an acquisition time of 568 ms. Data were processed using a non-shifted sine-bell window function followed by a tilting process.

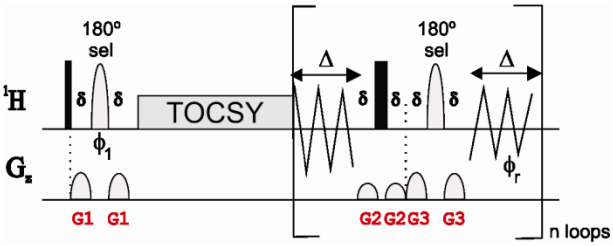

Figure S3: Pulse scheme for the selective and homodecoupled 1D TOCSY experiment. A minimum four-step phase cycle is used: ϕ_1=x,y,-x,-y and ϕ_r=x,-x. In contrast to the original homodecoupled SPFGE scheme (Fig. 1 of the manuscript), the features of the two selective 180º pulses are here different: the first selective 180º pulse is applied to an isolated resonance whereas the selective 180º pulse applied during the detection period is applied to a relayed resonance. Therefore, the selectivity and the offset of these pulses must be determined in each case according to the required selectivity.

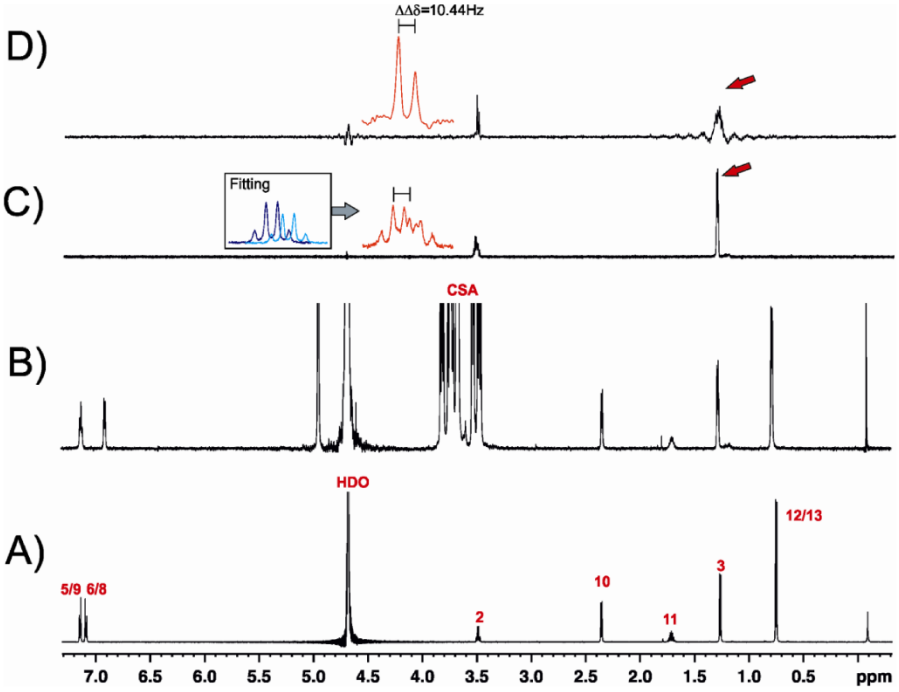

Figure S4: 600MHz ^{1}H NMR spectra of (*R,S*)-ibruprofen (35:65) in D_2O: A) before and B) after the addition of 3.6 equivalents of β-CD; C) conventional selective 1D TOCSY spectrum after initial selection of the H3 proton; D) broadband homodecoupled selective 1D TOCSY spectrum acquired using the pulse sequence of Fig. S3. Spectra C and D were recorded under the same experimental conditions: the H3 proton was selective excited by a 20ms Gaussian-shaped 180º ^{1}H pulse, and the H2 proton was fully homodecoupled during the acquisition period (Gaussian shaped pulse of 20 ms, Δ=14.2 ms, n=20 and AQ=568 ms) in D). Four scans were collected for each experiment using a recycle delay of 1s, a TOCSY mixing time (MLEV-17) of 60 ms and the same receiver gain value. Data were Fourier transformed without any window function.

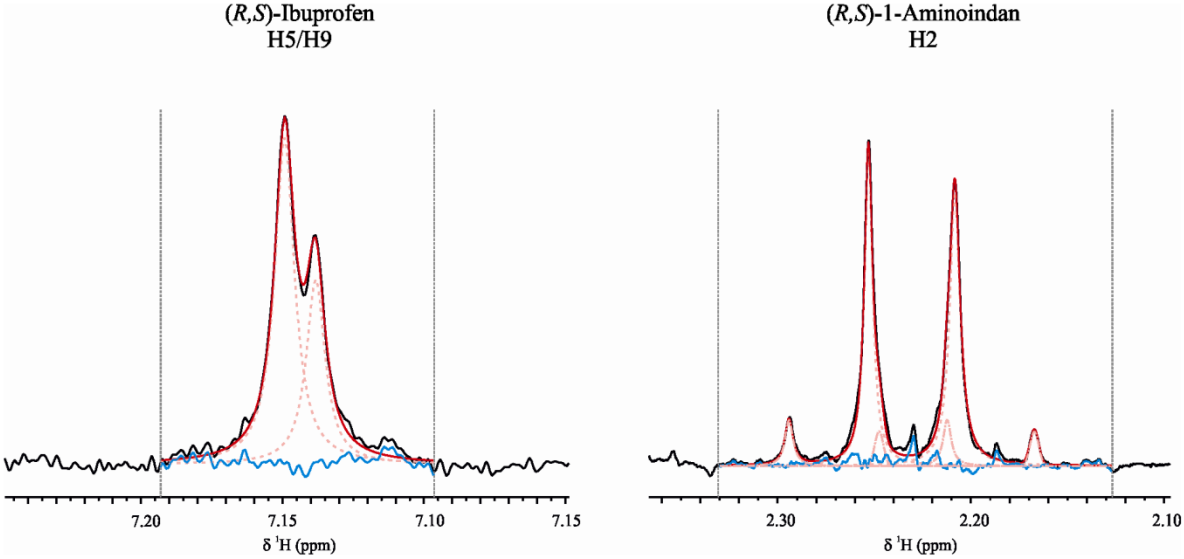

Figure S5: Examples of line fitting achieved for the singlets obtained from the HOBS spectra after selection the H5/H9 protons of (*R,S*)-ibuprofen (35:65) and H2' in (*RS*)-1-aminoindan samples. The experimental results are listed in Table S1.

Table S1: ΔΔδ and *S/R* molar ratio values for the samples studied in this work.

Sample	Experiment	Nucleus	Enantiodifferentiation			R/S molar ratio			
Theoretical S/R ratio (S:R)			ΔΔδ (Hz)	W[a] (Hz)	E[a]	Measurement by integration	Error[b] (%)	Measurement by line fitting[c]	Error[b] (%)
(*RS*)-Ibuprofen 1,85 (65:35)	^{1}H-NMR	H3	3.84	9.79	0.4	1.691[d]	8.6	1.648	11.3
		H5/9	7.32	10.79	0.7	1.780[d]	3.8	1.747	5.9
	$^1H_{sel}$-HOBS	H3	3.78	2.06	1.8	1.869	1.1	1.806	2.8
		H5/9	6.48	2.06[e]	3.1	1.859	0.5	1.875	1.0
(*RS*)-1-Aminoindan 1 (50:50)	^{1}H-NMR	H2'	33,43	32.91	1	0.953[f]	4.7	[g]	-
		H2	[h]	40.11	-	0.804[f]	19.6	[g]	-
		H3'	14.13[i]	35.32	0.4	[j]	-	[g]	-
		H3	32.83[i]	30.23	1.1	1.098	9.8	[g]	-
	$^1H_{sel}$-HOBS	H2'	33.34	3.58	9.3	1.014[k]	1.4	1.041[k]	4.1
		H2	26.83	3.11	8.6	0.994[k]	0.6	1.019[k]	1.9
		H3'	13.53	3.64	9.0	[j]	-	[j]	-
		H3	32.73	4.01	3.4	[j]	-	0.987[k]	1.3

[a] The enantiodifferentiation quotient, E, for an enantiodifferentiated signal is defined as ΔΔδ/W; where ΔΔδ is the chemical shift non-equivalence of that signal in presence of the CSA and W is de overall width of the same signal (singlet or multiplet) before adding the CSA. For more details see Pérez-Trujillo et al. Anal. Chem. 85 (2013) 10887-10894.

[b] Error calculated as the absolute value of (measured value - theoretical value)*100/theoretical value.

[c] Line fitting (deconvolution) done based on a Lorentzian/Gaussian function using MestreNova software (Mestrelab Research S. L., Santiago de Compostela, Spain).

[d] Measurement done by integrating the end peaks of the partially enantioresolved multiplet.

[e] This value was not possible to be measured, due to the proximity of H5/9 signal to H6/8 peak. An estimated value (the same than that obtained for H3 signal) was used for the determination of E.

[f] Measurement done by integrating each half of the partially enantioresolved multiplet from the central point.

[g] Not possible due to complex multiplicity.

[h] Not possible to measure due to severe overlap.

[i] Measurement done by superposing and shifting the ^{1}H NMR spectrum without CSA.

[j] Overlapped with an impurity.

[k] Sidebands have been included in determination of R/S molar ratio

Table S2: Comparison of R/S molar ratios obtained from the HOBS and the pseudo-2D ZS methods for the (*RS*)-1-aminoindan sample.

Sample	Experiment	Nucleus	R/S molar ratio[a]			
Theoretical S/R ratio (S:R)			Measurement by integration	Error[a] (%)	Measurement by line fitting[b]	Error[a] (%)
(*RS*)-1-Aminoindan 1 (50:50)	$^{1}H_{sel}$-HOBS	H2'	1.014 [c]	1.4	1.041[c]	4.1
		H2	0.994 [c]	0.6	1.019[c]	1.9
		H3'	[d]	-	[d]	-
		H3	[d]	-	0.987[c]	1.3
	pseudo-2D ZS experiment	H2'	1,001	0,1	1,014	1,4
		H2	1,007	0,7	1,026	2,6
		H3'	[d]	-	[d]	-
		H3	0,993	0,7	0,991	1,1

Values extracted from spectra of Fig. S2C and S2E

[a] Error calculated as the absolute value of (measured value - theoretical value)*100/theoretical value.

[b] Line fitting (deconvolution) done based on a Lorentzian/Gaussian function using MestreNova software (Mestrelab Research S. L., Santiago de Compostela, Spain).

[c] Sidebands have been included in determination of R/S molar ratio.

[d] Overlapped with an impurity.

PUBLICATION 5

Simultaneous ^{1}H and ^{13}C NMR enantiodifferentiation from highly-resolved pure shift HSQC spectra

Miriam Pérez-Trujillo, Laura Castañar, Eva Monteagudo, Lars T. Khun, Pau Nolis, Albert Virgili, Robert Thomas Williamson and Teodor Parella.

Chem. Commun., **2014**, *50*, 10214-10217.

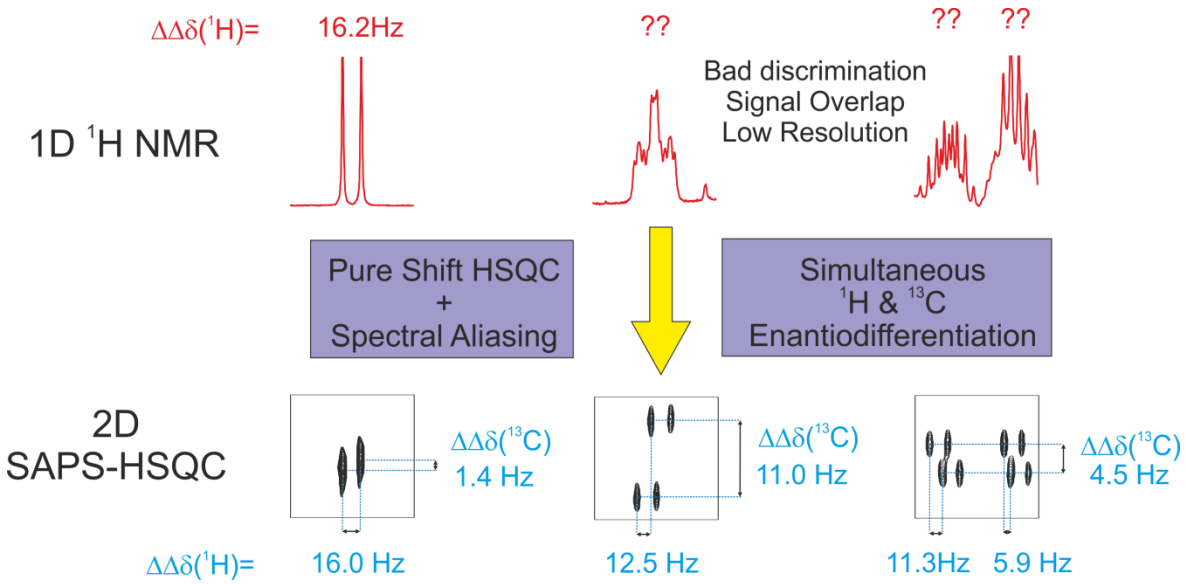

Introduction

In the previous work (**Publication 4**), the practical usefulness of 1D HOBS pure shift ^{1}H NMR experiments in enantiodifferentiation studies to distinct signals separated by more than 2 Hz in a 600 MHz spectrometer has been reported. On the other hand, recently, the conventional fully decoupled 1D ^{13}C{^{1}H} spectrum, one of the oldest pure shift NMR experiments, has successfully been applied in enantiodifferentiation studies.[91]

In this publication a new pure shift NMR approach is report to carry out enantiodifferentiation studies using CSAs. The proposed experiment is a highly-resolved 2D HSQC where the complementary features of the pure shift and spectral aliasing[92] approaches are combined in a single NMR experiment. As it is shown along this thesis work, the pure shift methodology highly improves signal resolution along the ^{1}H dimension simplifying the typical J_{HH} multiplicity pattern of ^{1}H signals to singlets. Spectral aliasing methodology is a very straightforward method that allows the increase of digital resolution along the indirect dimension within the same total experimental time. This method does not required any change in the pulse sequence and experimentally is easily implementable reducing the ^{13}C spectral width in HSQC experiments (for instance, from the typical 160 ppm to 5 ppm). In that manner, it is possible improve digital resolution and signal dispersion by one or two orders of magnitude along the ^{13}C dimension compared to classical acquisition when SNR is not a limiting factor. The experimental consequence to apply spectral aliasing is the temporary loss of the real chemical shift value along the indirect dimension. The new position of each aliased ^{13}C peak is exactly a multiple of the spectral width (SW_C) and its real position (δ_r) can be determined from the relationship:

$$\delta_r = \delta_{obs} + (K.SW_C)$$

where δ_{obs} is the experimental $\delta(^{13}C)$ measured in the aliased spectra using a given ^{13}C offset Ω_c and K is the aliasing factor which can be determined, for instance, from a reference non-aliased HSQC spectrum using a moderate number of t_1 increments. Several automated strategies have been proposed to determine the correct ^{13}C δ_r values and to reconstruct the entire spectrum.[92]

[91] M. Pérez-Trujillo, E. Monteagudo, T. Parella, *Anal. Chem.,* **2013***, 85,* 10887.

[92] a) D. Jeannerat, *Magn. Reson. Chem.,* **2003**, *41*, 3. b) I. Baskyr, T. Brand, M. Findeisen, S. Berger, *Angew. Chem. Int. Ed.,* **2006**, *45*, 7821. c) D. Jeannerat, *J. Magn. Reson.,* **2007**, *186*, 112. d) B. Vitorge, S. Bieri, M. Humam, P. Christen, K. Hostettmann, O. Muñoz, S. Loss, D. Jeannerat, *Chem. Commun.,* **2009**, 950. e) G. B. B. Njock, D. E. Pegnyem, T. A. Bartholomeusz, P. Christen, B. Vitorge, J. M. Nuzillard, R. Shivapurkar, M. Foroozandeh, D. Jeannerat, *Chimia,* **2010**, *64*, 235. f) M. Foroozandeh, D. Jeannerat, *ChemPhysChem,* **2010**, *11*, 2503. g) A. Cotte, M. Foroozandeh, D. Jeannerat, *Chimia,* **2012**, *66*, 764.

This new *Spectral Aliasing Pure Shift* HSQC (SAPS-HSQC) method has been successfully applied to enantiodifferentiation studies and it has been proved that it is a fast and very efficient tool for the detection and accurate differentiation and quantification of very small $\Delta\Delta\delta$ values, simultaneously for ^{1}H and ^{13}C. Enantiodifferentiation analysis through the SAPS-HSQC spectrum has been shown to be superior to the conventional 1D ^{1}H, the conventional ^{13}C or even the broadband homodecoupled 1D ^{1}H ZS spectrum. It is also important to remark that the relative sensitivity of standard HSQC experiment is retained in SAPS-HSQC experiments and even improved due to the collapse of the signals to singlets.

ChemComm

COMMUNICATION

View Article Online
View Journal | View Issue

Cite this: *Chem. Commun.*, 2014, 50, 10214

Received 28th May 2014,
Accepted 14th July 2014

DOI: 10.1039/c4cc04077e

www.rsc.org/chemcomm

Simultaneous ^{1}H and ^{13}C NMR enantiodifferentiation from highly-resolved pure shift HSQC spectra†

Miriam Pérez-Trujillo,[a] Laura Castañar,[a] Eva Monteagudo,[a] Lars T. Kuhn,[b] Pau Nolis,[a] Albert Virgili,[a] R. Thomas Williamson[c] and Teodor Parella*[a]

NMR enantiodifferentiation studies are greatly improved by the simultaneous determination of ^{1}H and ^{13}C chemical shift differences through the analysis of highly resolved cross-peaks in spectral aliased pure shift (SAPS) HSQC spectra.

The determination of enantiomeric purity can be accomplished by NMR spectroscopy using a great variety of auxiliary chiral sources.[1] Of these, chiral solvating agents (CSAs), such as the so-called Pirkle alcohol (PA) or cyclodextrins (CDs), have been widely used. They do not typically introduce significant line-broadening, the sample is easily prepared and the analysis is quickly performed by observing chemical shift differences ($\Delta\Delta\delta$) between the resulting diasteromeric complexes in conventional ^{1}H NMR spectra. However, signal enantiodifferentiation using CSAs is not uniform for all protons and in many cases, low $\Delta\Delta\delta$ values and signal overlap caused by complex multiplets lead to the lack of spectral signal dispersion that preclude a straightforward analysis. Alternatively, enantiodifferentiation using ^{13}C NMR spectroscopy can be more advantageous because singlet signals are analyzed, although its routine use is limited by its low sensitivity.[2] Another strategy to deconvolute these enantiodifferentiated data is to take advantage of improved signal dispersion offered by multidimensional spectra as shown for instance in the chiral recognition of camphor and α-pinene enantiomers with CDs made through HSQC spectra.[3] Recently, pure shift NMR spectroscopy has emerged as a promising tool to simplify the typical J(HH) multiplicity pattern of ^{1}H signals to singlets.[4–8] This affords a general improvement on signal dispersion that allows an improved analysis of complex and overcrowded resonances. Recently, this concept has proved its usefulness in the detection of $\Delta\Delta\delta$ values between diastereosiomeric complexes involving CSAs.[8]

In this study we utilized a racemic mixture of compound (**1**), a precursor for a series of diarylether lactams as cancer chemotherapeutic agents,[9] complexed with *R*-PA as a CSA. Its ^{1}H NMR spectrum (Fig. 1A) does show some well-differentiated signals (for instance, H12 appears at around 7.10–7.15 ppm as two triplet signals separated by 20.9 Hz or 34.8 ppb), but most of the signals cannot be individually distinguished. For example, H13 is hidden under the stronger H2 signal from *R*-PA (6.6 ppm), and the splitting in signals resonating in the congested

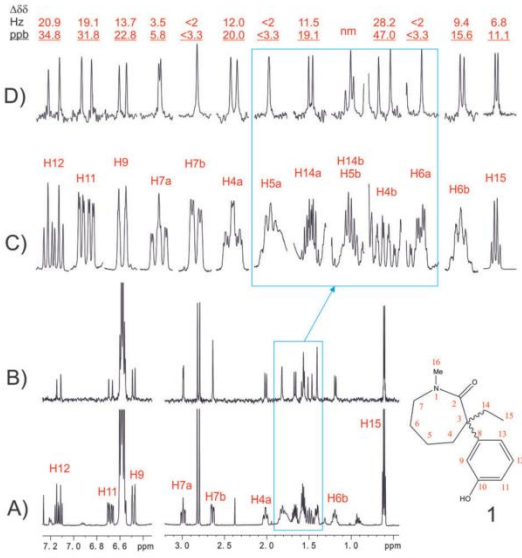

Fig. 1 600.13 MHz (A) conventional and (B) pure shift ^{1}H NMR spectra of 29 mM racemic compound **1** complexed with 9.6 equiv. of *R*-PA in $CDCl_3$. (C and D) Comparison of expanded ^{1}H multiplets for determining accurate $\Delta\Delta\delta(^{1}H)$ values (shown in Hz and ppb).

[a] *Servei de Ressonància Magnètica Nuclear and Departament de Química, Universitat Autònoma de Barcelona, E-08193 Bellaterra, Barcelona, Spain. E-mail: teodor.parella@uab.cat; Tel: +34 935812291*
[b] *DFG Research Center Molecular Physiology of the Brain (CMPB) & European Neuroscience Institute Göttingen (ENI-G), Göttingen, Germany*
[c] *NMR Structure Elucidation, Process and Analytical Chemistry, Merck & Co. Inc., 126 E. Lincoln Avenue, Rahway, NJ 07065, USA*

† Electronic supplementary information (ESI) available: Experimental details and NMR spectra. See DOI: 10.1039/c4cc04077e

aliphatic area at 1.4–1.8 ppm cannot be clearly observed due to spectral overlap. Other protons present complex multiplet patterns (H4a or H6b) or are poorly resolved (H7a), hindering their direct analysis. On the other hand, up to 9 signals appear split in the conventional ^{13}C spectrum of racemic **1** acquired after 9 hours, with a maximum $\Delta\Delta\delta(^{13}C)$ of 84.1 ppb (Fig. S3, ESI†). As an alternative to the acquisition and analysis of 1D ^{13}C NMR data, pure shift 1D ^{1}H NMR experiments can be employed to simplify the analysis and provide a much more sensitive approach in the determination of small $\Delta\Delta\delta(^{1}H)$ values (Fig. 1B). In this 1D pure shift ^{1}H spectrum acquired in 9 min using the pseudo-2D Zangger–Sterk (ZS) method,[4] the separation of each individual signal can be visualized allowing the accurate measurement of $\Delta\Delta\delta(^{1}H)$ as small as 2 Hz (3.3 ppb), even for signals that would exhibit very complex multiplets and serious overlapping in a standard 1D ^{1}H NMR (Fig. 1C *vs.* D).

In this communication, we show how highly resolved 2D HSQC spectra can be an efficient tool for enantiodifferentiation studies and also for the detection and accurate quantification of very small $\Delta\Delta\delta$ values. Traditionally, attempts to obtain highly resolved HSQC spectra over the entire ^{13}C spectral width involved an enormous investment in instrument time. Our method is based on the concerted leveraging of several approaches to improve signal dispersion in 2D HSQC spectra. First, spectral aliasing (SA) is incorporated to improve resolution along the indirect dimension by one or two orders of magnitude without increasing the total experimental time by using a reduced ^{13}C spectral width.[10] Secondly, a sensitivity-improved version[11] of the pure shift (PS) HSQC experiment (Fig. 2A),[6] referred to as psHSQCsi, is applied to enhance the resolution in the alternate ^{1}H dimension. This experiment applies 180°(^{1}H)-BIRD modules for homodecoupling and also heteronuclear decoupling during the τ acquisition periods to obtain fully decoupled ^{1}H singlet signals. Diastereotopic protons belonging to methylene AB spin systems appear as doublets because geminal ^{2}J(HH) magnetization is inverted together during the BIRD filter and is therefore not decoupled.[5] Finally, resolution can be further improved using non-uniform sampling[12] in combination with zero-filling and linear prediction during data processing.

Fig. 2B compares a portion of the SAPS-HSQC *vs.* SA-HSQC spectra of **1**, in order to evaluate multiplet simplification, signal dispersion and relative sensitivity. These data, acquired using a reduced ^{13}C spectral width of 2.5 ppm in a 600 MHz spectrometer with 256 t_1 increments per 2046 points each, provide a digital resolution of around 2–3 Hz pt^{-1} in both dimensions before data processing. It is shown that improved signal dispersion due to the combined effects of ^{1}H and ^{13}C δ differentiation is further enhanced by the multiplet pattern simplification provided by homo- and heteronuclear decoupling. The pure shift approach can afford a general sensitivity enhancement by 10–40% through the collapse of the multiplet structure. As expected, the proposed psHSQCsi version affords a substantial SNR improvement for CH cross-peaks when compared to the psHSQC (Fig. S4, ESI†). In terms of spectral quality, homodecoupling during acquisition in psHSQC/psHSQCsi experiments generates small sidebands at specific frequencies around the main signal

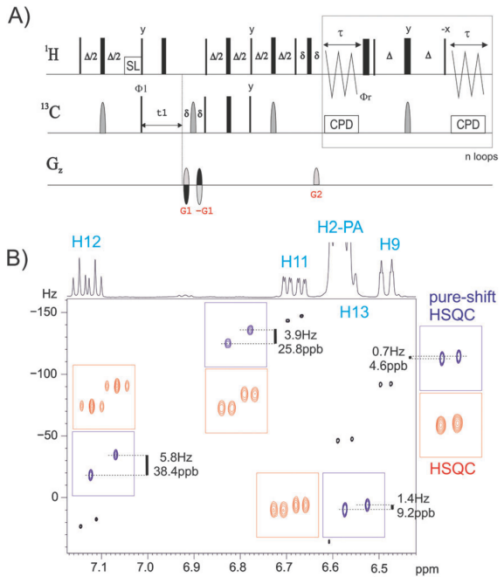

Fig. 2 (A) Pulse scheme of the pure shift sensitivity-improved HSQC experiment (Δ = 1/(2 × ^{1}J(CH))); (B) expanded areas comparing some cross-peaks in SA- (red) and SAPS-HSQC (blue) spectra of the racemic compound **1**–*R*-PA mixture acquired with a reduced ^{13}C spectral width of 2.5 ppm.

and a minimum broadening of the signal (~3 Hz *vs.* ~3.5 Hz) when compared to traditional experiments (Fig. S4, ESI†).[6] In practice, this does not affect the $\Delta\Delta\delta$ determination, and signal discrimination less than 0.5 Hz (0.8 ppb for ^{1}H and 3.3 ppb for ^{13}C) can typically be achieved (Table 1), even for NMR signals with no apparent splitting in the ^{13}C spectrum.

The analyzed sample contains several examples that illustrate the power of the proposed method which, *a priori*, could detect enantiodifferentiated signals even in the case that $\Delta\Delta\delta(^{1}H)$ or $\Delta\Delta\delta(^{13}C)$ is close to 0, whenever one of the two are sufficiently dispersed. In the example shown, of the 16 available proton signals, 5 are detected as enantiodifferentiated in the ^{1}H spectrum, 10 in the 1D ZS and 15 in the psHSQCsi. In addition, of the 11 signals of protonated carbons, 6 are detected as enantiodifferentiated in the 1D ^{13}C spectrum and 10 in the psHSQCsi (Table 1). A new parameter $\Delta\Delta\delta(CH)^2 = \Delta\Delta\delta(^{1}H)^2 + \Delta\Delta\delta(^{13}C)^2$ is defined to describe mathematically the signal dispersion in HSQC cross-peaks (Fig. S5, ESI†). In general, we can say that both $\Delta\Delta\delta(^{1}H)$ and $\Delta\Delta\delta(^{13}C)$ values can be measured when $\Delta\Delta\delta(CH) > 5$ ppb (Table 1). For instance, the two singlets corresponding to the NMe group in **1** (H16) are well resolved in the regular ^{1}H spectrum (27.0 ppb) whereas the corresponding C16 carbon is not resolved in the ^{13}C spectrum (<13.2 ppb). From the HSQC cross-peak an accurate value of $\Delta\Delta\delta$(C16) = 9.9 ppb can be obtained. Similar analysis can be made for the H9/C9 and H13/C13 pairs where the carbon signals do not appear split in the 1D ^{13}C spectrum but values of 4.6 ppb and 9.2 ppb, respectively, can be extracted from the 2D analysis (Fig. 2B and Fig. S8, ESI†). Another challenging

Table 1 ^{1}H and ^{13}C NMR chemical shift differences ($\Delta\Delta\delta(^{1}H)$ and $\Delta\Delta\delta(^{13}C)$) of the racemic compound 1 (29 mM) enantiodifferentiated with *R*-PA (9.6 equiv.) measured at 600 MHz and 298 K

	$\Delta\Delta\delta(^{1}H)$ [in ppb]			$\Delta\Delta\delta(^{13}C)$ [in ppb]			
Label	1D ^{1}H	1D ZS-^{1}H	SAPS-HSQC[c]	1D ^{13}C	SAPS-HSQC[c]	SA-HSQMBC[b,c]	$\Delta\Delta\delta$(CH) [in ppb]
2	—	—	—	14.5	—	14.5	30.3[b]
3	—	—	—	<13.2	—	3.3	12.4[b]
4a/4b	x[a]/x[a]	20.0/47.0	20.8/46.1	72.9	73.5	—	76.4/86.7
5a/5b	x[a]/x[a]	<3.3/x[a]	2.5/21.0	<13.2	5.3	—	5.9/21.7
6a/6b	x[a]/x[a]	<3.3/15.6	<3.3/16.7	<13.2	<3.3	—	<4.7/17.0
7a/7b	x[a]/x[a]	5.8/<3.3	4.6/1.2	13.9	13.2	—	14.0/13.2
8	—	—	—	84.1	—	84.1	90.9[b]
9	22.4	22.8	23.3	<13.2	4.6		23.7
10	—	—	—	43.7	—	44.4	56.2[b]
11	30.8	31.8	30.6	27.1	25.8	—	40.0
12	34.4	34.8	34.5	39.0	38.4	—	51.6
13	x[a]	x[a]	32.0	<13.2	9.2	—	33.3
14a/14b	x[a]/x[a]	19.1/x[a]	18.8/9.8	30.4	29.8	—	35.2/31.3
15	11.5	11.1	12.0	21.2	18.5	—	22.0
16	27.0	27.1	26.6	<13.2	9.9	—	28.4

[a] Not determined. [b] Only relevant data on quaternary carbons are shown. [c] Digital resolution of ±0.5 and ±2.6 ppb for ^{1}H and ^{13}C, respectively.

analysis involves the H7a/H7b protons and their C7 carbon, which present very low resolution. A very small $\Delta\Delta\delta$(H7b) = 1.2 ppb, which is not distinguishable in the ZS ^{1}H spectrum, can be measured from the highly resolved 2D cross-peak.

The same strategy can be followed to determine $\Delta\Delta\delta$ on quaternary carbons from an aliased non-refocused HSQMBC experiment.[13] Unfortunately, broadband homodecoupling in a similar manner as that described for the psHSQC experiment cannot be achieved because the detected signals correspond to ^{1}H–^{12}C magnetization that is homonuclear *J* coupled to other protons with the same ^{1}H–^{12}C topology. Although at least one pure shift HMBC approach has been reported, this technique requires long acquisition times and a complex processing protocol.[7] Fig. S9 (ESI†) shows some HSQMBC cross-peaks for the four quaternary carbons of **1** where a very small value of $\Delta\Delta\delta$(C3) = 3.3 ppb can be measured.

In all these spectra, each aliased ^{13}C peak appears without sign inversion at a position that is exactly a multiple of the spectral width (SW_c) from its real position (δ_r) that can be determined from the relationship $\delta_r = \delta_{obs} + (K \times SW_c)$, where δ_{obs} is the experimental $\delta(^{13}C)$ measured in the aliased spectra using a given ^{13}C offset Ω_c and *K* is the fold number which can be determined from reference non-aliased HSQC or HSQMBC spectra using a moderate number of t_1 increments (Fig. S10, ESI†). Several automated strategies that have been proposed to determine the correct ^{13}C δ_r values and to reconstruct the entire spectrum could also be applied here.[10] The enantiodifferentiation from highly resolved HSQC spectra allows the unambiguous ^{1}H and ^{13}C chemical shift assignment that is not available from the exclusive use of 1D spectra and, in addition, the pure shift nature of cross-peaks makes the proposed technique highly suitable for the quantitative determination of enantiomeric excess by 2D volume integration, because equivalent signals from both diastereoisomers have practically similar *J*(CH) coupling and T_2 relaxation values.

In summary, the combination of spectral aliasing and pure shift HSQC experiments represents an excellent routine tool for NMR enantiodifferentiation studies, yielding simultaneous ^{1}H and ^{13}C enantiodifferentiated data ($\Delta\Delta\delta(^{1}H)$ and $\Delta\Delta\delta(^{13}C)$) in short times and with high digital resolution and signal dispersion for both ^{1}H and ^{13}C nuclei. Its use increases significantly the probability to detect an enantiodifferentiated nucleus since more signals are observed (^{1}H and ^{13}C nuclei), overlapping problems of common 1D ^{1}H experiments are overcome, and poor enantiodifferentiation in 1D experiments can now be detected, allowing the study of cases abandoned in the past for reasons of poor enantioresolution and/or long experimental times. Alternatively, aliased long-range heteronuclear correlation experiments can be used to measure accurately such $\Delta\Delta\delta$ values for quaternary carbons. The method is compatible with other heteronuclei and with the use of other chiral auxiliaries, and it can be of special interest for chiral metabonomic studies, where chiral molecules in complex mixtures are enantiodifferentiated and small chemical shifts need to be resolved in overcrowded spectra.[14]

Financial support for this research provided by MINECO (project CTQ2012-32436) is gratefully acknowledged. We also thank the Servei de Ressonància Magnètica Nuclear, Universitat Autònoma de Barcelona, for allocating instrument time to this project.

Notes and references

1 (*a*) T. J. Wenzel, *Top. Curr. Chem.*, 2013, **341**, 1–68; (*b*) G. Uccello-Barretta and F. Balzano, *Top. Curr. Chem.*, 2013, **341**, 69–131.
2 (*a*) M. Palomino-Schätzlein, A. Virgili, S. Gil and C. Jaime, *J. Org. Chem.*, 2006, **71**, 8114–8120; (*b*) M. Pérez-Trujillo, E. Monteagudo and T. Parella, *Anal. Chem.*, 2013, **85**, 10887–10894.
3 (*a*) H. Dodziuk, A. Ejchart, O. Lukin and M. O. Vysotsky, *J. Org. Chem.*, 1999, **64**, 1503–1507; (*b*) H. Dodziuk, W. Koźmiński, O. Lukin and D. Sybilska, *J. Mol. Struct.*, 2000, **523**, 205–212.
4 (*a*) K. Zangger and H. Sterk, *J. Magn. Reson.*, 1997, **124**, 486–489; (*b*) N. H. Meyer and K. Zangger, *Angew. Chem., Int. Ed.*, 2013, **52**, 7143–7146; (*c*) N. H. Meyer and K. Zangger, *ChemPhysChem*, 2014, **15**, 49–55; (*d*) J. A. Aguilar, S. Faulkner, M. Nilsson and G. A. Morris, *Angew. Chem., Int. Ed.*, 2010, **49**, 3901–3903; (*e*) G. A. Morris, J. A. Aguilar, R. Evans, S. Haiber and M. Nilsson, *J. Am. Chem. Soc.*, 2010, **132**, 12770–12772.
5 J. R. Garbow, D. P. Weitekamp and A. Pines, *Chem. Phys. Lett.*, 1982, **93**, 504–509.

6 L. Paudel, R. W. Adams, P. Király, J. A. Aguilar, M. Foroozandeh, M. J. Cliff, M. Nilsson, P. Sándor, J. P. Waltho and G. A. Morris, *Angew. Chem., Int. Ed.*, 2013, **52**, 11616–11619.
7 P. Sakhaii, B. Haase and W. Bermel, *J. Magn. Reson.*, 2013, **228**, 125–129.
8 L. Castañar, M. Pérez-Trujillo, P. Nolis, E. Monteagudo, A. Virgili and T. Parella, *ChemPhysChem*, 2014, **15**, 854–857.
9 (*a*) S. J. deSolms, T. M. Ciccarone, S. C. MacTough, A. W. Shaw, C. A. Buser, M. Ellis-Hutchings, C. Fernandes, K. A. Hamilton, H. E. Huber, N. E. Kohl, R. B. Lobell, R. G. Robinson, N. N. Tsou, E. S. Walsh, S. L. Graham, L. S. Beese and J. S. Taylor, *J. Med. Chem.*, 2003, **46**, 2973–2984; (*b*) M. Pérez-Trujillo and A. Virgili, *Tetrahedron: Asymmetry*, 2006, **17**, 2842–2846.
10 (*a*) D. Jeannerat, *Magn. Reson. Chem.*, 2003, **41**, 3–7; (*b*) D. Jeannerat, *Rapid Multidimensional NMR: High Resolution by Spectral Aliasing*, Encyclopedia of Magnetic Resonance, John Wiley, Chichester, 2011; (*c*) B. Vitorge, S. Bieri, M. Humam, P. Christen, K. Hostettmann, O. Muñoz, S. Loss and D. Jeannerat, *Chem. Commun.*, 2009, 950–952; (*d*) M. Foroozandeh, P. Giraudeau and D. Jeannerat, *ChemPhysChem*, 2011, **12**, 2409–2411.
11 L. Kay, P. Keifer and T. Saarinen, *J. Am. Chem. Soc.*, 1992, **114**, 10663–10665.
12 K. Kazimierczuk and V. Y. Orekhov, *Angew. Chem., Int. Ed.*, 2011, **50**, 5556–5559.
13 R. T. Williamson, B. L. Márquez, W. H. Gerwick and K. E. Kövér, *Magn. Reson. Chem.*, 2000, **38**, 265–273.
14 M. Pérez-Trujillo, J. C. Lindon, T. Parella, H. C. Keun, J. K. Nicholson and T. J. Athersuch, *Anal. Chem.*, 2012, **84**, 2868–2874.

Electronic Supplementary Material (ESI) for ChemComm.

Supporting Information

Simultaneous ^{1}H and ^{13}C NMR enantiodifferentiation from highly resolved pure shift HSQC spectra

Míriam Pérez-Trujillo, Laura Castañar, Eva Monteagudo, Lars T. Kuhn, Pau Nolis, Albert Virgili, R. Thomas Williamson, and Teodor Parella*

Table of Contents:

Experimental Section

NMR experiments were performed on a Bruker Avance 600 spectrometer (Bruker AG, Rheinstetten, Germany) equipped with TXI HCN z-grad probes. The temperature for all measurements was set to 298 K and data were acquired and processed with TOPSPIN 3.1 (Bruker AG, Rheinstetten, Germany).

All spectra were recorded on a 600 μL fresh solution stock of racemic 3-ethyl-3-(3-hydroxyphenyl)-1-methylazepan-2-one (compound **1**, 29 mM) in $CDCl_3$, containing 9.6 equiv. (46.2 mg) of *R*-Pirkle alcohol (PA). Ii is referred to as compound **1** throughout the manuscript and this SI.

Slice selection in the 1D Zangger-Sterk (ZS) experiment (Fig. 1B) was performed using a selective 180 ^{1}H R-Snob pulse of 60 ms applied simultaneously to a weak rectangular gradient of 2%. Data was acquired in a pseudo 2D mode using 4 scans for each one of the 16 t_1 increments and a recycle delay of 1s. The FID reconstruction was performed with the AU program pshift (available at http://nmr.chemistry-manchester.ac.uk), followed by conventional Fourier transformation. The total experimental time was of 9 minutes.

The 2D ^{1}H-^{13}C pure shift HSQC spectrum (pulse scheme of Fig. 2A) was recorded as described in ref. 6. Pulse phases are x unless indicated otherwise and a basic two-step phase cycling scheme is applied: Φ_1=x,-x, Φ_r=x,-x. ^{13}C 180º pulses are applied as CHIRP inversion and refocusing pulses of 500 μs and 2000 μs of duration, respectively. The recycle delay was 3 s and the interpulse delays in the INEPT and BIRD modules were optimized for 140 Hz (Δ=3.57 ms). 2 scans were accumulated for each one of the 256 t_1 increments (512 experiments defined applying 50% non-uniform sparse sampling), the spectral windows in F1 and F2 dimensions were 377 Hz (2.5 ppm) and 4200 Hz, respectively, the number of data points in t_2 was set to 2048 and the acquisition time (AQ) was 0.24 s giving a FID resolution of 1.47 and 4.10 Hz, respectively. The total experimental time was of 30 min. Homodecoupling during acquisition was achieved applying 130 loops (n) with τ=7.7 ms. Broadband heteronuclear decoupling was applied during the τ periods using 1.5 ms chirped pulses combined in a p5m4 supercycle scheme. The ratio between the G1:G2 gradients were 40:20.1, measured as percentage of the absolute gradient strength of 53.5 G/cm. Data were acquired and processed using the echo/anti-echo protocol. Sine bell shaped gradients of 1 ms duration were used, followed by a recovery delay of 20 μs

(δ=1.02ms). Prior to Fourier-transformation of each data, zero filling to 1024 in F1, 8192 points in F2, linear prediction in F1 and a π/2-shifted sine squared window function in both dimensions were applied. The final digital resolution was of 0.51 and 0.36 Hz in F2 and F1 dimensions, respectively.

To determine ΔΔδ on quaternary carbons, a conventional non-refocused gradient-enhanced HSQMBC experiment optimized to 8 Hz was collected with the same acquisition and processing parameters described for the HSQC experiments. 16 scans were acquired per t_1 increment giving a total experimental time of 4 hours. Conventional 2D HSQC experiments were recorded under the same conditions as described previously for the pure shift analogues. HSQC and HSQMBC experiments were also recorded with ^{13}C spectral windows of 5 ppm (Fig. S6 and S9-10).

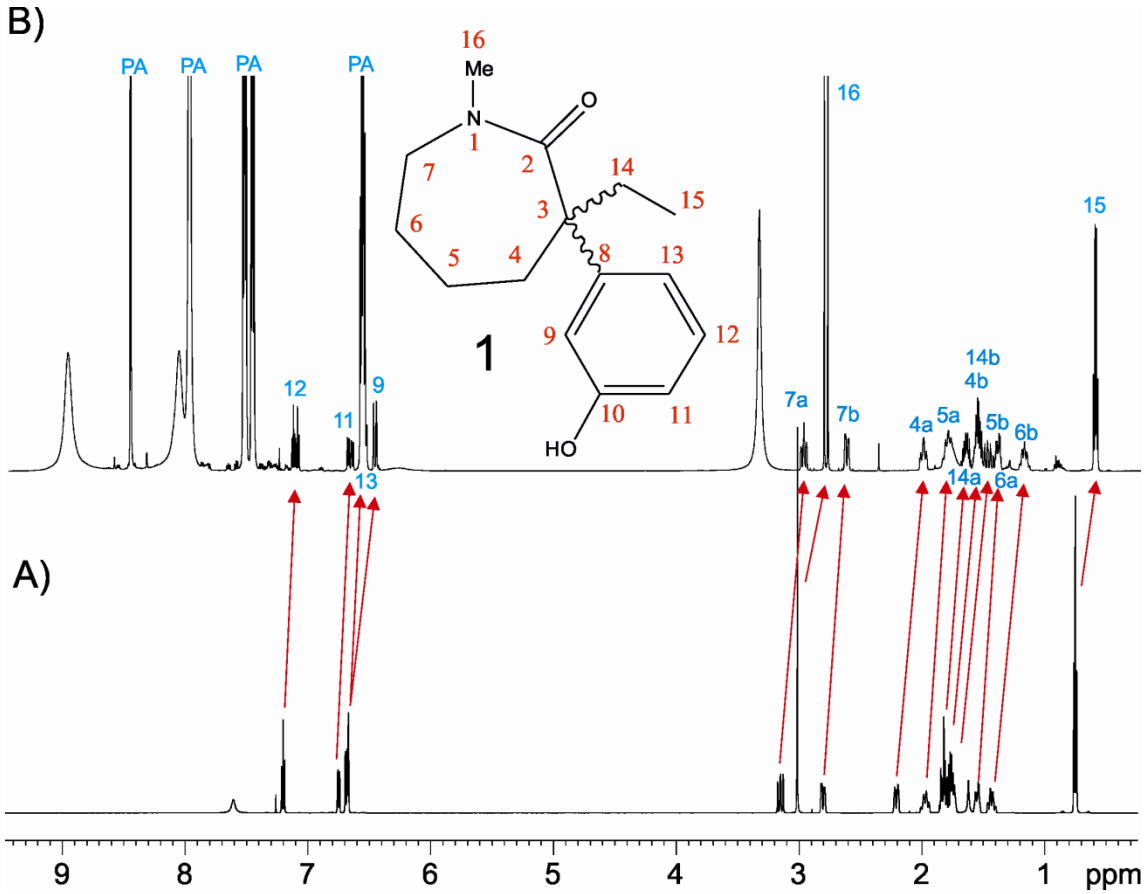

Figure S1: A) ^{1}H NMR spectrum of racemic compound (**1**) in $CDCl_3$; B) Resulting ^{1}H NMR spectrum after adding 9.6 equivalents of Pirkle Alcohol (*R*-PA).

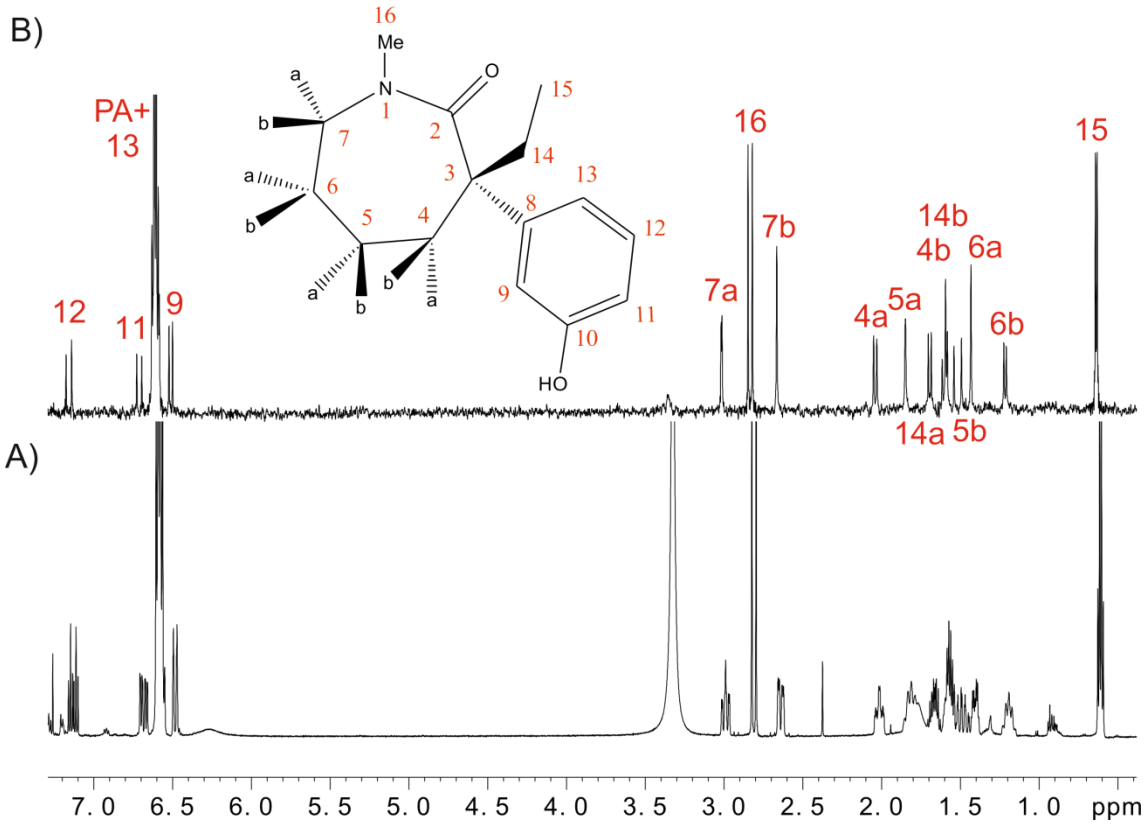

Figure S2: A) 1D conventional and B) pure shift ^{1}H spectrum of racemic compound **1** and *R*-PA. The structure of the *R*-**1** enantiomer is shown for stereoassignment purposes. See Fig. 1C and 1D for selected expansions and experimental $\Delta\Delta\delta(^{1}H)$ values.

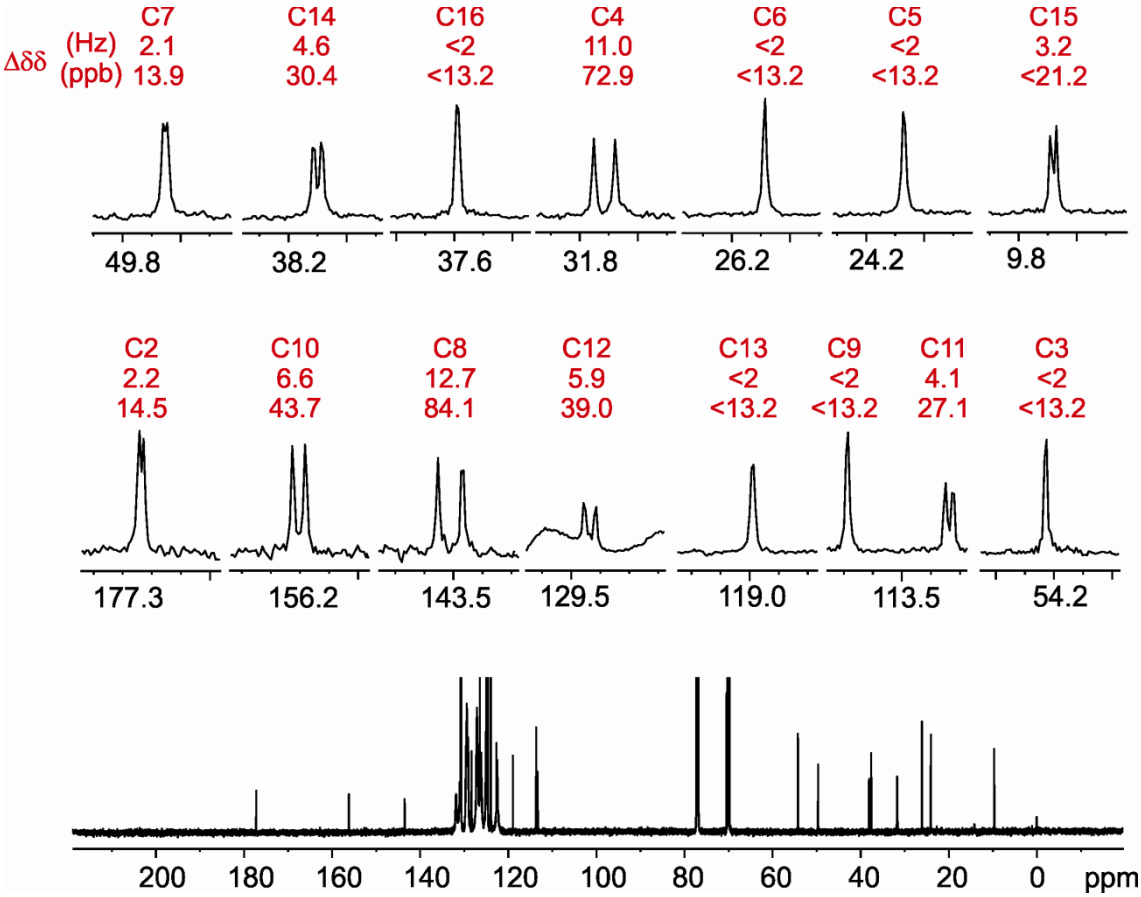

Figure S3: (Bottom) 150.9 MHz Broadband heterodecoupled ^{13}C NMR spectrum of racemic compound **1** and *R*-PA; (top) expanded multiplets to show individual signal splitting (in Hz and ppb) due to the enantiodifferenation.

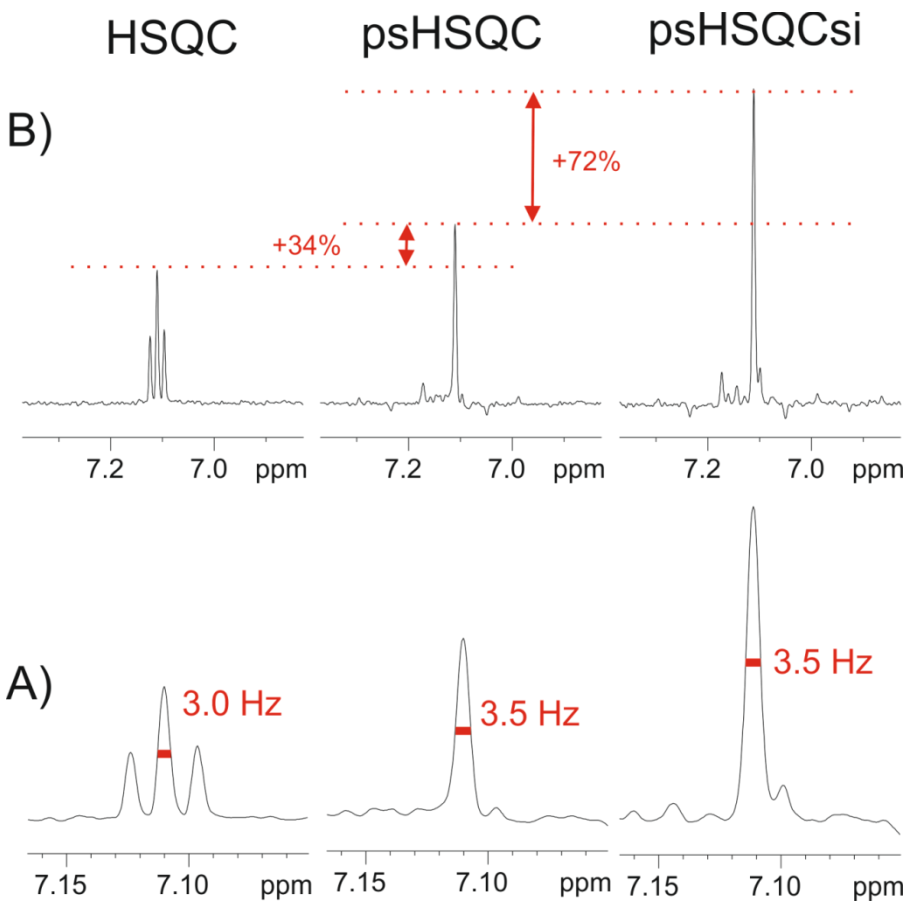

Figure S4: (A) Experimental line widths and B) relative sensitivities obtained in conventional HSQC, pure shift HSQC (psHSQC) and pure shift sensitivity-improved HSQC (psHSQCsi) experiments. 1D traces correspond to the upfield H12/C12 carbon frequency.

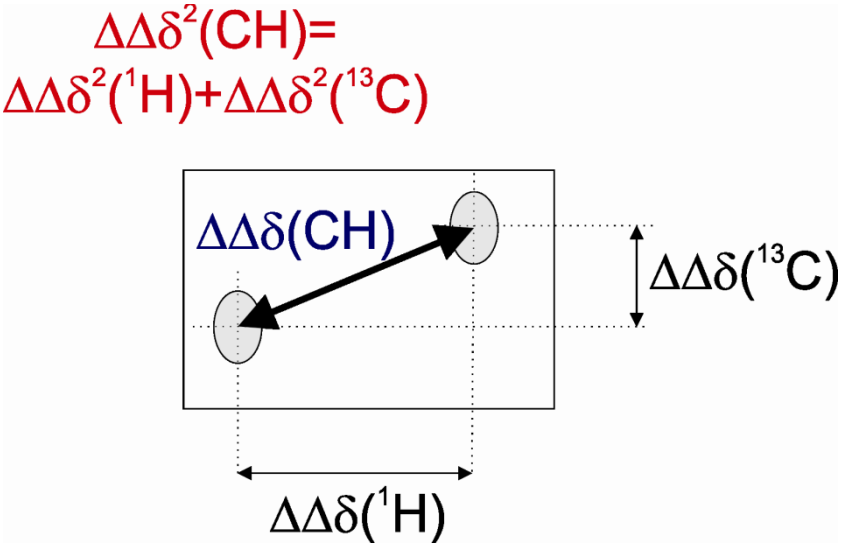

Figure S5: Schematic representation of the new parameter ΔΔδ(CH) that defines the separation between two cross-peaks from the individual ΔΔδ(^{1}H) and ΔΔδ(^{13}C) separations along each dimension of a 2D map.

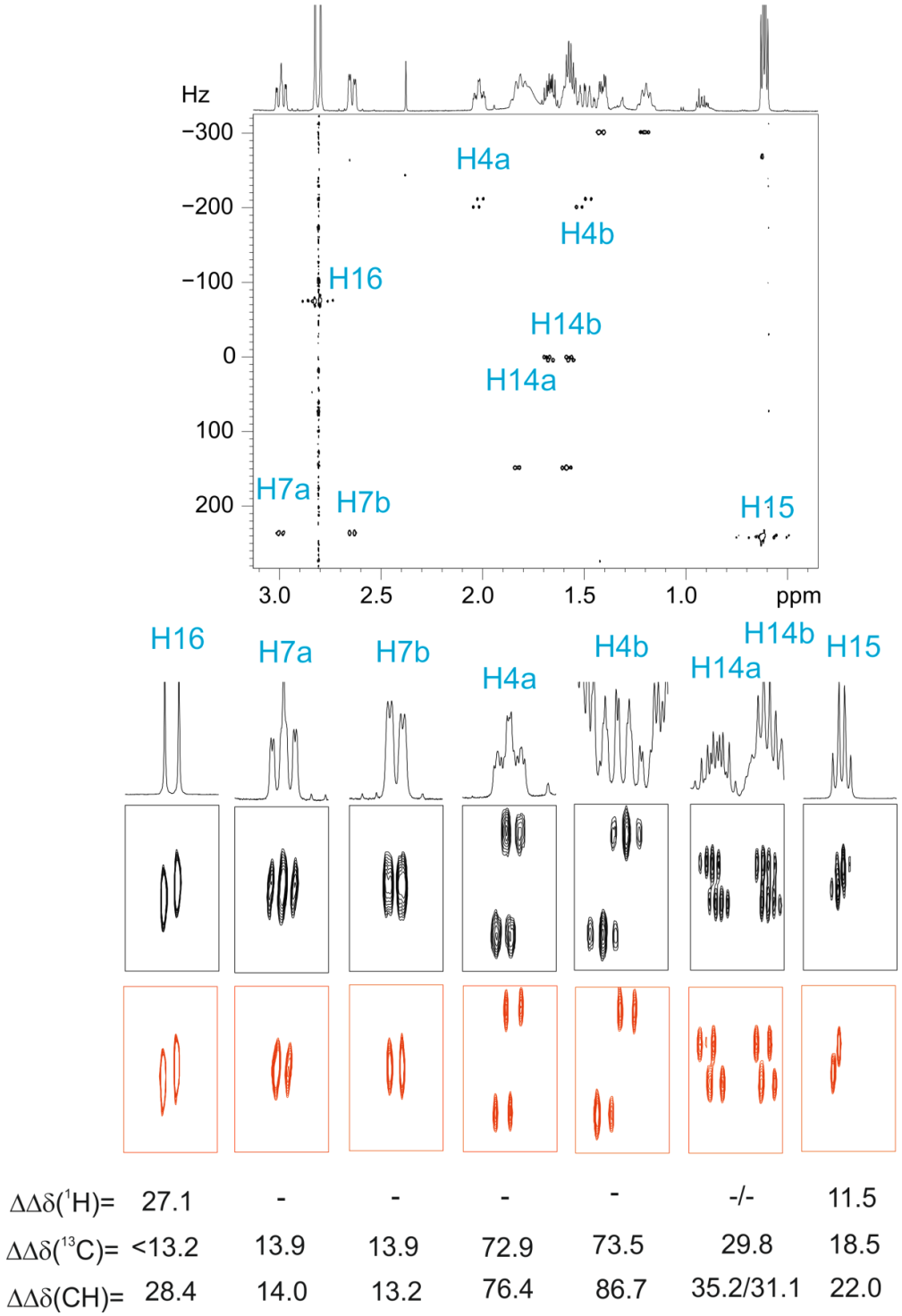

ΔΔδ(^{1}H)=	27.1	-	-	-	-	-/-	11.5
ΔΔδ(^{13}C)=	<13.2	13.9	13.9	72.9	73.5	29.8	18.5
ΔΔδ(CH)=	28.4	14.0	13.2	76.4	86.7	35.2/31.1	22.0

Figure S6: (Top) Expanded area corresponding to the 0.4-3.2 ppm region of the 2D psHSQCsi spectrum of **1** acquired with SW(^{13}C)=5 ppm; (medium) Expanded cross-peaks show the distinction between enantiomeric signals in 1D ^{1}H, conventional HSQC and psHSQCsi spectra; (bottom) experimental values extracted from the conventional ^{1}H spectrum (ΔΔδ(^{1}H)), 1D ^{13}C spectrum (ΔΔδ(^{13}C)) and calculated (ΔΔδ(CH)) values calculated from the splitting measured in the 2D spectrum.

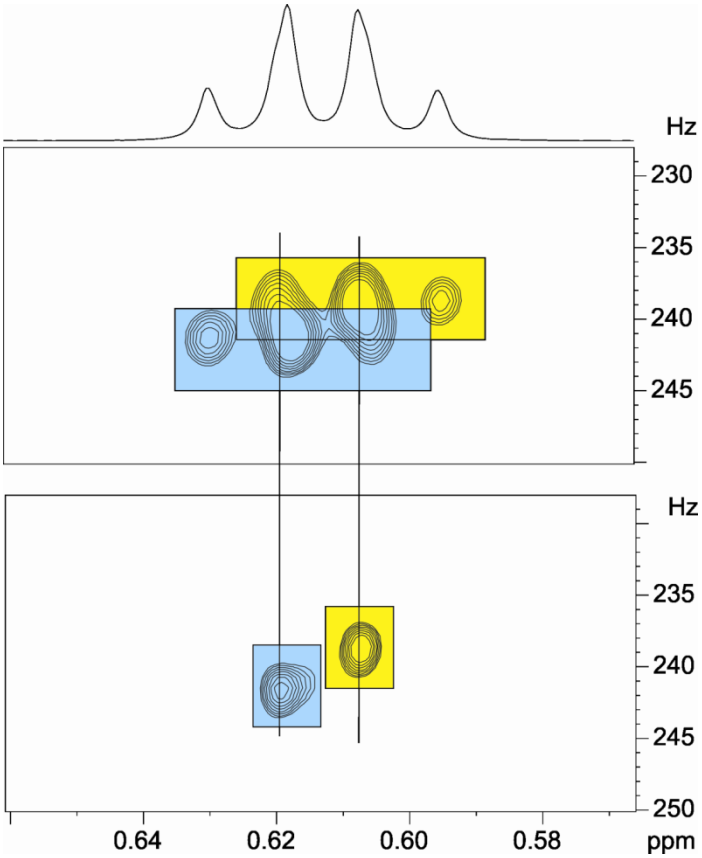

Figure S7: Expanded area corresponding to the C15/H15 cross-peak in (top) SA-HSQC and B) SAPS-HSQC spectra. The H15 signal consists of two overlapped triplets where is difficult to extract the exact ^{1}H chemical shift in both 1H and conventional HSQC spectra. Note the superior features of the SAPS approach to perform: i) automatic peak picking, ii) accurate and simultaneous determination of ^{1}H and ^{13}C chemical shift differences, and iii) an improved quantification by peak volume integration of each individual singlet signal.

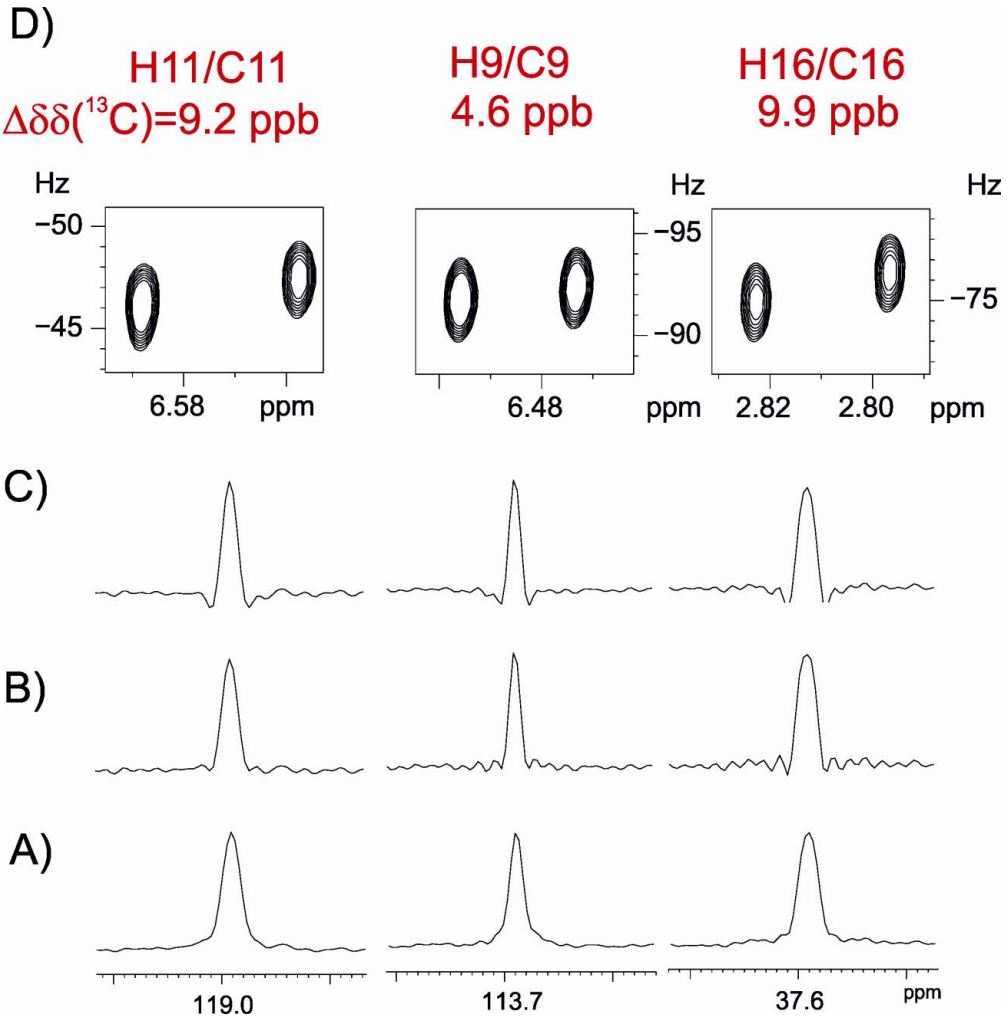

Figure S8: Example showing how the good dispersion along the detected ^{1}H dimensions allows the differentiation of small chemical shift differences along the indirect ^{13}C dimension, even smaller than the line width observed in the conventional ^{13}C spectrum. A-C) show some not resolved ^{13}C signals obtained in the conventional ^{13}C spectrum of 2mM racemic compound 1 complexed with R-PA. Data were acquired with 32K data points and an spectral width of 36057 Hz and further processed with a zero filling up to 64K giving a digital resolution of 0.6 Hz: A) processed with an exponential multiplication with a line broadening of 1 Hz; B) processed without any window function; C) processed with a Gaussian function with LB=-2 Hz and GB=0.5. The line widths at the half of well resolved signals in spectra B was about 1.7 Hz. D) Expansions of the corresponding cross-peaks obtained from the SAPS-HSQC spectra.

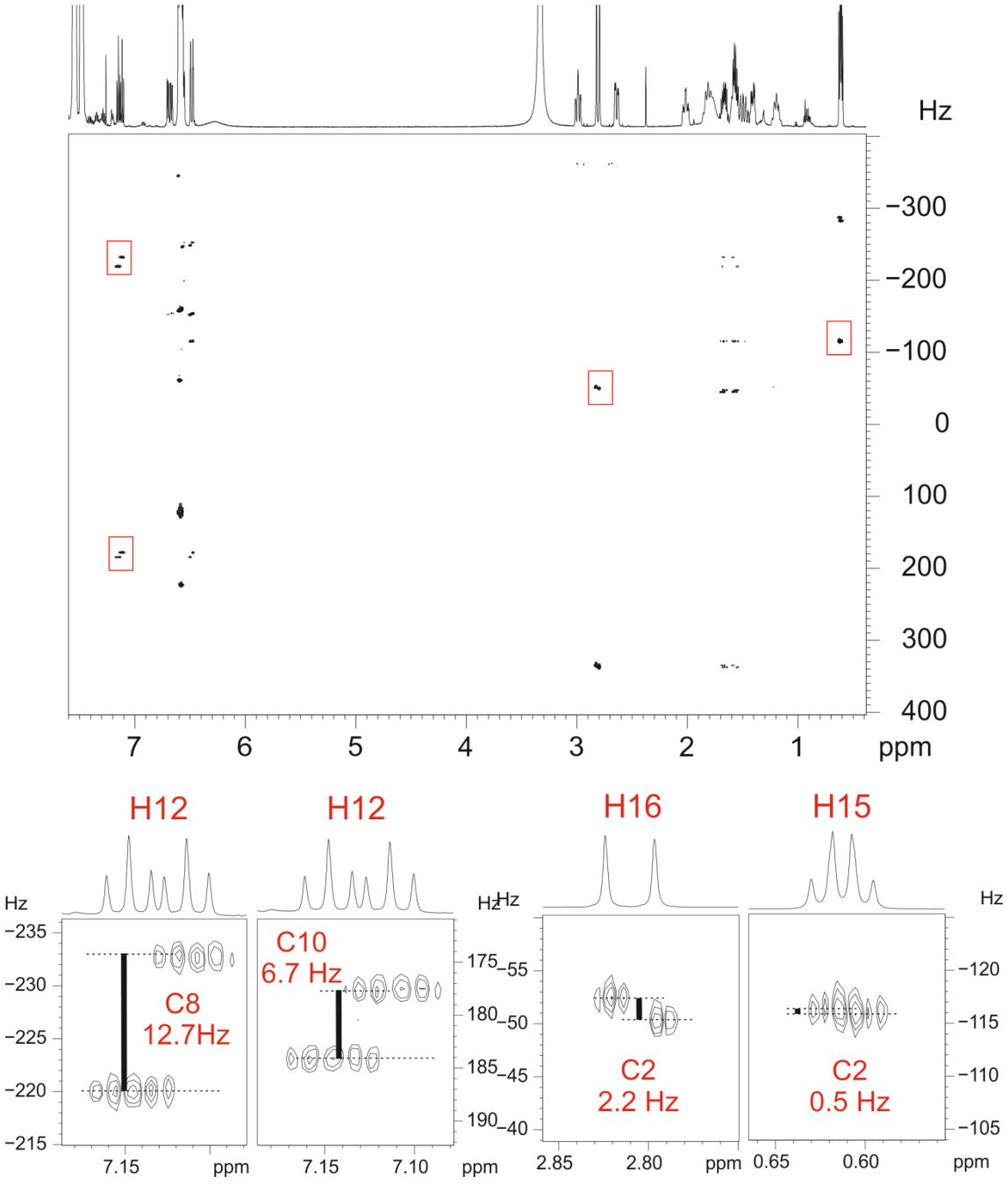

Figure S9: (top) Aliased 2D HSQMBC spectrum of **1**, acquired with a ^{13}C spectral width of 5.0 ppm. (bottom) Some selected 2D cross-peaks corresponding to quaternary carbons where $\Delta\Delta\delta(^{13}C)$ values ranging from 12.7 to 0.5 Hz (84.1 to 3.3 ppb, respectively) can be extracted from the F1 dimension.

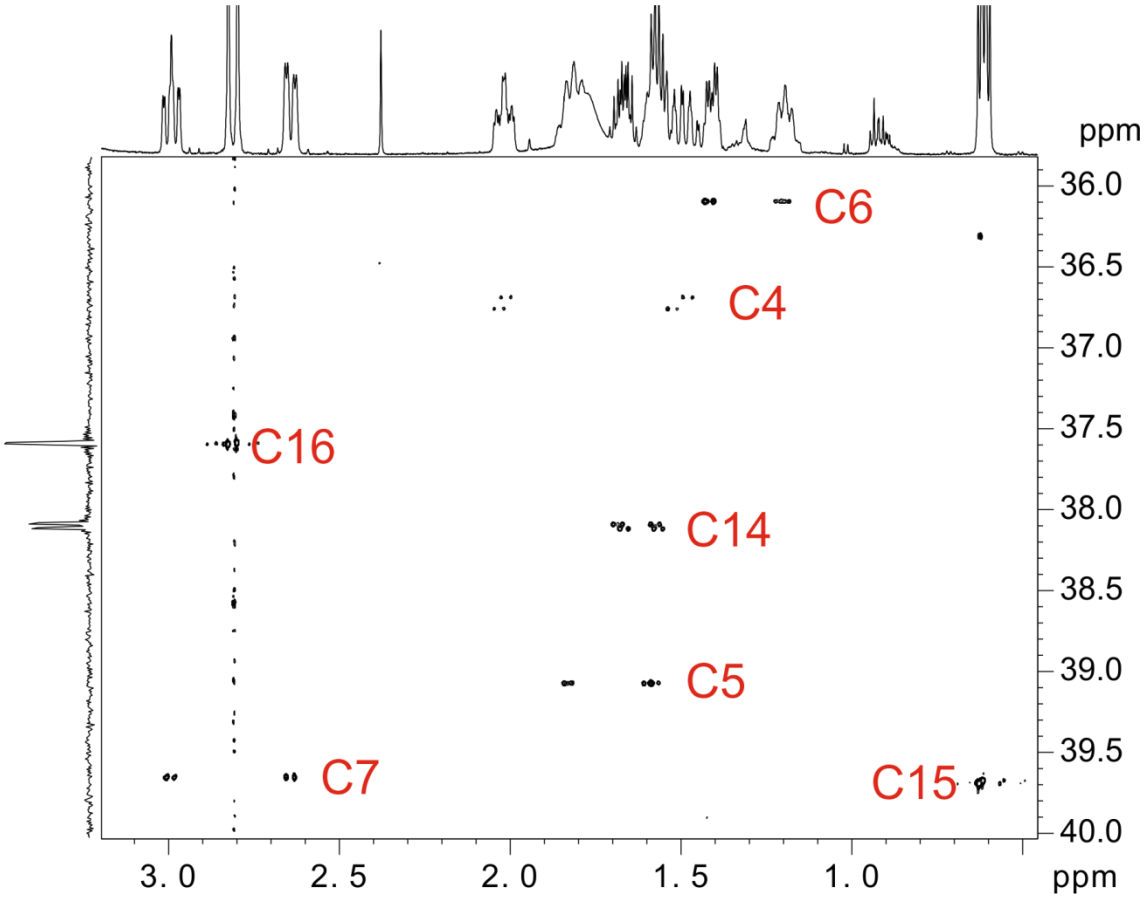

Position	δ(^{13}C) Aliased HSQC	δ(^{13}C) HSQC	K factor
C6	36.08	26.08	-2
C4	36.67/36.75	31.67/31.75	-1
C16	37.60	37.60	0
C14	38.08/38.11	38.08/38.11	0
C15	39.06	24.06	-3
C7	39.64/39.65	49.64/49.65	2
C15	39.67/39.69	9.67/9.69	-6

Figure S10: Chemical shifts in aliased and conventional 2D psHSQCsi spectra. Experimental parameters in the indirect dimension: carrier frequency= 38.0 ppm and ^{13}C spectral width= 5 ppm.

Table S1: ^{1}H and ^{13}C NMR chemical shift differences (($\Delta\Delta\delta(^{1}H)$ and $\Delta\Delta\delta(^{13}C)$ in Hz) of racemic compound **1** (2 mM) enantiodifferentiated with *R*-PA (9.6 equiv.) measured from different NMR experiments at 600MHz.

Position	**$\Delta\Delta\delta(^{1}H)$ [in Hz]**			**$\Delta\Delta\delta(^{13}C)$ [in Hz]**			**$\Delta\Delta\delta$ (CH) [in Hz]**
	1D ^{1}H	1D ZS-^{1}H	Pure shift HSQC[c]	1D ^{13}C	Pure shift HSQC[c]	HSQMBC[b]	
2	-	-	-	2.2	-	2.2	16.1
3	-	-	-	<2	-	0.5	7.2
4a/4b	x[a]/x[a]	12.0/28.2	12.5/27.7	11.0	11.1	-	16.7/29.8
5a/5b	x[a]/x[a]	<2/ x[a]	1.5/12.6	<2	0.8	-	1.7/12.6
6a/6b	x[a]/x[a]	<2/9.4	<2/10.0	<2	<0.5	-	<1/10.0
7a/7b	x[a]/x[a]	3.5/<2	2.8/0.7	2.1	2.0	-	3.4/2.1
8	-	-	-	12.7	-	12.7	24.3
9	13.5	13.7	14.0	<2	0.7		14.0
10	-	-	-	6.6	-	6.7	21.7
11	18.5	19.1	18.4	4.1	3.9	-	18.8
12	20.7	20.9	20.7	5.9	5.8	-	21.4
13	x[a]	x[a]	19.2	<2	1.4	-	19.2
14a/14b	x[a]/x[a]	11.5/ x[a]	11.3/5.9	4.6	4.5	-	12.1/7.4
15	6.9	6.7	7.2	3.2	2.8	-	7.7
16	16.2	16.3	16.0	<2	1.5	-	16.1

[a] Not determined
[b] Only relevant data on quaternary carbons is shown
[c] Digital resolution of ±0.3 and ±0.4 Hz for ^{1}H and ^{13}C respectively.

PUBLICATION 6

Implementing homo- and heterodecoupling in region-selective HSQMBC experiments

Laura Castañar, Josep Saurí, Pau Nolis, Albert Virgili and Teodor Parella.
J. Magn. Reson., **2014**, *238*, 63-69.

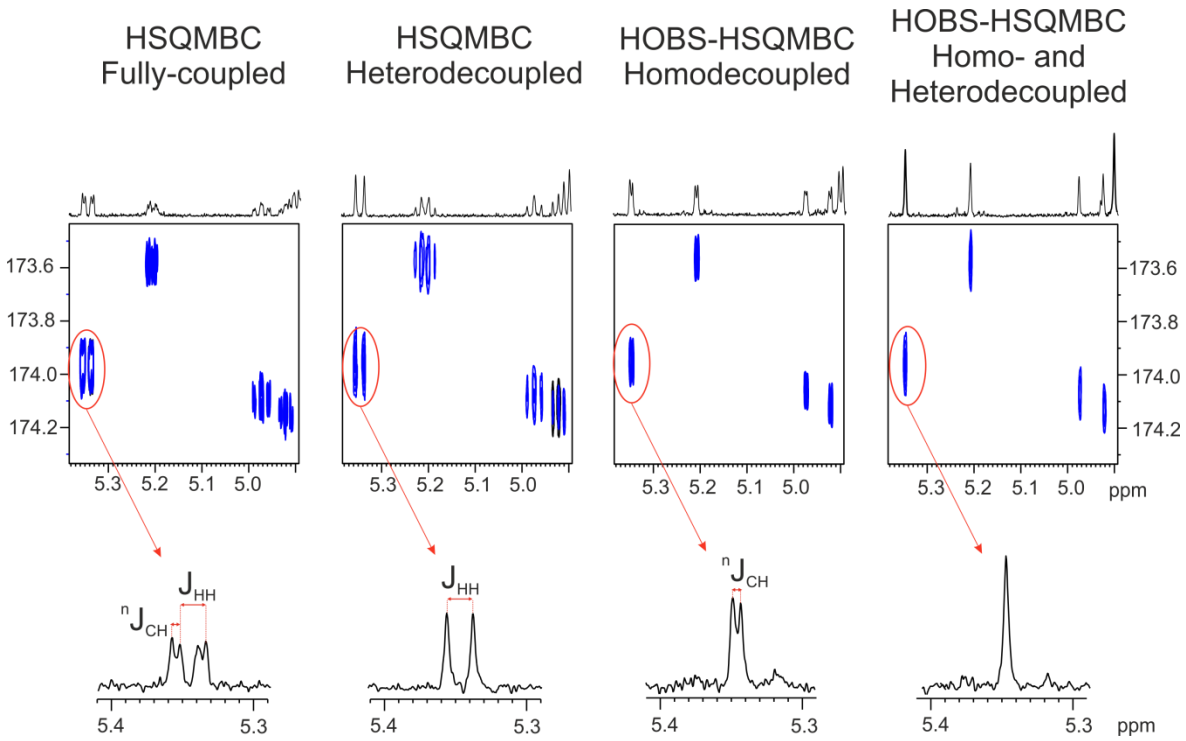

Introduction

As it was mention in the Introduction (see section 1.2.2) the HSQMBC[73] experiment allows obtain correlations between protons and both protonated and non-protonated carbon atoms separated by more than one bond. The main drawback of the conventional HSQMBC experiment is that cross-peaks show important AP contributions due to the J_{HH} evolution during the long INEPT periods (60-70 ms). A series of modified HSQMBC-like experiments have been proposed to obtain IP multiplets which allow measure the $^{n}J_{CH}$ in a more straightforward way (see section 1.2.2.2). It has been show that pure-phase cross-peaks can be obtain from selHSQMBC experiments using region-selective 180^{o} ^{1}H pulses at the middle of the INEPT periods.[78,80] The excellent IP multiplet structure with respect to J_{HH} allows the quantitative and accurate measurement of $^{n}J_{CH}$ from non-distorted pure-phase multiplets along the detected dimension. Importantly, to carry out the measure of the $^{n}J_{CH}$ without additional post-processing fitting or IPAP procedures, high digital resolution levels in the detected dimension is mandatory.

On the other hand, the pure shift methodology greatly improves the spectral resolution in the proton dimension removing the typical J_{HH} multiplet pattern. The incorporation of broadband homodecoupling in experiments detecting AP HH magnetization components, like the regular HSQMBC experiments, fails because multiplet structures should be partially or fully cancelled. However, the excellent IP nature demonstrated for the selHSQMBC experiment allows that homonuclear and/or heteronuclear decoupling can be implemented along the detected dimension using the HOBS technique (see **Publication 2**), obtaining simplified cross-peaks without their characteristic multiplet J_{HH} patterns.

In this article a new method to obtain ^{1}H-homodecoupled long-range ^{1}H-^{13}C correlations from a selected area of a 2D spectrum has been developed. The new HOBS-HSQMBC experiment shows higher resolution and sensitivity than the original selHSQMBC version and represents a completely new way to measure $^{n}J_{CH}$. In the F2-heterocoupled HOBS-HSQMBC version all cross-peaks appear homodecoupled from other protons resonating outside of the selected area, only displaying an IP doublet corresponding to the active $^{n}J_{CH}$ splitting. The semi-automated extraction of $^{n}J_{CH}$ can be made by direct analysis of cross-peaks if the multiplet is resolved enough. In cases of poor resolved multiplets or when the accuracy of the measurements may be doubtful, the application of the IPAP methodology can offer a better solution. The HOBS-HSQMBC method is fully compatible with simultaneous heteronuclear decoupling, leading to complete pure shift NMR spectra with enhanced resolution and maximum sensitivity.

Journal of Magnetic Resonance 238 (2014) 63–69

Contents lists available at ScienceDirect

Journal of Magnetic Resonance

journal homepage: www.elsevier.com/locate/jmr

Implementing homo- and heterodecoupling in region-selective HSQMBC experiments

Laura Castañar, Josep Saurí, Pau Nolis, Albert Virgili, Teodor Parella *

Servei de Ressonància Magnètica Nuclear and Departament de Química, Universitat Autònoma de Barcelona, E-08193 Bellaterra (Catalonia), Spain

ARTICLE INFO

Article history:
Received 21 September 2013
Revised 27 October 2013
Available online 15 November 2013

Keywords:
Pure-shift
Band-selective HSQMBC
Proton–carbon coupling constants
Homonuclear decoupling
Sensitivity improvement
Resolution enhancement

ABSTRACT

An NMR method to enhance the sensitivity and resolution in band-selective long-range heteronuclear correlation spectra is proposed. The excellent in-phase nature of the selHSQMBC experiment allows that homonuclear and/or heteronuclear decoupling can be achieved in the detected dimension of a 2D multiple-bond correlation map, obtaining simplified cross-peaks without their characteristic fine J multiplet structure. The experimental result is a resolution improvement while the highest sensitivity is also achieved. Specifically, it is shown that the ^{1}H-homodecoupled band-selective (HOBS) HSQMBC experiment represents a new way to measure heteronuclear coupling constants from the simplified in-phase doublets generated along the detected dimension.

1. Introduction

Long-range heteronuclear correlation experiments are key NMR tools for the structural characterization of small molecules and natural products in solution. The widely used HMBC/HSQMBC pulse schemes have been modified in several ways in order to improve their success application on a wide range of issues [1–2]. For instance, band-selective excitation in the indirect carbon dimension allows use very reduced spectral widths, and therefore the resolution/dispersion between ^{13}C signals can be strongly increased [3–7]. On the other hand, different attempts have been made to remove the undesired effects due to the evolution of J(HH) that generate cross-peaks with complex phase multiplets. This is particularly severe in HMBC experiments because J(HH) evolves during all the evolution periods, yielding an additional characteristic skew of the cross-peaks that can compromise peak analysis. Constant-time versions of the HMBC experiment have been proposed to remove such inconvenience and their combination with band-selective excitation affords better defined spectra [8–9]. It has been shown that pure-phase cross-peaks can be obtained from HSQMBC experiments using region-selective 180° ^{1}H pulses at the middle of the INEPT periods [10–11]. The excellent in-phase (IP) multiplet structure with respect to J(HH) allows the quantitative and accurate measurement of ^{n}J(CH) from non-distorted pure-phase multiplets along the detected dimension. Furthermore, the easy implementation of the IPAP methodology affords a powerful way to extract them, even when J coupling values are smaller than the linewidth, by analyzing the relative displacement between separate α/β multiplet components [10].

On the other hand, the concept of pure-shift NMR has been introduced in multidimensional NMR experiments as a method to simplify the J(HH) multiplet structure of proton resonances [12–21]. Most of these experiments rely in spatial encoding selection and their reliable applicability strongly depends on the experimental sensitivity. For this reason, pure-shift experiments have been mainly reported for homonuclear applications because its implementation into heteronuclear inverse-detected experiments suffers of important sensitivity success. Using a different concept, a tilted pseudo-3D HMBC experiment has been proposed to achieve ^{1}H-homodecoupling along the detected dimension by incorporating a J-resolved dimension into the HMBC pulse scheme [22].

Recently, a new detection scheme to obtain HOmodecoupled Band-Selection (HOBS) in the detected dimension of multidimensional NMR experiments has been reported [23]. It has been successfully implemented in homonuclear (TOCSY) and heteronuclear (HSQC) experiments involving in-phase HH magnetization. However, the incorporation of this technique in experiments involving anti-phase HH magnetization, like the regular COSY, HMBC or HSQMBC experiments, fail because the evolution of J(HH) generates anti-phase components that would cancel under homodecoupling conditions. Here we show how the HOBS methodology can be implemented in the pure-phase selHSQMBC experiment in order to obtain pure-shift heteronuclear correlation spectra that offer a considerable enhancement in both resolution

* Corresponding author.
E-mail address: teodor.parella@uab.cat (T. Parella).

1090-7807/$ - see front matter © 2013 Elsevier Inc. All rights reserved.
http://dx.doi.org/10.1016/j.jmr.2013.10.022

and sensitivity. In addition, the method is also fully compatible with band-selective excitation in the indirect dimension and with broadband heteronuclear decoupling during detection to obtain high-resolved pure-shift region-selective HSQMBC spectra. It will be shown that the method is also amenable to measure small heteronuclear coupling constants from the pure-phase doublet cross-peaks originated along the detected dimension and also fully compatible with the IPAP methodology described early [24]. All these features will be illustrated using the cyclic undecapeptide cyclosporine as test sample.

2. Results and discussion

Fig. 1 displays two basic pulse schemes of the selHSQMBC experiment [10] that incorporates band-selective homodecoupling during the acquisition period using the HOBS technique. Fig. 1A is a conventional experiment offering broadband ^{13}C excitation in the indirect dimension, whereas Fig. 1B is a ^{13}C band-selective version where the original G1-180°(^{13}C)-δ period during the t_1 period has been replaced by a G1∗0.5-180°($^{13}C_{sel}$)–G1∗(−0.5) block. As in the original experiment, the region-selective 180° ^{1}H pulses applied on non-mutually coupled protons during the long INEPT delays avoid any J(HH) evolution. Just prior to acquisition, signals present pure IP properties with respect to J(HH) coupling constants that are amenable for the application of the HOBS detection scheme to collapse the multiplet J structure. The HOBS scheme consists of n concatenated loops that includes a pair of hard/region-selective 180° ^{1}H pulses (each one flanked by the G3 and G4 gradients) applied at intervals of 2Δ period (Δ is set to AQ/$2n$) as shown in the box of Fig. 1. The selective 180° pulses applied in the INEPT and during detection have the same shape and duration, minimizing the requirements for additional experimental setup. Thus, all protons selected by the region-selective 180° ^{1}H pulse appear homodecoupled from all other protons that do not experience this pulse, and the result is a band-selective homodecoupled observation of a specific region of the ^{1}H spectrum. The method is also fully compatible with optional broadband heteronuclear ^{13}C decoupling which is applied only during the FID acquisition periods (Δ), as shown in Fig. 1. We refer to this technique as a BEHOBS (Broadband-hEterodecoupled and HOmodecoupled Band-Selective) and it affords fully homo- and heteronuclear decoupled spectra consisting only of singlet cross-peaks.

Fig. 2A shows the refocused IP version of the conventionally detected selHSQMBC spectrum of cyclosporine after applying a 5 ms REBURP 180° pulse as a band-selective 180° ^{1}H pulse on its H_α proton region [10–11]. Clearly, all expected long-range correlations are observed showing perfect IP multiplets with respect to both J(HH) and J(CH) coupling constants along the detected dimension. Fig. 2B shows the analog HOBS-HSQMBC spectrum acquired using the scheme of Fig. 1A but without heteronuclear decoupling. We

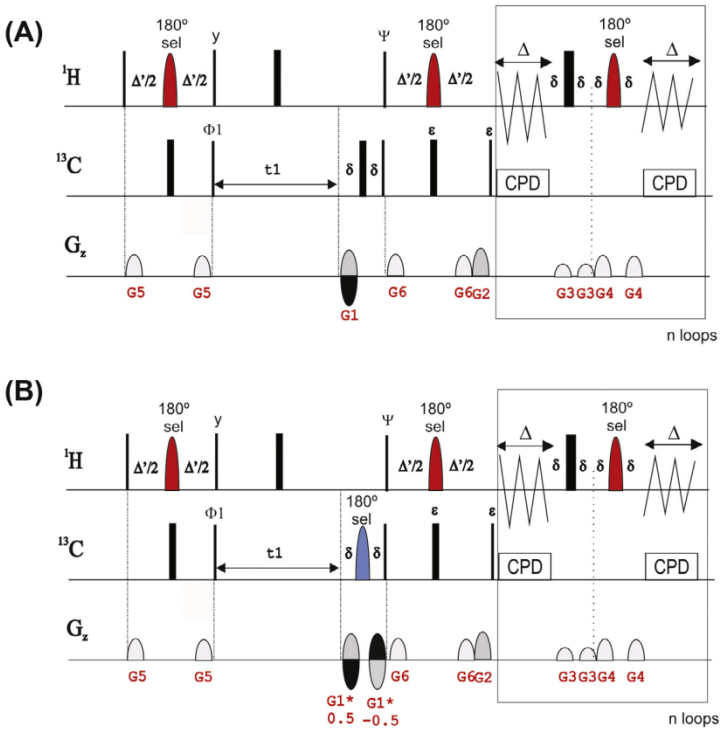

Fig. 1. Experimental pulse schemes for the (A) ^{13}C-broadband and (B) ^{13}C region-selective HOBS-HSQMBC experiment. Thin and thick bars represent broadband 90° and 180° pulses, respectively, whereas shaped pulses are region-selective 180° pulses. The selective 180° ^{1}H pulse applied at the middle of INEPT periods and during detection have the same shape and duration (p_{180}) and we found that REBURP pulses in the order of 3–10 ms provides the best result as a function of the required selectivity. The INEPT delays are set to $\kappa = \Delta' + p_{180} = 1/(2 * {}^{n}J_{CH})$. The basic phase cycling is $\Phi_1 = x, -x$ and Φ(receiver) = $x, -x$; all other unlabeled pulses are from the x-axis. Homonuclear decoupling during the acquisition time (AQ) is performed using a refocusing blocks including a pair of hard/selective 180° ^{1}H pulses applied at intervals of 2Δ = AQ/n, where n is the number of loops. Optional heteronuclear decoupling (CPD) during data collection can also be applied as shown in the scheme. For the measurement of proton-carbon coupling constants, the IPAP methodology can be applied: two different IP and AP data are recorded without heteronuclear decoupling as a function of the last 90° and 180° ^{13}C pulses (IP: $\Psi = y$, ε = on; AP: $\Psi = x$, ε = off) and then they are added/subtracted to afford to separate α/β subspectra. More details in the experimental section.

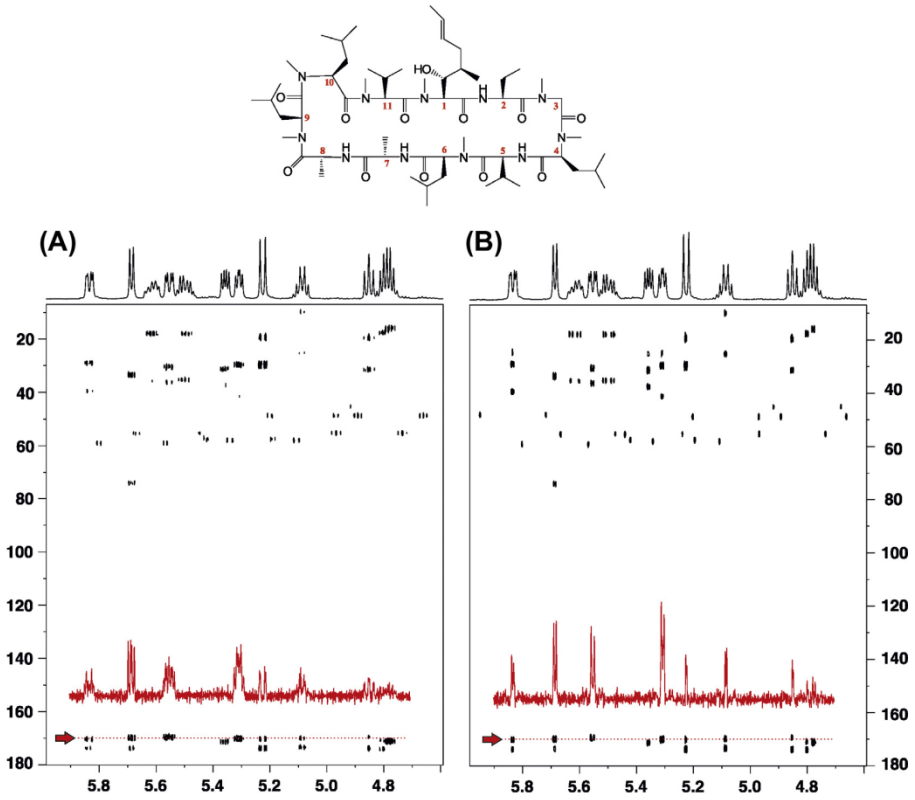

Fig. 2. Practical effects of broadband homodecoupling in the selHSQMBC experiment: (A) Conventional and (B) HOBS HSQMBC spectra of cyclosporine acquired under the same experimental time of 20 min. A selected 1D slice is plotted for each spectrum at the same absolute scale to compare the relative sensitivity and resolution achieved in the 2D spectra. The standard 1D spectrum is shown on top of the 2D plot.

can observe how the J(HH) multiplet structures of all H_α resonances along the detected dimension are collapsed because of the effective homodecoupling of H_α-NH and H_α–H_β coupling constants. A more detailed analysis of a 1D row reveals the enhanced resolution and improved sensitivity achieved with the simple implementation of the HOBS technique.

Fig. 3 shows the improved spectral resolution achieved after combining the band-selective ^{13}C excitation of the carbonyl region in conjunction with the HOBS detection scheme, with simultaneous application of homo- and/or heteronuclear decoupling during data acquisition (see pulse scheme of Fig. 1B): non-decoupled (Fig. 3A), with ^{13}C-decoupling (BEBS, Fig. 3B), with ^{1}H-decoupling (HOBS, Fig. 3C) and with simultaneous ^{13}C and ^{1}H-decoupling (BEHOBS, Fig. 3D) HSQMBC spectra. The analysis of 1D row confirms the enhanced resolution and the improved sensitivity by gradual J multiplet simplification, without affecting spectral quality (Fig. 4). The individual analysis of the SNR for each of the observed 19 cross-peaks affords an average enhancement by factors of 1.2 (with heteronuclear decoupling), 1.6 (with homonuclear decoupling) and 2.4 (with both homo- and heteronuclear decoupling) when compared with fully coupled data (normalized average factor of 1).

Of particular interest is the HOBS-HSQMBC spectrum (Fig. 3C) because all cross-peaks are present as pure IP doublets along the F2 dimension. This represents a completely new way to measure coupling constants, because all cross-peaks appear homodecoupled from other protons resonating outside of the selected area, and therefore they only display the active $^{n}J_{CH}$ splitting (Fig. 5). The direct extraction of these couplings can be made by direct analysis of cross-peaks if the multiplet is resolved enough. Because we are dealing with band-selective experiments, the spectral width in the direct dimension can be set to a reduced value and therefore, it is relatively easy to achieve high levels of spectral resolution. It can be shown that direct CH correlations are also observed because any low-pass J filtering method is applied, and therefore the magnitude of one-bond proton–carbon coupling constants, $^{1}J(CH)$, can be determined from the well separated singlet satellite lines. Until now, these scalar 1J(CH) and residual dipolar $^{1}D(CH)$ coupling constants have been measured from F1- or F2-coupled HSQC experiments [25–29] but the advent of new pure-shift NMR methods will offer a new way to perform this [30–32].

In cases of poor resolved multiplets or when the accuracy of the measurements may be doubtful, the IPAP methodology can offer a better solution. The technique is based in the acquisition of separate IP and AP data as a function of the application of the last 90° and 180° ^{13}C pulses in schemes of Fig. 1 (labeled with ε) followed by time domain IP ± AP data addition/subtraction. In this way, each individual α and β component of the doublet is obtained in two separate subspectra, rendering the measurement easier by simple determination of their relative mutual shift (Fig. 6). Table 1 shows a perfect agreement between the J(CH) values measured directly from the proposed HOBS and HOBS-IPAP methods with those ex-

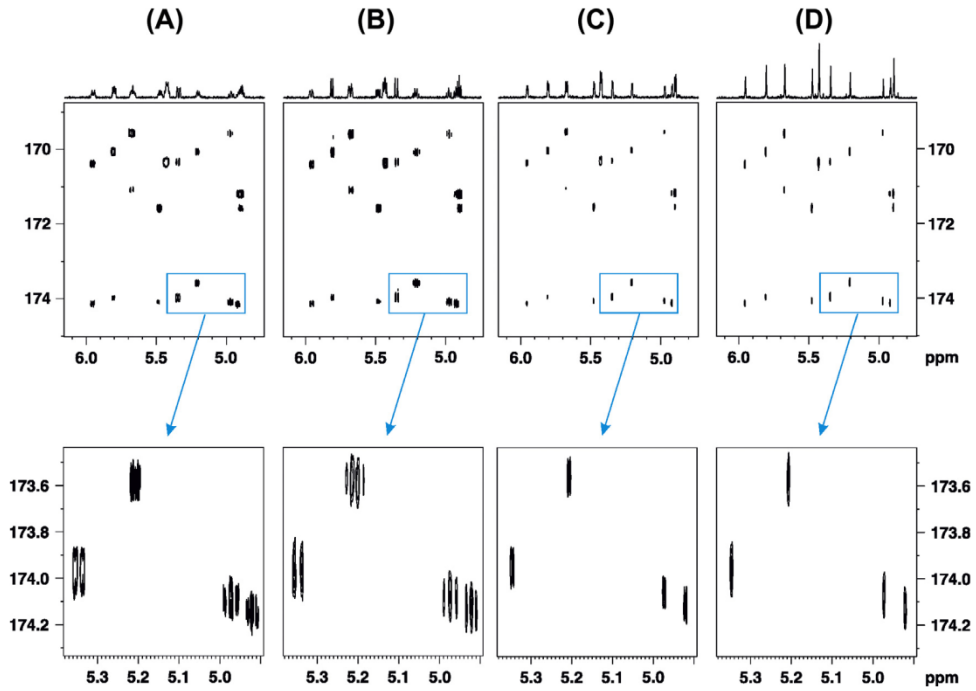

Fig. 3. Resolution enhancement effects after incorporation of homo or/and heteronulear decoupling in region-selected $^{1}H_{\alpha}$–^{13}CO HSQMBC spectra of cyclosporine: (A) conventional; (B) broadband ^{13}C-decoupled (BEBS); (C) ^{1}H-decoupled (HOBS) and (D) ^{1}H and broadband ^{13}C-decoupled (BEHOBS). The internal projection along the detected dimension is shown on top of each 2D plot and all they are plotted with the same absolute scale to compare the relative sensitivity and resolution.

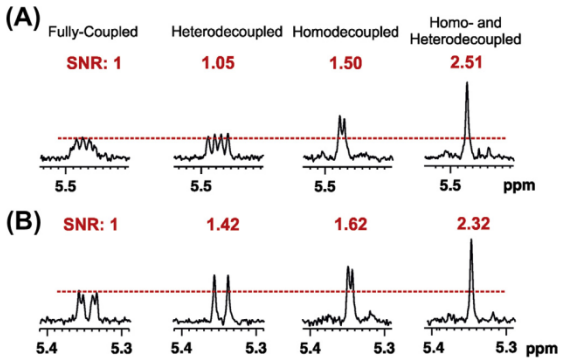

Fig. 4. 1D multiplets corresponding to the (A) C6Hα6 and (B) C11Hα11 cross-peaks obtained from the four different HSQMBC spectra of Fig. 3. The experimental SNR for each signal is shown taking the fully coupled peak (normalized value set to 1) as a reference.

tracted from HSQMBC-TOCSY spectra [33]. The simplicity of the resulting cross-peaks and their IP nature allows an automated peak picking and an easy extraction of $^{n}J(CH)$ values.

3. Conclusions

To conclude, a new method to obtain ^{1}H-homodecoupled long-range ^{1}H–^{13}C correlations from a selected area of a 2D spectrum has been developed. The method is fully compatible with simultaneous heteronuclear decoupling, leading to pure-shift NMR spectra, with enhanced resolution and maximum sensitivity. HOBS experiments have the restriction that full broadband homodecoupling can only be accomplished in regions containing non-mutually J coupled protons. As shown for cyclosporine, peptides are excellent targets for their success because NH, H_{α} and other aliphatic protons resonate in characteristic regions of the ^{1}H spectrum and there is usually no J interference between them. Alternatives to obtain HOBS spectra for the complete ^{1}H spectral range could be feasible by applying spatial-encoded techniques, as reported for broadband Zangger–Sterk (ZS) techniques [14–17], but this would be related to significant reductions in sensitivity.

In addition, we have focused on the success measurement of long-range heteronuclear coupling constants from the resulting in-phase doublet signals along the high-resolved direct dimension. Implementation of the HOBS and related techniques to other experiments is under development and the application to determine coupling constants from ultra simplified multiplets will be further evaluated.

4. Experimental

NMR experiments were performed on a Bruker Avance 600 spectrometer (Bruker Biospin, Rheinstetten, Germany) equipped with TXI HCN z-grad probes. The temperature for all measurements was set to 298 K. All spectra were recorded on a 25 mM sample of cyclosporine in C_6D_6 and processed with TOPSPIN 2.1 (Bruker Biospin, Rheinstetten, Germany).

The conventional 2D ^{1}H–^{13}C region-selective HSQMBC spectrum of Fig. 2A was recorded using the pulse scheme of Fig. 1A with a normal detection period [10]. The recycle delay was 1 s,

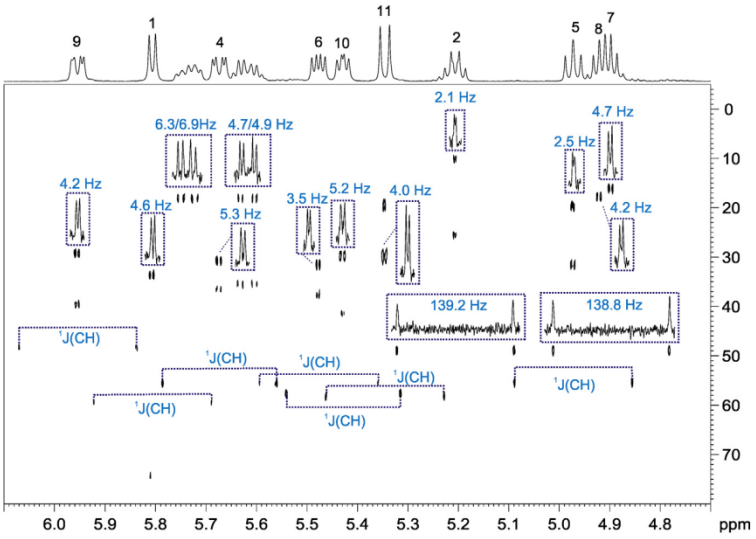

Fig. 5. In-phase HOBS-HSQMBC spectra of cyclosporine showing how the value of J(CH) for all direct and long-range cross-peaks can be extracted directly from the analysis of the clean doublet along the detected dimension (see the extracted value in each individual 1D inset). Note that only the AB spin system (protons resonating at 5.62 and 5.73 ppm) appears as a double of doublets due to their mutual J(HH).

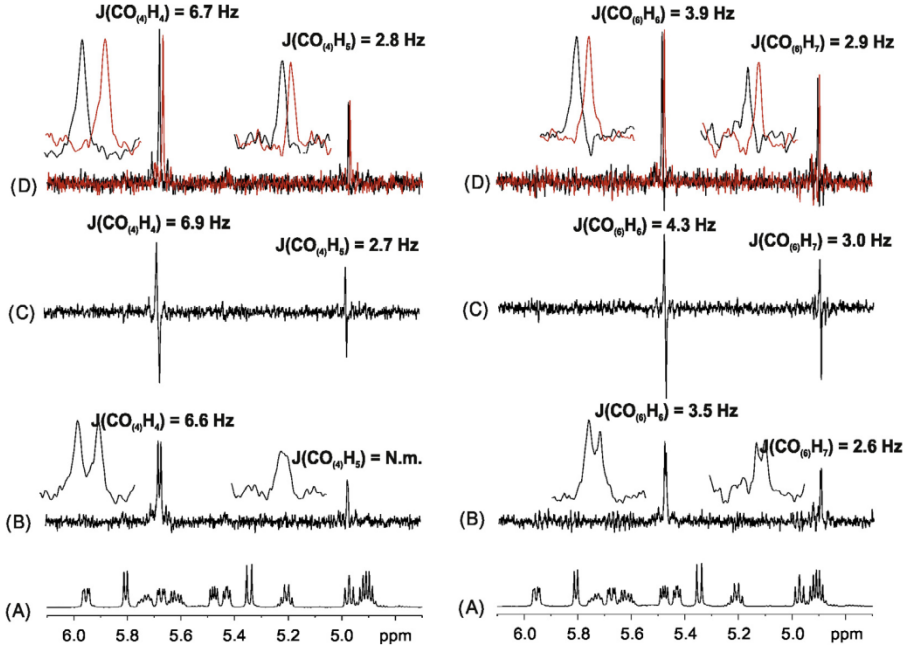

Fig. 6. α/β HOBS-HSQMBC spectra of cyclosporine after applied the IPAP techonology. The separate α and β sub-spectra generated after a combination IP ± AP are overlayed in black/red colors to distinguish the relative shifts along the detected dimension. (B–D) are 1D slices extracted at two different CO(4) (169.5 ppm) and CO(6) (171.6 ppm) carbonyl frequencies corresponding to the (B) in-phase, (C) anti-phase and (D) α/β multiplets. (For interpretation of the references to color in this figure legend, the reader is referred to the web version of this article.)

the region-selective 180° ^{1}H pulse was a REBURP shape of 5 ms of duration (p_{180}), and the interpulse INEPT delays ($\kappa = \Delta' + p_{180} = 1/(2 * {}^{n}J_{CH})$ were optimized for 8 Hz. 4 scans were accumulated for each one of the 128 t_1 increments, the spectral windows in F1 and F2 dimensions were 30,180 Hz and 1800 Hz, respectively, the number of data points in t_2 was set to 4096 and the acquisition time (AQ) was 1.13 s. The total experimental time was of 20 min. The ratio between the G1:G2:G3:G4:G5:G6 gradients were 80:20.1:41:63:11:17, measured as percentage of the absolute gradient strength of 53.5 G/cm. Data were acquired and

Table 1
Proton-carbon coupling constant values (in Hz) in cyclosporine measured from the (A) in-phase HOBS-selHSQMBC, (B) IPAP HOBS-selHSQMBC, and (C) IPAP selHSQMBC-TOCSY [33] experiments. Only the small two- and three-bond proton-carbon coupling constants marked in grey have been represented in the upper graph. The experimental error was of ±0.4 Hz.

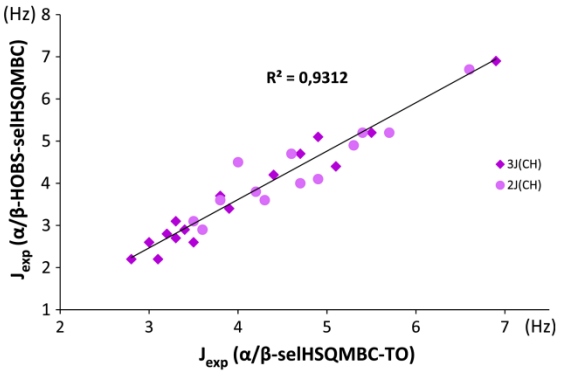

J(C–H_α)	IP HOBS-selHSQMBC (in Hz)	α/β HOBS-selHSQMBC (in Hz)	α/β selHSQMBC-TOCSY (in Hz)
^{3}JC2γ–H2	2.1	2.6	3.0
^{2}JC7β–H7	4.7	4.7	4.6
^{3}JC1η–H1a(olef)	6.3	6.9	6.9
^{2}JC1η–H1b(olef)	4.7	4.9	5.3
^{2}JC8β–H8	4.2	4.5	4.0
^{3}JC11γ–H11	2.0	2.2	2.8
^{3}JC5γ–H5	2.5	3.1	3.3
^{3}JNMe–H9	4.2	4.4	5.1
^{3}JNMe–H10	5.2	5.2	5.5
^{3}JNMe–H11	4.0	4.2	4.4
^{3}JNMe–H4	5.3	5.1	4.9
^{3}JNMe–H6	3.5	3.7	3.8
^{2}JC5β–H5	4.1	4.1	4.9
^{3}JNMe–H1	4.6	4.7	4.7
^{1}JC8H8	142.5	142.2	–
^{1}JC9H9	139.3	139.2	139.5
^{1}JC2H2	139.2	139.1	138.9
^{1}JC7H7	138.8	138.1	–
^{1}JC5H5	139.6	139.6	–
^{1}JC4H4	135.8	135.6	135.9
^{1}JC11H11	140.4	140.4	140.3
^{1}JC10H10	135.5	135.6	135.8
^{1}JC6H6	141.1	141.0	–
^{1}JC1H1	139.9	139.8	140.1
^{2}JCO4–H4	6.8	6.7	6.6
^{3}JCO4–H5	–	2.8	3.2
^{2}JCO1–H1	5.0	5.2	5.4
^{3}JCO1–H2	3.1	3.4	3.9
^{2}JCO9–H9	–	4.0	4.7
^{3}JCO3–H4	–	3.1	3.5
^{2}JCO10–H10	5.8	5.2	5.7
^{3}JCO10–H11	2.3	2.2	3.1
^{2}JCO6–H6	3.8	3.8	4.2
^{3}JCO6–H7	2.5	2.9	3.4
^{2}JCO7–H7	4.9	4.4	ov.
^{2}JCO11–H11	3.7	3.6	3.8
^{3}JCO11–H1	1.9	2.7	3.3
^{2}JCO2–H2	3.7	3.6	4.3
^{2}JCO5–H5	2.6	2.9	3.6
^{3}JCO5–H6	–	2.6	3.5
^{2}JCO8–H8	3.1	3.1	3.5
^{3}JCO8–H9	2.2	3.1	–

processed using the echo/anti-echo protocol. Sine bell shaped gradients of 1 ms duration were used, followed by a recovery delay of 20 μs. Prior to Fourier-transformation of each data, zero filling to 1024 in F1, 8192 points in F2 and a sine squared window function in both dimensions were applied. The analog 2D ^{1}H–^{13}C HOBS-HSQMBC spectrum of Fig. 2B was recorded as described for Fig. 2A using the detection period represented in Fig. 1A, with 20 loops (n), Δ = 28.25 ms and with the same selective pulse applied in the INEPT period.

All four spectra of Fig. 3 were recorded using the pulse sequence of Fig. 1B using only 64 t_1 increments, 4096 data points in t_2, a 2.5 ms REBURP pulse as a region-selected ^{13}C pulse applied at

the CO region (172 ppm) to excite the carbonyl carbons and reducing the spectral width in the indirect F1 dimension to 1800 Hz. 2 scans were collected for each t_1 increment and the overall experimental time for each 2D spectrum was about 5 min. In (A) a conventional detection period was used, in (B) and (D) broadband heteronuclear decoupling was achieved using a 4 kHz GARP scheme applied on-resonance to the carbonyl region, in (C) and (D) ^{1}H homodecoupling (HOBS) was achieved using the detection period represented in Fig. 1A with 20 loops (n) and Δ = 28.25 ms and with an acquisition time of 1.13 s. The spectrum of Fig. 5 was recorded as Fig. 3C but using 128 t_1 increments (experimental time of 10 min). The IPAP 2D subspectra of Fig. 6 were generated from the corresponding IP and AP-HSQMBC experiments separately acquired in the same conditions as described for Fig. 5, and data were added/subtracted in the time-domain without any scaling factor to provide spin-state selective data.

Acknowledgments

Financial support for this research provided by MINECO (Project CTQ2012-32436) is gratefully acknowledged. We also thank to the Servei de Ressonància Magnètica Nuclear, Universitat Autònoma de Barcelona, for allocating instrument time to this project.

References

[1] A. Bax, M.F. Summers, J. Am. Chem. Soc. 108 (1986) 2093–2094.
[2] R.T. Williamson, B.L. Márquez, W.H. Gerwick, K.E. Kövér, Magn. Reson. Chem. 38 (2000) 265–273.
[3] R.C. Crouch, T.D. Spitzer, G.E. Martin, Magn. Reson. Chem. 30 (1992) 595–605.
[4] C. Gaillet, C. Lequart, P. Debeire, J.M. Nuzillard, J. Magn. Reson. 139 (1999) 454–459.
[5] S. Yang, J.K. Gard, G. Harrigan, B. Parnas, J. Likos, R. Crouch, Magn. Reson. Chem. 41 (2003) 42–48.
[6] K. Krishnamurthy, J. Magn. Reson. 153 (2001) 144–150.
[7] R. Crouch, R.D. Boyer, R. Johnson, K. Krishnamurthy, Magn. Reson. Chem. 42 (2004) 301–307.
[8] T.D.W. Claridge, I. Pérez-Victoria, Org. Biomol. Chem. 1 (2003) 3632–3634.
[9] J. Furrer, Chem. Comm. 46 (2010) 3396–3398.
[10] S. Gil, J.F. Espinosa, T. Parella, J. Magn. Reson. 207 (2010) 312–321.
[11] J. Saurí, J.F. Espinosa, T. Parella, Org. Biomol. Chem. 11 (2013) 4473–4478.
[12] A.J. Pell, J. Keeler, J. Magn. Reson. 189 (2007) 293–299.
[13] B. Luy, J. Magn. Reson. 201 (2009) 18–24.
[14] K. Zangger, H. Sterk, J. Magn. Reson. 124 (1997) 486–489.
[15] N.H. Meyer, K. Zangger, Angew. Chem. Intl. Ed. 52 (2013) 7143–7146.
[16] M. Nilsson, G.A. Morris, Chem. Comm. 9 (2007) 933–935.
[17] J.A. Aguilar, S. Faulkner, M. Nilsson, G.A. Morris, Angew. Chem. Intl. Ed. 49 (2010) 3901–3903.
[18] G.A. Morris, J.A. Aguilar, R. Evans, S. Haiber, M. Nilsson, J. Am. Chem. Soc. 132 (2010) 12770–12772.
[19] J.A. Aguilar, A.A. Colbourne, J. Cassani, M. Nilsson, G.A. Morris, Angew. Chem. Intl. Ed. 51 (2012) 6460–6463.
[20] A. Lupulescu, G.L. Olson, L. Frydman, J. Magn. Reson. 218 (2012) 141–146.
[21] J.A. Aguilar, M. Nilsson, G.A. Morris, Angew. Chem. Intl. Ed. 50 (2011) 9716–9717.
[22] P. Sakhaii, B. Haase, W. Bermel, J. Magn. Reson. 228 (2013) 125–129.
[23] L. Castañar, P. Nolis, A. Virgili, T. Parella, Chem. Eur. J. (2013) in press. http://dx.doi.org/10.1002/chem.201303235.
[24] T. Parella, J.F. Espinosa, Prog. Nucl. Magn. Reson. Spectrosc. 73 (2013) 17–55.
[25] B. Yu, H. van Ingen, S. Vivekanandan, C. Rademacher, S.E. Norris, D.I. Freedberg, J. Magn. Reson. 215 (2012) 10–22.
[26] B. Yu, H. van Ingen, D.I. Freedberg, J. Magn. Reson. 228 (2013) 159–165.
[27] J. Farjon, W. Bermel, C. Griesinger, J. Magn. Reson. 180 (2006) 72–82.
[28] V.M. Marathias, I. Goljer, A.C. Bach II, Magn. Reson. Chem. 43 (2005) 512–519.
[29] C.M. Thiele, W. Bermel, J. Magn. Reson. 216 (2012) 134–143.
[30] L. Paudel, R.W. Adams, P. Kiraly, J.A. Aguilar, M. Foroozandeh, M.J. Cliff, M. Nilsson, P. Sandor, J.P. Waltho, G.A. Morris, Angew. Chem. Int. Ed. 52 (2013) 11616–11619.
[31] L. Kaltschnee, A. Kolmer, I. Timári, R.W. Adams, M. Nilsson, K.E. Kövér, G.A. Morris, C.M. Thiele, Pure Shift HSQC Measurements with Perfect BIRD Decoupling – A Method to Decouple Diastereotopic Protons, Poster No. 391 Presented at 9th European Magnetic Resonance Conference EUROMAR, 2013.
[32] I. Timári, L. Kaltschnee, A. Kolmer, R.W. Adams, M. Nilsson, C.M. Thiele, G.A. Morris, K.E. Kövér, J. Magn. Reson., in press. http://dx.doi.org/10.1016/j.jmr.2013.10.023.
[33] J. Saurí, J.F. Espinosa, T. Parella, Angew. Chem. Intl. Ed. 51 (2012) 3919–3922.

PUBLICATION 7

Disentangling complex mixture of compounds with near-identical ^{1}H and ^{13}C NMR spectra using pure shift NMR spectroscopy

Laura Castañar, Raquel Roldán, Pere Clapés, Albert Virgili and Teodor Parella.
Chem. Eur. J., **2015**, *21*, 7682-7685.

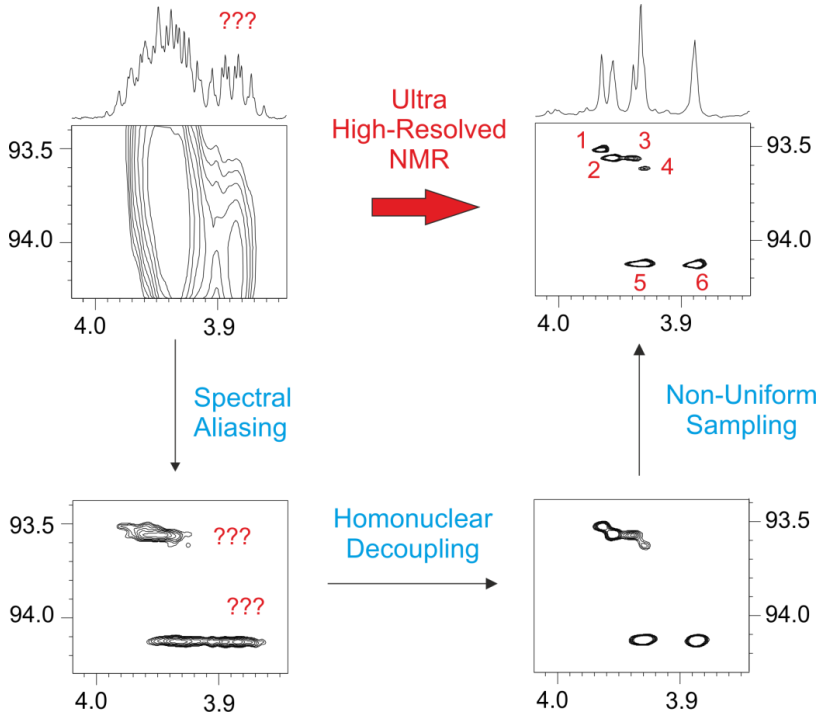

Introduction

As illustrated in **Publication 5**, the incorporation of broadband ^{1}H homodecoupling in the acquisition F2 dimension is fully compatible with other resolution-enhanced NMR techniques, such as spectral aliasing along the indirect F1 dimension,[92] opening the door to the design of ultra-high-resolved 2D NMR experiments in reasonable acquisition times. As it was previously shown, a common feature of spectral aliasing is its general and very easy implementation, improving the attainable resolution along the F1 dimension up to two orders of magnitude by a simple change of the ^{13}C spectral width in HSQC experiments.

In the last years, *Non-Uniform Sampling* (NUS)[68] has emerged as a very powerful tool to significantly speed up the acquisition of multidimensional NMR experiments due to the fact that only a subset of the usual linearly sampled data in the Nyquist grid is measured. For small molecules, NUS can facilitate significant reductions (~50%) in the time needed to collect 2D HSQC spectra, or otherwise offering gains in spectral resolution along the indirect ^{13}C dimension by recording less number of t_1 increments. Some of these algorithms are already implemented in modern NMR software packages, and NMR users can use them in a fully transparent and automatic way without any further modification of the standard pulse programs or general setup parameters. The quality of the resulting spectra depends crucially on the sampling schedules and the algorithms for data reconstruction. However, precaution should be taken for the presence of unwanted artifacts that can generate distorted or false cross-peaks.

In the present article, the combination of these two enhanced resolution approach (NUS and spectral aliasing) with the HOBS methodology (**Publication 2**) into a single 2D NMR experiment is reported for the development and application of ultra-high-resolved HSQC experiments to analyze highly complex mixtures of similar isomers exhibiting near-identical ^{1}H and ^{13}C NMR spectra. The whole ensemble of enhancements applied enables the in-situ distinction and assignment of similar organic compounds exhibiting near-identical ^{1}H and ^{13}C chemical shift and *J* coupling patterns in the same mixture. Very small $\Delta\delta(^{1}H)$ and $\Delta\delta(^{13}C)$ have been distinguished and precisely determined, even in the presence of highly overlapped signals or severe chemical shift degeneracy in conventional 1D ^{1}H and $^{13}C\{^{1}H\}$ NMR spectra. Whereas $\Delta\delta(^{1}H)$ and $\Delta\delta(^{13}C)$ up to 3 and 17 ppb, respectively, can be established from the singlets obtained in 1D HOBS and ^{13}C NMR spectra, the high signal dispersion achieved in spectral-aliased 2D HOBS-HSQC spectra allows an improved detection level to 1 and 5 ppb, respectively. This strategy combined with the use of HOBS versions into the HSQC-TOCSY and HSQMBC experiments has

enabled the unambiguous assignment of ^{1}H and ^{13}C chemical shifts for all peaks of different components of a complex mixture of isomers. The proposed strategy will prove to be very useful to facilitate the analysis of highly complex spectra, as found in many daily situations that exhibit high degeneracy of chemical shifts or severe signal overlap, such as the analysis of crude reactions, detection and characterization of intermediates, or reaction monitoring.

ChemPubSoc Europe

DOI: 10.1002/chem.201500521

CHEMISTRY A European Journal Communication

NMR Spectroscopy

Disentangling Complex Mixtures of Compounds with Near-Identical ^{1}H and ^{13}C NMR Spectra using Pure Shift NMR Spectroscopy

Laura Castañar,[a] Raquel Roldán,[b] Pere Clapés,[b] Albert Virgili,[a] and Teodor Parella*[a]

Abstract: The thorough analysis of highly complex NMR spectra using pure shift NMR experiments is described. The enhanced spectral resolution obtained from modern 2D HOBS experiments incorporating spectral aliasing in the ^{13}C indirect dimension enables the distinction of similar compounds exhibiting near-identical ^{1}H and ^{13}C NMR spectra. It is shown that a complete set of extremely small $\Delta\delta(^{1}H)$ and $\Delta\delta(^{13}C)$ values, even below the natural line width (1 and 5 ppb, respectively), can be simultaneously determined and assigned.

NMR spectroscopy is the most powerful analytical tool to characterize the structure and dynamics of organic molecules in solution. A high spectral resolution is mandatory for identifying individual resonances and to perform accurate measurements of chemical shifts or coupling constants. In past decades, NMR has demonstrated its tremendous capacity to analyze complex mixtures of compounds, where a large number of overlapping signals can be present. However, direct NMR analysis is often limited by the lack of appropriate signal dispersion due to small chemical-shift differences ($\Delta\delta$), the wide J_{HH} coupling patterns that expand the overall multiplet over a range of frequencies, and the natural linewidth ($\Delta\nu_{1/2}$) of each individual NMR signal. A successful characterization can be further complicated when trying to differentiate structural compounds exhibiting extremely small $\Delta\delta$ values and similar *J*-coupling patterns between analogous protons, due to the superposition of near-identical NMR spectra. This can be particularly difficult in ^{1}H NMR spectroscopy, because protons resonate in a relatively narrow range of frequencies (for instance, around 6000 Hz in a 600 MHz spectrometer) whereas each individual multiplet pattern can have a width of some tens of Hz. In contrast, the signal dispersion achieved in standard broadband heteronuclear decoupled ^{13}C NMR spectra is an illustrative example demonstrating how a simple and rapid spectral analysis can be performed when simplified singlet signals are available.

It is known that different molecules have different physical properties and therefore they show different NMR spectra. However, under some conditions, NMR spectra of two different molecules can become nearly identical with a high degree of apparent chemical shift degeneracy, even including the possibility that they are indistinguishable.[1] Several approaches have been reported for discerning compounds with very similar NMR spectra.[2,3] In this work we present a simple but very useful experimental NMR strategy that greatly facilitates the analysis of highly congested spectral regions. We will show here how a mixture of compounds with near-identical ^{1}H and ^{13}C NMR spectra can be distinguished using high-resolution NMR methods based on the combination of pure shift NMR[4–10] and spectral aliasing techniques.[11–16] The power of the proposed method is illustrated with the analysis of a challenging real sample from our lab, consisting of a mixture of several unknown compounds that were finally determined as three pairs of diastereoisomeric derivatives. These compounds were the result of a nonselective homoaldol addition of acetaldehyde, followed by the ketalization of the aldehyde group of the homoaldol adduct by its hydrate form (Scheme 1 and Scheme S1 in the Supporting Information).[17]

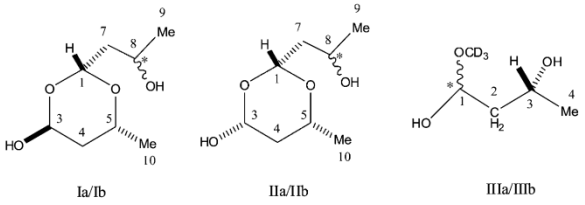

Scheme 1. Structures and numbering of the three pairs of diastereoisomer compounds present in the mixture.

We use a suite of modern pure shift NMR methods based on the homonuclear decoupling band-selective (HOBS) technique[18–21] in order to obtain fully homodecoupled signals for a set of nonmutually *J*-coupled protons resonating in a selected region of the ^{1}H spectrum. The choice of the HOBS over other existing pure shift techniques has been done for various reasons: i) with the aim to maximize sensitivity and to save spectrometer time; ii) the basic set-up is reduced to a simple cali-

[a] L. Castañar, Prof. A. Virgili, Dr. T. Parella
Servei de RMN and Departament de Química
Universitat Autònoma de Barcelona
08193 Bellaterra, Barcelona (Spain)
E-mail: teodor.parella@uab.cat

[b] R. Roldán, Dr. P. Clapés
Biotransformation and Bioactive Molecules Group
Instituto de Química Avanzada de Cataluña, IQAC-CSIC
Jordi Girona 18-26, 08034 Barcelona (Spain)

Supporting information for this article is available on the WWW under http://dx.doi.org/10.1002/chem.201500521.

ChemPubSoc Europe

CHEMISTRY
A European Journal
Communication

bration of a selective 180° ^{1}H pulse according to a selected ^{1}H NMR region; iii) HOBS allows a facile implementation into 2D experiments, as shown for a family of HOBS versions of standard 2D HSQC,[18] HSQC-TOCSY, and HSQMBC[22] experiments for unambiguous assignment purposes. Additionally, it is shown here that using a reduced ^{13}C spectral width of a few ppm, optionally combined with nonuniform sampling (NUS), can produce high-resolution 2D HOBS spectra in conventional acquisition times (Figure 1).

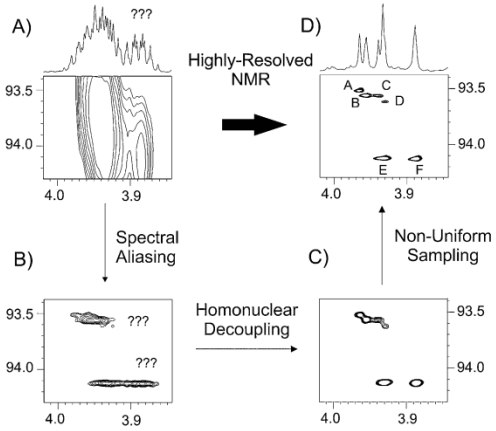

Figure 1. Schematic illustration of the resolution enhancements achieved after combining B) spectral aliasing in the indirect dimension, C) broadband homodecoupling in the detected dimension and D) nonuniform sampling into a single high-resolution HSQC experiment.

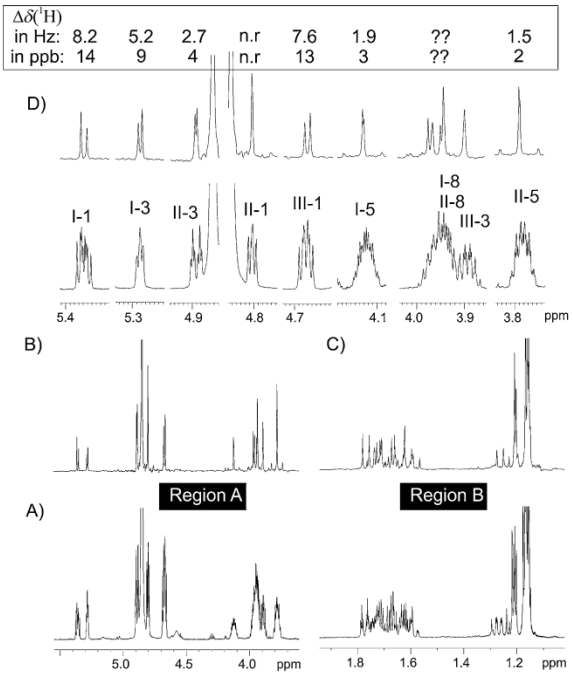

Figure 2. 600 MHz A) conventional and B–C) HOBS ^{1}H NMR spectra of the mixture; D) expanded ^{1}H multiplets of region A showing their $\Delta\delta(^{1}H)$.

At first glance, the conventional analysis of the ^{1}H (Figure 2A) and routine homo- and heteronuclear 2D spectra of the mixture does not provide any evidence of their high complexity, mainly due to the lack of sufficient digital and signal resolution. The presence of multiple components was confirmed from the standard 1D ^{13}C{^{1}H} spectrum, by virtue of its pure chemical shift nature, where all decoupled signals yield highly disperse singlet lines that usually avoid accidental signal overlap. In our sample, most of the ^{13}C signals appear split in a range of $\Delta\delta(^{13}C) = 15$ to 350 ppb (Figure S1 in the Supporting Information), although some peaks did not show observable splitting ($\Delta\delta(^{13}C) < 15$ppb) or, in other cases, the presence of multiple peaks in a narrow range of frequencies limited the possibility to differentiate pairs of signals and therefore to determine $\Delta\delta(^{13}C)$.

Four set of signals could be clearly classified and assigned after examination of ^{1}H, ^{13}C, and HSQC datasets: A) CH signals resonating at δ 4.65–5.38 (carbons between δ 91–97); B) CH signals resonating at δ 3.75-4.16 (carbons between δ 65–73); C) a large number of highly overlapping diastereotopic CH_2 signals resonating at δ 1.56-1.80 with an additional proton at δ 1.26 (carbons between δ 39–47); D) a large number of CH_3 signals resonating at δ 1.14–1.22 ppm (carbons at δ 21–24). The existence of different CH–CH_2–CH–CH_3 subunits was confirmed by the COSY experiment (data not shown).

To get more insight into the analysis of the ^{1}H spectrum, we collected two separate 1D HOBS spectra with full sensitivity in region A around δ 3.5–5.5 (Figure 2B) and region B at δ 1.0–1.8 (Figure 2C), respectively, using a 2.5 ms REBURP 180° ^{1}H pulse. As a first goal, a quick view of the HOBS spectrum of region A (see Figure 2B and its expanded image in Figure 2D), acquired in just half a minute, shows an excellent simplification of all ^{1}H multiplets to homodecoupled singlet signals with $\Delta\nu_{1/2}$ about 1.5 Hz (Figure S10 in the Supporting Information). Most of the ^{1}H signals appear doubled and the fast distinction of extremely small $\Delta\delta(^{1}H)$ values, ranging between 2 and 14 ppb, confirmed the presence of very similar species and the strong requirement for a third decimal place in the description of ^{1}H and ^{13}C NMR data of very similar compounds.[2] It can be observed that some signals are not differentiated (see, for instance, II-1 in Figure 2D) and, in other cases, the presence of multiple and complex overlapping resonances (six different signals appear at δ 3.86–3.99) prevents the identification of pairs of diastereoisomeric resonances and therefore the determination and assignment of $\delta(^{1}H)$.

The next step was to perform a complete ^{1}H/^{13}C chemical shift assignment by a spectral-aliased HOBS-HSQC experiment incorporating NUS (a compromise of 50% of sample points was used; see Figure 3). Data were recorded in about 14 min with a reduced spectral width of 5 ppm (754 Hz at 600 MHz) in the ^{13}C dimension. The expanded areas comparing standard versus pure shift 2D aliased multiplets exemplifies the significant enhanced signal dispersion achieved in broadband homodecoupled single-component cross-peaks, allowing the differ-

ChemPubSoc Europe

CHEMISTRY A European Journal Communication

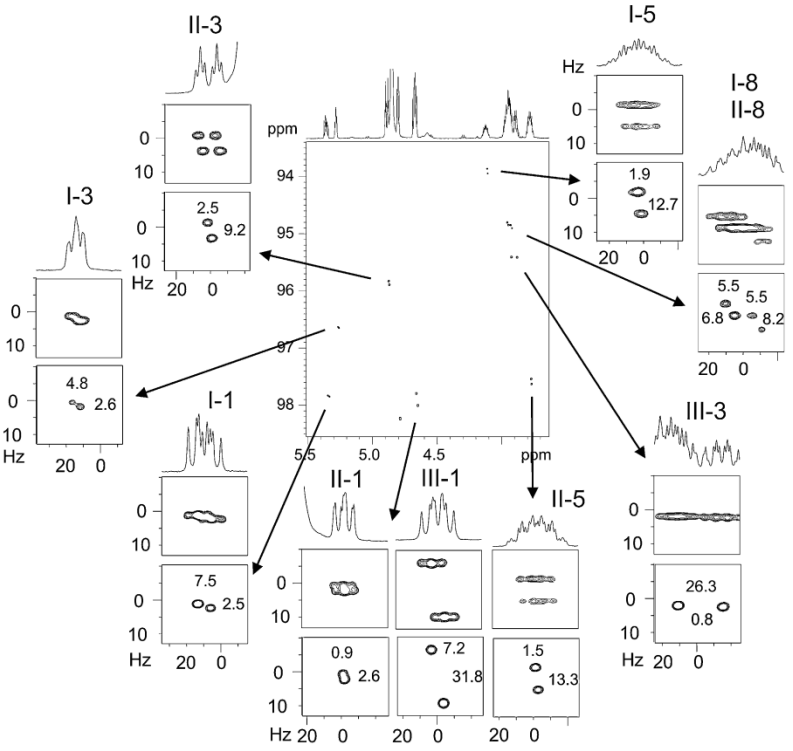

Figure 3. 2D HOBS-HSQC spectrum of region A acquired with SW(^{13}C) = 5 ppm. Expanded 2D cross-peaks corresponding to the (top) spectral-aliased HSQC and (bottom) spectral-aliased HOBS-HSQC spectra are shown for comparison. Experimental $\Delta\delta(^1H)$ and $\Delta\delta(^{13}C)$ are expressed in Hz.

entiation of signals that were not resolved in conventional 1D ^{1}H, 1D HOBS and ^{13}C spectra. It is very important to note that, in addition to the unambiguous chemical shift assignment for all resonances, determinations of $\Delta\delta(^1H)$ and $\Delta\delta(^{13}C)$ to minimum levels of 1 and 5 ppb, respectively, could be done. For instance, protons IIa-1 and IIb-1 which cannot be distinguished in standard and 1D HOBS ^{1}H spectra, are separated by 0.9 Hz (1 ppb) in the HOBS-HSQC spectrum by the small but sufficient signal dispersion of their directly attached carbon (2.7 Hz or 18 ppb). Moreover, all $\delta(^1H)$ and $\delta(^{13}C)$ for the six overlapped I-8, II-8, and III-3 protons could be clearly distinguished and assigned. Finally, as a good example showing the power to analyze high-resolution 2D cross-peaks over conventional 1D ^{13}C data, $\Delta\delta(^{13}C)$ of III-3 was determined to be 5 ppb (0.8 Hz) thanks to its highly dispersed directly attached protons (26.3 Hz or 44 ppb). The excellent signal dispersion achieved between equivalent cross-peaks can allow their quantitative measurements by 2D volume integration. If needed, higher levels of resolution could be achieved using a more drastic reduction of SW(^{13}C) up to 1–2 ppm (Figure S2 in the Supporting Information, SW = spectral width).

As a result of introducing spectral aliasing in HSQC experiments, ^{13}C chemical shift information is initially lost. Each cross-peak will show an experimental chemical shift value (δ_{obs}) that is exactly a multiple of SW(^{13}C) from its real position (δ_r) and it can be determined from the relationship $\delta_r = \delta_{obs} \pm (K*SW(^{13}C))$, where K is the aliasing factor. The true ^{13}C chemical shift values can be deciphered by comparing data from a previously acquired reference 1D ^{13}C or HSQC spectra, or from some reconstruction method. For instance, Figure S3 (in the Supporting Information) shows how K can be easily determined by comparing two different HSQC datasets recorded with F1 spectral widths of 5 and 4.9 ppm.[12]

After the unequivocal assignment of each C/H pair, a complete correlation between all ^{1}H and ^{13}C signals was necessary. Spectral aliasing has been previously reported for traditional HSQC, HSQC-TOCSY, and HMBC experiments,[15] but pure shift experiments retaining the maximum sensitivity are only available for some versions of the HSQC[18,19] and HSQMBC[22] experiments. As another novelty of this work, a HOBS-HSQC-TOCSY experiment is proposed here to assign protons and carbons belonging to the same spin system, in this case, to correlate each one of the two different I-3 signals with the two different I-5 protons. Thus, to completely assign all spin systems, spectral-aliased HSQC-TOCSY (Figure 4 A), HOBS-HSQC-TOCSY (Figure 4 B and S4), and HOBS-HSQMBC (Figure S5 in the Supporting Information) experiments were collected with the same spectral resolution conditions as described for the analogous HOBS-HSQC experiment. The HOBS-HSQMBC spectrum was decisive to determine the long-range correlations through the oxygen atoms between protons 1 and 3/5 in diastereoisomers I and II.

A special mention is required for the analysis of the 20 different resonances of the diastereotopic CH_2 protons appearing in region B at δ 1.6–1.8 region (Figure 2 A, C). The full simplification of this region was more complicated, because these signals cannot be converted to singlets with the HOBS technique, with the remaining active $^2J_{HH}$ observable because the pairs of methylene protons all lie within the same spectral region and hence are not affected by the selective 180° pulse that causes decoupling. Attempts to apply other pure shift methods including BIRD-based HSQC,[10] or the recently proposed PSYCHE experiment,[4] also failed (Figure S11 in the Supporting Information). However, the spectral-aliased HSQC-TOCSY experiment (Figure 4 A and S12 in the Supporting Information) was the most useful tool to determine the CH_2 assignments. A complete list of $\delta(^1H)$, $\delta(^{13}C)$, $\Delta\delta(^1H)$, and $\Delta\delta(^{13}C)$ for all compo-

ChemPubSoc Europe

CHEMISTRY
A European Journal
Communication

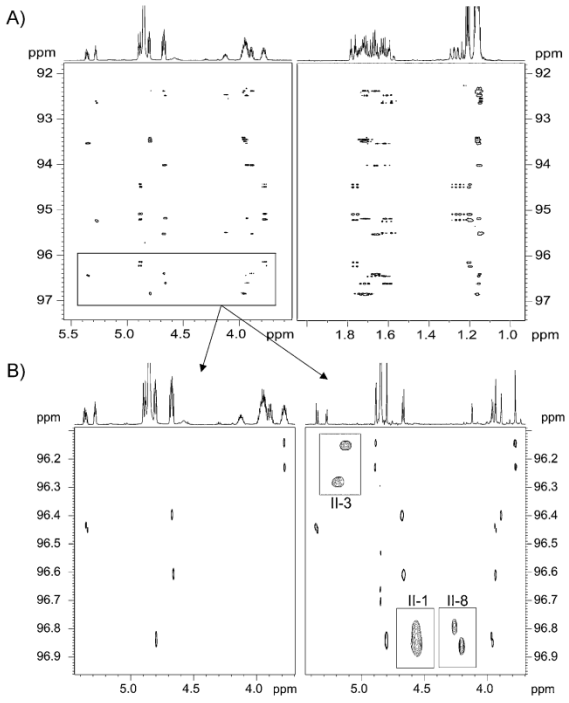

Figure 4. A) Spectral-aliased HSQC-TOCSY spectrum of the mixture acquired with SW(^{13}C) = 5 ppm; B) Expansions to compare the spectral-aliased HOBS-HSQC vs. HOBS-HSQC-TOCSY spectra on region A. In addition to proper assignments, note that relayed cross-peaks can visualize splitting that is not observed with direct correlations.

nents of the mixture are available in Tables S1–S3 in the Supporting Information. Unfortunately, the free rotation of the acyclic subunit makes it virtually impossible to determine the relative configuration of the C8 center in I-II and C1 in III and, therefore, the challenge to completely characterize each individual diastereoisomer remains with us.

In summary, it has been shown that the full sensitivity and the excellent spectral resolution obtained from spectral-aliased 2D HOBS spectra makes it possible to enable the in situ distinction and assignment of similar organic compounds exhibiting near-identical ^{1}H and ^{13}C NMR spectra in the same mixture. Very small $\Delta\delta(^{1}H)$ and $\Delta\delta(^{13}C)$ values can be distinguished and precisely determined, even in the presence of highly overlapping signals or severe chemical shift degeneracy, in conventional 1D ^{1}H and ^{13}C NMR spectra. Whereas $\Delta\delta(^{1}H)$ and $\Delta\delta(^{13}C)$ up to 3 and 17 ppb, respectively, can be established in 1D HOBS and ^{13}C NMR spectra, the excellent signal dispersion achieved in 2D experiments improves the level of detection to 1 and 5 ppb, respectively, as well as to unambiguously assign all peaks for the different components of a mixture. The proposed strategy could be very useful to facilitate the analysis of highly complex spectra, as found in many situations where significant degeneracy of chemical shifts or severe signal overlap is present. There is also potential to use the method with other applications, such as the analysis of crude reactions and detection of intermediates, reaction monitoring, or the analysis of complex mixtures.

Acknowledgements

Financial support for this research, provided by MINECO (projects CTQ2012-32436 and CTQ2012-31605), is gratefully acknowledged. We also thank the Servei de Ressonància Magnètica Nuclear, Universitat Autònoma de Barcelona, for allocating instrument time to this project.

Keywords: homodecoupling · mixture analysis · NMR spectroscopy · pure shift NMR · spectral aliasing

[1] G. Saielli, A. Bagno, *Org. Lett.* **2009**, *11*, 1409 – 1412.
[2] J. G. Napolitano, D. C. Lankin, T. N. Graf, J. Brent Friesen, S. N. Chen, J. B. McAlpine, N. H. Oberlies, G. F. Pauli, *J. Org. Chem.* **2013**, *78*, 2827 – 2839.
[3] N. Basar, K. Damodaran, H. Liu, G. A. Morris, H. M. Sirat, E. J. Thomas, D. P. Curran, *J. Org. Chem.* **2014**, *79*, 7477 – 7490.
[4] M. Foroozandeh, R. W. Adams, N. J. Meharry, D. Jeannerat, M. Nilsson, G. A. Morris, *Angew. Chem. Int. Ed.* **2014**, *53*, 6990 – 6992; *Angew. Chem.* **2014**, *126*, 7110 – 7112.
[5] M. Foroozandeh, R. W. Adams, M. Nilsson, G. A. Morris, *J. Am. Chem. Soc.* **2014**, *136*, 11867 – 11869.
[6] J. A. Aguilar, S. Faulkner, M. Nilsson, G. A. Morris, *Angew. Chem. Int. Ed.* **2010**, *49*, 3901 – 3903; *Angew. Chem.* **2010**, *122*, 3993 – 3995.
[7] N. H. Meyer, K. Zangger, *ChemPhysChem* **2014**, *15*, 49 – 55.
[8] K. Zangger, H. Sterk, *J. Magn. Reson.* **1997**, *124*, 486 – 489.
[9] N. H. Meyer, K. Zangger, *Angew. Chem. Int. Ed.* **2013**, *52*, 7143 – 7146; *Angew. Chem.* **2013**, *125*, 7283 – 7286.
[10] L. Paudel, R. W. Adams, P. Király, J. A. Aguilar, M. Foroozandeh, M. J. Cliff, M. Nilsson, P. Sándor, J. P. Waltho, G. A. Morris, *Angew. Chem. Int. Ed.* **2013**, *52*, 11616 – 11619; *Angew. Chem.* **2013**, *125*, 11830 – 11833.
[11] D. Jeannerat, *Magn. Reson. Chem.* **2003**, *41*, 3 – 17.
[12] I. Baskyr, T. Brand, M. Findeisen, S. Berger, *Angew. Chem. Int. Ed.* **2006**, *45*, 7821 – 7824; *Angew. Chem.* **2006**, *118*, 7985 – 7988.
[13] D. Jeannerat, *J. Magn. Reson.* **2007**, *186*, 112 – 122.
[14] G. B. B. Njock, D. E. Pegnyem, T. A. Bartholomeusz, P. Christen, B. Vitorge, J.-M. Nuzillard, R. Shivapurkar, M. Foroozandeh, D. Jeannerat, *Chim. Int. J. Chem.* **2010**, *64*, 235 – 240.
[15] A. Cotte, M. Foroozandeh, D. Jeannerat, *Chim. Int. J. Chem.* **2012**, *66*, 764 – 769.
[16] M. Pérez-Trujillo, L. Castañar, E. Monteagudo, L. T. Kuhn, P. Nolis, A. Virgili, R. T. Williamson, T. Parella, *Chem. Commun.* **2014**, *50*, 10214 – 10217.
[17] M. Vogel, D. Rhum, *J. Org. Chem.* **1966**, *31*, 1775 – 1780.
[18] L. Castañar, P. Nolis, A. Virgili, T. Parella, *Chem. Eur. J.* **2013**, *19*, 17283 – 17286.
[19] J. Ying, J. Roche, A. Bax, *J. Magn. Reson.* **2014**, *241*, 97 – 102.
[20] R. W. Adams, L. Byrne, P. Király, M. Foroozandeh, L. Paudel, M. Nilsson, J. Clayden, G. A. Morris, *Chem. Commun.* **2014**, *50*, 2512 – 2514.
[21] L. Castañar, M. Pérez-Trujillo, P. Nolis, E. Monteagudo, A. Virgili, T. Parella, *ChemPhysChem* **2014**, *15*, 854 – 857.
[22] L. Castañar, J. Saurí, P. Nolis, A. Virgili, T. Parella, *J. Magn. Reson.* **2014**, *238*, 63 – 69.

Received: February 8, 2015
Published online on March 27, 2015

CHEMISTRY
A European Journal

Supporting Information

Disentangling Complex Mixtures of Compounds with Near-Identical ^{1}H and ^{13}C NMR Spectra using Pure Shift NMR Spectroscopy

Laura Castañar,[a] Raquel Roldán,[b] Pere Clapés,[b] Albert Virgili,[a] and Teodor Parella*[a]

chem_201500521_sm_miscellaneous_information.pdf

Table of Contents

Experimental Section

Compounds were obtained by stirring an aqueous solution acetaldehyde (20 mL, 5 % v/v) in aqueous buffer trietanolamine (50 mM, pH 8.0) during 48 hours. Then the pH was adjusted to pH 5.6, the aqueous solvent was evaporated under vacuum and then purified by column chromatography on silica. The formation of the compunds Ia/Ib and IIa/IIb (Scheme S1) consists first in the dimerization of acetaldehyde to produce **S1** via aldol addition with an ensuing formation of a ketal between the aldehyde group of **S1** and the hydrate form of the dimer **S2**.

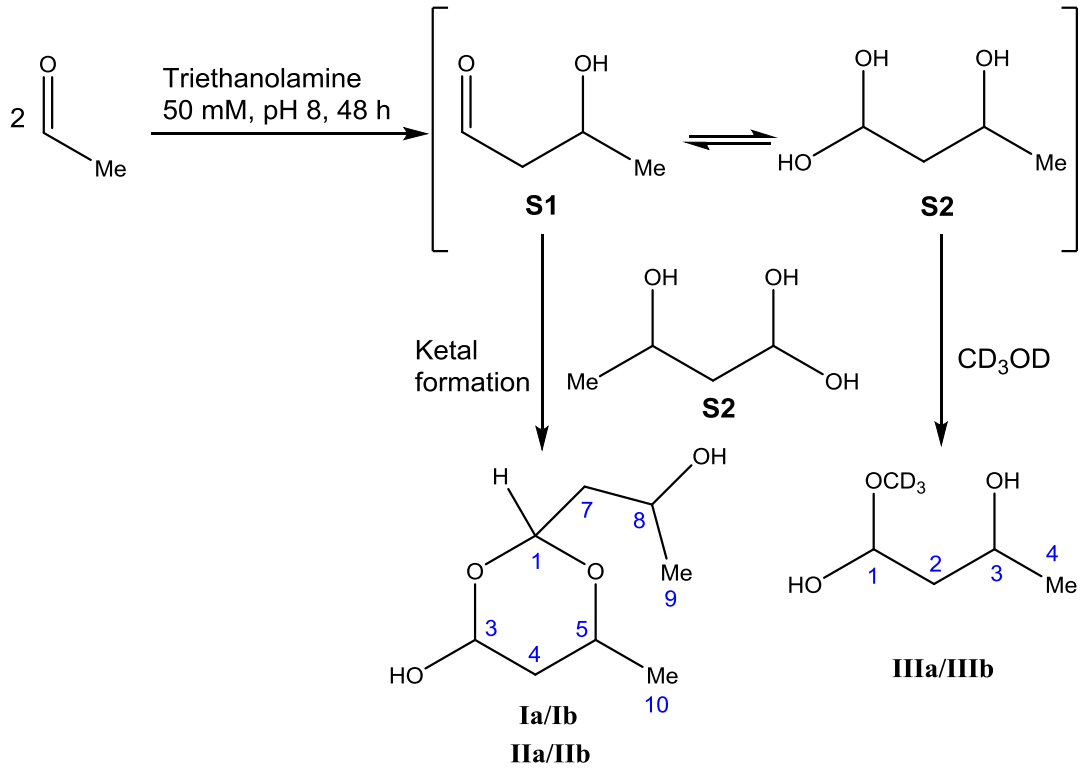

Scheme S1. Formation of **Ia/Ib**, **IIa/IIb** and **IIIa/IIIb** compunds from acetaldehyde.

The conformation and relative configurations of isomers Ia/Ib and IIa/IIb (see 3D views in tables S1-S2) have been determined using several NMR evidences:

- Key 1,3-diaxial NOEs were observed between H1 and H5 in derivatives Ia/Ib and between H1 and both H3/H5 in compounds IIa/IIb (see Figures S7 and S8)

- The effect of the hydroxyl group on the C3 position in isomers I and II is clearly observed in δ(H5) and δ(H1) values.
- The different axial/equatorial position of the H3 proton is evidenced from their δ values.
- Due to the high level of multiplet overlapping of protons H3 and H5, the accurate measurement of the corresponding J(H3-H4) and J(H5-H4) was not an easy task. However, it is evident from the 1H spectrum large J(H3-H4ax) values for isomers IIa/IIb (H3 is a double-doublet with 2.5 and 9.7 Hz) and small for isomers Ia/Ib (H3 is a double-doublet with 1.3 and 3.5 Hz) which were confirmed by a J-resolved experiments.

All experiments were acquired on a Bruker AVANCE spectrometer (Bruker BioSpin, Rheinstetten, Germany) operating at 600.13 MHz proton frequency, equipped with a 5 mm triple resonance inverse probe and a z-axis pulsed field gradient accessory (maximum strength of 53.5 G/cm). The spectra were collected on sample containing a mixture of unknown compounds dissolved in CD_3OD at a temperature T = 298 K, and processed with the software TOPSPIN 3.1.

The non-selective ^1H 180 pulses were of 8.6 μs duration. For all 1D and 2D HOBS experiments, a 180º band-selective REBURP shaped pulse of 2.5 ms was used for both excitation and homodecoupling. The strengths of the G3, G4 and G5 gradients were set to 21.9, 33.7 and 12.3 G/cm, respectively, with durations of 500 μs followed by a recovery delay of 20 μs.

1D HOBS spectra of Fig. 2B and 2C were recorded using the pulse sequence displayed in Fig. S7A, with four scans and 1 s of recycle delay. The spectral width was 7200 Hz, and 16K complex points were recorded during an acquisition time of 1.13 s. 40 loops (n) were concatenated with τ=AQ/2n=7.2 ms. The 1D time-domain data were directly transformed without any sensitivity or resolution enhancement.

The 2D ^1H-^{13}C HOBS-HSQC spectrum (Fig. 4A) was acquired using the pulse sequence displayed in Fig. S6B, optimized to 140 Hz ($\Delta=1/(2*J_{CH})$). Two scans of 2048 complex points were collected over an observed ^1H spectral width of 3600 Hz for each of the 256 t_1

values. The gradient ratio G1:G2 was set to 80:20.1 (percentage of the maximum strength of 53.5 G/cm). The acquisition time was of 0.284 ms. Data of Fig. 3 were acquired with SW(^{13}C)=5ppm (754 Hz) and transformed with a shifted sine window function along both the F1 and F2 dimensions and with a zero-filling to 8K in F2 and 1K in F1. Final resolution was 0.44 and 0.73 Hz/Pt in the F2 and F1 dimensions, respectively. The initial 90º band-selective pulses was a EBURP-2 shaped pulse of 1.75 ms. For homonuclear decoupling, 130 loops (n) were concatenated with τ=AQ/2n=9 ms. NUS was applied with a sampling density of 50%. The total experimental time was about 14 minutes.

The 2D ^{1}H-^{13}C HOBS-HSQC-TOCSY spectrum was acquired using the pulse sequence displayed in Fig. S6C with a mixing time of 60 ms. The number of scans was 8 per t_1 increment and all other acquisition and processing parameters as described for the HSQC experiment. The total experimental time was about 60 minutes. The 2D ^{1}H-^{13}C HOBS-selHQMBC spectrum was acquired using the pulse sequence displayed in Fig. S6D, with 32 scans per t_1 increment and optimized to $1/(2*J_{CH})$=8 Hz. All other parameters as described for the HSQC experiment. The total experimental time was about 2 hours. Standard HSQC, HSQC-TOCSY and selHSQMBC experiments were recorded with the same pulse schemes of Fig. S6 and the same conditions, but including a standard FID period as acquisition.

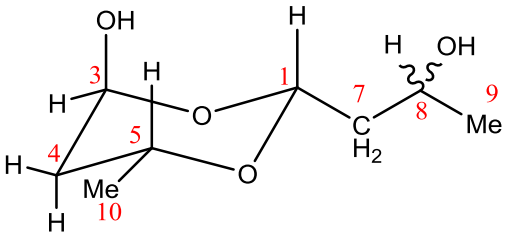

Table S1: ^{1}H and ^{13}C chemical shift values (in ppm) and $\Delta\delta(^{1}H)$ and $\Delta\delta(^{13}C)$ (in ppm and Hz) of the two distinguished diastereoisomers Ia/Ib.

	Ia		Ib		1D HOBS[a]	1D ^{13}C[a]	HOBS-HSQC[c]	
	^{1}H	^{13}C	^{1}H	^{13}C	$\Delta\Delta\delta(^{1}H)$	$\Delta\Delta\delta(^{13}C)$	$\Delta\Delta\delta(^{1}H)$	$\Delta\Delta\delta(^{13}C)$
1	5.365	92.802	5.351	92.820	0.014 (8.2)	0.019 (2.2)	0.012 (7.5)	0.016 (2.4)
3	5.278	91.629	5.287	91.611	0.009 (5.2)	0.018 (2.7)	0.008 (4.8)	0.018 (2.7)
4	1.629 1.582	39.024	1.629- 1.583	38.981	n.d	0.039 (5.9)	n.d	0.043 (6.5)
5	4.126	68.851	4.123	68.937	0.003 (1.9)	0.086 (12.7)	0.003 (1.9)	0.084 (12.7)
7	1.665 1.638	44.919	1.703- 1.617	44.919	n.d	n.d	n.d	n.d
8	3.944	64.825	3.938	64.879	n.d	n.d	0.009 (5.5)	0.054 (8.1)
9	1.166	23.692	1.166	23.692	n.d	n.d	n.d	n.d
10	1.156	21.862	1.159	21.862	n.d	n.d	n.d	n.d

a) Resolution in HOBS and ^{13}C after processing were 0.11 and 0.38 Hz/pt, respectively.
b) Resolution in the F2 and F1 dimension of the 2D HOBS-HSQC was 0.43 and 0.73 Hz/pt, respectively, after processing.
c) n.d=not determined; by signal overlap or lack of resolution

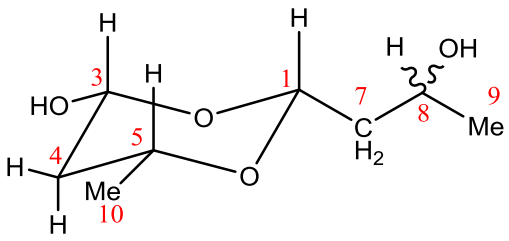

Table S2: ^{1}H and ^{13}C chemical shifts values (in ppm) and $\Delta\delta(^{1}H)$ and $\Delta\delta(^{13}C)$ (in ppm and Hz) of the two distinguished diastereosiomers IIa/IIb.

	IIa		IIb		1D HOBS[a]	1D ^{13}C[a]	HOBS-HSQC[c]	
	^{1}H	^{13}C	^{1}H	$\Delta\Delta\delta(^{13}C)$	$\Delta\Delta\delta(^{1}H)$	$\Delta\Delta\delta(^{13}C)$	$\Delta\Delta\delta(^{1}H)$	$\Delta\Delta\delta(^{13}C)$
1	4.805	98.194	4.804	98.215	<0.002 (<2)	0.021 (2.6)	0.001 (0.9)	0.018 (2.7)
3	4.892	95.810	4.888	95.874	0.004 (2.7)	0.062 (9.1)	0.004 (2.5)	0.061 (9.3)
4	1.774 1.267	41.466	1.774 1.267	41.466	n.d	n.d	n.d	n.d
5	3.781	72.616	3.783	72.528	0.002 (1.5)	0.092 (13.2)	0.002 (1.6)	0.088 (13.3)
7	1,745 1.710	44.876	1.736 1.717	44.829	n.d	n.d	n.d	0.045 (6.8)
8	3.970	64.780	3.961	64.825	n.d	n.d	0.009 (5.4)	0.048 (7.2)
9	1.173	23.776	1.172	23.742	n.d	n.d	n.d	0.038 (5.7)
10	1.209	21.586	1.214	21.572	n.d	0.017(2.7)	0.009 (5.4)	0.014 (2.3)

a) Resolution in HOBS and ^{13}C after processing were 0.11 and 0.38 Hz/pt, respectively.
b) Resolution in the F2 and F1 dimension of the 2D HOBS-HSQC was 0.43 and 0.73 Hz/pt, respectively, after processing.
c) n.d=not determined; by signal overlap or lack of resolution

Table S3: ^{1}H and ^{13}C chemical shift values (in ppm) and $\Delta\delta(^{1}H)$ and $\Delta\delta(^{13}C)$ (in ppm and Hz) of the two distinguished diastereosiomers IIIa/IIIb.

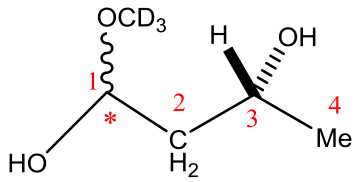

	IIIa		IIIb		1D HOBS[a]	1D ^{13}C[a]	HOBS-HSQC[c]	
	^{1}H	^{13}C	^{1}H	^{13}C	$\Delta\Delta\delta(^{1}H)$	$\Delta\Delta\delta(^{13}C)$	$\Delta\Delta\delta(^{1}H)$	$\Delta\Delta\delta(^{13}C)$
1	4.680	97.759	4.667	97.974	0.013 (7.59)	0.216 (31.6)	0.012 (7.16)	0.210 (31.75)
2	1.679 1.663	46.923	1.727 1.612	46.577	n.d	0.350 (51.6)	n.d	0.343 (51.7)
3	3.894	65.393	3.938	65.385	n.d	n.d	0.044 (26.31)	0.005 (0.81)
4	1.162	23.745	1.166	23.845	n.d	n.d	0.004 (2.4)	0.110 (16.7)

a) Resolution in HOBS and ^{13}C after processing were 0.11 and 0.38 Hz/pt, respectively.
b) Resolution in the F2 and F1 dimension of the 2D HOBS-HSQC was 0.43 and 0.73 Hz/pt, respectively, after processing.
c) n.d=not determined; by signal overlap or lack of resolution

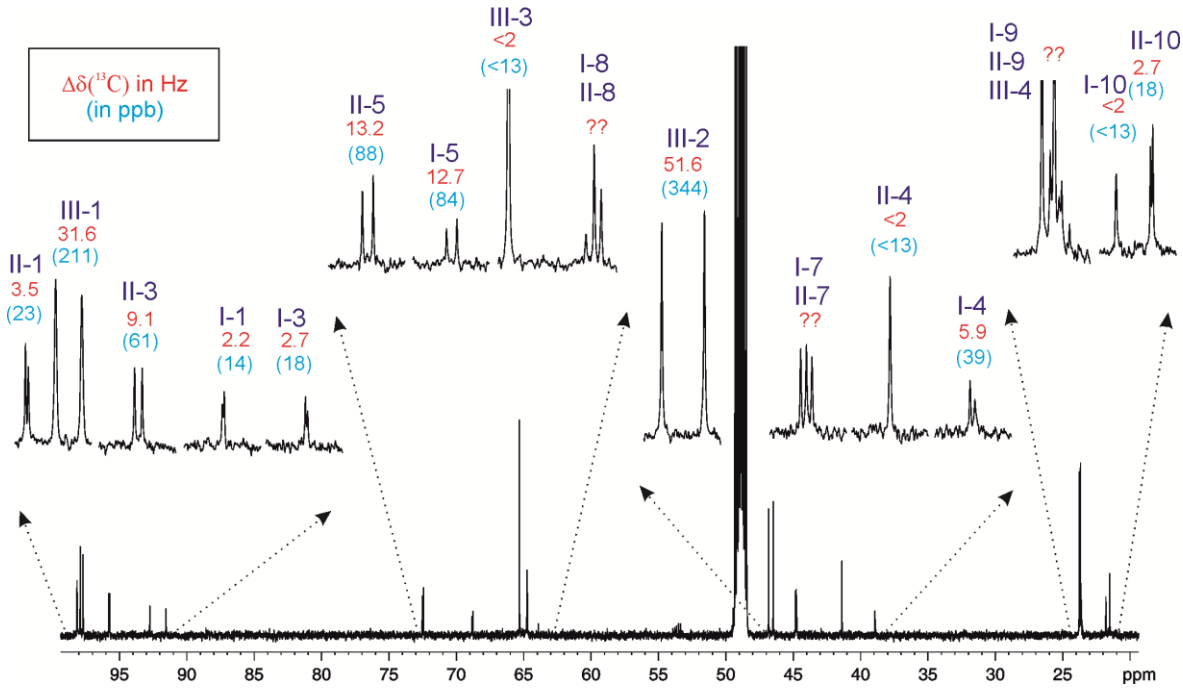

Figure S1: 150.62 MHz 1D ^{13}C NMR spectrum of the mixture. Expanded areas shows the chemical shift differences (in Hz and ppb) observed for analog carbons in the mixture of the diastereoisomers Ia/Ib, IIa/IIb and IIIa/IIIb.

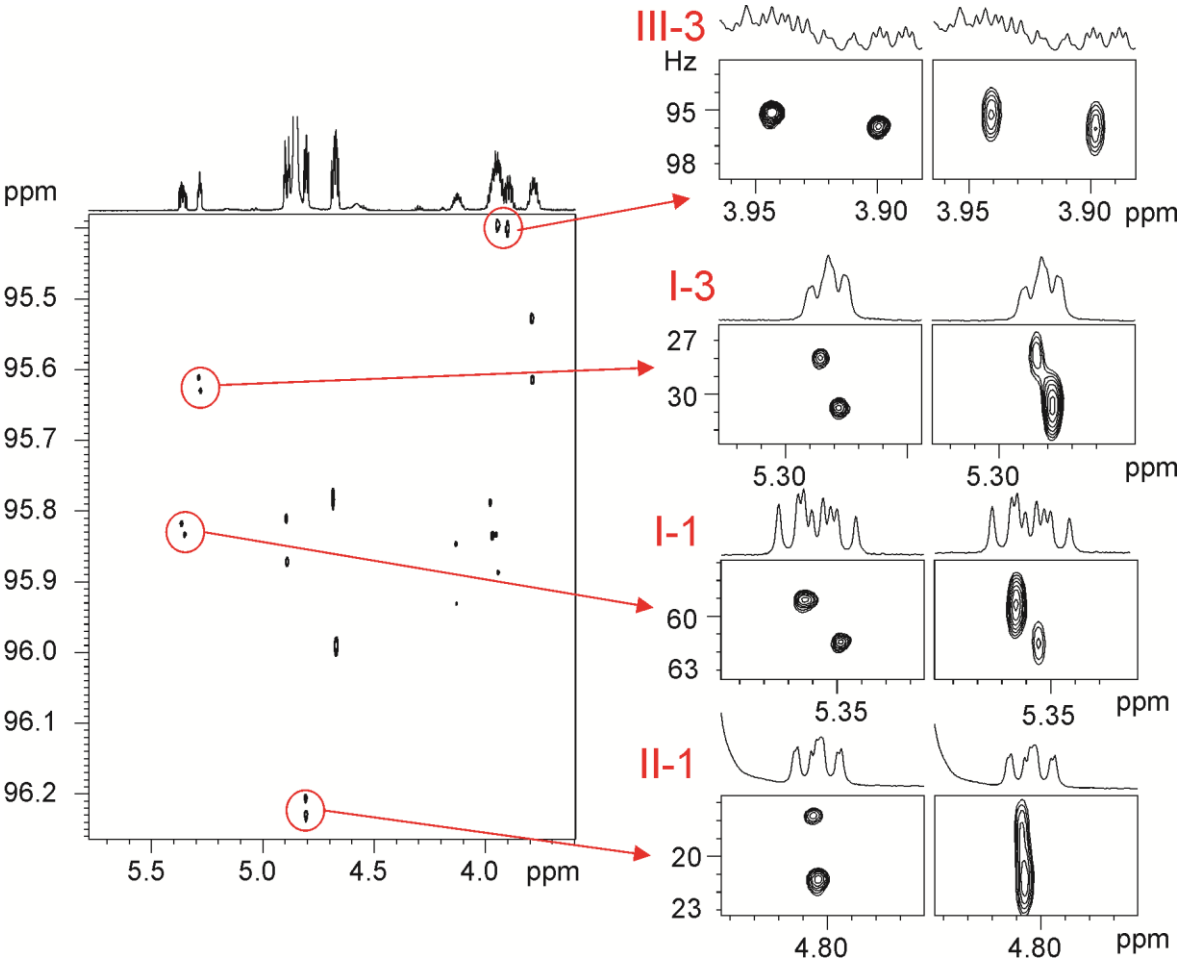

Figure S2: (left) 2D HOBS-HSQC spectrum of the region I acquired with a SW(^{13}C)=1 ppm. (right) Comparison of some expanded cross-peaks in HOBS-HSQC spectra acquired with SW(^{13}C)=1 and 5 ppm, respectively.

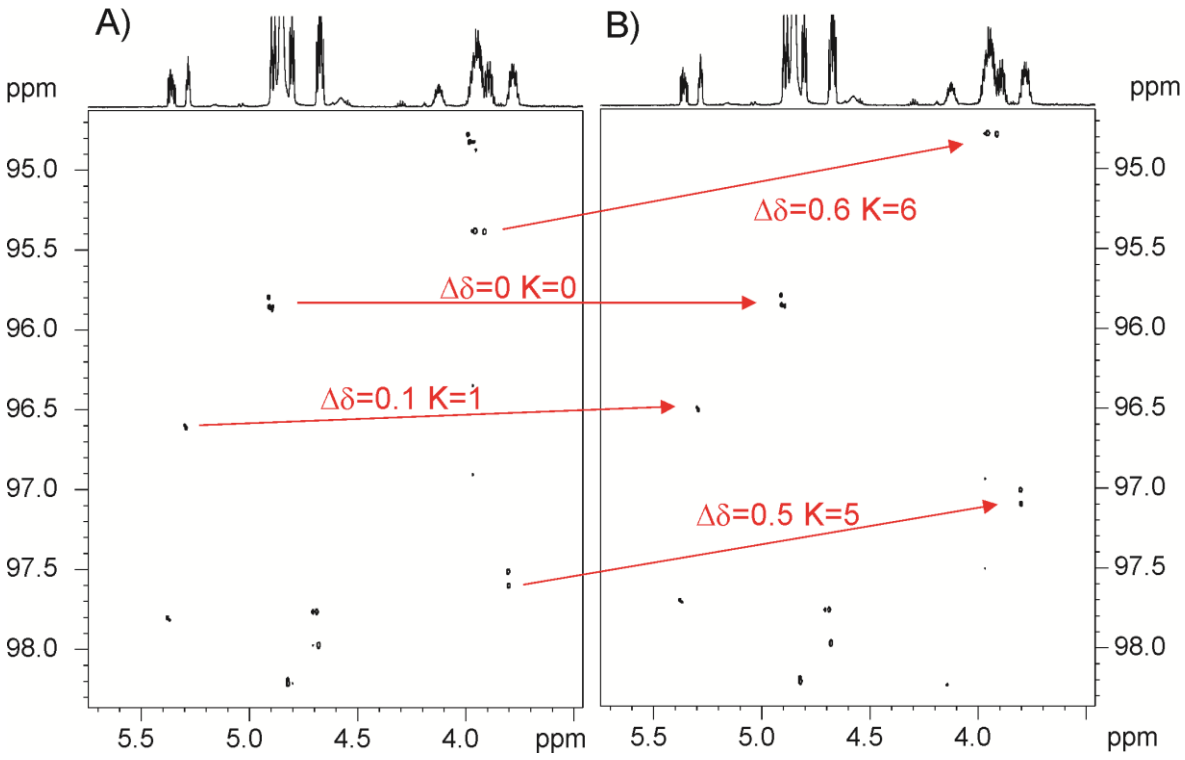

Figure S3: Spectral-aliased HSQC spectra acquired with SW(^{13}C) of A) 5 ppm and B) 4.9 ppm. The comparison of the observed chemical shift values allows determine the aliasing K factor and the real chemical shift value according to the relationship δ(obs)=δ(real)±K*SW(^{13}C).

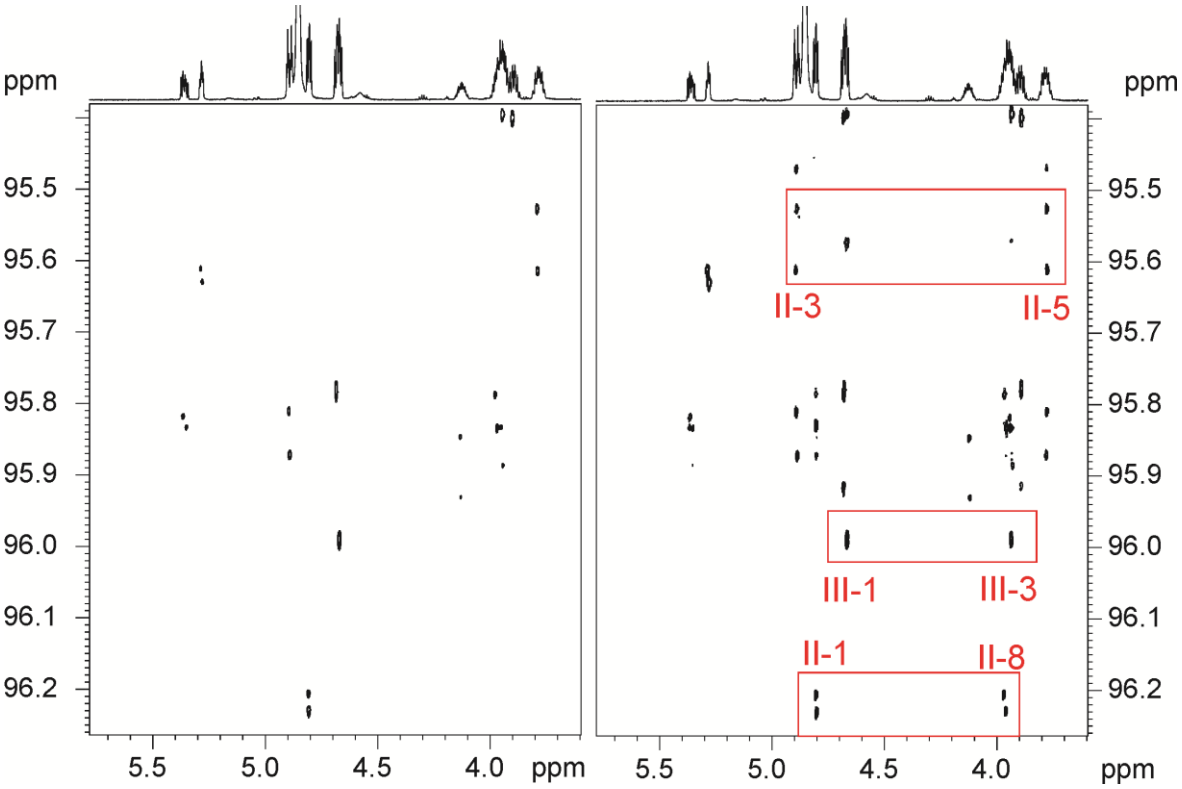

Figure S4: Comparison of spectral-aliased HOBS-HSQC (left) vs HOBS-HSQC-TOCSY (right) spectra of region A acquired with SW(^{13}C)=1 ppm. Some key correlations are marked for assignment of protons belonging to the same spin system. Experimental parameters as described for spectra in Figure 4.

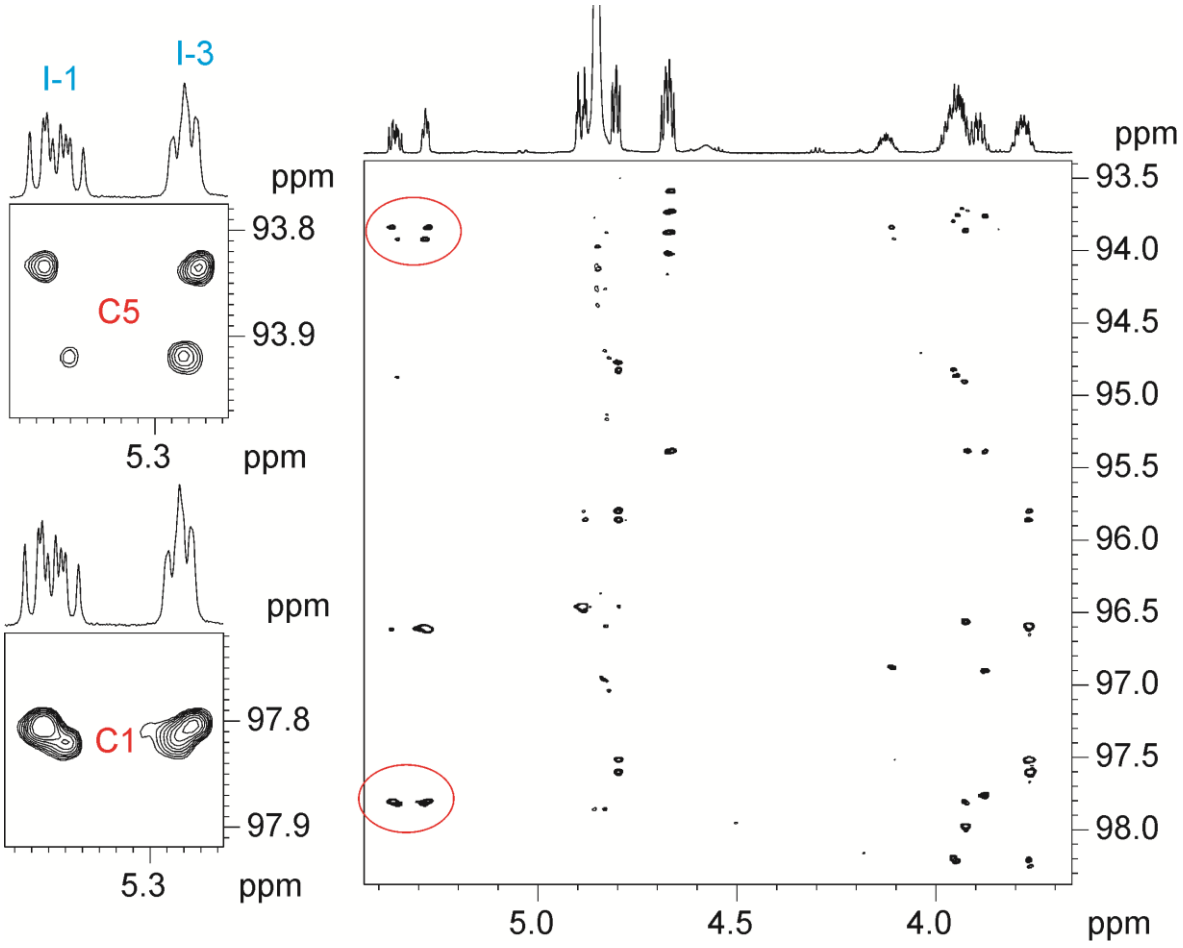

Figure S5: Spectral-aliased 2D ^{1}H-^{13}C HOBS-HSQMBC spectrum acquired with SW(^{13}C)=5 ppm. Note the key long-range H3-C1, H1-C5 and H3-C5 correlations in the expansions.

A)

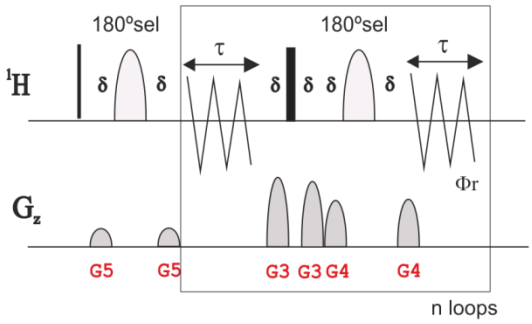
180°sel
180°sel
τ
τ
δ
δ
δ
δ
δ
δ
Φr
^{1}H
G_z
G5
G5
G3 G3 G4
G4
n loops

B)

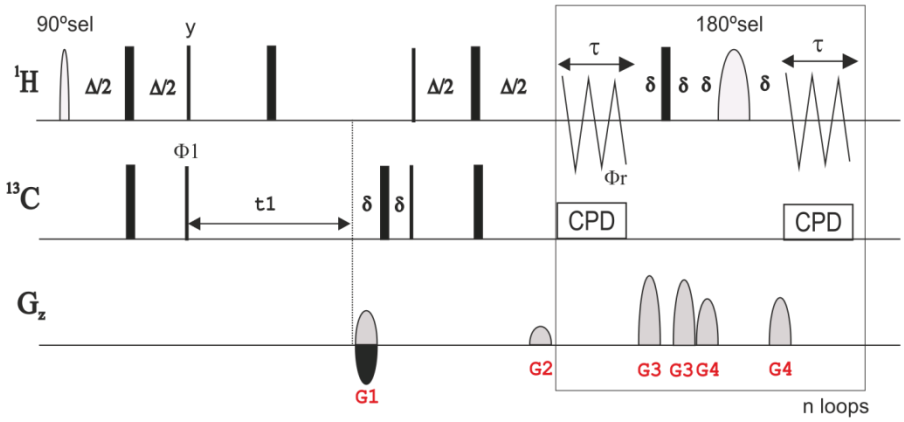
90°sel
y
180°sel
τ
τ
Δ/2
Δ/2
Δ/2
Δ/2
δ
δ
δ
δ
Φ1
Φr
^{1}H
^{13}C
t1
δ
δ
CPD
CPD
G_z
G1
G2
G3 G3 G4
G4
n loops

C)

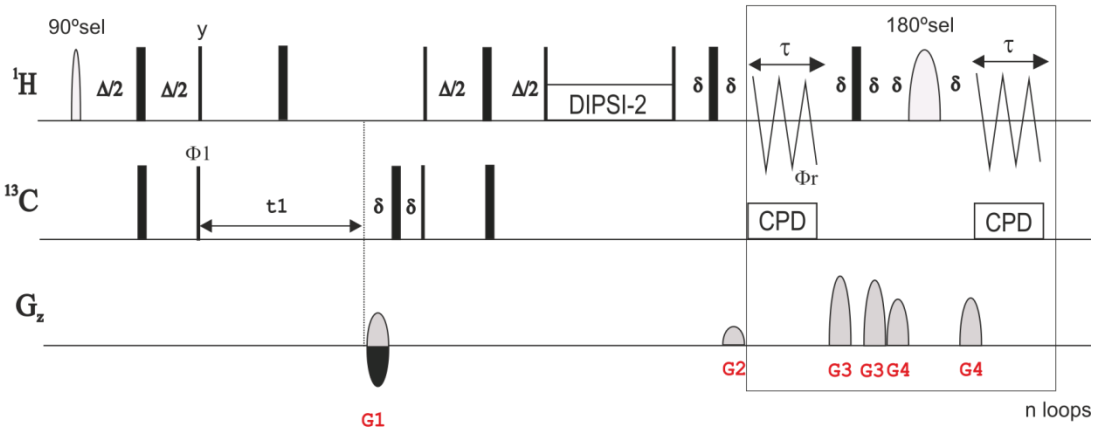
90°sel
y
180°sel
τ
τ
Δ/2
Δ/2
Δ/2
Δ/2
DIPSI-2
δ
δ
δ
δ
δ
Φ1
Φr
^{1}H
^{13}C
t1
δ
δ
CPD
CPD
G_z
G1
G2
G3 G3 G4
G4
n loops

D)

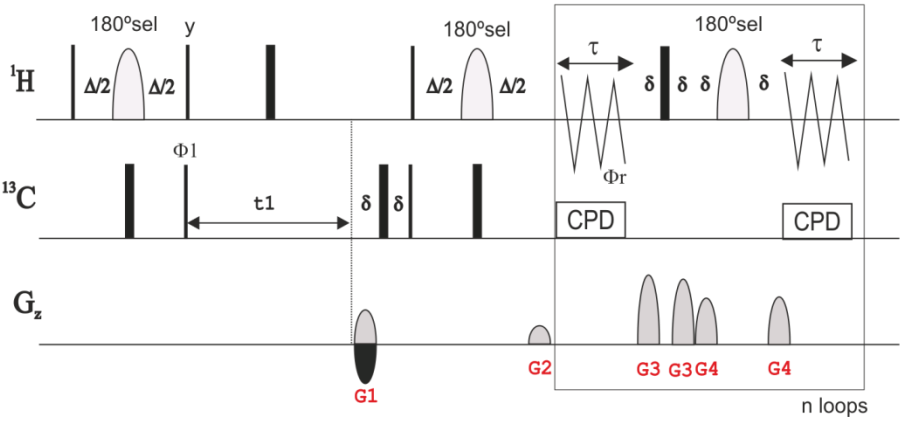
180°sel
y
180°sel
180°sel
τ
τ
Δ/2
Δ/2
Δ/2
Δ/2
δ
δ
δ
δ
Φ1
Φr
^{1}H
^{13}C
t1
δ
δ
CPD
CPD
G_z
G1
G2
G3 G3 G4
G4
n loops

Figure S6: NMR pulse sequences used in this work: A) 1D HOBS; B) 2D ^{1}H-^{13}C HOBS-HSQC; C) 2D ^{1}H-^{13}C HOBS-HSQC-TOCSY; D) 2D ^{1}H-^{13}C HOBS-HSQMBC. Thin and thick bars represent broadband 90º and 180º pulses, respectively, whereas shaped pulses are region-selective 180º pulses. The basic phase cycling is Φ_1=x,-x and Φr=x,-x; all other unlabeled pulses are from the x-axis. Homonuclear decoupling during the acquisition time (AQ) is performed using a refocusing blocks including a pair of hard/selective 180º ^{1}H pulses applied at intervals of 2τ=AQ/n, where n is the number of loops. Heteronuclear decoupling (CPD) during data collection is applied as shown in the scheme. δ is the duration of gradients and the recovery delay. The selective 180º ^{1}H pulse applied at the middle of INEPT periods and during detection have the same shape and duration (p_{180}). The INEPT delays are set to $\Delta = 1/2 * {}^{1}J_{CH}$ in HSQC and HSQC-TOCSY experiment and to $\Delta + p_{180} = 1/2 * {}^{n}J_{CH}$ in selHSQMBC experiments. Other details can be found into the experimental section.

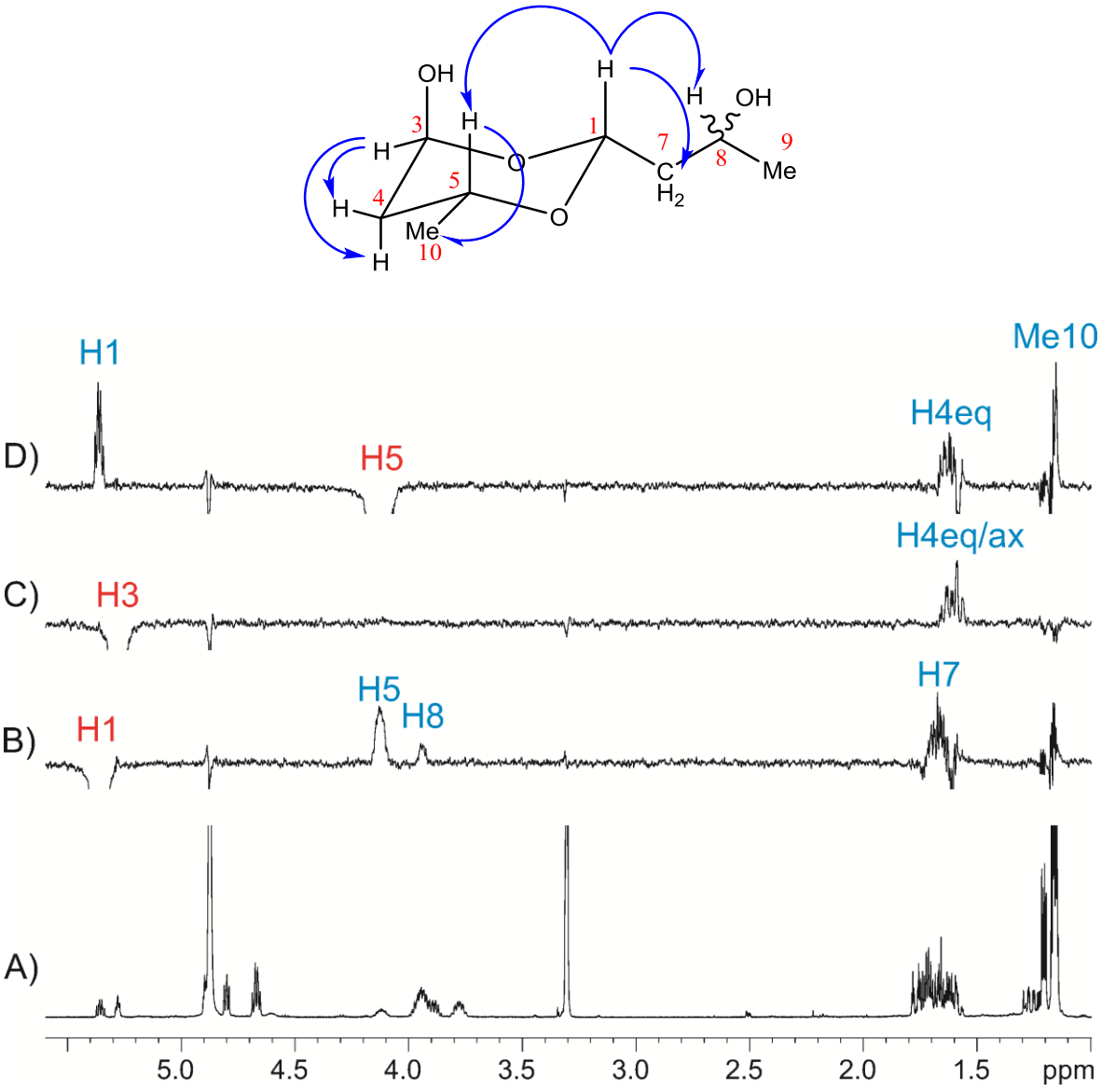

Figure S7: Selective 1D NOESY spectra after selective excitation of some protons belonging to isomers Ia/Ib.

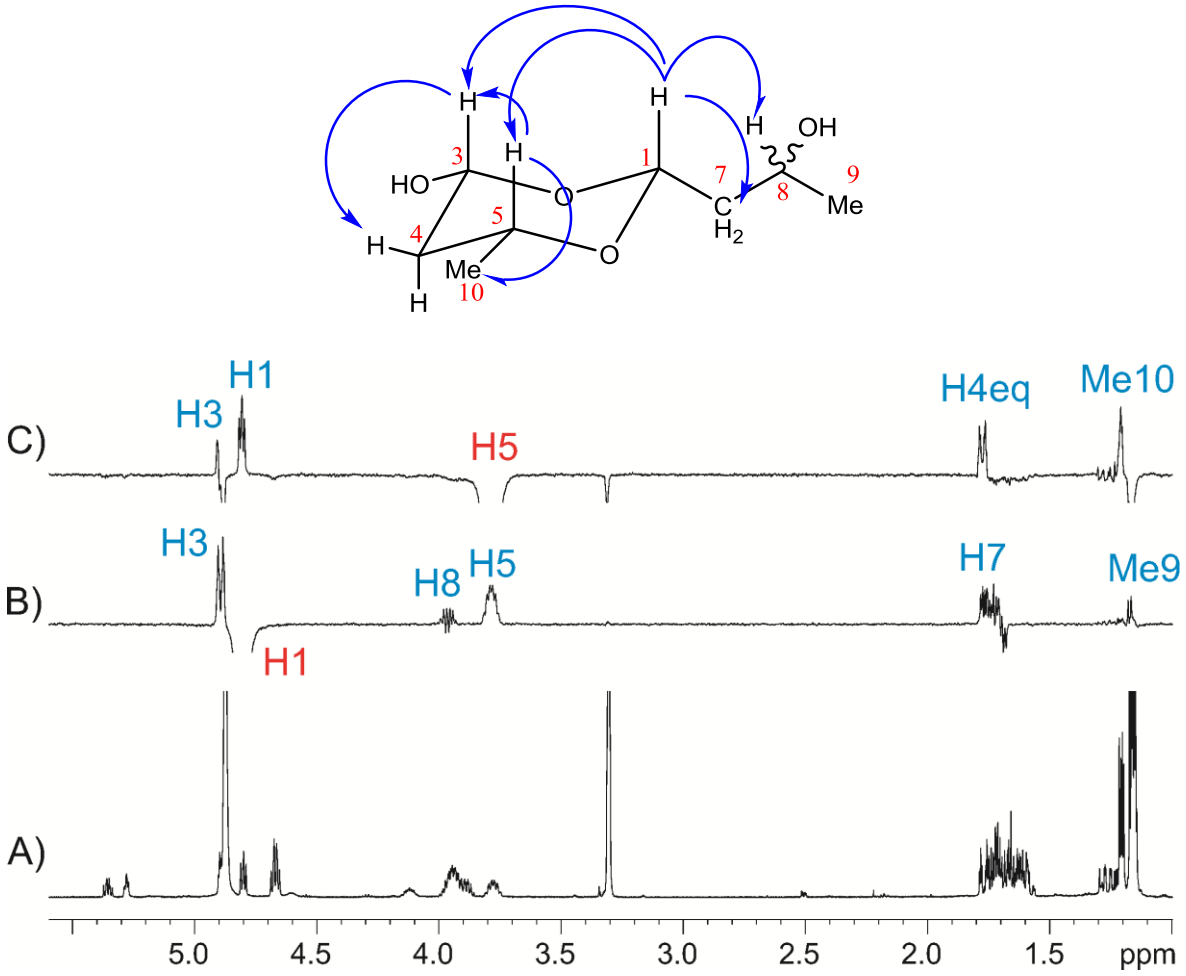

Figure S8: Selective 1D NOESY spectra after selective excitation of some protons belonging to isomers IIa/IIb.

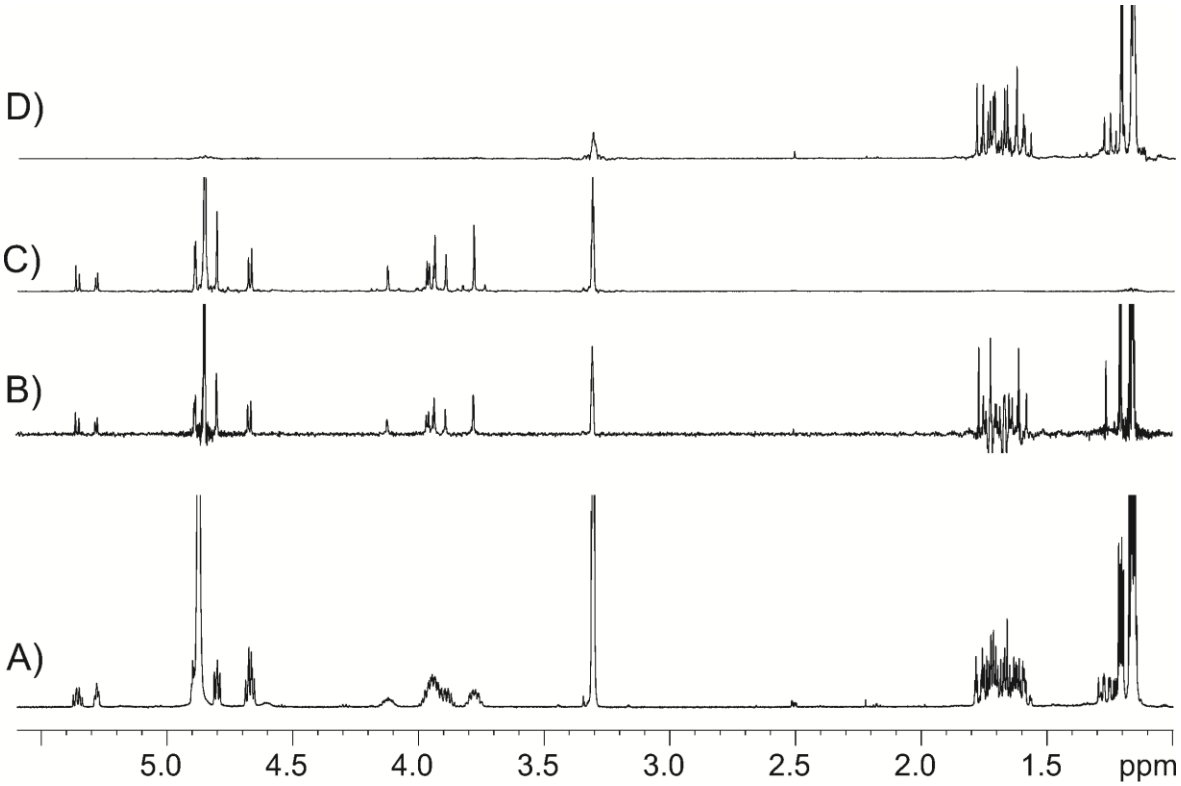

Figure S9: Comparison between the B) PSYCHE (2D acquisition mode using 1 scan per 16 t_1 increments)[4] and the C-D) individual 1D HOBS experiments (acquired only with 4 scans each one, as shown in Figure 2). All spectra were processed without any window function before Fourier transformation. See expanded areas in Figures S10 and S11 for more details.

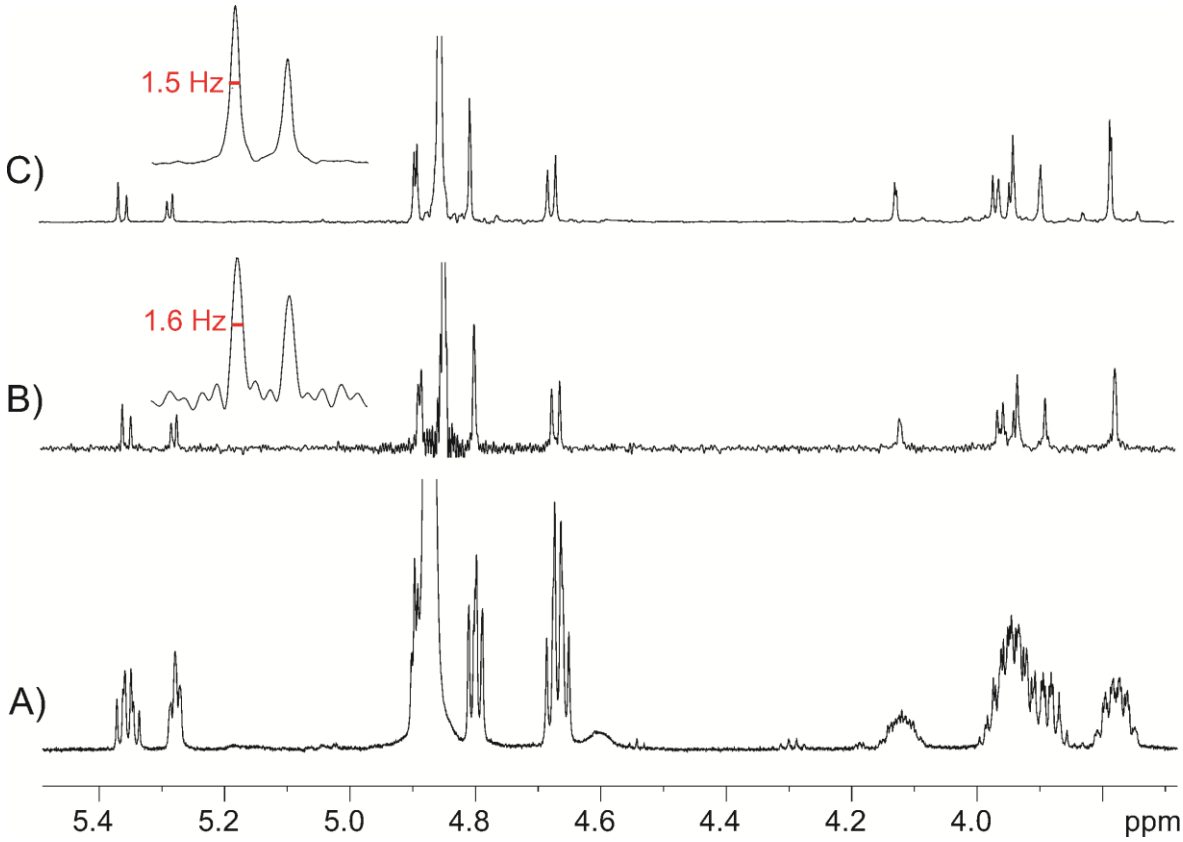

Figure S10: Expanded area between 3.7-5.5 ppm comparing the experimental sensitivity and natural line widths achieved in B) PSYCHE and C) HOBS spectra of Figure S9. Whereas similar spectral quality and experimental line widths (about 1.5-1.6 Hz) were obtained in both experiments, the 1D HOBS spectrum shows an enhanced sensitivity by two orders of magnitude.

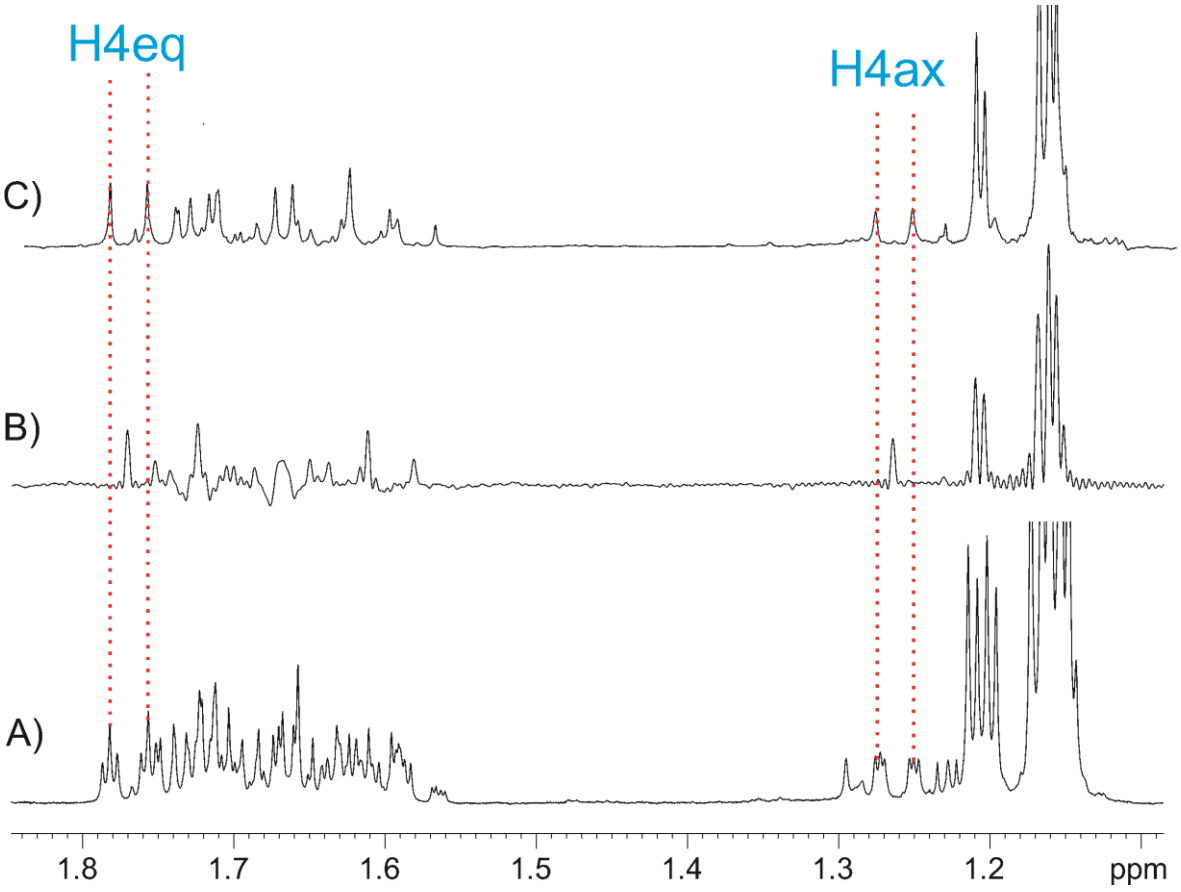

Figure S11: Expanded area between 1.1-1.8 ppm comparing the experimental sensitivity, multiplet simplification and line widths achieved in B) PSYCHE and C) HOBS spectra of Figure S9. As shown in Figure S9 and S10, the 1D HOBS spectrum shows a sensitivity enhancement by two orders of magnitude. Note the partial multiplet simplification of diastereotopic CH_2 protons, exemplified with the H4 protons of isomers IIa/IIb, where the geminal ^2J(HH) splitting remains. In addition, also note how the PSYCHE experiment fails to homodecouple all strongly-coupled geminal protons resonating around 1.6-1.8 ppm.

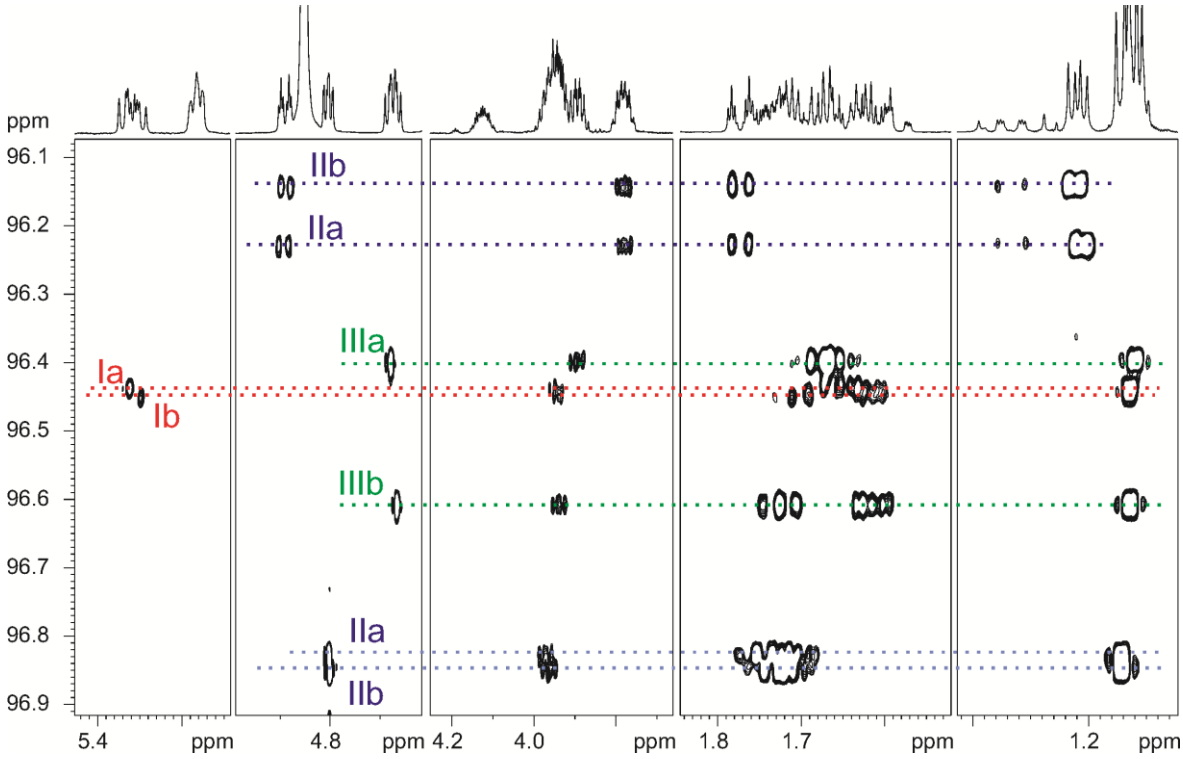

Figure S12: Expansion of the spectral aliased HSQC-TOCSY of Figure 4A. Note how eight different spin systems can be distinguished and assigned.

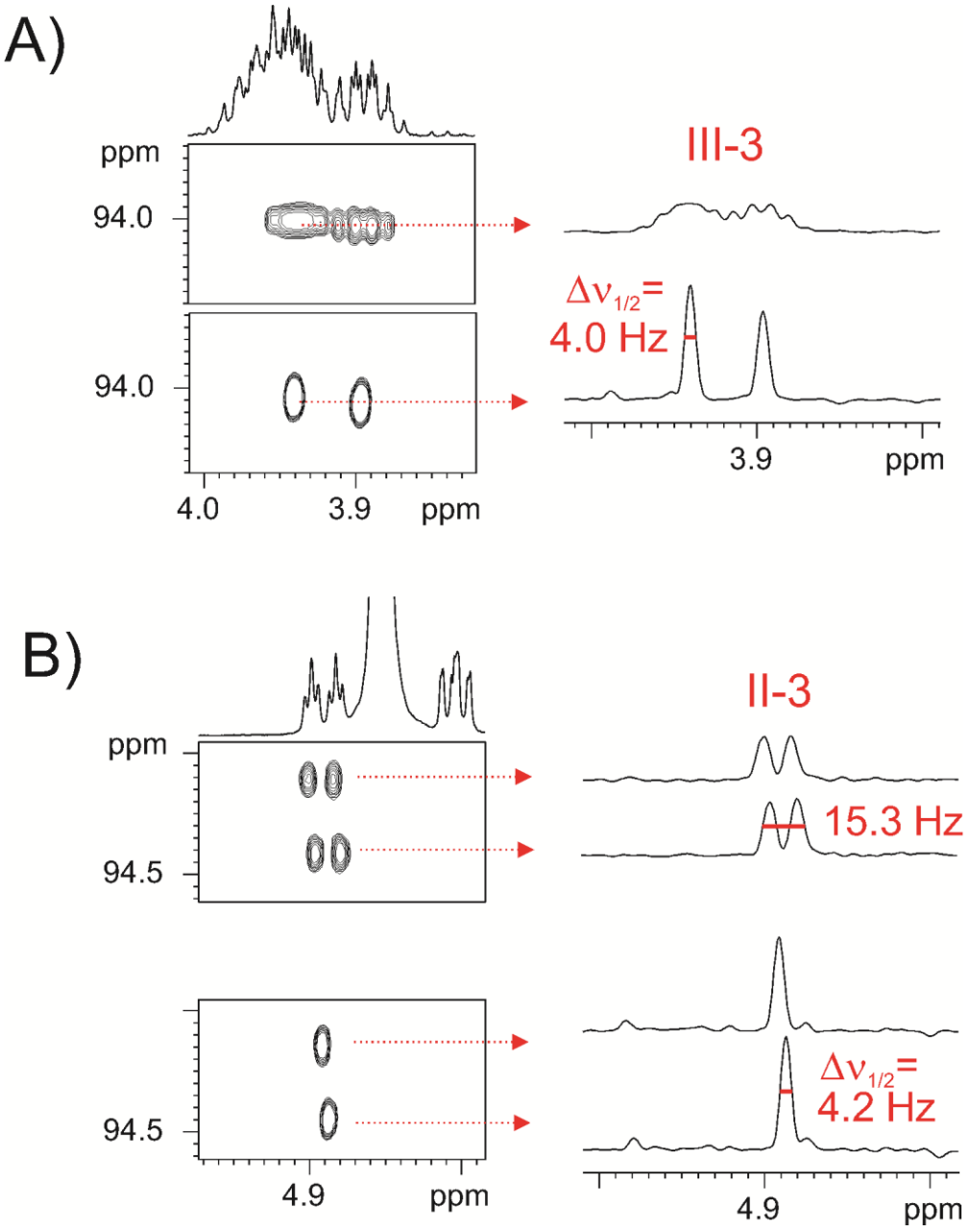

Figure S13: (top) Conventional and (bottom) broadband homodecoupled HSQC A) III-3 and B) II-3 cross peaks. 1D slices on the right allow to compare the relative sensitivity, the multiplet simplification and the experimental line widths achieved in both experiments.

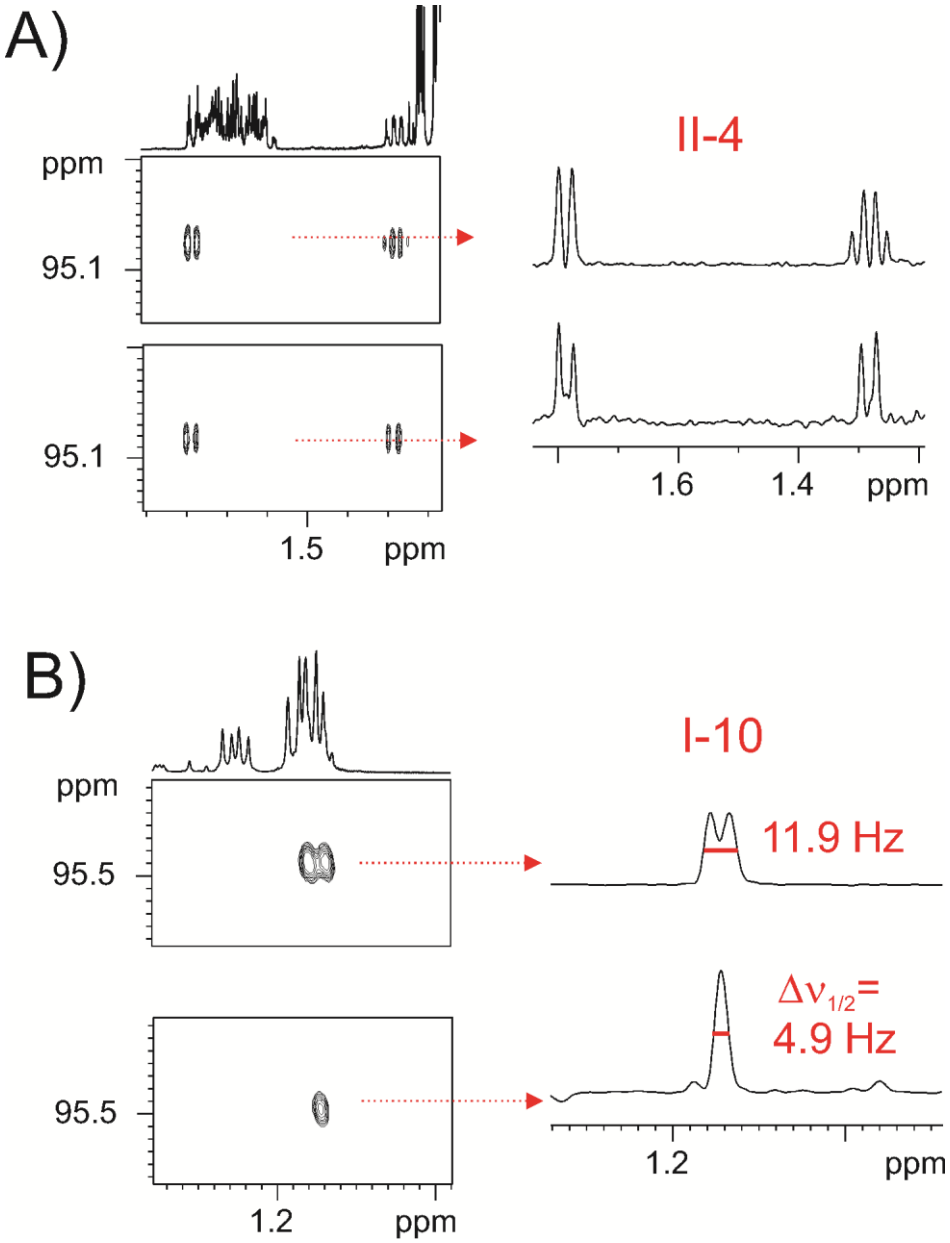

Figure S14: (top) Conventional and (bottom) broadband homodecoupled HSQC A) II-4 (diastereotopic CH_2) and B) I-10 (CH_3) cross peaks. 1D slices on the right allow to compare the relative sensitivity, the multiplet simplification and the experimental line widths achieved in both experiments.

PUBLICATION 8

Pure in-phase heteronuclear correlation NMR experiments

Laura Castañar, Josep Saurí, Robert Thomas Williamson,
Albert Virgili and Teodor Parella.
Angew. Chem. Int. Ed., **2014**, *53*, 8379-8382.

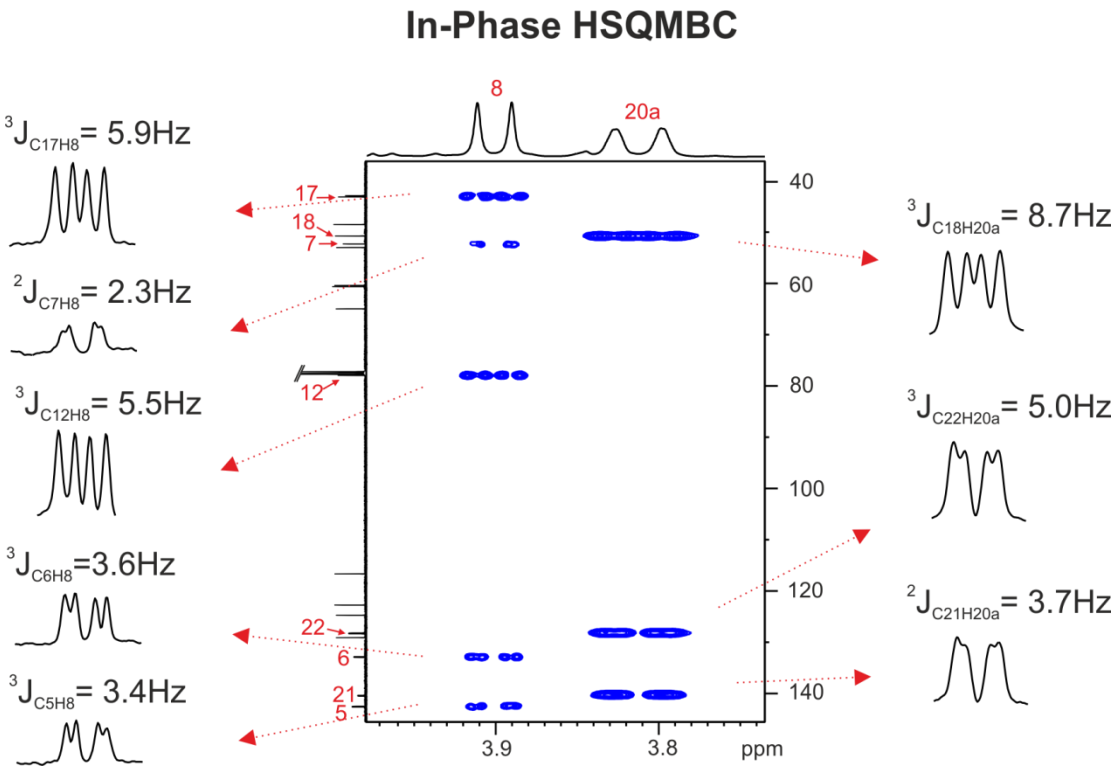

Introduction

The most serious drawback of HSQC and HSQMBC experiments is that the phase of 2D cross-peaks appears strongly distorted due to that the observable magnetization just before acquisition is a mixture of IP and AP components (see Eq.1.12 in section 1.2.1.1). This communication reports a simple and general solution to obtain heteronuclear correlation spectra that yield truly pure absorption lineshapes and IP multiplet structures for all available cross-peaks with respect to both J_{CH} and all the passive J_{HH} coupling constants along the detected dimension. The proposal is based on a conventional HSQC/HSQMBC pulse train with an adiabatic *z*-filter[93] applied just before acquisition.

The use of adiabatic *z*-filters was proposed to remove the *Zero-Quantum Coherences* (ZQCs) which give rise to AP dispersive components, thereby reducing the effective resolution, introducing misleading correlation, and obscuring wanted features. Although ZQCs are not detected, they can be transferred into observables signals producing AP dispersive components in the final spectrum. This ZQ filter is based on the simultaneously application of a swept-frequency 180° pulse (CHIRP pulse) and a soft PFG flanked by two 90° ^{1}H pulses (Figure 22).

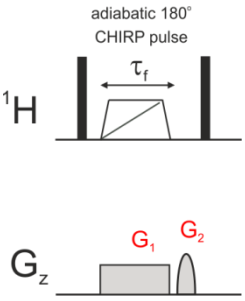

Figure 22: ZQ-filter scheme that consists of a simultaneous CHIRP 180° ^{1}H pulse and a purging gradient (G_1) followed by a single short gradient (G_2), all they placed between two 90° ^{1}H pulses.

The way in which this swept-pulse/gradient pair works can be envisaged in the following way. The application of the gradient (along the *z*-axis) results in that the Larmor frequency becomes a function of the *z*-position into the NMR tube. The swept-frequency 180° pulse will therefore flip the spins at different positions in the sample at different times. Thus, the top of the sample might experience the 180° pulse at the start of the sweep, the middle of the sample at time $\tau_f/2$, and the bottom at time τ_f, where τ_f is the duration of the sweep. The result is that in different parts of the sample the zero-quantum has evolved for different times, and so has acquired a different phase. If

[93] M. Thrippleton, J. Keeler. *Angew. Chem. Int. Ed.*, **2003**, *42*, 3938.

the range of these phases across the sample is large enough, the net result will be the cancelation of the ZQCs.

The experimental results shown in this publication confirm that the adiabatic *z*-filter incorporated at the end of the conventional HSQC/HSQMBC pulse train is an efficient tool to suppress unwanted homo- and heteronuclear AP contributions. The proposed PIP-HSQC and PIP-HSQMBC experiments yield undistorted in-phase cross-peaks that are amenable for a more accurate extraction of small coupling constant values. All these methods can be recorded in full automation mode without any prior calibration and they offer a general implementation on a large variety of isotropic and anisotropic sample conditions.

Angewandte International Edition Chemie

NMR Spectroscopy

DOI: 10.1002/anie.201404136

Pure In-Phase Heteronuclear Correlation NMR Experiments**

*Laura Castañar, Josep Saurí, Robert Thomas Williamson, Albert Virgili, and Teodor Parella**

Abstract: *A general NMR approach to provide pure in-phase (PIP) multiplets in heteronuclear correlation experiments is described. The implementation of a zero-quantum filter efficiently suppresses any unwanted anti-phase contributions that usually distort the multiplet pattern of cross-peaks and can hamper their analysis. The clean pattern obtained in PIP-HSQMBC experiments is suitable for a direct extraction of coupling constants in resolved signals, for a peak-fitting process from a reference signal, and for the application of the IPAP technique in non-resolved multiplets.*

Long-range proton–carbon correlations routinely extracted from HMBC spectra are key elements in the structural characterization of small and medium-sized molecules in solution.[1] However, the accurate quantitation of such interactions from these spectra has been problematic due to the characteristic mixed phases of the resulting HMBC cross-peaks, which lead to difficult data analysis.[2] As an alternative, the long-range optimized HSQC experiment, referred to as HSQMBC,[3] has been preferred to measure small proton–carbon coupling constants, $^{n}J(CH)$ ($n>1$), although it is not free of inconveniences. In both HMBC and HSQMBC experiments, the main source of problems arises from the fact that proton–proton coupling constants, $J(HH)$, that have similar magnitudes to $^{n}J(CH)$ (typically ranging from 0–15 Hz), also evolve during the defocusing/refocusing periods. This unwanted modulation can introduce undesired effects in both the multiplet phase and the transfer efficiency. In order to avoid or minimize such interferences, several approaches have been reported such as the use of a BIRD-INEPT element,[4] CPMG pulse trains,[5] or selective 180° ^{1}H pulses.[6]

HMBC and HSQMBC experiments are usually recorded under non-refocusing conditions and the resulting cross-peaks are related to anti-phase (AP) multiplet patterns. Recently, a frequency-selective CLIP-HSQMBC experiment has been proposed to obtain undistorted pure in-phase (PIP) patterns that are easier to analyze but this approach requires the recording of multiple experiments to monitor all protons in the molecule of interest.[7] Here we report a simple and general solution to obtain heteronuclear correlation spectra that yield truly pure absorption lineshapes and IP multiplet structures for all available cross-peaks with respect to both $J(CH)$ and all passive $J(HH)$ coupling constants along the detected dimension (Figure 1). The proposal is based on a conventional HSQC pulse train with an appended adiabatic z-filter[8] applied just before a refocusing gradient perfect-echo element[9] and acquisition. Modification of HSQC and HSQMBC pulse sequences to include a PIP-module affords experiments that can be referred to as PIP-HSQC when the Δ delay is optimized as a function of $^{1}J(CH)$ or as PIP-HSQMBC when Δ is optimized as a function of $^{n}J(CH)$.

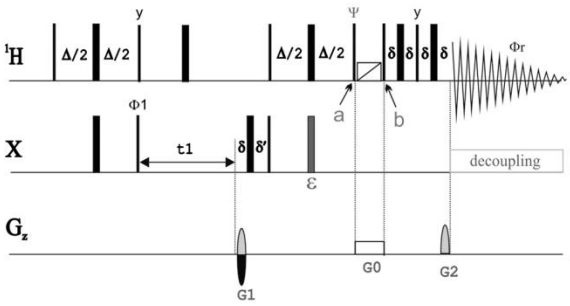

Figure 1. Pulse sequence designed to obtain pure in-phase (PIP) cross-peaks in heteronuclear correlation experiments. The delay Δ is set to $1/[2\,^{1}J(CH)]$ or $1/[2\,^{n}J(CH)]$ in PIP-HSQC or PIP-HSQMBC experiments, respectively. The z-filter includes a chirped adiabatic 180° ^{1}H pulse applied simultaneously with a purging G0 gradient, and broadband heteronuclear decoupling during proton acquisition is optional. A complete detailed description of the experiment can be found in the Supporting Information.

The HSQC scheme is easily analyzed by product operator formalism considering a heteronuclear three-spin H_1, H_2 and C system, with $J(H_1H_2)$ and $J(CH_1)$ coupling values. At the end of the refocusing INEPT period (point a in Figure 1), the magnetization of spin H_1 can be described as a mixture of IP and AP components:

$$H_{1x}\,c^2s'^2 - 2\,H_{1y}C_z\,c^2s'c' + 2\,H_{1y}H_{2z}css'^2 + 4\,H_{1x}H_{2z}C_z\,csc's' \qquad (1)$$

where c is $\cos(\pi J(H_1H_2)\Delta)$, s is $\sin(\pi J(H_1H_2)\Delta)$, c′ is $\cos(\pi J(CH_1)\Delta)$, s′ is $\sin(\pi J(CH_1)\Delta)$, and Δ is the J evolution period. The last three terms explain why cross-peaks appear strongly distorted in F2-coupled HSQC spectra of a test sample of the alkaloid strychnine (**1**) (Figure 2 A). The use of the CLIP technique (a 90° ^{13}C purging pulse applied just before the acquisition)[10] or heteronuclear decoupling during acquisition

[*] L. Castañar, J. Saurí, Prof. A. Virgili, Dr. T. Parella
Servei de RMN and Departament de Química
Universitat Autònoma de Barcelona
08193 Bellaterra (Spain)
E-mail: teodor.parella@uab.cat
Dr. R. T. Williamson
NMR Structure Elucidation, Process & Analytical Chemistry
Merck & Co. Inc.
126 E. Lincoln Avenue, Rahway, NJ 07065 (USA)

[**] Financial support provided by MINECO of Spain (project CTQ2012-32436) is gratefully acknowledged. We thank SeRMN, Universitat Autònoma de Barcelona, for allocating instrument time to this project and R. R. Gil for a sample of PMMA gel.

Supporting information for this article is available on the WWW under http://dx.doi.org/10.1002/anie.201404136.

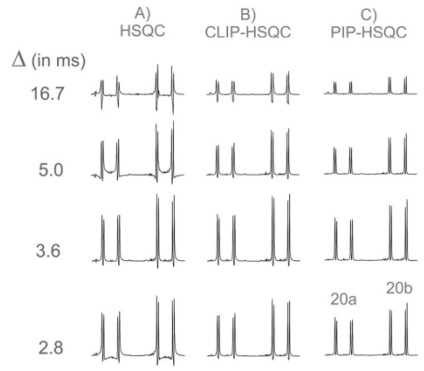

Figure 2. 1D traces extracted at the C20 chemical shift of (**1**) showing the phase distortions in A) conventional HSQC, B) CLIP-HSQC, and C) PIP-HSQC spectra with Δ optimized to several ^{1}J(CH) values: 2.8 ms (180 Hz), 3.6 ms (140 Hz), 5 ms (100 Hz), and 16.7 ms (30 Hz). Experimental values of the diastereotopic CH_2 group: ^{2}J(H20a-H20b) = 14.9 Hz, ^{1}J(C-H20a) = 138.8 Hz, ^{1}J(C-H20b) = 138.7 Hz.

efficiently removes the second and the fourth terms, but a mixture consisting of $H_{1x} + 2H_{1y}H_{2z}$ still remains (Figure 2B). In practice, due to the difference of magnitudes between ^{1}J(CH) and J(HH), these unwanted contributions are small and they have been traditionally omitted in cross-peak analysis in CLIP-HSQC or in conventional decoupled HSQC experiments. It is shown experimentally and by simulations that a gradient-based ^{1}H z-filter before acquisition[11] would improve the result by partially removing the double-quantum contribution in the third term but PIP peaks are still not achieved (Supporting Information, Figures S1–S6). These perturbations could become critical when measuring ^{1}J(CH) in the presence of large J(HH) values (Figure S3), as could be found in the measurement of Residual Dipolar Couplings (RDCs) for weakly aligned samples in anisotropic media, or in experiments involving longer Δ delays (Figures S4–S6). For instance, for J(HH) = 5 Hz and ^{1}J(CH) = 140 Hz, the contribution of the ZQ term is only about 3% in a 140 Hz optimized HSQC experiment. However, in the case that ^{n}J(CH) = 8 Hz, this percentage increases to 75% in an 8 Hz optimized experiment.

As a further enhancement, it is shown here that all unwanted homo- and heteronuclear dispersive AP contributions are completely removed (Figure 2C) by applying a z-filter consisting of a 90°$_y$(^{1}H)–[adiabatic 180° ^{1}H pulse/purge gradient]–90°$_x$(^{1}H) element.[8] The remarkable benefits from the use of a z-filter for obtaining high-quality spectra has already been demonstrated for a number of NMR experiments.[9,12] Thus, after the 90°$_y$(^{1}H) pulse the above four components are converted to

$$-H_{1z}\,c^2s'^2 - 2H_{1y}C_z\,c^2s'c' + 2H_{1y}H_{2x}\,css'^2 - 4H_{1z}H_{2x}C_z\,csc's' \qquad (2)$$

where the second and fourth terms represent transverse AP heteronuclear magnetization and the third element represents a mixture of homonuclear ZQ and DQ coherences, which are also eliminated by the effect of the simultaneous adiabatic 180° ^{1}H pulse and the purging G0 gradient pair. As a result, only the first term representing the desired IP magnetization remains detectable after the z-filter (point b in Figure 1). To maintain the pure IP character during detection, the classical δ-180°$_x$(^{1}H)-G2 block has been replaced by a perfect gradient echo element, in the form of δ-180°$_x$(^{1}H)–δ-90°$_y$(^{1}H)–δ-180°$_x$(^{1}H)-G2, where J(HH) should be fully refocused.[9] Using gradients with a duration of 1 ms, the unwanted anti-phase J(HH) contribution should be about 3% for a J(HH) = 5 Hz using a conventional gradient echo (Figure S7).

The interference of J(HH) effects is more obvious when the size of J(CH) and J(HH) are of the same order, as found in long-range heteronuclear correlation experiments. The importance of the z-filter is illustrated with the superior IP performance of the 8 Hz PIP-HSQMBC experiment over conventional, CLIP and z-filtered HSQMBC experiments acquired under the same conditions (Figure 3). It must be emphasized that the apparent reduced sensitivity of the PIP spectrum is not due to relaxation associated to the z-filter, but rather to the elimination of all dispersive components.

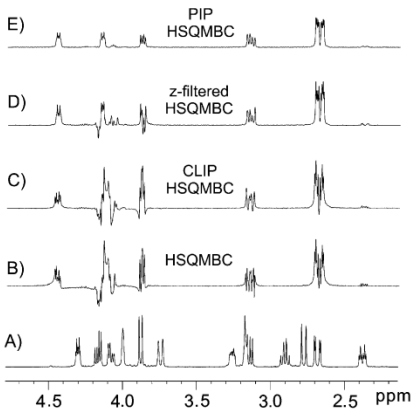

Figure 3. A) ^{1}H NMR spectrum of (**1**); B–E) 1D traces extracted at the C12 chemical shift showing the signal distortions in B) HSQMBC, C) CLIP-HSQMBC, D) z-filtered HSQMBC, and E) PIP-HSQMBC spectra (all experiments were optimized to 8 Hz (Δ = 62.5 ms)).

The inspection of some selected traces along the F2 dimension belonging to the 8 Hz PIP-HSQMBC spectrum of (**1**) clearly reveals that all cross-peaks display a clean IP character (Figure 4B). The expansion observed for the H8 and H20a cross-peaks (Figure 4C) exhibits well resolved multiplets, where the additional IP splitting (in these simple signals all observed cross-peaks become double-doublets) allows a direct and easy determination of the ^{n}J(CH) value, analogous to measuring J(HH) in conventional 1D ^{1}H spectra. Note the rough proportionality between signal intensity and ^{n}J(CH) values. Under these conditions, even a small coupling value of 2.3 Hz can be directly measured for the two-bond C7/H8 correlation. Experimentally, a different delay optimization can be useful in the event that expected correlations are missing (Figure S8).

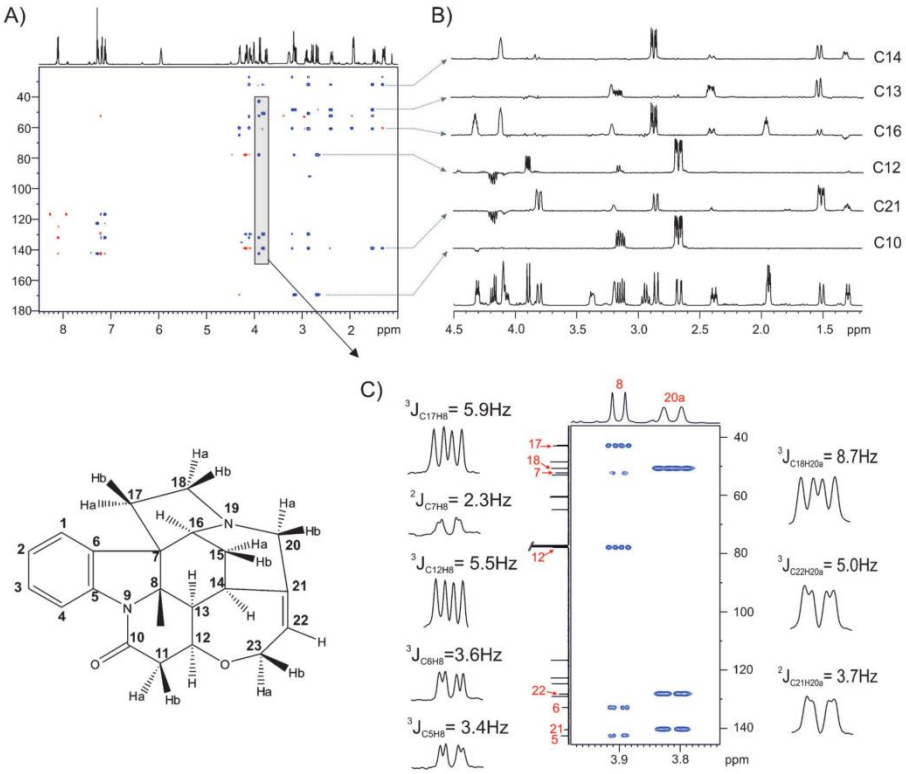

Figure 4. A) 8 Hz optimized PIP-HSQMBC spectrum of (**1**) acquired with a BIRD cluster in the initial INEPT period to minimize direct responses. B) 1D row slices taken at different ^{13}C frequencies showing in-phase multiplet patterns for all observed cross-peaks. C) Expanded area showing how the magnitude of $^nJ(CH)$ can be easily determined from direct analysis of undistorted and resolved IP peaks.

The extraction of $^nJ(CH)$ in more complex or non-resolved multiplets can be performed with several established methods: 1) measuring overall multiplet widths, 2) fitting/matching them to an external reference cross-peak obtained from the same sequence with broadband ^{13}C-decoupling during acquisition,[13] or 3) from the internal satellite lines corresponding to the direct $^1J(CH)$ responses, if available, without need to acquire a second reference spectrum. Alternatively, a simple approach relies on the implementation of the IPAP technique,[6] which is achieved by recording two separate IP and AP datasets as a function of the last 180° ^{13}C pulse (marked with ε in Figure 1). Figure 5 and S9–S10 compare the success of all these analytical methods from some selected cross-peaks. Similar results are obtained in experiments where the basic INEPT period has been replaced by other heteronuclear echo periods such as INEPT-BIRD,[4] CPMG,[5] or CPMG-BIRD[5] elements (Figures S11–S14).

The performance of the proposed PIP methods has been also verified under anisotropic conditions, using a sample of **1** weakly aligned in a reversible compressed poly(methyl methacrylate (PMMA) gel swollen in $CDCl_3$ (Figures S15–S17).[14] Although broader and more complex ^1H signals are typical for RDC experiments, experimental splittings arising from CH couplings in the range 110–190 Hz and to large HH

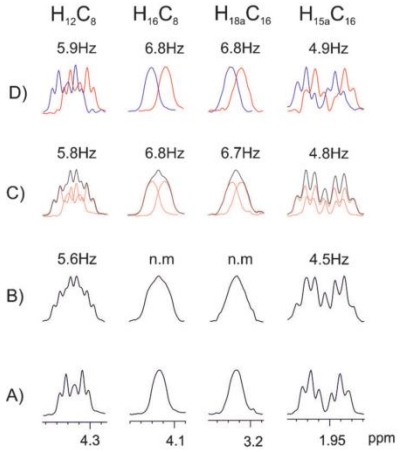

Figure 5. Comparison of several methods for the measurement of $^nJ(CH)$ values in non-resolved or complex multiplets. PIP-HSQMBC cross-peaks obtained A) with and B) without ^{13}C decoupling during acquisition; C) fitting process performed from the decoupled multiplets in A to match the experimental coupled multiplets in B; D) overlaid α and β multiplets obtained after IP±AP data combination in an IPAP experiment, respectively.

couplings up to 35 Hz can be measured (Tables S1–S3). In particular, special focus is made for the analysis and precise determination of $^{1}D(CH)$ and $^{2}D(HH)$ RDCs from undistorted cross-peaks belonging to diasterotopic CH_2 groups. The H11a/H11b protons of **1** are a good example to evaluate the more accurate measurement of their homonuclear ($^{2}D(HH) = -12.5$ Hz) and heteronuclear ($^{1}D(C_{11}H_{11a}) = +7.7$ Hz and $^{1}D(C_{11}H_{11b}) = -18.2$ Hz) RDCs, facilitating determination of their unequivocal orientation and stereoselective assignment. It is shown that errors in the measurement of up to 10% Hz can be introduced from distorted cross-peaks in conventional F2-coupled CLIP-HSQC and F2-decoupled HSQC spectra. These errors are avoided in the undistorted PIP-HSQC cross-peaks. In addition, a PIP-HSQMBC spectrum has been recorded under these challenging conditions to quantitatively measure a number of small long-range CH RDCs values, thus opening the door for the application of these parameters to superior structure determination and refinement (Figures S19–S21).

In conclusion, it has been shown that a *z*-filter is an extremely efficient tool to suppress unwanted homo- and heteronuclear anti-phase contributions in HSQC-like experiments. The proposed PIP-HSQC and PIP-HSQMBC experiments yield undistorted in-phase cross-peaks that are amenable for a more accurate extraction of small coupling constant values. All these methods can be recorded in full automation mode without any prior calibration and they offer a general implementation on a large variety of isotropic and anisotropic sample conditions. In addition, the method can be implemented in other inverse-detected NMR experiments, including HMQC-type experiments or involving other heteronuclei than carbon.

Received: April 9, 2014
Published online: June 24, 2014

Keywords: coupling constants · heteronuclear long-range correlation · HSQC · HSQMBC · pure in-phase NMR

[1] a) A. Bax, M. F. Summers, *J. Am. Chem. Soc.* **1986**, *108*, 2093–2094; b) R. C. Breton, W. F. Reynolds, *Nat. Prod. Rep.* **2013**, *30*, 501–524.
[2] a) T. Parella, J. F. Espinosa, *Prog. Nucl. Magn. Reson. Spectrosc.* **2013**, *73*, 17–55; b) B. L. Márquez, W. H. Gerwick, R. T. Williamson, *Magn. Reson. Chem.* **2001**, *39*, 499–530.
[3] a) R. T. Williamson, B. L. Márquez, W. H. Gerwick, K. E. Kövér, *Magn. Reson. Chem.* **2000**, *38*, 265–273.
[4] a) J. R. Garbow, D. P. Weitekamp, A. Pines, *Chem. Phys. Lett.* **1982**, *93*, 504–509; b) V. Lacerda, Jr., G. V. J. da Silva, M. G. Constantino, C. F. Tormena, R. T. Williamson, B. L. Márquez, *Magn. Reson. Chem.* **2006**, *44*, 95–98.
[5] a) H. Koskela, I. Kilpelainen, S. Heikkinen, *J. Magn. Reson.* **2003**, *164*, 228–232; b) K. E. Kövér, G. Batta, K. Fehér, *J. Magn. Reson.* **2006**, *181*, 89–97; c) K. Kobzar, B. Luy, *J. Magn. Reson.* **2007**, *186*, 131–141.
[6] a) S. Gil, J. F. Espinosa, T. Parella, *J. Magn. Reson.* **2010**, *207*, 312–313; b) S. Gil, J. F. Espinosa, T. Parella, *J. Magn. Reson.* **2011**, *213*, 145–150; c) J. Saurí, J. F. Espinosa, T. Parella, *Angew. Chem.* **2012**, *124*, 3985–3988; *Angew. Chem. Int. Ed.* **2012**, *51*, 3919–3922.
[7] J. Saurí, T. Parella, J. F. Espinosa, *Org. Biomol. Chem.* **2013**, *11*, 4473–4478.
[8] M. J. Thrippleton, J. Keeler, *Angew. Chem.* **2003**, *115*, 4068–4071; *Angew. Chem. Int. Ed.* **2003**, *42*, 3938–3941.
[9] A. M. Torres, G. Zheng, W. S. Price, *Magn. Reson. Chem.* **2010**, *48*, 129–133.
[10] A. Enthart, J. C. Freudenberger, J. Furrer, H. Kessler, B. Luy, *J. Magn. Reson.* **2008**, *192*, 314–322.
[11] K. E. Kövér, O. Prakash, V. J. Hruby, *J. Magn. Reson.* **1993**, *103*, 92–96.
[12] a) Ref [5c]; b) A. J. Pell, R. A. E. Edden, J. Keeler, *Magn. Reson. Chem.* **2007**, *45*, 296–316; c) B. Luy, *J. Magn. Reson.* **2009**, *201*, 18–24; d) A. M. Torres, R. D. Cruz, W. S. Price, *J. Magn. Reson.* **2008**, *193*, 311–316.
[13] K. E. Kövér, V. J. Hruby, D. Uhrín, *J. Magn. Reson.* **1997**, *129*, 125–129.
[14] J. D. Snider, E. Troche-Pesqueira, S. R. Woodruff, C. Gayathri, N. V. Tsarevsky, R. R. Gil, *Magn. Reson. Chem.* **2012**, *50*, S89–S91.

Angewandte Chemie
Eine Zeitschrift der Gesellschaft Deutscher Chemiker

Supporting Information

69451 Weinheim, Germany

Pure In-Phase Heteronuclear Correlation NMR Experiments**

*Laura Castañar, Josep Saurí, Robert Thomas Williamson, Albert Virgili, and Teodor Parella**

anie_201404136_sm_miscellaneous_information.pdf

Table of Contents:

- **Figure S17:** Comparison of 1D traces extracted from F2-decoupled (A) conventional HSQC and (B) PIP-HSQC spectra in anisotropic conditions.
- **Table S1:** ^{1}J(CH)/ ^{1}T(CH) values extracted from the PIP-HSQC spectra of strychnine recorded in isotropic and anisotropic conditions.
- **Table S2:** ^{2}J(HH)/ ^{2}T(HH) vàlues of diasterotopic CH_2 groups extracted from the PIP-HSQC spectra of strychnine recorded in isotròpic and anisotropic conditions.
- **Table S3:** Comparison of ^{2}J(HH)/ ^{2}T(HH) values extracted from the conventional HSQC, CLIP-HSQC and PIP-HSQC spectra of strychnine recorded in isotropic and anisotropic conditions.
- **Figure S18:** Plot showing the correlation between the experimental and calculated ^{1}D(CH) data for strychnine.
- **Figure S19:** 8-Hz optimized PIP-HSQMBC spectrum of strychnine in anisotropic conditions
- **Figure S20:** Comparison of 1D traces extracted from (B) HSQMBC, (C) CLIP-HSQMBC and (D) PIP-HSQMBC spectra in anisotropic conditions.
- **Figure S21:** Measurement of $^{n}T_{CH}$ values of (**1**) in anisotropic conditions in complex multiplets.
- Pulse program code for Bruker spectrometers.

Experimental Section

All NMR experiments were recorded on a BRUKER DRX-500 spectrometer equiped with a 3-channel 5-mm cryoprobe incorporating a z-gradient coil. The test sample was 25 mg of strychnine (**1**) in 0.6 ml of $CDCl_3$.

Details of pulse sequence of Fig. 1: Pulse phases are x unless indicated otherwise (Ψ=y) and a basic two-step phase cycling scheme is applied: Φ_1=x,-x, Φ_r=x,-x. The z-filter includes a chirped adiabatic 180º ^{1}H pulse applied simultaneously with a purging G0 gradient. Gradient echo/anti-echo and coherence selection was achieved by switching gradients according to G1/G2=γ_H/γ_X, where γ is the gyromagnetic ratio. δ stands for the duration of the gradient and its recovery delay and $\delta'=\delta+t_1$. TPPI-like incrementation with the echo/anti-echo recording scheme was achieved by simultaneous inversion of ^{13}C pulses applied prior to the variable t_1 period. Broadband heteronuclear decoupling during proton acquisition is optional. The IPAP technique can be applied by recording separately two complementary IP (ε=on; Ψ=y) and AP (ε=off; Ψ=x) data sets, which are further added/subtracted in the time domain followed by conventional processing to give two separate α/β spectra.

PIP-HSQC and PIP-HSQMBC spectra were recorded using the same pulse program (see Fig. 1), with an interpulse delay optimized to 140 Hz ($\Delta=1/2*{}^1J_{CH}$=3.57 ms) and 8 Hz (($\Delta=1/2*{}^nJ_{CH}$=62.5 ms), respectively. The recycle delay was of 1 s and 4 scans were collected for each one of the 128 t_1 increments, with 4096 data points in each t_1 increment. Prior to Fourier-transformation, zero-filling to 1024 points in F1, 8192 points in F2 and a squared sine-bell apodization phase-shifted 90º in both dimensions were applied. The final resolution along the detected F2 dimension was of 0.4 Hz. The total experimental time was about 13 min. Gradients G1 and G2 with a duration of 1 ms (δ) are used for echo-antiecho coherence selection, and G0 is applied simultaneously to a CHIRP pulse (30 ms) to remove undesired transverse and ZQ contributions. The proportionality between gradients G1:G2:G0 were set to ±80:20.1:3. ^{13}C 180º pulses are applied as CHIRP inversion and refocusing pulses of 500 μs and 2000 μs of duration, respectively. For the IPAP technique, IP and AP-HSQMBC datasets were separately recorded and then added/subtracted in the time-domain to provide two separate α/β data. Several fitting processes, simulations, some experimental spectra and the pulse sequence code are contained in the Supporting information.

We have also evaluated other possible long-range correlation pulse schemes where the basic INEPT period has been replaced by other heteronuclear echo periods such as INEPT-BIRD, CPMG, or CPMG-BIRD elements (Fig. S11). In all of these approaches and in the absence of the z-

filter, a severe degree of multiplet distortions were always observed due to dispersive AP contributions. These interferences occurred even when using a CPMG element with short inter-pulse delays but these approaches are particularly problematic because the consecutive application of simultaneous ^{1}H and ^{13}C pulses at high rates can produce sample heating and signal distortion. A comparison of all these versions shows that the z-filter completely removes any unwanted AP contribution and, in all cases, the resulting IP signals can be analyzed with superior accuracy (Fig. S12-S14).

For the measurement of RDCs, 4 mg of strychnine was weakly aligned in a poly(methyl methacrylate) (PMMA) gel swollen in 200ml of $CDCl_3$ using the reversible compression relaxation method. The ^{2}H quadrupolar splitting ($\Delta\upsilon_Q$) for the $CDCl_3$ signal was of 26 Hz. PIP-HSQC and PIP-HSQMBC experiments were recorded using the same pulse program, with an interpulse delay optimized to 140 Hz ($\Delta=1/2*{}^{1}J_{CH}$=3.57 ms) and 8 Hz (($\Delta=1/2*{}^{n}J_{CH}$=62.5 ms), respectively. The recycle delay was of 1 s and 64 scans were collected for each one of the 128 t_1 increments, with 4096 data points in each t_1 increment. Prior to Fourier-transformation, zero-filling to 1024 points in F1, 8192 points in F2 and a squared sine-bell apodization phase-shifted 90º in both dimensions were applied. The final resolution along the detected F2 dimension was of 0.4 Hz. The total experimental time was about 3h 30min. All spectra and experimental and calculated values can be found in figures S15-S21 and tables S1-S3.

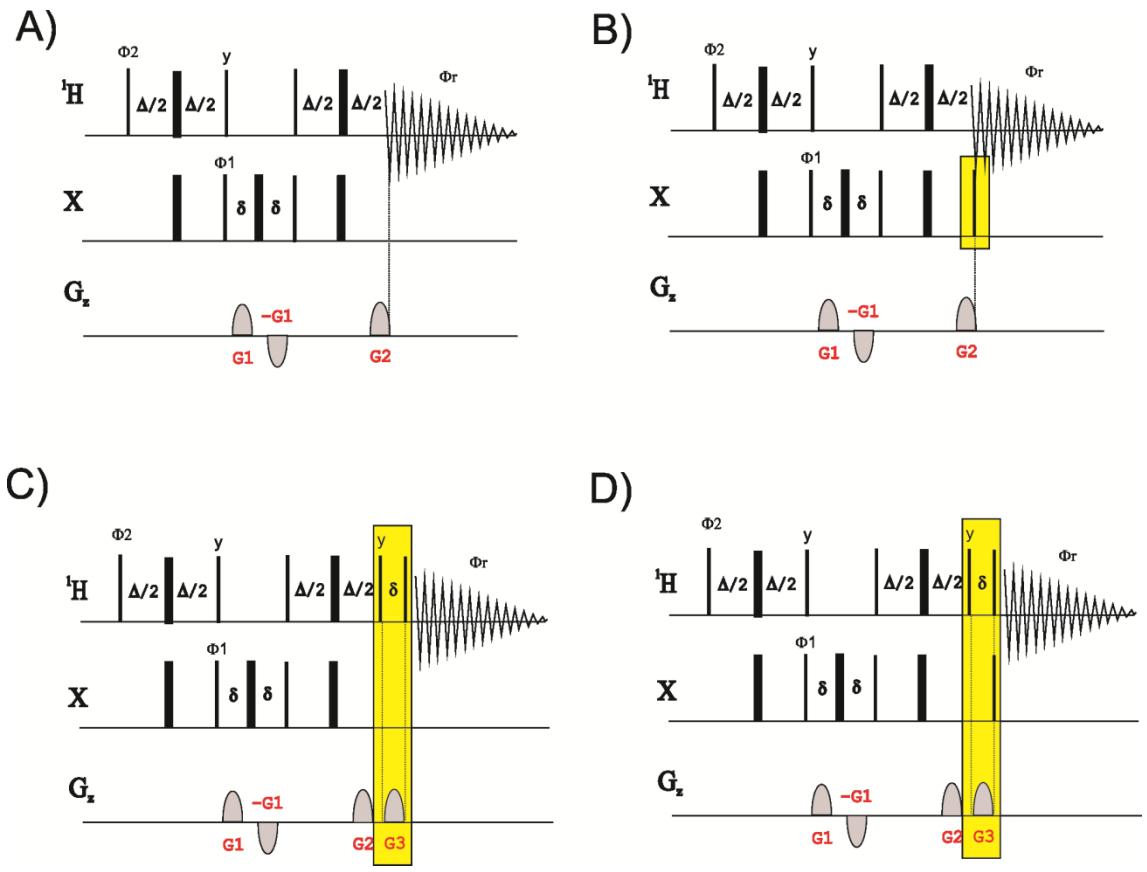

Figure S1: 1D HSQC pulse sequences used in the simulations: A) Conventional F2-coupled HSQC; B) CLIP-HSQC; C) HSQC including a z-filter, and D) HSQC including a z-filter and a CLIP ^{13}C pulse. All simulations were performed using the NMRSIM module included into the Bruker's Topspin (v3.1) software package. Pulse phases are x unless indicated otherwise. A basic four-step phase cycle was applied: Φ1=x,-x,x,-x; Φ2=x,x-x,-x; Φ r=x,-x,-x,x. Gradient ratios with a duration of 1 ms (δ) were set to G1:G2:G3=2:1:0.3 and the inter-pulse delay was optimized to Δ=1/[2*(J(CH)]. Simulations of the z-filter including the adiabatic pulse were not possible with this program.

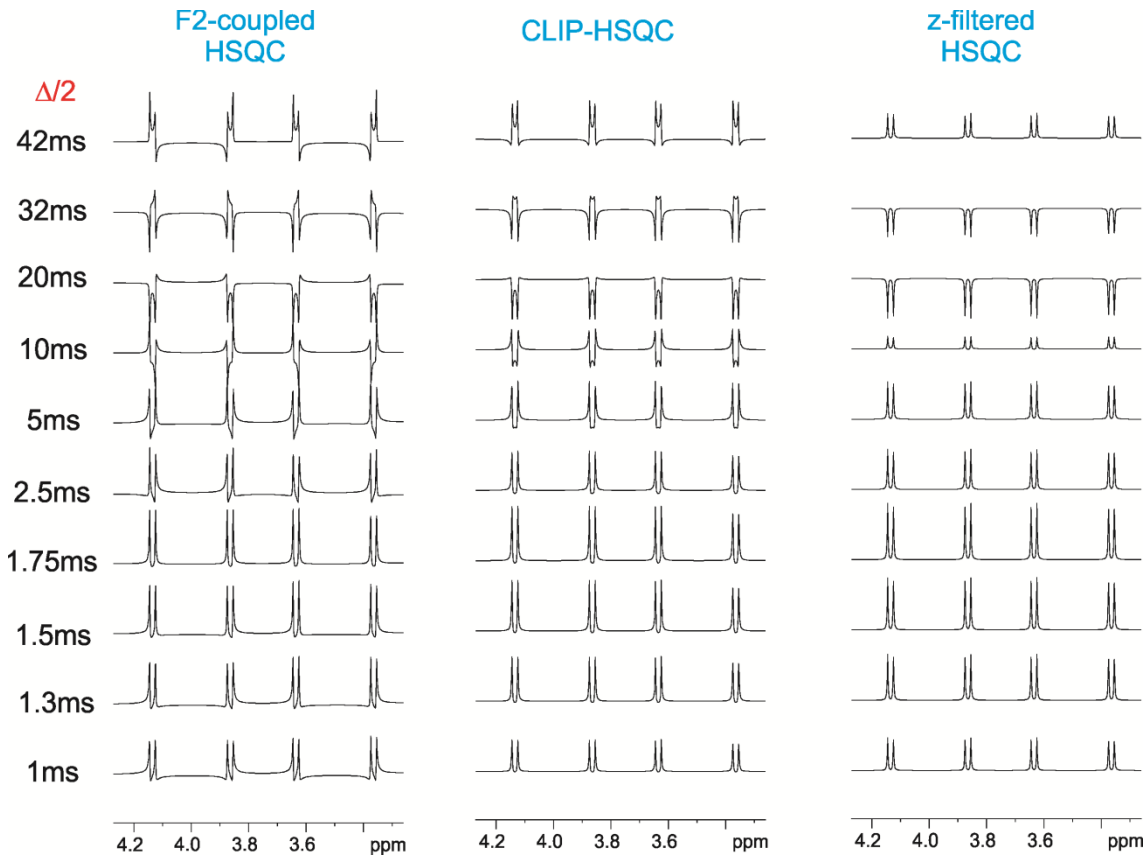

Figure S2: Simulations showing the effects of J(HH) as a function of the inter-pulse delay optimization in 1D F2-coupled A) conventional HSQC, B) CLIP-HSQC and C) z-filtered HSQC experiments (see pulse schemes in Fig. S1). Simulation parameters of the diastereotopic CH_2 group: $\delta(H_A)$=4.0 ppm, $\delta(H_A)$=3.5 ppm, $J(H_AH_B)$=10 Hz, $^1J(CH_A)$= $^1J(CH_B)$=135 Hz.

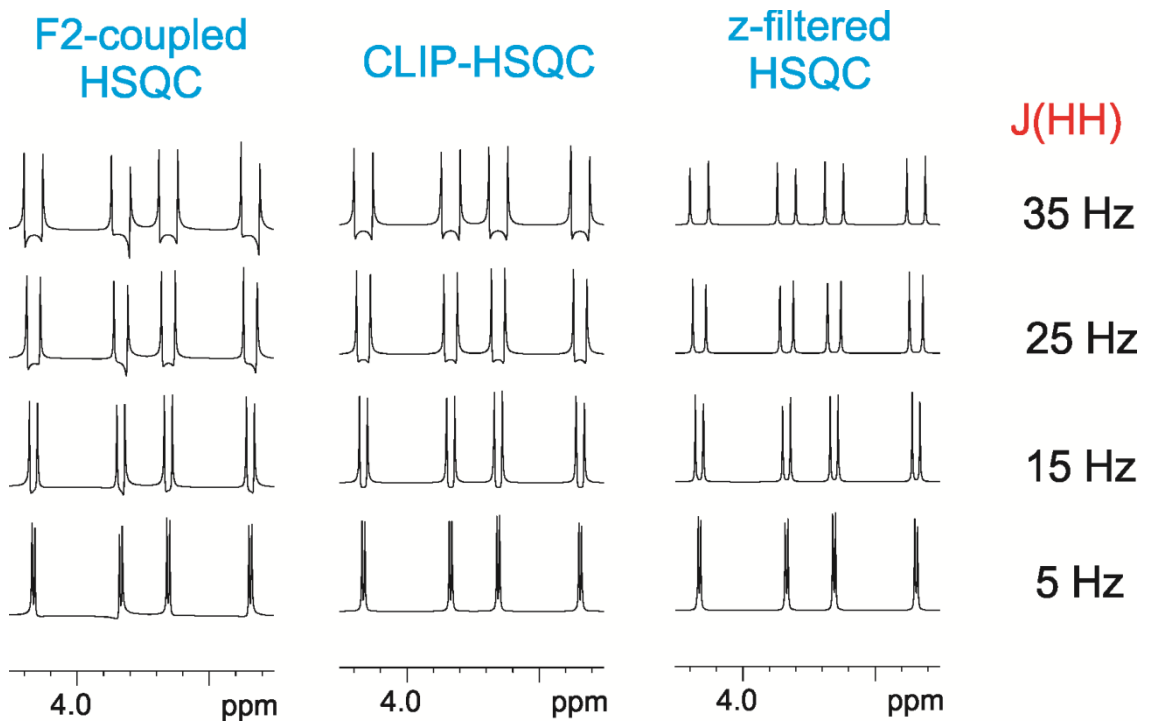

Figure S3: Simulations showing the effects of the size of J(HH) in 140-Hz optimized F2-coupled HSQC, CLIP-HSQC and z-filtered HSQC experiments. Simulation parameters: $\delta(H_A)$=4.0 ppm, $\delta(H_A)$=3.5 ppm, $^1J(CH_A)$=155 Hz, $^1J(CH_B)$=165 Hz and Δ=3.5 ms.

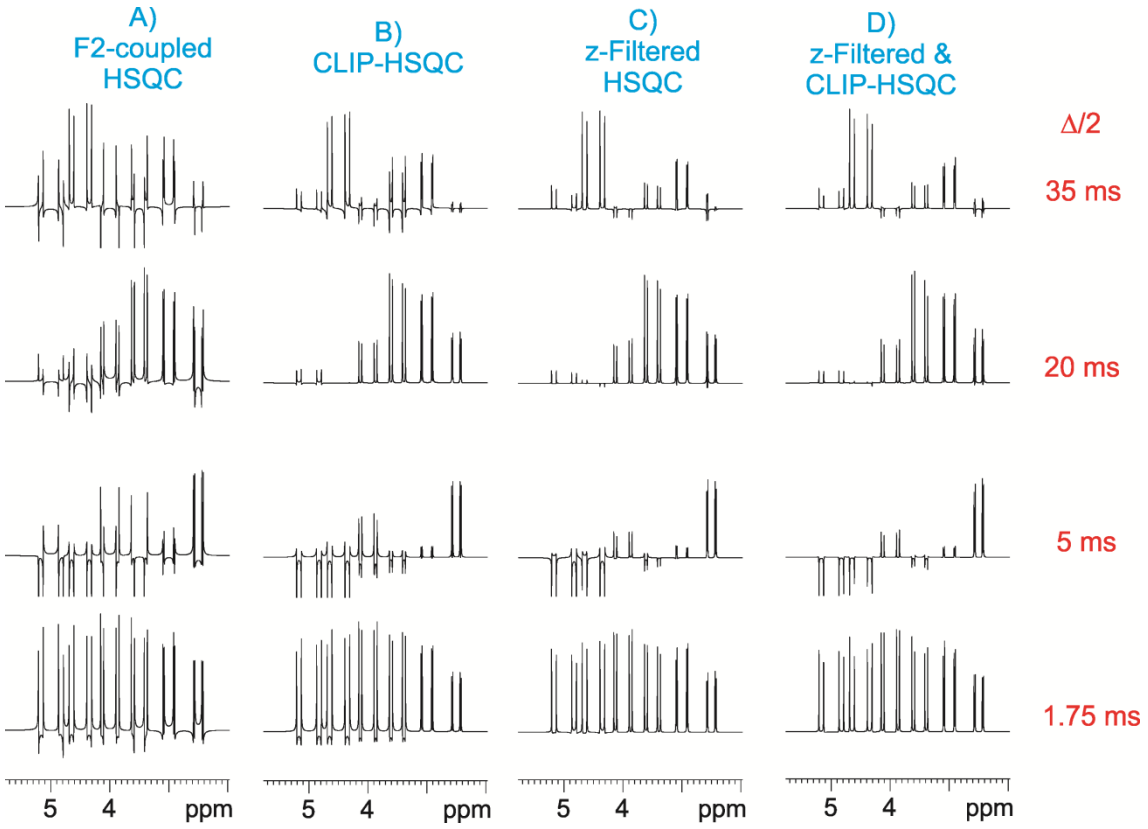

Figure S4: Simulations showing the effects of a wide range of J(HH) and J(CH) values in F2-coupled A) HSQC, B) CLIP-HSQC, C) z-filtered HSQC and D) z-filtered & CLIP-HSQC experiments as a function of the inter-pulse delay optimization. Simulation parameters: $\delta(H_A)$=2.5, $\delta(H_B)$=3.0, $\delta(H_C)$=3.5, $\delta(H_D)$=4.0, $\delta(H_E)$=4.5, $\delta(H_F)$=5; $^1J(CH_A)$=70 Hz, $^1J(CH_B)$=90 Hz, $^1J(CH_C)$=110 Hz, $^1J(CH_D)$=130 Hz, $^1J(CH_E)$=150 Hz, $^1J(CH_F)$=170Hz; $^2J(H_AH_B)$=10 Hz, $^2J(H_CH_D)$= 25 Hz, $^2J(H_EH_F)$=40 Hz.

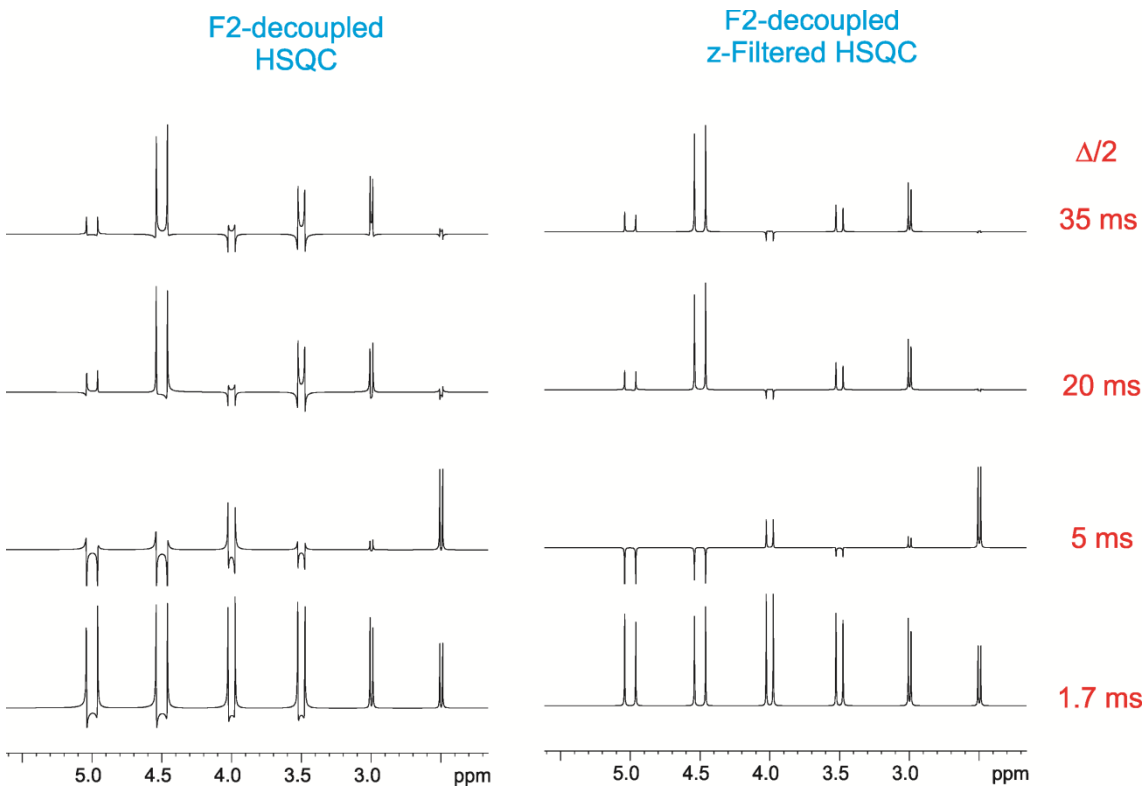

Figure S5: Simulations showing the effects of a wide range of J(HH) and J(CH) values in broadband decoupled HSQC and z-filtered HSQC experiment as a function of the inter-pulse delay optimization. We used the same spin system as described in Fig. S4.

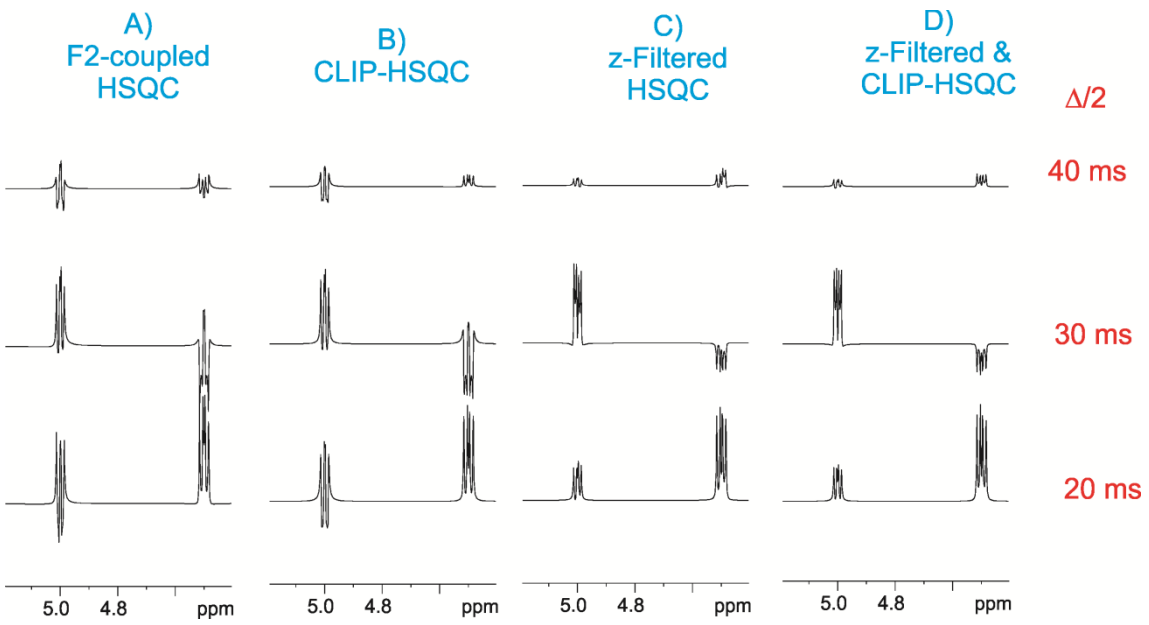

Figure S6: Simulations showing the effects of the inter-pulse delay optimization on small long-range J(CH) coupling constants in A) F2-coupled HSQC, B) CLIP-HSQC, C) z-filtered HSQC and D) z-filtered & CLIP-HSQC experiments. Simulation parameters: $\delta(H_A)$=4, $\delta(H_B)$=4.5, $\delta(H_C)$=5.0; $^{1}J(CH_A)$=140 Hz, $^{n}J(H_AH_B)$=6 Hz, $^{n}J(H_AH_C)$= 5 Hz, $^{n}J(CH_B)$=10 Hz, $^{n}J(CH_C)$=8 Hz.

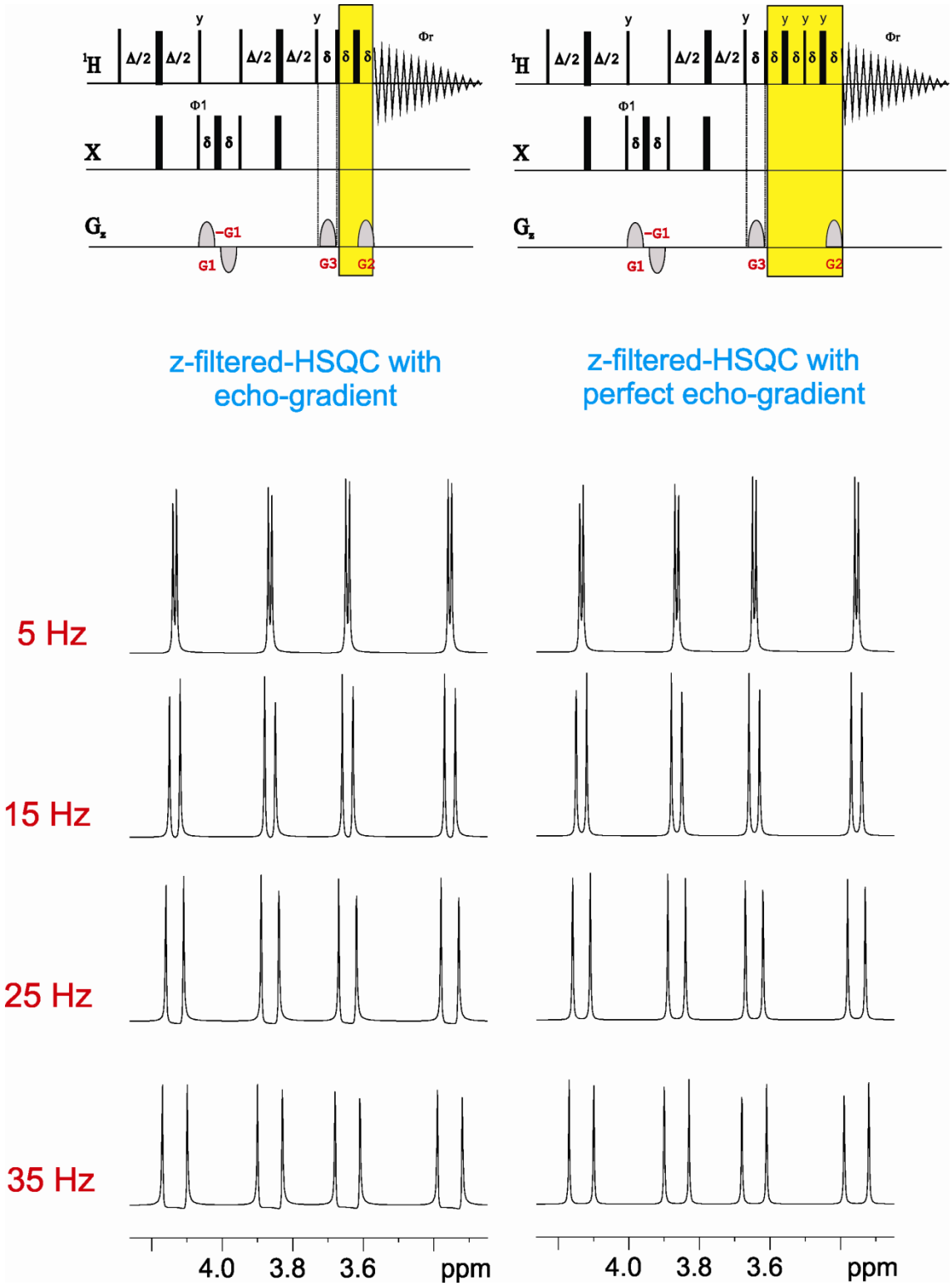

Figure S7: Simulations showing the effects of J(HH) evolution in a F2-coupled z-filtered HSQC experiment with A) a conventional echo gradient and B) a perfect-echo gradient. Simulation parameters: $\delta(H_A)$=4.0 ppm, $\delta(H_A)$=3.5 ppm, $^1J(CH_A)$=135 Hz, $^1J(CH_B)$=145 Hz,Δ=3.57 ms (optimized to 140 Hz), the duration of the gradient was 1ms and the recovery delay was set to 100µs (δ=1.1ms).

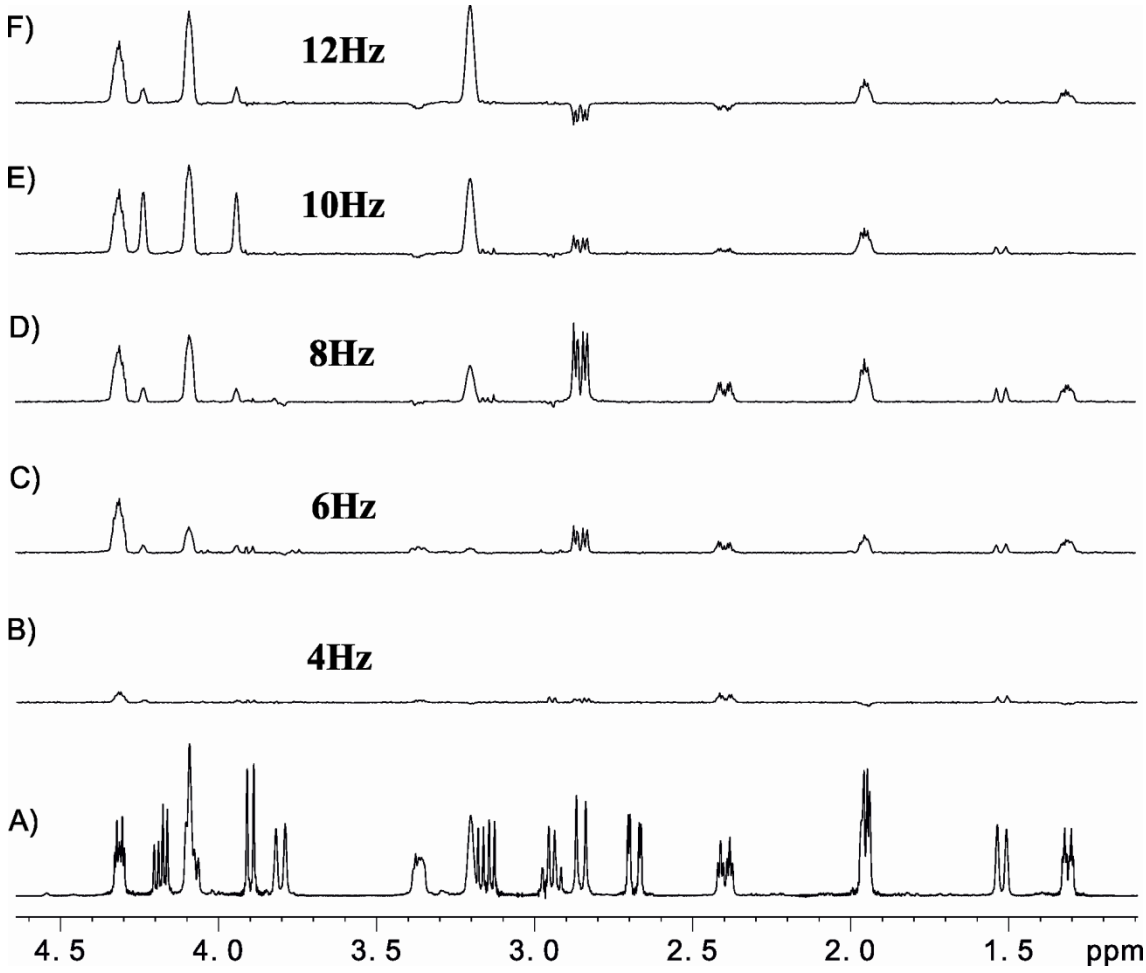

Figure S8: 1D traces extracted at 60.1 ppm (corresponding to the C8 and C16 carbons) as a function of inter-pulse Δ delay optimization in the PIP-HSQMBC experiment. A) Conventional ^{1}H, B) 4 Hz (Δ=125 ms), C) 6 Hz (Δ=83.3 ms), D) 8 Hz (Δ=62.5 ms), E) 10 Hz (Δ=50 ms) and E) 12 Hz (Δ=41.7 ms).

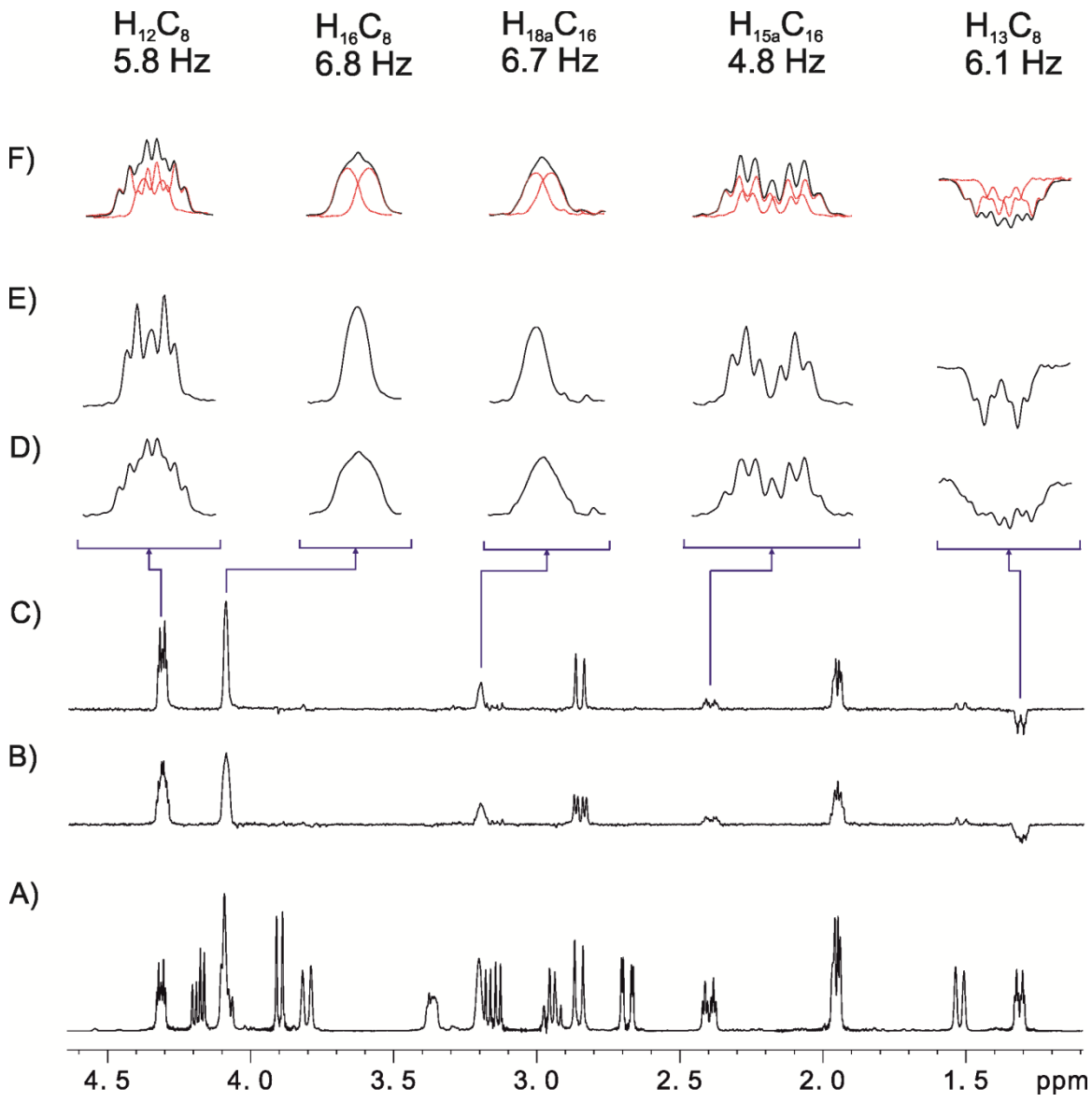

Figure S9: A) ^{1}H spectrum of strychnine at 500.13MHz. B-C) Comparison of the 1D slices extracted at 60.1 ppm (C8 and C16 carbons) from PIP-HSQMBC spectra acquired without (B) and with (C) heteronuclear decoupling during proton acquisition in Fig. 1 (Δ=62.5 ms). D-E) Expansion of some signals extracted from B and C, respectively. F) The decoupled multiplets can be used as a reference for a fitting process in cases where the additional splitting due to the active ^{n}J(CH) cannot be directly extracted from the non-decoupled multiplet.

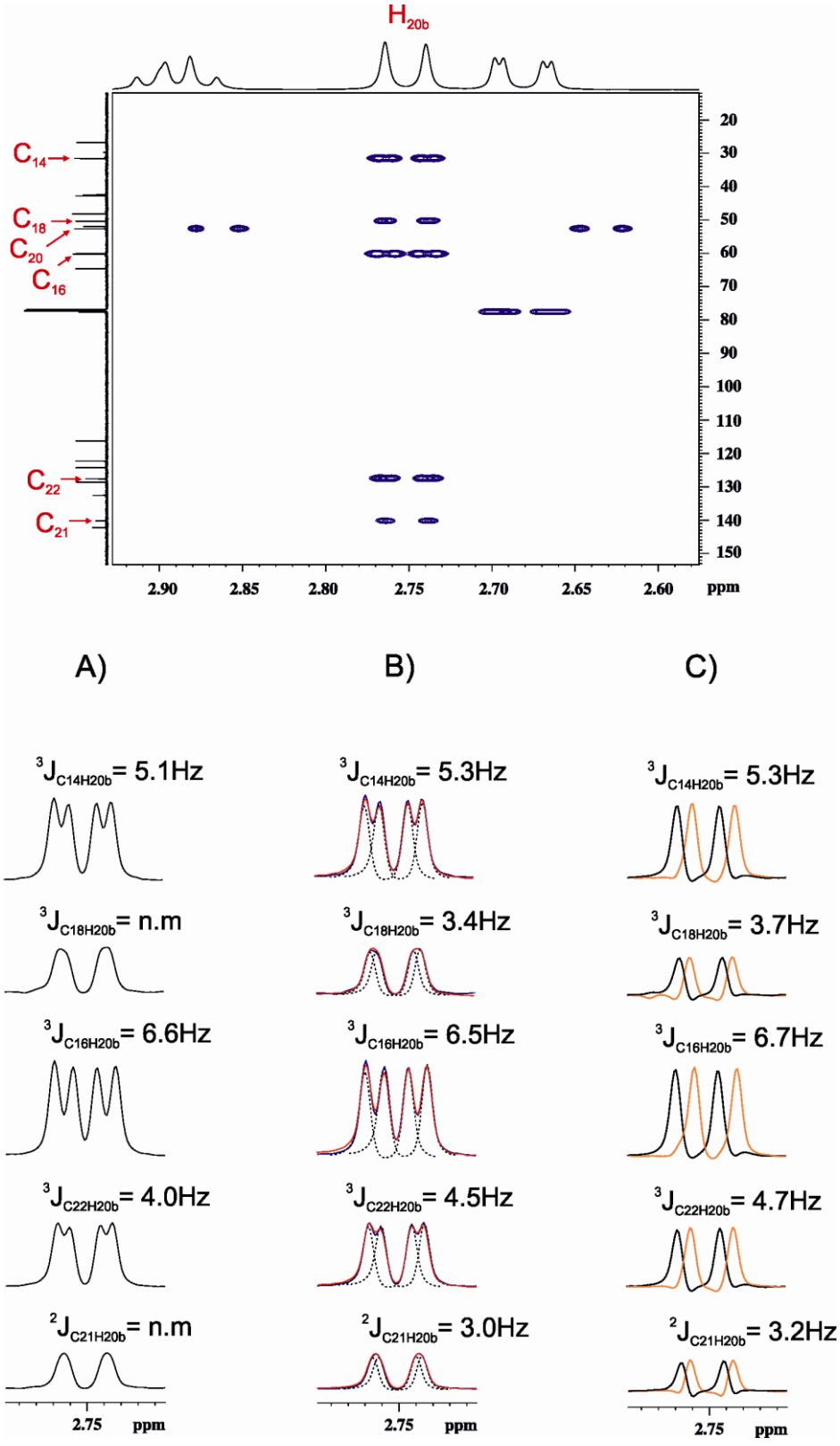

Figure S10: Comparison of methods for the measuring of small heteronuclear coupling constants taking some multiplet patterns from an 8 Hz optimized PIP-HSQMBC spectrum: A) direct extraction, B) fitting from the internal satellite lines and, C) IPAP methodology. The resolution along the detected F2 dimension was of 0.4Hz.

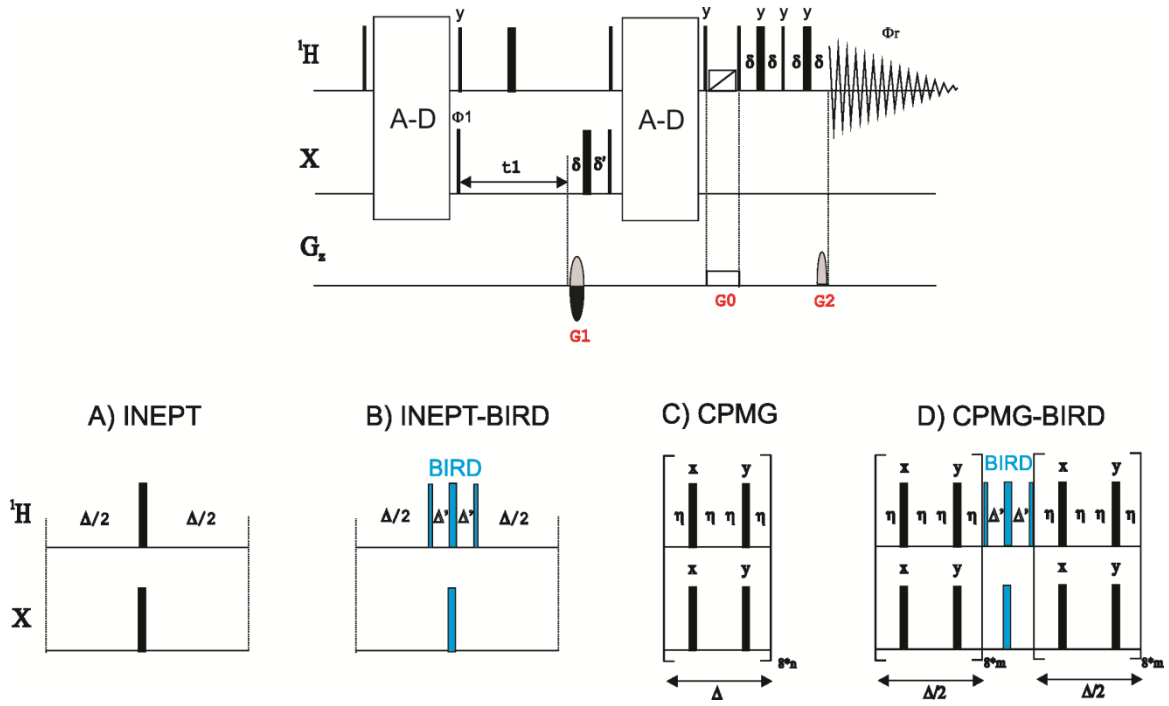

Figure S11: 2D pulse schemes to obtain PIP heteronuclear long-range correlation spectra. All these variants use the basic HSQMBC pulse train with a final zero-quantum filter after the refocusing period and just before the refocusing gradient echo and the acquisition. Several elements have been evaluated for the defocusing/refocusing of the heteronuclear coupling constants during the period $\Delta=1/[2*^{n}J(CH)]$: A) the basic INEPT; B) the INEPT-BIRD block ($\Delta'=1/[2*^{1}J(CH)]$); C) the CPMG XY-16 super cycle consisting of simultaneous ^{1}H and ^{13}C pulses applied at intervals 2η; D) the CPMG-BIRD element combining the features of B and C.

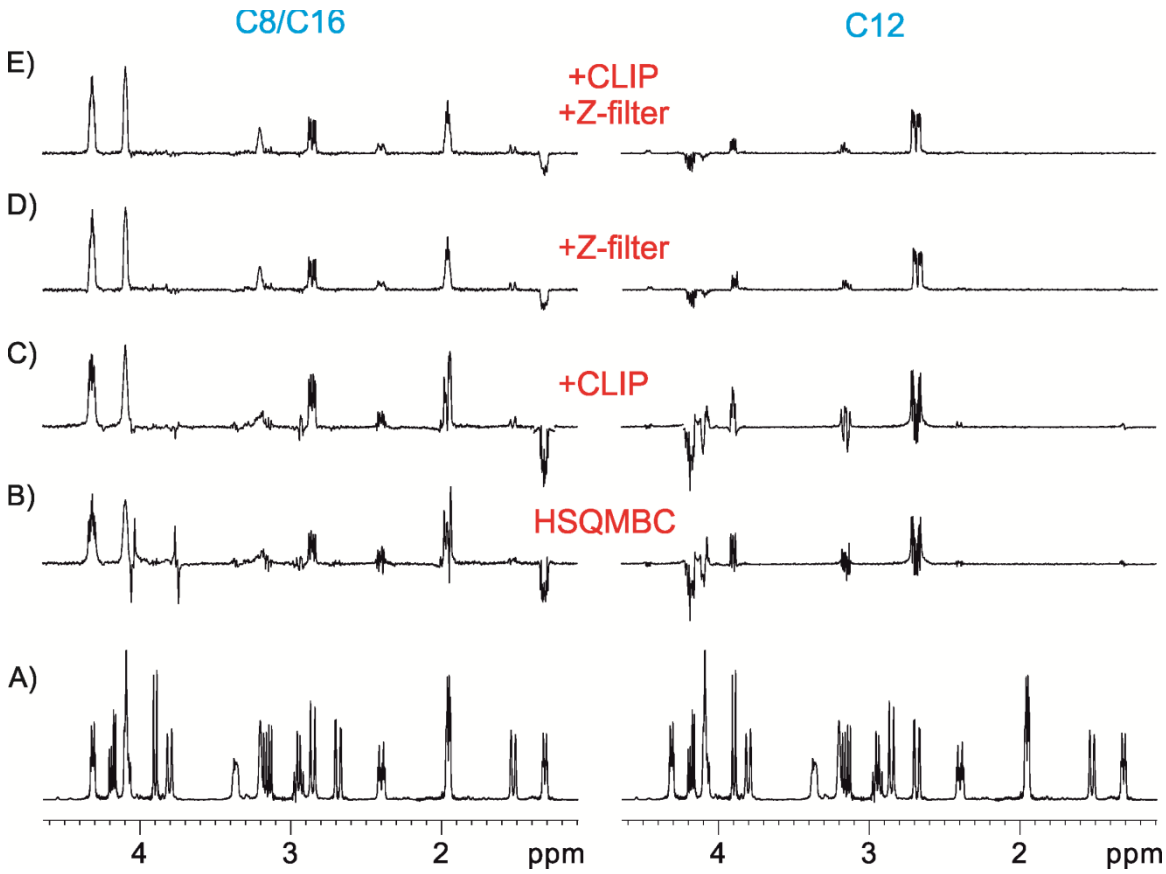

Figure S12: A) ^{1}H spectrum of strychnine at 500.13 MHz. B-E) Experimental effects on the application of the z-filter and a purging 90º ^{13}C pulse just before acquisition. 1D slices were extracted at 60.1 and 77.7 ppm (C8/C16 and C12 carbons, respectively) corresponding to the following 8 Hz optimized PIP-HSQMBC experiments: B) without adiabatic z-filter and CLIP pulse; C) with CLIP pulse; D) with adiabatic z-filter; E) with CLIP pulse and adiabatic z-filter. In all cases, data were acquired and processed under the same conditions (see experimental section) and the corresponding slices have been plotted at the same vertical scale to compare real sensitivity levels.

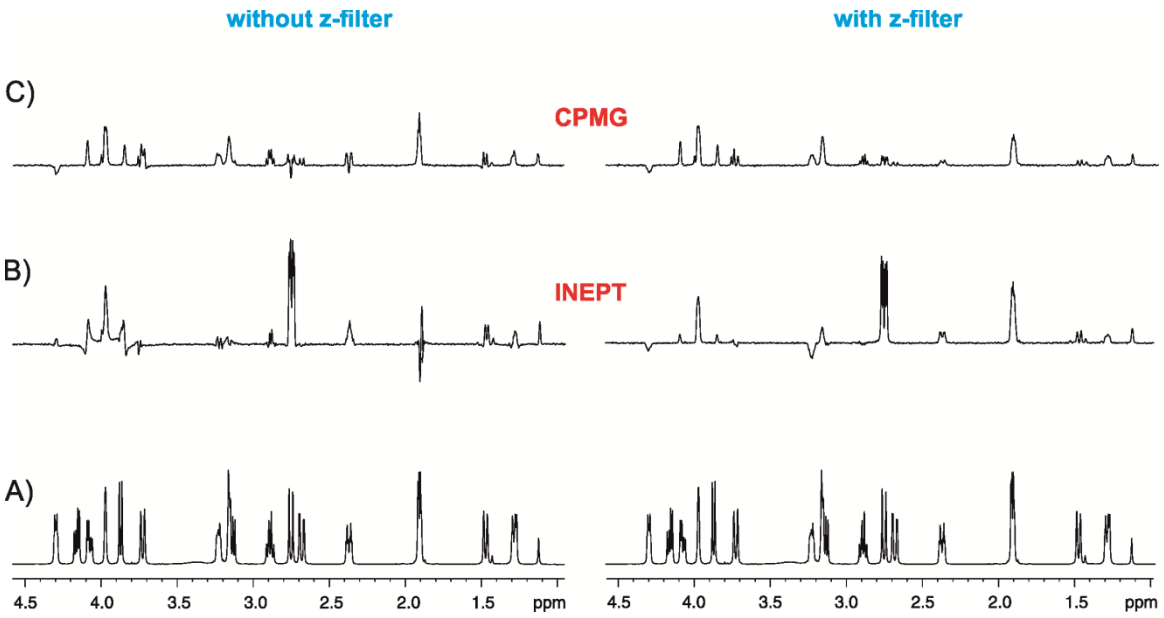

Figure S13: A) Conventional ^{1}H NMR; B-D) 1D slices extracted at 60.1 ppm (C8 and C16 carbons), corresponding to the following 8-Hz optimized PIP-HSQMBC experiments with and without z-filter: B) HSQMBC with INEPT (Fig. S11A); C) HSQMBC with CPMG (Fig. S11C with η=300 μs). In all cases, data were acquired and processed under the same conditions (see experimental section). The corresponding slices have been plotted at the same vertical scale to compare real sensitivity levels.

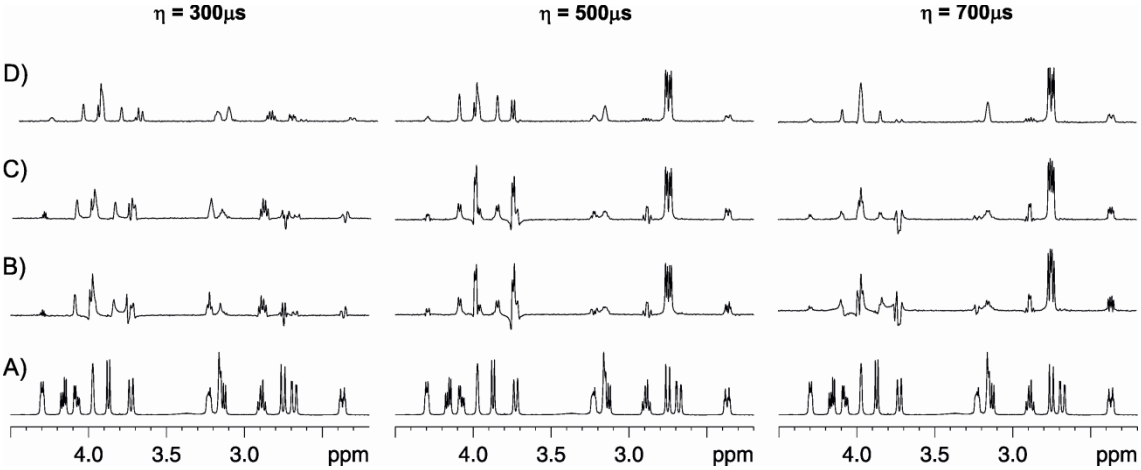

Figure S14: Experimental effects on the influence of the inter-pulse delay setting (η) in the success of the 8 Hz optimized B) HSQMBC-CPMG, C) HSQMBC-CPMG-CLIP and D) PIP-HSQMBC-CPMG experiment. All NMR experiments were acquired with the same experimental conditions described in figure S13.

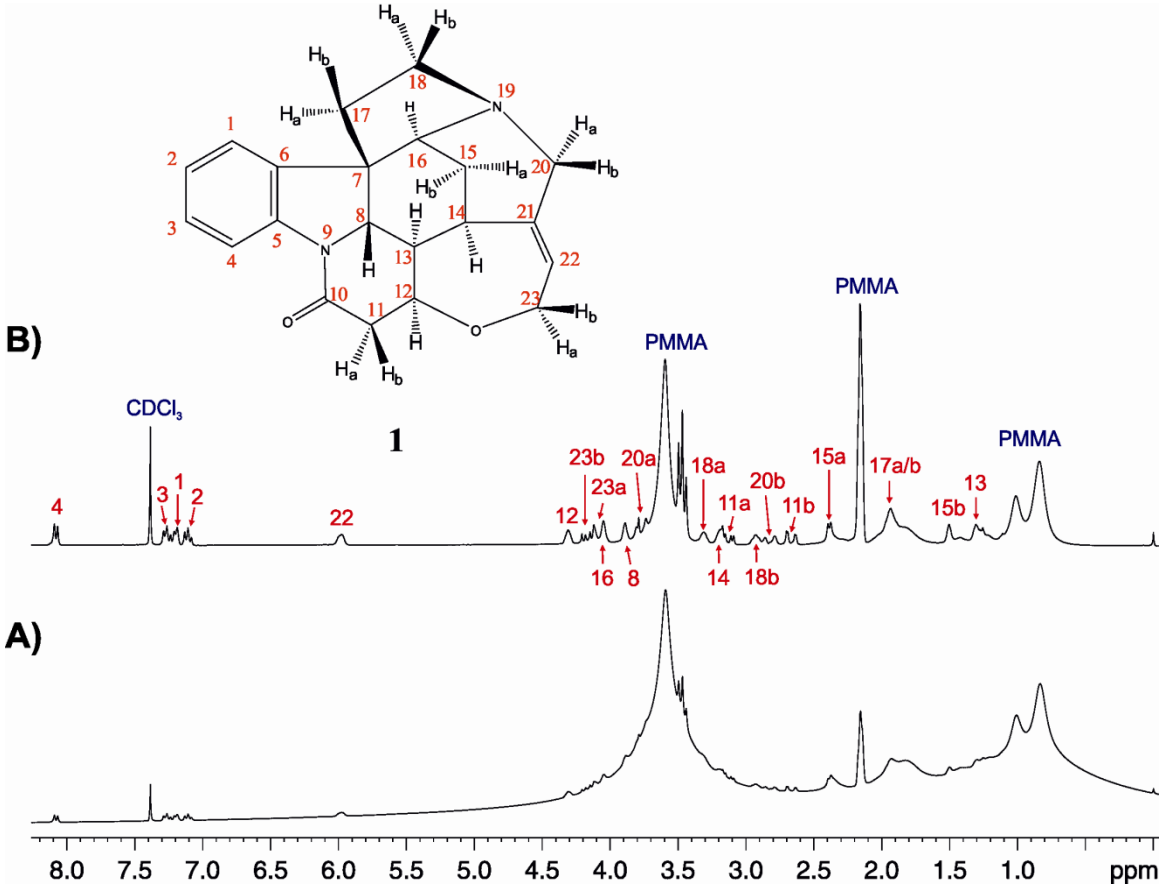

Figure S15: (A) conventional ^{1}H and (B) CPMG-PROJECT spectra of 4 mg of strychnine weakly aligned in PMMA gel swollen in $CDCl_3$. The 1D CPMG spectrum was acquired with a total echo time of 12 ms. Both experiments were collected using 4 scans.

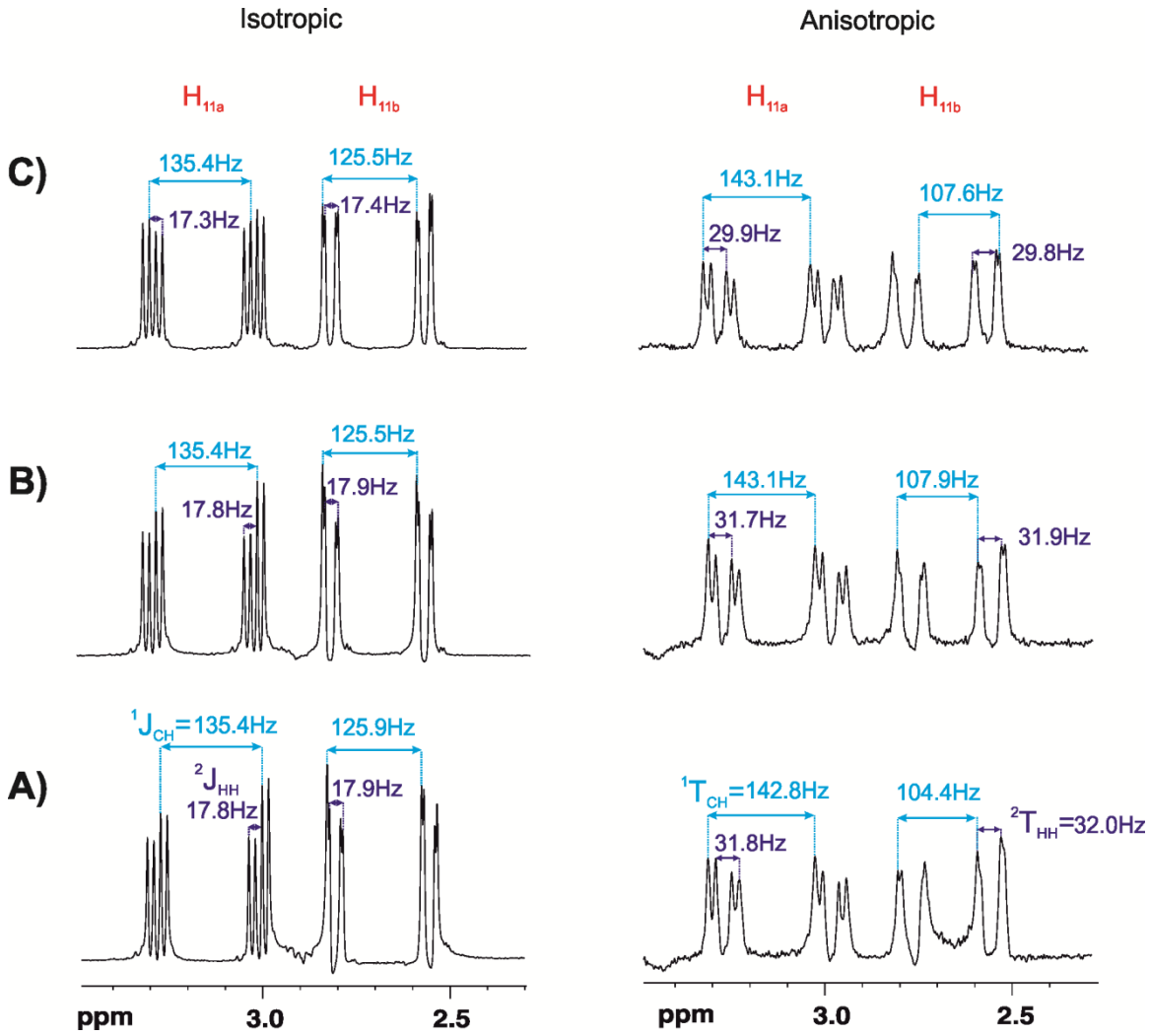

Figure S16: 1D traces extracted at the C11 chemical shift of (**1**) in isotropic and anisotropic conditions showing the signal distortions originated in (A) conventional HSQC, (B) CLIP-HSQC, and (C) PIP-HSQC spectra recorded with Δ set to 3.6 ms ($^{1}J_{CH}$=140 Hz).

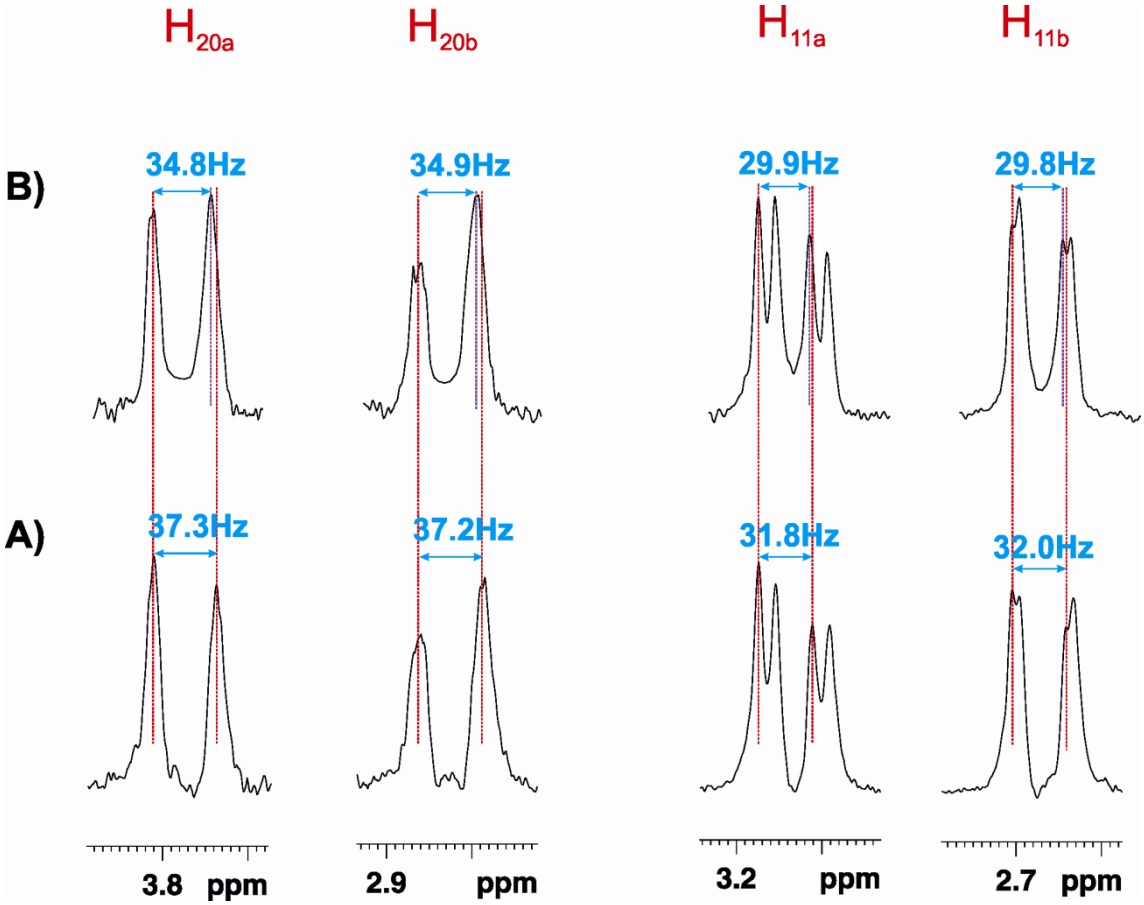

Figure S17: 1D traces extracted at the C11 and C20 chemical shift of (**1**) in anisotropic conditions from F2-decoupled (A) conventional HSQC and (B) PIP-HSQC spectra with Δ optimized 3.6 ms ($^{1}J_{CH}$=140 Hz). The elimination of all dispersive components in (B) allows carrying out the measurement of ^{n}JHH more accurately. J_{HH} splittings extracted from ^{1}H-PROJECT spectrum were $^{2}J_{H20aH20b}$=34.8Hz and $^{2}J_{H11aH11b}$=30.0Hz.

Table S1: Experimental $^{1}J(CH)$/ $^{1}T(CH)$ values extracted from the PIP-HSQC spectra of strychnine recorded in isotropic and anisotropic conditions.

				PIP-HSQC				
				Isotropic	**Anisotropic**		**Predicted**[c]	**Others** [ref.1]
C	δ (ppm)	H	δ (ppm)	$^{1}J_{CH}$ (Hz)	$^{1}T_{CH}$ (Hz)	$^{1}D_{CH}$ (Hz)	$^{1}D_{CH}$ (Hz)	$^{1}D_{CH}$ (Hz)
C_1	122.3	H_1	7.16	158.3	174.8	+16.5	+12.2	+21.0
C_2	124.2	H_2	7.09	160.8[a]	163.7[a]	+2.9	+2.2	+12.3
C_3	128.6	H_3	7.25	159.2[a]	163.5[a]	+4.3	+3.2	+10.0
C_4	116.2	H_4	8.08	168.4	187.1	+18.7	+13.9	+21.6
C_8	60.1	H_8	3.86	144.9	133.7	-11.2	-8.6	-9.8
C_{11}	42.5	H_{11a}	3.12	135.4	143.1	+7.7	+5.9	+10.0
		H_{11b}	2.66	125.5	107.6	-18.2	-14.1	-18.0
C_{12}	77.6	H_{12}	4.28	150.0	134.2	-15.8	-12.3	-20.6
C_{13}	48.2	H_{13}	1.27	124.8	118.9	-5.9	-4.6	-4.9
C_{14}	31.6	H_{14}	3.15	131.3	117.9	-13.4	-10.4	-20.7
C_{15}	26.8	H_{15a}	2.36	130.9	135.0	+4.1	+3.2	+2.0
		H_{15b}	1.47	129.9	131.0	+1.1	+0.9	+4.5
C_{16}	60.2	H_{16}	3.98	146.7	158.2	+11.5	+9.0	+14.0
C_{17}	42.8	$H_{17a/b}$	1.90	133.2	139.1	+5.9	+4.6	+1.38
C_{18}	50.3	H_{18a}	3.25	146.3	148.1	+1.8	+1.4	0.0
		H_{18b}	2.88	131.7	143.4	+11.7	+9.0	+13.0
C_{20}	52.7	H_{20a}	3.73	138.8	ov[b]		-7.7	-10.0
		H_{20b}	2.76	138.7	132.9	-6.2	-4.6	-6.0
C_{22}	127.6	H_{22}	5.93	158.8	156.4	-2.4	-1.8	-1.1
C_{23}	64.6	H_{23b}	4.15	145.5	148.9	+3.4	+2.6	+8
		H_{23a}	4.05	137.2	111.7	-25.5	-19.4	--

[a] Strong coupling effect
[b] Overlapped with PMMA signals
[c] The predicted values have been calculated with MSpin program (MESTREALAB RESEARCH SL, Santiago de Compostela, Spain. http://www.mestrelab.com).

[1] J. D. Snider, E.Troche-Pesqueira, S. R. Woodruff, C.Gayathri, N. V. Tsarevsky and R. R. Gil, *Magn. Reson. Chem*. **2012**, 50, S89-S91.

Table S2: $^{2}J(HH)/ {}^{2}T(HH)$ values extracted from the PIP-HSQC spectra of strychnine recorded in isotropic and anisotropic conditions.

		^{1}H NMR	CPMG-PROJECT	PIP-HSQC				
		Isotropic[a]	Anisotropic[a]	Isotropic[a]	Anisotropic[a]		Predicted[c]	Others [ref.2]
H	δ (ppm)	$^{2}J_{HH}$ (Hz)	$^{2}T_{HH}$ (Hz)	$^{2}J_{HH}$ (Hz)	$^{2}T_{HH}$ (Hz)	$^{2}D_{HH}$ (Hz)	$^{2}D_{HH}$ (Hz)	$^{2}D_{HH}$ (Hz)
H_{11a}	3.12	-17.3	-30.1	-17.3	-29.9	-12.6	-9.9	-12.5
H_{11b}	2.66	-17.4	-30.0	-17.4	-29.8	-12.4		-12.6
H_{15a}	2.36	-14.4	-n.m	-14.5	n.m	--	+10.2	+13.2
H_{15b}	1.47	-14.4	-n.m	-14.6	n.m	--		+13.3
H_{18a}	3.25	n.m	-n.m	n.m	n.m	--	+7.1	+8.8
H_{18b}	2.88	-9.6	-n.m	-9.6	n.m	--		+8.9
H_{20a}	3.73	-14.8	-34.7	-15.0	-34.8	-19.8	-15.3	-20.1
H_{20b}	2.76	-14.8	-34.9	-14.9	-34.9	-20.0		-20.1
H_{23b}	4.15	-13.8	-30.1	-13.7	-29.7	-16.0	-12.7	-16.2
H_{23a}	4.05	-13.8	ov[b]	-13.8	-29.8	-16.0		-16.3

n.m: not measured due to signal widening caused by $^{n}J_{HH}/ {}^{n}T_{HH}$ splitting.

[a] The sign of the measure has been extrapolated from ω1-iINEPT experiments [2].

[b] Overlapped with H_{23a} and H_{16} signals.

[c] The predicted values have been calculated with MSpin program (MESTREALAB RESEARCH SL, Santiago de Compostela, Spain. http://www.mestrelab.com).

[2] Measuring from the ω1-iINEPT experiment in isotropic and anisotropic media: J. Saurí, L. Castañar, P. Nolis, A. Virgili, T. Parella, *J. Magn. Reson*. 242 (2014) 33–40.

Table S3: Comparison of $^{2}J(HH)$/ $^{2}T(HH)$ values extracted from the conventional HSQC, CLIP-HSQC and PIP-HSQC spectra of strychnine recorded in isotropic and anisotropic conditions.

		^{1}H NMR	CPMG-PROJECT	HSQC		CLIP-HSQC		PIP-HSQC	
		Isotropic	Anisotropic	Isotropic	Anisotropic	Isotropic	Anisotropic	Isotropic	Anisotropic
H	δ (ppm)	$^{2}J_{HH}$ (Hz)	$^{2}T_{HH}$ (Hz)	$^{2}J_{HH}$ (Hz)	$^{2}T_{HH}$ (Hz)	$^{2}J_{HH}$ (Hz)	$^{2}T_{HH}$ (Hz)	$^{2}J_{HH}$ (Hz)	$^{2}T_{HH}$ (Hz)
H_{11a}	3.12	-17.3	-30.1	-17.8	-31.8	-17.8	-31.7	-17.3	-29.9
H_{11b}	2.66	-17.4	-30.0	-17.9	-32.0	-17.9	-31.9	-17.4	-29.8
H_{15a}	2.36	-14.4	-n.m	-15.1	n.m	-15.1	n.m	-14.5	n.m
H_{15b}	1.47	-14.4	-n.m	-15.3	n.m	-15.4	n.m	-14.6	n.m
H_{18a}	3.25	-n.m	-n.m	n.m	n.m	n.m	n.m	n.m	n.m
H_{18b}	2.88	-9.6	-n.m	-9.9	n.m	-10.0	n.m	-9.6	n.m
H_{20a}	3.73	-14.8	-34.7	-15.6	-37.3	-15.7	-37.2	-15.0	-34.8
H_{20b}	2.76	-14.8	-34.9	-15.6	-37.2	-15.6	-37.4	-14.9	-34.9
H_{23b}	4.15	-13.8	-30.1	-13.6	-32.1	-13.6	-32.2	-13.7	-29.7
H_{23a}	4.05	-13.8	-ov[b]	-13.9	-32.2	-13.9	-32.2	-13.8	-29.8

n.m: not measured due to signal widening caused by $^{n}J_{HH}$/ $^{n}T_{HH}$ splitting.

[a] The sign of the measure has been extrapolated from ω1-iINEPT experiments [2].

[b] Overlapped with H_{23a} and H_1 signals.

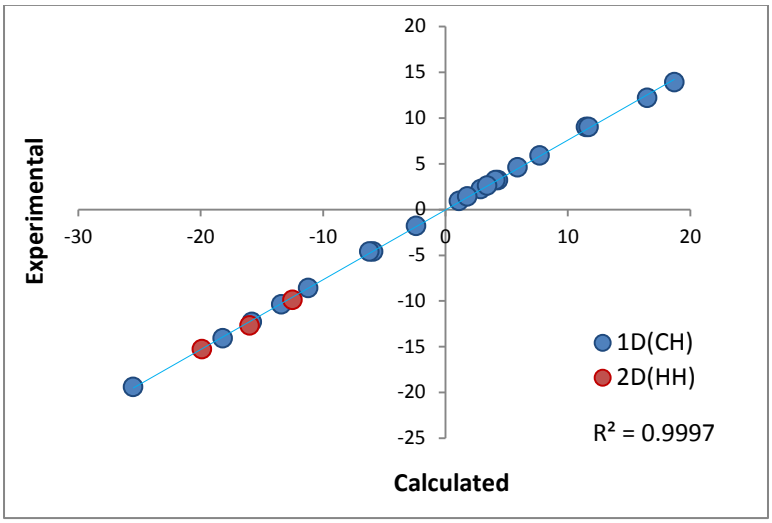

Figure S18: Plot showing the correlation between the experimental and calculated ^{1}D(CH) data for strychnine described in Table S1.

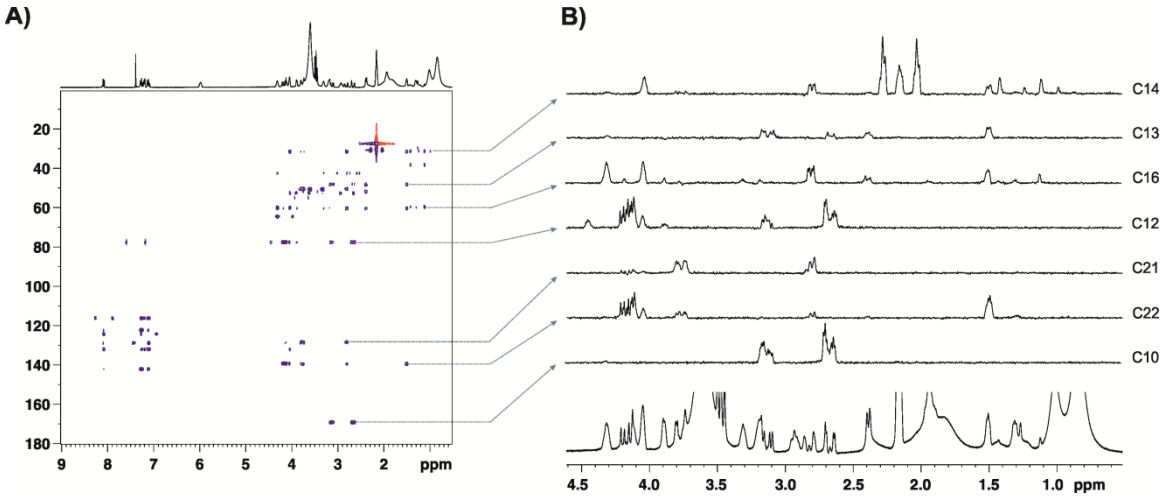

Figure S19: (A) 8-Hz optimized PIP-HSQMBC spectrum of (**1**) in anisotropic conditions; (B) 1D row slices taken at different ^{13}C frequencies showing in-phase multiplet patterns for all observed cross-peaks.

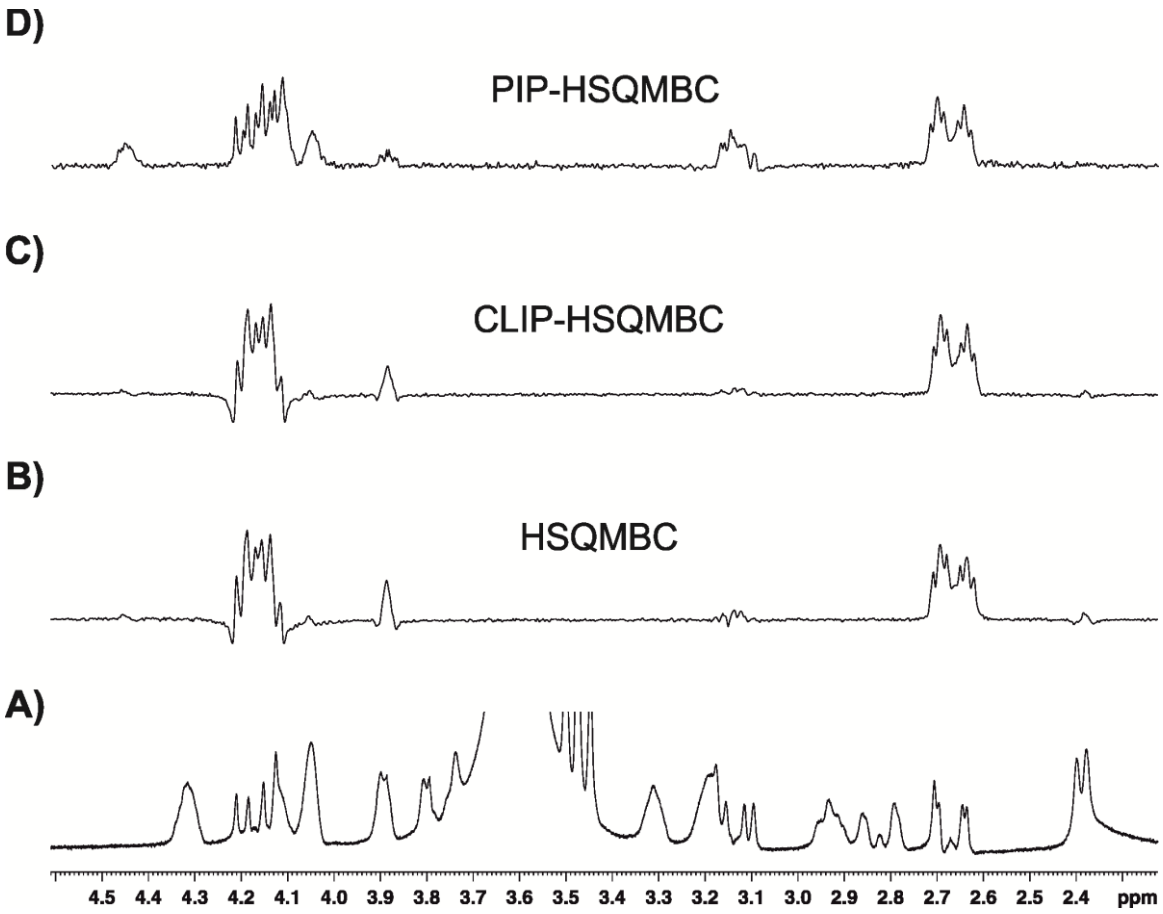

Figure S20: (A) ^{1}H-PROJECT spectrum of (**1**) in anisotropic conditions; (B-D) 1D traces extracted at the C12 chemical shift showing the signal distortions in (B) HSQMBC, (C) CLIP-HSQMBC and (D) PIP-HSQMBC spectra (all experiments were optimized to 8 Hz (Δ=62.5 ms)).

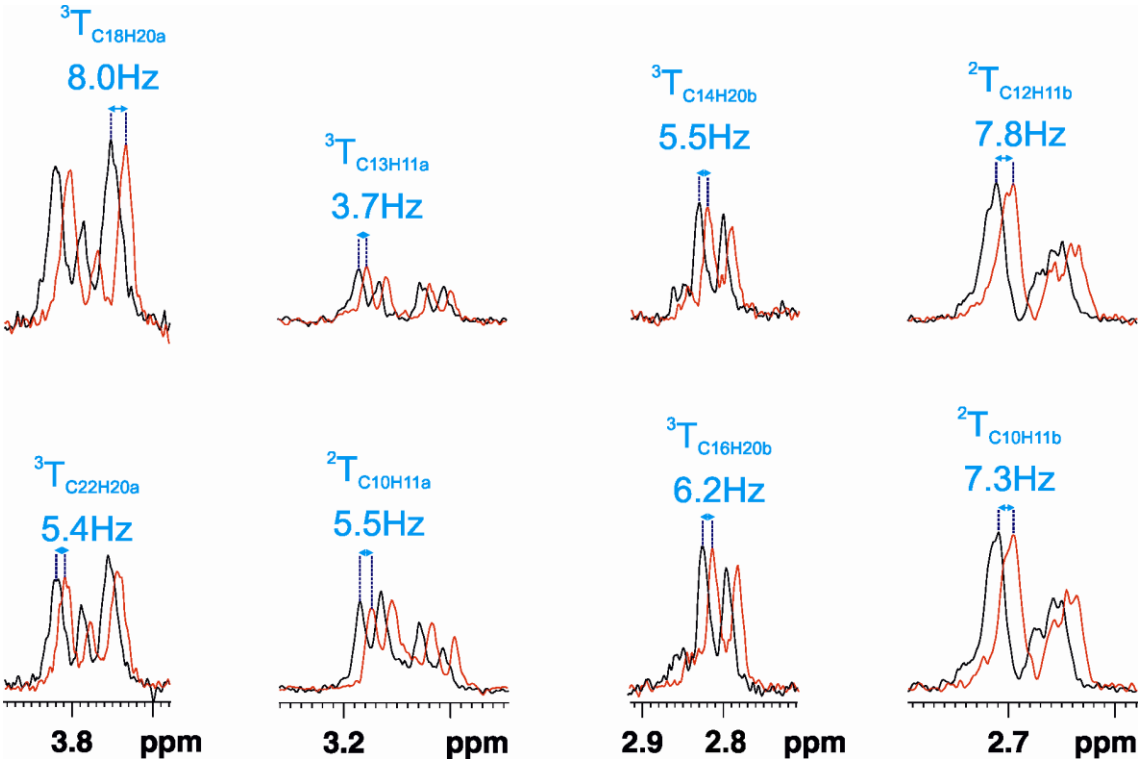

Figure S21: Measurement of $^{n}T_{CH}$ values of (**1**) in complex multiplets obtained under anisotropic conditions. 1D traces show overlaid α and β multiplets obtained in an IPAP PIP-HSQC experiment after IP±AP data combination.

Pulse Program code for Bruker spectrometers:

```
; PIPhsqmbc
;Pure In-Phase HSQMBC  with final adiabatic z-filter and perfect echo gradient
;optional IPAP using const25

#include <Avance.incl>
#include <Grad.incl>
#include <Delay.incl>

"p2=p1*2"
"d6=1s/(cnst2*4)"
"d0=3u"
"in0=inf1/2"

"DELTA2=d6-larger(p2,p14)/2"
"DELTA=p16+d16+p2+d0*2"
"DELTA4=p16+d16"

1 ze
2 d1 pl1:f1
3 (p1 ph1)

  DELTA2 pl0:f2
  (center (p2 ph1) (p14:sp3 ph6):f2 )
  DELTA2 pl2:f2 UNBLKGRAD

  (p1 ph2) (p3 ph3):f2
  d0
  (p2 ph5)
  d0
  p16:gp1*EA
  d16 pl0:f2
  (p24:sp7 ph4):f2
  DELTA pl2:f2
  (ralign (p1 ph1) (p3 ph4):f2 )

if "cnst25==0"
          {
          DELTA2 pl0:f2
          (center (p2 ph1) (p14:sp3 ph1):f2 )
          DELTA2 pl2:f2
          }
          else
          {
            d6
           (p2 ph2)
           d6
          }

  if "cnst25==0"
```

```
        {
        (p1 ph2):f1
        }
        else
        {
        (p1 ph1):f1
        }

 d12 pl0:f1
 300u gron0
 (p32:sp29 ph1):f1
 300u groff
 d12 pl1:f1
 p1 ph1

 DELTA4
 p2 ph1
 DELTA4
 p1 ph2
 DELTA4
 p2 ph1
 p16:gp2
 d16 BLKGRAD

 go=2 ph31
 d1 mc #0 to 2
   F1EA(calgrad(EA), caldel(d0, +in0) & calph(ph3, +180) & calph(ph6, +180) & calph(ph31, +180))
exit

ph1=0
ph2=1
ph3=0 2
ph4=0
ph5=0
ph6=0
ph31=0 2

;pl0 : 0W
;pl1 : f1 channel - power level for pulse (default)
;pl2 : f2 channel - power level for pulse (default)
;sp3: f2 channel - shaped pulse 180 degree
;sp7: f2 channel - shaped pulse 180 degree
;sp29: f2 channel - shaped adiabatic pulse 180 degree
;p1 : f1 channel -  90 degree high power pulse
;p2 : f1 channel - 180 degree high power pulse
;p3 : f2 channel -  90 degree high power pulse
;p4 : f2 channel - 180 degree high power pulse
;p14: f2 channel - 180 degree shaped pulse for inversion
;p24: f2 channel - 180 degree shaped pulse for refocusing
;p32: f2 channel - 180 degree shaped pulse for adiabatic z-filter
;p16: homospoil/gradient pulse
```

```
;d0 : incremented delay (2D)                    [3 usec]
;d1 : relaxation delay; 1-5 * T1
;cnst25=0 (IP) 1 (AP)
;cnst2= 8Hz
;d6 : 1/(4J)XH (long range coupling constant)
;d16: delay for homospoil/gradient recovery
;inf1: 1/SW(X) = 2 * DW(X)
;in0: 1/(2 * SW(X)) = DW(X)
;nd0: 2
;NS: 2 * n
;DS: >= 2
;td1: number of experiments
;FnMODE: echo-antiecho

;use gradient ratio:       gp 1 : gp 2
;                           80 : 20.1    for C-13
;                           80 :  8.1    for N-15

;for z-only gradients:
;gpz1: 80%
;gpz2: 20.1% for C-13, 8.1% for N-15
;gpz0: 3%

;use gradient files:
;gpnam1: SMSQ10.100
;gpnam2: SMSQ10.100
```

PUBLICATION 9

Suppression of phase and amplitude J_{HH} modulations in HSQC experiments

Laura Castañar, Eduard Sistaré, Albert Virgili, Robert Thomas Williamson and Teodor Parella.

Magn. Reson. Chem., **2014**, *53*, 115-119.

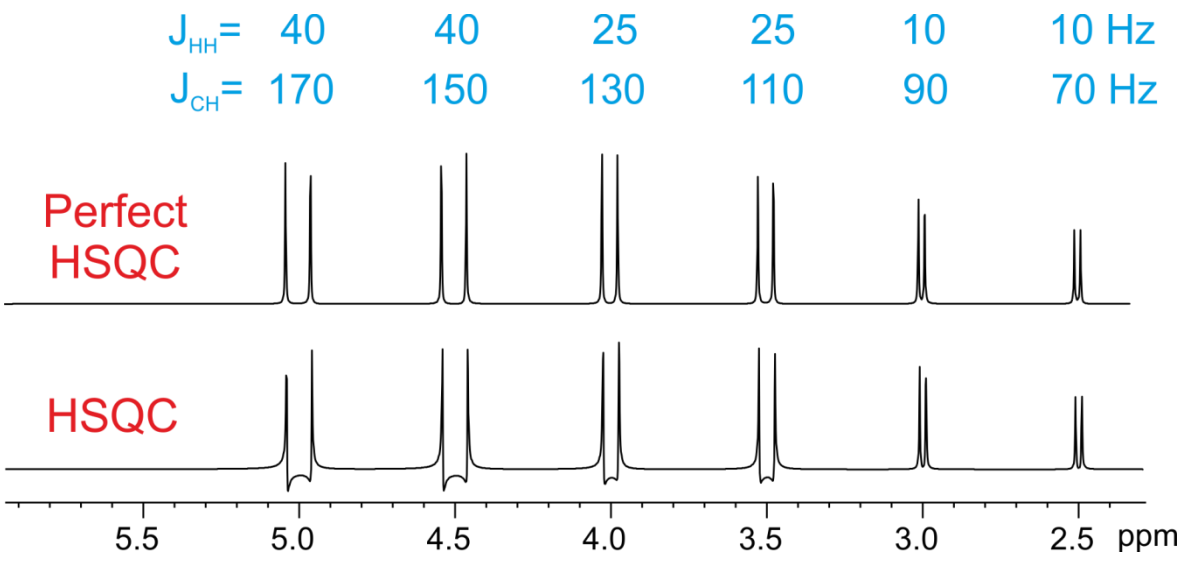

Introduction

There is an enormous interest in the use of the HSQC experiment as a quantitative NMR tool, as demonstrated for the many different approaches proposed in the last years.[94] In conventional HSQC and HSQMBC spectra, peak volumes of different protons are modulated according to each individual J_{HH} coupling pattern by the $\cos^2(\pi J_{H_1H_2}\Delta)$ function (see Eq.1.21 in section 1.2.1.1.). This non-uniform dependence causes a common source of error during volume integration and quantification.

In the previous publication has been demonstrated that the unwanted homo- and heteronuclear AP contributions in HSQC and HSQMBC experiments can be removed by applying an adiabatic *z*-filter, and the resulting PIP-HSQC and HSQCMBC spectra display undistorted in-phase cross-peaks. However, in these experiments the evolution under the J_{HH} takes place during the INEPT period and the final IP detected signal is still modulated by a $\cos^2(\pi J_{H_1H_2}\Delta)$ factor.

In this publication, it is shown experimentally and by simulation that the typical J_{HH} interferences present in conventional HSQC experiments can be efficiently suppressed using an improved perfect-HSQC pulse scheme. The proposal is based on the conventional HSQC pulse scheme where the standard INEPT block is replaced by a J_{HH}-compensated perfect-echo INEPT[95] module consisting of a double echo period in both defocusing/refocusing heteronuclear transfer periods. J_{HH} is refocused at the end of each double echo period, and therefore, the signal amplitude is only modulated by the effect of $^1J_{CH}$.

The resulting 2D perfect-HSQC spectra afford pure IP cross-peaks with respect to both $^1J_{CH}$ and J_{HH} rendering practical applications such as phase correction and multiplet analysis more convenient and accurate. There is a second and very significant positive consequence for removing J_{HH} interferences: signal intensity is amplitude modulated only by a $\sin^2(\pi J_{CH}\Delta)$ factor, and therefore the perfect-HSQC experiment is an excellent candidate to design future strategies for quantitative NMR studies. The proposed method is less aggressive than the use of CPMG-INEPT blocks where a train of simultaneous ^{1}H/^{13}C pulses are applied at high repetition rates, and where the resulting peaks can include

[94] a) H. Koskela, T. Väänänen, *Magn. Reson. Chem.,* **2002**, *40*, 705. b) S. Heikkinen, M. M. Toikka, P. T. Karhunen, A. Kilpeläinen, *J. Am. Chem. Soc.,* **2003**, *125*, 4362. c) H. Koskela, I. Kilpeläinen, S. Heikkinen, *J. Magn. Reson*., **2005**, *174*, 237. d) D. J. Peterson, N. M. Loening, *Magn. Reson. Chem.,* **2007***, 45*, 937. e) H. Koskela, O. Heikkilä, I. Kilpeläinen, S. Heikkinen, *J. Magn. Reson*., **2010**, *202*, 24.

[95] B. Baishya, C. L. Khetrapal. *J. Magn. Reson*., **2014**, *242*, 143.

unwanted dependences from offset effects or the presence of TOCSY contributions as well as deleterious effects on sample heating under extreme fast pulsing conditions.

The main disadvantage of the perfect-HSQC experiment arises from the longer duration of the perfect-echo INEPT versus the conventional INEPT (2Δ *vs*. Δ, respectively) that can lead to some signal loss due to additional T_2 relaxation. The overall duration of the sequence is extended about 3.6 ms for each perfect-echo INEPT period in a 140-Hz optimized experiment but this does not represent a serious issue for small molecules having reasonably long T_2 relaxation times (some hundreds of milliseconds).

Research article

MRC

Received: 10 May 2014 Revised: 11 July 2014 Accepted: 25 August 2014 Published online in Wiley Online Library: 3 October 2014

(wileyonlinelibrary.com) DOI 10.1002/mrc.4149

Suppression of phase and amplitude J(HH) modulations in HSQC experiments

Laura Castañar,[a,b] Eduard Sistaré,[a,b] Albert Virgili,[a,b] R. Thomas Williamson[c] and Teodor Parella[a,b]*

The amplitude and the phase of cross peaks in conventional 2D HSQC experiments are modulated by both proton–proton, J(HH), and proton–carbon, ^{1}J(CH), coupling constants. It is shown by spectral simulation and experimentally that J(HH) interferences are suppressed in a novel perfect-HSQC pulse scheme that incorporates perfect-echo INEPT periods. The improved 2D spectra afford pure in-phase cross peaks with respect to ^{1}J(CH) and J(HH), irrespective of the experiment delay optimization. In addition, peak volumes are not attenuated by the influence of J(HH), rendering practical issues such as phase correction, multiplet analysis, and signal integration more appropriate. Copyright © 2014 John Wiley & Sons, Ltd.

Keywords: NMR; HSQC; pure in-phase signals; perfect HSQC; J(HH) modulation

Introduction

Heteronuclear multiple-quantum correlation (HMQC)[1] and heteronuclear single-quantum correlation (HSQC)[2] experiments have become the most popular pulse schemes to obtain heteronuclear chemical-shift correlation NMR spectra. Both techniques use a similar logical concept based on a ^{1}H-to-^{13}C-to-^{1}H out-and-back magnetization transfer via the one-bond proton–carbon coupling constants, ^{1}J(CH).[3] The HMQC scheme is simpler in terms of the number of pulses, but its major complication relies on that proton magnetization is located in the transverse plane during the entire pulse sequence. Additionally, proton–proton coupling constants, J(HH), also evolve during the variable t_1 period. As a result, cross peaks present strongly distorted twist-phased patterns along the detected F2 dimension and a characteristic skew shape along the indirect F1 dimension of the two-dimensional (2D) map. On the other hand, the HSQC experiment uses INEPT blocks for heteronuclear magnetization transfer, and the evolution during the t_1 period is not affected by J(HH). However, J(HH) couplings evolve during the INEPT periods, and their influences on the phase and amplitude signal modulation must be considered when a detailed analysis is required. In practice, the magnitudes of ^{1}J(CH) (120–250 Hz) are generally more than one order of magnitude larger than J(HH) (0–15 Hz), and therefore, the prejudicial effects of J(HH) on the detected signal have usually been neglected.

On the other hand, the concept of perfect echo[4] has been successfully implemented in a series of NMR applications to solve some traditional issues, such as the elimination of peak distortion caused by homonuclear J-coupling in diffusion NMR experiments,[5] the determination of T_2 relaxation times from undistorted multiplets in 'perfect-echo Carr–Purcell–Meiboom–Gill (CPMG)' experiments,[6] the suppression of J(HH) evolution during the solvent-suppression period in a 'perfect water suppression by gradient tailored excitation' method,[7] or during the t_1 period in 'perfect-HMQC' experiments.[8] This concept has also been used in an effort to improve long-range heteronuclear transfers by means of a 'perfect-echo INEPT' element.[9]

Many chemists use the HSQC experiment in a qualitative way to correlate the chemical shifts of carbon and attached protons. For these applications, the issues with phase distortion caused by J(HH) are for the most part invisible and therefore irrelevant. However, these effects are present in the form of antiphase components and become highly relevant when trying quantitative measurements in terms of J or intensity measurements because they do not cancel out. It is shown here, experimentally and by simulation, that the typical J(HH) interferences present in conventional HSQC experiments can be efficiently suppressed in an improved perfect-HSQC pulse scheme (Fig. 1), which replaces the classical INEPT ($\Delta/2\text{-}180_x(^1H,^{13}C)\text{-}\Delta/2$) by a perfect-echo INEPT module consisting of a double echo period ($\Delta/2\text{-}180_x(^1H)\text{-}\Delta/2\text{-}90_y(^1H)\text{-}\Delta/2\text{-}180_x(^1H,^{13}C)\text{-}\Delta/2$) in both defocusing/refocusing heteronuclear transfer periods. The resulting 2D perfect-HSQC spectra afford pure in-phase cross peaks with respect to both ^{1}J(CH) and J(HH), and in addition, peak volumes are not influenced by J(HH), rendering practical applications such as phase correction, signal integration, and multiplet analysis more convenient and accurate.

Results and discussion

Figure 1 shows the pulse sequences of the F2-coupled and F2-heterodecoupled perfect-HSQC experiments. As a major novelty,

* *Correspondence to: Teodor Parella, Servei de Ressonància Magnètica Nuclear, Universitat Autònoma de Barcelona, 08193 Bellaterra, Barcelona, Spain. E-mail: teodor.parella@uab.cat*

a *Servei de Ressonància Magnètica Nuclear, Facultat de Ciències, Universitat Autònoma de Barcelona, 08193 Bellaterra, Barcelona, Catalonia, Spain*

b *Departament de Química, Facultat de Ciències, Universitat Autònoma de Barcelona, 08193 Bellaterra, Barcelona, Catalonia, Spain*

c *NMR Structure Elucidation, Process and Analytical Chemistry, Merck & Co. Inc., 126 E. Lincoln Avenue, Rahway, NJ, 07065, USA*

MRC

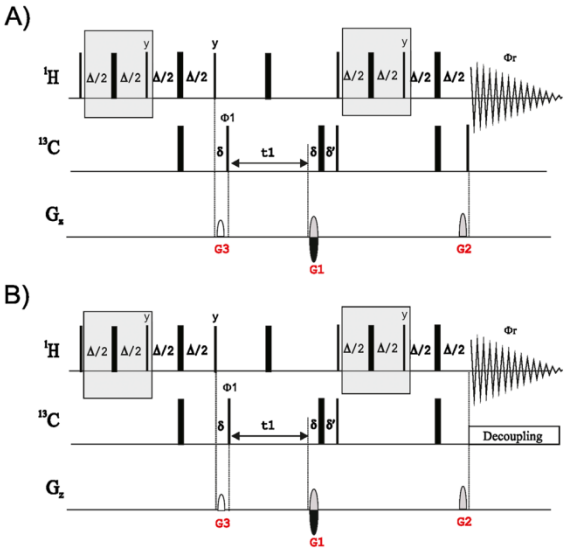

Figure 1. Pulse schemes of the (A) F2-coupled perfect-CLIP-HSQC and (B) broadband F2-heterodecoupled perfect-HSQC experiments designed to provide pure in-phase multiplet patterns with respect to ^{1}J(CH) and J(HH). Narrow and wide filled rectangles represent 90° and 180° pulses, respectively. Pulse phases are along the *x*-axis if not stated otherwise. Phase cycles were ϕ_1 = x, −x and ϕ_r = x, −x. The interpulse delay Δ is set to 1/(2 * ^{1}J(CH)), and coherence selection is performed using the echo/antiecho protocol, with the G1 : G2 : G3 gradient ratio set to ±80:20.1:33. δ stands for the duration of the gradient and its recovery delay, and $\delta' = \delta + t_1 + p4$, where *p*4 is the duration of the 180° ^{1}H pulse. TPPI-like incrementation with the echo/antiecho recording scheme was achieved by simultaneous inversion of ^{13}C pulses applied prior to the variable t_1 period. Conventional HSQC experiments were recorded without the ^{1}H pulses and delays marked into the boxes.

the ^{1}H pulses and delays marked into the boxes represent the additional elements incorporated in the new perfect-HSQC schemes compared with conventional HSQC experiments. The F2-^{1}J(CH)-coupled version is obtained by inserting a 90° ^{13}C pulse just prior to acquisition and omitting the heteronuclear decoupling as described for the clean in-phase (CLIP)-HSQC experiment.[10]

First of all, spectral simulations have been performed to assess the signal amplitude and phase dependence with respect to both J(HH) and ^{1}J(CH) evolution in several 1D HSQC pulse schemes, neglecting relaxation effects (Fig. S1 in the Supporting information). To illustrate such effects for a wide range of coupling constant values, three independent diastereotopic CH_2 spin systems with J (HH) values of 10, 25, and 40 Hz, respectively, and ^{1}J(CH) magnitudes covering 70–150 Hz have been defined. The choice of this wide range of values has been made to demonstrate the features of the HSQC even under extreme conditions. Although organic compounds under isotropic conditions present a narrower range of J values, these intervals are commonly found when measuring J splittings in anisotropic conditions. For instance, it has been reported that experimental ^{2}T(HH) (^{2}J(HH) + ^{2}D(HH)) coupling values up to 30–40 Hz in magnitude and ^{1}T(CH) (^{1}J(CH) + ^{1}D(CH)) in the range of 100–180 Hz are measured in the case of strychnine dissolved in a $CDCl_3$/poly-methylmethacrylate gel.[11]

For the theoretical analysis using the product operator formalism,[12] an isolated heteronuclear three-spin system consisting of a directly attached C–H_1 pair with ^{1}J(CH_1) and a third H_2 proton nucleus with J(H_1H_2) is considered. The magnetization just prior to the acquisition period in a conventional HSQC can be described as a mixture of in-phase and antiphase homonuclear and heteronuclear components:

$$H_{1x}c^2s'^2(\text{term I}) - 2H_{1y}C_zc^2s'c'(\text{term II}) + 2H_{1y}H_{2z}css'^2(\text{term III}) + 4H_{1x}H_{2z}C_zcsc's'(\text{term IV})$$

where c is cos(πJ(H_1H_2)Δ), s is sin(πJ(H_1H_2)Δ), c′ is cos(π^{1}J(CH_1)Δ), s′ is sin(π^{1}J(CH_1)Δ), and Δ is the echo period. Thus, the phase anomalies observed in F2-heterocoupled HSQC spectra (Fig. 2A) result from two independent effects: (i) the mismatch between the optimized Δ delay and the active ^{1}J(CH) value (terms II and IV) and (ii) the evolution of J(HH) during the echo INEPT periods (term III). Such anomalies prevent any attempt of accurate analysis in terms of quantification via integration or direct J measurement. A simple solution to partially solve these drawbacks was proposed with the CLIP-HSQC experiment,[10] which applies a 90° ^{13}C pulse just prior the acquisition. In this way, the antiphase contributions as a result of ^{1}J(CH) (terms II and IV) are converted to multiple-quantum coherence, and apparently, clean phase patterns are obtained although this is only true in the case of the presence of small J(HH) splittings (Fig. 2B). However, the effects of J(HH) evolution are still present (term III) although they have traditionally been omitted because of their relative low percentage compared with the desired response (term I). A simple calculation shows that these effects may become important. For instance, the relative percentage of the term III with respect term I in a 140-Hz optimized CLIP-HSQC experiment is of 5.6 and 17% for J(HH) values of 5 and 15 Hz, respectively. Such percentages can be more pronounced when measuring residual dipolar couplings in anisotropic media, where higher values can be involved.[13]

It has been shown that two major conclusions can be extracted from the analysis of the perfect-echo INEPT:[9] J(HH) is refocused at the end of the double-echo period, and the signal amplitude is only modulated by the effect of ^{1}J(CH), if relaxation is neglected. Thus, the magnetization just prior to acquisition in the perfect-HSQC experiment is defined exclusively by only two components:

$$H_{1x}s'^2 - 2H_{1y}C_zs's'$$

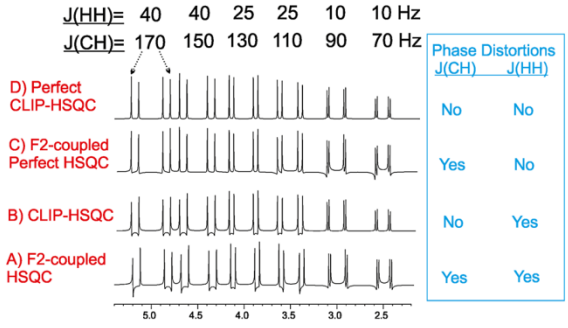

Figure 2. Simulated spectra showing the phase peak distortion effects in several 140-Hz optimized F2-heterocoupled HSQC experiments: (A) conventional HSQC, (B) CLIP-HSQC, (C) perfect-HSQC, and (D) perfect CLIP-HSQC. Six protons have been simulated with different J(HH) and ^{1}J(CH) values, as shown in the upper part.

Figure 2C shows that an F2-coupled perfect-HSQC spectrum without the CLIP pulse still shows phase distortions provided that Δ does not match the corresponding ^{1}J(CH) value. For instance, deviations of 10 and 20 Hz between ^{1}J(CH) and the Δ delay optimization generate antiphase contributions of about 11 and 23%, respectively, in a 140-Hz optimized experiment. Such distortions are efficiently suppressed using the perfect-CLIP-HSQC pulse scheme, affording perfect pure in-phase multiplet patterns for all peaks independent of their J(HH) and J(CH) values (Fig. 2D). Similar conclusions are also obtained from the analysis of broadband heterodecoupled HSQC and perfect-HSQC versions (Fig. 3). Note the perfect in-phase nature of all cross peaks in the perfect-HSQC spectra independent of experiment optimization.

A series of 2D F2-coupled and decoupled HSQC experiments have been experimentally recorded on a test sample of strychnine to verify the theoretical predictions. We have focused our attention on several diastereotopic CH_2 groups because the nonequivalent geminal protons present large mutual ^{2}J(HH) values (10–16 Hz). Figure 4 shows some multiplets extracted from equivalent 140-Hz optimized heteronuclear decoupled HSQC and perfect-HSQC spectra, and similar conclusions can be extracted analyzing the F2-coupled versions (Figs S2–S3 in the Supporting information). Significant antiphase contributions are clearly observed in some HSQC peaks that distort the signal phase and decrease their relative intensities. The H16 proton can be taken as a reference for a resonance that does not show large values, and therefore, a practically equal multiplet pattern and signal intensity are obtained in both spectra. However, differences up to 20% in signal intensity were observed for the diastereotopic H15a and H15b protons, and also, distortions can be observed for methine and methyl peaks, as shown for the H8 proton.

These distortions also introduce a source of error when an accurate measurement of J(HH) by direct peak maxima analysis is performed. In Fig. 5, it is shown that whereas the same J(HH) value is obtained from the conventional ^{1}H and the perfect-HSQC peak, considerable errors are made when direct peak picking on distorted HSQC and HSQC preservation of equivalent pathway (PEP) multiplets is applied. This perfect phase behavior is not achieved in the sensitivity-improved PEP version of the perfect-HSQC experiment,[14] where stronger phase distortions as a result of J(HH) are obtained (Figs S2–S4 in the Supporting information). In this case, two different magnetization components are involved, and the perfect INEPT block does not avoid the J(HH) modulation for both contributors. It is important to highlight that the perfect INEPT element could be implemented as a general building block in a large number of multidimensional NMR experiments that use the classical INEPT and HSQC pulse timings for the quantitative measurement of coupling constants.

In conventional HSQC spectra, peak volumes of different protons are variably modulated as a function of each individual J(HH)

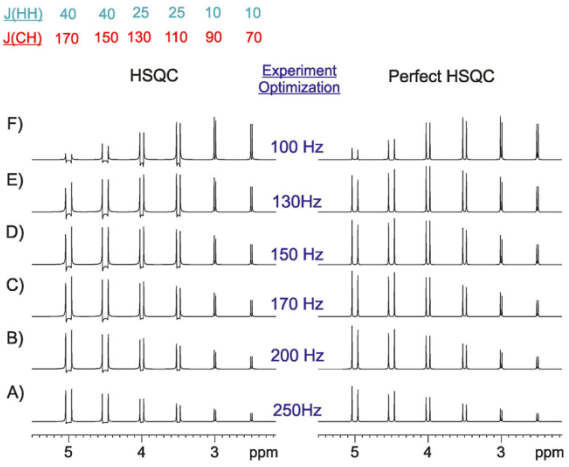

Figure 3. Simulated spectra showing the peak phase and intensity dependence in HSQC and perfect-HSQC experiments. Pure in-phase patterns are achieved for all signals in all perfect-HSQC spectra, independent to J(HH), ^{1}J(CH), and delay optimization ($\Delta = 1/(2 * {}^{1}JCH)$). From bottom to the top, (A) 250 Hz ($\Delta = 2.0$ ms), (B) 200 Hz ($\Delta = 2.5$ ms), (C) 170 Hz ($\Delta = 2.94$ ms), (D) 150 Hz ($\Delta = 3.33$ ms), (E) 130 Hz ($\Delta = 3.84$ ms), and (F) 100 Hz ($\Delta = 5.0$ ms).

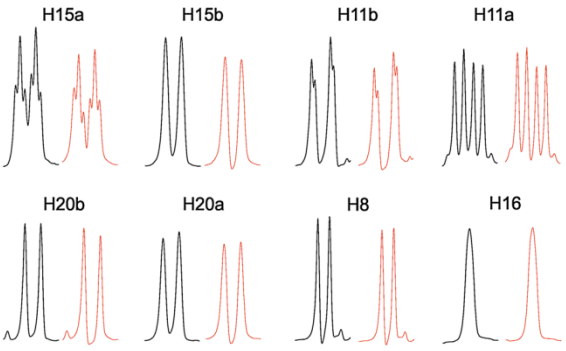

Figure 4. Comparison of some perfect-HSQC (left) and conventional HSQC (right) multiplets obtained from F2-heterodecoupled of strychnine. Note the evident phase distortions and decreased sensitivity in signals presenting large J(HH) values. The H16 proton can be taken as an undistorted reference signal not showing large J(HH) values.

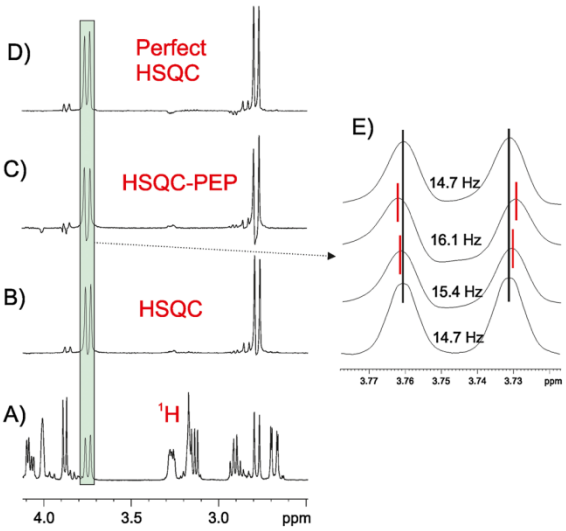

Figure 5. (A) Expanded area of the 500.13-MHz ^{1}H NMR spectrum of strychnine; (B–D) 1D traces extracted at the C20 carbon frequency of the following broadband F2-heterodecoupled 2D experiments: (B) conventional HSQC, (C) conventional HSQC-PEP, and (D) perfect-HSQC. (E) Experimental determination of J(HH) in H20a by using direct peak-maxima analysis.

coupling pattern. This nonuniform dependence causes a common source of error during integration and quantification of response intensities. In the perfect-HSQC experiment, there is a second and very significant positive consequence for removing J(HH) interferences: Signal intensity is amplitude modulated only by the $\sin^2(\pi J(CH)\Delta)$ factor (Fig. S4 in the Supporting information) and is therefore an excellent candidate to design future strategies for quantitative NMR studies.[15] The proposed method is less aggressive than the use of CPMG-INEPT blocks where a train of simultaneous $^1H/^{13}C$ pulses are applied at high repetition rates and where the resulting peaks can include unwanted dependence from offset effects or the presence of TOCSY contributions as well as deleterious effects on sample heating under extreme fast-pulsing conditions.[15c,15f]

To evaluate the $^1J(CH)$-compensated intensity strategy based on the proper selection of multiple polarization transfer values,[15b] we have simulated the perfect-HSQC spectrum of a spin system consisting of several protons having J(HH) in the extreme range between 10 and 30 Hz and $^1J(CH)$ ranging between 120 and 180 Hz. From a single-Δ 140-Hz perfect-HSQC experiment, a pure in-phase spectrum with peak volume differences up to 25% is obtained (Fig. 6A). On the other hand, Fig. 6B shows the $^1J(CH)$-compensated perfect-HSQC spectrum after combining four datasets acquired with Δ values of 2.94 ms (170 Hz), 2.86 ms (175 Hz), 2.86 ms (175 Hz), and 5.88 ms (85 Hz). Note that intensity differences below 2% are obtained in the complete $^1J(CH)$ range between 120 and 180 Hz. Of course, these simulations have been performed neglecting differential relaxation effects between different protons and carbons. A more exhaustive and detailed analysis is out of the scope of this communication but may be considered in the future.

The only apparent disadvantage of the perfect-HSQC experiment arises from the longer duration of the perfect-echo INEPT *versus* the conventional INEPT (2Δ vs Δ, respectively) that can lead to some signal loss as a result of relaxation losses. The duration of the sequence is extended about 3.6 ms for each perfect-echo INEPT period in a 140-Hz optimized experiment, but this is not a serious problem for small molecules having reasonably long T_2 relaxation times. For example, the experimental T_2 relaxation times for strychnine are about 0.35–0.50 s for aliphatic protons and around 0.6–0.7 s for aromatic protons as measured on a 20-mg sample in a 500-MHz spectrometer at 298 K (refer to Table S1 in the Supporting information). These values become larger in more dilute samples or at lower magnetic fields.[16]

In conclusion, a 2D perfect-HSQC experiment has been proposed that avoids any interference as a result of J(HH) coupling constants. The method is very simple to implement, and it can be recorded with and without broadband heteronuclear decoupling during acquisition. The resulting cross peaks exhibit pure in-phase multiplet patterns, irrespective of the experiment optimization. These uniform and predictable responses are more amenable to an accurate and quantitative analysis than what is encountered with the results of standard HSQC pulse sequences, with particular emphasis in the determination of $^1J(CH)$ and J(HH) coupling values. In addition, signal intensity is not modulated by J(HH), which opens the opportunity to design quantitative NMR applications based on perfect-HSQC datasets.

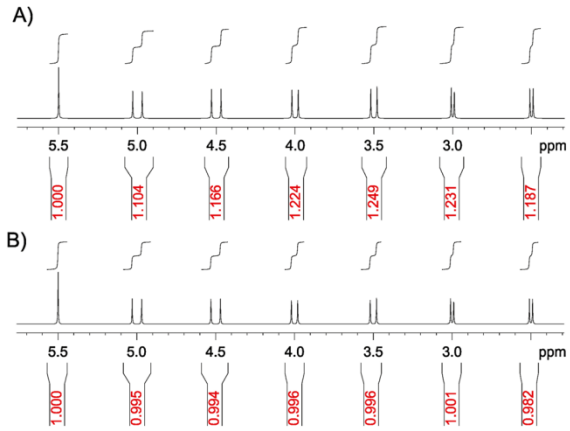

Figure 6. Spectral simulations showing integration ratios in heterodecoupled perfect-HSQC spectra: (A) optimized to a single Δ value of 3.6 ms, corresponding to 140 Hz; (B) average spectrum after combining four datasets acquired with Δ values of 2.94 ms (170 Hz), 2.86 ms (175 Hz), 2.86 ms (175 Hz), and 5.88 ms (85 Hz). The simulated protons have J(HH) and $^1J(CH)$ values in the range between 10-30 Hz and 120–180 Hz, respectively.

Methods and materials

NMR experiments were collected at 298 K on a Bruker AVANCE spectrometer (Bruker BioSpin, Rheinstetten, Germany) operating at 500.13-MHz proton frequency, equipped with a 5-mm TXI cryoprobe probe including a *z*-axis pulsed field gradient accessory (maximum strength of 53.5 G/cm). Experimental data were acquired with a sample of 20 mg of strychnine (Scheme 1) dissolved in 600 µl $CDCl_3$ and processed using the TOPSPIN v3.1 software package (Bruker BioSpin, Rheinstetten, Germany).

For the conventional HSQC and HSQC-PEP experiments, the standard hsqcetgpsp and hsqcetgpsisp2 pulse programs (Bruker library) were used. The corresponding F2-heterodecoupled and CLIP versions were created from these pulse programs, by adding a hard 90° ^{13}C pulse just before acquisition and omitting the decoupling during acquisition. For all conventional HSQC and perfect-HSQC experiments, ^1H and ^{13}C carrier frequencies were set at 4.5 and 90 ppm, respectively. Spectra were acquired with spectral windows of 8 (^1H dimension) and 160 (^{13}C dimension) ppm, using a prescan delay of 1 s and two scans per t_1 increment. Data were acquired with 2048 complex points in the ^1H dimension and 128 complex points in the ^{13}C dimension using the echo/antiecho detection mode. Zero filling up to 4 * 1 K was used prior to Fourier transformation using a 90° phase-shifted squared sine-bell apodization in both dimensions. Gradients G1 and G2 with a duration of 1 ms (δ) were used for echo–antiecho coherence selection. The proportionality between gradients G1 : G2 was set to ±80:20.1. ^{13}C 180° pulses are applied as CHIRP inversion and refocusing pulses of 500 µs and 2 ms of duration, respectively.

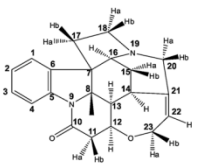

Scheme 1. Chemical structure and numbering of Strychnine

NMR simulations

Spectral simulations were performed using the NMRSIM v5.4 module included in the TOPSPIN (Bruker BioSpin, Rheinstetten, Germany). 1D pulse scheme equivalents to the first increment of the 2D pulse schemes shown in Figure 1 were used for simulations. The linewidth for all peaks used in the simulations is 0.2 Hz, and all 1D data were processed using an exponential function with a line broadening of 3 Hz prior to Fourier transformation.

For the spectral simulations of Figs 2, 3, S4, and S5, three independent diastereotopic CH_2 spin systems were defined, with different values of J(HH) and ^{1}J(CH), for studying the performance of the proposed perfect-HSQC experiment *versus* conventional HSQC and HSQC-PEP experiments. Spin system: $\delta(H_A) = 2.5$ ppm, $\delta(H_B) = 3.0$ ppm, $\delta(H_C) = 3.5$ ppm, $\delta(H_D) = 4.0$ ppm, $\delta(H_E) = 4.5$ ppm, $\delta(H_F) = 5$ ppm; $\delta(C_1) = 30$ ppm, $\delta(C_2) = 40$ ppm, and $\delta(C_3) = 50$ ppm; $^1J(C_1H_A) = 70$ Hz, $^1J(C_1H_B) = 90$ Hz, $^1J(C_2H_C) = 110$ Hz, $^1J(C_2H_D) = 130$ Hz, $^1J(C_3H_E) = 150$ Hz, and $^1(C_3H_F) = 170$ Hz; $^2J(H_AH_B) = 10$ Hz, $^2J(H_CH_D) = 25$ Hz, and $^2J(H_EH_F) = 40$ Hz.

Spectral simulations shown in Fig. 6 were performed on the following spin system: $\delta(H_A) = 2.5$ ppm, $\delta(H_B) = 3.0$ ppm, $\delta(H_C) = 3.5$ ppm, $\delta(H_D) = 4.0$ ppm, $\delta(H_E) = 4.5$ ppm, $\delta(H_F) = 5$ ppm, and $\delta(H_G) = 5.5$ ppm; $\delta(C_1) = 30$ ppm, $\delta(C_2) = 40$ ppm, $\delta(C_3) = 50$ ppm, and $\delta(C_4) = 35$ ppm; $^1J(C_1H_A) = 120$ Hz, $^1J(C_1H_B) = 130$ Hz, $^1J(C_2H_C) = 140$ Hz, $^1J(C_2H_D) = 150$ Hz, $^1J(C_3H_E) = 160$ Hz, $^1J(C_3H_F) = 170$, and $^1J(C_4H_G) = 180$ Hz; $^2J(H_AH_B) = 10$ Hz, $^2J(H_CH_D) = 20$ Hz, and $^2J(H_EH_F) = 30$ Hz.

Acknowledgements

Financial support for this research provided by Ministerio de Economía y Competitividad (project CTQ2012-32436) is gratefully acknowledged. We also thank the Servei de Ressonància Magnètica Nuclear, Universitat Autònoma de Barcelona, for allocating instrument time to this project.

References

[1] (a) L. Muller. *J. Am. Chem. Soc.* **1979**, *101*, 4481–4484;
(b) A. Bax, R. Griffey, B. Hawkins. *J. Magn. Reson.* **1983**, *55*, 301–315.
[2] G. Bodenhausen, D. J. Ruben. *Chem. Phys. Lett.* **1980**, *69*, 185–189.
[3] P. K. Mandal, A. Majumdar. *Conc. Magn. Reson. Part A* **2004**, *20A*, 1–23.
[4] K. Takegoshi, K. Ogura, K. Hikichi. *J. Magn. Reson.* **1989**, *84*, 611–615.
[5] A. M. Torres, G. Zheng, W. S. Price. *Magn. Reson. Chem.* **2010**, *48*, 129–133.
[6] J. A. Aguilar, M. Nilsson, G. Bodenhausen, G. A. Morris. *Chem. Commun.* **2012**, *48*, 811–813.
[7] R. W. Adams, C. M. Holroyd, J. A. Aguilar, M. Nilsson, G. A. Morris. *Chem. Commun.* **2013**, *49*, 358–360.
[8] B. Baishya, C. L. Khetrapal, K. K. Dey. *J. Magn. Reson.* **2013**, *234*, 67–74.
[9] B. Baishya, C. L. Khetrapal. *J. Magn. Reson.* **2014**, *242*, 143–154.
[10] A. Enthart, J. C. Freudenberger, J. Furrer, H. Kessler, B. Luy. *J. Magn. Reson.* **2008**, *192*, 314–322.
[11] J. D. Snider, E. Troche-Pesqueira, S. R. Woodruff, C. Gayathri, N. V. Tsarevsky, R. R. Gil. *Magn. Reson. Chem.* **2012**, *50*, S89–S91.
[12] O. W. Sørensen, G. W. Eich, M. H. Levitt, G. Bodenhausen, R. R. Ernst. *Prog. Nucl. Magn. Reson. Spectrosc.* **1983**, *16*, 163–192.
[13] (a) T. Carlomagno, W. Peti, C. Griesinger. *J. Biomol. NMR* **2000**, *17*, 99–109;
(b) P. Permi. *J. Magn. Reson.* **2001**, *153*, 267–272;
(c) P. Permi. *J. Biomol. NMR* **2002**, *22*, 27–35;
(d) E. Miclet, E. O'Neil-Cabello, E. P. Nikonowicz, D. Live, A. Bax. *J. Am. Chem. Soc.* **2003**, *125*, 15740–15741;
(e) C. M. Thiele. *J. Org. Chem.* **2004**, *69*, 7403–7413;
(f) P. Tzvetkova, S. Simova, B. Luy. *J. Magn. Reson.* **2007**, *186*, 193–200;
(g) J. Saurí, L. Castañar, P. Nolis, A. Virgili, T. Parella. *J. Magn. Reson.* **2014**, *242*, 33–40.
[14] L. E. Kay, P. Keifer, T. Saarinen. *J. Am. Chem. Soc.* **1992**, *114*, 10663–10665.
[15] (a) H. Koskela, T. Väänänen. *Magn. Reson. Chem.* **2002**, *40*, 705–715;
(b) S. Heikkinen, M. M. Toikka, P. T. Karhunen, A. Kilpeläinen. *J. Am. Chem. Soc.* **2003**, *125*, 4362–4367;
(c) H. Koskela, I. Kilpeläinen, S. Heikkinen. *J. Magn. Reson.* **2005**, *174*, 237–244;
(d) D. J. Peterson, N. M. Loening. *J. Magn. Reson.* **2007**, *45*, 937–941;
(e) A. Lewis, R. H. Karsten, M. E. Norton, M. Tonelli, W. M. Westler, J. L. Markley. *Anal. Chem.* **2010**, *82*, 4558–4563;
(f) H. Koskela, O. Heikkilä, I. Kilpeläinen, S. Heikkinen. *J. Magn. Reson.* **2010**, *202*, 24–33;
(g)P. Giraudeau. *Magn. Reson. Chem.* **2014**; In press. DOI 10.1002/mrc.4068.
[16] R. T. Williamson, G. E. Martin, A. Buevich, T. Parella. *J. Org. Chem.* **2014**, *79*, 3887–3894.

Supporting information

Additional supporting information may be found in the online version of this article at the publisher's website

Supporting Information

Suppression of phase and amplitude J(HH) modulations in HSQC experiments

Laura Castañar, Eduard Sistaré, Albert Virgili, R. Thomas Williamson and Teodor Parella*

Table of Contents

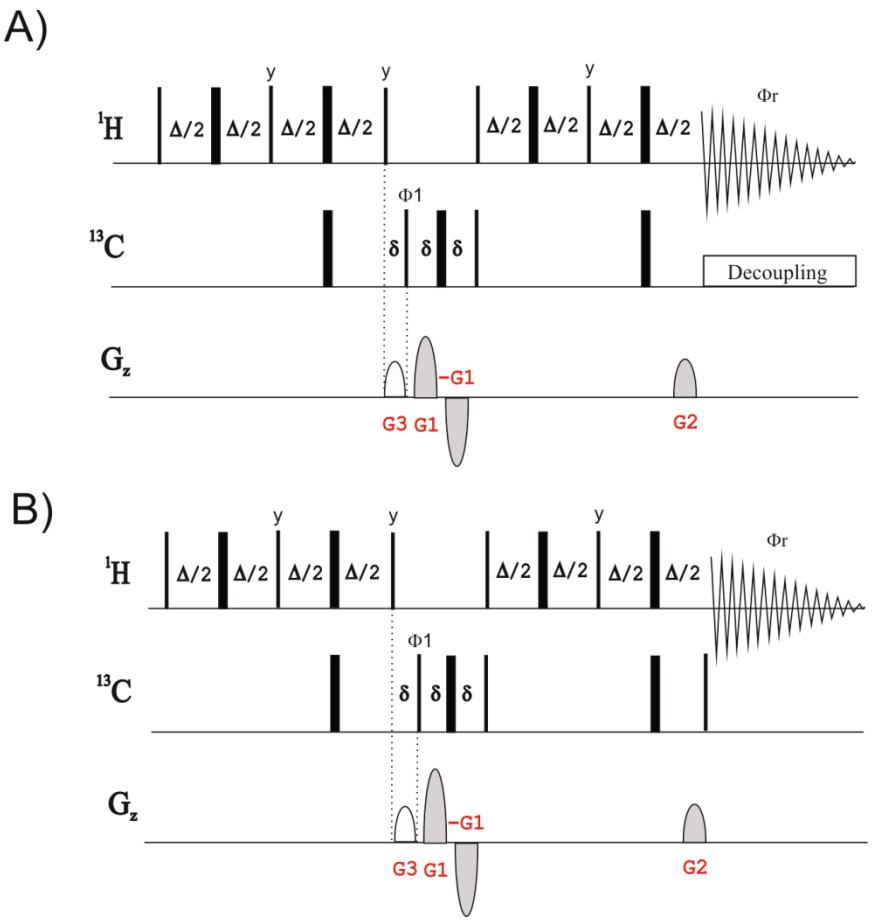

Figure S1: 1D Pulse schemes used in simulations. The recycle delay was set to 1s and the inter-pulse delay Δ was optimized to $1/(2*{}^{1}J(CH))$. Gradients G1:G2 with a duration of 1 ms followed by a recovery time the 100µs (δ=1.1ms) were set to a 80:20.1 ratio. The purge gradient G3 applied during the zz filter was set to 33%. 2 scans were recorded with ϕ_1=x,-x and ϕ_r=x,-x, using the spin systems defined in the experimental section. Data were processed by Fourier transformation without any window function.

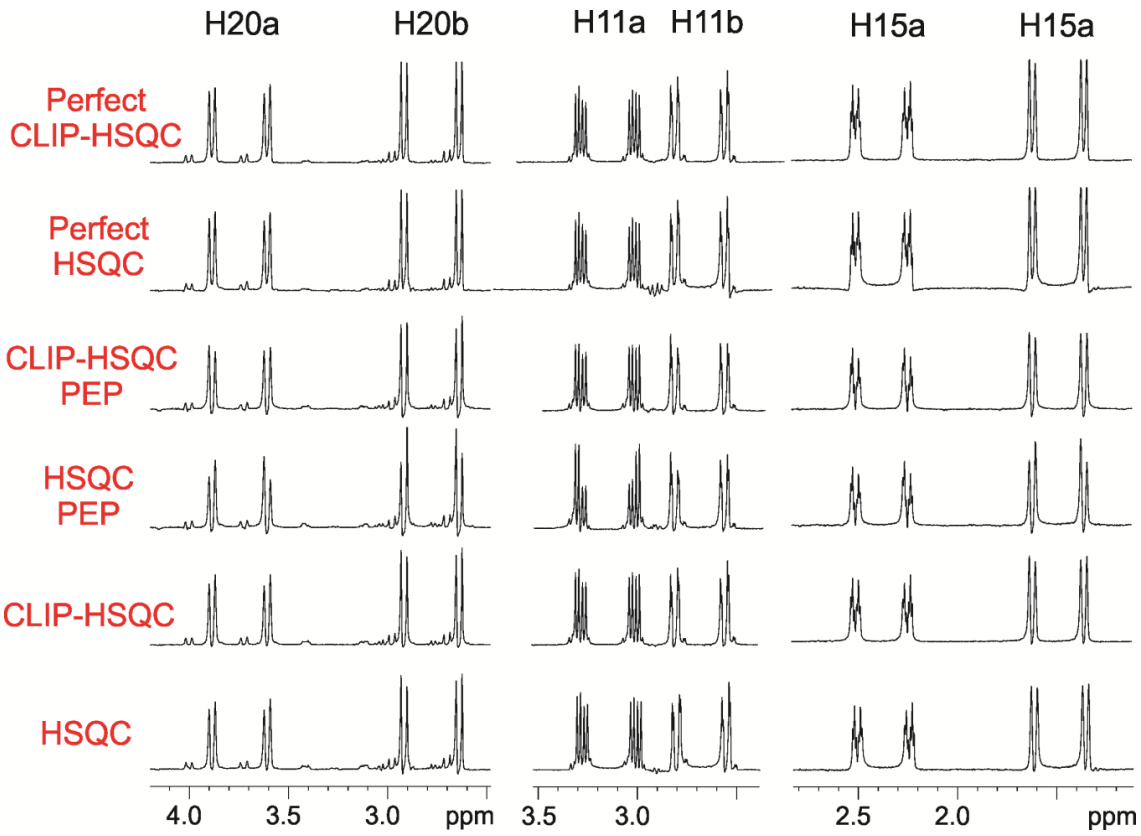

Figure S2: 1D traces extracted at C20, C11 and C15 carbon frequencies of several F2-coupled HSQC experiments. Note the perfect phase for all peaks in the perfect-CLIP-HSQC experiment when compared to all other experiments.

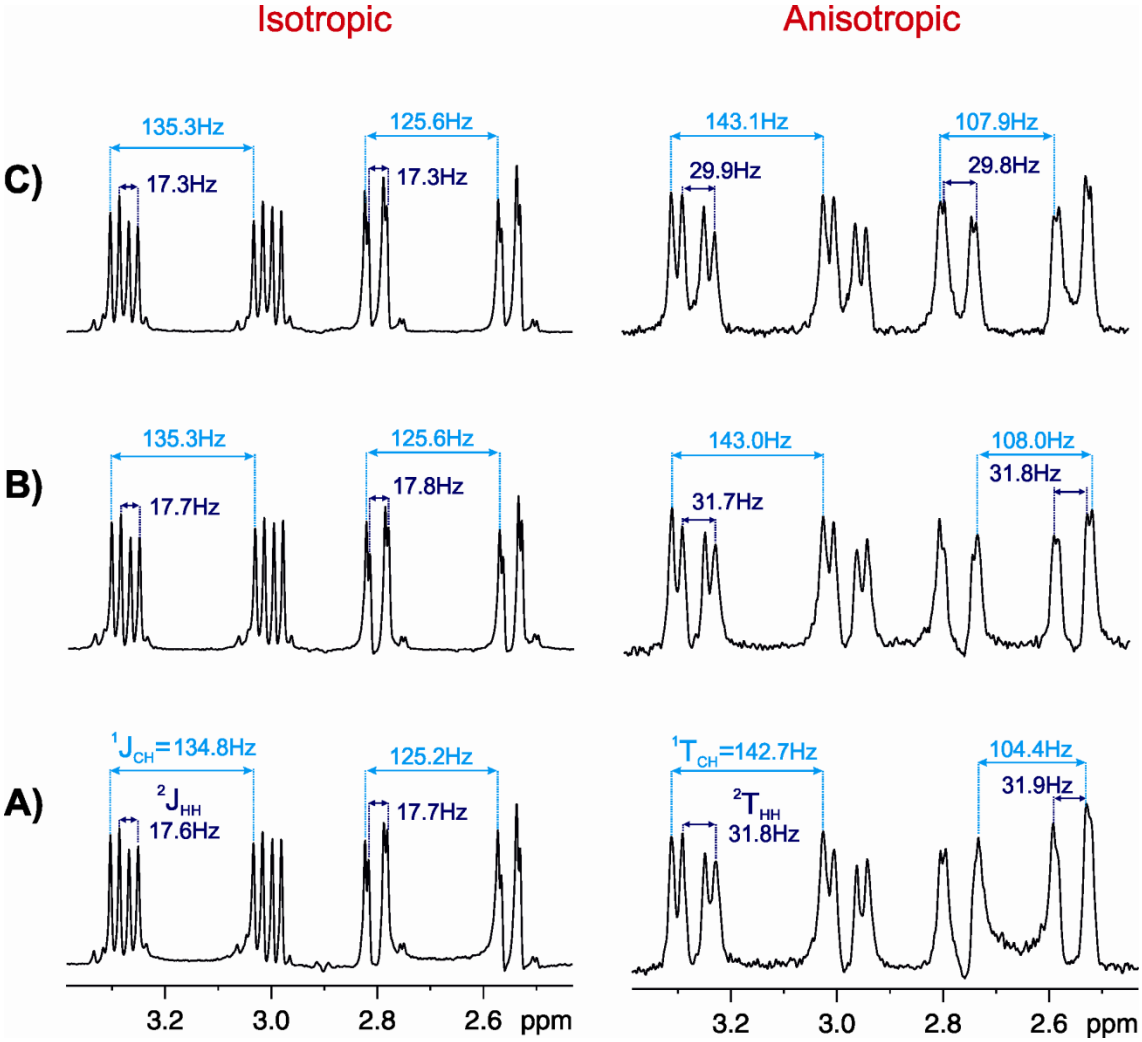

Figure S3: Comparison of the experimental measurement of J(HH)/T(HH) and ^{1}J(CH)/ ^{1}T(CH) from direct peak maxima analysis in A) HSQC, B) CLIP-HSQC, C) perfect CLIP-HSQC cross-peaks corresponding to the 11-CH_2 group of strychnine in both conventional isotropic and also non-isotropic conditions. For the measurement of RDCs in the anisotropic media, 4 mg of strychnine was weakly aligned in a poly(methylmethacrylate) (PMMA) gel swollen in 200µl of $CDCl_3$ using the reversible compression relaxation method. The ^{2}H quadrupolar splitting ($\Delta\upsilon_Q$) for the $CDCl_3$ signal was of 26 Hz.

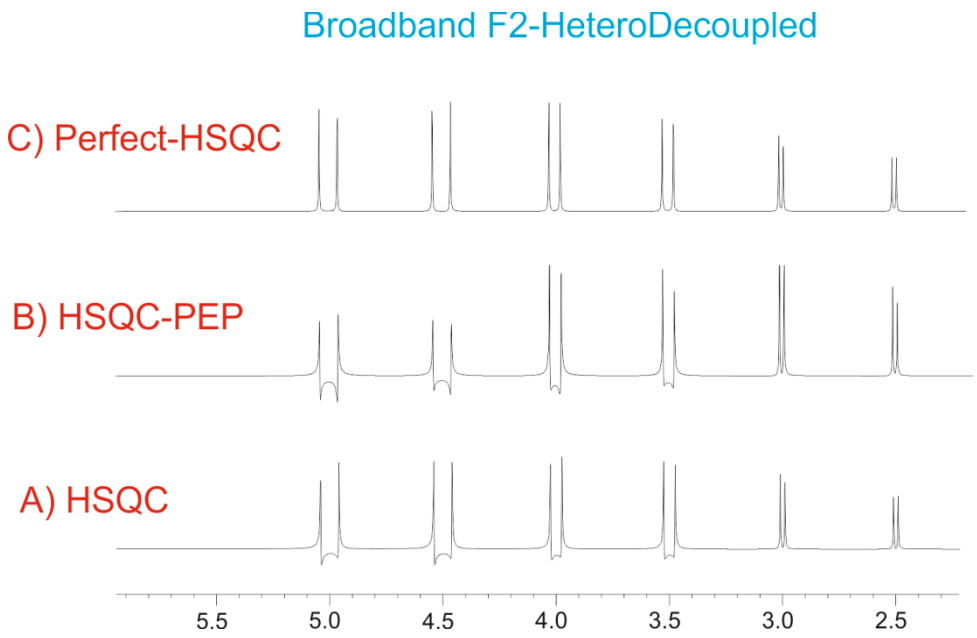

Figure S4: Spectral simulations showing the exclusive effects of J(HH) in several 140-Hz optimized broadband F2-heterodecoupled HSQC experiments: A) Conventional HSQC, B) HSQC-PEP and C) perfect-HSQC. Same conditions as Fig. 3 but using heteronuclear decoupling during acquisition.

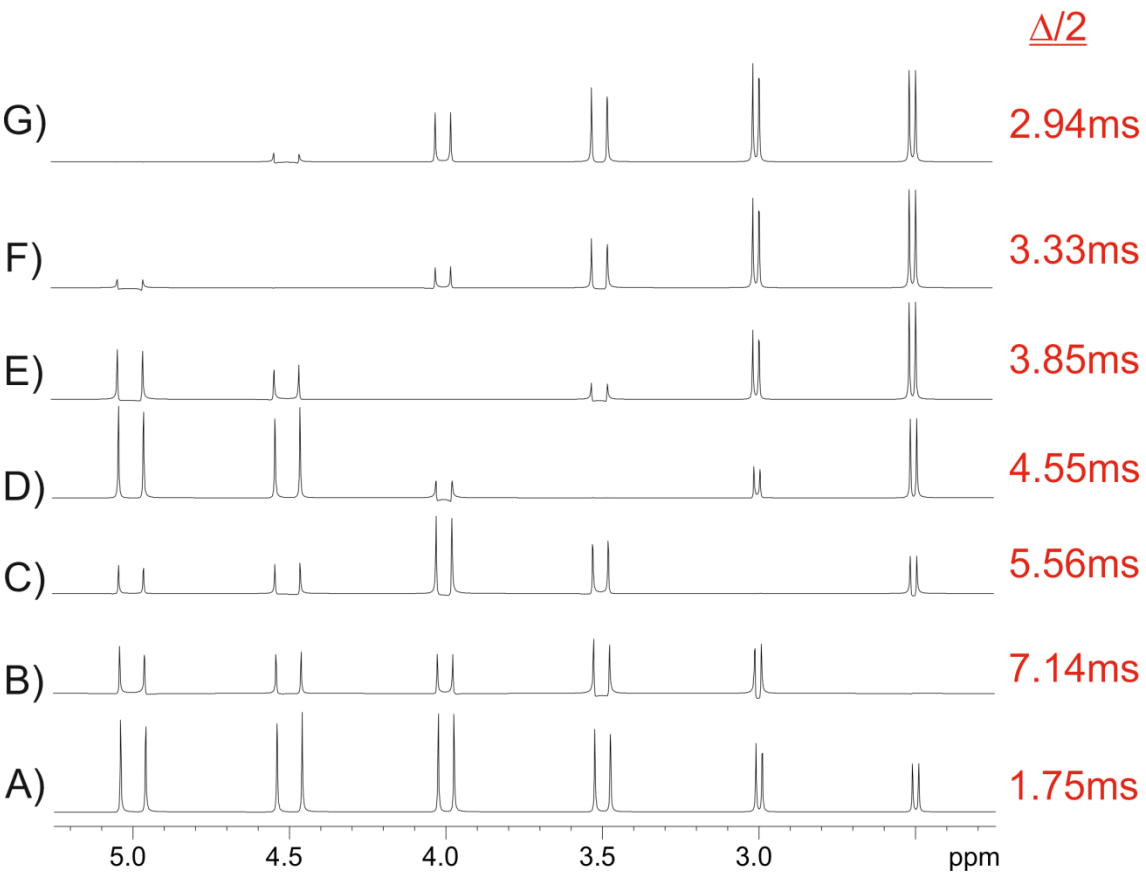

Figure S5: Spectral simulations showing the exclusive signal intensity dependence with respect to the $\sin^2(\pi J\Delta)$ function. A) is the regular experiment optimized to $\Delta/2=1/(4*{}^1J_{CH})=1.75$ ms. Spectra B-F) are delivery optimized to specific $\Delta/2=1/(2*{}^1J_{CH})$ values to demonstrate that null intensities are obtained when Δ exactly match ${}^1J_{CH}$, independent of the involved J(HH) values. For instance, B) is the 35-Hz optimized perfect-HSQC spectrum where the signal having ${}^1J(CH)=70$ Hz (2.5ppm) shows null intensity. In the same way, G) corresponds to the 75-Hz optimized perfect-HSQC spectrum and therefore signals with ${}^1J(CH)$ values of 70 and 90 Hz (2.5 and 3.0 ppm, respectively) shows maximum intensity whereas that with ${}^1J(CH)=150$ Hz (5.0 ppm) is perfectly nulled.

	T_2 (s)	r^2		T_2 (s)	r^2
H1	0.6268	0.9999	H15a	0.3699	0.9969
H2	0.6176	0.9992	H15b	0.3638	0.9944
H3	0.7161	0.9995	H17	0.3101	0.9981
H4	0.7321	0.9996	H18a	0.3295	0.9793
H8	0.5232	0.9981	H18b	0.3443	0.9588
H11a	0.4755	0.9889	H20a	0.3630	0.9877
H11b	0.4495	0.9991	H20b	0.3545	0.9797
H12	0.4865	0.9968	H22	0.4128	0.9983
H13	0.4986	0.9996	H23a	0.4006	0.9941
H14	0.4466	0.9972			

Table S1: Experimental T2 values measured for a sample of 20 mg strychnine in $CDCl_3$ in a 500 MHz spectrometer at 298K. Ten different CPMG-PROJECT spectra were recorded using an inter-pulse time of 1.5ms (n=4) and a different number of loops: 1, 10, 25, 50, 100, 150, 200, 250, 375 and 500, with a total echo time of 0.012 s, 0.066 s, 0.157 s, 0.306 s, 0.609 s, 0.911 s, 1.212 s, 1.514 s, 2.267 s and 3.021 s respectively.

PUBLICATION 10

Recent advances in small molecule NMR: Improved HSQC and HSQMBC experiments

Laura Castañar and Teodor Parella.
Annu. Rep. NMR Spectrosc., **2015**, *84*, 163-232.

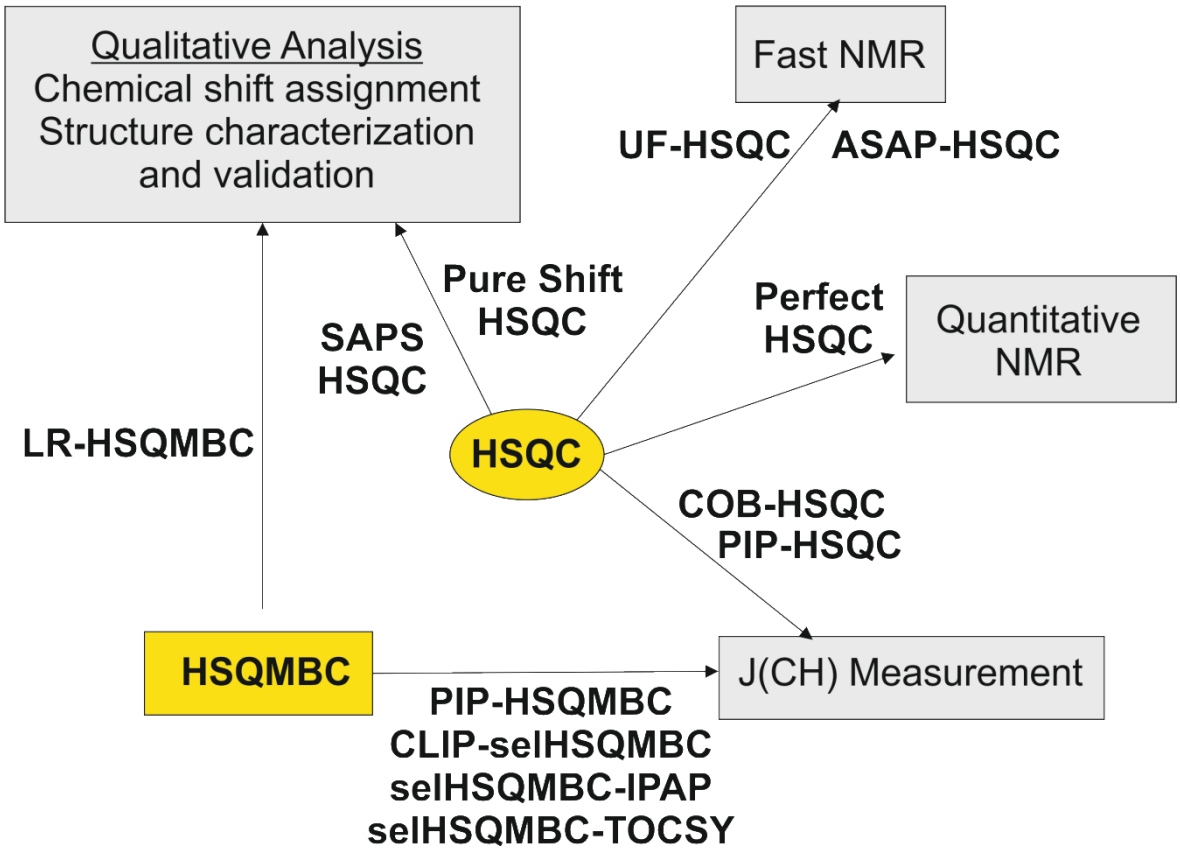

Introduction

This publication is a chapter of the book entitled “Annual Reports on NMR Spectroscopy”. It is a review work where a deeply discussion about the recent developments introduced into novel HSQC and HSQMBC pulse sequences (including all the publications related with HSQC/HSQMBC experiments with and without pure shift methodology discussed in this doctoral thesis). Special emphasis is made on modern concepts such as fast NMR, pure shift NMR, and also on robust techniques affording pure in-phase multiplet patterns, which are amenable for a simpler and a more accurate analysis.

This publication is also focused on the different practical applications of these modern HSQC and HSQMBC experiments, with special emphasis in the measurement of homo- and heteronuclear coupling constants. The suitability of some of these methods for the quantitative measurement of one-bond and long-range proton–carbon coupling values in molecules in isotropic and weakly aligned anisotropic conditions is illustrated.

CHAPTER FOUR

Recent Advances in Small Molecule NMR: Improved HSQC and HSQMBC Experiments

Laura Castañar, Teodor Parella
Servei de Ressonància Magnètica Nuclear and Departament de Química, Universitat Autònoma de Barcelona, Bellaterra, Catalonia, Spain

Contents

Annual Reports on NMR Spectroscopy, Volume 84
ISSN 0066-4103
http://dx.doi.org/10.1016/bs.arnmr.2014.10.004

Abstract

A general description of the latest developments in heteronuclear single-quantum correlation and heteronuclear single-quantum multiple bond correlation experiments designed for small molecules at the natural isotopic abundance is reported. A discussion is made on the details introduced into novel NMR pulse sequences with special emphasis on modern concepts such as fast NMR or pure shift NMR and also on robust techniques affording pure in-phase multiplet patterns, which are amenable for a simpler and a more accurate analysis. The suitability of some of these methods for the quantitative measurement of one-bond and long-range proton–carbon coupling values in molecules in isotropic and weakly aligned anisotropic conditions is also reviewed.

Keywords: NMR, HSQC, HSQMBC, Proton–carbon coupling constants, Pure Shift NMR, Pulse sequence development

1. INTRODUCTION

Proton-detected two-dimensional (2D) NMR experiments, essentially based on two different pulse schemes referred to as heteronuclear single-quantum correlation (HSQC) [1] and heteronuclear multiple-quantum correlation (HMQC) [2], have been key NMR tools during many years for chemists and biochemists to provide valuable structural information on $^{1}H–^{13}C$ (and $^{1}H–^{15}N$) chemical bonds in a molecule. Nowadays, these experiments are usually performed in a complete automation mode in both data acquisition and processing steps, practically without any need for direct user intervention. The resulting 2D maps are very simple to analyze and to interpret, even for non-experienced NMR users, typically displaying well-dispersed cross-peaks that correlate ^{1}H (direct F2 dimension) and ^{13}C (indirect F1 dimension) chemical shifts between directly attached $^{1}H–^{13}C$ groups, through the one-bond proton–carbon coupling constant ($^{1}J(CH)$) transfer mechanism. Compared to HMQC, the standard HSQC presents a better defined pulse scheme with characteristic steps which can be individually analyzed and modified in a straightforward way. Thus, heteronuclear magnetization transfers performed by INEPT elements and the evolution of single-quantum ^{13}C coherences to generate the indirect F1 dimension are the two main features that define the HSQC experiment.

Since its introduction, the HSQC pulse scheme has been modified in so many different ways in order to improve important experimental aspects such as sensitivity, resolution, efficiency, robustness, and performance. A recommendable work to understand the fundamentals and the different features, options and practical details of both HMQC and HSQC experiments is available as a comprehensive reading and as a complementary

reference to this article [3]. Historically, a major development in pulse sequence design was the incorporation of pulsed field gradients (PFGs) for coherence pathway selection. In both HSQC and HMQC experiments, PFGs allow a clear distinction between $^{1}H–^{12}C$ versus $^{1}H–^{13}C$ magnetization, which results in the collection of high-quality free-artifacts NMR spectra under standard routine conditions [4,5]. In addition, the use of PFGs reduces the requirement for an extensive number of phase cycles to be executed, significantly reducing the overall experiment time when sensitivity is not the limiting factor. PFGs have also been used as purge zz and refocusing elements, and further combination with water suppression strategies extent its applicability for biomolecules working in H_2O solutions. Two additional enhancements of the basic HSQC pulse scheme involved the modification of the last retro-INEPT element: (i) the incorporation of the preservation of equivalent pathways (PEP) technique that afford an important sensitivity improvement for CH and NH spin systems [6] and (ii) the use of the transverse relaxation optimized spectroscopy (TROSY) strategy enables a better sensitivity and resolution for large biomolecules and complexes in high magnetic fields [7]. All these improvements have been successfully incorporated in a large number of multidimensional NMR experiments designed to detect NH groups on isotopically labeled proteins and nucleic acids [8].

Nowadays, clean $^{1}H–^{13}C$ HSQC spectra can be obtained in minutes using conventional hardware configurations and with only some milligrams of a sample at natural isotopic abundance. The availability of high magnetic fields, cryogenically cooled radiofrequency (rf) coils and preamplifier components, and low-volume tube and capillary probes has dramatically improved the detection limits of the NMR spectroscopy, allowing to obtain such 2D spectra even for very low concentrated samples. These innovations can lead to an approximate 20-fold increase in mass sensitivity compared with conventional NMR instrumentation at the same field, providing chemists with new capabilities for exploration of submilligram natural product samples [9]. For instance, it has been reported that a conventional $^{1}H–^{13}C$ HSQC spectrum of 7.5 μg of a natural product dissolved in 30 μl of solvent can be obtained in 15–30 min in a 1.7-mm microcryoprobe at 600 MHz [10] or the measurement of ^{1}J(CH) values from an F2-coupled $^{1}H–^{13}C$ HSQC spectrum has been accomplished with 90 μg of the natural product muironolide in an overnight acquisition [11]. Less-sensitive $^{1}H–^{15}N$ HSQC of natural products can be obtained from about 1 mg samples using a 1.7-mm microcryoprobe within 4 h.

Over the years, the original HSQC pulse scheme has also been largely modified to provide additional and complementary information from a

single NMR experiment. For instance, the multiplicity-edited HSQC (ME-HSQC) experiment [12] is a common and very useful technique used in routine NMR protocols to additionally obtain information about the carbon multiplicity (distinction of CH/CH_3 vs. CH_2 spin systems) as a function of the relative positive/negative phase of HSQC cross-peaks. The experiment uses an extended ^{13}C echo period during the evolution of ^{13}C single-quantum coherences (SQCs) that minimally affect the overall sensitivity and therefore, in practical terms, the ME-HSQC can be preferred to the standard HSQC to trace out connectivities and to obtain multiplicity information in an unique spectrum. The HSQC-TOCSY experiment [13] is another simple but complementary extension of the HSQC experiment which provides the simultaneous information of ^{1}H and ^{13}C chemical shifts into a complete *J*-coupled spin system, offering a relevant interest in the analysis and unambiguous assignments of complex spin systems. The experiment relies in a consecutive and sensitive $^{1}J(CH) + J(HH)$ transfer mechanism but, as a main drawback, only works for protonated carbons. On the other hand, and in analogy to the classical heteronuclear multiple bond connectivity (HMBC) experiment [14,15], the long-range optimized HSQC experiment (referred to as heteronuclear single-quantum multiple bond correlation or HSQMBC) [16] provides information about protons and carbons separated by more than one-bond, typically two- and three-bond connectivities. In its basic form, the regular HSQC pulse timing is executed with a different setting of the interpulse delay (typically 50–75 ms) to match the smallest long-range proton–carbon coupling constant ($^{n}J(CH)$; $n > 1$) values, typically in the range of 0–15 Hz. The less-sensitive ADEQUATE experiments [17] are based on extended $J(CH) + J(CC)$ transfer mechanisms, where the main features of the HSQC experiment are combined with an intermediate ^{13}C double-quantum mixing period. The basic 1,1-ADEQUATE experiment provides two-bond connectivities according to a $^{1}H–^{13}C–^{13}C$ spin system, and complementary 1,*n*-, *n*,1-, and *n*,*n*-ADEQUATE versions have been also useful to trace out longer $^{1}H/^{13}C$ correlations [18].

In addition to the tremendous potential of the HSQC experiment as an analytical method for unambiguous chemical shift assignment, structure characterization and validation, and mixture analysis, it has also demonstrated to be very efficient for other purposes, such as the quantitative measurement of $^{1}J(CH)$ couplings, the determination of T_1/T_2 relaxation times, or for quantitative studies by peak volume integration. For small molecules in isotropic conditions, $^{1}J(CH)$ values are large in magnitude (in the range of ~120–250 Hz) and positive in sign, and they can be quickly measured for

the large doublet observed in coupled HSQC spectra. ^{1}J(CH) has been found to have interesting applications in many constitutional, configurational, and conformational studies [19–22] and, in the last decade, a renewed interest for the measurement of one-bond proton–carbon residual dipolar coupling (RDC) constants (^{1}D(CH)) has appeared when working in weakly aligned anisotropic media [23–27]. The magnitude and the relative sign of ^{1}D(CH) are determined from the differences obtained from the experimental isotropic versus anisotropic values according to $^{1}D(\mathrm{CH}) = {}^{1}J(\mathrm{CH}) - {}^{1}T(\mathrm{CH})$, and they are strongly related to the CH bond orientation with respect to the molecular tensor and the permanent magnetic field. On the other hand, related NMR experiments based on the HSQC-TOCSY and HMBC/HSQMBC pulses schemes have been proposed for the quantitative measurement of smaller ^{n}J(CH) couplings.

The aim of this article is to compile all new HSQC-related NMR experiments published in the last years that have been specifically designed and applied to small molecules at natural abundance (Scheme 1). Special focus will be made on novel HSQC schemes including concepts such as fast NMR and pure shift NMR. In addition, reference to improved *J*-compensated HSQC sequences will be made, discussing the effects of the intensity and phase signal modulation dependence with respect to ^{1}J(CH) and/or *J*(HH) which are generated during INEPT periods. A particular analysis will be also made on modern NMR methods designed for the quantitative measurement of ^{1}J(CH) and/or ^{1}D(CH) and, by

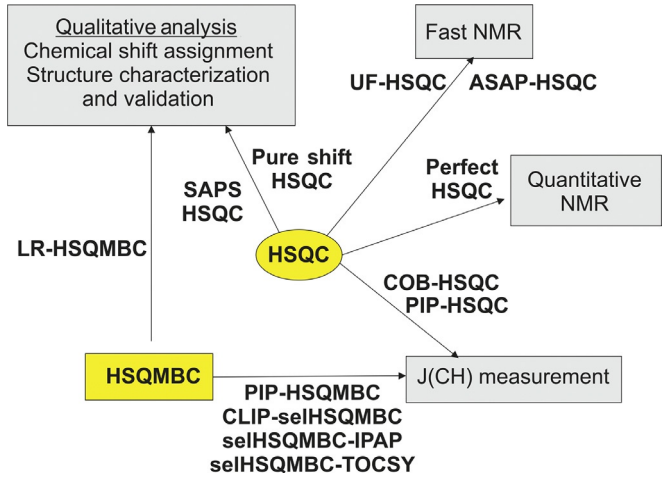

Scheme 1 Graphical representation of some recently reported HSQC/HSQMBC-related NMR methods.

extrapolation, for the determination of the magnitude and/or the sign of small ^{n}J(CH) coupling constants. Finally, miscellaneous HSQC/HSQMBC methods to obtain semiquantitative spectra suitables for a direct peak volume integration, to achieve optimum signal resolution in F1 and/or F2 dimensions, or to observe very long-range heteronuclear connectivities will be commented.

2. THE BASIC HSQC EXPERIMENT

Figure 1 shows the five basic independent steps that can be identified in a standard 2D gradient-selected HSQC pulse scheme. *Step 1*: The pre-scan period is usually defined by a long recycle delay (some seconds of duration, accordingly to the existing $T_1(^1H)$ relaxation times) to allow the recovery of the ^1H magnetization to a pre-equilibrium state just before to start the sequence. *Step 2*: After the initial ^1H excitation, heteronuclear transfer via J(CH) takes place using an INEPT element. *Step 3*: Antiphase (AP) ^{13}C SQC evolves during a variable t_1 period under the effect of ^{13}C chemical shift, whereas the evolution of heteronuclear J(CH) couplings is

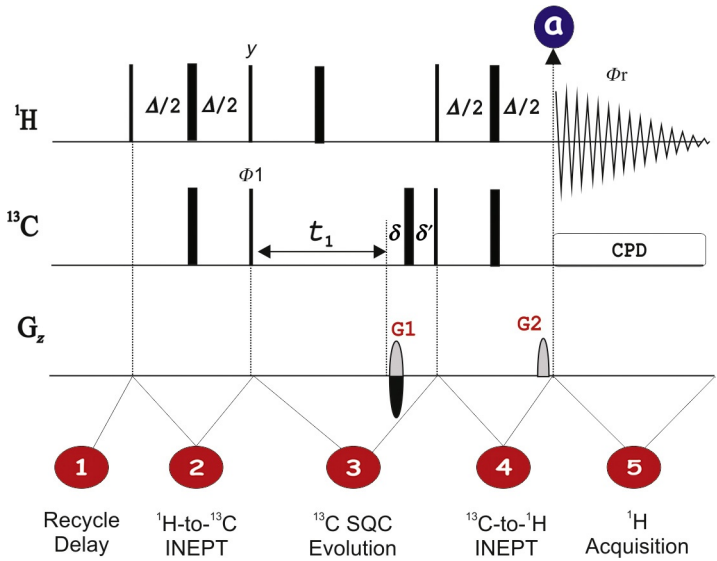

Figure 1 Schematic representation of the different steps involved in a standard 2D ^1H–^{13}C HSQC pulse sequence. Thin and thick vertical rectangles represent 90° and 180° hard pulses, respectively. The delay Δ should be set to $1/(2*^1J(CH))$, and δ represents the duration of the PFG and its recovery delay. In this scheme, coherence selection is performed by the gradient pair G1/G2 using the echo–antiecho protocol.

decoupled by the central 180° ^{1}H pulse. *Step 4*: During the retro-INEPT element, ^{13}C magnetization is initially reconverted to ^{1}H magnetization, whereas the subsequent J(CH) evolution generates in-phase (IP) magnetization prior to acquisition. *Step 5*: The sequence ends with a ^{1}H detection period under optional broadband heteronuclear composite pulse decoupling (CPD). This scheme deserves some additional comments because it is used as a pattern for most experiments described in this report. First, it uses coherence selection by PFGs using the echo–antiecho approach, where the encoding gradient G1 (of duration δ) is located into a ^{13}C spin-echo period to avoid any evolution during this application. The decoding gradient G2 applied during the last evolution period is optimized according to the refocusing gradient condition ($G1 = (\gamma_H/\gamma_C)$*G2).

The interpulse INEPT delay is optimized to a single J value, according to $\Delta = 1/(2*^{1}J(CH))$, and therefore, the cross-peak intensities do not show an uniform response owing to the variable and wide range of ^{1}J(CH) coupling values. The magnitude of ^{1}J(CH) is a direct measurement for the degree of hybridization of the involved carbon atom, presenting approximate values of ~120–140 Hz for aliphatic sp^3 carbons, ~150–170 Hz for olefinic systems or 240–270 Hz for acetylenic functional groups. The practical use of ^{1}J(CH) has found a wide interest for structural analysis of small molecules including, for instance, the distinction of axial and equatorial protons in cyclic systems, of anomeric protons in carbohydrates, or the use of RDCs as angular constraints, among other.

For a proper knowledge how the HSQC pulse scheme works, the signal intensity and phase dependences generated during the INEPT periods can be easily analyzed by the product operator formalism [28]. At the end of the refocusing ^{13}C-to-^{1}H INEPT period and just before acquisition (point **a** in Fig. 1), the observable ^{1}H magnetization for an isolated ^{1}H–^{13}C two-spin system, with a mutual coupling of ^{1}J(CH), can be described as a mixture of IP and AP components:

$$H_x s'^2 (\text{Term I}) - 2H_y C_z s' c' (\text{Term II}) \quad (1)$$

where c' is $\cos(\pi J(CH)\,\Delta)$, s' is $\sin(\pi J(CH)\,\Delta)$, and Δ is the J evolution INEPT period. The term II in Eq. (1) can be removed by heteronuclear CPD during acquisition. To understand the effects of J(HH) in an HSQC experiment, each INEPT block can be considered as an spin-echo period for protons and therefore, the undesired J(HH) evolution during the overall Δ period can be assessed by considering a heteronuclear three-spin H_1, H_2, and

C system, with active $J(H_1H_2)$ and $J(CH_1)$ couplings. In this case, the magnetization of spin H_1 at point **a** in Fig. 1 can be now described as:

$$H_{1x}c^2s'^2(\text{Term I}) - 2H_{1y}C_zc^2s'c'(\text{Term II}) + 2H_{1y}H_{2z}css'^2(\text{Term III}) + 4H_{1x}H_{2z}C_zcsc's'(\text{Term IV}) \quad (2)$$

where c' is $\cos(\pi J(CH_1)\,\Delta)$, s' is $\sin(\pi J(CH_1)\,\Delta)$, c is $\cos(\pi J(H_1H_2)\Delta)$, and s is $\sin(\pi J(H_1H_2)\,\Delta)$. Although that terms II and IV in Eq. (2) can be removed by heteronuclear CPD during acquisition, this more complex signal intensity dependence usually hinders any attempt for the quantitative use of standard HSQC data, requiring the design of more robust J(HH)- and J(CH)-compensated INEPT sequences to improve/avoid such anomalies (see Section 5.1.2).

3. SPEEDING-UP HSQC DATA ACQUISITION

There has always been a general interest to develop fast NMR methods to reduce the experimental time required for a complete 2D acquisition and to economize valuable spectrometer time. There are two main factors that determine the overall duration of a given 2D experiment: (i) the long recycle delay (typically in the order of some seconds) needed to achieve a preequilibrium proton polarization and (ii) the number of variable linearly sampled t_1 increments required for an optimum resolution in the indirect F1 dimension. Several approaches to accelerate data acquisition in HSQC experiments have been reported.

3.1. ASAP-HSQC Experiment

In conventional HSQC experiments, the preparatory recycle period is determined as a function of the $T_1(^1H)$ values, typically 1–2 s in routine analysis. Thus, a simple solution to speed up data acquisition should be the reduction of the recycle delay between scans to some milliseconds. However, fast pulsing generates partial signal saturation and the overall sensitivity can be significantly decreased.

Fast acquisition of ^1H–^{15}N HSQC spectra in proteins has been performed using the SOFAST or BEST approaches, which is based on the replacement of all hard ^1H pulses by region-selective 90° and 180° ^1H (^{15}N) pulses in order to reduce the longitudinal $T_1(^1HN)$ relaxation [29,30]. This allows the combined use of very short recycle delays with an optimized Ernst-angle excitation to achieve optimal sensitivity per time unit. However, this region-selective excitation strategy is not of general

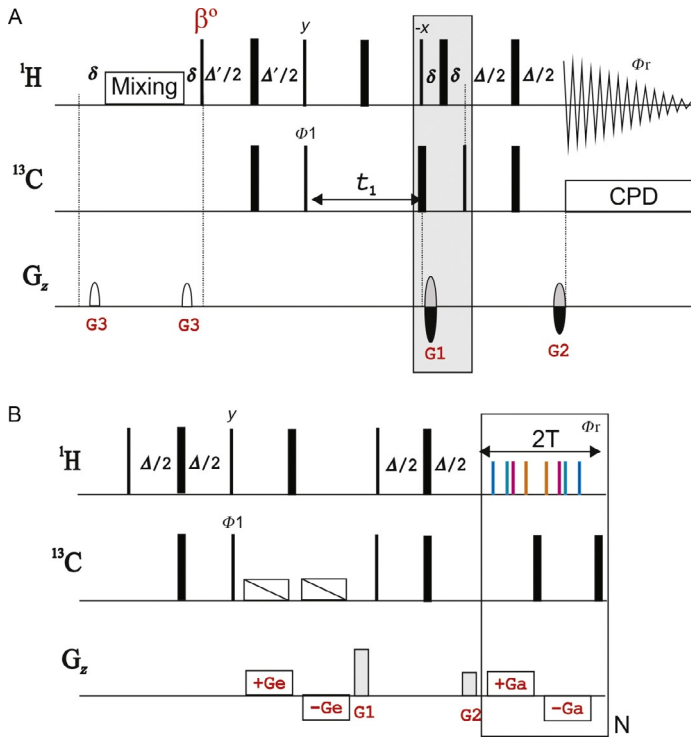

Figure 2 Two different approaches to achieve fast recording of HSQC spectra: (A) ASAP-HSQC experiment and (B) single-scan Ultrafast HSQC (UF-HSQC) experiment.

application to small molecules. Recently, a fast ASAP-HSQC experiment [31] (ASAP stands for Acceleration by Sharing Adjacent Polarization) (Fig. 2A) has been proposed to quickly obtain a 2D HSQC map in less than 30 s for relatively concentrated samples, and it has been demonstrated that better spectral and cross-peak quality is obtained than a previous ASAP-HMQC experiment [32]. The ASAP method [33] uses a short (40 ms) PFG-flanked isotropic mixing period instead of the conventional long recycle delay and it can be combined with the use of an optimized Ernst-angle pulse excitation (β) and shorter Δ' delays during the first defocusing INEPT periods. The main originality of the sequence relies in the management of ^{1}H magnetization just after the evolution of ^{13}C SQC during the variable t_1 period, which retains the polarization reservoir for all the passive spins not directly bound to the NMR-active heteronucleus. This modified experiment applies a 90°(^{1}H) pulse of the backtransfer step with $-x$ phase before the actual coherence order selection and echo–antiecho encoding. As described in the original publication, this

way the polarization reservoir is flipped along z, ensuring that it is not affected by the gradients. Coherence order selection is then achieved by dephasing either zero-quantum or double-quantum coherences with a proper setting of the involved gradient strengths. The fast acquisition of HSQC spectra allows the averaging over many more scans or to acquire a large number of t_1 increments for the same experiment time. Overall, the ASAP-HSQC shows a moderate gain in SNR per time unit when compared to the standard HSQC recorded into the same experimental time. It must be emphasized that for long acquisitions, precautions should be taken because rapid pulsing could generate sample heating and damage probe components.

The original ASAP-HMQC pulse sequence has been evaluated for rapid screening of natural products [34], and an ASAP version of the HMBC experiment (defined as IMPACT-HMBC) has been also reported and further tested for analyzing silylated derivatives [35] and for monitoring hydrogen bonding in peptides [36].

3.2. Non-uniform Sampling

It is recognized that one of the major inconveniences of any 2D experiment is the need to record a minimum number of t_1 increments, which determines the resolution achieved in the indirect dimension and also influences the overall experimental time. Several approaches have been proposed to improve the resolution along the indirect dimension of an HSQC experiment and to reduce spectrometer times: (i) the use of band selection in the indirect dimension that allows the use of a reduced ^{13}C spectral width [37,38]; (ii) the application of data processing techniques such as zero-filling or linear prediction; (iii) the use of a deliberate reduced ^{13}C spectral width to achieve spectral folding or spectral aliasing which depends on the acquisition mode [39–42]; or (iv) the use of non-uniform sampling (NUS) [43,44] techniques. For small molecules, NUS can facilitate significant reductions (~50%) in the time needed to collect 2D HSQC spectra by using ~50% of sampling density, or otherwise offering gains in spectral resolution along the indirect ^{13}C dimension by recording less number of t_1 increments. Some of these algorithms are already implemented in modern NMR software packages, and non-experienced users can use them in a fully transparent and automatic way without any further modification of the standard pulse programs or general setup parameters. The quality of the resulting spectra depends crucially on the sampling schedules and the algorithms for data reconstruction. However,

precaution should be taken for the presence of unwanted artifacts that can generate distorted or false cross-peaks.

An accelerated 3D HSQC-DOSY experiment has been proposed to obtain individual 2D HSQC maps of each component in a mixture by joint sparse sampling of the diffusion and time dimensions [45].

3.3. Ultrafast HSQC

The spatially encoded single-scan or Ultrafast (UF) NMR technique allows performing 2D experiments in a single scan, within a few seconds, provided that sensitivity and sample concentration are sufficient [46–49]. Since its earliest days, an important number of new developments and applications have converted UF-NMR as a powerful analytical tool for real-time monitoring of chemical and biochemical processes [50–52]. Several UF-HSQC pulse sequences have been proposed where the key elements are the use of spatially encoding gradients during Step 3 of the basic HSQC scheme (see Fig. 1) and an echo planar imaging acquisition mode as traditionally implemented in magnetic resonance imaging applications (Fig. 2B). In practice, a general applicability of the UF-HSQC experiment in routine protocols of small molecules is hampered because the UF dimension window is limited by the strength of the encoding/decoding gradients and also by the severe sensitivity losses due to slice selection. Experimentally, the spectral width observable in the ^{13}C dimension is limited to a few tens of ppm [53,54] although that an improved version has been reported that combines spatial encoding with iterative compressed-sensed reconstruction [55]. UF-HSQC has been successfully applied for the real-time mechanistic monitoring of chemical reactions [56], for the fast measurement of $^{1}J(CH)/^{1}D(CH)$ in oriented media [57] and combined with *ex situ* dynamic nuclear polarization (DNP) [58]. Although these experiments can be currently defined as non-routine techniques due to their apparent complexity, valuable documentation describing the experimental details (the step-by-step protocol, pulse sequences and processing programs) required to implement UF-HSQC experiments in modern spectrometers is available [59–61].

4. HIGH-RESOLVED HSQC USING PURE SHIFT NMR

4.1. PS-HSQC Experiments

In the last years, the old idea of broadband homodecoupling [62] has emerged in the field of small molecule ^{1}H NMR spectroscopy under the acronym of pure shift NMR. [63–66] A number of homodecoupled

versions of the most traditional 1D and 2D NMR experiments have been proposed providing the collapse of the typical *J*(HH) multiplet patterns to simplified singlet lines along the detected dimension. Among the different homodecoupling approaches developed over the years, the Zangger–Sterk (ZS) experiment has become one of the most powerful approaches to efficiently improve signal resolution. It is based on the combination of a hard 180° pulse and a selective inversion element applied in the center of an echo period to allow the exclusive evolution of ^{1}H chemical shifts of the active protons (those experiencing the selective inversion perturbation), whereas all their passive *J*(HH) couplings are refocused. The implementation of the ZS method involves a pseudo-2D acquisition scheme that usually requires the collection of 16–32 measurements and a special free induction decay (FID) reconstruction of an 1D homodecoupled FID from the concatenation of the initial chunk of each increment with a duration $1/SW_1$, where SW_1 is about twice the width of the widest multiplet to be decoupled (typically about 10 ms) [63,67]. Alternatively, a real-time 1D acquisition scheme that requires conventional data processing offers a considerable gain of sensitivity per time unit ratios but at some cost in spectral quality and resolution and limited to the use of short selective pulses [62,64,68]. In principle, the direct implementation of these ZS methods should be suitable for all known 1D and 2D experiments involving IP magnetization with respect to *J*(HH), such as TOCSY, NOESY, ROESY, and HSQC experiments, but would fail for those involving AP magnetization such as traditional COSY or HMBC/HSQMBC experiments. Thus, HSQC has been a good target to evaluate the performance, the advantages, and also the limitations of such implementations, and a number of different pure shift HSQC (PS-HSQC) experiments have been reported incorporating the pseudo-2D or real-time acquisition strategies, using either a BIRD element to invert selectively ^{1}H–^{12}C versus ^{1}H–^{13}C [62] or spatially encoded frequency-selective pulses.

The first proposal RESET-HSQC experiment [69] implemented the original pseudo-2D ZS element just prior to acquisition, using a BIRD element as selective inversion module to homodecouple ^{1}H–^{13}C protons from those belonging to ^{1}H–^{12}C. An improved version offering better suppression of strong coupling effects and better tolerance to the mismatch INEPT/BIRD delays optimization has been further proposed (Fig. 3A) [70]. As a main drawback, this approach uses a 3D acquisition scheme, and therefore, the gains associated with multiplet collapsing are strongly minimized by the need of extra spectrometer time to record

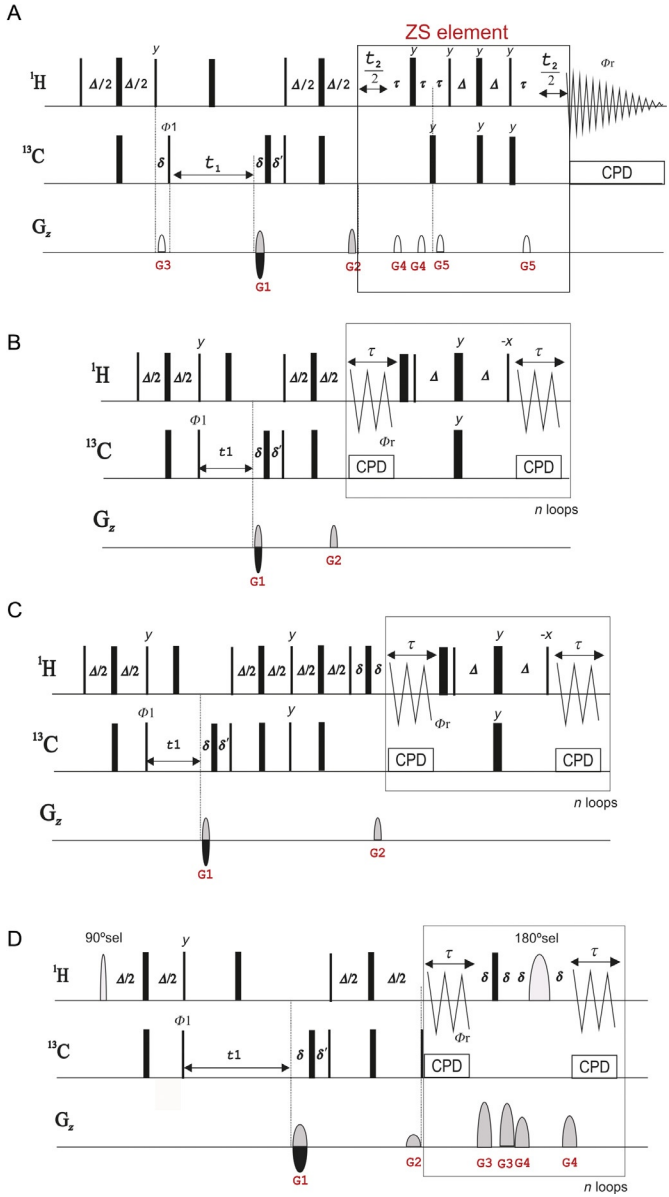

Figure 3 Pulse schemes to obtain pure shift HSQC spectra. (A) HSQC-RESET experiment which uses a pseudo-3D BIRD-based ZS acquisition scheme; (B) PS-HSQC experiment using real-time homodecoupling by the combination of a hard 180°(^{1}H)-BIRD element during data acquisition; (C) sensitivity-improved PS-HSQC; (D) HOBS-HSQC experiment using real-time homodecoupling during detection achieved by applying a pair of hard/band-selective 180° ^{1}H pulses (represented as solid and shaded shapes). In (B–D), the homodecoupling element is applied at the middle of $2\tau = AQ/n$ periods, where AQ is the acquisition time and n is the number of concatenated loops. See original publications for a more detailed description.

the homodecoupled ^{1}H dimension. F2-heterocoupled versions of the RESET-HSQC experiment have been also reported for the measurement of ^{1}J(CH) couplings (see Section 5.1.5).

An enhanced approach of the PS-HSQC experiment uses the real-time detection method where the homodecoupled BIRD-based inversion element is applied into short echo periods during the acquisition period (Fig. 3B) [71]. This real-time BIRD-based technique was initially proposed as a 1D method [62,68] to avoid the strong coupling effects associated with slice selection, but it also delivers two orders of magnitude of sensitivity lost when compared to a conventional ^{1}H spectrum due to the unavoidable editing of ^{1}H–^{13}C magnetization at natural abundance (1%). However, the incorporation of this module in a 2D HSQC scheme affords the maximum attainable sensitivity and improved resolution than the regular experiment because the HSQC pulse train by itself acts as a ^{1}H–^{13}C filter and the homodecoupled element applied during the acquisition period only decouples these selected protons from the passive ^{1}H–^{12}C. It is important to mention that real-time broadband homodecoupling is fully compatible with classical broadband heteronuclear decoupling which is applied during the FID periods.

Experimentally, it has been shown that pure-shift approach can afford a general sensitivity enhancement by 10–40% through collapse of the multiplet structure, and a substantial signal enhancement for CH cross-peaks can be achieved with the sensitivity-improved PS-HSQC experiment (Fig. 3C) [72]. However, the BIRD cluster is not able to suppress the effects of geminal homonuclear couplings and protons belonging to diastereotopic CH_2 groups appear partially homodecoupled with characteristic doublets due to the active ^{2}J(HH) splitting (Fig. 4). Broadband homodecoupling could be incorporated in any type of HSQC-like experiments as reported originally with the multiplicity-edited HSQC (PS-edHSQC) experiment [71].

4.2. HOBS-HSQC: Homodecoupled Band-Selective HSQC

Band-selective NMR spectroscopy experiments are really useful for peptides and proteins because a set of equivalent spins (amide NH, H_α, or aliphatic side-chain protons) appear in well-separated regions. Another alternative to obtain PS-HSQC spectra is by implementing the HOmodecoupled Band-Selective (HOBS) detection scheme [73,74]. This technique has been successfully implemented in a suite of NMR experiments involving IP ^{1}H magnetization, such as Inversion-Recovery and CPMG-Project experiments

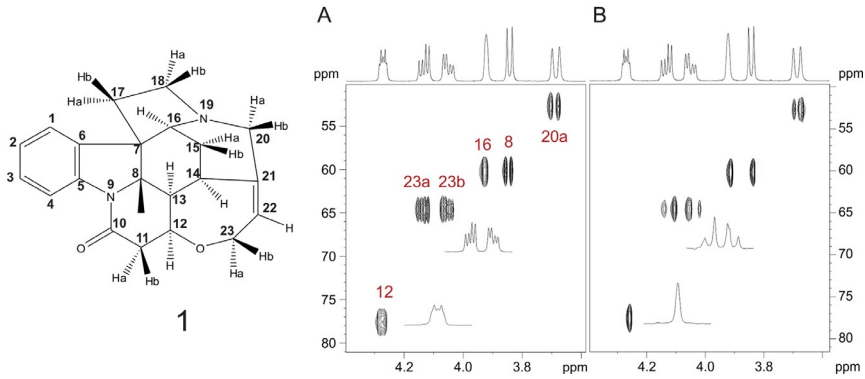

Figure 4 Selected areas corresponding to the (A) conventional HSQC and (B) pure-shift HSQC spectra of strychnine (**1**). One-dimensional traces are shown for selected CH and CH_2 spin systems. Data were acquired, processed, and displayed with the same conditions to allow a quantitative comparison.

to measure T_1 and T_2 relaxation times in overlapped signals [75] or in homonuclear 2D TOCSY [73], NOESY [74], and ROESY [76] experiments. Similarly, a band-selective version of the PS-HSQC experiment has been also reported, the so-called HOBS-HSQC experiment [73,74], where a region-selective 180° ^{1}H pulse is used instead of the BIRD element as a selective inversion element (Fig. 3D). The HOBS method is based on the real-time instant ZS experiment proposed by Meyer and Zangger [64] but yields full sensitivity because the original spatially encoding gradient applied simultaneously to the selective 180° ^{1}H pulse is omitted. Similarly as described above for the BIRD element, the homodecoupling scheme consists of n concatenated loops that include a pair of hard/region-selective 180° ^{1}H pulses (each one flanked by strong G1 and G2 gradients) applied at intervals of 2τ period (τ is set to AQ/2n).

The HOBS-HSQC experiment has demonstrated its usefulness for a natural-abundance sample of cyclosporine (**2**) (Fig. 5). The collected data allow conventional data processing and the best results in terms of selectivity and optimum relaxation were obtained using 180° REBURP semiselective ^{1}H pulses of 5–7.5 ms and decoupling intervals of $2\tau = 10$–15 ms. The method affords broadband homodecoupling for all protons into the selected region, except those that are mutually J coupled which will show their corresponding doublet pattern, as shown for the excitation of the H_α region in **2**. Note the improved sensitivity and signal resolution obtained from the selected 1D slice in Fig. 5. In a similar implementation, a ^{1}H–^{15}N HSQC technique for measuring ^1D(NH) RDCs in protonated ^{15}N/^{13}C-enriched ubiquitin weakly aligned in Pf1 has been reported [74]. A spatial-encoded

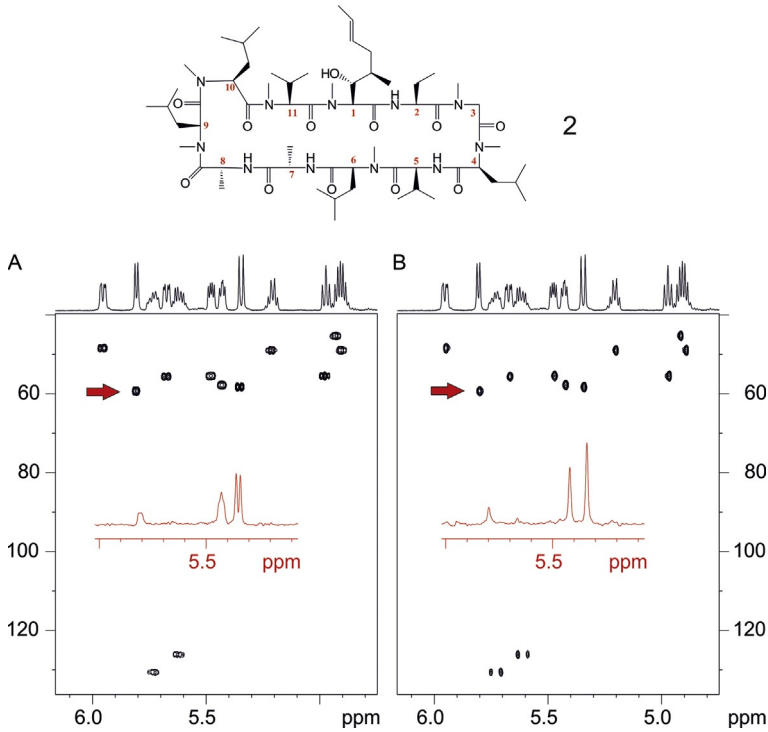

Figure 5 (A) Conventional and (B) fully homo- and heteronuclear decoupled HOBS-HSQC spectra of the peptide cyclosporine (**2**) after selection of the H_α region. Note the residual doublet splitting of the two mutually *J*(HH) coupled olefinic protons belonging to the residue 1 in (B). *Adapted from Ref. [73].*

homodecoupled version of a constant-time HSQC experiment has been also proposed using the instant detection technique and applied to a ^{13}C-labeled intrinsically disordered protein but this approach suffers from high levels of sensitivity losses due to slice selection [77].

4.3. SAPS-HSQC: Spectral Aliasing and Pure-Shift NMR

A very simple experimental trick based on the reduction of the ^{13}C spectral width in HSQC experiments (for instance, from the typical 160 to 5 ppm) is extremely useful to improve digital resolution and signal dispersion by one or two orders of magnitude (for a given number of t_1 increments) along the indirect dimension of an HSQC map, without a substantial modification of the total experimental time. Signals outside of the selected spectral width appear folded or aliased depending on the acquisition scheme [42,78–80]. Recently, a highly resolved Spectral Aliased Pure Shift

(SAPS-HSQC) [72] method has proved to be a fast and very efficient tool for the detection and accurate differentiation and quantification of very small $\Delta\Delta\delta$ values simultaneously for ^{1}H and ^{13}C (Fig. 6). The method combines the complementary features of the pure shift approach that enhances signal resolution in the alternate ^{1}H dimension with those related to spectral aliasing in the ^{13}C dimension. This approach has been successfully applied to enantiodifferentiation studies and it can found interest in the analysis of complex mixtures or the distinction of isomers with very similar NMR spectra.

Enantiodifferentiation analysis through the SAPS-HSQC spectrum has been shown to be superior than the conventional 1D ^{1}H, the conventional ^{13}C, or even the broadband homodecoupled 1D ^{1}H ZS spectra. SAPS-HSQC data allow the detection of enantiodifferentiated signals even in the case that $\Delta\Delta\delta(^{1}H)$ or $\Delta\Delta\delta(^{13}C)$ is close to 0, whenever one of these two values is sufficiently dispersed. In a previous work, 1D pure shift ^{1}H NMR already demonstrated its practical usefulness in enantiodifferentiation studies to distinct signals separated by more than

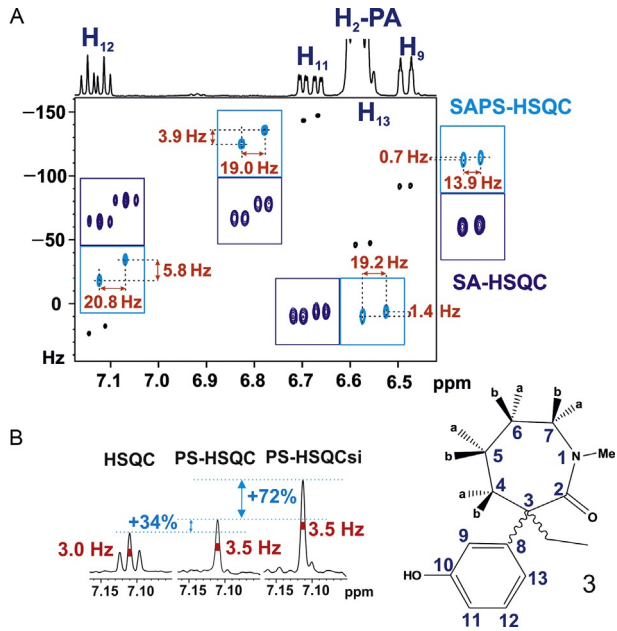

Figure 6 (A) Expanded areas comparing some cross-peaks in SA- and SAPS-HSQC spectra of the racemic compound (**3**)/*R*-PA (Pirkle Alcohol) mixture acquired with a reduced ^{13}C spectral width of 2.5 ppm. (B) Experimental line widths and relative sensitivities obtained in conventional HSQC, pure shift HSQC (PS-HSQC) and pure shift sensitivity-improved HSQC (PS-HSQCsi) experiments. One-dimensional traces correspond to the H12/C12 cross-peak. *Adapted from Ref. [72].*

2 Hz [81]. Similarly, a conventional fully decoupled 1D ^{13}C spectrum is one of the oldest pure shift experiment and it has been shown that enantiodifferentation can also be accomplished with signals above 2 Hz in a 600-MHz spectrometer [82]. To quantify the better enantiodifferentiation and signal dispersion achieved in a 2D HSQC cross-peak, a new parameter $\Delta\Delta\delta(CH)^2 = \Delta\Delta\delta(^1H)^2 + \Delta\Delta\delta(^{13}C)^2$ has been defined. It can be stated that both $\Delta\Delta\delta(^1H)$ and $\Delta\Delta\delta(^{13}C)$ values can be measured when $\Delta\Delta\delta(CH) > 5$ ppb, even in the case that signals are not differentiated in the conventional 1D ^{1}H or ^{13}C spectra. In terms of spectral quality, homodecoupling during acquisition in PS-HSQC experiments generates sidebands at specific frequencies around the main signal and a slight broadening of the signal (~3 vs. ~3.5 Hz) when compared to regular experiments (Fig. 6B). In practice, this does not affect the $\Delta\Delta\delta$ determination, and signal discrimination less than 1 Hz can be achieved in a 600-MHz spectrometer, even for those NMR signals with no apparent splitting in the ^{1}H and/or in the ^{13}C spectrum (<2 Hz). For instance, the H9/C9 and H13/C13 signals are two excellent examples showing how two carbon signals that do not appear split in the 1D ^{13}C spectrum can be clearly distinguished with $\Delta\Delta\delta(^{13}C)$ values of 0.7 and 1.4 Hz (4.6 and 9.2 ppb), respectively, from the 2D cross-peak analysis. In the example shown in Fig. 6A, only 5 of the 16 available proton signals were clearly enantiodifferentiated in the conventional ^{1}H spectrum, 10 in the 1D ZS spectrum, and 15 in the SAPS-HSQC spectrum. On the other hand, 6 of the 11 protonated carbons were enantiodifferentiated in the 1D ^{13}C spectrum acquired overnight, whereas 10 signals were distinguished in the SAPS-HSQC data collected in only 10 min.

The improved signal dispersion achieved due to the combined effects of ^{1}H and ^{13}C δ differentiation and the enhanced multiplet pattern simplification provided by both homo- and heteronuclear decoupling in both dimensions is also illustrated in Fig. 7. The H-15 methyl signal consists of two overlapped triplets where it is difficult to extract the exact chemical shift values in both ^{1}H and conventional HSQC spectra. Note the superior performance of the SAPS approach for an automated peak picking to determine a more accurate and simultaneous determination of $\delta(^{13}H)$, $\delta(^{13}C)$, $\Delta\Delta\delta(^1H)$, and $\Delta\Delta\delta(^{13}C)$ and to quantify each individual singlet signal by direct peak volume integration.

In analogy, small ^{13}C chemical shift differences for quaternary carbons can also be determined by implementing spectral aliasing in HSQMBC experiments. Unfortunately, a real-time broadband homodecoupling

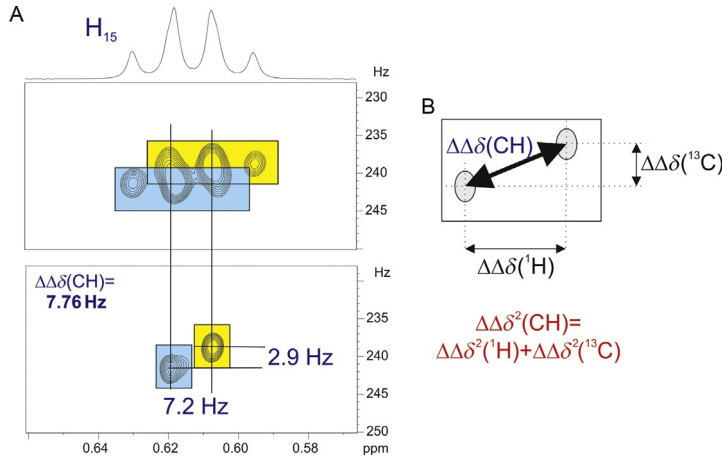

Figure 7 (A) Expanded area showing the C15/H15 cross-peak enantiodifferentiation of (**3**) by using in (top) SA-HSQC and (bottom) SAPS-HSQC spectra. (B) Definition of the new $\Delta\Delta\delta$(CH) enantiodifferentation parameter. *Adapted from Ref. [72].*

acquisition scheme as described previously for the HSQC scheme cannot be implemented in conventional HSQMBC sequences because the detected ^{1}H signals are directly attached to ^{12}C and the BIRD element is not able to distinguish between different *J*(HH)-coupled ^{1}H(^{12}C) protons. However, two different approaches have been reported to achieve pure shift long-range heteronuclear correlation experiments: (i) A band-selective version based on the HOBS technique (HOBS-HSQMBC), which is described in detail in Section 6.5 and (ii) a broadband homodecoupled HMBC spectrum based on a 3D *J*-resolved HMBC experiment [83]. In this latter case, a special data processing and the requirement for a longer 3D acquisition time can limit its practical use.

Finally, the incorporation of spectral aliasing in HSQC-TOCSY experiments also shows to be complementary to the HSQC counterparts for unambiguous chemical shift assignments of signals belonging to each enantiomer. As discussed before, it has not been reported any NMR method incorporating broadband homodecoupling in the HSQC-TOCSY experiment, mainly due to the same reasons as given for the long-range correlation experiments. However, broadband homodecoupled HSQMBC and HSQC-TOCSY experiments could be designed using the real-time instant or the pseudo-2D ZS strategy based on slice selection but they would become prohibitive in terms of sensitivity and overall experimental time.

5. HSQC METHODS FOR MEASURING ^1J(CH)

The HSQC experiment has been largely used for the sensitive measurement of ^1J(CH)/^1D(CH) coupling constants in solution and anisotropic media, respectively, of both small molecules at natural abundance and large labeled biomolecules [84–86]. A comparison of standard F1- and F2-coupled HSQC methods to measure ^1J(CH) and ^1T(CH) in diastereotopic protons of strychnine was reported some years ago [87], and more recently, the pros and cons of new HSQC methods have been evaluated, with special focusing on the design of robust NMR methods to perform such measurements in an easy, user-friendly, and accurate way, and considering some relevant aspects such as (i) the discussion about whether the ^1J(CH) splitting should be measured from the direct F2 (^{1}H) or the indirect F1 (^{13}C) dimension of a 2D HSQC spectrum, (ii) the optimum measurement when a large variation of ^1J(CH)/^1T(CH) values are present, (iii) the determination of ^1J(CH) for individual protons in diastereotopic CH_2 or NH_2 groups, (iv) the simultaneous determination of additional coupling constants from the analysis of the same cross-peak, being the maximum interest the sign-sensitive determination of geminal ^2J(HH) values, and (v) the detection and recognition of the presence of undesired strong coupling effects and evaluation of their influence on the accuracy of the measurement.

5.1. F2-Coupled HSQC Experiments

The easier method to measure ^1J(CH) is from the detected dimension of a conventional HSQC experiment recorded without heteronuclear decoupling during proton acquisition, referred here to as F2-HSQC experiment (Fig. 8A). The main advantages of such an approach are its easy and direct measurement due to the presence of large doublets (Fig. 9A), the high levels of digital resolution readily available in the proton dimension and different peaks belonging to diastereotopic CH_2 groups can be individually analyzed. The drawbacks are that signals exhibit the typical J(HH) multiplet pattern structure, and therefore, the lack of a well-defined multiplicity J substructure or undesired line broadening effects can preclude accurate determinations, factors that are emphasized in anisotropic media due to the important HH dipolar contribution. In addition, strong coupling effects can be quickly recognized by the distortions observed in one of the two components, as shown in Fig. 9B, hindering an accurate measurement.

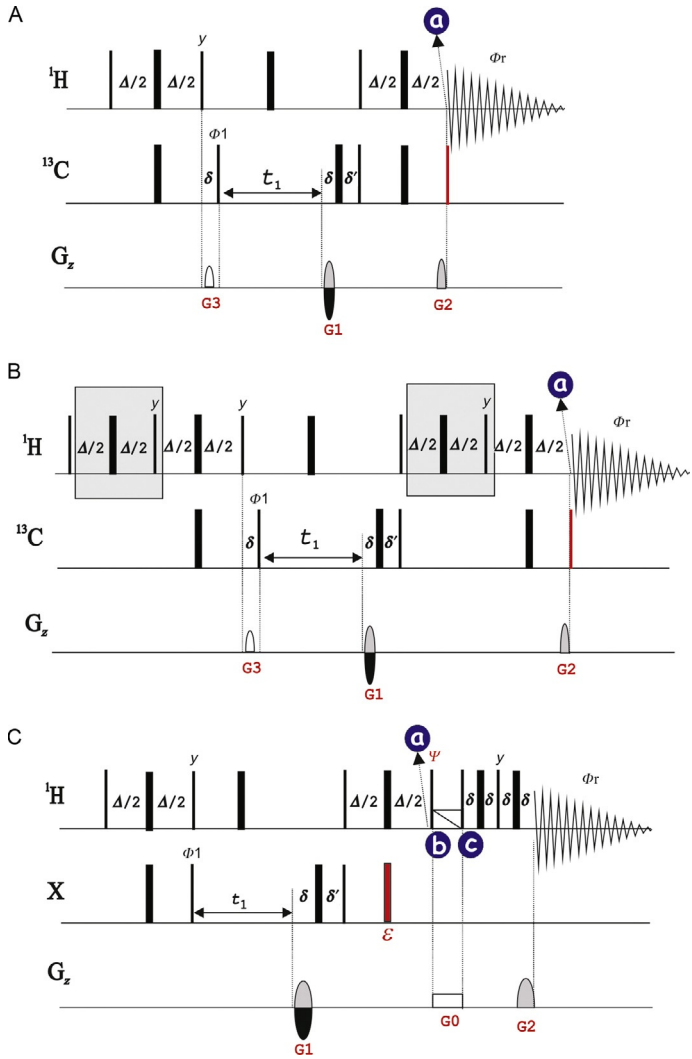

Figure 8 Basic pulse schemes to obtain F2-heterocoupled two-dimensional ^{1}H–^{13}C HSQC spectra: (A) CLIP-HSQC, (B) perfect-CLIP-HSQC, and (C) PIP-HSQC experiments. Narrow and broad pulses represent 90° and 180° pulses, respectively, with phase *x*, unless specified explicitly. The interpulse delay Δ is set to $1/(2^{*1}J(\mathrm{CH}))$ and a basic two-step phase cycling is executed with $\phi_1 = x,-x$ and receiver $\phi_r = x,-x$. Gradients for coherence selection using the echo–antiecho protocol are represented by G1 and G2 and δ stands for the duration and the gradient and its recovery delay. A purge gradient G3 is placed for zz-filtering whereas the final and optional 90°(^{13}C) stands for the so-called CLIP pulse to remove heteronuclear AP contributions. F2-heterodecoupled versions of all three HSQC schemes should be obtained by applying broadband heterodecoupling during the acquisition period. In such cases, the CLIP pulse in (A) and (B) is not required.

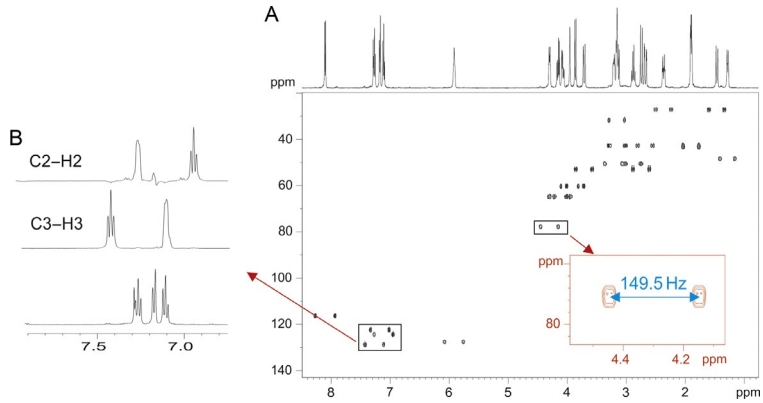

Figure 9 (A) Conventional F2-coupled CLIP-HSQC spectrum of (**1**) recorded in a 500-MHz spectrometer. ^{1}J(CH) can be easily measured from the large doublet along the detected dimension, as shown in the inset. (B) One-dimensional slices showing distorted signals due to the presence of strong-coupling effects.

The effects on the phase and the intensity observed in different HSQC cross-peaks as a function of the magnitudes of J(HH), ^{1}J(CH), and the delay Δ optimization for several F2-HSQC schemes have been studied by 1D spectral simulations (Fig. 10). Thus, the phase anomalies observed in conventional F2-HSQC cross-peaks (Fig. 10A) result from the mismatch between the optimized Δ delay and the active ^{1}J(CH) value (terms II and IV derived in Eq. 2), and from the evolution of J(HH) during the echo INEPT periods (term III in Eq. 2). Such distortions limit any attempt to realize an accurate analysis in terms of signal quantification via peak integration or direct ^{1}J(CH) and J(HH) measurements.

5.1.1 CLIP-HSQC

A simple solution to partially solve these phase distortions was proposed with the CLean IP HSQC (CLIP-HSQC) experiment [88], which applies a 90° ^{13}C pulse (from the x-axis) just prior the acquisition (Fig. 8A). In this way, the AP contributions due to ^{1}J(CH) are converted to multiple-quantum coherences (terms II and IV) and, apparently, clean IP patterns should be obtained in the absence of any J(HH) coupling.

$$\text{Eq. (2)} \xrightarrow{90°(x,^{13}\text{C})} \begin{aligned} &\mathrm{H}_{1x}\, c^2 s'^2\,(\text{Term I}) + 2\mathrm{H}_{1y}\mathrm{C}_y c^2 s' c'\,(\text{Term II}) \\ &+ 2\mathrm{H}_{1y}\mathrm{H}_{2z} c s s'^2\,(\text{Term III}) - 4\mathrm{H}_{1x}\mathrm{H}_{2z}\mathrm{C}_y c s c' s'\,(\text{Term IV}) \end{aligned} \tag{3}$$

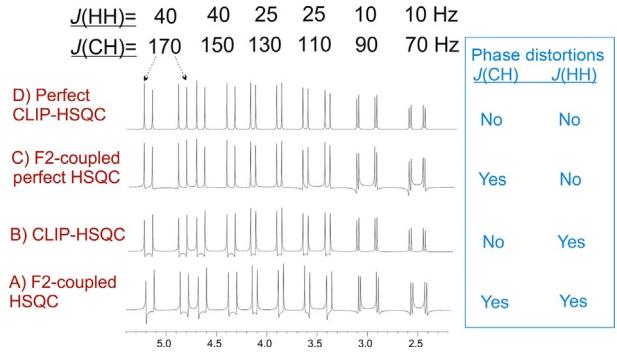

Figure 10 Simulated 1D spectra showing the phase peak distortion effects in several 140-Hz optimized F2-heterocoupled HSQC experiments: (A) Conventional HSQC, (B) CLIP-HSQC, (C) perfect-HSQC, and (D) perfect CLIP-HSQC. Six protons belonging to three different diastereotopic CH_2 groups have been simulated with a wide range of *J*(HH) and ^1J(CH) values, as shown in the upper part. *Adapted from Ref. [95].*

However, in the presence of *J*(HH), a mixture of observable IP and AP components ($H_{1x} + 2H_{1y}H_{2z}$) are still active, as shown in the simulated spectrum of Fig. 10B. In practice, due to the large difference of magnitudes between ^1J(CH) and *J*(HH), these unwanted contributions are small and they have been traditionally omitted in cross-peak analysis in CLIP-HSQC or in conventional decoupled HSQC experiments. A simple calculation shows that these effects may become important. For instance, the relative percentage of the term III with respect to term I in an 140-Hz optimized CLIP-HSQC experiment is of 5.6% and 17% for *J*(HH) values of 5 and 15 Hz, respectively. Such percentages can be more pronounced when measuring RDCs in anisotropic media, where higher values of HH couplings are usually involved.

Enthart *et al.* also introduced the IPAP technique into the F2-HSQC (CLIP/CLAP-HSQC experiment) [88] to edit the two components of the doublet in two separate spin-state selective α/β spectra in order to avoid accidental signal overlap. Similar IPAP techniques have been also implemented in broadband homodecoupled F2-HSQC (see Section 5.1.5) and selHSQMBC (see Section 6) experiments. The robustness of the CLIP/CLAP experiments has been also tested using optimized designed broadband 90° and 180° pulses.

5.1.2 J(HH)-Compensated INEPT: Perfect-HSQC

The evolution of *J*(HH) during homonuclear or heteronuclear echo periods also generates AP components that distort the phase of the signal. The

product operator analysis of a conventional echo element (Fig. 11A) for a weakly coupled AX H_1/H_2 two-spin system, with a mutual $J(H_1H_2)$ coupling, can be summarized as:

$$-H_{1y}-H_{2y}\xrightarrow{\Delta-180-\Delta}\begin{array}{l}-H_{1y}\cos(\pi J\Delta)+2H_{1x}H_{2z}\sin(\pi J\Delta)\\-H_{2y}\cos(\pi J\Delta)+2I_{2x}I_{1z}\sin(\pi J\Delta)\end{array} \quad (4)$$

An interesting general NMR building block, referred to as perfect echo, has shown a renewed interest in the last years because the J(HH) effects generated during a spin-echo period can be efficiently refocused for a spin AX system (Eq. 5). Basically, it is a double spin-echo scheme separated by an orthogonal J-refocusing 90° pulse, with the interpulse delay set to $\Delta \ll 1/J(\mathrm{HH})$ (Fig. 11B) [89].

$$\begin{aligned}\mathrm{Eq.}(4)&\xrightarrow{90(y)}-H_{1y}\cos(\pi J\Delta)-2H_{1z}H_{2x}\sin(\pi J\Delta)-H_{2y}\cos(\pi J\Delta)\\&\quad-2H_{2z}H_{1x}\sin(\pi J\Delta)\\&\xrightarrow{\Delta-180-\Delta}-H_{1y}\cos^2(\pi J\Delta)+2H_{1x}H_{2z}\cos(\pi J\Delta)\sin(\pi J\Delta)\\&\quad-2H_{1z}H_{2x}\sin(\pi J\Delta)\cos(\pi J\Delta)-H_{2y}\sin^2(\pi J\Delta)\\&\quad-H_{2y}\cos^2(\pi J\Delta)+2H_{2x}H_{1z}\cos(\pi J\Delta)\sin(\pi J\Delta)\\&\quad-2H_{2z}H_{1x}\sin(\pi J\Delta)\cos(\pi J\Delta)-H_{1y}\sin^2(\pi J\Delta)\\&=-H_{1y}-H_{2y}\end{aligned} \quad (5)$$

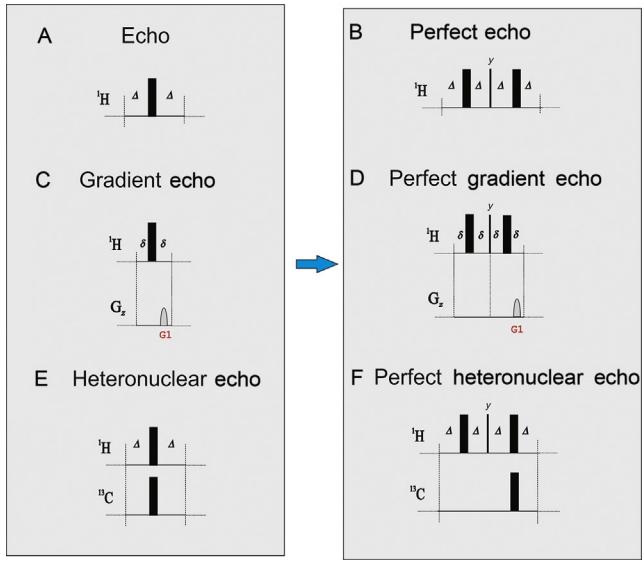

Figure 11 NMR building blocks comparing conventional versus J(HH)-compensated spin-echo elements.

The concept of perfect echo has been successfully implemented in a series of NMR applications to solve some traditional issues, such as the determination of T_2 relaxation times from undistorted multiplets in "perfect-echo CPMG" experiments [90], the elimination of peak distortion caused by J(HH) in diffusion NMR experiments [91], the suppression of J(HH) evolution during the solvent-suppression period in a "perfect WATERGATE" method [92], or during the variable t_1 period in "perfect-HMQC" experiments to remove the typical cross-peak tilting along the indirect dimension [93]. In the heteronuclear case, a J(HH)-compensated INEPT sequence called "perfect-echo INEPT" element (Fig. 11F) has been introduced to refocus J(HH) modulations appeared during INEPT elements and it has been applied to improve long-range heteronuclear transfers in conventional 1D refocused ^{13}C INEPT experiments [94].

The J(HH) interferences present in conventional HSQC experiments have been efficiently minimized in a perfect-HSQC pulse scheme (Fig. 8B) which replaces the classical INEPT by a J(HH)-compensated perfect-echo INEPT module consisting of a double echo period in both defocusing/refocusing heteronuclear transfer periods [95]. J(HH) is refocused at the end of each double echo period, and therefore, the signal amplitude is only modulated by the effect of ^1J(CH). Thus, in contrast to the conventional HSQC experiment (see Eq. 2), the magnetization just prior to acquisition in the perfect-HSQC experiment is defined exclusively by only two components, as similarly described in Eq. (1). The resulting 2D perfect-HSQC spectra afford pure IP cross-peaks with respect to both ^1J(CH) and J(HH) and, in addition, peak volumes are not influenced by J(HH), rendering practical applications such as phase correction, signal integration, and multiplet analysis more convenient and accurate.

Figure 10C shows that the simulated F2-coupled perfect-HSQC spectrum without the CLIP pulse still shows some phase distortions provided Δ does not match the corresponding ^1J(CH) value. For instance, deviations of 10 and 20 Hz between ^1J(CH) and the Δ delay optimization generate antiphase contributions of about 11% and 23%, respectively, in a 140-Hz optimized experiment. Such distortions can be efficiently suppressed using the perfect-CLIP-HSQC pulse scheme (Fig. 8B), affording perfect pure IP multiplet patterns for all peaks independent of their J(HH) and J(CH) values (Fig. 10D).

Figure 12 compares some experimental multiplets extracted from equivalent 140-Hz optimized heteronuclear decoupled HSQC and perfect-HSQC spectra. Significant AP J(HH) contributions are observed in those HSQC peaks presenting large J(HH) values that distort the signal phase

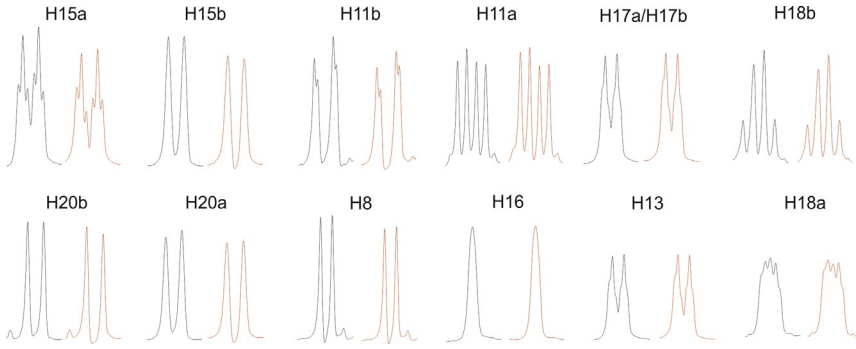

Figure 12 Comparison of perfect-HSQC (left) and HSQC (right) signals of (**1**), both acquired under the same experimental conditions. Phase distortions and decreased sensitivity in conventional HSQC multiplets are due to *J*(HH) modulation during the INEPT blocks. *Adapted from Ref. [95].*

and decrease their relative intensities. The H16 proton can be taken as a reference for a resonance which does not show large values, and therefore, a practically equal multiplet pattern and signal intensity are obtained in both spectra. For instance, differences up to 20% in signal intensity were observed for the diastereotopic H15a and H15b protons and distortions could be also observed for the methine H8 peak.

The main disadvantage of the perfect-HSQC experiment arises from the longer duration of the perfect-echo INEPT versus the conventional INEPT (2Δ vs. Δ, respectively) that can lead to some signal loss due to additional T_2 relaxation. The overall duration of the sequence is extended about 3.6 ms for each perfect-echo INEPT period in a 140-Hz optimized experiment but this does not represent a serious issue for small molecules having reasonably long T_2 relaxation times (some hundreds of milliseconds).

5.1.3 J(CH)-Compensated INEPT: COB-HSQC

Traditional HSQC experiments use a single heteronuclear echo element for both defocusing and refocusing magnetization transfer which are optimized for a single ^1J(CH) value. Thus, the efficiency of such transfer and therefore the observed signal intensities can vary considerably depending on the matching between the interpulse delay optimization and the active ^1J(CH). Several attempts have been made to compensate for variation of ^1J(CH) values in HSQC experiments: (i) by adding data acquired with different delays, (ii) by exploiting the time-dependent inversion that is characteristic of adiabatic inversion pulses to apply different refocusing delays to

different ^{13}C chemical shifts [96,97], or (iii) by designing alternative *J*-compensated INEPT sequences that usually require a much number of rf pulses and delays, increasing the overall duration of the element and making it more sensitivity to rf inhomogeneities (Fig. 13B) [98,99]. Signal intensity also depends on the imperfections due to carbon chemical shift offsets and B_1 field inhomogeneities, and all these can be improved by replacing the hard rectangular 180° ^{13}C pulse by adiabatic or broadband inversion pulses [100].

In order to improve the broadband response in HSQC experiments, several modified INEPT transfer elements that compensate for a wide range of couplings, offsets, and B_1-inhomogeneities (COB) have been reported [101]. The initial COB-INEPT element (Fig. 13C) takes profit on the availability of effective optimization of shaped broadband pulses and the compensation covers all the needs of HSQC-type experiments of small molecules with, e.g., scalar coupling constants in the range of 120–250 Hz [102]. The same authors have recently proposed improved COB3-INEPT elements that are able to cover a much wider range of ^1J(CH) couplings (120–750 Hz) for all different CH, CH_2, and CH_3 multiplicities (Fig. 13D) [103]. In general, it has been shown that these *J*(CH)-compensated sequences strongly require the use of broadband, specifically

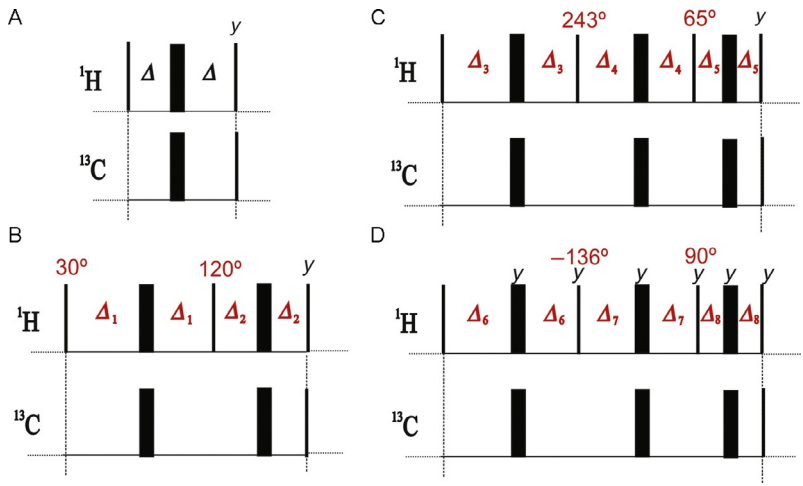

Figure 13 Basic ^1J(CH)-compensated INEPT elements using hard pulses: (A) conventional; (B) J45+90A INEPT; (C) COB-INEPT, and (D) COB3-INEPT. Delays: $\Delta = 1/(4*{}^1J(CH))$; $\Delta_1 = 2.68/{}^1J(CH)$; $\Delta_2 = 1.34/{}^1J(CH)$; $\Delta_3 = 1.469/{}^1J(CH)$; $\Delta_4 = 2.134/{}^1J(CH)$; $\Delta_5 = 0.394/{}^1J(CH)$; $\Delta_6 = 1.07$ ms; $\Delta_7 = 1.065$ ms; and $\Delta_8 = 0.54$ ms. All original COB-INEPT elements were described using shaped-optimized ^1H and ^{13}C pulses.

designed, and optimized broadband pulses for an optimum and uniform intensity response. These transfer elements are quite robust due to the application of offset and field B_1-compensated point-to-point (PP) pulses such as BEBOP [104–107] universal rotation (UR) pulses such as BURBOP [108,109], and broadband excitation (BEBE) and broadband UR and broadband inversion (BUBI) pulses [110]. Potential applications of such methods have been proposed for the measurement of any type of heteronuclear coupling constants with particular emphasis to the determination of ^1D(CH) RDCs of partially oriented molecules in anisotropic media. For instance, it has been shown that whereas in a 145-Hz optimized conventional HSQC experiment only cross-peaks corresponding to couplings up to 200 Hz are visible, signals corresponding to couplings up to 375–400 Hz are observed with optimum sensitivity in a COB3-HSQC spectrum of a partially aligned sample of a tetrasubstituted pyrrolidine dissolved in a liquid crystalline PBLG/$CDCl_3$ phase. However, all these approaches do not consider the effect of J(HH) modulation and they are not suitable as an accurate quantitative NMR method.

5.1.4 PIP-HSQC Experiment

Another simple and general solution to obtain heteronuclear correlation spectra that yield truly pure absorption line shapes and IP multiplet structures for all available cross-peaks with respect to both J(CH) and all passive J(HH) coupling constants along the detected dimension is the so-called Pure In-Phase HSQC (PIP-HSQC) experiment [111]. The key point is an appended adiabatic zero-quantum filter (ZQF) [112] applied just before a refocusing gradient perfect-echo element and the acquisition. Thus, after the $90°_y(^1\mathrm{H})$ pulse (point **b** in Fig. 8C) the above four components derived from Eq. (2) are converted to

$$\begin{aligned}\text{Eq. (2)} \rightarrow\ & -\mathrm{H}_{1z}c^2s'^2(\text{Term I}) - 2\mathrm{H}_{1y}\mathrm{C}_z c^2 s' c'(\text{Term II}) \\ & + 2\mathrm{H}_{1y}\mathrm{H}_{2x}css'^2(\text{Term III}) - 4\mathrm{H}_{1z}\mathrm{H}_{2x}\mathrm{C}_z csc's'(\text{Term IV})\end{aligned} \tag{6}$$

where the second and fourth terms represent transverse AP heteronuclear magnetization and the third element represents a mixture of homonuclear ZQ and DQ coherences, which are also eliminated by the effect of the simultaneous adiabatic 180° ^{1}H pulse and the purging G0 gradient pair. As a result, only the first term representing the desired IP magnetization remains detectable after the z-filter (point **c** in Fig. 8C). To maintain the pure IP character during detection, the classical gradient echo block has been

replaced by a perfect gradient echo element (see Fig. 11C vs. D) where J(HH) should be fully refocused. Such distortions could become critical when measuring J(CH) in the presence of large J(HH) values, as could be found in the measurement of RDCs, or in experiments involving longer Δ delays (see PIP-HSQMBC experiment in Section 6.6). Table 1 shows the experimental ^1J(CH)/^1D(CH) values obtained for a sample of strychnine weakly aligned in a poly(methyl methacrylate) (PMMA) gel swollen in $CDCl_3$ using the reversible compression relaxation method (Fig. 14). It has been shown that errors up to 10% Hz can be introduced from the analysis of distorted cross-peaks in conventional F2-coupled CLIP-HSQC and F2-decoupled HSQC spectra.

5.1.5 F2-Coupled Pure Shift HSQC Experiments

Several F2-coupled versions of the previously described PS-HSQC schemes (see Section 4) have also been proposed for the measurement of ^1J(CH) from simplified homodecoupled doublets (Fig. 15A–C). As discussed before, the use of a pseudo-3D acquisition mode produces long acquisition times when compared to 2D HSQC analogs but the obtention of simplified doublets can facilitate the semi-automated peak picking and the measurement from simple frequency differences between singlet peak maxima. Two very similar schemes of the real-time PS-HSQC experiment using a BIRD element with broadband pulses that is not compensated for ^1J(CH) variations have been simultaneously reported [70,113]. The CLIP/CLAP-RESET HSQC method (Fig. 15A) [113] leads to complete homonuclear decoupling for CH groups and CH_3 groups in isotropic samples but leaves residual splittings with AP contributions for CH_2 groups due to ^2J(HH) coupling evolution that is not decoupled by the BIRD element. In terms of experimental times, whereas a conventional HSQC was obtained in 6 min, the corresponding CLIP-RESET spectrum acquired with 16 increments of the homodecoupled dimension required 1 h and 25 min. Pure shift HSQC versions using the COB-INEPT element and broadband-shaped excitation, inversion and refocusing pulses were also introduced to provide a much better uniform response and to obtain a much cleaner IPAP editing (COB-CLIP-RESET experiment) [113]. Alternatively, a more sophisticated constant-time version (CT-CLIP-RESET experiment) was also proposed with full homonuclear decoupling for weakly coupled CH_2 spin systems, but sensitivity was further compromised. Unfortunately, J(CH)-compensated BIRD elements are not yet available. The authors make a comparative study between different CLIP methods to

Table 1 Experimental ^1J(CH)/^1T(CH) values extracted from the PIP-HSQC spectra of strychnine (**1**) recorded in isotropic and anisotropic conditions.

				Isotropic	Anisotropic		Predicted[a]
C	δ (ppm)	H	δ (ppm)	$^1J_{CH}$ (Hz)	$^1T_{CH}$ (Hz)	$^1D_{CH}$ (Hz)	$^1D_{CH}$ (Hz)
C1	122.3	H1	7.16	158.3	174.8	+16.5	+12.2
C2	124.2	H2	7.09	160.8[b]	163.7[b]	+2.9	+2.2
C3	128.6	H3	7.25	159.2[b]	163.5[b]	+4.3	+3.2
C4	116.2	H4	8.08	168.4	187.1	+18.7	+13.9
C8	60.1	H8	3.86	144.9	133.7	−11.2	−8.6
C11	42.5	H11a	3.12	135.4	143.1	+7.7	+5.9
		H11b	2.66	125.5	107.6	−18.2	−14.1
C12	77.6	H12	4.28	150.0	134.2	−15.8	−12.3
C13	48.2	H13	1.27	124.8	118.9	−5.9	−4.6
C14	31.6	H14	3.15	131.3	117.9	−13.4	−10.4
C15	26.8	H15a	2.36	130.9	135.0	+4.1	+3.2
		H15b	1.47	129.9	131.0	+1.1	+0.9
C16	60.2	H16	3.98	146.7	158.2	+11.5	+9.0
C17	42.8	H17a/b	1.90	133.2	139.1	+5.9	+4.6
C18	50.3	H18a	3.25	146.3	148.1	+1.8	+1.4
		H18b	2.88	131.7	143.4	+11.7	+9.0
C20	52.7	H20a	3.73	138.8	ov[c]		−7.7
		H20b	2.76	138.7	132.9	−6.2	−4.6
C22	127.6	H22	5.93	158.8	156.4	−2.4	−1.8
C23	64.6	H23b	4.15	145.5	148.9	+3.4	+2.6
		H23a	4.05	137.2	111.7	−25.5	−19.4

[a]The predicted values have been calculated with MSpin program (MESTREALAB RESEARCH SL, Santiago de Compostela, Spain. http://www.mestrelab.com).
[b]Strong coupling effect.
[c]Overlapped with PMMA signals.

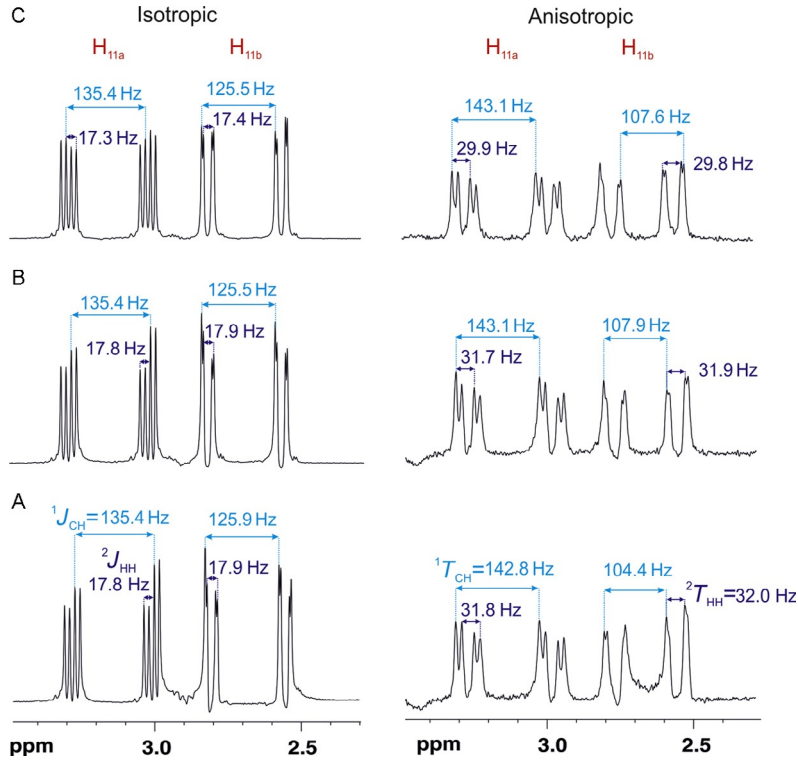

Figure 14 1D traces extracted at the C11 chemical shift of (**1**) in isotropic and anisotropic conditions showing the signal distortions originated in (A) conventional HSQC, (B) CLIP-HSQC, and (C) PIP-HSQC spectra recorded with Δ set to 3.6 ms ($^1J_{CH} = 140$ Hz). *Adapted from Ref. [111].*

measure ^1J(CH) on a sample of menthol, and some guidelines to identify the effects of strong coupling effects were presented and discussed.

Non-refocused and refocused versions of the F2-coupled HOBS-HSQC experiment described in Section 4.2 have also been reported (see pulse diagram in Fig. 15C), and the important sensitivity and resolution enhancements as well as the multiplet simplification can be quickly evidenced when comparing the selected 1D slices in Fig. 15D versus E. In addition, analogs counterparts of the previously described 2D perfect-HSQC (Section 5.1.2) and PIP-HSQC (Section 5.1.4) experiments could be easily designed by incorporating BIRD-based or HOBS broadband homodecoupling as outlined in Fig. 15B and C, respectively.

A modified version of the non-refocused HMQC pulse train has been proposed to measure ^1J(CH) from the direct dimension using a pseudo-homodecoupling approach based on the scaled evolution of J(HH) during

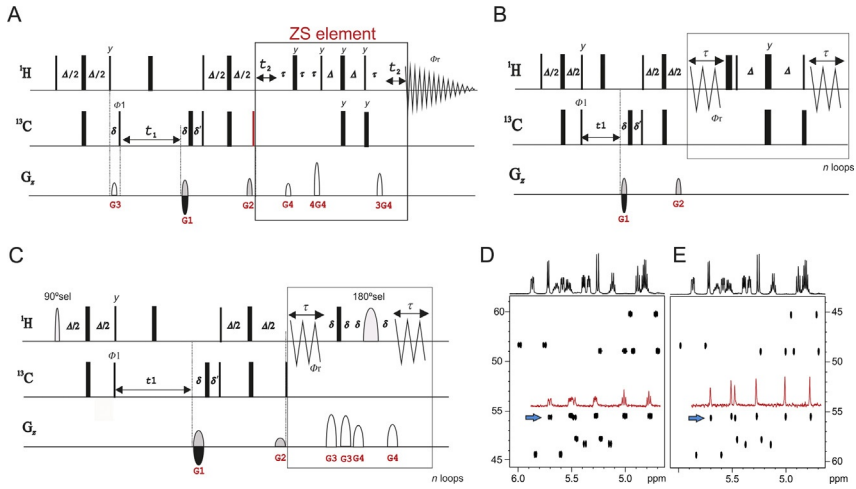

Figure 15 F2-heterecoupled PS-HSQC experiments: (A) pseudo 3D RESET-HSQC; (B) PS-HSQC using a BIRD inversion element during acquisition; (C) HOBS-HSQC using a band-selective pulse as the inversion element; (D,E) F2-coupled conventional HSQC and HOBS-HSQC spectra of (**2**). *Figure partially adapted from Ref. [73].*

the indirect t_1 period. In this HR-HSBC experiment [114], which is based on an early HR-HMBC experiment [115], the analysis of the resulting tilted cross-peaks in a specific row of the detected dimension avoids the complexity of the overall multiplet substructure.

5.2. F1-Coupled HSQC Experiments

The measurement of ^1J(CH) exclusively along the indirect F1 dimension of a HSQC spectrum is recommended to avoid the interferences of J(HH) splittings, but a major inconvenient arises for the need of a large number of t_1 increments, and therefore longer acquisition times. The successful use of NUS, J scaling factors or spectral folding/aliasing can speed up data acquisition and/or increase the digital resolution in the F1 dimension. Several F1-coupled HSQC pulse schemes have been compared and evaluated by Thiele and Bermel [116]. The most simple approach results from the removing of the central 180° ^{1}H pulse placed in the middle of the t_1 evolution period in the conventional HSQC experiment, referred to as F1-HSQC experiment (Fig. 16A). A more convenient method incorporates a G-BIRD^r module to allow the simultaneous evolution of both ^1J(CH) and ^{13}C chemical shift evolution while contributions from ^nJ(CH) are efficiently refocused [117]. The better line shapes along the indirect dimension allow

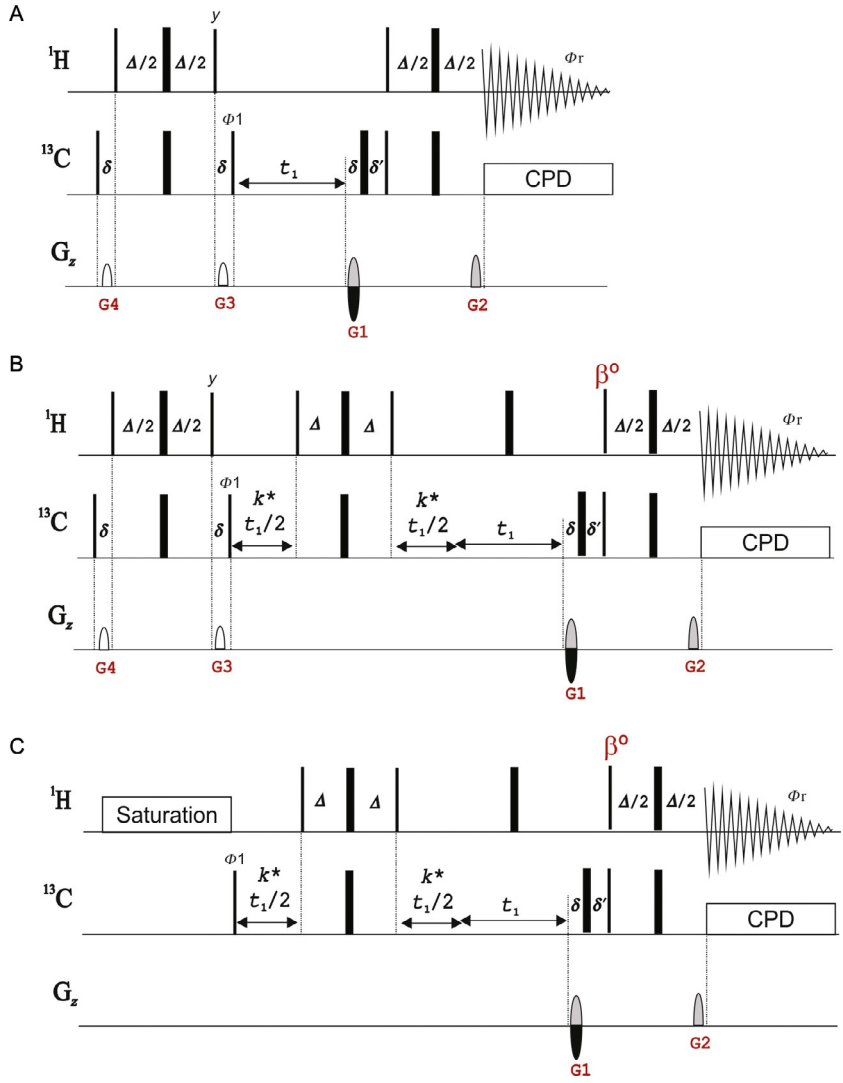

Figure 16 Several pulse schemes to achieve F1-heterocoupled HSQC spectra: (A) F1-HSQC, (B) BIRD-HSQC, and (C) F1-iINEPT experiments. Inversion and refocusing 180° ^{13}C pulses can be applied as adiabatic or BIP pulses and the $\delta(^{13}C)$ evolution period is optional. The interpulse delays in INEPT and BIRD elements are optimized according to $\Delta = 1/(2*^1J(CH))$ and a small flip angle ($\beta = 36^\circ$) generates E.COSY cross-peaks for $^2J(HH)$ couplings.

the determination of ^1J(CH) by simply measuring the frequency difference between the peak maxima of singlets instead of the centers of complex multiplets.

The accurate measurement of the two ^1J(CH) values and particularly the geminal ^2J(HH) coupling in diastereotopic CH_AH_B groups has always been a challenging task, particularly for F1-HSQC experiments. Several methods have been proposed for measuring them either from the F1 or from the F2 dimension, but they all present some drawbacks that have prevented their general use. For instance, the passive $^1J(C\text{-}H_B)$ value can be separately measured into the active H_A cross-peak, and vice versa, along the F1 dimension of a *J*-resolved HMQC experiment [118]. In addition, the large doublet is further split by the $^2J(H_AH_B)$ coupling yielding a doublet of doublet. The disadvantage is that additional experiments can be required to measure ^1J(CH) for CH or CH_3 spin systems, and significant distortions on the cross-peaks (banana shape peaks) are frequently observed in the spectra of complex small molecules. Another important group of NMR experiments are those based on spin-state selection specifically designed for methylene groups that yield simplified coupling patterns, and where the sign and the magnitude of the geminal ^2J(HH) can sometimes be additionally extracted [119–129].

5.2.1 BIRD-HSQC Experiment

The BIRD-HSQC approach uses two sequential blocks to separate the contributions from $\delta(^{13}C)$ and ^1J(CH) evolution during the heteronucleus frequency labeling period (Fig. 16B) [116,130]. This strategy presents several advantages: (i) the *J*(CH) evolution period can incorporate a BIRD element to remove long-range contributions; (ii) the *J*(CH) splitting in the indirect dimension can be scaled by a factor **k**; and (iii) the experiment can be optionally recorded with a very narrow spectral width in the indirect dimension (about 500 Hz) by omitting the $\delta(^{13}C)$ evolution period, affording a *J*-resolved HSQC format [131] with a considerable resolution gain by one of two orders of magnitude, whereas a reasonable number of t_1 increments can be collected in a shorter experimental time. A similar procedure has been reported where the ^1J(CH) evolution period is inserted in the initial INEPT period [130]. The utility of these *J*-resolved HSQC-BIRD spectra has been demonstrated by differentiating enantiomeric derivatives dissolved in anisotropic media from their different ^1J(CH) splitting sizes along the indirect dimension [132,133].

A major inconvenient in all F1-HSQC experiments is that the central lines of the F1−multiplet corresponding to a CH_2 group are not observed, and therefore, only the sum of the two ^1J(CH) can be determined from the indirect dimension. The BIRD-HSQC experiment can be analyzed considering an isolated diastereotopic CH_AH_B spin system defined with three different $^1J(CH_A)$, $^1J(CH_B)$, and $^2J(H_AH_B)$ coupling constants. The sequence starts with an initial 90°(^{13}C)-gradient element to remove any contribution coming from the ^{13}C Boltzmann polarization. After the ^{1}H-to-^{13}C INEPT transfer, AP ^{13}C magnetization is present as a mixture of $2H_{Az}C_y+2H_{Bz}C_y$, which evolve under the effects of ^1J(CH) and $\delta(^{13}C)$ in a sequential mode, by using separated and synchronously incremented time periods. Thus, the magnetization evolves first under the effect of a BIRD^{d,X} element [134] flanked by a variable *J*-scaled t_1 evolution period (defined by a scaling factor *k*) to allow the exclusive evolution of ^1J(CH), whereas ^{13}C chemical shift and long-range CH contributions are refocused, and then ^{13}C chemical shift can evolve from an optional t_1 evolution period as usual. In the subsequent analysis, the scaling factor, which is set arbitrarily within the limits set by relaxation and/or signal overlapping, the effects of the labeling G1 gradient and the optional ^{13}C chemical shift t_1 evolution period are neglected for the sake of clarity. Thus, for a single H_A spin, the evolution during the variable BIRD-based t_1 period ($k=1$) is described by $2H_{Az}C_y\cos(\pi(^1J(CH_A+^1J(CH_B))t_1)$, meaning that only the outer lines of the theoretical triplet or double–doublet coupling pattern of the methylene proton cross-peak would be observed and, therefore, only the sum of the both couplings ($^1J(CH_A+^1J(CH_B)$) will be observed as an IP doublet along the indirect dimension. This signal dependence with respect to the cosine function makes that multiplet patterns with relative intensities of 1:1 for CH, 1:0:1 for CH_2, and 3:1:1:3 for CH_3 will be displayed along the F1 dimension. The combined use of the *J*-scaled BIRD-HSQC and *J*-scaled BIRD-HSQC/HMQC experiments have been used to define a new strategy to assign unambiguously the diastereotopic CH_2 protons of strychnine from RDC data [135].

An optional but very useful feature in the BIRD-HSQC experiment is the use of a small flip ^{1}H pulse angle ($\beta=36°$) in the last retro-INEPT block which generates simplified E.COSY multiplet patterns for non-equivalent protons in CH_2 and CH_3 spin systems, allowing the determination of the sign and the magnitude of ^2J(HH) in these spin systems as a function of multiplet pattern slope. This idea comes from a time-optimized non-refocused version of an F1–F2 fully coupled HSQC experiment which has been proposed to measure ^1J(CH) and ^2J(HH) in diastereotopic CH_2 systems. The

major inconvenient of this simple Pure Exclusive HSQC (P.E.HSQC experiment) scheme is the number of multiple lines into a single cross-peak, requiring high levels of digitization in both dimensions and increasing the probability of accidental signal overlapping [136].

5.2.2 iINEPT Experiment

A simple modification of the small flip-angle BIRD-HSQC experiment has been reported for detecting the missing central lines in diastereotopic CH_2 cross-peaks. The resulting cross-peaks in this new 2D F1-coupled inverse INEPT experiment (referred to as F1-iINEPT) [137] present a characteristic E.COSY multiplet pattern that facilitates the straightforward measurement of both individual $^1J(CH_A)$ and $^1J(CH_B)$ values, as well as the sign and magnitude of the geminal $^2J(HH)$ coupling. Figure 17A summarizes the expected cross-peak pattern for a single diastereotopic CH_AH_B proton using the different F1-HSQC and F1-iINEPT approaches with $\beta = 90°$ and 36° (compare Fig. 17A vs. B). The sequence avoids the initial INEPT transfer, starting exclusively from the ^{13}C Boltzmann polarization (Fig. 16C). The experiment works for all multiplicities and it is easily adapted for a *J*-resolved presentation (referred to as F1-iINEPT-*J*) which allows to obtain higher levels of resolution within the same experimental time by the use of a reduced spectral width in the indirect dimension (Fig. 17F).

The initial 90° ^{13}C pulse generates IP $-C_y$ magnetization which evolves under the effect of $^1J(CH)$ during the variable t_1 BIRD-based period:

$$\begin{aligned} &2H_{Az}C_x\left[\sin\left(\pi^1J(CH_A)t_1\right)\cos\left(\pi^1J(CH_B)t_1\right)\right. \\ &\left.-2H_{Bz}C_x\cos\left(\pi^1J(CH_A)t_1\right)\sin\left(\pi^1J(CH_B)t_1\right)\right] \end{aligned} \tag{7}$$

The resulting pure absorptive 2D F1-iINEPT spectra display double–doublet coupling patterns along the F1 dimension for each individual H_A or H_B cross-peaks, which initially would consist of eight different components as shown in Fig. 17C. Analyzing only the H_A spin will show an anti-phase doublet pattern with respect to $^1J(CH_A)$ (sine modulated) and an additional IP doublet pattern with respect to $^1J(CH_B)$ (cosine modulated) along the F1 dimension. As discussed before, the effect to apply a small flip angle ($\beta = 36°$) will generate a simplified four-component cross-peak with a characteristic E.COSY multiplet pattern due to the mutual $^2J(H_AH_B)$ (Fig. 17D), which facilitates both the multiplet interpretation and analysis. Thus, the active $^1J(CH_A)$ coupling is directly extracted from the antiphase 1:−1 pattern along the same row in F1, whereas the passive $^1J(CH_B)$

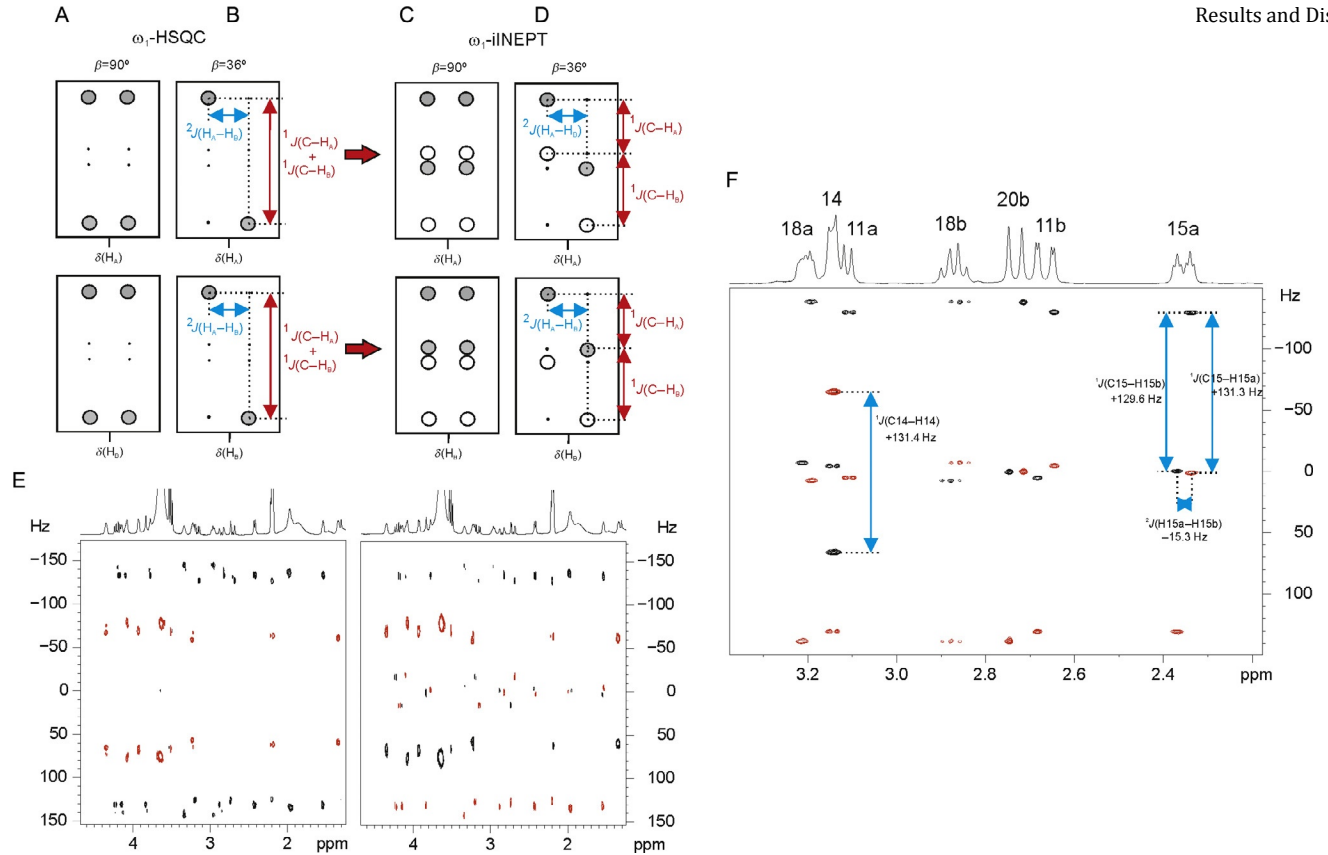

Figure 17 Schematic representation of the 2D multiplet pattern of each individual H_A and H_B proton belonging to a methylene CH_AH_B group. (A,B) ^{1}H-Boltzmann polarization driven (F1-HSQC) experiments using $\beta = 90°$ and 36°, respectively, and (C,D) ^{13}C-Boltzmann polarization driven experiments (F1-iINEPT) using $\beta = 90°$ and 36°, respectively. In (D), the magnitude and the sign of all involved couplings (defined as $^2J(H_AH_B)$ and assuming that $^1J(CH_A) < {}^1J(CH_B)$) can be readily extracted. Open and dotted circles represent peaks with opposite phase. (E) Comparison between the BIRD-HSQC and iINEPT *J*-resolved spectra of a sample of (**1**) in PMMA/$CDCl_3$. Note the appearance of the central lines for all diastereotopic CH_2 protons. (F) 2D ^{1}H–^{13}C F1-iINEPT-*J* spectra of (**1**) in $CDCl_3$ (scaling factor $k = 1$ and omission of the ^{13}C chemical shift t_1 evolution period). *Adapted from Ref. [137].*

coupling can be also extracted directly by measuring the IP components in each part of the E.COSY pattern. Otherwise, the sign and the magnitude of ^{2}J(HH) are easily extracted from the frequency separation between tilted peaks along the F2 dimension (Fig. 17F). For CH groups, a doublet with relative 1:−1 intensities is obtained whereas a 1:1:−1:−1 coupling pattern is displayed for a CH_3 group. A related HSQC sequence using a refocused INEPT as a preparation period has been also published providing a 1:3:3:1 quartet for AX_3 spin system and a 1:2:1 triplet for AX_2. Experimental results are illustrated for NH_2 and NH_3^+ groups in ^{15}N-labeled proteins [138]. The success of the method has been demonstrated for the measurement of small ^{1}D(CH) and ^{2}D(HH) values of **1** in PMMA/$CDCl_3$ (Fig. 17E). Of the five diastereotopic CH_2 groups, three have negative ^{2}D(HH) values (^{2}D(H11a–H11b) = − 12.5 Hz, ^{2}D(H20a–H20b) = − 20.1 Hz, and ^{2}D(H23a–H23b) = − 16.2), whereas two are positive (^{2}D(H15a–H15b) = + 13.2 Hz and ^{2}D(H18a–H18b) = + 8.9 Hz), clearly evidencing their relative orientation with respect to the molecular tensor and the magnetic field. Similarly, ^{1}J(CH) provides distinctive results between diastereotopic protons (^{1}D(C11–H11a) = + 7.7 Hz vs. ^{1}D(C11–H11b) = − 18.2 Hz, and ^{1}D(C23–H23a) = + 3.4 Hz vs. ^{1}D(C23–H23b) = − 25.5 Hz).

Pure shift versions of the F1-HSQC and F1-iINEPT experiments have not been published but they are easy to design and implement with the aim to achieve automated peak picking and automated extraction of ^{1}J(CH) and ^{2}J(HH) coupling constants.

5.3. Strong Coupling Effects in HSQC Experiments

It has been recognized that strong J(HH) coupling effects can introduce severe systematic errors in the measurement of ^{1}J(CH) from F2-coupled HSQC spectra because a certain degree of asymmetry between the high- and low-field multiplet lines can be introduced. This is due to changes in the resonance frequency and relative intensities, line shapes, and/or phases of cross-peaks. Freedberg and coworkers have demonstrated by product operator formalism and spectral simulations that these effects can be present either in the direct or in the indirect dimension of an HSQC spectrum [139]. They reported errors by up to 4 Hz when comparing experimental ^{1}J(CH) measured from the F1 and F2 dimensions of HSQC spectra. In addition, strong discrepancies up to 7 Hz were found between values measured in the ^{1}H dimension versus those in the ^{13}C dimension. However, from an experimental point of view, the use of this strategy based on spectral

simulations and fitting can become time-consuming, and the requirement for individual simulations for each particular case severely limits its widespread use, particularly when applied to the measurement of RDCs.

To avoid a direct measurement by determining frequency differences, a ^1J(CH)-modulated constant-time INEPT CT-HSQC (CTi-CT-HSQC) method has been proposed to measure experimentally accurate ^1J(CH)/^1D(CH) in the presence of strong J(HH) coupling effects [140]. This method avoids the phase distortions of the signals of interest or the presence of spurious peaks due to strong coupling, and also improves the analysis of the multiplet structure in broad or complex signals or when large contributions of RDCs can generate poorly defined multiplets that difficult accurate measurements.

The originality of the method relies in a CT-INEPT transfer module with a constant duration of Δ, where the 180° ^{13}C pulse is moved away from the central 180° ^{1}H pulse for a period τ. Thus, ^1J(CH) evolves only during a $(\Delta - 2\tau)$ period. Signal intensity during the INEPT element depends on three variables: $T_2(^1\text{H})$ relaxation times, ^1J(CH), and J(HH) modulations. Thus, recording multiple datasets with different τ optimizations, a pure signal intensity dependence with respect to $\sin^2(\pi J(\text{CH})(\Delta - 2\tau))$ is obtained keeping the relaxation effects and the J(HH) modulation during the overall period Δ independent of τ for all data. It has been shown that the fitting of the J-modulation curve yields accurate ^1J(CH) values with minimum deviations due to strong J(HH) coupling interference. Experimentally, the major inconvenience is the requirement for a collection of multiple 2D J-modulated data that means large experimental times [114].

6. HSQMBC EXPERIMENTS FOR MEASURING ^nJ(CH)

The measurement of ^nJ(CH) in small molecules at the natural abundance has been another hot topic of interest in small molecule NMR. [141] A comprehensive overview on the different NMR methods and applications to structural, configurational, and conformational studies appeared in the last decade has been recently published [142]. Most of these available long-range methods rely on the basic HMQC and HSQC pulse schemes where the interpulse delay is optimized to a ^nJ(CH) value instead of the original ^1J(CH), or on related hybrid HSQC-TOCSY experiments with a limited application to protonated carbons. Figure 18 shows different spin topologies defining the transfer mechanism followed in HSQC/HSQMBC-based experiments designed to measure J(CH). The HMBC experiment

[143–145] usually gives better sensitivity ratios but, in many cases, the equivalent HSQMBC is the preferred technique because it generally affords a better performance in terms of simplicity, peak phase behavior, and pulse sequence analysis.

The basic HSQC pulse train can be easily tuned to detect and measure quantitatively long-range proton–carbon interactions, which typically are in the range of 0–15 Hz in magnitude. In its basic form, the only requirement is the re-optimization of the interpulse Δ delay to a small coupling value, about typically 6–10 Hz. Under these conditions, the undesired effects of J(HH) evolution during the long INEPT periods (typically about 50–80 ms) become very important because the magnitude of J(HH) and ^{n}J(CH) coupling values is similar in size. The HSQMBC experiment has been traditionally used in a non-refocused mode [16]. This minimizes losses by T_2 relaxation but multiplet patterns appear strongly phase distorted because of the AP character with respect to ^{n}J(CH) and the mixed phase due to the effects of J(HH) modulation during the long INEPT period. In addition, cross-peak intensities strongly depend on the mismatch between this Δ optimization and the corresponding ^{n}J(CH) values and also of the potential losses by relaxation. The experimental result is the obtention of highly distorted cross-peaks with complex phase and variable intensities, even for some of the expected cross-peaks that can be missing in the final spectrum. The hard analysis of these complex multiplets has prevented its general use in a routine and easy task.

With the main objective to develop simpler methods, a suite of new HSQMBC pulse schemes have been proposed to measure ^{n}J(CH) in a more straightforward way, without need of sophisticated and time-consuming post-processing tasks [146,147]. These new selHSQMBC methods (Fig. 19) avoid all typical problems associated with accidental line cancelation or complex analysis of AP multiplets, work for both protonated and non-protonated carbons, and the measurement is performed along the detected F2 dimension where resolution is not critical and therefore the number of required t_1 increments is only dependent on signal congestion in the ^{13}C dimension. The selHSQMBC experiment is basically a standard HSQC pulse train in which the central hard 180° ^{1}H pulse in the INEPT periods has been replaced by frequency-selective 180° ^{1}H pulses to prevent the undesired J(HH) coupling evolution, whereas selective heteronuclear polarization transfer for the selected protons is achieved. The main limitation of these experiments relies on the selective concept because not all the protons can be simultaneously excited/observed or decoupled/unmodulated at

the same time and several experiments may be needed to measure all the targeted couplings. However, multiple protons can be simultaneously studied in a single experiment using region-selective or multiple frequency-selective pulses, provided that all excited protons are not mutually *J*-coupled.

6.1. CLIP-HSQMBC

The basic selHSQMBC experiment is the 2D CLean In-Phase HSQMBC (CLIP-HSQMBC)] [148] (Fig. 19A) that yields undistorted IP ^{1}H multiplets with pure absorptive line shapes along the detected dimension from which the easy, direct, and accurate measurement of ^{n}J(CH) can be performed. The resulting cross-peaks show an additional splitting compared to the conventional ^{1}H multiplet arising from the active proton–carbon coupling because proton acquisition is performed without heteronuclear decoupling. As discussed before for other CLIP experiments, the key point of this sequence is the 90° ^{13}C pulse applied just prior to acquisition, which efficiently converts the existing dispersive AP contribution to non-observable multiple-quantum coherences. Figure 20 clearly shows that for simple and well-resolved multiplets, the magnitude of ^{n}J(CH) can be extracted directly by analyzing peak frequency separation as usually made for conventional ^{1}H multiplets. The phase properties of the multiplet and therefore the accurate extraction of ^{n}J(CH) are independent of experiment optimization, with a small uncertainty of 0.1–0.2 Hz, but important errors of 20–30% should be easily introduced when omitting the CLIP pulse. In practice, a perfect match between ^{n}J(CH) and the experiment optimization is not critical, cross-peaks show a clear dependence with the $\sin^2(\pi^{n}J(\mathrm{CH})\Delta)$ function, and ^{n}J(CH) values in the range 3–10 Hz can be measured in a 6–8 Hz optimized selHSQMBC experiment.

For more complex multiplets, the separation of the outer peaks of the multiplet can be compared to that in the ^{1}H spectrum to indirectly extract the additional splitting or, alternatively, a simple fitting procedure taking the internal satellite ^{1}J(CH) component as decoupled reference multiplet can be applied. On the other hand, a double-selective 1D version of a refocused HSQMBC experiment has been also proposed for the fast and accurate measurement of specific ^{n}J(CH) values from pure IP 1D multiplets [149].

6.2. selHSQMBC-IPAP

A powerful alternative for the simple and direct of ^{n}J(CH) in broad, unresolved, or highly selHSQMBC multiplets is based on the incorporation of

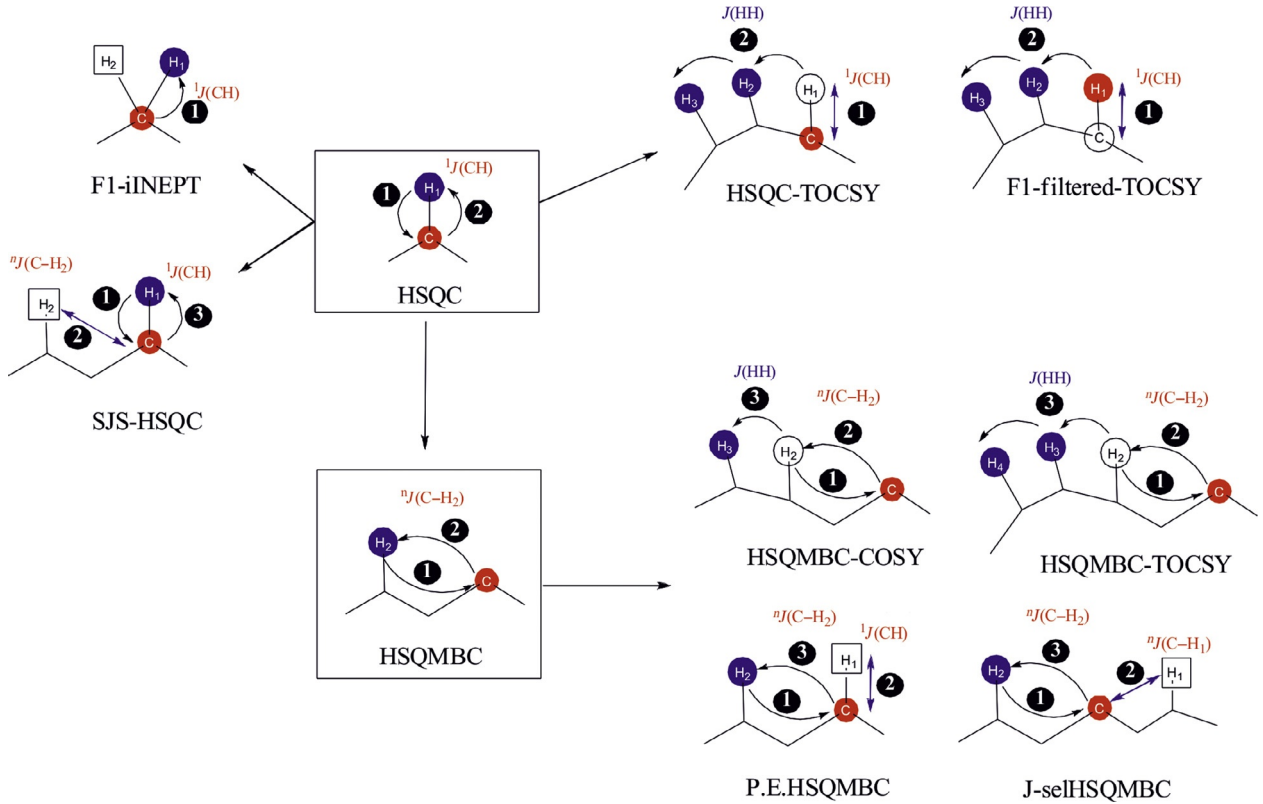

Figure 18 Schematic representation of several spin systems and NMR experiment names that can be studied by HSQC and HSQMBC type experiments.

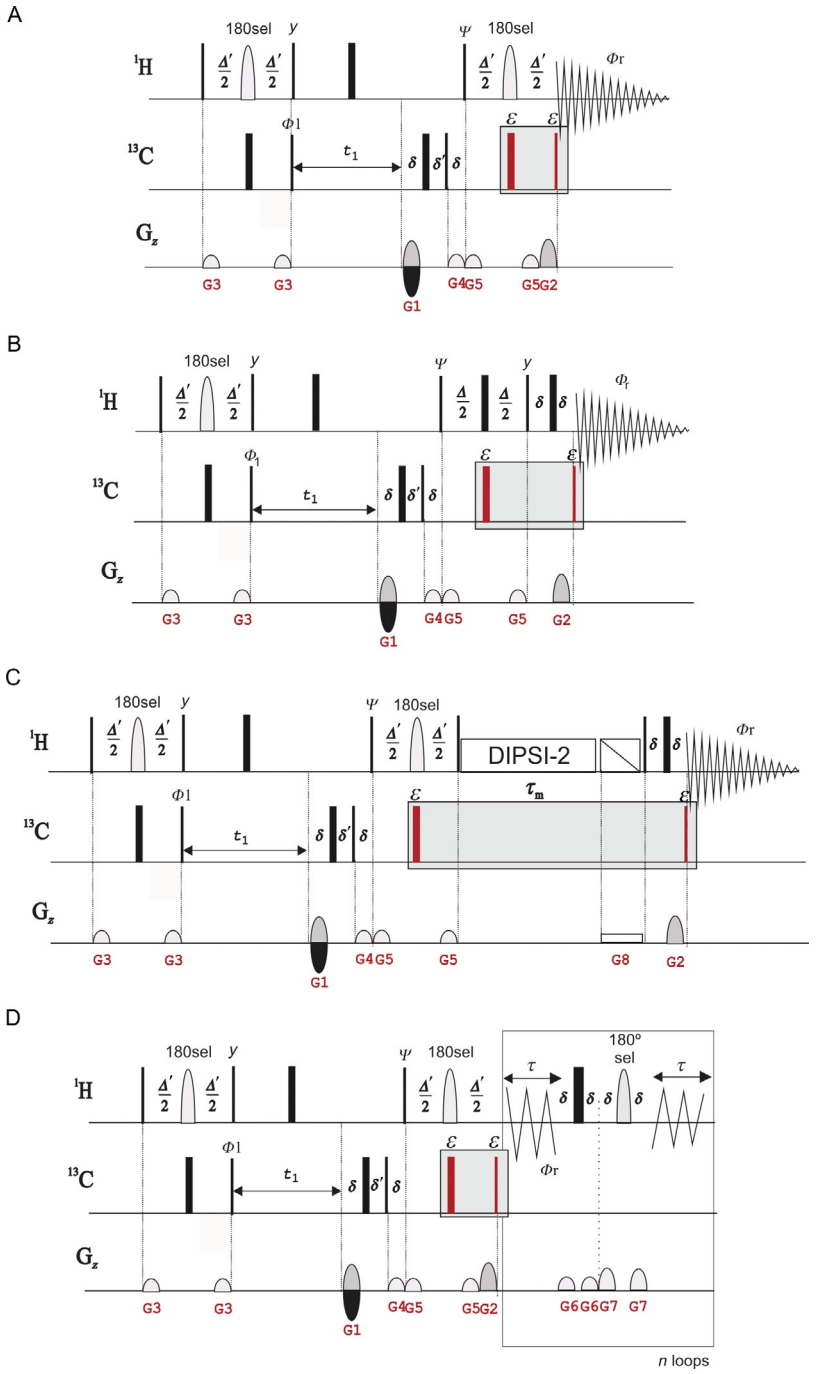

Figure 19 See legend on next page.

the IPAP principle (selHSQMBC-IPAP) that relies on the separate acquisition of complementary IP and AP datasets [150,151]. The IP data are generated as described for the CLIP-HSQMBC experiment ($\Psi = y$ and $\varepsilon =$ on), whereas the AP data (with a $\sin(\pi {}^{n}J(\mathrm{CH})\Delta)$ signal intensity dependence) are obtained using the same scheme with $\Psi = x$ and omitting the last 180° and 90° ^{13}C pulses to avoid ${}^{n}J(\mathrm{CH})$ refocusing ($\varepsilon =$ off). Time-domain data combination (IP ± AP) affords two separate pure-phase α− and β-selHSQMBC subspectra where the ${}^{n}J(\mathrm{CH})$ value can be extracted by direct analysis of the relative frequency displacement between these α/β cross-peaks along the highly resolved F2 dimension. Figure 21 summarizes this protocol for the broad pseudo-triple H22 proton of **1**. Accurate ${}^{n}J(\mathrm{CH})$ values can be easily extracted, irrespective of the multiplet complexity and avoiding the typical overestimation associated to the direct analysis of AP signals or the lack of multiplet definition in IP signals.

The success of the IPAP technique relies on the complementarity between the IP and AP data, and the percentage of undesired cross-talk generated during IP±AP data combination will be proportional to a $\sin^2(\pi {}^{n}J(\mathrm{CH})\Delta)$-$\sin(\pi {}^{n}J(\mathrm{CH})\Delta)$ factor. The use of individualized scaling factor (AP ± k*IP) factors can compensate unbalanced IPAP cross-peaks. As a

Figure 19—Cont'd Several ^{1}H-selective 2D HSQMBC schemes designed to measure long-range proton–carbon coupling constants: (A) selHSQMBC, (B) selHSQMBC-COSY, (C) selHSQMBC-TOCSY, and (D) HOBS-selHSQMBC experiments. Frequency-selective 180° ^{1}H pulses represented as shaped pulses are applied in the middle of the INEPT blocks ($\Delta = 1/(2*{}^{n}J(\mathrm{CH})) = \Delta'$+p180 where p180 is the duration of the selective 180° ^{1}H pulse that must be set accordingly to the required selectivity in each case). ^{1}H data are acquired without ^{13}C decoupling. CLIP versions of the experiments are obtained using ($\Psi = y$ and $\varepsilon =$ on). Alternatively, the IPAP methodology can be applied: Two independent IP and AP data are separately collected as a function of the pulses marked with ε: IP ($\Psi = y$ and $\varepsilon =$ on) and AP ($\Psi = x$ and $\varepsilon =$ off). α/β data are obtained after time-domain addition/subtraction data (AP ± IP). A minimum two-step phase cycle was applied: $\phi_1 = x,-x$ and $\phi_{rec} = x,-x$, all other unlabeled pulses are from the x-axis. In (A–C) gradients G1 and G2 are used for coherence selection using echo–antiecho, G4 acts as a zz-filter, G3 and G5 flank the inversion proton pulses to generate pure refocusing elements and G8 is simultaneously applied to a and adiabatic CHIRP pulse to remove undesired ZQ contributions. In (D), the selective 180° ^{1}H pulse applied at the middle of INEPT periods and during detection have the same shape and duration and we found that REBURP pulses in the order of 3–7.5 ms provides the best result as a function of the required selectivity. Homonuclear decoupling during the acquisition time (AQ) is performed using a refocusing blocks including a pair of hard/selective 180°^{1}H pulses flanked with gradient G6 and G7 and applied at intervals of $2\tau =$ AQ/n, where n is the number of loops.

bonus, the IPAP methodology offers additional controls to confirm the accuracy of the measurement or the presence of cross-talking. Three different multiplets (IP, AP, and α/β) are available for independent measurements and proper data comparison and validation.

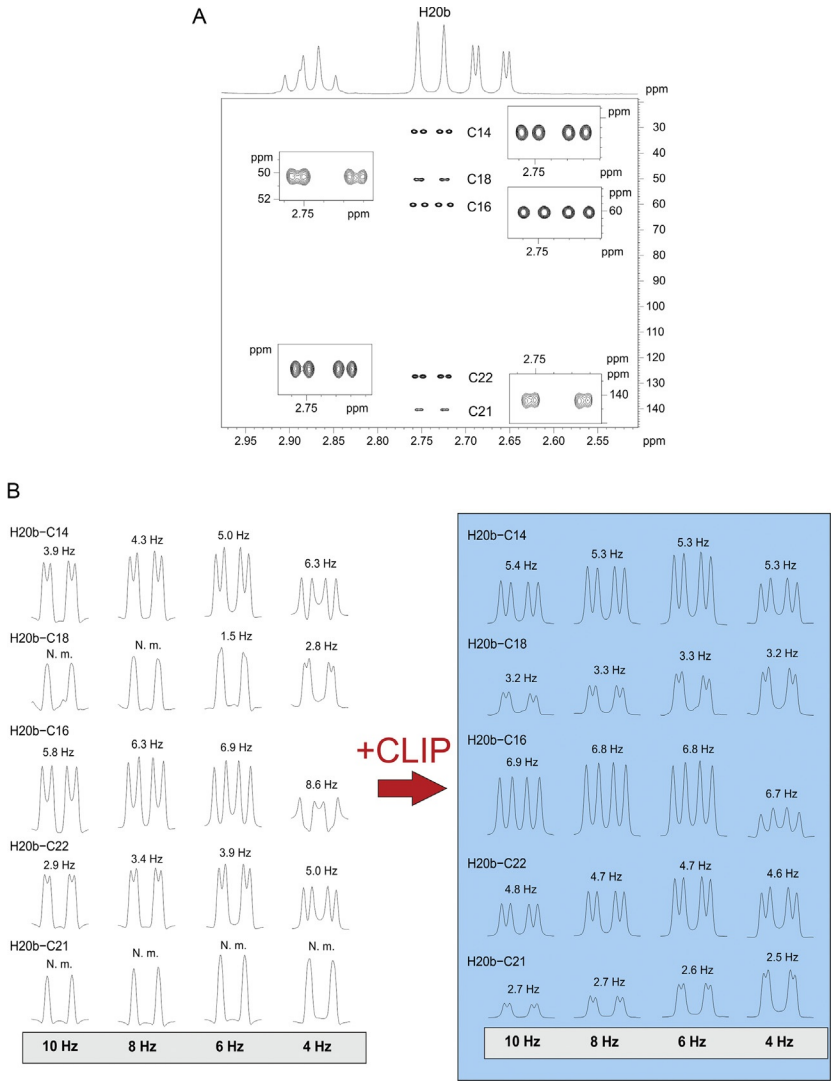

Figure 20 (A) 2D CLIP-selHSQMBC spectrum after selective excitation of the H-20b proton of (**1**). (B) Direct extraction ^{n}J(CH) can be made from pure in-phase cross-peaks, independent of experiment optimization (from 4 to 10 Hz). *Adapted from Ref. [148].*

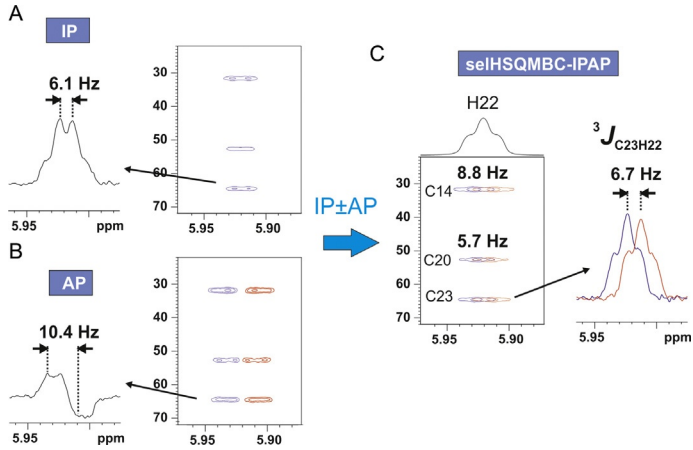

Figure 21 selHSQMBC-IPAP experiments after selective excitation of the olefinic H-22 proton in **1**: The acquired (A) IP and (B) AP datasets are added/subtracted to provide (C) separate α/β subspectra. The relative displacement between α/β cross-peaks along the F2 dimension provides a direct measurement of ^nJ(CH) without any posterior analysis. *Adapted from Ref. [142].*

6.3. selHSQMBC-TOCSY

An enhanced CLIP-selHSQMBC-TOCSY experiment [148] has been proposed where an appended TOCSY period consisting of a DIPSI mixing element included into a ZQF [112] is inserted just prior to acquisition (Fig. 19C). The method expands and improves the features of the original selHSQMBC experiment because it uses a sequential transfer mechanism based on a dual step via $^nJ(CH_1)+J(H_1H_2)$. Thus, starting from a selected H1 proton, a relayed C-H2 cross-peak can be observed with an intensity independent to its $^nJ(CH_2)$ coupling value. Due to the IP nature of the TOCSY transfer, the resulting cross-peaks will also show IP multiplet patterns from which small ^nJ(CH) values could be determined. A simple comparison between selHSQMBC and selHSQMBC-TOCSY spectra acquired under the same experimental conditions (Fig. 22) reveals a major number of cross-peaks to be analyzed from a single experiment, even for those signals appearing in overlapped regions where selective irradiation should not be feasible.

The IPAP technique can be also implemented to yield a robust selHSQMBC-TOCSY-IPAP experiment to determine coupling values smaller than the linewidth [152]. As a major enhancement, the method allows additionally the easy and direct determination of the relative sign

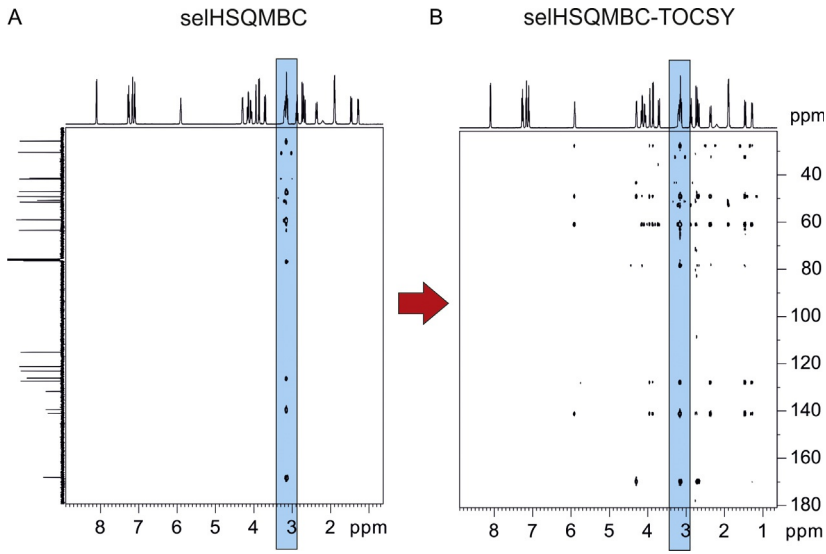

Figure 22 Comparison between a (A) 2D selHSQMBC and (B) selHSQMBC-TOCSY spectra of (**1**) after selective refocusing of the three overlapped protons (H14, H11a, and H18a) resonating at 3.15 ppm. The mixing time in TOCSY was of 60 ms. *Adapted from Ref. [142].*

of ^{n}J(CH) by analyzing the relative left–right or right–left displacement of α/β multiplets, avoiding any complex and time-consuming fitting procedure. The extraction of relative signs is only applicable when signals from the same row are compared (the same carbon) but not for peaks of the same column but different rows (different carbons). Figure 23 demonstrates the powerful of the selHSQMBC-TOCSY-IPAP experiment by analyzing the 1D traces from the carbonyl C10 carbon. Large negative values are revealed for H11a and H11b protons (−6.3 and −7.9 Hz, respectively) and a small positive value for H12 (+2.0 Hz). On the other hand, the olefinic C21 carbon at 140.5 ppm presents positive values for H13 (+7.6 Hz), H15b (+6.5 Hz) and H15a (+1.3 Hz) and negative values for the two-bond H14 (−5.8 Hz) and even for the tiny four-bond H16 (−1.0 Hz) correlations. In addition, the optimum performance to work with IP multiplets rather from AP multiplets is clearly evidenced by the better sensitivity of the IP multiplets and the important cancelation effects in AP multiplets, as shown for the H12 proton.

Related 1D versions of the selHSQMBC-TOCSY experiment have been published to measure the sign and the magnitude of heteronuclear coupling constants in other nuclei than ^{13}C in a very fast and efficient way [153].

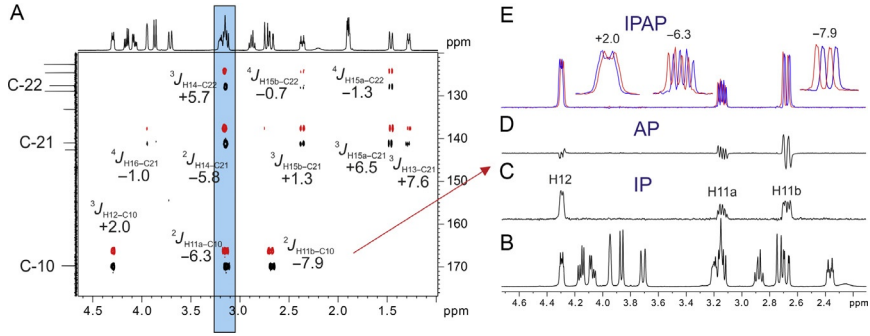

Figure 23 (A) Expanded area corresponding of the 2D selHSQMBC-TOCSY-IPAP spectra of (**1**). (B) Conventional 1D ^{1}H NMR spectrum and (C–E) 1D slices extracted at the C10 frequency showing the excellent pure-phase properties of (C) IP, (D) AP, and (E) overlayed α/β data. *Adapted from Ref. [152].*

Two different approaches have been reported: (i) the Up&Down technique relies on the direct analysis of antiphase multiplets whereas (ii) the Left&Right technique is based on the relative displacement between separate IPAP components. Examples are provided for high-abundant (^{19}F and ^{31}P) and low-abundant (^{77}Se, ^{29}Si, and ^{119}Sn) heteronuclei demonstrating that small *J*(XH) couplings and their corresponding signs can be determined between remote spins separated for more than the conventional two- and three-bond connectivities.

6.4. selHSQMBC-COSY-IPAP

The IPAP methodology also works when two mutually *J*-coupled protons are simultaneously excited in selHSQMBC experiments. IP and AP data only differ in the application of ^{13}C pulses, and therefore, the resulting α/β cross-peaks present the same relative phase distortion because *J*(HH) modulation does not affect the addition/subtraction procedure [154]. Based on this premise, a selHSQMBC-COSY-IPAP experiment has been derived by replacing the selective 180° ^{1}H pulse in the refocusing INEPT period by a hard 180° ^{1}H pulse (Fig. 19B) [155]. In this way, simultaneous *J*(HH) and ^{n}*J*(CH) evolution takes place during this period that generates COSY transfer when a last 90°(*y*) ^{1}H pulse is applied. The experiment retains the simplicity in both acquisition and processing steps and maintains the same overall duration of the original selHSQMBC experiment. Similarly as discussed by the TOCSY transfer, an increased number of coupling values with their corresponding signs can be measured. Although the mixed phases are present in the corresponding α- and β-COSY multiplets, this does not affect

the direct measurement because only the relative displacement between α/β signals is of interest. Very importantly, the sign of ^{n}J(CH) is also encoded as the relative left/right (negative) or right/left (positive) frequency peak displacement. Based on these fundamentals, broadband versions of the HMBC-IPAP and HSQMBC-IPAP experiments have been reported which do not require the use of selective pulses [156]. In addition, an excellent complementarity has been demonstrated between HMBC/HSQMBC and its counterparts HMBC-COSY/HSQMBC-COSY experiments which are designed by simply adding a 90° ^{1}H pulse at the end of the sequence. This complementarity can be an interesting alternative to other approaches to retrieve some missing cross-peaks, such as the use of different delay-optimized experiments or the use of accordion spectroscopy.

6.5. HOBS-selHSQMBC

The incorporation of broadband homodecoupling in experiments detecting antiphase HH magnetization components, like the regular COSY, HMBC, or HSQMBC experiments, fails because multiplet components should be partially or fully canceled. However, the excellent IP nature demonstrated for the selHSQMBC experiment allows that homonuclear and/or heteronuclear decoupling can be implemented along the detected dimension using the HOBS technique (see Section 4.2), obtaining simplified cross-peaks without their characteristic fine J multiplet structure. Figure 19D shows the ^{1}H-homodecoupled band-selective HSQMBC (HOBS-selHSQMBC) pulse scheme, which represents a new way to measure ^{n}J(CH) from the simplified IP doublets generated along the detected dimension [157]. The selective 180° pulses applied in the INEPT and during detection have the same shape and duration, minimizing the requirements for additional experimental setup. Thus, all protons selected by the region-selective 180° ^{1}H pulse appear homodecoupled from all other protons that do not experience this pulse, and the result is a band-selective homodecoupled observation of a specific region of the ^{1}H spectrum. Figure 24 compares the band-selective CLIP-HSQMBC versus CLIP-HOBS-selHSQMBC spectra of cyclosporine after applying a 5 ms REBURP 180° pulse on the H_α proton region. It can be observed how the ^{1}H–^{1}H J multiplet structures of all H_α resonances along the detected dimension are collapsed because of the effective homodecoupling of H_α–NH and H_α–H_β coupling constants, affording enhanced resolution and improved sensitivity as shown from the 1D slices.

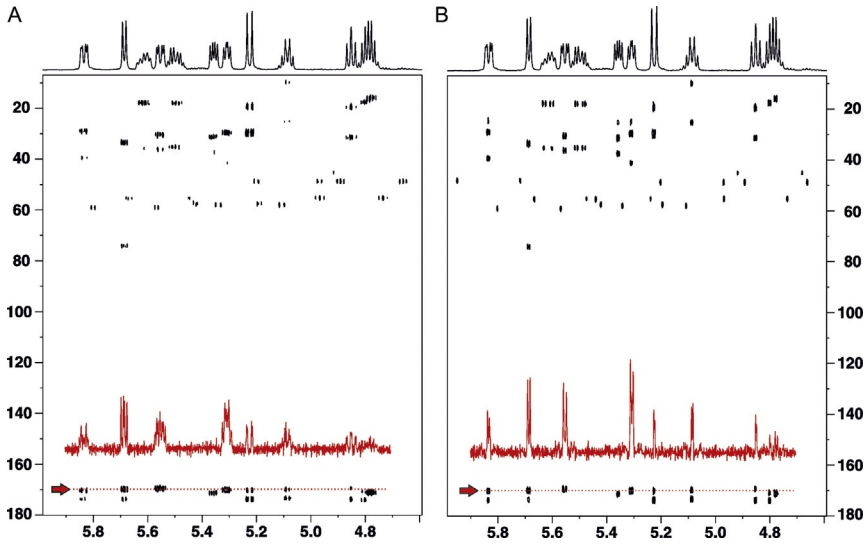

Figure 24 (A) Conventional band-selective HSQMBC and (B) HOBS-selHSQMBC spectra of (**2**) acquired under the same experimental conditions. A selected 1D slice is plotted for each spectrum at the same absolute scale to compare the relative sensitivity and resolution achieved in the 2D spectra. *Adapted from Ref. [157].*

A detailed inspection shows that HOBS-HSQMBC cross-peaks are simplified to IP doublets due to the active ^{n}J(CH) coupling (Fig. 25). The direct and semi-automated extraction of the ^{n}J(CH) can be made by direct analysis of cross-peaks if the multiplet is resolved enough. In cases of poor resolved multiplets or when the accuracy of the measurements may be doubtful, the application of the IPAP methodology described above can offer a better solution. A perfect agreement between the ^{n}J(CH) values measured directly from the proposed HOBS and HOBS-IPAP methods with those extracted from selHSQMBC-TOCSY spectra has been reported.

The HOBS-selHSQMBC experiment is also compatible for broadband heteronuclear decoupling during acquisition. Figure 26 shows the substantial sensitivity and resolution enhancements achieved by sequential implementation of hetero- and homodecoupling in a regular selHSQMBC experiment. An average enhancement by factors of 1.2 (with heteronuclear decoupling), 1.6 (with homonuclear decoupling), and 2.4 (with both homo- and heteronuclear decoupling) when compared with fully coupled data (normalized average factor of 1) has been reported.

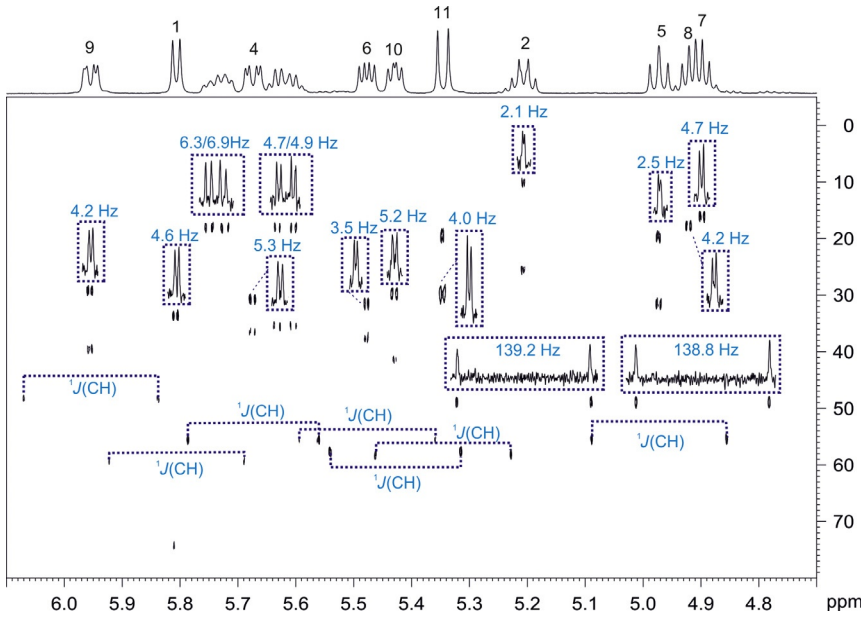

Figure 25 In-phase HOBS-selHSQMBC spectra of (**2**) showing how the value of *J*(CH) for all direct and long-range cross-peaks can be extracted directly from the analysis of the clean IP doublets along the detected dimension. *Adapted from Ref. [157].*

6.6. PIP-HSQMBC

A broadband Pure In-Phase HSQMBC (PIP-HSQMBC) experiment yielding pure IP multiplet patterns for all long-range cross-peaks has been recently reported (Fig. 27) [111]. It is an extension of the PIP-HSQC experiment described in Section 5.1.4, where the interference due to undesired *J*(HH) evolution during the longer heteronuclear transfer periods is more pronounced than the HSQC counterpart because the size of ^{n}J(CH) and *J*(HH) is of the same order. As largely reported for older HSQMBC experiments, the standard INEPT transfer can be replaced by other schemes such as INEPT-BIRD, CPMG, or CPMG-BIRD elements (Fig. 27B–D). In all these versions, pure IP multiplets would be obtained but with a different signal intensity dependence as a function of the chosen transfer element. As shown previously for PIP experiments, the key element is the adiabatic *z*-filter that removes any AP contribution due to *J*(HH) and unmatched ^{n}J(CH) couplings evolution. The importance of the adiabatic z-filter is illustrated with the superior performance of the 8-Hz PIP module over conventional, CLIP, and z-filtered HSQMBC experiments acquired under the

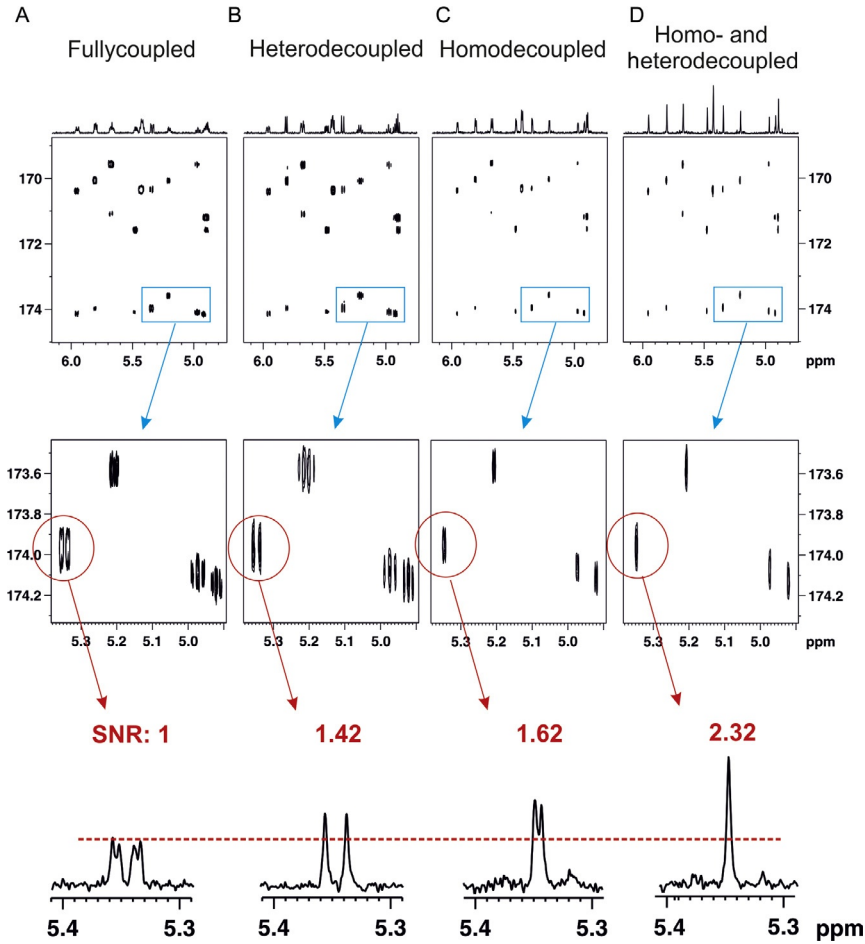

Figure 26 Resolution enhancement effects after incorporation of homo or/and heteronuclear decoupling in $^{1}H_{\alpha}$–^{13}CO HSQMBC spectra (2): (A) Conventional; (B) broadband ^{13}C-decoupled, (C) HOBS-selHSQMBC, and (D) broadband ^{13}C-decoupled HOBS-selHSQMBC. At the bottom, 1D slices showing the experimental SNR and multiplet simplification. *Adapted from Ref. [157].*

same conditions (Fig. 28). Note that dispersive components are observed in all cases rendering complicated the cross-peak analysis, except in the PIP-HSQMBC trace where pure IP pattern are observed for all signals.

Analysis of some selected 1D traces in the PIP-HSQMBC spectrum of strychnine reveals that all cross-peaks display a clean IP character (Fig. 29B). For instance, all PIP-HSQMBC cross-peaks belonging to the H8 and H20a protons show well-resolved multiplets (Fig. 29C) that allow direct and easy

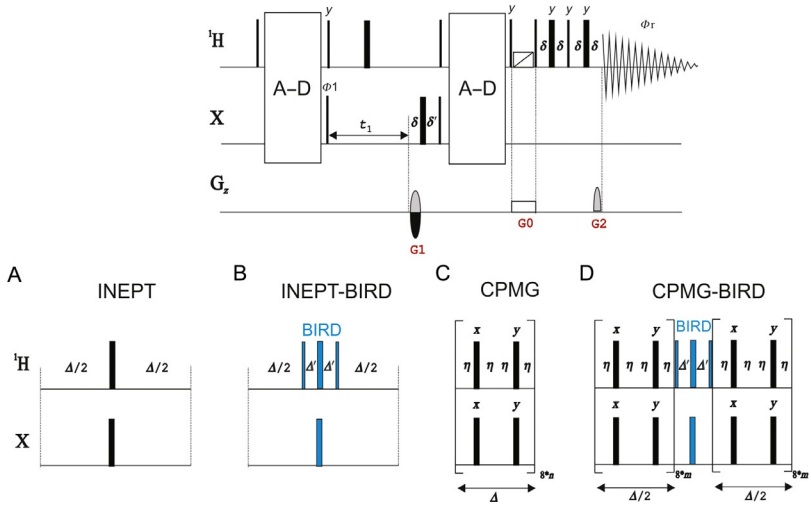

Figure 27 Basic pulse schemes to collect PIP-HSQMBC spectra. Several modules can be used for heteronuclear transfer elements ($\Delta = 1/[2{*}^{n}J(\mathrm{CH})]$): (A) the basic INEPT; (B) the INEPT-BIRD block ($\Delta' = 1/[2{*}^{1}J(\mathrm{CH})]$); (C) the CPMG XY-16 super cycle consisting of simultaneous ^{1}H and ^{13}C pulses applied at intervals 2η; and (D) the CPMG-BIRD element. All these variants use the same scheme with an adiabatic z-filter after the refocusing period and just before the refocusing gradient echo and the acquisition.

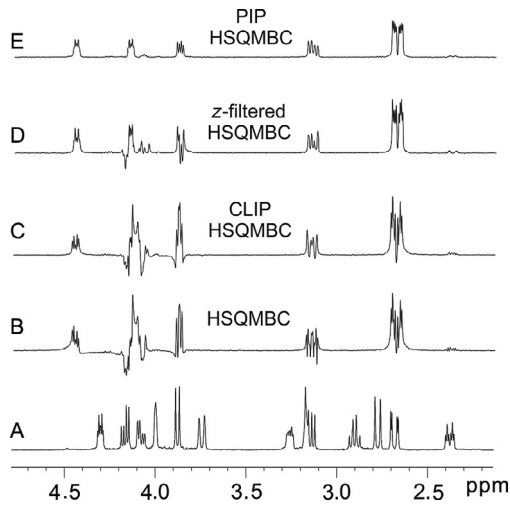

Figure 28 (A) ^{1}H NMR spectrum of (**1**); (B–E) 1D traces extracted at the C12 of (**1**) in 8-Hz optimized (B) HSQMBC, (C) CLIP-HSQMBC, (D) *z*-filtered HSQMBC, and (E) PIP-HSQMBC spectra. *Adapted from Ref. [111].*

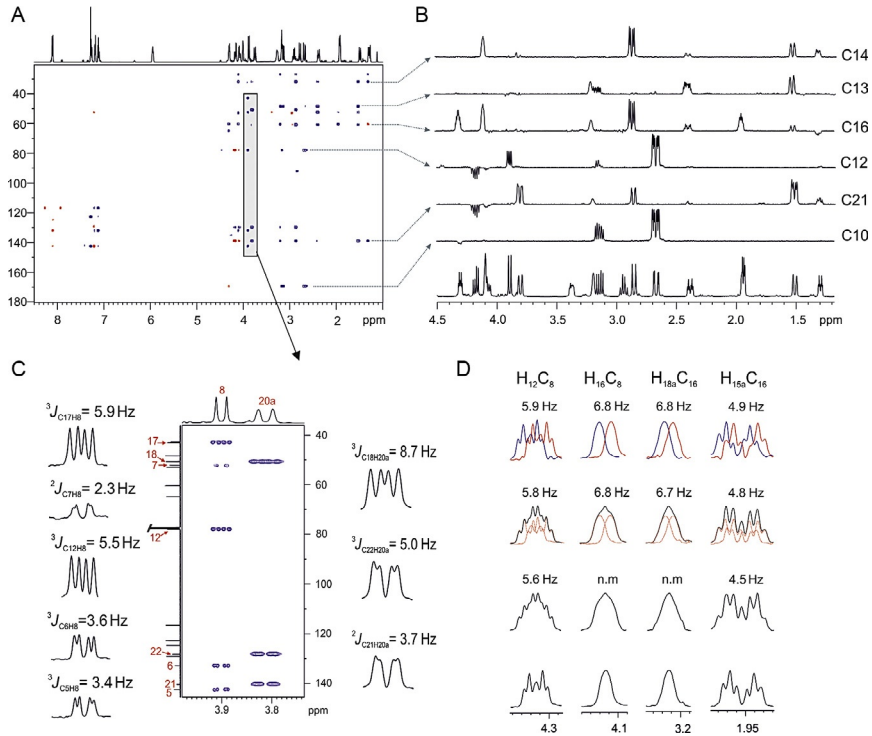

Figure 29 (A) 8-Hz optimized PIP-HSQMBC spectrum of (**1**); (B) 1D row slices taken at different ^{13}C frequencies showing in-phase multiplet patterns for all observed cross-peaks; (C) Expanded area showing how the magnitude of $^nJ(CH)$ can be easily determined from direct analysis of undistorted and resolved IP peaks. (D) Comparison of several methods for the extraction of $^nJ(CH)$ values in non-resolved or complex PIP-HSQMBC multiplets: (from bottom to top) multiplets obtained with and without ^{13}C decoupling during acquisition; fitting process performed from the decoupled multiplets in (A) to match the experimental coupled multiplets in (B); overlaid α and β multiplets obtained after IP ± AP data combination in a HSQMBC-IPAP experiment, respectively. *Adapted from Ref. [111].*

measurements of $^nJ(CH)$ values up to 2–3 Hz. Doublets in the conventional ^1H spectrum for these protons are converted to IP double of doublets for the corresponding HSQMBC cross-peaks. As discussed previously, the extraction of $^nJ(CH)$ in more complex or non-resolved multiplets becomes more complicated but it can be performed (i) by measuring overall multiplet widths, (ii) fitting/matching them to an external reference cross-peak obtained from the same sequence with broadband ^{13}C-decoupling during acquisition, (iii) from the internal satellite lines corresponding to the direct $^1J(CH)$ responses, if available, without need to acquire a second reference spectrum,

or (iv) by implementing the IPAP technique. Figure 29D shows some examples to measure ^{n}J(CH) by using the coupled/decoupled fitting or the IPAP approach. The performance of the PIP-HSQC and PIP-HSQMBC methods has been also verified for the efficient measurement of RDCs under anisotropic conditions.

6.7. Simultaneous Measurement of Multiple Coupling Constants

The selHSQMBC pulse scheme has also been modified to allow the simultaneous measurement of multiple homo- and heteronuclear coupling constants from a single 2D cross-peak, thanks to the complementarity between the E.COSY and the IPAP principles. In the P.E.HSQMBC experiment, the sign and the magnitude of J(HH) can be measured along the direct dimension from the relative E.COSY-type multiplet pattern displacement due to the passive ^{1}J(CH) splitting generated in the indirect dimension [158]. On the other hand, the corresponding ^{n}J(CH) is independently determined in the detected dimension from the IPAP multiplet displacement. The sequence combines in a single experiment (a) the accurate measurement of ^{1}J(CH) along the indirect dimension described for F1-coupled HSQC schemes; (b) the sign-sensitive measurement of ^{1}J(CH) and ^{2}J(HH) in E.COSY multiplets similarly as reported in the P.E.HSQC experiment, and (c) the precise measurement of ^{n}J(CH) using the IPAP methodology. The P.E.HSQMBC sequence (Fig. 30) is basically a selHSQMBC applied on an H_A proton and signal intensity will depend on the $\sin^2(\pi^{n}J(CH_A)\Delta')$ function. As an essential feature, a ^{n}J(CH)-scaling BIRD element is applied during the evolution of the transverse ^{13}C magnetization and the last step a selective 90° pulses on H_A proton is employed to provide a characteristic E.COSY-like transfer.

In a similar way, a new *J*-selHSQMBC-IPAP experiment has been proposed for the independent measurement of two different long-range $^{n}J(CH_A)$ and $^{n}J(CH_B)$ coupling constants from the same 2D cross-peak [159]. In addition, the E.COSY pattern provides additional information about the magnitude and relative sign between $J(H_AH_B)$ and $^{n}J(CH_B)$ coupling constants. The sequence is a selHSQMBC applied on an H_A proton, and a selective inversion element on a different H_B proton is applied during the evolution of the transverse ^{13}C magnetization (Fig. 31). Thus, whereas ^{13}C chemical shift is encoded in the usual way during the t_1 period, signal is also modulated by a $\cos((\pi^{n}J(CH_B)kt_1)$ factor that will cause an IP splitting due to $k^{*n}J(CH_B)$ in the F1 dimension. Each correlation can also show an additional doublet with an apparent $k^{*}J(CH_B)$ splitting in the F1 dimension.

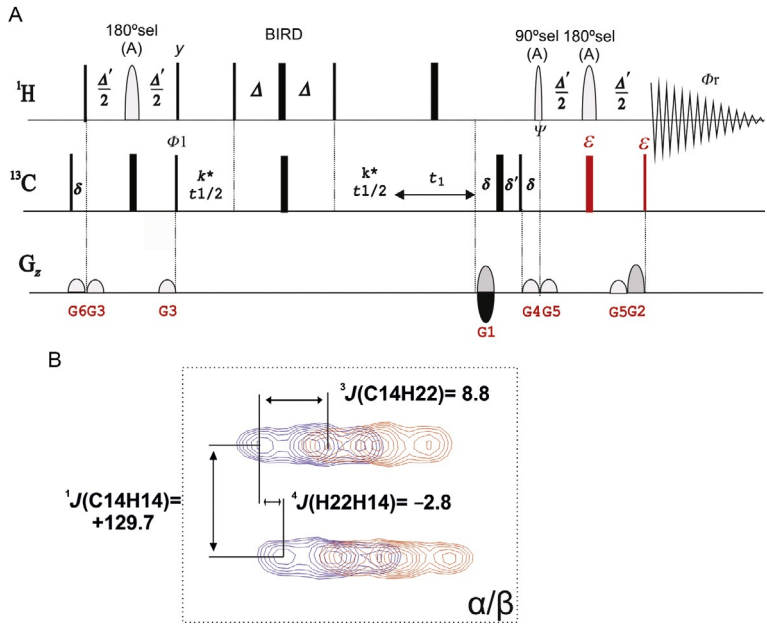

Figure 30 (A) Pulse scheme for the P.E.HSQMBC experiment. (B) Typical multiplet pattern of a P.E.HSQMBC cross-peak, where three couplings (^1J(CH), J(HH), and ^nJ(CH)) can be measured from a single cross-peak. General scheme of the IPAP procedure and the corresponding IP, AP, and α/β multiplet patterns obtained from this experiment. *Adapted from Ref. [158].*

Thus, two independent $^nJ(CH_A)$ and $^nJ(CH_B)$ coupling constants on the same carbon can be independently measured from the analysis of a single 2D cross-peak. Moreover, additional information about $J(H_AH_B)$ and the relative sign between $J(H_AH_B)$ and $^nJ(CH_B)$ can be also extracted from the E.COSY pattern generated by the passive H_B proton.

This same inversion element has also been implemented in a high-sensitive selective *J*-scaled sensitivity-improved HSQC (SJS-HSQC) experiment [160], which allows the simultaneous determination of the magnitude and sign of both $J(H_AH_B)$ and $^nJ(CH_B)$ in a CH_A HSQC cross-peak. The success of this experiment has been demonstrated by determining the relative configuration of the natural product 10-*epi*-8-deoxycumambrin B using long-range CH RDCs.

A suite of coupled/decoupled versions of fluorine-detected triple resonance $^{19}F–^{13}C\{^1H\}$ HSQMBC and HMBC spectra of fluorinated compounds to determine the size and the sign of *J*(CH), *J*(CF), and *J*(HF) coupling constants from E.COSY multiplet patterns has been also reported [161].

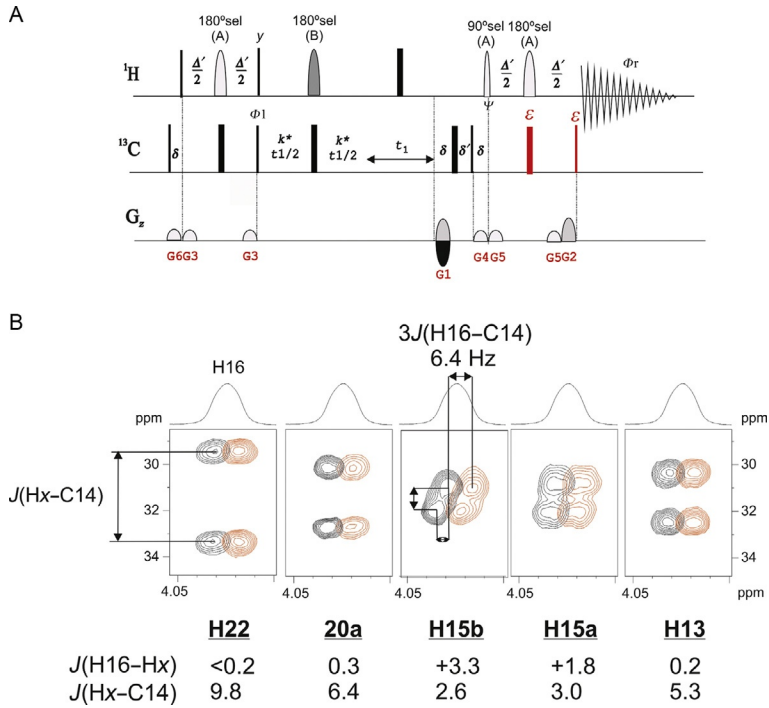

	H22	20a	H15b	H15a	H13
J(H16–H*x*)	<0.2	0.3	+3.3	+1.8	0.2
J(H*x*–C14)	9.8	6.4	2.6	3.0	5.3

Figure 31 (A) Pulse scheme for the J-selHSQMBC-IPAP experiment. (B) Several multiplet patterns corresponding to the H16–C14 cross-peak of (**1**) after selective excitation of a second proton. *Adapted from Ref. [159].*

7. OTHER METHODS

7.1. Quantitative HSQC

There is an enormous interest in the use of the HSQC experiment as a quantitative NMR tool and many different approaches have been proposed in the last years [162–169]. In conventional HSQC spectra, peak volumes of different protons are variably modulated as a function of each individual *J*(HH) coupling pattern. This non-uniform dependence causes a common source of error during integration and quantification of response intensities. In the perfect-HSQC experiment described in Section 5.1.2, there is a second and very significant positive consequence for removing *J*(HH) interferences: signal intensity is amplitude modulated only by the $\sin^2(\pi J(\mathrm{CH})\Delta)$ factor, and is therefore an excellent candidate to design future strategies for quantitative NMR studies. The proposed method is less aggressive than the use of

CPMG-INEPT blocks where a train of simultaneous $^{1}H/^{13}C$ pulses are applied at high repetition rates, and where the resulting peaks can include unwanted dependences from offset effects or the presence of TOCSY contributions as well as deleterious effects on sample heating under extreme fast-pulsing conditions.

To evaluate the ^{1}J(CH)-compensated intensity strategy based on the proper selection of multiple polarization transfer values, the perfect-HSQC spectrum of a spin system consisting of several protons having J(HH) in the extreme range between 10 and 30 Hz and ^{1}J(CH) ranging between 120 and 180 Hz has been simulated. From a single-Δ 140-Hz perfect-HSQC experiment, a pure IP spectrum with peak volume differences up to 25% is obtained (Fig. 32A). On the other hand, Fig. 32B shows the ^{1}J(CH)-compensated perfect-HSQC spectrum after combining four datasets acquired with Δ values of 2.94 ms (170 Hz), 2.86 ms (175 Hz), 2.86 ms (175 Hz), and 5.88 ms (85 Hz). Note that intensity differences below 2% are obtained in the complete ^{1}J(CH) range between 120 and 180 Hz.

7.2. LR-HSQMBC

HMBC and HSQMBC are traditionally used to trace out long-range proton–carbon correlations. Most of the observed cross-peaks correspond

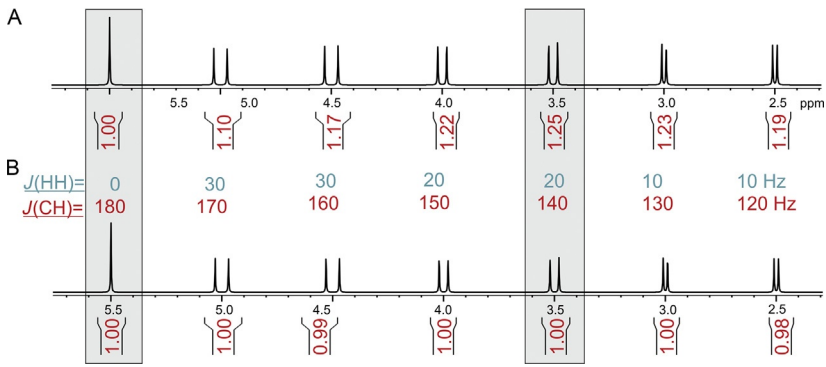

Figure 32 Spectral simulations showing integration ratios in heterodecoupled perfect-HSQC spectra: (A) optimized to a single Δ value of 3.6 ms, corresponding to 140 Hz; (B) average spectrum after combining four datasets acquired with Δ values of 2.94 ms (170 Hz), 2.86 ms (175 Hz), 2.86 ms (175 Hz), and 5.88 ms (85 Hz). The simulated protons have J(HH) and ^{1}J(CH) values in the range between 10–30 Hz and 120–180 Hz, respectively. Enhanced boxes compare signal intensity integration for two different protons. *Adapted from Ref. [95].*

to two- and three-bond away connectivities and attempt to use a 2- to 4-Hz optimized HMBC experiment to find longer correlations results in a considerable loss in sensitivity due to AP cancelation of responses. Classical alternatives such as HSQC-TOCSY or ADEQUATE experiments present some limitations for a widespread use. Thus, a long-range HSQMBC (LR-HSQMBC) experiment [170] has been proposed as a complement to the classical HMBC to overcome its typical $^{2,3}J$(CH) limitation, by extending the visualization of long-range correlation data to four-, five-, and even six-bond long-range ^{n}J(CH) heteronuclear couplings, in a similar way as achieved by 1,*n*-ADEQUATE experiments. This technique should prove to be an effective experiment to complement HMBC for testing the structure of proton-deficient molecules.

The pulse sequence itself is a refocused and heterodecoupled modification of the G-BIRD^{r,x}-HSQMBC pulse sequence optimized for the observation of very long-range correlations. Refocusing the desired ^{n}J(CH) magnetization after the t_1 evolution time provides two advantages. First, it generates IP ^{n}J(CH) correlations which avoid the AP cancelation of responses with very small coupling constants. Second, refocusing the heteronuclear coupling allows the application of ^{13}C decoupling during the acquisition time. This operation collapses the heteronuclear coupling of the response and partially recovers some of the SNR lost as a result of relaxation processes encountered during the long duration of the delays optimized for detection of very small ^{n}J(CH) couplings.

It has been reported that the 2-Hz optimized LR-HSQMBC experiment acquired a provided a major number of very long-range correlations than analogs HMBC and D-HMBC experiments. These data could be obtained in 2–3 h from a 4.9 mg sample of strychnine (10.5 μmol) dissolved in 40 μL of $CDCl_3$ in a 600-MHz spectrometer equipped with a 1.7-mm MicroCryoProbe. Data were also compared with an equivalent dual optimization inverted ^{1}J(CC) 1,*n*-ADEQUATE spectrum acquired in about 24 h [171]. In comparison, 29 of the ADEQUATE correlations were missing in the LR-HSQMBC data (23.6%), but additional 62 new correlations (50.4%) not observed in the inverted ^{1}J(CC) 1,*n*-ADEQUATE data were visualized in the LR-HSQMBC experiment. While drawing comparisons, the sole negative attribute of the LR-HSQMBC experiment relative to dual optimization inverted ^{1}J(CC) 1,*n*-ADEQUATE is that the former does not allow the unequivocal differentiation of ^{1}J(CC) from ^{n}J(CC) (^{2}J(CH) vs. ^{n}J(CH) where $n \geq 3$) afforded by the latter experiment [172–175].

The recently reported LR-HSQMBC experiment has been optimized for $^{1}H–^{15}N$ long-range heteronuclear couplings [176]. Several previously unreported four-bond correlations, consistent with the predicted by DFT calculations (0.2–0.3 Hz ^{4}J(NH) couplings), have been observed for strychnine using 2 Hz optimization of the LR-HSQMBC experiment. The $^{1}H–^{15}N$ LR-HSQMBC experiment affords a viable, high sensitivity alternative to HMBC and the accordion-optimized IMPEACH and CIGAR experiments when long-range correlations to nitrogen must be established for either small couplings or in proton-deficient molecules such as might be encountered in natural products or pharmaceuticals.

A triple-resonance 2D H(C)N experiment, referred to as HCNMBC [177], based on the sequential transfer mechanism via ^{1}J(CH)+J(NC) has been recently proposed as an alternative to $^{1}H–^{15}N$ HMBC or HSQMBC experiments to detect multiple-bond proton–nitrogen correlations. It has been shown that clean HCNMBC spectra despite the extremely low content of the isotopomers containing both ^{15}N and ^{13}C isotopes in the same molecule can be obtained if cryogenically cooled probes are available. Because of the similarity between ^{1}J(CN) and ^{2}J(CN) in a variety of nitrogen containing molecules, the experiment is not quite as straightforward to interpret as, for example, an 1,1-ADEQUATE.

8. CONCLUSION

Since its introduction 30 years ago, the HSQC pulse scheme has been modified in a large number of varieties and even now, the existing sequences can be improved in many different aspects. The last developments in HSQC and HSQMBC experiments have been described in this revision covering new NMR methodologies for a faster acquisition, more uniform response for a wide range of ^{1}J(CH) values, the obtention of pure IP undistorted multiplets or improved resolution and/or enhanced sensitivity achieved from broadband homodecoupled signals. It has also described a suite of robust NMR methods designed for the accurate quantitative determination of ^{1}J(CH) and small ^{n}J(CH) scalar and RDCs and also complementary tools to the current techniques that allow one to trace out ultralong range heteronuclear correlations among others. All these methods are a demonstration that the development of new pulse sequences is still a very active and attractive area of interest in the field of small molecule NMR.

ACKNOWLEDGMENTS

Financial support for this research provided by the Spanish MINECO (project CTQ2012-32436) is gratefully acknowledged. We also thank the Servei de Ressonància Magnètica Nuclear, Universitat Autònoma de Barcelona, for allocating instrument time to this project.

REFERENCES

[1] G. Bodenhausen, D.J. Ruben, Natural abundance nitrogen-15 NMR by enhanced heteronuclear spectroscopy, Chem. Phys. Lett. 69 (1980) 185–189.
[2] A. Bax, R. Griffey, B. Hawkins, Correlation of proton and nitrogen-15 chemical shifts by multiple quantum NMR, J. Magn. Reson. 55 (1983) 301–315.
[3] P.K. Mandal, A. Majumdar, A comprehensive discussion of HSQC and HMQC pulse sequences, Concepts Magn. Reson. 20A (2004) 1–23.
[4] T. Parella, Pulsed-field gradients: a new tool for routine NMR, Magn. Reson. Chem. 36 (1998) 467–495.
[5] W. Willker, D. Leibfritz, R. Kerssebaum, W. Bermel, Gradient selection in inverse heteronuclear correlation spectroscopy, Magn. Reson. Chem. 31 (1993) 287–292.
[6] L. Kay, P. Keifer, T. Saarinen, Pure absorption gradient enhanced heteronuclear single quantum correlation spectroscopy with improved sensitivity, J. Am. Chem. Soc. 114 (1992) 10663–10665.
[7] K. Pervushin, R. Riek, G. Wider, K. Wüthrich, Attenuated T_2 relaxation by mutual cancellation of dipole-dipole coupling and chemical shift anisotropy indicates an avenue to NMR structures of very large biological macromolecules in solution, Proc. Natl. Acad. Sci. U. S. A. 94 (1997) 12366–12371.
[8] I. Bertini, K.S. McGreevy, G. Parigi, NMR of Biomolecules: Towards Mechanistic Systems Biology, Wiley-VCH, Weinheim, 2012.
[9] T.F. Molinski, NMR of natural products at the nanomole-scale, Nat. Prod. Rep. 27 (2010) 321–329.
[10] Y. Liu, M.D. Green, R. Marques, T. Pereira, R. Helmy, R.T. Williamson, W. Bermel, G.E. Martin, Using pure shift HSQC to characterize microgram samples of drug Metabolites, Tetrahedron Lett. 55 (2014) 5450–5453.
[11] D.S. Dalisay, B.I. Morinaka, C.K. Skepper, T.F. Molinski, A tetrachloro polyketide hexahydro-^{1}H-isoindolone, muironolide A, from the marine sponge Phorbas sp. natural products at the nanomole scale, J. Am. Chem. Soc. 131 (2009) 7552–7553.
[12] R.D. Boyer, R. Johnson, K. Krishnamurthy, Compensation of refocusing inefficiency with synchronized inversion sweep (CRISIS) in multiplicity-edited HSQC, J. Magn. Reson. 165 (2003) 253–259.
[13] L. Lerner, A. Bax, Sensitivity-enhanced two-dimensional heteronuclear relayed coherence transfer NMR spectroscopy, J. Magn. Reson. 69 (1986) 375–380.
[14] J. Furrer, Recent developments in HMBC studies, Annu. Rep. NMR Spectrosc. 74 (2011) 293–354.
[15] W.F. Reynolds, D.C. Burns, Getting the most out of HSQC and HMBC spectra, Annu. Rep. NMR Spectrosc. 76 (2012) 1–21.
[16] R.T. Williamson, B.L. Márquez, W.H. Gerwick, K.E. Kövér, One- and two-dimensional gradient-selected HSQMBC NMR experiments for the efficient analysis of long-range heteronuclear coupling constants, Magn. Reson. Chem. 38 (2000) 265–273.
[17] B. Reif, M. Köck, R. Kerssebaum, J. Schleucher, C. Griesinger, Determination of ^{1}J, ^{2}J, and ^{3}J carbon–carbon coupling constants at natural abundance, J. Magn. Reson. B 112 (1996) 295–301.

[18] G.E. Martin, Using 1,1- and 1, n-ADEQUATE 2D NMR Data in structure elucidation protocols, Annu. Rep. NMR Spectrosc. 74 (2011) 215–291.
[19] I. Tvaroska, F.R. Taravel, One-bond carbon-proton coupling constants—angular-dependence in alpha-linked oligosaccharides, Carbohydr. Res. 221 (1991) 83–94.
[20] I. Tvaroska, F.R. Taravel, One-bond carbon-proton coupling constants—angular-dependence in beta-linked oligosaccharides, J. Biomol. NMR 2 (1992) 421–430.
[21] N.C. Maiti, Y.P. Zhu, I. Carmichael, V.E. Anderson, $^{1}J_{CH}$ correlates with alcohol hydrogen bond strength, J. Org. Chem. 71 (2006) 2878–2880.
[22] S. Uhrinova, D. Uhrin, T. Liptaj, J. Bella, J. Hirsch, Measurement of one-bond proton-carbon coupling constants of saccharides, Magn. Reson. Chem. 29 (1991) 912–922.
[23] C.M. Thiele, Use of RDCs in rigid organic compounds and some practical considerations concerning alignment media, Concepts Magn. Reson. Part A 30 (2007) 65–80.
[24] R.R. Gil, Constitutional, configurational, and conformational analysis of small organic molecules on the basis of NMR residual dipolar couplings, Angew. Chem. Int. Ed. 50 (2011) 7222–7224.
[25] C.M. Thiele, Residual dipolar couplings (RDCs) in organic structure determination, Eur. J. Org. Chem. 34 (2008) 5673–5685.
[26] G. Kummerlowe, B. Luy, Residual dipolar couplings as a tool in determining the structure of organic molecules, Trends Anal. Chem. 28 (2009) 483–493.
[27] G. Kummerlowe, B. Luy, Residual dipolar couplings for the configurational and conformational analysis of organic molecules, Annu. Rep. NMR Spectrosc. 68 (2009) 193–232.
[28] O.W. Sørensen, G.W. Eich, M.H. Levitt, G. Bodenhausen, R.R. Ernst, Product operator formalism for the description of NMR pulse experiments, Prog. NMR Spectrosc. 16 (1983) 163–192.
[29] P. Schanda, H. Van Melckebeke, B. Brutscher, Speeding up three-dimensional protein NMR experiments to a few minutes, J. Am. Chem. Soc. 128 (2006) 9042–9043.
[30] J. Farjon, J. Boisbouvier, P. Schanda, A. Pardi, J.P. Simorre, B. Brutscher, Longitudinal-relaxation-enhanced NMR experiments for the study of nucleic acids in solution, J. Am. Chem. Soc. 131 (2009) 8571–8577.
[31] D. Schulze-Sünninghausen, J. Becker, B. Luy, Rapid heteronuclear single quantum correlation NMR spectra at natural abundance, J. Am. Chem. Soc. 136 (2014) 1242–1244.
[32] J. Furrer, A robust, sensitive, and versatile HMBC experiment for rapid structure elucidation by NMR: IMPACT-HMBC, Chem. Commun. 46 (2010) 3396–3398.
[33] E. Kupce, R. Freeman, Fast multidimensional NMR by polarization sharing, Magn. Reson. Chem. 45 (2007) 2–4.
[34] W.F. Reynolds, R.C. Breton, D.C. Burns, Evaluating ASAP-HMQC and PS-HSQC NMR pulse sequences with non-uniform sampling for rapid screening of natural products, Planta Med. 80 (2014) IL26.
[35] J. Farjon, A. Giros, S. Deloisy, L. Blanco, J. Hannedouche, E. Schulz, D. Merlet, ^{29}Si-^{1}H IMPACT HMBC: a suitable tool for analyzing silylated derivatives, Magn. Reson. Chem. 51 (2013) 230–233.
[36] A. Altmayer-Henzien, V. Declerck, D.J. Aitken, E. Lescop, D. Merlet, J. Farjon, Fast-pulsing NMR techniques for the detection of weak interactions: successful natural abundance probe of hydrogen bonds in peptides, Org. Biomol. Chem. 11 (2013) 7611–7615.
[37] C. Gaillet, C. Lequart, P. Debeire, J.M. Nuzillard, Band-Selective HSQC and HMBC experiments using excitation sculpting and PFGSE, J. Magn. Reson. 139 (1999) 454–459.

[38] S.A. Bradley, K. Krishnamurthy, A modified CRISIS-HSQC for band-selective IMPRESS, Magn. Reson. Chem. 43 (2005) 117–123.
[39] D. Jeannerat, High resolution in heteronuclear ^{1}H-^{13}C NMR experiments by optimizing spectral aliasing with one-dimensional carbon data, Magn. Reson. Chem. 41 (2003) 3–7.
[40] M. Foroozandeh, D. Jeannerat, Deciphered chemical shifts in aliased spectra recorded with two slightly different narrow windows or differential chemical shift evolution, ChemPhysChem 12 (2011) 2409–2411.
[41] D. Jeannerat, Rapid multidimensional NMR: high resolution by spectral aliasing, in: R.K. Harris, R.E. Wasylishen (Eds.), Encyclopedia of Magnetic Resonance, John Wiley, Chichester, 2011.
[42] B. Vitorge, S. Bieri, M. Humam, P. Christen, K. Hostettmann, O. Muñoz, S. Loss, D. Jeannerat, High-precision heteronuclear 2D NMR experiments using 10-ppm spectral window to resolve carbon overlap, Chem. Commun. (2009) 950–952.
[43] K. Kazimierczuk, V.Y. Orekhov, Accelerated NMR spectroscopy by using compressed sensing, Angew. Chem. Int. Ed. 50 (2011) 5556–5559.
[44] K. Kazimierczuk, W. Koźmiński, I. Zhukov, Two-dimensional Fourier transform of arbitrarily sampled NMR data sets, J. Magn. Reson. 179 (2006) 323–328.
[45] M. Urbanczyk, W. Kozminski, K. Kazimierczuk, Accelerating diffusion-ordered NMR spectroscopy by joint sparse sampling of diffusion and time dimensions, Angew. Chem. Int. Ed. 53 (2014) 6464–6467.
[46] L. Frydman, T. Scherf, A. Lupulescu, The acquisition of multidimensional NMR spectra within a single scan, Proc. Natl. Acad. Sci. 99 (2002) 15858–15862.
[47] P. Pelupessy, Adiabatic single scan two-dimensional NMR spectrocopy, J. Am. Chem. Soc. 125 (2003) 12345–12350.
[48] A. Tal, L. Frydman, Single-scan multidimensional magnetic resonance, Prog. Nucl. Magn. Reson. Spectrosc. 57 (2010) 241–292.
[49] P. Giraudeau, L. Frydman, Ultrafast 2D NMR: an emerging tool in analytical spectroscopy, Annu. Rev. Anal. Chem. 7 (2014) 129–161.
[50] A. Herrera, E. Fernández-Valle, R. Martínez-Álvarez, D. Molero, Z.D. Pardo, E. Sáez, M. Gal, Real-time monitoring of organic reactions with two-dimensional Ultrafast TOCSY NMR Spectroscopy, Angew. Chem. Int. Ed. 48 (2009) 6274–6277.
[51] Z.D. Pardo, G.L. Olsen, M.E. Fernández-Valle, L. Frydman, R. Martínez-Álvarez, A. Herrera, Monitoring mechanistic details in the synthesis of pyrimidines via real-time, ultrafast multidimensional NMR spectroscopy, J. Am. Chem. Soc. 134 (2012) 2706.
[52] I. Fernández, M.E. Fernández-Valle, R. Martínez-Álvarez, D. Molero-Vílchez, Z.D. Pardo, E. Sáez-Barajas, E. Sánchez, A. Herrera, Discovering mechanistic insights by application of *tandem* ultrafast multidimensional NMR techniques, J. Org. Chem. 79 (2014) 8086–8093.
[53] P. Giraudeau, S. Akoka, A new gradient-controlled method for improving the spectral width of ultrafast 2D NMR experiments, J. Magn. Reson. 205 (2010) 171–176.
[54] Y. Shrot, B. Shapira, L. Frydman, Ultrafast 2D NMR spectroscopy using a continuous spatial encoding of the spin interactions, J. Magn. Reson. 171 (2004) 162–169.
[55] Y. Shrot, L. Frydman, Compressed sensing and the reconstruction of ultrafast 2D NMR data: principles and biomolecular applications, J. Magn. Reson. 209 (2011) 352–358.
[56] L.H.K. Queiroz, P. Giraudeau, F.A.B. dos Santos, K.T. Oliveira, A.G. Ferreira, Real-time mechanistic monitoring of an acetal hydrolysis using ultrafast 2D NMR, Magn. Reson. Chem. 50 (2012) 496–501.
[57] P. Giraudeau, T. Montag, B. Charrier, C.M. Thiele, Fast access to residual dipolar couplings by single-scan 2D NMR in oriented media, Magn. Reson. Chem. 50 (2012) S53–S57.

[58] L. Frydman, D. Blazina, Ultrafast two-dimensional nuclear magnetic resonance spectroscopy of hyperpolarized solutions, Nat. Phys. 3 (2007) 415–419.
[59] L.H.K. Queiroz, A.G. Ferreira, P. Giraudeau, Optimization and practical implementation of ultrafast 2D NMR experiments, Quim. Nova 4 (2013) 577–581.
[60] http://www.sciences.univ-nantes.fr/CEISAM/ebsi/ultrafast/uf_acq.html.
[61] M. Pathan, B. Charrier, I. Tea, S. Akoka, P. Giraudeau, New practical tools for the implementation and use of ultrafast 2D NMR experiments, Magn. Reson. Chem. 51 (2013) 168–175.
[62] J.R. Garbow, D.P. Weitekamp, A. Pines, Bilinear rotation decoupling of homonuclear scalar interactions, Chem. Phys. Lett. 93 (1982) 504–509.
[63] K. Zangger, H. Sterk, Homonuclear broadband-decoupled NMR spectra, J. Magn. Reson. 124 (1997) 486–489.
[64] N.H. Meyer, K. Zangger, Simplifying proton NMR spectra by instant homonuclear broadband decoupling, Angew. Chem. Int. Ed. Engl. 52 (2013) 7143–7146.
[65] J.A. Aguilar, S. Faulkner, M. Nilsson, G.A. Morris, Pure shift ^{1}H NMR: a resolution of the resolution problem? Angew. Chem. Int. Ed. Engl. 49 (2010) 3901–3903.
[66] G.A. Morris, J.A. Aguilar, R. Evans, S. Haiber, M. Nilsson, True chemical shift correlation maps: a TOCSY experiment with pure shifts in both dimensions, J. Am. Chem. Soc. 132 (2010) 12770–12772.
[67] J.A. Aguilar, M. Nilsson, G.A. Morris, Simple proton spectra from complex spin systems: pure shift NMR spectroscopy using BIRD, Angew. Chem. Int. Ed. 50 (2011) 9716–9717.
[68] A. Lupulescu, G. Olsen, L. Frydman, Toward single-shot pure-shift solution ^{1}H NMR by trains of BIRD-based homonuclear decoupling, J. Magn. Reson. 218 (2012) 141–146.
[69] P. Sakhaii, B. Haase, W. Bermel, Experimental access to HSQC spectra decoupled in all frequency dimensions, J. Magn. Reson. 199 (2009) 192–198.
[70] I. Timári, L. Kaltschnee, A. Kolmer, R.W. Adams, M. Nilsson, C.M. Thiele, G.A. Morris, K.E. Kövér, Accurate determination of one-bond heteronuclear coupling constants with pure shift broadband proton-decoupled CLIP/CLAP-HSQC experiments, J. Magn. Reson. 239 (2014) 130–138.
[71] L. Paudel, R.W. Adams, P. Király, J.A. Aguilar, M. Foroozandeh, M.J. Cliff, M. Nilsson, P. Sándor, J.P. Waltho, G.A. Morris, Simultaneously enhancing spectral resolution and sensitivity in heteronuclear correlation NMR spectroscopy, Angew. Chem. Int. Ed. 52 (2013) 11616–11619.
[72] M. Pérez-Trujillo, L. Castañar, E. Monteagudo, L.T. Kuhn, P. Nolis, A. Virgili, R.T. Williamson, T. Parella, Simultaneous ^{1}H and ^{13}C NMR enantiodifferentiation from highly-resolved pure shift HSQC spectra, Chem. Commun. 50 (2014) 10214–10217.
[73] L. Castañar, P. Nolis, A. Virgili, T. Parella, Full sensitivity and enhanced resolution in homodecoupled band-selective NMR experiments, Chem. Eur. J. 19 (2013) 17283–17286.
[74] J. Ying, J. Roche, A. Bax, Homonuclear decoupling for enhancing resolution and sensitivity in NOE and RDC measurements of peptides and proteins, J. Magn. Reson. 241 (2014) 97–102.
[75] L. Castañar, P. Nolis, A. Virgili, T. Parella, Measurement of T_1/T_2 relaxation times in overlapped regions from homodecoupled ^{1}H singlet signals, J. Magn. Reson. 244 (2014) 30–35.
[76] V.M.R. Kakita, J. Bharatam, Real-time homonuclear broadband and band-selective decoupled pure-shift ROESY, Magn. Reson. Chem. 52 (2014) 389–394.

[77] N.H. Meyer, K. Zangger, Enhancing the resolution of multi-dimensional heteronuclear NMR spectra of intrinsically disordered proteins by homonuclear broadband decoupling, Chem. Commun. 50 (2014) 1488–1490.
[78] B. Vitorge, D. Jeannerat, NMR diffusion measurements in complex mixtures using constant-time-HSQC-IDOSY and computer-optimized spectral aliasing for high resolution in the carbon dimension, Anal. Chem. 78 (2006) 5601–5606.
[79] D. Jeannerat, Computer optimized spectral aliasing in the indirect dimension of ^{1}H–^{13}C heteronuclear 2D NMR experiments. A new algorithm and examples of applications to small molecules, J. Magn. Reson. 186 (2007) 112–122.
[80] W.F. Reynolds, R.G. Enriquez, The advantages of forward linear prediction over multiple aliasing for obtaining high-resolution HSQC spectra in systems with extreme spectral crowding, Magn. Reson. Chem. 41 (2003) 927–932.
[81] L. Castañar, M. Pérez-Trujillo, P. Nolis, E. Monteagudo, A. Virgili, T. Parella, Enantiodifferentiation through frequency-selective pure-shift ^{1}H Nuclear Magnetic Resonance spectroscopy, ChemPhysChem 15 (2014) 854–857.
[82] M. Pérez-Trujillo, E. Monteagudo, T. Parella, Evaluation of ^{1}H and ^{13}C NMR spectroscopy for the differentiation of enantiomeric molecules by chiral solvating agents, Anal. Chem. 85 (2013) 10887–10894.
[83] P. Sakhaii, B. Haase, W. Bermel, Broadband homodecoupled heteronuclear multiple bond correlation spectroscopy, J. Magn. Reson. 228 (2013) 125–129.
[84] M.H. Lerche, A. Meissner, F.M. Poulsen, O.W. Sorensen, Pulse sequences for measurement of one-bond ^{15}N-^{1}H coupling constants in the protein backbone, J. Magn. Reson. 140 (1999) 259–263.
[85] M. Ottiger, F. Delaglio, A. Bax, Measurement of J and dipolar couplings from simplified two-dimensional NMR spectra, J. Magn. Reson. 131 (1998) 373–378.
[86] L.S. Yao, J.F. Ying, A. Bax, Improved accuracy of ^{15}N-^{1}H scalar and residual dipolar couplings from gradient-enhanced IPAP-HSQC experiments on protonated proteins, J. Biomol. NMR 43 (2009) 161–170.
[87] C.M. Thiele, Simultaneous assignment of all diastereotopic protons in strychnine using RDCs: PELG as alignment medium for organic molecules, J. Org. Chem. 69 (2004) 7403–7413.
[88] A. Enthart, J.C. Freudenberger, J. Furrer, H. Kessler, B. Luy, The CLIP/CLAP HSQC: pure absorptive spectra for the measurement of one-bond couplings, J. Magn. Reson. 192 (2008) 314–322.
[89] K. Takegoshi, K. Ogura, K. Hikichi, A perfect spin echo in a weakly homonuclear J-coupled spin=1/2 system, J. Magn. Reson. 84 (1989) 611–615.
[90] J.A. Aguilar, M. Nilsson, G. Bodenhausen, G.A. Morris, Spin echo NMR spectra without J modulation, Chem. Commun. 48 (2012) 811–813.
[91] A.M. Torres, G. Zheng, W.S. Price, J-compensated PGSE: an improved NMR diffusion experiment with fewer phase distortions, Magn. Reson. Chem. 48 (2010) 129–133.
[92] R.W. Adams, C.M. Holroyd, J.A. Aguilar, M. Nilsson, G.A. Morris, "Perfecting" WATERGATE: clean proton NMR spectra from aqueous solution, Chem. Commun. 49 (2013) 358–360.
[93] B. Baishya, C.L. Khetrapal, K.K. Dey, "Perfect Echo" HMQC: sensitivity and resolution enhancement by broadband homonuclear decoupling, J. Magn. Reson. 234 (2013) 67–74.
[94] B. Baishya, C.L. Khetrapal, "Perfect Echo" INEPT: more efficient heteronuclear polarization transfer by refocusing homonuclear J-coupling interaction, J. Magn. Reson. 242 (2014) 143–154.

[95] L. Castañar, E. Sistaré, A. Virgili, R.T. Williamson, T. Parella, Suppression of phase and amplitude in J(HH) modulations in HSQC experiments. Magn. Reson. Chem. (2014), http://dx.doi.org/10.1002/mrc.4149, in press.
[96] K. Hallenga, G.M. Lippens, A constant time ^{13}C,^{1}H HSQC with uniform excitation over the complete 13C chemical shift range, J. Biomol. NMR 5 (1995) 59–66.
[97] P.W.A. Howe, Compensating for variation in ^{1}JCH coupling constants in HSQC spectra acquired on small organic molecules, Magn. Reson. Chem. 48 (2010) 837–841.
[98] S. Wimperis, G. Bodenhausen, Heteronuclear coherence transfer over a range of coupling constants. A broadband-INEPT experiment, J. Magn. Reson. 69 (1986) 264–282.
[99] V.S. Manu, A. Kumar, Fast and accurate quantification using Genetic Algorithm optimized ^{1}H-^{13}C refocused constant-time INEPT, J. Magn. Reson. 234 (2013) 106–111.
[100] E. Kupce, R. Freeman, Compensated adiabatic inversion pulses: broadband INEPT and HSQC, J. Magn. Reson. 187 (2007) 258–265.
[101] S. Ehni, B. Luy, A systematic approach for optimizing the robustness of pulse sequence elements with respect to couplings, offsets, and B_1-field inhomogeneities (COB), Magn. Reson. Chem. 50 (2012) S63–S72.
[102] T.E. Skinner, T.O. Reiss, B. Luy, N. Khaneja, S.J. Glaser, Application of optimal control theory to the design of broadband excitation pulses for high resolution NMR, J. Magn. Reson. 163 (2003) 8–15.
[103] S. Ehni, B. Luy, Robust INEPT and refocused INEPT transfer with compensation of a wide range of couplings, offsets, and B_1-field inhomogeneities (COB3), J. Magn. Reson. 247 (2014) 111–117. http://dx.doi.org/10.1016/j.jmr.2014.07.01.
[104] K. Kobzar, T.E. Skinner, N. Khaneja, S.J. Glaser, B. Luy, Exploring the limits of broadband excitation and inversion pulses, J. Magn. Reson. 170 (2004) 236–243.
[105] K. Kobzar, T.E. Skinner, N. Khaneja, S.J. Glaser, B. Luy, Exploring the limits of broadband excitation and inversion pulses II: RF-power optimized pulses, J. Magn. Reson. 194 (2008) 58–66.
[106] N.I. Gershenzon, K. Kobzar, B. Luy, S.J. Glaser, T.E. Skinner, Optimal control design of excitation pulses that accomodate relaxation, J. Magn. Reson. 188 (2007) 330–336.
[107] K. Kobzar, B. Luy, N. Khaneja, S.J. Glaser, Pattern pulses: design of arbitrary excitation profiles as a function of pulse amplitude and offset, J. Magn. Reson. 173 (2005) 229–235.
[108] T.E. Skinner, N.I. Gershenzon, M. Nimbalkar, W. Bermel, B. Luy, S.J. Glaser, New strategies for designing robust universal rotation pulses: application to broadband refocussing at low power, J. Magn. Reson. 216 (2012) 78–87.
[109] K. Kobzar, S. Ehni, T.E. Skinner, S.J. Glaser, B. Luy, Exploring the limits of broadband 90° and 180° universal rotation pulses, J. Magn. Reson. 225 (2012) 142–160.
[110] S. Ehni, B. Luy, BEBE^{tr} and BUBI: J-compensated concurrent shaped pulses for ^{1}H-^{13}C experiments, J. Magn. Reson. 232 (2013) 7–17.
[111] L. Castañar, J. Saurí, R.T. Williamson, A. Virgili, T. Parella, Pure in-phase heteronuclear correlation NMR experiments, Angew. Chem. Int. Ed. 53 (2014) 8379–8382.
[112] M.J. Thrippleton, J. Keeler, Elimination of zero-quantum interference in two-dimensional NMR spectra, Angew. Chem. Int. Ed. 86 (2003) 3938–3941.
[113] T. Reinsperger, B. Luy, Homonuclear BIRD-decoupled spectra for measuring one-bond couplings with highest resolution: CLIP/CLAP-RESET and constant time-CLIP/CLAP-RESET, J. Magn. Reson. 239 (2014) 110–120.
[114] B. Görling, S. Bräse, B. Luy, HR-HSBC: measuring heteronuclear one-bond couplings with enhanced resolution, Magn. Reson. Chem. 50 (2012) S58–S62.

[115] K. Furihata, M. Tashiro, H. Seto, High resolution-HMBC (HR-HMBC), a new method for measuring heteronuclear long-range coupling constants, Magn. Reson. Chem. 48 (2010) 179–183.
[116] C.M. Thiele, W. Bermel, Speeding up the measurement of one-bond scalar (^{1}J) and residual dipolar couplings (1D) by using non-uniform sampling (NUS), J. Magn. Reson. 216 (2012) 134–143.
[117] K. Fehér, S. Berger, K.E. Kövér, Accurate determination of small one-bond heteronuclear residual dipolar couplings by F1 coupled HSQC modified with a G-BIRD^r module, J. Magn. Reson. 163 (2003) 340–346.
[118] K.E. Kövér, K. Fehér, Measurement of one-bond heteronuclear dipolar coupling contributions for amine and diastereotopic protons, J. Magn. Reson. 168 (2004) 307–313.
[119] M. Ottiger, F. Delaglio, J.L. Marquardt, N. Tjandra, A. Bax, Measurement of dipolar couplings for methylene and methyl sites in weakly oriented macromolecules and their use in structure determination, J. Magn. Reson. 124 (1998) 365–369.
[120] P. Nolis, T. Parella, Solution-state NMR experiments based on heteronuclear cross-polarization, Curr. Anal. Chem. 3 (2007) 47–68.
[121] T.N. Pham, T. Liptaj, K. Bromek, D. Uhrin, Measurement of small one-bond proton-carbon residual dipolar coupling constants in partially oriented ^{13}C natural abundance oligosaccharide samples. Analysis of heteronuclear $^1J_{CH}$-modulated spectra with the BIRD inversion pulse, J. Magn. Reson. 157 (2002) 200–209.
[122] T. Carlomagno, W. Peti, C. Griesinger, A new method for the simultaneous measurement of magnitude and sign of $^1D_{CH}$ and $^1D_{HH}$ dipolar couplings in methylene groups, J. Biomol. NMR 17 (2000) 99–109.
[123] P. Permi, A spin-state-selective experiment for measuring heteronuclear one-bond and homonuclear two-bond couplings from an HSQC-type spectrum, J. Biomol. NMR 22 (2002) 27–35.
[124] E. Miclet, D.C. Williams Jr., G.M. Clore, D.L. Bryce, J. Boisbouvier, A. Bax, Relaxation-optimized NMR spectroscopy of methylene groups in proteins and nucleic acids, J. Am. Chem. Soc. 126 (2004) 10560–10570.
[125] G. Guichard, A. Violette, G. Chassaing, E. Miclet, Solution structure determination of oligoureas using methylene spin state selective NMR at ^{13}C natural abundance, Magn. Reson. Chem. 46 (2008) 918–924.
[126] T. Parella, M. Gairí, Simultaneous recording of spin-state-selective NMR spectra for different InS spin systems, J. Am. Chem. Soc. 126 (2004) 9821–9826.
[127] P. Permi, Two simple NMR experiments for measuring dipolar couplings in asparagine and glutamine side chains, J. Magn. Reson. 153 (2001) 267–272.
[128] E. Miclet, E. O'Neil-Cabello, E.P. Nikonowicz, D. Live, A. Bax, ^{1}H-^{1}H dipolar couplings provide a unique probe of RNA backbone structure, J. Am. Chem. Soc. 125 (2003) 15740–15741.
[129] P. Nolis, J.F. Espinosa, T. Parella, Optimum spin-state-selection for all multiplicities in the acquisition dimension of the HSQC experiment, J. Magn. Reson. 180 (2006) 39–50.
[130] J. Furrer, M. John, H. Kessler, B. Luy, J-spectroscopy in the presence of residual dipolar couplings: determination of one-bond coupling constants and scalable resolution, J. Biomol. NMR 37 (2007) 231–243.
[131] M. Liu, R.D. Farrant, J.M. Gillam, J.K. Nicholson, J.C. Lindon, Selective inverse-detected long-range heteronuclear J-resolved NMR spectroscopy and its application to the measurement of $^3J_{CH}$, J. Magn. Reson. B 109 (1995) 275–283.
[132] L. Ziani, J. Courtieu, D. Merlet, Visualisation of enantiomers via insertion of a BIRD module in X-H correlation experiments in chiral liquid crystal solvent, J. Magn. Reson. 183 (2006) 60–67.

[133] K. Kobzar, H. Kessler, B. Luy, Stretched gelatin gels as chiral alignment media for the discrimination of enantiomers by NMR spectroscopy, Angew. Chem. Int. Ed. 44 (2005) 3145–3147.
[134] D. Uhrin, T. Liptaj, K.E. Kövér, Modified BIRD pulses and design of heteronuclear pulse sequences, J. Magn. Reson. A 101 (1993) 41–46.
[135] J.D. Snider, E. Troche-Pesqueira, S.R. Woodruff, C. Gayathri, N.V. Tsarevsky, R.R. Gil, New strategy for RDCs assisted diastereotopic protons assignment using a combination of J-scaled BIRD HSQC and J-scaled BIRD HMQC/HSQC, Magn. Reson. Chem. 50 (2012) S86–S91.
[136] P. Tzvetkova, S. Simova, B. Luy, P.E. HSQC: a simple experiment for the simultaneous and sign-sensitive measurement of ($^1J_{CH}$ + D_{CH}) and ($^2J_{HH}$ + D_{HH}) couplings, J. Magn. Reson. 186 (2007) 193–200.
[137] J. Saurí, L. Castañar, P. Nolis, A. Virgili, T. Parella, Straightforward measurement of individual ^{1}J(CH) and ^{2}J(HH) in diastereotopic CH2 groups, J. Magn. Reson. 232 (2014) 33–40.
[138] Y. Takayama, D. Sahu, J. Iwahara, Observing in-phase single-quantum ^{15}N multiplets for NH_2/NH_3^+ groups with two-dimensional heteronuclear correlation spectroscopy, J. Magn. Reson. 194 (2008) 313–316.
[139] B.W. Yu, H. van Ingen, S. Vivekanandan, C. Rademacher, S.E. Norris, D.I. Freedberg, More accurate $^1J_{CH}$ coupling measurement in the presence of $^3J_{HH}$ strong coupling in natural abundance, J. Magn. Reson. 215 (2012) 10–22.
[140] B.W. Yu, H. van Ingen, D.I. Freedberg, Constant time INEPT CT-HSQC (CTi-CT-HSQC)—a new NMR method to measure accurate one-bond J and RDCs with strong ^{1}H-^{1}H couplings in natural abundance, J. Magn. Reson. 228 (2013) 159–165.
[141] B.L. Márquez, W.H. Gerwick, R.T. Williamson, Survey of NMR experiments for the determination of nJ(C, H) heteronuclear coupling constants in small molecules, Magn. Reson. Chem. 39 (2001) 499–530.
[142] T. Parella, J.F. Espinosa, Long-range proton-carbon coupling constants: NMR methods and applications, Prog. NMR Spectrosc. 73 (2013) 17–55.
[143] A. Bax, M. Summers, Sensitivity-enhanced detection of heteronuclear multiple-bond connectivity by 2D multiple quantum NMR, J. Am. Chem. Soc. 108 (1986) 2093–2094.
[144] J. Furrer, A comprehensive discussion of HMBC pulse sequences, part 1: the classical HMBC, Concepts Magn. Reson. 40A (2012) 101–127.
[145] J. Furrer, A comprehensive discussion of HMBC pulse sequences, part 2: some useful variants, Concepts Magn. Reson. 40A (2012) 146–169.
[146] J.M. Richardson, J.J. Titman, J. Keeler, D. Neuhaus, Assessment of a method for the measurement of long-range heteronuclear coupling constants, J. Magn. Reson. 93 (1991) 533–553.
[147] R.A.E. Edden, J. Keeler, Development of a method for the measurement of long-range ^{13}C–^{1}H coupling constants from HMBC spectra, J. Magn. Reson. 166 (2004) 53–68.
[148] J. Saurí, T. Parella, J.F. Espinosa, CLIP-HSQMBC: easy measurement of small proton-carbon coupling constants in organic molecules, Org. Biomol. Chem. 11 (2013) 4473–4478.
[149] J.F. Espinosa, P. Vidal, T. Parella, S. Gil, Measurement of long-range proton–carbon coupling constants from pure in-phase 1D multiplets, Magn. Reson. Chem. 49 (2011) 502–507.
[150] S. Gil, J.F. Espinosa, T. Parella, Accurate measurement of small heteronuclear coupling constants from pure-phase α/β HSQMBC cross-peaks, J. Magn. Reson. 213 (2011) 145–150.

[151] D. Uhrín, V. Varma, J.R. Brisson, A Method for measurement of long-range heteronuclear coupling constants from 2D HMQC spectra, J. Magn. Reson. A 119 (1996) 120–124.
[152] J. Saurí, J.F. Espinosa, T. Parella, A definitive NMR solution for a simple and accurate measurement of the magnitude and the sign of small heteronuclear coupling constants on protonated and non-protonated carbon atoms, Angew. Chem. Int. Ed. 51 (2012) 3919–3922.
[153] J. Saurí, P. Nolis, T. Parella, Efficient and fast sign-sensitive determination of heteronuclear coupling constants, J. Magn. Reson. 236 (2013) 66–69.
[154] J. Saurí, T. Parella, On the interference of J_{HH} in HSQMBC-IPAP and HMBC-IPAP experiments, Magn. Reson. Chem. 51 (2013) 509–513.
[155] J. Saurí, T. Parella, Efficient measurement of the sign and the magnitude of long-range proton-carbon coupling constants from a spin-state-selective HSQMBC-COSY experiment, Magn. Reson. Chem. 50 (2012) 717–721.
[156] S. Gil, J.F. Espinosa, T. Parella, IPAP–HSQMBC: measurement of long-range heteronuclear coupling constants from spin-state selective multiplets, J. Magn. Reson. 207 (2010) 312–321.
[157] L. Castañar, J. Saurí, P. Nolis, A. Virgili, T. Parella, Implementing homo- and heterodecoupling in region-selective HSQMBC experiments, J. Magn. Reson. 238 (2014) 63–69.
[158] J. Saurí, L. Castañar, P. Nolis, A. Virgili, T. Parella, P.E. HSQMBC: simultaneous measurement of proton-proton and proton-carbon coupling constants, J. Magn. Reson. 224 (2012) 101–106.
[159] J. Saurí, T. Parella, Simultaneous measurement of J(HH) two different ^{n}J(CH) coupling constants from a single multiple-edited 2D cross-peak, Magn. Reson. Chem. 51 (2013) 397–402.
[160] P. Trigo-Mouriño, A. Navarro-Vázquez, J. Ying, R.R. Gil, A. Bax, Structural discrimination in small molecules by accurate measurement of long-range proton-carbon NMR residual dipolar couplings, Angew. Chem. Int. Ed. 50 (2011) 7576–7580.
[161] K.A.M. Ampt, R.L.E.G. Aspers, P. Dvortsak, R.M. van der Werf, S.S. Wijmenga, M. Jaeger, Determination of size and sign of hetero-nuclear coupling constants from 2D ^{19}F-^{13}C correlation spectra, J. Magn. Reson. 215 (2012) 27–33.
[162] H. Koskela, T. Väänänen, Quantitative determination of aliphatic hydrocarbon compounds by 2D NMR, Magn. Reson. Chem. 40 (2002) 705–715.
[163] S. Heikkinen, M.M. Toikka, P.T. Karhunen, A. Kilpeläinen, Quantitative 2D HSQC (Q-HSQC) via suppression of J-dependence of polarization transfer in NMR spectroscopy: application to wood lignin, J. Am. Chem. Soc. 125 (2003) 4362–4367.
[164] H. Koskela, I. Kilpeläinen, S. Heikkinen, Some aspects of quantitative 2D NMR, J. Magn. Reson. 174 (2005) 237–244.
[165] D.J. Peterson, N.M. Loening, QQ-HSQC: a quick, quantitative heteronuclear correlation experiment for NMR spectroscopy, Magn. Reson. Chem. 45 (2007) 937–941.
[166] H. Koskela, O. Heikkilä, I. Kilpeläinen, S. Heikkinen, Quantitative two-dimensional HSQC experiment for high magnetic field NMR spectrometers, J. Magn. Reson. 202 (2010) 24–33.
[167] P. Giraudeau, Quantitative 2D liquid-state NMR, Magn. Reson. Chem. 52 (2014) 259–272.
[168] E. Martineau, S. Akoka, R. Boisseau, B. Delanoue, P. Giraudeau, Fast quantitative ^{1}H-^{13}C two-dimensional NMR with very high precision, Anal. Chem. 85 (2013) 4777–4783.

[169] A. Mäkelä, I. Kilpeläinen, S. Heikkinen, Quantitative ^{13}C NMR spectroscopy using refocused constant-time INEPT, Q-INEPT-CT, J. Magn. Reson. 204 (2010) 124–130.
[170] R.T. Williamson, A.V. Buevich, G.E. Martin, T. Parella, LR-HSQMBC: a sensitive NMR technique to probe very long-range heteronuclear coupling pathways, J. Org. Chem. 79 (2014) 3887–3894.
[171] M. Reibarkh, R.T. Williamson, G.E. Martin, W. Bermel, Broadband inversion of 1J(CC) responses in 1, n-ADEQUATE spectra, J. Magn. Reson. 236 (2013) 126–133.
[172] G.E. Martin, R.T. Williamson, P.G. Dormer, W. Bermel, Inversion of 1J(CC) correlations in 1, n-ADEQUATE spectra, Magn. Reson. Chem. 50 (2012) 563–568.
[173] M.M. Senior, R.T. Williamson, G.E. Martin, Using HMBC and ADEQUATE NMR data to define and differentiate long-range coupling pathways: is the Crews rule obsolete? J. Nat. Prod. 76 (2013) 2088–2093.
[174] G.E. Martin, K.A. Blinov, M. Reibarkh, R.T. Williamson, 1JCC-edited HSQC-1, n-ADEQUATE: a new paradigm for simultaneous direct and long-range carbon–carbon correlation, Magn. Reson. Chem. 50 (2012) 722–728.
[175] G.E. Martin, B.D. Hilton, K.A. Blinov, HSQC-1,1-ADEQUATE and HSQC-1, n-ADEQUATE: new methods for establishing adjacent and long-range carbon-carbon networks, J. Nat. Prod. 74 (2011) 2400–2407.
[176] R.T. Williamson, A.V. Buevich, G.E. Martin, Using LR-HSQMBC to observe long-range $^{1}H–^{15}N$ correlations, Tetrahedron Lett. 55 (2014) 3365–3366.
[177] S. Cheatham, P. Gierth, W. Bermel, E. Kupče, HCNMBC—a pulse sequence for H-(C)-N multiple bond correlations at natural isotopic abundance, J. Magn. Reson. 247 (2014) 38–41.

4. Summary and Conclusions

In summary, a novel set of modern pure shift NMR and HSQC/HSQMBC experiments have been developed for helping chemists to solve common problems encountered in their daily NMR activities.

Bellow, a brief summary with the main conclusions extracted from the experimental results is exposed:

- A new data collection technique to improve the SNR by one order of magnitude in slice-selective NMR experiments has been presented (**Publication 1**). The method is based on multiple-slice selection into a NMR tube by applying a multiple-frequency pulse simultaneously with a spatial encoding gradient. The experimental procedure to fulfill the sampled frequency requirement is simple and the results can be immediately adapted to a wide range of applications, such as demonstrated for pure shift ZS experiments.

- A new band-selective detection scheme (HOBS) has been proposed to collect homodecoupled NMR spectra of specific regions without sacrificing sensitivity (**Publication 2**). HOBS is especially useful in spectra presenting a set of equivalent spin systems in well-separated and defined regions (for instance, peptides and proteins). The main advantages of HOBS method are:
  - It is a full sensitivity experiment. The sensitivity of standard 1D ^{1}H NMR experiments is retained and even improved because to the collapse of the multiplet pattern to simplified singlets.
  - HOBS spectra present an excellent spectral quality.
  - Data collection is carry out in real-time mode without need of additional reconstruction methods, allowing a conventional FID data processing.

- The implementation of the HOBS approach is easy and reliable for a large number of standard mono- and multidimensional NMR experiments, as reported for:
  - HOBS-TOCSY and HOBS-HSQC (**Publication 2**)
  - HOBS-IR and HOBS-CPMG-PROJECT (**Publication 3**)
  - HOBS-selTOCSY (**Publication 4**)

- HOBS-HSQMBC (**Publication 6**)
- HOBS-HSQC-TOCSY (**Publication 7**)

- The HOBS experiments developed during this work has been used for several practical applications, as for example:
  - The simple measurement of T_1 and T_2 NMR relaxation times in overlapped areas without need of multi-exponential decay analysis or deconvolution methods. (**Publication 3**)
  - To carry out fast enantiodifferentiation studies in presence of CSAs. (**Publication 4**)
  - The direct measurement of heteronuclear coupling constants from simplified in-phase doublets. (**Publication 6**)
  - To carry out the distinction and assignment of highly complex mixtures of similar compounds exhibiting near-identical ^{1}H and ^{13}C NMR spectra. (**Publication 7**)

- The combination of spectral aliasing and pure shift HSQC approaches in SAPS-HSQC experiments represents an excellent routine tool for NMR enantiodifferentiation studies. The enantiodifferentiated data is obtained in short acquisition times and with high signal dispersion for both ^{1}H and ^{13}C nuclei. Overlapping problems of common 1D ^{1}H experiments are overcome, and poor enantiodifferentiation in 1D experiments can now be detected, allowing the study of cases abandoned in the past for reasons of poor enantioresolution and/or long experimental times. (**Publication 7**)

- In **Publication 8**…
  - It has been demonstrated that the use of an adiabatic *z*-filter is an extremely useful NMR element to suppress unwanted homo- and heteronuclear anti-phase contributions in HSQC and HSQMBC experiments. The improvement achieved is more spectacular in the long-range heteronuclear correlation experiments where the effects of the J_{HH} evolution are more pronounced.

- The proposed broadband PIP-HSQC and PIP-HSQMBC experiments yield undistorted in-phase cross peaks, which improve spectral quality and facilitate spectral analysis.

- PIP-HSQC and PIP-HSQMBC experiments have been applied to the measurement of homonuclear (J_{HH}) and direct ($^{1}J_{CH}$) and long-range ($^{n}J_{CH}$; n>1) heteronuclear scalar and residual (D_{HH}; $^{1}D_{CH}$; $^{n}D_{CH}$) coupling constants in isotropic and/or anisotropic media. The clean in-phase character displayed by the cross-peaks allows a direct and easy determination of $^{1}J_{CH}/^{n}J_{CH}$ and $^{1}D_{CH}/^{n}D_{CH}$. The proposed experiments are fully compatible with the IPAP methodology allowing the measurement of small coupling heteronuclear constants even in complex or non-resolved multiplets.

- The proposed methods can be recorded in full automation mode without any prior calibration and they offer a general implementation on a large variety of isotropic and anisotropic sample conditions.

- In **Publication 9**…

  - A perfect-INEPT block has been implemented in HSQC experiments to avoid any interference as a result of J_{HH} coupling constant evolution. It has been shown theoretically and experimentally that during the perfect-INEPT element the magnetization evolution under the effect of the J_{HH} is refocused.

  - It has been show that the resulting cross-peaks of the perfect-HSQC spectra exhibit pure in-phase multiplet pattern, irrespective of the experiment optimization. These uniform and predictable responses are more amenable to an accurate and quantitative analysis than what is encountered with the results of standard HSQC pulse sequence.

  - Particular emphasis has been made in the application of the proposed perfect-HSQC experiment in the accurate determination of homonuclear (J_{HH}) and one-bond heteronuclear scalar ($^{1}J_{CH}$) and residual (D_{HH}; $^{1}D_{CH}$) coupling constants in isotropic and/or anisotropic media.

  - It has been demonstrated that in perfect-HSQC experiments the final in-phase detected signal is only modulated by $\sin^2(\pi^n J_{H_1C}\Delta)$, which opens the opportunity to design quantitative NMR application.

- In **Publication 10**…
  - A compilation of novel HSQC experiments have been made, including a discussion of the new family of HSQC experiments developed in this thesis: pure shift HSQC (ps-HSQC-PEP, HOBS-HSQC, SAPS-HSQC) as well as the perfect-HSQC and PIP-HSQC experiments.
  - Similarly, a comprehensive analysis of HSQMBC experiments has been also performed, with detailed discussion on the new HOBS-HSQMBC and PIP-HSQMBC experiments developed in this thesis.

5. APPENDIX

This section contains some work carried out along this doctoral thesis which cannot be included as Publications. The reasons for which have not been included are:

- **Publication 11** and **Publication 12** were part of the Ph.D. thesis of Dr. Josep Saurí entitled "*Modern NMR methodologies for the measurement of homo- and heteronuclear coupling constants in small molecules*" which was presented in May 2014.

- **Publication 13** is a complete revision work about the recent developments and application of modern pure shift NMR experiments.

PUBLICATION 11

P.E.HSQMBC: Simultaneous measurement of proton-proton and proton-carbon coupling constants

Josep Saurí, Pau Nolis, Laura Castañar, Albert Virgili and Teodor Parella.
J. Magn. Reson., **2012**, *224*, 101-106.
DOI: 10.1016/j.jmr.2012.09.007

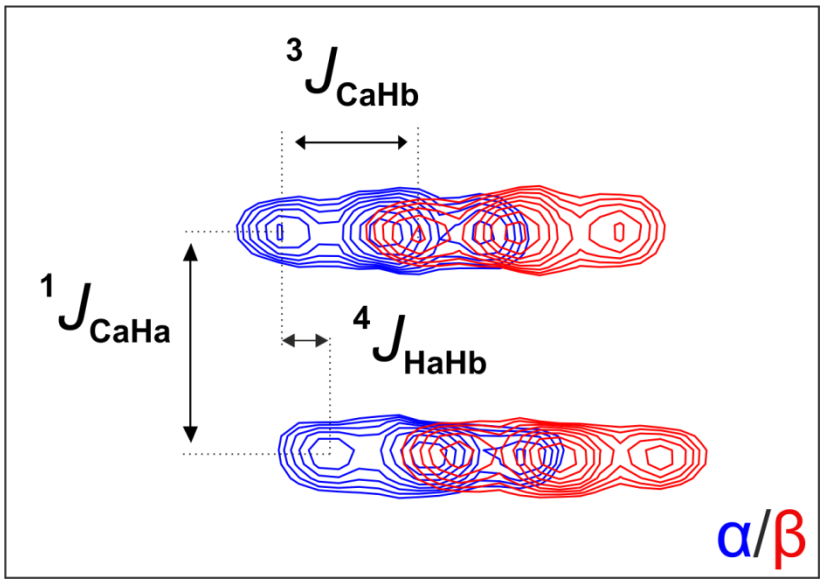

Introduction

In this publication, a new proton-selective NMR experiment, denoted as *Pure Exclusive* HSQMBC (P.E.HSQMBC), is presented to measure simultaneously $^{n}J_{HH}$, $^{1}J_{CH}$ and $^{n}J_{CH}$ coupling constants in a three $^{1}H_{a}$-$^{1}H_{b}$-^{13}C spin system. In addition, the experiment is also able to extract the relative sign of the $^{n}J_{HH}$ coupling constants.

The pulse scheme is based on the existing P.E.HSQC experiment,[67d] but optimized to long-range proton-carbon correlations instead of one-bond correlations. The experiment uses selective proton pulses to avoid any unwanted J_{HH} modulation during the INEPT periods. Additionally, it is shown how the concepts of *J*-resolved spectroscopy and the *Exclusive COrrelation SpectroscopY* (E.COSY) principle[96] can be fully complementary to the IPAP technique and they all can be incorporated into the same NMR experiment. In this way, several coupling constants can be simultaneous measured from a single 2D cross-peak.

The main goal of the P.E.HSQMBC experiment is to take profit of the large $^{1}J_{CH}$ value, which is used as a passive coupling constant, to generate a large splitting in the indirect dimension of 2D cross-peaks. The E.COSY pattern, which is generated by a small-flip (36^{o}) ^{1}H pulse, allows extract the magnitude and the sign of J_{HH}. The method also uses the IPAP technique along the detected dimension to get an accurate measurement of $^{n}J_{CH}$, as described in the original selHSQMBC experiment.[78]

[96] a) C. Griesinger, O. W. Sørensen, R. R. Ernst. *J. Am. Chem. Soc.*, **1985**, *107*, 6394. b) C. Griesinger, O. W. Sørensen, R. R. Ernst. *J.Chem. Phys.*, **1986**, *852*, 6837.

Journal of Magnetic Resonance 224 (2012) 101–106

Contents lists available at SciVerse ScienceDirect

Journal of Magnetic Resonance

journal homepage: www.elsevier.com/locate/jmr

P.E.HSQMBC: Simultaneous measurement of proton–proton and proton–carbon coupling constants

Josep Saurí [a], Pau Nolis [a], Laura Castañar [a,b], Albert Virgili [b], Teodor Parella [a,b,*]

[a] Servei de Ressonància Magnètica Nuclear, Universitat Autònoma de Barcelona, E-08193 Bellaterra, Barcelona, Spain
[b] Departament de Química, Universitat Autònoma de Barcelona, E-08193 Bellaterra, Barcelona, Spain

ARTICLE INFO

Article history:
Received 12 July 2012
Revised 10 September 2012
Available online 25 September 2012

Keywords:
HSQMBC
E.COSY
Proton–proton coupling constants
Long-range proton–carbon coupling constants
IPAP

ABSTRACT

A long-range optimized P.E.HSQC experiment, named P.E.HSQMBC, is proposed for the simultaneous measurement of a complete set of homonuclear and heteronuclear coupling constants from a single 2D cross-peak. The sign and the magnitude of proton–proton coupling constants are measured along the direct dimension from the relative E.COSY-type multiplet pattern displacement due to the passive one-bond coupling constant splitting generated in the indirect dimension. On the other hand, long-range proton–carbon coupling constants are independently determined in the detected dimension from a traditional fitting analysis of antiphase multiplet patterns or, more conveniently, from the IPAP multiplet displacement obtained from extended HSQMBC experiments.

1. Introduction

The determination of homonuclear and heteronuclear coupling constants is of prime importance in the structural and conformational studies of molecules in solution. Not only do *J*-couplings contain information about chemical connectivity, they also contain structural information as known for the typical Karplus-like dependence that exhibits ^3J vs dihedral angles. In addition, it has well been recognized during the last years that residual dipolar couplings (RDCs), as measured by solution state NMR, carry important structural information regarding internuclear vector orientation relative to the principal axis system of the molecule's alignment tensor [1].

Homonuclear proton–proton coupling constants, *J*(HH), can usually be determined by a variety of simple NMR methods, but the precise measurement of heteronuclear small long-range (^nJ(CH); $n > 1$) has not been so evident [2,3]. HSQC-TOCSY experiments becomes a sensitive and accurate approach to provide both the sign and the magnitude of ^nJ(CH) for protonated carbons [4–6]. On the other hand, NMR pulse schemes mainly based on the HMBC and HSQMBC experiments have been widely accepted to determine them on quaternary carbons [6–8]. However, the major inconvenient of this latter approach is the need for a post-processing fitting procedure by using the shape and intensity of signals simultaneously [6,9] to analyze the anti-phase nature of each multiplet pattern and the accuracy of the measurement is often questioned. Recently, IPAP versions have been suggested to avoid this fitting analysis by recording a series of refocused HSQMBC experiments to obtain complementary In-Phase (IP) and Anti-Phase (AP) data that are suitable to provide simplified spin-state selective multiplets after data addition/subtraction [10–13]. In this way, accurate and direct measurement of ^nJ(CH) can be made with simplicity even for complex multiplets. This IPAP approach has been also proposed to measure carbon–carbon coupling constants [14,15].

In addition to the IPAP technique, other different NMR approaches have been proposed to extract homo- and heteronuclear coupling constants from heteronuclear correlations experiments as, for instance, the elegant E.COSY (Exclusive Correlation Spectroscopy) principle [16]. The major advantages to analyze E.COSY-type multiplets are: (i) very easy interpretation; (ii) are suited equally well for the measurement of small and large coupling values, (iii) it provides information about the sign analyzing the relative slope of cross peaks components, (iv) works well even for coupling constants smaller than the NMR line width, (v) *J* values are measured from the direct dimension where good resolution requirements are more easily reached. Several E.COSY-type methods have been proposed for the simultaneous measurement of different scalar and residual dipolar couplings in small molecules. For instance, a simple and sensitive P.E.HSQC experiment, closely related to a fully coupled non-refocused HSQC pulse scheme, has been proposed to determine the sign and the magnitude of one-bond proton–carbon

* Corresponding author at: Servei de Ressonància Magnètica Nuclear, Universitat Autònoma de Barcelona, E-08193 Bellaterra, Barcelona, Spain.
E-mail address: teodor.parella@uab.cat (T. Parella).

1090-7807/$ - see front matter © 2012 Elsevier Inc. All rights reserved.
http://dx.doi.org/10.1016/j.jmr.2012.09.007

(^1J(CH) and ^{1}D(CH)) and two-bond proton–proton (^2J(HH) and ^{2}D(HH)) coupling constants from a single 2D spectrum [17]. Recently a spin-flip HSQC experiment has also been proposed for the simultaneous measurement of J(HH) and ^nJ(CH) [18]. Although this later technique is a proton-selective method that only works for protonated carbons, it has been proved that the addition of accurate long-range CH RDCs can significantly improve the structural discrimination power in complex small molecules with multiple stereogenic centers.

In what follows, we show a variant of the mentioned P.E.HSQC experiment, referred here as P.E.HSQMBC, for the simultaneous and accurate measurement of multiple J(HH), ^1J(CH) and ^nJ(CH) coupling constants. In this long-range ^{1}H–^{13}C correlation experiment, the large heteronuclear ^1J(CH) coupling constant is employed for separating two multiplet patterns along the indirect F_1 dimension while homonuclear HH couplings can be accurately measured from their relative E.COSY-type displacements in the detected F_2 dimension. The experiment closely relates to the XLOC experiment, a long-range correlation experiment designed to measure J(HH) in a similar E.COSY way [19–21]. Furthermore, we also present and discuss several options to extract ^nJ(CH) values at the same time and it will be shown that both E.COSY and IPAP principles can be implemented into the same pulse scheme to simultaneous measure different coupling constants from the same 2D multiplet with an extreme simplicity.

2. Results and discussion

Three different NMR pulse sequences suitable for an E.COSY version of the HSQMBC experiment are presented in Fig. 1. They combine the main features of three different older methods in a single experiment: (a) the accurate measurement of ^1J(CH) along the indirect dimension from F1-coupled HSQC schemes [22–25]; (b) the sign-sensitive measurement of ^1J(CH) and ^2J(HH) in E.COSY multiplets as reported in the P.E.HSQC experiment [17], and (c) the precise measurement of ^nJ(CH) using the IPAP technology in selHSQMBC experiments [11]. For the present work, we have chosen the general application of selective 180° ^{1}H pulses as a refocusing element in the INEPT block because this affords pure-phase multiplets and completely avoids any signal modulation due to J(HH).

The simplest pulse sequence is essentially a small-flip-angle non-refocused HSQC experiment where all CH coupling constants evolve freely during the entire t_1 period and the read ^{1}H pulse before acquisition is set to $\beta = 36°$ to achieve simplified multiplet structure. As described in the original P.E.HSQC experiment [17], instead of the long phase cycling schemes used in classical experiments, a simple small-angle pulse is used to generate the E.COSY-like pattern (Fig. 1A). In order to explain how pulse sequences work and describe the nature of multiplets generated in the proposed P.E.HSQMBC experiment, we concentrate the description on a heteronuclear three-spin system involving two active (H2 and C1) and a single passive (H1) spins (Scheme 1). These active spins having a long-range ^nJ(H2–C1) coupling determine the position of the cross-peak multiplet at (δ(H2), δ(C1)) which consists of two different components separated by the large ^1J(H1–C1) splitting along the F1 dimension. The magnitude and the sign of the J(H2–H1) coupling constant can be easily extracted comparing the relative displacement and the slope, respectively, between these two different rows in the detected F2 dimension (Fig. 2A). On the other hand, each row component of these E.COSY multiplets will present the characteristic antiphase pattern with respect to ^nJ(H2–C1) and pure in-phase character with respect all passive J(HH) couplings. The magnitude of ^nJ(H2–C1) must be extracted using well-established fitting algorithms that will not be discussed in detail here [6–9].

A modified P.E.HSQMBC version in where a BIRD^r cluster is incorporated into the carbon evolution period to suppress unwanted ^nJ(CH) contributions in the indirect dimension is shown in Fig. 1B. This option also offers the possibility to scale the ^1J(CH) splitting by a scaling factor k that strongly minimizes the resolution requirements and the number of t_1 increments to be acquired. This approach becomes particularly useful to obtain well defined multiplets in the indirect dimension that lead to precise measurement of scalar ^1J(CH) and/or dipolar ^{1}D(CH) values for weakly aligned samples. In analogy to the above description, this version also provides two separate cross peaks separated by $k * {}^1J$(CH) in the F1 dimension whereas ^nJ(CH) present the same AP features described above (Fig. 2B).

Finally, a refocused P.E.HSQMBC version has been developed to facilitate the measurement of ^nJ(CH) using the IPAP technique (Fig. 1C). Filtering the downfield and upfield doublet components into separate spectra is a successful concept to avoid the tedious analysis of anti-phase multiplets. This version can be understood as a F1-coupled analog of the recently proposed selHSQMBC experiment and although it suffers of a worse sensitivity due to the additional refocusing period, the magnitude of ^nJ(CH) can be extracted more accurately by the analysis of relative displacement of α/β cross-peaks in the detected dimension (see Fig. 2C). This more user-friendly method combines the principles of E.COSY and IPAP methodologies into a single NMR experiment whereas retains all the benefits described for the original selHSQMBC experiment [11].

Several details about sensitivity, multiplet patterns and relative pulse phases must be highlighted in order to explain the observed experimental data. Very importantly, two different mechanisms are present in the basic pulse scheme of Fig. 1A. First, the traditional pathway generated from the initial ^{1}H Boltzmann magnetization through the initial proton-selective INEPT transfer leads to two observable terms at the end of the t_1 period:

$$2H_{2y}C_{1z}\ \sin(\pi J_{H2-C1}\Delta)\ \cos(\pi J_{H2-C1}t_1)\ \cos(\pi J_{H1-C1}t_1) \quad (1a)$$

$$2H_{1y}C_{1z}\ \sin(\pi J_{H2-C1}\Delta)\ \sin(\pi J_{H2-C1}t_1)\ \sin(\pi J_{H1-C1}t_1) \quad (1b)$$

Thus, two different cross-peaks at δ(C1) appear showing pure anti-phase character with respect to J(H2–C1) in the F2 dimension: (i) a long-range H2–C1 correlation showing in-phase ^1J(CH) pattern and (ii) a direct H1–C1 cross-peak showing anti-phase ^1J(CH) pattern in the F1 dimension. The number of lines in the indirect dimension will depend on carbon multiplicity: CH appears as doublets, CH_2 as triplets and CH_3 as quartets with their intensities as described previously whereas quaternary carbons will not show splitting.

On the other hand, the original magnetization belonging to ^{13}C Boltzmann distribution also contributes to the final spectrum independently of the Δ delay and the selective proton pulse, in the form of the following term:

$$2H_{1y}C_{1z}\ \sin(\pi J_{H1-C1}t_1) \quad (2)$$

This pathway provides all direct correlations showing antiphase pattern with respect to ^1J(CH) in both dimensions independently of the selective nature of the INEPT block and therefore, the measurement of the sign and the magnitude of all ^1J(CH) and ^2J(HH) couplings can be performed as exactly described for the regular P.E.HSQC experiment [17].

These two different pathways can be separately obtained by a proper phase cycling of the 90° proton pulse labeled with ϕ_2 phase. Thus, the separate acquisition of two complementary data acquired with the pulse scheme of Fig 1A and with $\phi_2 = y$ and $\phi_2 = -y$ afford the same spectrum but with inverted phase for components coming from INEPT transfer (Fig. 3A and B, respectively). Conventional data addition/subtraction affords independent

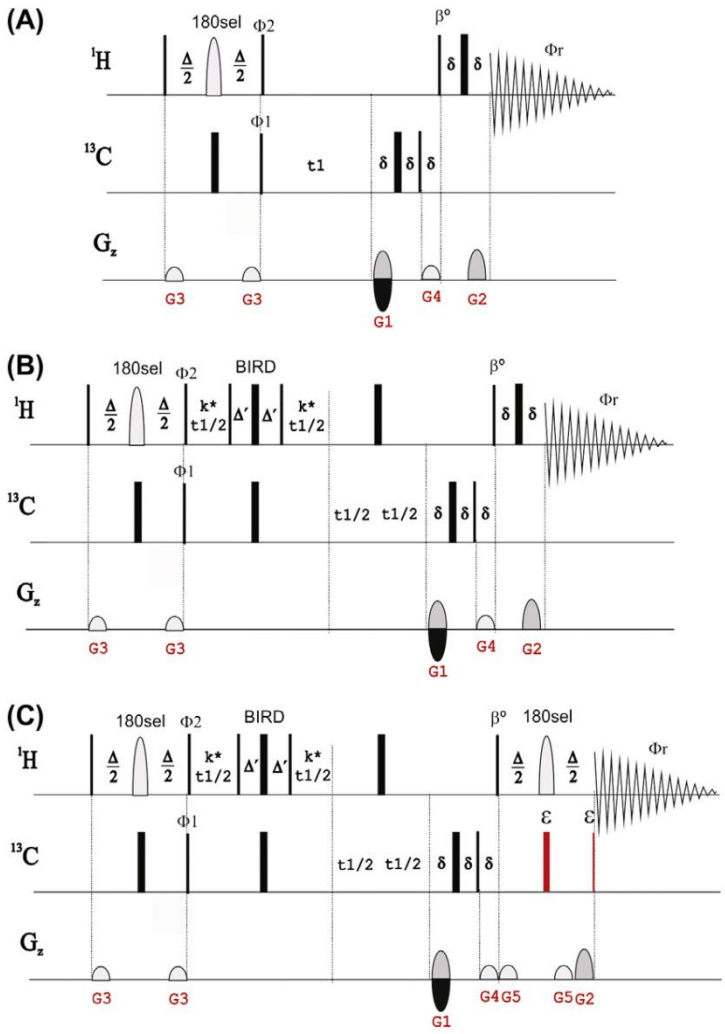

Fig. 1. Pulse sequences for the simultaneous determination of J(HH) and ^{n}J(CH). Narrow and wide filled bars represent 90° and 180° pulses (unless the flip angle $\beta = 36°$ is indicated), respectively, while half-ellipsoids denote ^{1}H-selective 180° pulses (p_{180}): (a) non-refocused fully-coupled P.E.HSQMBC sequence; (b) non-refocused fully-coupled P.E.HSQMBC sequence incorporating an ^{1}J(CH)-scalable BIRD^{r} module (scaling factor k) that allows the selective evolution of ^{1}J(CH) whereas refocuses all ^{n}J(CH) components during the variable evolution t_1 period; (c) refocused IPAP version based on the separate acquisition of In-Phase (IP:ε = on) and Anti-Phase (AP:ε = off) data that are further combined to provide separate α- and β-P.E.HSQMBC spectra. The interpulse delays are optimized to $\Delta + p_{180} = 1/(2 * {}^{n}J(\mathrm{CH}))$ and $\Delta' = 1/(2 * {}^{1}J(\mathrm{CH}))$. δ stands for the duration of each gradient and the recovery delay. The minimum phase cycle is $\phi_1 = x,-x$ and $\phi_r = x,-x$. See text for the importance of the phase ϕ_2: it is set to $\phi_2 = y$ for non-editing and $\phi_2 = y,y,-y,-y$ for editing of P.E.HSQC and P.E.HSQMBC data. Gradients G1 and G2 are used for coherence selection using echo-antiecho protocol, G3 and G5 are used for proper refocusing and G4 for zz-selection.

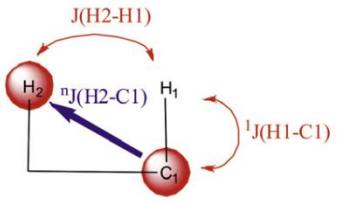

Scheme 1. Schematic representation of the spin-coupling networks involved in the simultaneous determination of ^{1}J(CH), J(HH) and ^{n}J(CH). The blue arrow indicates the active H2–C1 coupling which is essential for coherence transfer. The desired E.COSY multiplet structure is caused by the large splitting of ^{1}J(H1C1) due to the spin passive H1 along the indirect dimension. Fig. 2 summaries the multiplet patterns obtained from each proposed experiment and how couplings can be measured. (For interpretation of the references to color in this figure legend, the reader is referred to the web version of this article.)

P.E.HSQC (Fig. 3C) and P.E.HSQMBC (Fig. 3D) spectra. Otherwise, the corresponding P.E.HSQMBC spectra could also be obtained directly by performing the subtraction during acquisition by applying a four-step phase cycling with $\phi_2 = y,y,-y,-y$. In this case, a 90°(^{13}C)-gradient element just before the initial 90° ^{1}H pulse helps to efficiently remove unwanted ^{13}C Boltzmann contribution.

P.E.HSQC data are analyzed exactly as described in the original experiment and no more details will be given here. On the other hand, Fig. 4 shows an expansion of the column corresponding to the H15b proton in the P.E.HSQMBC spectrum. The direct correlation, that is visible because the selective pulse also excites the satellite lines, shows pure in-phase character in the indirect F1 dimension. It is clearly shown that is possible to differentiate the corresponding active ^{1}J(H15b–C15) and the passive ^{1}J(H15a–C15)

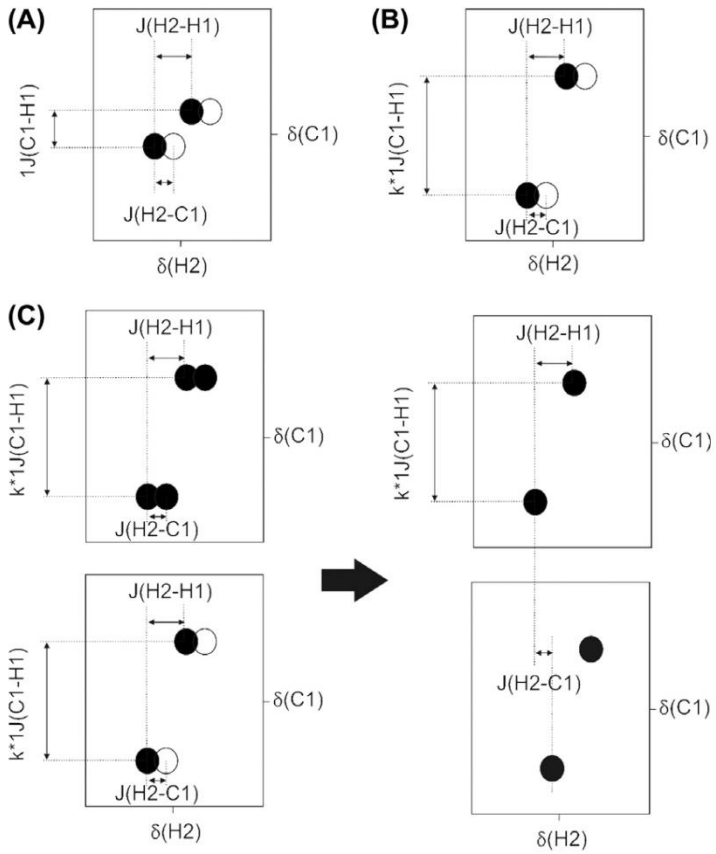

Fig. 2. (A–C) Schematics representing the expected multiplet patterns obtained from sequences of Fig. 1A, B and C, respectively. Filled and open circles represent multiplet components with opposite phase. In all cases, J(HH) is measured from the E.COSY pattern. On the other hand, ^{n}J(CH) must be extracted from the analysis of anti-phase multiplet patterns in the same row (in A and B), or from the relative displacement between two components that are separated in two separate spin-state selected spectra (see C).

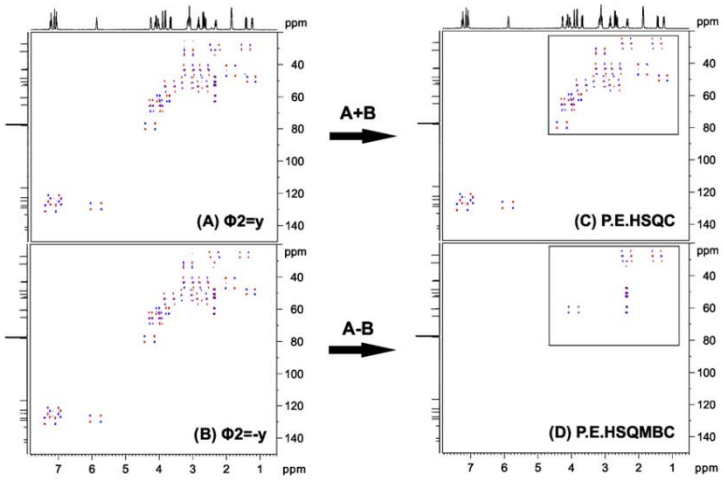

Fig. 3. General scheme to obtain separate P.E.HSQC and P.E.HSMBC spectra after selective refocusing of H15b proton (resonating at 2.35 ppm) of strychnine using the scheme of Fig. 1B. Two different data are independently acquired only changing the phase of the 90° proton pulse just applied after the t_1 period (A) using $\Phi_2 = y$ and (B) $\Phi_2 = -y$ whereas other relevant phase remain unchanged ($\Phi_1 = x,-x$ and $\Phi_r = x,-x$). After addition and subtraction of these data, two separate (C) P.E.HSQC and (D) P.E.HSQMBC spectra are obtained to determine ^{1}J(CH), J(HH) and ^{n}J(CH). The scaling factor was set to $k = 3$ and the experiment optimized to 8 Hz.

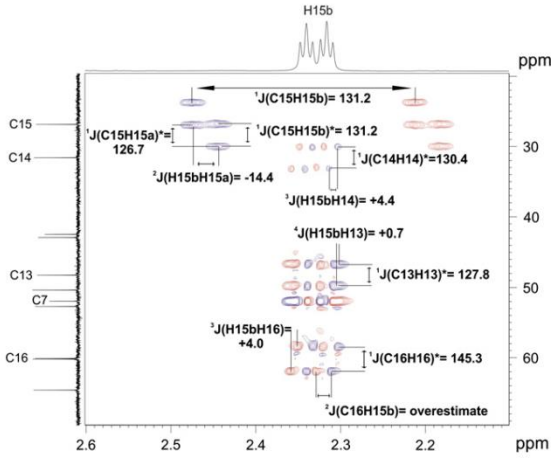

Fig. 4. Expanded region of the P.E.HSQMBC spectrum showing the column corresponding to the H15b proton (see Fig. 3D). Note that from the direct correlation, the relative sign between ^{2}J(HH) and ^{1}J(CH) can be obtained. From the other cross-peaks the sign and magnitude of ^{3}J(HH) can be extracted. The analysis of an specific row for the direct determination of ^{n}J(CH) is not advisable due to an overestimation and a conventional fitting procedure is required.

in diastereotopic CH_2 spin systems as well as to the sign and magnitude of the geminal and passive J(H15b–H15a) coupling value. Additional H15b cross-peaks are also observed for the methines C14, C13 and C16 carbons and for the quaternary C7 carbon. The well-resolved doublets in F1 for each CH cross-peak evidences the relative displacement between them along the F2 dimension, allowing the measurement of both magnitude and sign of the corresponding J(HH) as a function of the observed signal tilting. On the other hand, each individual row displays a pure anti-phase pattern with respect to the active ^{n}J(CH) that can be analyzed accordingly. The anti-phase nature structure of cross-peaks can cause partial intensity losses when the active scalar coupling is within the line width.

For this reason, a refocused version that uses the IPAP principle is proposed (Fig. 1C) for a much better and more user-friendly measurement on ^{n}J(CH). Fig. 5 illustrates the experimental protocol to acquire, to process and to analyze these P.E.HSQMBC data taking the H15b–C16 cross-peak as an example. Two complementary IP and AP data are separately acquired as shown in Fig. 5A and B, respectively. Although J(HH) could already be measured in any of these spectra from the E.COSY pattern, the extraction of ^{n}J(CH) would usually require an individual fitting analysis for each cross-peak. Sum and difference data (Fig. 5C and D) contain only the upfield and downfield components of the active doublet which makes it possible the straightforward measurement of ^{n}J(CH) by analyzing the relative displacement between them. However, in analogy to the regular selHSQMBC experiment the sign information of ^{n}J(CH) is not available from this analysis. In our hands, the use of a scaling factor of $k = 3$ is a good compromise to clearly resolve ^{1}J(CH) multiplet components in the indirect dimension using 256 t_1 increments. On the other hand, the non-equivalence between IP and AP data can afford undesired J-cross talk contributions that can introduce some error in the measurement. The use of an individualized scaling k' factor in the form of AP $\pm$ $k' * $ IP can be used to correct them. The tolerance on these cross-talk effects has already been discussed previously [10,11].

A limitation of the proposed experiments is its ^{1}H-selective nature and therefore multiple experiments should be needed for a global determination of coupling values in a molecule. However, the extraction of ^{n}J(CH) from multiple protons can be simultaneously obtained by applying the principles of multiple-site or band-selective excitation. Fig. 6 shows an example after selective refocusing of several protons that are not mutually coupled and acquired under the same experimental conditions as described in Fig. 3.

In summary, it has been shown that the concepts of J-resolved, E.COSY and IPAP principles can be mixed all together into the same pulse scheme in order to measure multiple coupling constants from a single 2D cross-peak analysis. We have developed a method that leads to the accurate measurement of both J(HH) and ^{n}J(CH)

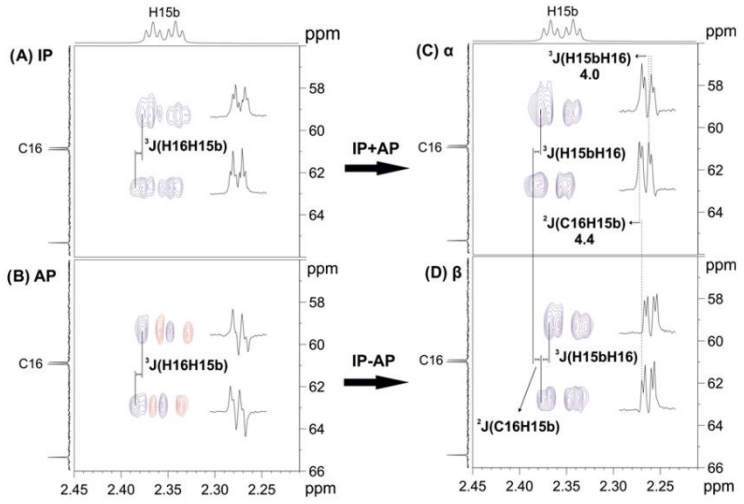

Fig. 5. Expanded areas corresponding to the H15b–C16 cross peak in the IPAP-selHSQMBC-E.COSY experiment acquired with the same experimental conditions as discussed in Fig. 3 and using pulse scheme of Fig. 1C. Two different data are acquired using the IPAP principle: (A) IP with the phase of β° pulse set to y and applying the pulses labeled with ε (on); (B) AP with the phase of β° pulse set to x and omitting the pulses ε (off). Time-domain data addition/subtraction followed by conventional processing afford complementary (C) α- and (D) β-selHSQMBC-E.COSY spectra from which the ^{n}J(CH) value can be directly extracted in a simple way by analyzing the relative left/right displacement of signals in the F2 dimension.

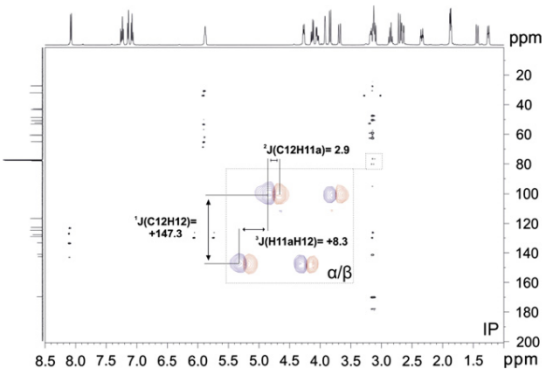

Fig. 6. Example showing the advantage to use multiple-site selective excitation in the P.E.HSQMBC experiment using shifted laminar pulses of non-mutually coupled protons. Different protons (H4 (8.15 ppm), H22 (5.9 ppm) and H11a/H18a/H14 (all three resonating near to 3.15 ppm)) were simultaneously refocused using a 40 ms Gaussian-shaped 180° proton pulse. The 2D spectrum corresponds to the In-Phase (IP) data and the inset shows the separate α/β data corresponding to the H11a–C12 cross peak.

from the high resolution obtained in the detected dimension whereas ^1J(CH) is precisely resolved in the indirect dimension. The proper combination of multiple proton excitation and non-uniform sampling can allow a faster measurement of all these couplings in small and medium size molecules. Alternatively, the experiment could be also implemented in a broadband mode, using for instance a CPMG-BIRD element instead of the selective INEPT block [26–28]. However, complete suppression of proton–proton coupling evolution and undesired sample heating remains to be solved. Much work is in progress to extrapolate all these concepts to the simultaneous measurement of the sign and magnitude of different types of heteronuclear coupling constants.

3. Methods and materials

All NMR experiments have been recorded on a BRUKER DRX-500 spectrometer equiped with a 3-channel 5-mm cryoprobe incorporating a *z*-gradient coil on a sample of 25 mg of strychnine, **1**, dissolved in 0.6 ml of $CDCl_3$. All experiments were optimized to 8 Hz, that means that ^nJ(CH) evolves during a period of $\Delta + p_{180} = 1/(2 * {}^nJ_{CH})$; where p_{180} is a selective 180° ^{1}H pulse. A Gaussian-shaped 180° pulse of duration of 20 ms (p_{180}) was used as a selective refocusing. The recycle and the interpulse BIRD^r ($\Delta' = 1/(2 * {}^1J(CH))$ delays were set to 1 s and 3.6 ms, respectively. An scaling factor $k = 3$ were used. Sine bell shaped gradients of 1 ms duration (δ) were used, followed by a recovery delay of 100 μs. Gradient ratios for G1:G2:G3:G4:G5:G6 were 80:20.1:33:50:11:17, measured as percentage of the absolute gradient strength of 5.35 G/cm.

All experiments were acquired and processed using the echo/anti-echo protocol. Quadrature detection is achieved inverting the G1and G2 gradient pulses for every second FID. Four scans were accumulated for each one of the 256 t_1 increments and the number of data points in t_2 was set to 4096. Spectral windows in both dimensions were 22500 (F1) and 4500 (F2) Hz, respectively. Prior to Fourier-transformation of each data, zero filling to 1024 in F1, 8192 points in F2 and a sine squared function in both dimensions were applied.

2D ^{1}H–^{13}C IP and AP-HSQMBC experiments of Fig. 5 were separately recorded using the same experimental conditions described in Fig. 4. The overall acquisition time for each individual IP and AP data was about 26 min which were added/subtracted in the time-domain without any scaling factor to provide spin-state selective data. Finally, the same conditions were applied for the spectra shown in Fig. 6 except for the selective refocusing. A 40 ms multiple-site pulse applied to three different frequencies was automatically generated using the shape tool package included into Tospin software (see captions for more details).

Acknowledgments

Financial support for this research provided by MICINN (Projects CTQ2009-08328 and Consolider Ingenio-2010 CSD2007-00006) and Bruker Española S.A. is gratefully acknowledged. We also thank to the Servei de Ressonància Magnètica Nuclear, Universitat Autònoma de Barcelona, for allocating instrument time to this project.

References

[1] C. Thiele, Eur. J. Org. Chem. (2008) 5673–5685.
[2] B.L. Márquez, W.H. Gerwick, R.T. Williamson, Magn. Reson. Chem. 39 (2001) 499–530.
[3] T. Parella, 2D methods for the measurement of long-range proton–carbon coupling constants, in: G.A. Morris, J.W. Emsley (Eds.), Multidimensional NMR Methods for the Solution State, vol. 305, John Wiley & Sons Ltd., Chichester, UK, 2010.
[4] P. Nolis, J.F. Espinosa, T. Parella, J. Magn. Reson. 180 (2006) 39–50.
[5] W. Koźmiński, J. Magn. Reson. 137 (1999) 408–412.
[6] K. Kobzar, B. Luy, J. Magn. Reson. 186 (2007) 131–141.
[7] M.J. Thrippleton, J. Keeler, Angew. Chem., Int. Ed. 42 (2003) 3938–3941.
[8] R.T. Williamson, B.L. Márquez, W.H. Gerwick, K.E. Kövér, Magn. Reson. Chem. 38 (2000) 265–273.
[9] L. Verdier, P. Sakhaii, M. Zweckstetter, C. Griesinger, J. Magn. Reson. 163 (2003) 353–359.
[10] S. Gil, J.F. Espinosa, T. Parella, J. Magn. Reson. 207 (2010) 312–321.
[11] S. Gil, J.F. Espinosa, T. Parella, J. Magn. Reson. 213 (2011) 145–150.
[12] J. Saurí, J.F. Espinosa, T. Parella, Angew. Chem., Int. Ed. 51 (2012) 3919–3922.
[13] D. Uhrín, V. Varma, J.R. Brisson, J. Magn. Reson. A 119 (1996) 120–124.
[14] K.E. Kövér, M. Lenoir, D. Uhrín, J. Magn. Reson. 190 (2008) 171–182.
[15] L. Jin, D. Uhrín, Magn. Reson. Chem. 45 (2007) 628–633.
[16] C. Griesinger, O.W. Sørensen, R.R. Ernst, J. Am. Chem. Soc. 107 (1985) 6394–6396.
[17] P. Tzvetkova, S. Simova, B. Luy, J. Magn. Reson. 186 (2007) 193–200.
[18] P. Trigo-Mouriño, A. Navarro-Vázquez, J. Ying, R.R. Gil, A. Bax, Angew. Chem., Int. Ed. 50 (2011) 7576–7580.
[19] M.D. Sørensen, J.J. Led, O.W. Sørensen, J. Biomol. NMR 4 (1994) 135–141.
[20] A. Meissner, O.W. Sørensen, Magn. Reson. Chem. 39 (2001) 49–52.
[21] A. Meissner, J.ø Duus, O.W. Sørensen, J. Magn. Reson. 128 (1997) 92–97.
[22] C. Thiele, W. Bermel, J. Magn. Reson. 216 (2012) 134–143.
[23] J. Furrer, M. John, H. Kessler, B. Luy, J. Biomol. NMR 37 (2007) 231–243.
[24] K. Fehér, S. Berger, K.E. Kövér, J. Magn. Reson. 163 (2003) 340–346.
[25] K.E. Kövér, K. Fehér, J. Magn. Reson. 168 (2004) 307–313.
[26] H. Koskela, I. Kilpeläinen, S. Heikkinen, J. Magn. Reson. 164 (2003) 228–232.
[27] K.E. Kövér, G. Batta, K. Fehér, J. Magn. Reson. 181 (2006) 89–97.
[28] S. Boros, K.E. Kövér, Magn. Reson. Chem. 49 (2011) 106–110.

PUBLICATION 12

Straightforward measurement of individual $^1J_{CH}$ and $^2J_{HH}$ in diastereotopic CH_2 groups

Josep Saurí, Laura Castañar, Pau Nolis, Albert Virgili and Teodor Parella.
J. Magn. Reson. ,**2014**, *242*, 33-40.
DOI: 10.1016/j.jmr.2014.02.003

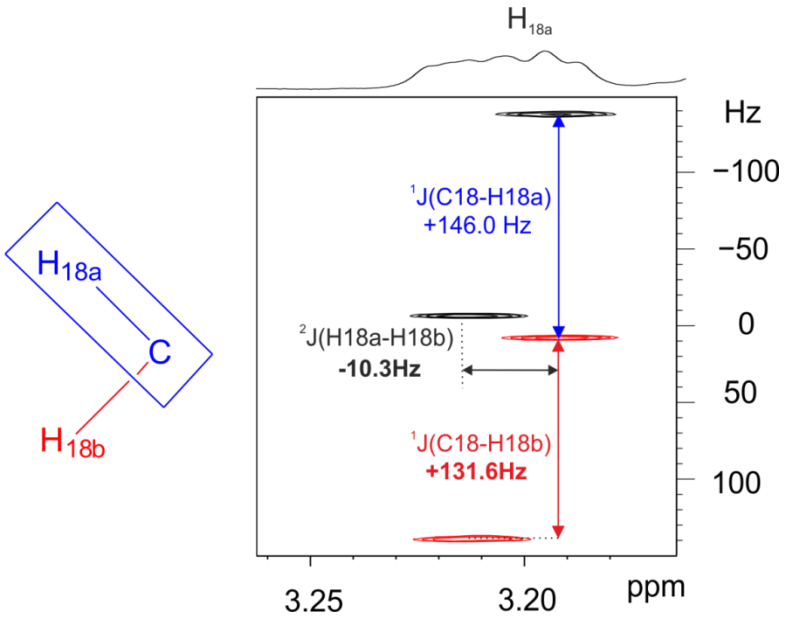

Introduction

The accurate measurement of $^{1}J_{CH}/^{1}T_{CH}$ for individual protons in diastereotopic CH_AH_B groups has been a challenging task. Several NMR methods has been proposed to measure them from the F1 or F2 dimension of HSQC spectra, but they all present some drawback that can prevent their general use.

In this publication, a new 2D ω_1-coupled inverse INEPT experiment (referred to as ω_1-iINEPT) is proposed for the simultaneous measurement of individual $^{1}J_{CH}/^{1}T_{CH}$ as well as the magnitude and the sign of geminal proton-proton coupling constants ($^{2}J_{HH}/^{2}T_{HH}$) in diastereotopic methylene groups in isotropic and anisotropic conditions. The method is based on a F1-coupled HSQC spectra that uses the initial ^{13}C Boltzmann polarization instead of the conventional INEPT transfer. The experiment is easily adapted for a *J*-resolved presentation (referred to as ω_1-iINEPT-*J*) which allows to obtain higher levels of resolution within the same experimental time by the use of a reduced spectral width in the indirect dimension. The success of the method is illustrated for several samples in isotropic conditions and also for the accurate measurement of $^{1}D_{CH}$ and $^{2}D_{HH}$ RDCs in diastereotopic CH_2 groups for samples aligned in anisotropic media. These measurements are also feasible for CH and CH_3 multiplicities.

Journal of Magnetic Resonance 242 (2014) 33–40

Contents lists available at ScienceDirect

Journal of Magnetic Resonance

journal homepage: www.elsevier.com/locate/jmr

Straightforward measurement of individual $^1J(CH)$ and $^2J(HH)$ in diastereotopic CH_2 groups

Josep Saurí, Laura Castañar, Pau Nolis, Albert Virgili, Teodor Parella *

Servei de Ressonància Magnètica Nuclear and Departament de Química, Universitat Autònoma de Barcelona, E-08193 Bellaterra, Catalonia, Spain

ARTICLE INFO

Article history:
Received 17 December 2013
Revised 31 January 2014
Available online 12 February 2014

Keywords:
E.COSY
One-bond proton–carbon coupling constants
Two-bond proton–proton coupling constants
Methylene spin systems
Inverse INEPT
Residual dipolar couplings

ABSTRACT

The C–H_A cross-peak corresponding to a diastereotopic CH_AH_B methylene spin system exhibits a characteristic 1:0:1 multiplet pattern along the indirect dimension of a ω_1-coupled HSQC spectrum. It is shown here that the use of the initial ^{13}C Boltzmann polarization instead of the regular INEPT-based ^1H Boltzmann polarization makes visible the central lines of this multiplet pattern. A spin-state-selective method is proposed for the efficient measurement of both $^1J(CH_A)$ and $^1J(CH_B)$ along the indirect dimension of a 2D spectrum as well as to the magnitude and the sign of the geminal $^2J(H_AH_B)$ coupling constant from the straightforward analysis of a single four-component E.COSY cross-peak. Additionally, the extraction of $^1J(CH)$ values for CH and CH_3 multiplicities can be also performed from the same spectrum. The success of the method is also illustrated for the determination of residual dipolar $^1D(CH)$ and $^2D(HH)$ coupling constants in a small molecule weakly aligned in a PMMA swollen gel.

1. Introduction

In recent years, it has appeared an enormous interest for the measurement of scalar and residual dipolar (RDC) one-bond proton–carbon coupling constants ($^1J(CH)$ and $^1D(CH)$, respectively) in small molecules dissolved in weakly aligned anisotropic media [1–3]. HSQC-based pulse schemes have been generally chosen for this purpose and the accuracy and the simplicity on the experimental measurement of $^1J(CH)$ are subjects of discussion. Some topics of recent interest have been (i) the design of general and robust NMR methods that works efficiently for all multiplicities, (ii) the discussion about whether the $^1J(CH)$ splitting should be measured from the direct ω_2 (^1H) or the indirect ω_1 (^{13}C) dimension, (iii) the accurate measurement of $^1J(CH)$ for individual protons in diastereotopic CH_2 or NH_2 groups, or (iv) the simultaneous determination of additional coupling constants from the analysis of the same cross-peak, being the maximum interest the sign-sensitive determination of geminal $^2J(HH)$ values.

The measurement of $^1J(CH)$ from the detected dimension is relatively easy and high levels of digital resolution are readily available. For instance, the CLIP-HSQC experiment prove to be an efficient tool to determine the $^1J(CH)$ value from the resulting clean in-phase doublets [4]. However, strong J(HH) coupling effects can generate a high degree of asymmetry between the high- and low-field multiplet lines in ω_2-coupled HSQC spectra, which can preclude reliable determination of $^1J(CH)$ coupling constants values. In addition, broad signals and/or the large contributions of RDCs can generate poorly defined multiplets that make difficult accurate measurements. These drawbacks have already been described, particularly for CH spin systems in carbohydrates or on the typical strong geminal interaction found in diastereotopic CH_2 spin systems, and some practical solutions have been proposed [5–9]. To avoid such inconveniences, the measurement of $^1J(CH)$ along the ω_1 dimension have been advisable [9,10] although this requires the need for a large number of t_1 increments, and therefore longer acquisition times. The successful use of non-linear uniform sampling, J scaling factors or spectral folding can speed up data acquisition and/or increase the digital resolution in the ω_1 dimension [10].

The accurate measurement of $^1J(CH)$ for individual protons in diastereotopic CH_AH_B (or NH_AH_B) groups is one of the most challenging tasks in this field. Several methods have been proposed that measure them from the ω_1 or ω_2 dimension, but they all present some drawback that can prevent their general use [11–25]. For instance, the passive $^1J(C–H_B)$ value can be separately measured into the active H_A cross-peak, and vice versa, along the ω_1 dimension of a J-resolved HMQC experiment [11]. In addition, the large doublet is further split by the $^2J(H_AH_B)$ coupling yielding a double-doublet. The disadvantage is that additional experiments can

* Corresponding author.
E-mail address: teodor.parella@uab.cat (T. Parella).

http://dx.doi.org/10.1016/j.jmr.2014.02.003
1090-7807/

be needed to measure $^1J(CH)$ for CH or CH_3 spin systems. ^{13}C-edited versions of the 2D ^1H J-resolved experiment have been proposed to resolve enantiomeric derivatives dissolved in anisotropic media by visualizing their different $^1J(CH)$ splitting sizes along the indirect dimension [12,13]. Other related J-resolved HSQC experiments have been also described but they can require time-consuming 3D data acquisition [14] or the collection of multiple 2D J-modulated data [15,16]. An important group of NMR experiments are those based on spin-state selection specifically designed for methylene groups [8,17–25]. Some reported examples should be the P.E.HSQC [8] SPITZE [17] or CH_2-TROSY [19,20] experiments that yield simplified coupling patterns, and where the sign and the magnitude of the geminal $^2J(HH)$ can be additionally extracted. In all these cases, the central lines of the ω_1-multiplet corresponding to a CH_2 group are not observed, and therefore only the sum of the two $^1J(CH)$ can be determined from the indirect dimension.

In the present study, a new 2D ω_1-coupled inverse INEPT experiment (referred to as ω_1-iINEPT) is proposed for the observation of the missing central lines in diastereotopic CH_2 cross-peaks. The resulting cross-peak present a characteristic E.COSY multiplet pattern that facilitates the straightforward measurement of both individual $^1J(CH_A)$ and $^1J(CH_B)$ values, as well as the sign and magnitude of the geminal $^2J(HH)$ coupling. The method starts exclusively from ^{13}C Boltzmann polarization, it is driven with broadband ^{13}C decoupling during ^1H acquisition and, very importantly, also works for CH and CH_3 multiplicities. The experiment is easily adapted for a J-resolved presentation (referred to as ω_1-iINEPT-J) which allows obtain higher levels of resolution within the same experimental time by the use of a reduced spectral width in the indirect dimension [11–13,26,27]. The success of the method is illustrated for several samples and particular cases and as well as for the measurement of small residual coupling constants in small molecules dissolved in a weakly aligned media.

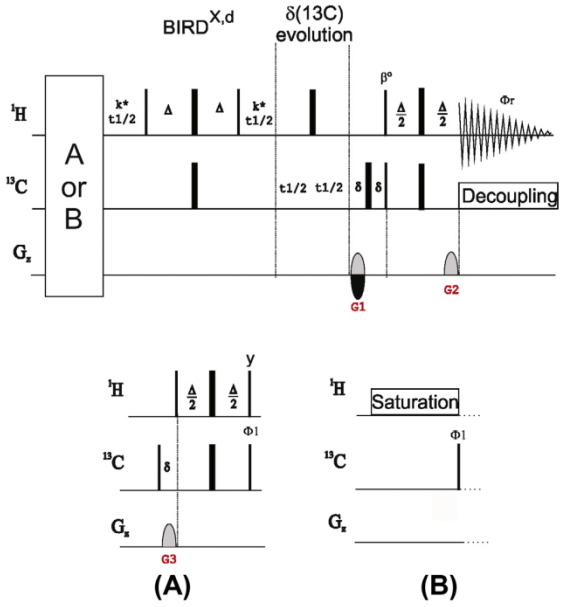

Fig. 1. Pulse sequences for the (A) ω_1-HSQC and (B) ω_1-iINEPT experiments. Thin and thick rectangles represent 90° and 180° rectangular pulses, respectively, applied along the x axis unless indicated differently. A basic two-step phase cycling is applied: $\varphi_1 = x,-x$; $\varphi_{rec} = x,-x$. A small flip angle ($\beta = 36°$) generates E.COSY cross-peaks. Inversion and refocusing 180° ^{13}C pulses can be applied as adiabatic pulses and the element labeled as $\delta(^{13}C)$ evolution period is optional. The inter-pulse delays in INEPT and BIRD elements are optimized according to $\Delta = 1/(2 * {}^1J(CH))$. The echo/anti-echo encoding of ω_1 frequencies was achieved by changing the sign of G1 between successive t_1 increments. The ratio between G1:G2:G3 were 80:20.1:13. The duration of a pulse-field gradient (PFG) and of the subsequent recovery delay amounts to δ.

2. Results and discussion

The idea to develop the ω_1-iINEPT experiment was born from the recent P.E.HSQMBC experiment, which was devised to measure three different $^1J(CH)$, $^2J(HH)$ and a $^nJ(CH)$ coupling constants from a single 2D cross-peak [28]. Other related works that have inspired us were the P.E.HSQC [8] and the BIRD-HSQC [9] experiments, this latter being further refined and evaluated by Thiele and Bermel (see Fig. 1c in Ref. [10]). The basic pulse scheme of the reference ω_1-coupled HSQC (ω_1-HSQC) experiment uses the traditional ^1H Boltzmann polarization as a starting point (Fig. 1A). In the following, we consider an isolated diastereotopic CH_AH_B spin system defined with three different $^1J(CH_A)$, $^1J(CH_B)$ and $^2J(H_AH_B)$ coupling constants. The sequence starts with an initial 90° (^{13}C)-gradient element to remove any contribution coming from the ^{13}C Boltzmann polarization. After the ^1H-to-^{13}C INEPT transfer, anti-phase ^{13}C magnetization is present as a mixture of $2H_{Az}C_y + 2H_{Bz}C_y$, which evolve under the effects of $^1J(CH)$ and $\delta(^{13}C)$ in a sequential mode, by using separated and synchronously incremented time periods. Thus, the magnetization evolves first under the effect of a $BIRD^{d,X}$ element [29,30] flanked by a variable J-scaled t_1 evolution period (defined by a scaling factor k) to allow the exclusive evolution of $^1J(CH)$ whereas ^{13}C chemical shift and long-range CH contributions are refocused, and then ^{13}C chemical shift can evolve from an optional t_1 evolution period as usual. In the subsequent analysis, the scaling factor, which is set arbitrarily within the limits set by relaxation and/or signal overlapping, the effects of the labeling G1 gradient and the optional ^{13}C chemical shift t_1 evolution period are neglected for the sake of clarity. Thus, for a single H_A spin, the evolution during the variable t_1 BIRD-based period ($k = 1$) is described as:

$$2H_{Az}C_y[\cos(\pi^1J(CH_A)t_1)\cos(\pi^1J(CH_B)t_1) - \sin(\pi^1J(CH_A)t_1) \times \sin(\pi^1J(CH_B)t_1)] \quad (1)$$

Applying the trigonometric relationship $\cos A\cos B - \sin A\sin B = \cos(A + B)$, we obtain

$$2H_{Az}C_y\cos(\pi^1J(CH_A + {}^1J(CH_B))t_1) \quad (2)$$

meaning that only the outer lines of the theoretical triplet or double-doublet coupling pattern of the methylene proton cross-peak would be observed and, therefore, only the sum of the both couplings ($^1J(CH_A + {}^1J(CH_B)$) will be observed as an in-phase doublet along the indirect dimension (Fig. 2A) [15]. This dependence with respect to the cosine function makes that multiplet patterns with relative intensities of 1:1 for CH, 1:0:1 for CH_2, and 3:1:1:3 for CH_3 will be displayed along the ω_1 dimension [8,34]. A key feature introduced in the last refocusing INEPT block is the small-flip ^1H pulse angle ($\beta = 36°$) which generates simplified E.COSY multiplet patterns for non-equivalent protons in CH_2 and CH_3 spin systems (Fig. 2B) [8,31–33].

To improve the appearance and usefulness of cross-peaks obtained from ω_1-iINEPT experiments, we propose to start the experiment with the initial ^{13}C Boltzmann polarization instead of the INEPT-based ^1H Boltzmann polarization because this leads to interesting changes in the central lines of methylene cross-peaks, as known for the analogous old ^{13}C-detected heteronuclear J-resolved 2D experiment [35]. The initial 90° ^{13}C pulse, applied after an

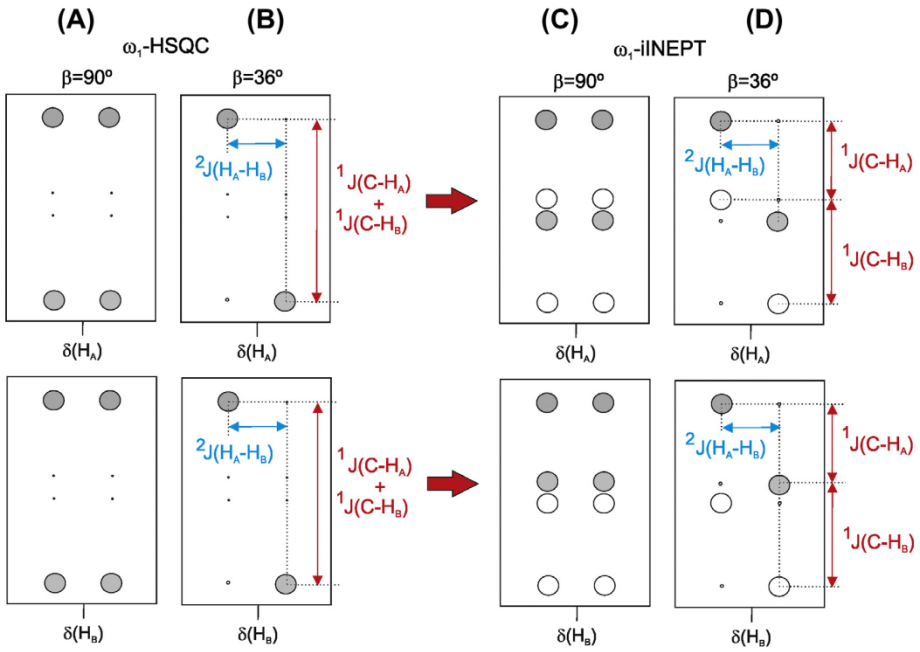

Fig. 2. Schematic representation of the 2D multiplet pattern of each individual H_A and H_B proton belonging to a methylene CH_AH_B group. (A and B) ^{1}H-Boltzmann polarization driven (ω_1-HSQC) experiments using $\beta = 90°$ and 36°, respectively, and (C and D) ^{13}C-Boltzmann polarization driven experiments (ω_1-iINEPT) using $\beta = 90°$ and 36°, respectively. In (D), the magnitude and the sign of all involved couplings (defined as $^2J(H_AH_B)$ and assuming $^1J(CH_A) < {}^1J(CH_B)$) can be readily extracted. Open and dotted circles represent peaks with opposite phase.

heteronuclear NOE enhanced pre-scan period by means of a ^{1}H WALTZ-16 pulse train saturation, generates in-phase $-C_y$ magnetization (Fig. 1B) which evolves under the effect of $^1J(CH)$ during the variable t_1 BIRD-based period:

$$-2H_{Az}C_x[\sin(\pi^1J(CH_A)t_1)\cos(\pi^1J(CH_B)t_1)] - 2H_{Bz}C_x[\cos(\pi^1J(CH_A)t_1)\sin(\pi^1J(CH_B)t_1)] \quad (3)$$

The result is a pure absorptive 2D ω_1-iINEPT spectra displaying double-doublet coupling patterns along the ω_1 dimension for each individual H_A or H_B cross-peaks, that initially would consist of eight different components as shown in Fig. 2C. Analyzing only the H_A spin, it will show an anti-phase doublet pattern with respect to $^1J(CH_A)$ (sine modulated) and an additional in-phase doublet pattern with respect to $^1J(CH_B)$ (cosine modulated) along the ω_1 dimension. As discussed before, the effect to apply a small flip angle ($\beta = 36°$) will generate a simplified four-component cross-peak with a characteristic E.COSY multiplet pattern due to the mutual $^2J(H_AH_B)$ (Fig. 2D), which facilites both the multiplet interpretation and analysis (see Fig. S1; supporting information). Thus, the active $^1J(CH_A)$ coupling is directly extracted from the anti-phase 1:−1 pattern along the same column in ω_1, whereas the passive $^1J(CH_B)$ coupling can be also extracted directly by measuring the in-phase components in each part of the E.COSY pattern. Otherwhise, the sign and the magnitude of $^2J(HH)$ is easily extracted from the frequency separation between tilted peaks along the w2 dimension. Fig. 2 summarizes the expected cross-peak pattern for a single diastereotopic CH_AH_B proton using the different ω_1-HSQC and ω_1-iINEPT approaches with $\beta = 90°$ and 36°. For CH groups, a doublet with relative 1:−1 intensities is obtained whereas a 1:1:−1:−1 coupling pattern will be displayed for a CH_3 group.

As a first example, Fig. 3A and B shows the equivalent ω_1-HSQC and ω_1-iINEPT correlation spectra, respectively, of strychnine (**1** in Scheme 1) acquired with the pulse schemes of Fig. 1, under the same experimental conditions and using a scaling factor of $k = 8$. The general coupling pattern for individual CH and CH_2 groups are marked with highlighted boxes. CH cross-peaks present the same doublet structure in both approaches. On the other hand, whereas the central lines for each individual CH_2 cross-peak are absent in the ω_1-HSQC spectrum, they are clearly distinguished in the ω_1-iINEPT version. A close inspection of the multiplet patterns for CH_2 cross-peaks in both spectra reveals the simplified E.COSY multiplet structure as described in other related experiments [8,19]. Also note the different in-phase *vs* anti-phase pattern behavior along the indirect dimension, although this is not relevant for the measurement. In cases where chemical shift assignment is already known and/or signal overlapping is not severe, the proposed method can be recorded in a J-resolved mode by simple omission of the ^{13}C chemical shift evolution period ($t_{1/2} - 180°(^1H) - t_{1/2}$). In this way the spectral width in the indirect dimension could be reduced by a factor of about 40, from 20,000 Hz (160 ppm at 500 MHz) to 500 Hz, and therefore the spectral resolution in ω_1 should be improved by a similar factor if all other experimental conditions remain the same. Fig. 3C and D shows the equivalent ω_1-HSQC-J and ω_1-iINEPT-J spectra, respectively, acquired with the same number of t_1 increments and using an scaling factor of $k = 1$. It can be observed that the absence of ^{13}C chemical shift signal dispersion does not introduce a serious problem on severe signal overlapping in a small molecule like **1**, where all cross-peaks can be succesfully analyzed. All the discussion and conclusions described in Ref. [10] about the application of non-linear sampling to accelerate data acquisition and/or to increase digital resolution in the indirect dimension could

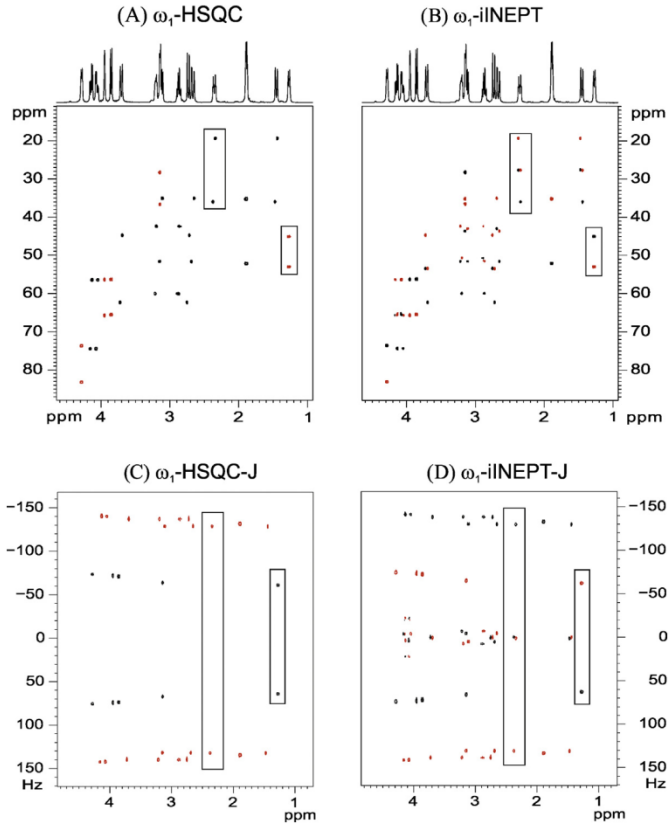

Fig. 3. 2D ^{1}H–^{13}C spectra of **1** acquired with the pulse sequences of Fig. 1. (A) ω_1-HSQC and (C) ω_1-HSQC-J spectra were obtained starting from ^{1}H Boltzmann magnetization, and (B) ω_1-iINEPT and (D) ω_1-iINEPT-J spectra were achieved starting from ^{13}C Boltzmann magnetization. (A) and (B) are heteronuclear correlation maps (acquired with an scaling factor of $k = 8$) whereas (C) and (D) are the corresponding J-resolved versions (scaling factor $k = 1$ and omission of the ^{13}C chemical shift t_1 evolution period). All spectra were acquired and processed under the same experimental conditions. 2 scans were collected for each one of the 256 t_1 increments using a pre-scan delay of 3 s. Squared boxes mark specific CH and diastereotopic CH_2 cross-peak as examples in each spectrum.

be extrapolated here for the proposed methods. Further increase of resolution by a factor of 3 can be additionally achieved by allowing signal folding in the indirect dimension (see Fig. S2 in the supporting information for an example provided using a reduced spectral width of 180 Hz).

Fig. 4 shows an expanded area of the 2D ω_1-iINEPT-J spectrum, where the clean tilt, the straightforward analysis and the excellent resolution of the resulting peak patterns can be quickly observed. Note the perfect equivalence between the cross peaks of diastereotopic protons (for instance H-18a *vs* H-18b or H-11a *vs* H-11b) which permit the easy and direct measurement of the same three different involved couplings ($^{1}J(CH_A)$ and $^{1}J(CH_B)$ as well as the geminal $^{2}J(HH)$) from two independent cross-peaks. The comparison of the experimental J values extracted from these two different measurements evaluates the accuracy of the measurement, and also ensures the measurement of all couplings even in the case of accidental signal overlapping of one of the two diastereotopic proton prevents its analysis. For well resolved $^{2}J(HH)$ values, the difference between diastereotopic $^{1}J(CH)$ values is quickly ascertained from the relative displacement between the two central lines and accurate $^{1}J(CH)$ values can be easily measured even in the case of minor differences between $^{1}J(CH_A)$ and $^{1}J(CH_B)$. For instance, whereas a small difference smaller than 2 Hz is measured for the H-15a/H-15b pair, a big difference about 14.5 Hz is found for H-18a/H-18b. Experimental $^{1}J(CH)$ and $^{2}J(HH)$ data extracted from these spectra for compound **1** are in agreement with those reported previously in other works (see Table S1 in the supporting information) [5,36–39]. Even in the case of signal overlapping, CH cross-peaks can be easily distinguished from those of CH_2 groups by their different doublet or double-doublet coupling patterns and also from the relative opposite phase of the anti-phase components for CH/CH_3 and CH_2 groups because the BIRD element acts as a multiplicity-editing element. For instance, note the clear distinction and straightforward measurement that can be performed for the three different protons resonating close to 3.1–3.2 ppm.

When two diastereotopic protons have similar chemical shift and $^{1}J(CH)$ values, the central lines can be partially or completely cancelled, as shown for the H-17a/H-17b protons resonating at 1.9 ppm in Fig. 3D. Another special case is when the geminal $^{2}J(HH)$ is near to 0 Hz, where the distinction of the four E.COSY components will depend of the different $^{1}J(CH)$ sizes. One illustrative example is the H-8a and H-8b olefinic protons belonging to the exocyclic CH_2 group in 5-methylene-2-norbornene (**2**) (Fig. 5A) which present unresolved signals in the conventional ^{1}H spectrum, and where the mutual $^{2}J(H8a–H8b)$ coupling can not be directly measured. The well differentiated four components observed in the ω_1-iINEPT-J spectra allow a measurement of $^{2}J(HH) = +1.1$ Hz,

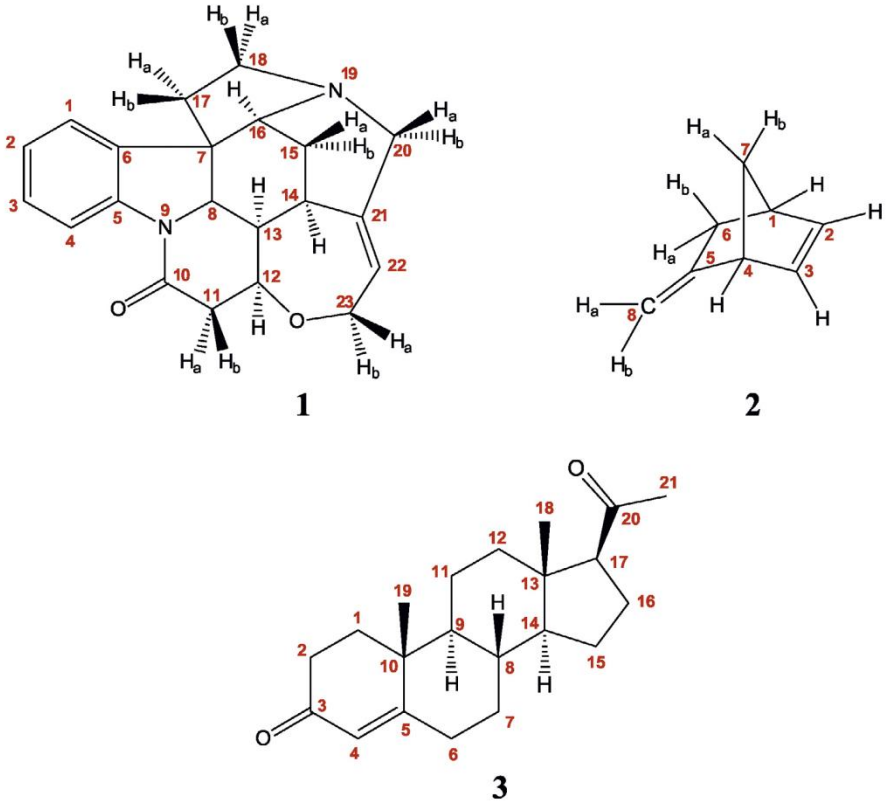

Scheme 1. Molecules used in this work.

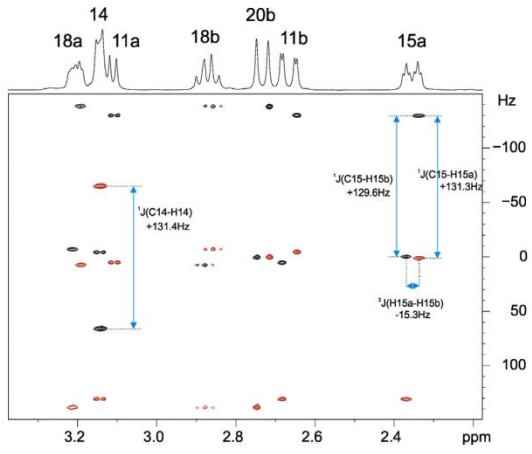

Fig. 4. Expanded area corresponding to the ω_1-iINEPT-J spectrum of Fig. 3D, where the different multiplet patterns for a CH group and several diastereotopic CH_2 spin systems can be clearly visualized and analyzed, and all ^{1}J(CH) and ^{2}J(HH) can be measured with simplicity and accuracy.

where the positive sign can be determined by comparison with the opposite E.COSY tilt presented by other diastereotopic H-6 and H-7 methylene protons, which have large negative ^{2}J(HH) values of −15.3 Hz and −8.1 Hz, respectively. Although there are small differences between the two central lines, the measurement of each individual ^{1}J(CH) (155.1 *vs* 157.1 Hz) can be performed twice, independently from each cross-peak and with a minimal deviation of ±0.1 Hz (Table S2; supporting information).

The simplicity of the proposed ω_1-iINEPT methods make them highly interesting for the measurement of small ^{1}D(CH) and ^{2}D(HH) RDCs, by comparison the difference between experimental measurements performed in isotropic *vs* anisotropic conditions ($D = T_{(aniso)} - J_{(is)}$). Compound **2** was weakly aligned in a poly(-methyl methacrylate) (PMMA) gel swollen in $CDCl_3$ using the reversible compression/relaxation method [40] , and ^{1}D(CH) and ^{2}D(HH) RDCs magnitudes and signs could be easily determined for all signals (see Fig. S3C; supporting information). Fig. 5 compares some cross-peaks obtained in both isotropic and anisotropic conditions. It can be seen how the relative orientation of each diastereotopic HH pair is clearly differentiated from their ^{2}D(HH) values: −0.2 Hz for H-8a/H-8b protons, −4.1 Hz for H-6a/H-6b protons and +3.1 Hz for H-7a/H-7b protons. A list of all measured scalar and residual dipolar coupling constants can be found in Table S2 of the supporting information.

The last example corresponds to a molecule having a more complex ^{1}H spectrum, progesterone (**3**), with high levels of signal overlapping in its aliphatic region. Fig. 6 shows an expanded area of the ω_1-iINEPT spectrum, where cross-peaks for all multiplicites can be distinguished and the corresponding ^{1}J(CH) and ^{2}J(HH) values conveniently measured (see Table S3 in the supporting information). For instance, note the excellent signal dispersion and multiplet editing for the five resonances fully overlapped in the 1.5–1.65 ppm area. Accidental overlapping of multiplet components

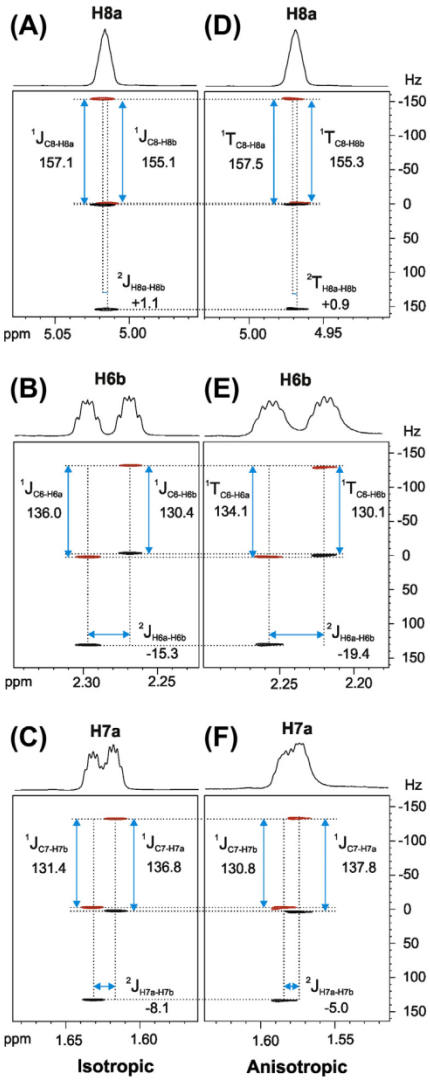

Fig. 5. Some illustrative 2D cross-peaks extracted from the ω_1-iINEPT-J spectra of **2** showing the easy measurement of the experimental $^1J(CH)/^1T(CH)$ and $^2J(HH)/^2T(HH)$ values measured in (A–C) isotropic ($CDCl_3$) and (D–F) anisotropic (weakly aligned in PMMA gel swollen in $CDCl_3$) conditions. Similar values for the same couplings are also measured from the cross-peaks of the other diastereotopic protons (see a complete set of coupling values in Table S2 in the Supporting information).

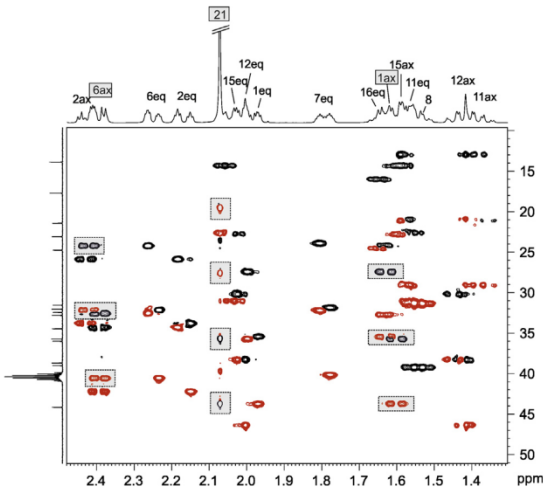

Fig. 6. Expanded area of the 2D ω_1-iINEPT spectrum of **3** acquired with 4 scans for each one of the 256 t_1 increments, and using a pre-scan delay of 3 s. Boxes enhance the different components corresponding to the H-6ax and H-1ax protons. In addition, the 1:1:−1:−1 multiplet corresponding to the methyl group 21 (at 2.08 ppm) is also highlighted.

can be overcomed by using the J-resolved version or by changing the scaling factor. The diastereotopicity in the three protons belonging to a methyl groups is not observed and they usually appear as a singlet due to their free rotation under isotropic conditions. However, in analogy with the discussion presented here for diastereotopic CH_2 spin systems, the same conclusions could be extracted from the analysis of a hypothetical non-equivalent protons in a CH_3 group [8,41]. Whereas isotropic CH_3 cross-peaks with no distinction between equivalent protons present a typical 3:1:1:3 multiplet pattern in ω_1-HSQC experiments [34], they display a symmetrical 1:1:−1:−1 coupling pattern in the ω_1-iINEPT, as seen for the Me-21 in Fig. 6. A modified HSQC experiment has been reported to recover the 1:2:1 and 1:3:3:1 pattern in NH_2 and NH_3^+ groups, respectively, and spin-state selected methods to study analysis have been used to study differential relaxation of the different line multiplets of methyl cross-peaks in proteins [41].

In terms of sensitivity, the ω_1-iINEPT experiment present a sensitivity decrease when compared to the analog ω_1-HSQC experiment, because of the differential signal enhancement achieved by heteronuclear polarization transfer via INEPT or by heteronuclear NOE effects. In addition, the pre-scan delay must be optimized as a function to the longer ^{13}C T_1 values, although that protonated carbons relax relatively fast. Our experimental data confirms such theoretical prediction and signal-to-noise enhancements by a factor of about 3 and 4 can be achieved for ω_1-iINEPT and ω_1-HSQC experiments, respectively, when compared with a reference non signal-enhanced ω_1-iINEPT experiment acquired without proton saturation and a pre-scan delay of 3 s (see Fig. S4 in the supporting information). Although the proposed methodology could distinguish diastereotopic protons in NH_2 groups, the large difference in sensitivity enhancement achieved by polarization transfer when compared with those obtained by direct ^{15}N Boltzmann magnetization without NOE enhancement (a theoretical factor about 10) makes the experiment of limited practical use due to its very low sensitivity. In addition, the two central lines are likely to be quite broad for large molecules.

In summary, a general and simple NMR method to obtain a characteristic spin-state-selected multiplet pattern for diastereotopic CH_AH_B methylene systems has been described. The magnitude and the sign of the three involved coupling values ($^1J(CH_A)$, $^1J(CH_B)$ and $^2J(H_AH_B)$) can be measured simultaneously from the analysis of a single and clean four-component E.COSY cross-peak. The method also measures $^1J(CH)$ for all other carbon multiplicities, and it is easily adapted for a J-resolved representation that allows the use of a more reduced spectral width in the carbon dimension, obtaining higher levels of resolution within the same experimental time. We have also shown that small $^1D(CH)$ and $^2D(HH)$ RDCs can be measured for small molecules weakly aligned in anisotropic media. The proposed techniques are appropriate for routine use because require minimum set-up and afford simple data analysis and interpretation.

3. Methods and materials

The isotropic samples used in this work were 0.12 M strychnine dissolved in $CDCl_3$ (**1**), 0.14 M 5-methylene-2-norbornene dissolved in $CDCl_3$ (**2**) and 0.13 M progesterone dissolved in DMSO (**3**) (see chemical structures in Scheme 1). For the measurement of RDCs, 10 mg of **2** was aligned in a poly(methyl methacrylate) (PMMA) gel swollen in $CDCl_3$ using the reversible compression/relaxation method [40]. The ^{2}H quadrupolar splitting ($\Delta\nu Q$) for the $CDCl_3$ signal was of 24 Hz. NMR experiments on **1** and **3** were recorded on a BRUKER DRX-500 spectrometer equipped with a 3-channel 5-mm cryoprobe incorporating a z-gradient coil. NMR experiments on **2** were carried out in a Bruker Avance 600 spectrometer equipped with a TXI HCN z-grad probe. The temperature for all measurements was set to 298 K.

In all experiments, the inter-pulse Δ (=1/(2 * ^{1}J(CH)) delays were set to 3.5 ms (optimized to ^{1}J(CH)=145 Hz). Gradient ratios for G1:G2:G3 were set to 80:20.1:13, measured as percentage of the absolute gradient strength of 53.5 G/cm. Sine bell shaped gradients of 1 ms of duration and followed by a recovery delay of 100 μs were used. ^{1}H saturation during the entire pre-scan delay was accomplished applying a 2.5 kHz WALTZ-16 modulated pulse train. Broadband ^{13}C decoupling during acquisition was achieved applying a 8 kHz GARP modulated pulse train. All experiments were acquired and processed using the echo/anti-echo protocol where the gradient G1 was inverted for every second FID. An scaling factor $k = 8$ were used for the correlation experiments for all compounds. The J-resolved spectra were acquired omitting the $t_{1/2} - 180(^1H) - t_{1/2}$ element in the pulse sequence of Fig. 1 and reducing the spectral width in the indirect ω_1 dimension to 500 Hz.

For spectra of Figs. 3, 2 scans were accumulated for each one of the 256 t_1 increments and the number of data points in t_2 was set to 2048. The recycle delay was set to 1 s for ω_1-HSQC type experiments (Fig. 3A and C) and 3 s for ω_1-iINEPT type experiments (Fig. 3B and D). Spectra 3A and 3B were acquired with an spectral window of 5000 Hz (in ω_2) and 20,000 Hz (in ω_1) giving a FID resolution of 2.4 and 9.8 Hz, respectively. Prior to Fourier-transformation of each data, zero filling to 4096 in ω_2, 1024 in ω_1 and a $\pi/2$-shifted sine-squared window function in both dimensions were applied. After applying zero filling the digital resolution was 1.2 and 2.4 Hz, respectively. In spectra of Figs. 3C and 3D, the spectral window in ω_1 dimension was reduced to 500 Hz giving a FID resolution of 2.4 Hz (in ω_2) and 1.9 Hz (in ω_1). After applying zero filling the digital resolution was 1.2 and 0.5 Hz, respectively.

In the ω_1-iINEPT-J experiments recorded on **2** in isotropic and anisotropic media (Fig. 5), a recycle delay of 3 s was used, 4 scans were accumulated for each one of the 256 t_1 increments and the number of data points in t_2 was set to 2048. Both of them were acquired with an spectral window of 3600 Hz (in ω_2) and 500 Hz (in ω_1) giving a FID resolution of 1.8 and 1.9 Hz, respectively. Prior to Fourier-transformation of each data, zero filling to 4096 in ω_2, 1024 in ω_1 and a $\pi/2$-shifted sine-squared window function in both dimensions were applied. After applying zero filling the digital resolution was 0.9 and 0.5 Hz, respectively. In the ω_1-iINEPT experiment recorded on **3** (Fig. 6), a recycle delay of 3 s was used, 4 scans were recorded for each one of the 256 t_1 increments and the number of data points in t_2 was set to 2048 in all the experiments. Data were acquired with an spectral window of 2000 Hz (in ω_2) and 12,500 Hz (in ω_1) giving a FID resolution of 1.0 and 6.1 Hz, respectively. Prior to Fourier-transformation of each data, zero filling to 4096 in ω_2, 1024 in ω_1 and a $\pi/2$-shifted sine-squared window function in both dimensions were applied. After applying zero filling the digital resolution was 0.5 and 1.5 Hz, respectively.

Acknowledgments

Financial support for this research provided by MINECO (project CTQ2012-32436) is gratefully acknowledged. Authors thanks to R.R. Gil and A. Navarro-Vázquez for a sample of PMMA gel. We also thank the Servei de Ressonància Magnètica Nuclear, Universitat Autònoma de Barcelona, for allocating instrument time to this project.

Appendix A. Supplementary material

Supplementary data associated with this article can be found, in the online version, at http://dx.doi.org/10.1016/j.jmr.2014.02.003.

References

[1] C.M. Thiele, Residual dipolar couplings (RDCs) in organic structure determination, Eur. J. Org. Chem. (2008) 5673–5685.
[2] G. Kummerlowe, B. Luy, Residual dipolar couplings for the configurational and conformational analysis of organic molecules, Annu. Rep. NMR Spectrosc. 68 (2009) 193–230.
[3] G. Kummerlowe, B. Luy, Residual dipolar couplings as a tool in determining the structure of organic molecules, Trend Anal. Chem. 28 (2009) 483–493.
[4] A. Enthart, J.C. Freudenberger, J. Furrer, H. Kessler, B. Luy, The CLIP/CLAP HSQC: pure absorptive spectra for the measurement of one-bond couplings, J. Magn. Reson. 192 (2008) 314–322.
[5] C.M. Thiele, Simultaneous assignment of all diastereotopic protons in strychnine using RDCs: PELG as alignment medium for organic molecules, J. Org. Chem. 69 (2004) 7403–7413.
[6] B.W. Yu, H. van Ingen, S. Vivekanandan, C. Rademacher, S.E. Norris, D.I. Freedberg, More accurate ^{1}JCH coupling measurement in the presence of ^{3}JHH strong coupling in natural abundance, J. Magn. Reson. 215 (2012) 10–22.
[7] B.W. Yu, H. van Ingen, D.I. Freedberg, Constant time INEPT CT-HSQC (CTi-CT-HSQC) – a new NMR method to measure accurate one-bond J and RDCs with strong 1H–1H couplings in natural abundance, J. Magn. Reson. 228 (2013) 159–165.
[8] P. Tzvetkova, S. Simova, B. Luy, P.E. HSQC: a simple experiment for the simultaneous and sign-sensitive measurement of (^{1}JCH + DCH) and (^{2}JHH + DHH) couplings, J. Magn. Reson. 186 (2007) 193–200.
[9] K. Fehér, S. Berger, K.E. Kövér, Accurate determination of small one-bond heteronuclear residual dipolar couplings by F1 coupled HSQC modified with a G-BIRD(r) module, J. Magn. Reson. 163 (2003) 340–346.
[10] C.M. Thiele, W. Bermel, Speeding up the measurement of one-bond scalar (1J) and residual dipolar couplings (1D) by using non-uniform sampling (NUS), J. Magn. Reson. 216 (2012) 134–143.
[11] K.E. Kövér, K. Fehér, Measurement of one-bond heteronuclear dipolar coupling contributions for amine and diastereotopic protons, J. Magn. Reson. 168 (2004) 307–313.
[12] L. Ziani, J. Courtieu, D. Merlet, Visualisation of enantiomers via insertion of a BIRD module in X-H correlation experiments in chiral liquid crystal solvent, J. Magn. Reson. 183 (2006) 60–67.
[13] U.R. Prabhu, S.R. Chaudhari, N. Suryaprakash, Visualization of enantiomers and determination of homo- and hetero-nuclear residual dipolar and scalar couplings: the natural abundant ^{13}C edited J/D-resolved NMR techniques, Chem. Phys. Lett. (2010) 334–341.
[14] J. Furrer, M. John, H. Kessler, B. Luy, J-spectroscopy in the presence of residual dipolar couplings: determination of one-bond coupling constants and scalable resolution, J. Biomol. NMR 37 (2007) 231–243.
[15] M. Ottiger, F. Delaglio, J.L. Marquardt, N. Tjandra, A. Bax, Measurement of Dipolar Couplings for methylene and methyl sites in weakly oriented macromolecules and their use in structure determination, J. Magn. Reson. 124 (1998) 365–369.
[16] T.N. Pham, T. Liptaj, K. Bromek, D. Uhrín, Measurement of small one-bond proton-carbon residual dipolar coupling constants in partially oriented ^{13}C natural abundance oligosaccharide samples. Analysis of heteronuclear ^{1}JCH-modulated spectra with the BIRD inversion pulse, J. Magn. Reson. 157 (2002) 200–209.
[17] T. Carlomagno, W. Peti, C. Griesinger, A new method for the simultaneous measurement of magnitude and sign of ^{1}DCH and ^{1}DHH dipolar couplings in methylene groups, J. Biomol. NMR 17 (2000) 99–109.
[18] P. Permi, A spin-state-selective experiment for measuring heteronuclear one-bond and homonuclear two-bond couplings from an HSQC-type spectrum, J. Biomol. NMR 22 (2002) 27–35.
[19] E. Miclet, D.C. Williams Jr., G.M. Clore, D.L. Bryce, J. Boisbouvier, A. Bax, Relaxation-optimized NMR spectroscopy of methylene groups in proteins and nucleic acids, J. Am. Chem. Soc. 126 (2004) 10560–10570.
[20] G. Guichard, A. Violette, G. Chassaing, E. Miclet, Solution structure determination of oligoureas using methylene spin state selective NMR at ^{13}C natural abundance, Magn. Reson. Chem. 46 (2008) 918–924.

[21] T. Parella, M. Gairí, Simultaneous recording of spin-state-selective NMR spectra for different I_nS spin systems, J. Am. Chem. Soc. 126 (2004) 9821–9826.
[22] P. Permi, Two simple NMR experiments for measuring dipolar couplings in asparagine and glutamine side chains, J. Magn. Reson. 153 (2001) 267–272.
[23] E. Miclet, E. O'Neil-Cabello, E.P. Nikonowicz, D. Live, A. Bax, ^{1}H–^{1}H dipolar couplings provide a unique probe of RNA backbone structure, J. Am. Chem. Soc. 125 (2003) 15740–15741.
[24] P. Nolis, J.F. Espinosa, T. Parella, Optimum spin-state-selection for all multiplicities in the acquisition dimension of the HSQC experiment, J. Magn. Reson. 180 (2006) 39–50.
[25] P. Nolis, T. Parella, Solution-state NMR experiments based on heteronuclear cross-polarization, Curr. Anal. Chem. 3 (2007) 47–68.
[26] M. Liu, R.D. Farrant, J.M. Gillam, J.K. Nicholson, J.C. Lindon, Selective inverse-detected long-range heteronuclear *J*-resolved NMR spectroscopy and its application to the measurement of ^{3}JCH, J. Magn. Reson. B 109 (1995) 275–283.
[27] K. Kobzar, H. Kessler, B. Luy, Stretched gelatin gels as chiral alignment media for the discrimination of enantiomers by NMR spectroscopy, Angew. Chem. Int. Ed. 44 (2005) 3145–3147.
[28] J. Saurí, L. Castañar, P. Nolis, A. Virgili, T. Parella, P.E. HSQMBC: simultaneous measurement of proton–proton and proton–carbon coupling constants, J. Magn. Reson. 224 (2012) 101–106.
[29] J.R. Garbow, D.P. Weitekamp, A. Pines, Bilinear rotation decoupling of homonuclear scalar interactions, Chem. Phys. Lett. 93 (1982) 504–509.
[30] D. Uhrín, T. Liptaj, K.E. Kövér, Modified BIRD pulses and design of heteronuclear pulse sequences, J. Magn. Reson. A 101 (1993) 41–46.
[31] C. Griesinger, O.W. Sørensen, R.R. Ernst, Two-dimensional correlation of connected NMR transitions, J. Am. Chem. Soc. 107 (1985) 6394–6396.
[32] L. Mueller, P.E-COSY, a simple alternative to E.COSY, J. Magn. Reson. 72 (1986) 191–196.
[33] C. Griesinger, O.W. Sørensen, R.R. Ernst, Practical aspects of the E.COSY technique. Measurement of scalar spin-spin coupling constants in peptides, J. Magn. Reson. 75 (1987) 474–492.
[34] Y. Takayama, D. Sahu, J. Iwahara, Observing in-phase single-quantum ^{15}N multiplets for NH_2/NH_3^+ groups with two-dimensional heteronuclear correlation spectroscopy, J. Magn. Reson. 194 (2008) 313–316.
[35] W.P. Aue, L. Muller, R.R. Ernst, Phase separation in two-dimensional spectroscopy, J. Magn. Reson. 28 (1977) 29–39.
[36] B. Luy, K. Kobzar, H. Kessler, An easy and scalable method for the partial alignment of organic molecules for measuring residual dipolar couplings, Angew. Chem. Int. Ed. 43 (2004) 1092–1094.
[37] A. Bagno, F. Rastrelli, G. Saielli, Toward the complete prediction of the ^{1}H and ^{13}C NMR spectra of complex organic molecules by DFT methods: application to natural substances, Chem. Eur. J. 12 (2006) 5514–5525.
[38] M. Misiak, W. Koźmiński, Determination of heteronuclear coupling constants from 3D HSQC-TOCSY experiment with optimized random sampling of evolution time space, Magn. Reson. Chem. 47 (2009) 205–209.
[39] J.C. Cobas, V. Constantino-Castillo, M. Martín-Pastor, F. del Río Portilla, A two-stage approach to automatic determination of 1H NMR coupling constants, Magn. Reson. Chem. 43 (2005) 843–848.
[40] C. Gayathri, N.V. Tsarevsky, R.R. Gil, RDCs analysis of small molecules made easy: fast and tuneable alignment by reversible compression/relaxation of reusable PMMA gels, Chem. Eur. J. 16 (2010) 3622–3626.
[41] G. Kontaxis, A. Bax, Multiplet component separation for measurement of methyl ^{13}C–^{1}H dipolar couplings in weakly aligned proteins, J. Biomol. NMR 20 (2001) 77–82.

Straightforward measurement of individual $^{1}J(CH)$ and $^{2}J(HH)$ in diastereotopic CH_2 groups.

Josep Saurí, Laura Castañar, Pau Nolis, Albert Virgili and Teodor Parella*

Supporting Information

Figure S1: Effect of the β angle in ω_1-iINEPT-J experiments.

Figure S2: Spectral Folding in ω_1-iINEPT-J experiment.

Figure S3: ω_1-iINEPT and ω_1-iINEPT-J spectra of 5–methylene-2-norbornene in isotropic and anisotropic media.

Figure S4: Intensity signal dependence with respect the pre-scan delay in ω_1-iINEPT and ω_1-HSQC experiments

Table S1: ^{1}J(CH) and ^{2}J(HH) coupling constants of strychnine measured from ω_1-iINEPT-J spectra and other published methods.

Table S2: ^{1}J(CH)/^{1}T(CH) and ^{2}J(HH)/^{2}T(HH) coupling constants of 5-methylene-2-norbornene measured from ω_1-iINEPT-J spectra.

Table S3: ^{1}J(CH) and ^{2}J(HH) coupling constants of progesterone measured from ω_1-iINEPT and ω1-HSQC spectra.

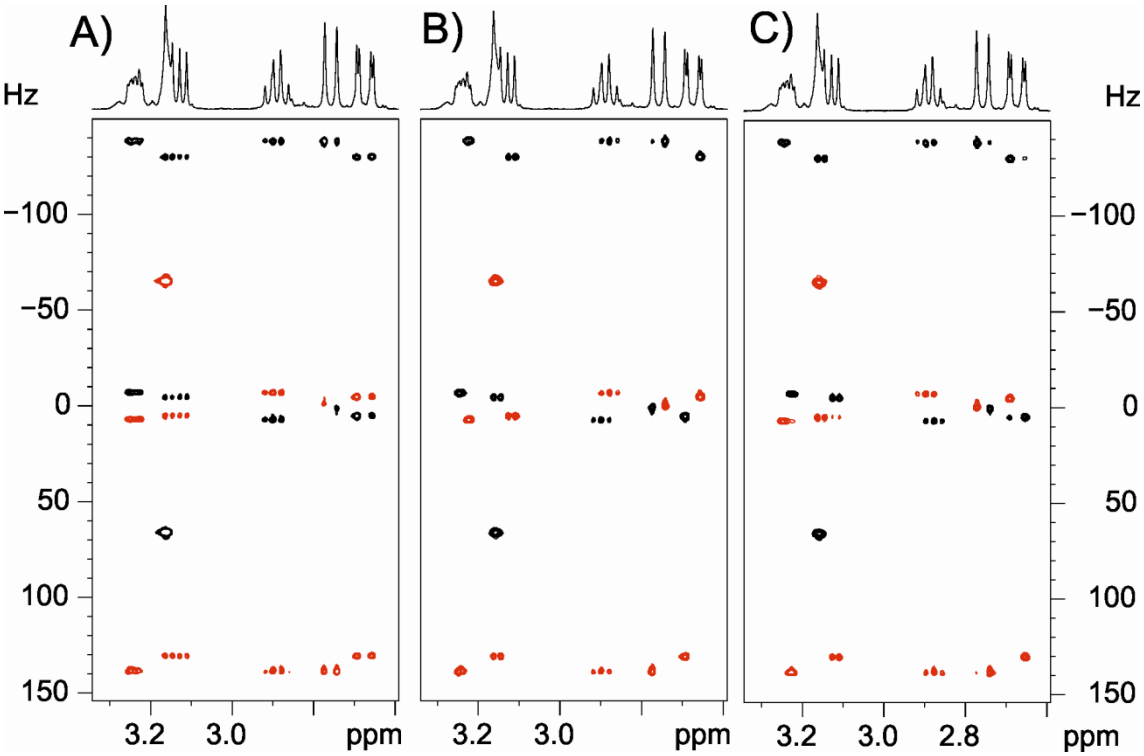

Figure S1: Effect of the β angle in ω_1-iINEPT-J experiments of **1**: A) β=90º, B) β=36º, and C) β=126º. Note the complementary spin-state selection in B *vs* C. Experimental conditions as described for Fig. 3D.

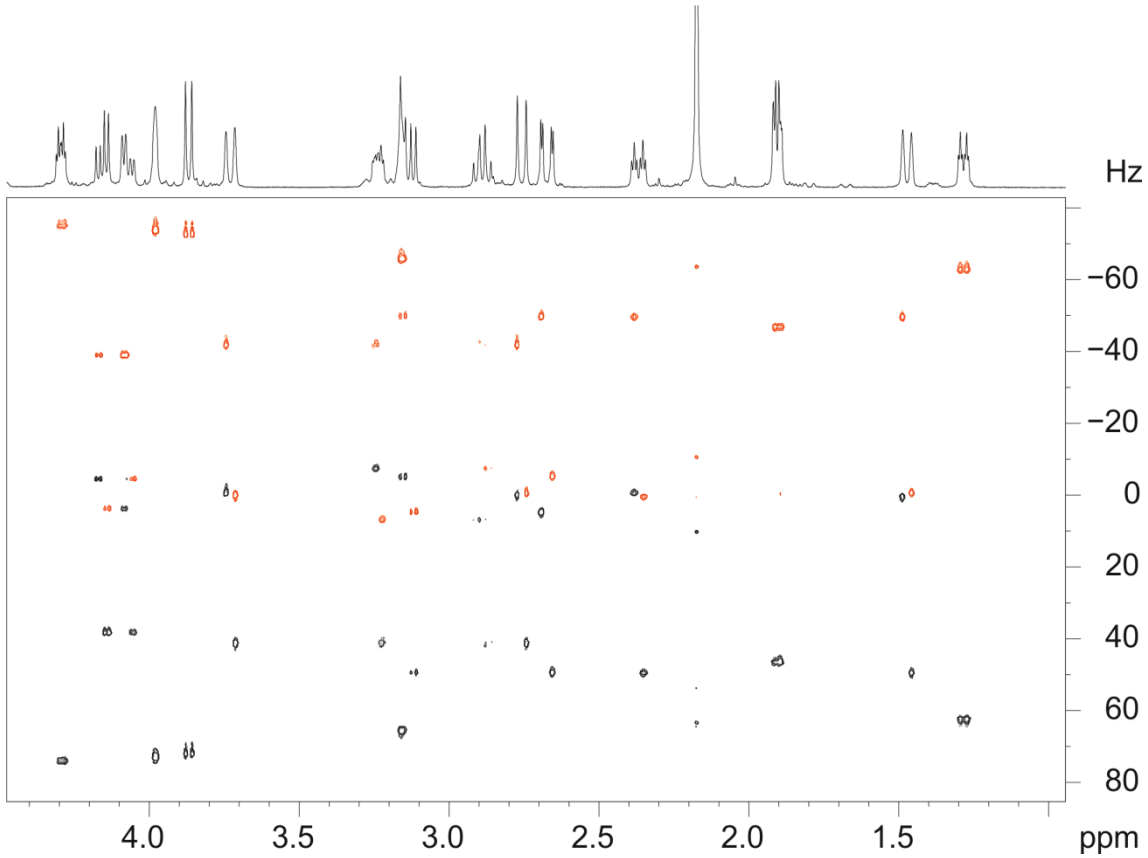

Figure S2: Spectral folding in the ω_1-iINEPT-J spectrum of **1**. 2 scans were collected for each one of the 256 t_1 increments using a spectral width (SW(F1)) of 180Hz in the indirect dimension. The digital resolution was of 0.18 Hz in the indirect dimension. All other experimental conditions as described in the Fig. 3D. ^{1}J(CH) coupling values are extracted from the relationship SW(F1)-$\Delta\nu(\omega_1)$, where $\Delta\nu(\omega_1)$ is the distance measured between individual components of a given cross-peak along the indirect dimension. Similarly, the distance between outer components allows to obtain the sum of the two coupling values, according to $^1J(CH_A)+ {}^1J(CH_B)=2*SW(F1)-\Delta\nu(F1)$.

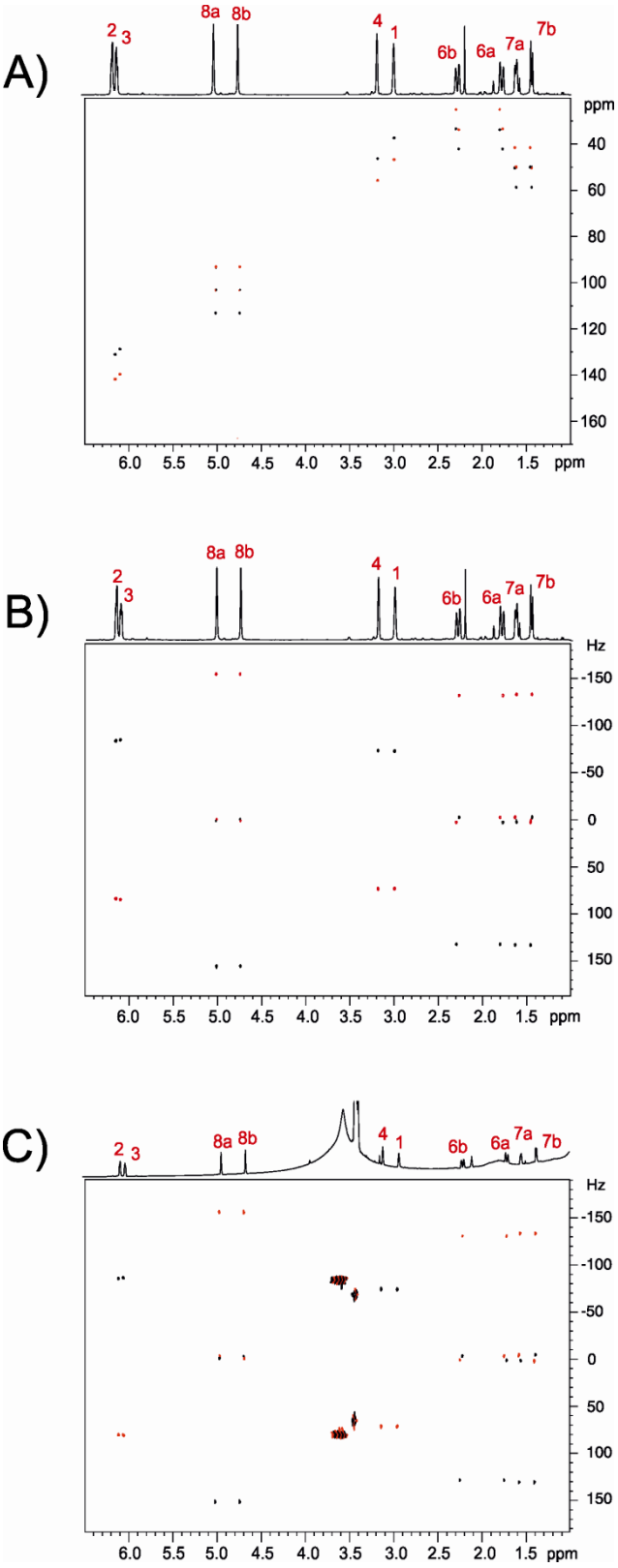

Figure S3: A) ω_1-iINEPT and B) ω_1-iINEPT-J spectra of **2** in isotropic $CDCl_3$ solution; C) ω_1-iINEPT spectra of **2** in anisotropic conditions (PMMA gel swollen in $CDCl_3$). ω_1-iINEPT experiment (A) was acquired with an scaling factor of k=8 whereas B) and C) used K=1. Other experimental conditions as described for Fig. 5.

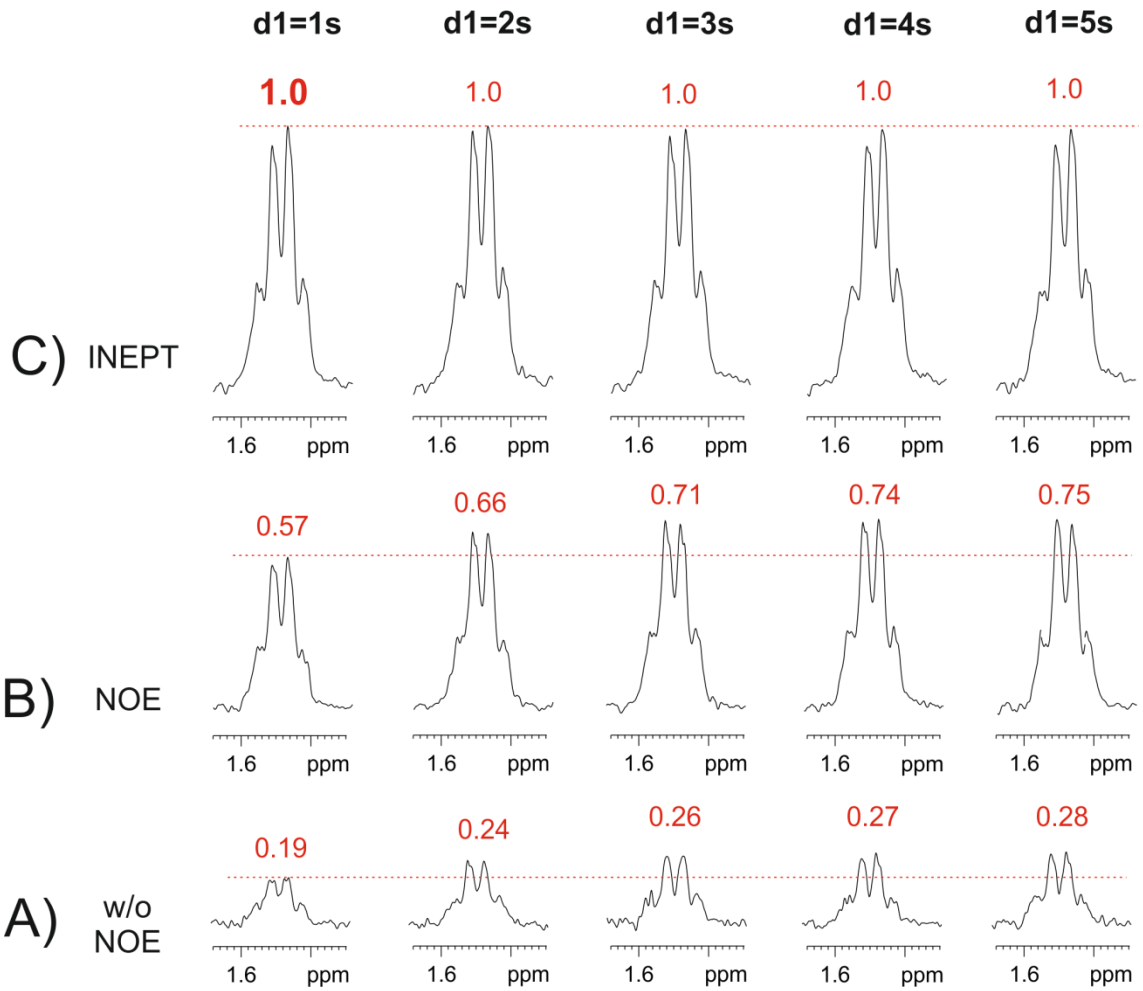

Figure S4: Signal intensity dependence of the H-8 proton in **3** as a function of the duration of the pre-scan delay: ω_1-iINEPT experiments A) without and B) with ^{1}H-saturation during the pre-scan delay, and c) ω_1-HSQC experiment using an initial INEPT transfer. As a reference, the intensity of the HSQC experiment using a recycle delay of 1 second has been normalized to 1.

Table S1: $^{1}J(CH)$ and $^{2}J(HH)$ coupling constants (in Hz) of strychnine (**1**) extracted from the ω_1-iINEPT-J spectrum.

		ω_1-iINEPT-J (This work)		**ref. [37]**	**ref. [36]**	**ref. [38]**	**ref. [5]**	**ref. [37]**	**ref. [39]**
		$^{1}J(CH)$	**$^{2}J(HH)$**	**$^{1}J(CH)$**				**$^{2}J(HH)$**	
C1	H1	158.9	-	158.0	158.8	159.0	159.0	-	-
C2	H2	161.7	-	162.0	160.7	161,3	161.56	-	-
C3	H3	160.3	-	159.0	-	159,4	159.85	-	-
C4	H4	169.1	-	168.2	168.7	168,6	168.4	-	-
C8	H8	144.9	-	145.1	144.7	144,9	144.89	-	-
C11 (from H11a)	H11a H11b	135.6 125.9	-18,1	133.8	134.9	135,3	135.06	-17,4	-17.38
C11 (from H11b)	H11a H11b	135.7 126.1	-18.3	125.2	125.8	125,5	126.08		
C12	H12	149.2	-	147.6	148.3	149,3	149.17	-	-
C13	H13	124.8	-	123.6	123.7	125,2	124.38	-	-
C14	H14	131.4	-	131.4	130.3	131,9	130.36	-	-
C15 (from H15a)	H15a H15b	131.3 129.6	-15.3	132.1	130.0	131,5	130.36	-14,5	-14.31
C15 (from H15b)	H15a H15b	130.7 129.6	-15.4	132.2	129.4	130,4	129.93		
C16	H16	146.8	-	146.9	145.9	146,3	146.6	-	-
C17	H17	133.1	-	134.0	134.2	133,1	132.93	-	-
C18 (from H18a)	H18a H18b	146.0 131.6	-10.3	139.7	147.1	147,6	146.17	-10,1	-
C18 (from H18b)	H18a H18b	146.1 131.3	-10.3	131.5	131.0	133,5	131.2		
C20 (from H20a)	H20a H20b	139.0 138.5	-15.6	137.7	138.4	139,7	138.91	-14,3	-14.74
C20 (from H20b)	H20a H20b	138.9 138.9	-15.5	137.7	138.7	139,9	138.91		
C22	H22	158.7	-	158.1	159.1	159,3	159.43	-	-
C23 (from H23a)	H23a H23b	145.1 137.3	-13.7	144.7	145.5	145,9	145.74	-13,7	-13.44
C23 (from H23b)	H23a H23b	145.6 137.2	-13.8	136.8	136.0	137,2	137.2		
Digital Resolution (Hz)		0.5	1.1	1.0	-	0.4	0.2	1.0	-

Table S2: $^{1}J(CH)$/ $^{1}T(CH)$ and $^{2}J(HH)$/$^{2}T(HH)$ coupling constants (in Hz) of 5–methylene-2-norbornene (**2**) measured from ω_1-iINEPT-J experiments in isotropic and anisotropic weakly aligned media.

		Isotropic		Anisotropic			
		$^{1}J_{CH}$	$^{2}J_{HH}$	$^{1}T_{CH}$	$^{2}T_{HH}$	$^{1}D_{CH}$[a]	$^{2}D_{HH}$[b]
C_1	H_1	147.2	-	147.9	-	0.7	-
C_2	H_2	168.9	-	168.2	-	-0.7	-
C_3	H_3	170.8	-	170.2	-	-0.6	-
C_4	H_4	148.3	-	148.8	-	0.5	-
C_6 (from H_{6a})	H_{6a}	136.0	-15.1	134.4	-18.9	-1.6	-3.8
	H_{6b}	130.7		130.1		-0.6	
C_6(from H_{6b})	H_{6a}	136.0	-15.3	134.1	-19.4	-1.9	-4.1
	H_{6b}	130.4		130.1		-0.3	
C_7 (from H_{7a})	H_{7a}	136.8	-8.1	137.8	-5.0	1.0	3.1
	H_{7b}	131.4		130.8		-0.6	
C_7 (from H_{7b})	H_{7a}	136.8	-8.1	137.9	-5.1	1.1	3.0
	H_{7b}	131.5		130.9		-0.6	
C_8 (from H_{8a})	H_{8a}	157.0	1.1	157.5	0.9	0.5	-0.2
	H_{8b}	155.1		155.3		0.2	
C_8 (from H_{8b})	H_{8a}	157.1	1.0	157.6	0.8	0.5	-0.2
	H_{8b}	155.1		155.4		0.3	
Digital Resolution (Hz)		0.5	0.9	0.5	0.9		

[a] RDCs ($^{1}D_{CH}$) values calculated from the different between the $^{1}T_{CH}$ values and the corresponding isotropic $^{1}J_{CH}$ values.

[b] RDCs ($^{2}D_{HH}$) values calculated from the different between the $^{2}T_{HH}$ values and the corresponding isotropic $^{2}J_{HH}$ values.

Table S3: $^{1}J(CH)$ and $^{2}J(HH)$ coupling constants of progesterone (**3**) measured from ω_1-iINEPT and ω_1-HSQC experiments.

		ω_1-iINEPT		**ω_1-HSQC**	
		$^{1}J(CH)$	**$^{2}J(HH)$**	**$^{1}J(CH)$ [a]**	**$^{2}J(HH)$**
C1 (from H1ax)	H1ax H1eq	126.8 129.9	-13.5	256.7	-13.8
C1 (from H1eq)	H1ax H1eq	126.5 127.7	-13.6	256.2	-13.3
C2 (from H2ax)	H2ax H2eq	123.9 132.1	-16.7	255.7	-16.6
C2 (from H2eq)	H2ax H2eq	124.3 132.3	-16.9	255.9	-16.9
C4	H4	158.8	-	158.7	-
C6 (from H6ax)	H6ax H6eq	124.8 130.6	-14.3	255.3	-14.5
C6(from H6eq)	H6ax H6eq	125.1 130.7	-14.4	255.1	-14.2
C7 (from H7ax)	H7ax H7eq	124.7 130.4	-13.2	254.5	-13.4
C7 (from H7eq)	H7ax H7eq	124.6 130.2	-13.3	254.5	-13.0
C8	H8	124.4	-	123.7	-
C9	H9	122.9	-	123.6	-
C11 (from H11ax)	H11ax H11eq	125.3 127.8	-9.5	253.7	-9.7
C11 (from H11eq)	H11ax H11eq	126.2 128.3	-10.8	253.8	-10.6
C12 (from H12ax)	H12ax H12eq	127.3 126.4	-13.7	256.2	-13.7
C12 (from H12eq)	H12ax H12eq	127.2 126.9	-13.5	256.1	-13.7
C14	H14	124.0	-	124.1	
C15 (from H15ax)	H15ax H15eq	130.7 132.4	-12.6	262.2	-12.9
C15 (from H15eq)	H15ax H15eq	ov 132.9	-13.7	262.1	-12.9
C16 (from H16ax)	H16ax H16eq	128.2 133.6	*	260.5	*
C16 (from H16eq)	H16ax H16eq	127.1 133.5	*	261.1	*
C17	H17	127.5	-	127.9	-
C18	H18	125.6	-	125.5	-
C19	H18	127.4	-	127.0	-
C21	H19	126.8	-	127.2	-
Digital Resolution (Hz)		1.5	0.5	1.5	0.5

[a] For diastereotopic CH_2 protons

PUBLICATION 13

Broadband ^{1}H homodecoupled NMR experiments: recent developments, methods and applications

Laura Castañar and Teodor Parella.
Mag. Reson. Chem., **2015**, *53*, 399-426.
DOI: 10.1002/mrc.4238

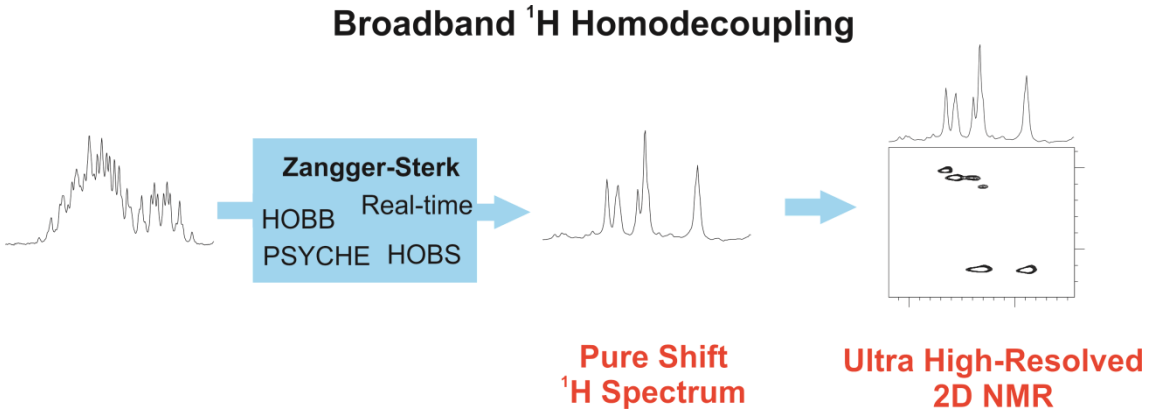

Introduction

In recent years, a great interest in the development of new broadband ^{1}H homonuclear decoupled techniques providing simplified J_{HH} multiplet patterns has emerged again in the field of small molecule NMR. The resulting highly resolved ^{1}H NMR spectra display resonances as collapsed singlets, therefore minimizing signal overlap and expediting spectral analysis. This publication is a complete revision work about modern pure shift NMR methodologies, with a particular emphasis to the Zangger–Sterk experiment.[3] A description of the most important broadband homodecoupling building blocks and their implementation on different versions of the ZS experiment is made. A detailed discussion about the most relevant practical aspects in terms of pulse sequence design, selectivity, sensitivity, spectral resolution and performance is provided. Finally, the implementation of the different reported strategies into traditional 1D and 2D NMR experiments is described while several practical applications are also reviewed, including (i) the measurement of homo- and heteronuclear coupling constants from simplified multiplets, (ii) the analysis of diffusion and relaxation data in overlapped regions, (iii) the pure shift versions of standard 2D experiments, and (iv) the combined use of different but complementary resolution-enhanced techniques into a single NMR experiment in order to have ultra-high-resolved spectra with standard hardware configurations and conventional acquisition times.

Feature article: review

MRC

Received: 21 January 2015 Revised: 23 February 2015 Accepted: 25 February 2015 Published online in Wiley Online Library: 21 April 2015

(wileyonlinelibrary.com) DOI 10.1002/mrc.4238

Broadband ^{1}H homodecoupled NMR experiments: recent developments, methods and applications

Laura Castañar and Teodor Parella*

In recent years, a great interest in the development of new broadband ^{1}H homonuclear decoupled techniques providing simplified J_{HH} multiplet patterns has emerged again in the field of small molecule NMR. The resulting highly resolved ^{1}H NMR spectra display resonances as collapsed singlets, therefore minimizing signal overlap and expediting spectral analysis. This review aims at presenting the most recent advances in pure shift NMR spectroscopy, with a particular emphasis to the Zangger–Sterk experiment. A detailed discussion about the most relevant practical aspects in terms of pulse sequence design, selectivity, sensitivity, spectral resolution and performance is provided. Finally, the implementation of the different reported strategies into traditional 1D and 2D NMR experiments is described while several practical applications are also reviewed. Copyright © 2015 John Wiley & Sons, Ltd.

Keywords: NMR spectroscopy; pure shift NMR; homonuclear decoupling; Zangger–Sterk; BIRD; HOBB; HOBS; PSYCHE

Introduction

NMR spectroscopy is one of the most powerful tools for determining structural, dynamic, chemical and physical properties of molecules under a great variety of sample conditions. The most significant aspects in NMR are sensitivity and spectral resolution. Advances in sensitivity have been occurring over the years by a multitude of different techniques intended to improve NMR data acquisition and processing. The development and the improvements in NMR instrumentation have also played a key role to enhance sensitivity, with a particular emphasis in the technical design of cryogenically cooled probes or higher magnetic fields. On the other hand, spectral resolution is also improved inherently in higher magnetic fields, which disperse the chemical shifts over a wider frequency range, although the effects of signal overlap can still be a limiting factor when analyzing complex NMR spectra. The continuous development of new pulse sequences and the improvement of the existing ones have been another very important factor to understand the enormous potential of the NMR spectroscopy, and the incorporation of multiple-frequency dimensions achieves a tremendous qualitative and quantitative leap, particularly when it comes to improving signal dispersion.

The associated benefits of decoupling through-bond interactions for the apparent simplification of scalar coupling constant splittings are easily understood when analyzing a typical ^{13}C spectrum, which is routinely recorded under broadband heteronuclear ^{1}H decoupling during data acquisition.[1–5] In a standard 1D ^{13}C{^{1}H} spectrum, all signals appear as single lines providing excellent signal dispersion, allowing the knowledge of the number of signals that are present and also measuring accurate chemical shift values in a very straightforward way. In contrast, despite using high magnetic fields, 1D ^{1}H NMR spectra often suffer of low signal resolution and severe signal overlap due to the limited range of ^{1}H chemical shifts and also to the additional J_{HH} splittings observed in each proton resonance. The analysis of the fine multiplet structure contains valuable structural information such as the number and knowledge of neighboring spins or dihedral angle constraints, but, in many cases, signal overlap hampers a definitive multiplet analysis or the accurate extraction of chemical shifts, which are also fundamental in the analysis and interpretation of NMR spectra. On the other hand, *J* information can become redundant when multidimensional NMR spectra are analyzed, because only the correlation between chemical shifts is usually of interest for assignment purposes. Complex multiplet structures also negatively impact the usage of Computer-Assited Structure Elucidation (CASE) programs for automated structure elucidation, a problem that can be largely ameliorated with pure shift experiments.

The advantages of obtaining homonuclear decoupled ^{1}H NMR spectra have been extensively recognized, although there is not an easy and general solution to achieve this. Only as an example, Fig. 1 shows how the simplified *J* multiplet structure achieved in a small molecule like progesterone is a clear proof of the excellent complementarity between the homodecoupled and the standard 1D ^{1}H spectra. The absence of scalar coupling splittings improves signal dispersion, facilitates and accelerates chemical shift recognition and simplifies the analysis and assignment of complex regions, as illustrated for the overlap signals resonating around 1.6 and 2 ppm. Several homonuclear decoupling strategies have been suggested to improve signal resolution in ^{1}H NMR spectra, which are briefly commented in Section on Classical Homodecoupling Techniques. In the last few years, there has been a revival in the development of the so-called pure shift NMR techniques based

* *Correspondence to: Teodor Parella, Servei de Ressonància Magnètica Nuclear, Universitat Autònoma de Barcelona, E-08193, Bellaterra, Barcelona, Catalonia, Spain. E-mail: teodor.parella@uab.cat*

Servei de Ressonància Magnètica Nuclear and Departament de Química, Facultat de Ciències, Universitat Autònoma de Barcelona, E-08193, Bellaterra, Barcelona, Catalonia, Spain

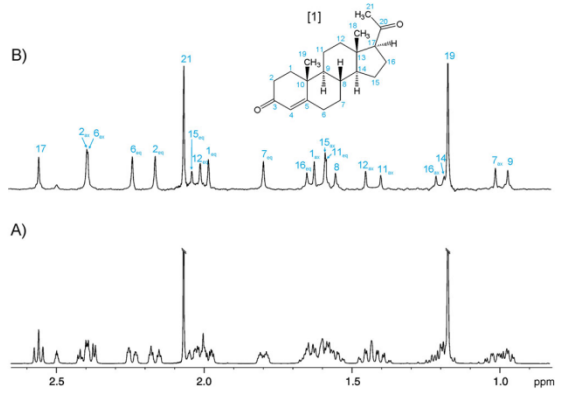

Figure 1. (A) 600-MHz conventional and (B) broadband homodecoupled 1D ^{1}H NMR spectra of the steroid progesterone [1] in dimethyl sulfoxide-d_6. Note how all simplified singlet resonances at their chemical shift frequencies can be distinguished in the pure shift spectrum, which was acquired in about 5 min using the PSYCHE experiment.

on the original *Zangger–Sterk* (ZS) experiment.[6] For this reason, we aim at presenting here the fundamentals and the recent progress in the design of new NMR pulse sequence elements to afford broadband homodecoupled ^{1}H NMR spectra. First, we describe some basic NMR building blocks designed to achieve broadband homodecoupling, discussing the pros and cons of each approach and introducing the most important practical aspects for a better performance. Then, the general strategies to implement these basic elements into standard 1D and 2D NMR experiments are introduced. Several recent applications are also highlighted showing the impact of these novel methodologies in the field of the small molecule NMR. At the time of writing this review, other excellent and complementary reviews about broadband homodecoupling NMR methods have also been published.[7–9] It is important to comment that the concept of homonuclear decoupling is also of high interest in other areas of the NMR spectroscopy, such as ^{13}C homodecoupling in experiments involving ^{13}C-labeled natural products,[10] proteins or nucleic acids,[11,12] or homonuclear decoupling of ^{1}H–^{1}H dipolar interactions when working in anisotropic media[13] or in solid-state NMR conditions,[14] but these descriptions are out of the scope of this review.

Broadband homodecoupling building blocks

The development and implementation of new homodecoupling building blocks into specific pulse schemes are nowadays an expanding area of research. Efforts are mainly concentrated in the design of methodologies that guarantee a routine use involving a simple and nonextended acquisition set-up, a standard and nonsophisticated data-processing procedure and general applicability in a wide range of NMR experiments.

Figure 2 illustrates a general building block to achieve broadband homodecoupling by combining the effects of a pair of NMR elements: a nonselective 180° pulse and a selective inversion element that affects only the so-called active spins. Some basic selective elements that perform such specific perturbation have been proposed: (i) a ^{12}C/^{13}C isotopic BIRD module (Fig. 2A),[15,16] (ii) frequency-selective 180° pulses (Fig. 2B–D), and (iii) spatially resolved elements consisting of a selective or adiabatic 180° pulse applied simultaneously to a weak *pulsed field gradient* (PFG) (Fig. 2E–H). In all these cases, the passive spins (decoupled spins) experience a 180° pulse whereas the active spins (detected spins) are unperturbed because they undergo an overall rotation of 360°. In practical terms, this means that chemical shift of active nuclei will not be affected and, therefore, it will evolve, while the homonuclear $J_{\mathrm{Hpassive-Hactive}}$ coupling will be efficiently refocused. The amount of active spins being inverted is typically much smaller

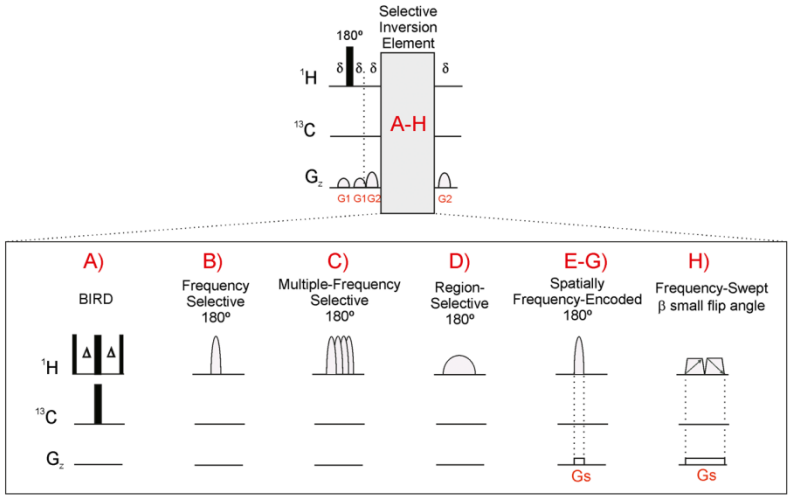

Figure 2. Basic NMR building blocks to perform broadband homonuclear decoupling, consisting of a nonselective 180° pulse and a selective inversion element: (A) BIRD cluster to selectively invert ^{1}H–^{13}C *versus* ^{1}H–^{12}C protons, or vice versa; (B–D) frequency-selective 180° pulses designed to invert/refocus a single or specific groups of signals; (E–G) slice-selective element to achieve spatially frequency-encoded perturbation along the *z*-axis, thanks to the simultaneously application of an encoding G_s gradient and a single-selective, multiple-selective or region-selective 180° pulse; (H) spatially selective element using a pair of small flip angle frequency-swept adiabatic pulses jointly with an encoding G_s gradient. The use of gradients (G1 and G2) flanking each inversion element can be optionally applied to remove improper refocusing/inversion. δ is the duration of the gradient and its recovery delay.

than the passive spins, entailing some cost in sensitivity that must be carefully evaluated in each case.

BIRD-based elements

A simple way to perform homonuclear decoupling is using the BIRD module, which is based on a different isotopic $^{12}C/^{13}C$ behavior. BIRD-based homodecoupling, introduced by Garbow and coworkers more than 30 years ago,[15] selectively inverts or refocuses all proton spins bounded to ^{13}C (active spins) while leaving ^{12}C bound protons (passive spins) unaffected ($BIRD^d$ element), or vice versa ($BIRD^r$ element), depending on the phases of BIRD pulses.[16] The basic homodecoupling block consists of the combination of a hard 180° ^1H pulse followed by a BIRD element (Fig. 2A), and the net effect is therefore a 360° rotation of protons directly bound to ^{12}C and a 180° rotation of the protons attached to ^{13}C. The main features of the success use of BIRD are as follows:

(i) Problems associated to strong J_{HH} coupling effects are minimized.
(ii) The geminal $^2J_{HH}$ interaction between diastereotopic protons is retained because the BIRD element cannot distinguish between protons directly bound to the same ^{13}C nucleus. As a practical consequence, BIRD-based pure shift spectra will show doublets for nonequivalent methylene protons. Recently, novel concepts based on constant-time BIRD[17] or perfect BIRD[18] elements have been proposed to refocus such $^2J_{HH}$ effects.
(iii) The ideal behavior expected for spins during the BIRD block can be compromised in real situations because of the single delay Δ (optimized to $1/2^{*1}J_{CH}$) that may not simultaneously satisfy the heteronuclear couplings arising for different spins of the molecules and because of imperfect inversions for ^{13}C sites spanning up to 200 ppm in their chemical shift range. Either of these two deviations can affect the behavior expected for the ^{13}C-bonded protons, leading to artifacts. In practice, a suitable compromise value of Δ can be found to minimize the J_{CH}-derived artifacts whereas the use of adiabatic-shaped 180° ^{13}C pulses eliminates off-resonance effects.[19]
(iv) The price to pay for applying BIRD-based homodecoupling is sensitivity. Natural abundance of ^{13}C is approximately 1.1%, and therefore, an unavoidable sensitivity loss of ~99% is obtained after using a BIRD filter. This sensitivity penalty is avoided in experiments that preselect ^1H–^{13}C magnetization, as carried out in pure shift HSQC experiments.[20]
(v) BIRD fails for fully ^{13}C-labeled compounds because of J_{CC} evolution.

The BIRD-based homodecoupling method has been further refined and adapted for pure shift 1D[19,21] and 2D HSQC experiments[20,22] and applied in a variety of structural problems.[17,23–27]

Use of frequency-selective pulses

The use of a frequency-selective 180° pulse is a simple option to achieve selective inversion on a single or multiple ^1H signals (Fig. 2B–D). The performance is under the control of the NMR user by an appropriate choice of the duration and shape of the selected 180° pulse that defines the effective bandwidth of the selective excitation. Several options are feasible, including single-frequency, multiple-frequency or band-selective excitation covering a specific region of the proton spectrum. The only requirement is that this selective pulse must not affect to mutually *J* coupled protons to avoid the evolution of this mutual coupling.

These building blocks were initially used to significantly increase the spectral resolution in the indirect F1 dimension of 2D experiments, by collapsing J_{HH} multiplets to singlets by *band-selective homonuclear decoupling* (BASHD) techniques,[28,29] as reported for BASHD-COSY,[30] BASHD-TOCSY,[29,31–35] BASHD-ROESY[32,33,35,36] and BASHD-HMBC[37] experiments. This strategy can be combined with other homodecoupling techniques along the detected F2 dimension in order to obtain ultra high resolution in both dimensions of fully homodecoupled 2D spectra.

Spatial encoding

Conventional NMR experiments involve the nonspecific excitation and detection of the NMR signal in the entire detector coil (Fig. 3A). The incorporation of the spatial encoding concept, traditionally used in magnetic resonance imaging applications, into high-resolution NMR spectroscopic techniques is attracting an increasingly larger interest. Several strategies have been developed to perform spatial encoding into an NMR tube (Fig. 3B–D):

(i) Data collection is focused on a specific *z*-slice along the NMR sample (Fig. 3B). Spatially resolved NMR applications have been reported for the analysis and characterization of heterogeneous samples, for instance, to study biphasic systems,[38–40] to detect and quantify sample inhomogeneities and spatial distribution in different alignment media such as gels or liquid crystals,[41,42] to investigate solvation and diffusion of CO_2 in ionic liquids,[43] to perform fast titrations and *in situ* reaction monitoring for obtaining information about reaction mechanisms and detecting intermediates[44] or to avoid *z*-gradient imperfections in diffusion NMR experiments.[45,46]
(ii) Signal excitation of different slices is executed in a sequential mode with the aim of reducing the long recycle delay and therefore shortening the overall acquisition time in 1D and 2D experiments (Fig. 3C). Examples have been reported to speed up data acquisition in 1D broadband homodecoupled,[47] 2D COSY[48] and 2D HMQC[49] experiments or to monitor fast reactions by sampling different parts of the NMR tube.[50]
(iii) Achievement of a selective and simultaneous signal perturbation, where each proton frequency is excited at different *z*-positions (Fig. 3D). This is the basis of the original ZS experiment,[6] and it has also been applied in single-scan T_1 relaxation time measurements,[51] to measure coupling constants,[52,53] or for the efficient diagonal peak suppression in 2D experiments.[54]
(iv) Use of selective multiple-frequency pulses in order to excite simultaneously a specific signal in different parts of the NMR tube (multislice selection) (Fig. 3E).[55,56]
(v) Simultaneous selection of multiple *z*-slices by using a concerted signal excitation and acquisition scheme (Fig. 3F), as traditionally performed in single-scan ultra-fast 2D NMR techniques where the t_1 increments sequentially recorded in a standard 2D experiment are simultaneously carried out along the length of the sample.[57]

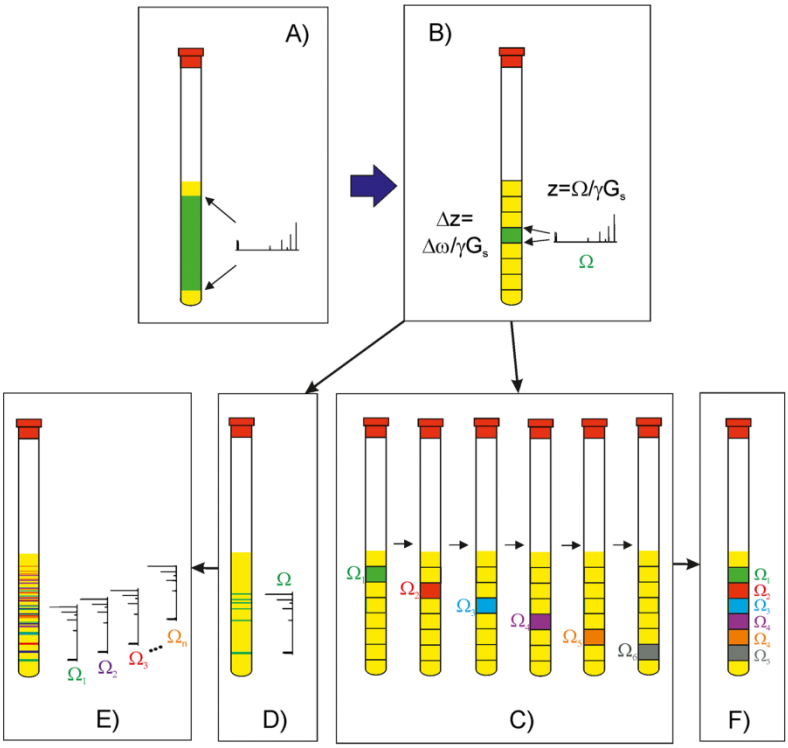

Figure 3. Different strategies to induce spatial selection along the *z*-axis of an NMR tube: (A) standard excitation/detection over the entire coil; (B) single-slice selection; (C) sequential spatial selection; (D) frequency-selective spatial selection; (E) simultaneous multiple frequency-selective spatial selection; (F) simultaneous multiple-slice excitation/detection.

Most of the reported slice-selective applications have been implemented in conventional liquid-state NMR spectrometers equipped with a basic hardware configuration; this is a direct or indirect detection probe incorporating a gradient coil that can deliver maximum gradient strengths around 50–60 G/cm along the *z*-axis. Experimentally, spatial frequency encoding is achieved by simultaneous application of a frequency-selective 90° or 180° pulses and a weak spatial-encoding PFG, G_s, both with the same duration (Fig. 2E–G).[6]

When a PFG is applied along the *z*-axis, the B_0 field is made spatially inhomogeneous by varying linearly along the applied dimension. Thus, during the application of a PFG, different parts of the sample experience a different magnetic field strength depending of its *z*-position, leading to a spatial-dependent frequency shift across the sample volume. Figure 4 compares the effects to apply a hard 90°, a frequency-selective 90° and a simultaneous selective 90°/gradient element. In the conventional ^{1}H spectrum, all signals from any part of the NMR tube into the active detector coil contribute to the observed signal (Fig. 4A). In the selective experiment, only those signals experiencing the selective pulse contribute to the detected data, although the maximum sensitivity for these signals is retained (Fig. 4B). In the slice-selective experiment, a complete ^{1}H spectrum can be obtained using optimized pulses and gradients, but each individual signal exclusively comes from a different part of the tube along the *z*-dimension (Fig. 4C). As an obvious consequence, a decrease of overall sensitivity is always associated with any slice-selective experiment, which is proportional to the number of generated *z*-slices.

Experimentally, the range of sampled frequencies or spectral width (SW_G) is defined by the strength of G_S according to

$$SW_G = \gamma.L.G_S \quad (1)$$

where γ is the gyromagnetic ratio of the spatially encoded nucleus and *L* is the active volume coil length. On the other hand, the carrier frequency (Ω) and the selective pulse bandwidth ($\Delta\omega$) determine the *z*-position of each nuclear spin (*z*) and the slice thickness (Δz) according to these two expressions, respectively:

$$z = \Omega/\gamma.G_S \quad (2)$$

$$\Delta z = \Delta\omega/\gamma.G_S \quad (3)$$

The SNR of slice-selective experiments depends on the active slice thickness because detected signal only comes from a selected *z*-slice. As shown, Δz depends both on the strength of G_S (which is proportional to the SW_G) and on the selectivity of the pulse (which should not exceed the smallest chemical shift difference expected between any coupled proton pairs). For instance, a typical 20-ms Gaussian-shaped 180° pulse (bandwidth of 60.7 Hz) applied simultaneously with a gradient G_S of 0.74 G/cm splits the sample height ($L = 1.8$ cm) into around 94 slices along the *z*-axis, defining a Δz of about 0.019 cm and covering an SW_G

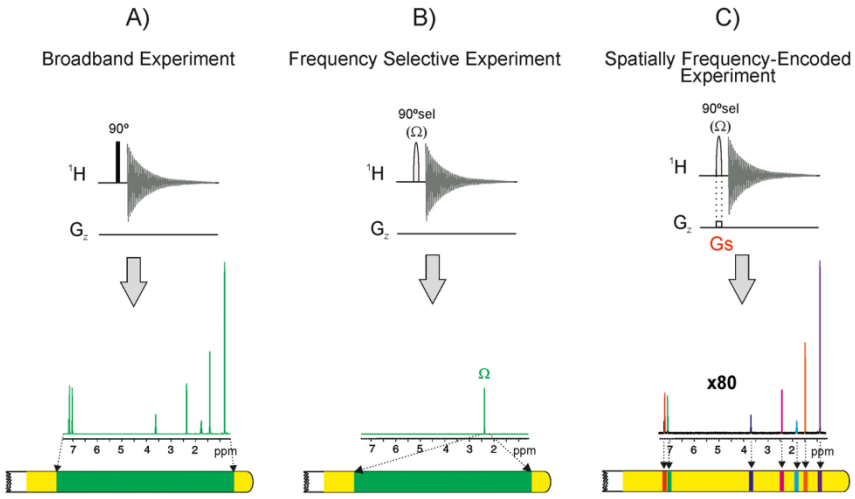

Figure 4. General illustration to understand slice-selective excitation: (A) conventional acquisition scheme to obtain an ^{1}H spectrum; (B) selective excitation using a 90° frequency-selective pulse; (C) slice selection consisting of the simultaneous application of a selective 90° pulse and a weak encoding gradient. In the latter case, the full spectrum is obtained, thanks to the spatial-dependent *z*-position of each individual resonance along the NMR tube.

of 5694 Hz (9.5 ppm in a 600-MHz spectrometer). Thus, under these general conditions, the single-slice selection procedure would afford only about 1% of the sensitivity of a conventional ^{1}H spectrum.

Several approaches have been reported to enhance SNR per time unit in slice-selective experiments:

(i) Sequential slice excitation (Fig. 3C) with the aim of reducing the long recycle delay and shortening the overall acquisition time in 1D and 2D experiments[47–49] or performing continuous data acquisition, as described in fast reaction monitoring studies.[50] This strategy uses a fast pulsing approach with around 100 ms of recycle delay, and after each scan, the offset of the selective shaped pulse is changed to access fresh equilibrium magnetization from adjacent frequency/spatial regions. Sakhaii *et al.* reported how an optimized division of the NMR tube in eight slices by changing the offset accordingly affords an experiment increment by a √8 factor in the original ZS experiment.[47] Similarly, spatially selective HMQC spectra have been rapidly recorded within 45–90 s dividing the NMR tube of protein samples in four *z*-slices.[49]

(ii) Use of multiple-frequency modulated pulses to simultaneously excite different slices in a single-NMR experiment (Fig. 5A).[55,56] This proposal is based on the careful setting of multiple offsets to avoid the excitation of mutually *J*-coupled protons within the same slice. Figure 5B shows different 1D *z*-profile images for a test sample of the anti-inflammatory drug ibuprofen acquired with a single scan, demonstrating that the user can have a full control on which signal and which *z*-position the excitation is performed. It can be shown how each individual signal in the conventional ^{1}H spectrum is excited in a particular *z*-position of the NMR tube. As predicted theoretically, an improved SNR by a factor of 4 is experimentally achieved using a four-site excitation (Fig. 5C).

(iii) It has been reported that the use of the so-called through-polarization sharing can afford an average enhancement by a factor of 2.[58] This approach is based on the original *acceleration by sharing adjacent polarization* (ASAP) technique that uses a short recycle delay consisting of a 40-ms isotropic DIPSI-2 (Decoupling In the Presence of Scalar Interactions) pulse train flanked by two gradients.[59] The method presents some limitations because sensitivity enhancement is not uniform for all signals and strongly dependent of the different relaxation properties of the excited protons while other spins remain unperturbed, preventing any attempt of quantification.

Slice selection works well for weakly coupled spin systems, but it can fail for strongly coupled signals. If the chemical shift difference ($\Delta\delta$) of coupled spins is less than the selective pulse bandwidth ($\Delta\omega$) but they are not very strongly coupled ($\Delta\omega > \Delta\delta > J$), couplings within $\Delta\omega$ become active, but the effects of couplings to other spins remain suppressed, retaining much of the resolution advantage. Where spins are fairly strongly coupled ($\Delta\omega > \Delta\delta \approx J$), weak extra signals appear at intermediate frequencies, and if they are very strongly coupled ($\Delta\omega > J > \Delta\delta$), it will typically yields distorted signals. The optimum selective 180° pulse and the encoding G_s gradient strength are quickly calibrated using a *slice-selective single-PFG echo* (ss-SPFGE) experiment. The excitation of two *J*-coupled protons into the same slice is observed as distorted multiplets in the corresponding 1D ss-SPFGE spectrum (Fig. 5C).[55]

Homodecoupling acquisition modes

Classical homodecoupling techniques

Each signal in an ^{1}H NMR spectrum exhibits a particular multiplet J_{HH} pattern as a result of its through-bond interactions with their neighboring protons. Thus, experimental issues such as signal dispersion, spectral resolution or signal overlap become very relevant to identify and assign each individual signal, in particular when a large number of resonances are present in a narrow range of frequencies. The use of NMR methods affording simplified multiplet structures are of interest because they can facilitate the

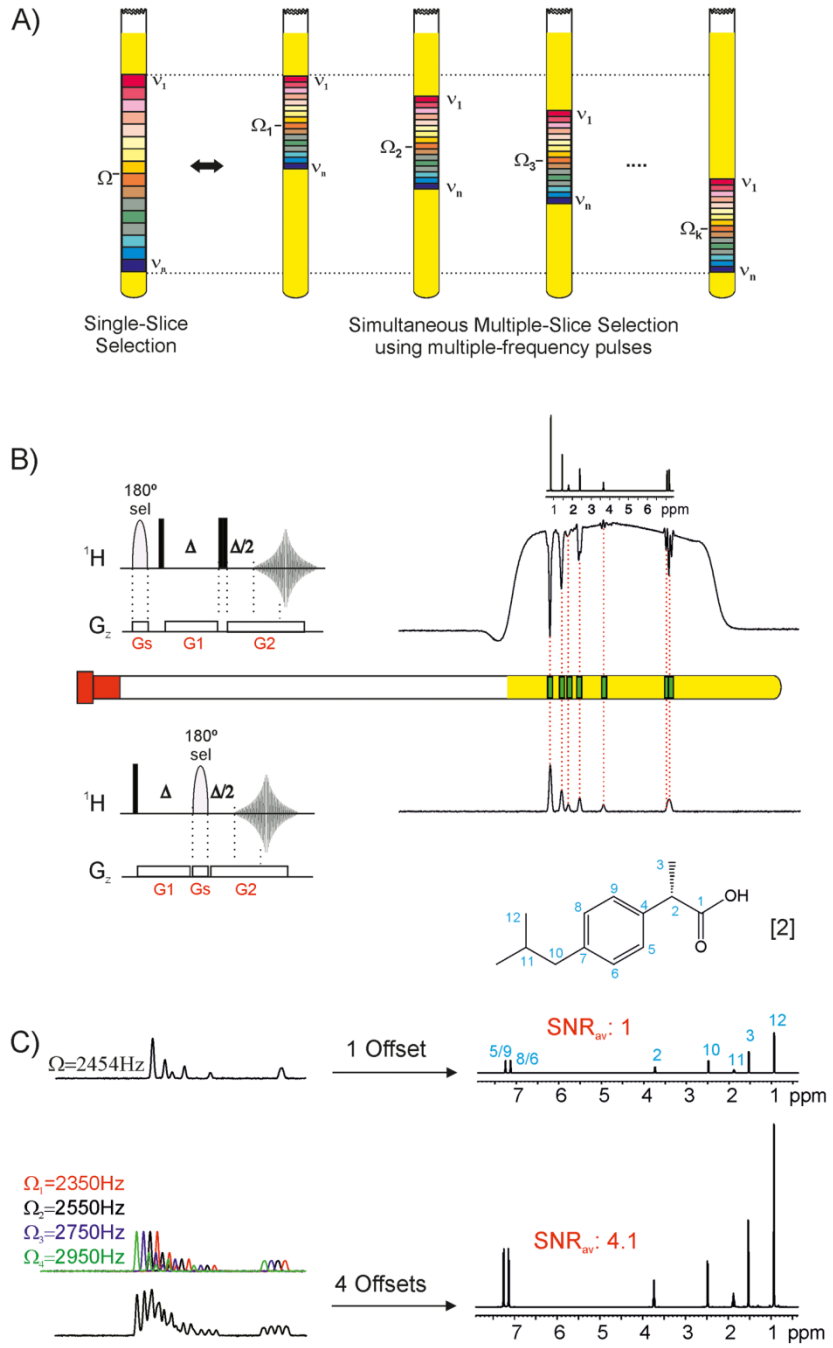

Figure 5. (A) Schematic illustration of the single *versus* multiple offset slice selection. (B) Pulse schemes to obtain 1D *z*-profile images of ibuprofen [2] along the NMR tube. (C) Experimental sensitivity enhancement obtained by a simultaneous four-site excitation. In (B) and (C), a selective 20-ms Gaussian-shaped 180° pulse was applied simultaneously with a square-shaped encoding gradient (G_S) of 0.742 G/cm. Figure adapted from reference.[55]

analysis and the interpretation of the corresponding spectra. The traditional way to achieve such simplification is by frequency-selective continuous-wave irradiation on a single-target signal during the acquisition period.[60] The method has been improved by multiple irradiation of different signals using multiple-frequency homodecoupling,[61] polychromatic pulses[62] or irradiating a group of signals resonating into the same region,[63–67] among others,[68] being the band-selective homodecoupling of the well-defined NH

or H_α regions in peptides and proteins one of the most reported applications.[69–72] All these approaches do not provide broadband homodecoupling in the entire spectrum, so only multiplet patterns of some signals are partially simplified according to the irradiated signals, and therefore, success is limited to specific and well-isolated spin systems.

A simple and classical approach to achieve a broadband homodecoupled ^{1}H spectrum is the 1D projection obtained along the detected dimension in a tilted homonuclear *J*-resolved experiment.[73–87] The standard experiment suffers of poor phase-twist lineshapes, and alternatives to obtain absorptive spectra such as the incorporation of spatial-selective encoding at expense of important sensitivity losses[83] or using a *z*-filter combined with a post-processing pattern recognition algorithm[84] have been proposed. Another drawback that has been recognized and evaluated in detail is the presence of extra peak artifacts due to strong coupling effects.[82] The use of appropriate data processing in *J*-resolved experiments has also been an interesting area to enhance sensitivity.[88] The *J*-resolved module has been appended as an NMR building block to standard 2D experiments, such as reported for homodecoupled versions of DOSY[89,90] and HMBC experiments,[87] although the resulting 3D experiments become more time consuming than the original ones. The *J*-resolved experiment has been successfully used in the determination of small chemical shift differences in complex mixtures, such as metabonomics[91] or enantiodifferentiation[86] studies, among others.

Separation of chemical shifts and *J* couplings while retaining absorption-mode lineshapes can also be obtained from the diagonal projected spectrum of a modified anti *z*-COSY experiment.[92] Another group of NMR experiments performs broadband homonuclear decoupling in the indirectly detected dimension of multidimensional experiments using time reversal,[93] constant-time evolution[94–102] or BIRD editing in the case of heteronuclear experiments.[103]

Pseudo-2D ZS experiment

Two different acquisition schemes are available to achieve broadband homodecoupling in the acquisition dimension: (i) a pseudo-2D acquisition mode where a homodecoupled FID is reconstructed by concatenating data chunks extracted from individual time domain datasets of a 2D experiment[6] (Fig. 6A) and (ii) a real-time acquisition mode that provides directly the homodecoupled FID (Fig. 6B).[19,104]

The original ZS experiment, reported in 1997,[6] uses a slice-selective 2D pulse timing where a variable delay is incremented stepwise as usual (Fig. 6A). The homodecoupling block (see several options in Fig. 2) is applied in the middle of this incremented delay to refocus any J_{HH} evolution. A special post-processing is needed, where the first data chunks of each FID are assembling to create a new reconstructed 1D FID that is processed and transformed by ordinary procedures to lead a homodecoupled ^{1}H NMR spectrum. A more robust ZS scheme has been proposed where the timing of the decoupling element was carefully designed to provide homodecoupling in the middle of each data chunk, where PFGs were also applied to suppress strong signals from passive spins.[105]

Experimentally, the evolution time (t_1) is incremented according to $1/SW_1$, where SW_1 is the defined spectral width in the indirect dimension (typically $SW_1 = 50–100$ Hz), and the first 10–20 ms of each individual FID are selected for a further FID reconstruction. In case of large scalar coupling constants, the increments must be set to smaller values ($SW_1 < J_{HH}$) in order to avoid scalar coupling evolution. This method produces small artifacts, typically in the form of weak sidebands at multiples of SW_1. The resolution of the signals is directly related with the number of increments in the indirect dimension. Normally, 16–32 increments are enough to obtain a high-quality 1D homodecoupled spectrum with optimum resolution and narrow line widths. Only as a reference, typical standard parameters to afford a nice 1D homodecoupled spectrum in ~5–10 min for a sample concentration about 10 mM would involve Gaussian or rSNOB shaped 180° ^{1}H pulses with a duration of 40–60 ms and an encoding G_s gradient around 0.5–1 G/cm. Under these general conditions, the pseudo-2D ZS method would afford only ~1–5% of the sensitivity of a conventional ^{1}H spectrum. SNR could be improved by using shorter and less selective pulses and/or less intense encoding gradients but always with an increased probability of accidental excitation of two coupled protons within the same slice. As discussed previously for slice-selective experiments, several ZS enhancements have been reported to improve this low SNR, including sequential slice selection,[47] multiple-slice selection[55,56] or ASAP enhancement[58] and to make these ZS experiments of practical use for moderately concentrated samples. For instance, Fig. 7 shows an example of multiple-slice

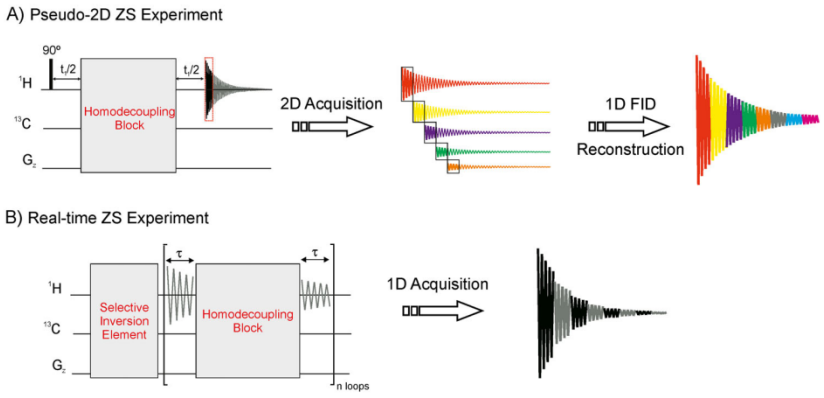

Figure 6. General schemes leading to 1D broadband homodecoupled ^{1}H NMR spectra: (A) The original ZS method is based on a 2D acquisition mode followed by an FID reconstruction from the initial data chunks of each increment; (B) the real-time ZS experiment incorporates periodically the homodecoupling block in the middle of the FID acquisition. The homodecoupling block can be any option described in Fig. 2.

selection where an experimental SNR enhancement by a factor of 7 achieved for the immunosuppressant drug cyclosporine by using a multiple frequency-modulated pulse at eight different offsets.[55]

The original ZS experiment was based on slice selection, and a BIRD-based ZS experiment has also been reported.[21] In a recent improvement, referred to as *pure shift yielded by chirp excitation* (PSYCHE) experiment (Fig. 8A),[106] a pair of low flip angle swept-frequency pulses and a weak PFG are used as a selective inversion element (Fig. 2H). By adjusting the pulse flip angle, it is possible to balance optimum sensitivity and full broadband homodecoupling for all signals in a given sample. PSYCHE can offer a sensitivity improvement of almost one order of magnitude in performance over conventional ZS methods performed by slice-selection or BIRD pulses (Fig. 8C–E).

The pseudo-2D ZS experiment has been applied to measure homonuclear[107] and heteronuclear[26,108,109] coupling constants, to detect small chemical shit differences in enantiodifferentiation studies,[24] and it has been implemented into 2D experiments, as reported for pure shift DOSY,[105,110,111] TOCSY,[112–114] NOESY,[102] HSQC[17,22,23] and Heteronuclear Single Quantum Multiple-Bond Correlation (HSQMBC).[109] The main drawback of these resulting pseudo-3D experiments is that their overall acquisition times can become extremely long for routine use.

Real-time ZS experiment

HOBB experiments

Real-time broadband homodecoupling was initially proposed using the BIRD element as homodecoupling block during data acquisition,[19] and shortly after, a slice selective version was also reported[104] using the general scheme of Fig. 6B. This new acquisition technique, referred to here as real-time ZS or *homodecoupled broadband* (HOBB) experiment, directly generates a single 1D FID that after standard processing leads to a broadband homodecoupled 1D ^{1}H NMR spectrum. This method offers instant and sped-up data acquisition and an improved SNR per time unit compared with the original ZS experiment, although the attainable sensitivity is still far from a regular ^{1}H spectrum because of the involved ^{13}C editing or slice selection procedures.

In the real-time ZS method, instead of recording each fraction of the FID in a series of individual experiments, a single FID is collected in each scan. The acquisition is interrupted after every τ period to perform either slice-selective or BIRD-based homodecoupling, as shown in Fig. 9A. Note that the first fraction of acquisition is only half as long as the subsequent ones. Thereby, full scalar decoupling is achieved in the middle of each fraction of the FID. These acquisition segments are assembled consecutively in a conventional FID, which can be treated like a regular 1D NMR experiment. The τ period is defined as $AQ/2n$ where AQ is the acquisition time and n the number of loops. As long as $\tau << 1/J_{HH}$, homonuclear J modulations occurring during these acquisition segments can be disregarded with no compromise in the final spectral resolution, leading to the potential collapse of all J_{HH} splittings. Deviations from this condition lead to incomplete homodecoupling and the appearance of distinct decoupling sidebands flanking each purely shifted resonance at spacing multiples of $2n/AQ$. On the other hand, while the acquisition is interrupted for decoupling, the magnetization is relaxing, and therefore, it is critical to keep the interruptions as short as possible, especially for larger molecules that have shorter T_2 relaxation times. Moreover, it is also important

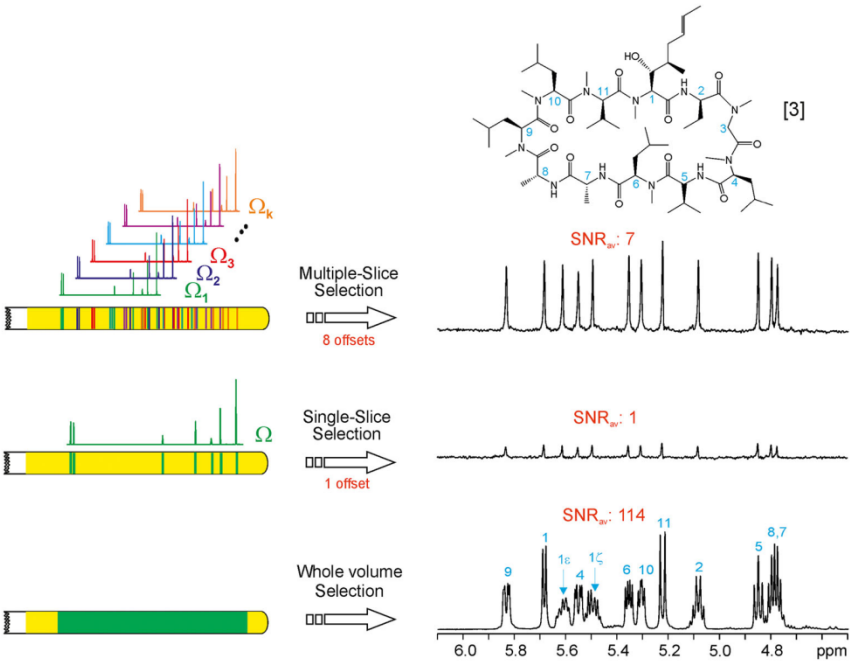

Figure 7. Comparison of the real SNR achieved in the pseudo-2D ZS experiment of cyclosporine [3], taking the standard ^{1}H spectrum as a reference. The pseudo-2D ZS experiment acquired with an rSNOB shaped pulse of 80 ms and a weak gradient of 1.13 G/cm affords an SNR factor of 1/114 whereas the use of an eight-site excitation improves SNR by an experimental factor of ~7. Figure reproduced with permission of reference.[55]

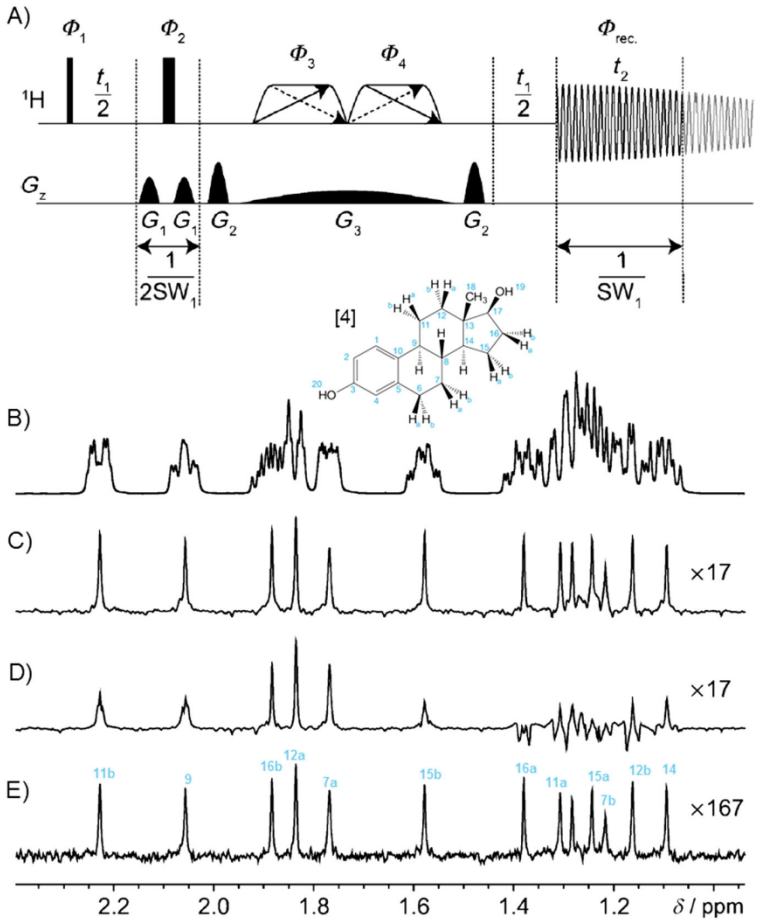

Figure 8. (A) Pulse scheme of the ZS-based PSYCHE experiment that uses a pair of low-power frequency-swept chirp pulses and a weak gradient as a selective inversion element. (B) 600-MHz ^{1}H NMR spectrum of the sex hormone estradiol [4] in $CDCl_3$; (C and D) original ZS spectra using 12- and 100-ms rSNOB 180° ^{1}H pulses, respectively; (E) PSYCHE spectrum obtained with two chirp pulses of 15 ms ($\beta = 20°$) and G3 = 0.75 G/cm. Each ZS spectrum in (C–E) was obtained in ~6 min. Adapted from reference.[106]

to minimize pronounced discontinuities during the FID that can lead to considerable sideband artifacts. If a BIRD-based homodecoupling block is used, the FID is interrupted about 6–8 ms (to $^1J_{CH}$ between 120 and 160 Hz). In the case of using a selective 180° pulse, a compromise duration of 5–10 ms balances between an optimum slice selection and an effective homodecoupling of nearby signals, while it minimizes the T_2 relaxation effects. In practice, real-time ZS acquisition reduces the overall experimental time and improves SNR per time unit but at some cost in spectral quality and the achievement of wider line widths. As an example, the HOBB spectrum of cyclosporine, quickly acquired in a single scan, shows full homodecoupling for most of the signals (except in some aliphatic CH_2 resonances), thanks to the well-dispersed spin systems (Fig. 9C). Importantly, the SNR of the HOBB experiment also suffers of the unavoidable losses due to slice selection (~8% of the maximum theoretical signal).

The real-time ZS acquisition mode becomes an attractive NMR building block for the design of pure shift methods, and, as a major advantage, it can be incorporated as a detection scheme in standard multidimensional experiments without increasing their original dimensionalities and continuing to use the same data-processing protocols. This represents a boost in SNR per time unit when compared with the pseudo-2D ZS experiment, as reported for HOBB-DOSY,[115] HOBB-TOCSY,[104] HOBB-ROESY[116] and HOBB-HSQC[20,24,25,117] experiments. From a strategic point of view, it is advisable to optimize first a 1D HOBB experiment in order to determine the best homodecoupling conditions for the sample under study. The signal simplification observed in 2D HOBB spectra will be the same obtained in a 1D HOBB spectrum recorded under the same conditions.

Recently, the sensitivity enhancement properties to the dissolution *dynamic nuclear polarization* combined with broadband homodecoupling techniques have been proposed to collect homonuclear decoupled proton NMR spectra with optimum sensitivity. This HyperBIRD experiment[27] is based on an initial ^{13}C *ex situ* hyperpolarization process, followed by a spontaneous ^{13}C-to-^{1}H polarization transfer via cross-correlation. Then, a rapid ^{1}H data collection using a 1D real-time BIRD-based ZS experiment exclusively detects ^{1}H directly attached to ^{13}C, whereas ^{1}H–^{12}C

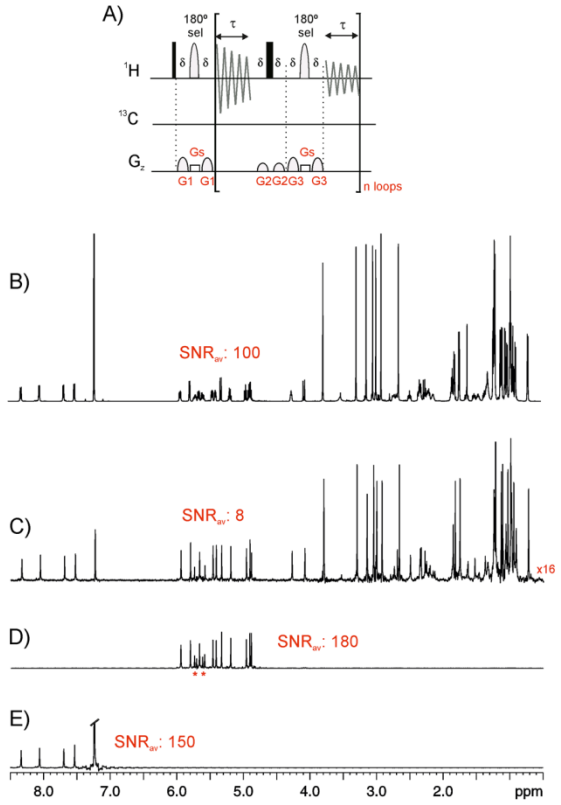

Figure 9. (A) General pulse scheme of the real-time 1D HOBB and HOBS experiments; (B) 600-MHz conventional ^{1}H spectrum of cyclosporine [3]; (C) 1D HOBB spectrum acquired with a REfocusing Band-selective Uniform-Response Pure-phase (RE-BURP) pulse of 5 ms for both excitation and decoupling and $G_s = 1.1$ G/cm. (D and E) 1D HOBS spectra acquired exactly as described for C but omitting the encoding gradient (G_s = off) and setting the frequency of the selective pulse on the H_α and NH regions, respectively. 8K data points were acquired using an acquisition time (*AQ*) of 576 ms [40 loops (*n*) were used with $\tau = 7.2$ ms] and a recycle delay of 1 s. For an objective comparison of real sensitivities, the experimental averaged SNR is indicated for each 1D dataset. All spectra have been recorded with the same receiver gain, using a single scan, processed with a Fourier transformation without any additional window function and plotted with the same absolute vertical scaling factor.

magnetization is efficiently suppressed. It has been shown that a 100-fold enhancement of the satellite ^{1}H–^{13}C signals can be reached about 5–10 s after injection when compared with the normal thermal sensitivity (Fig. 10).

HOBS experiments

A very simple modification of the slice-selective 1D HOBB experiment allows one the collection of broadband homodecoupled spectra of specific regions of the ^{1}H spectrum without sacrificing sensitivity. As a major feature, this *homodecoupled band-selective* (HOBS) NMR method[118–120] does not use the spatial encoding gradient G_s applied simultaneously with the selective pulses, and therefore, pure shift 1D spectra can be quickly recorded without the sensitivity losses characteristic of the slice selection. The main limitation of this frequency-selective experiment is that only a particular part of the ^{1}H spectrum is monitored in a single-NMR spectrum. However, HOBS promises to have a potential use in spectra presenting a set of equivalent spin systems in well-separated and defined regions, such as the typical NH or H_α protons in peptides and proteins or those found in nucleic acids. In the case that mutually *J*-coupled protons resonate into the same selected region, they will display a splitting due to their mutual coupling.

Similar to the HOBB experiment, HOBS offers a very simple and fast experimental implementation (pulse scheme in Fig. 9A with G_s = off) and is particularly useful for small molecules. It will likely have an impact similar to that of routinely use of key frequency-selective 1D experiments such as selective 1D TOCSY and selective 1D NOESY. Only two parameters need to be defined and calibrated in a single-scan 1D experiment: the offset and the bandwidth of the 180° ^{1}H pulse as a function of the area to be analyzed. The best results in terms of selectivity and optimum relaxation are obtained using semiselective 180° RE-BURP pulses of 5–10 ms for both region-selective excitation and homodecoupling and applied at intervals of $2\tau = 10$–20 ms. Pulses of longer duration than 10–20 ms introduce important penalties in T_2 relaxation and FID interruption that generates sensitivity losses, line widths broadening and sidebands artifacts. From Figs 9D and 9E, it is shown that HOBS spectra corresponding to the H_α and NH region of cyclosporine are one order of magnitude more sensitive than the equivalent HOBB spectrum and they show even better sensitivity than the conventional ^{1}H spectrum because of the complete collapsing of conventional multiplets to full homodecoupled singlets.

An important advantage of the HOBS technique is its easy and reliable implementation for a large number of homonuclear and heteronuclear multidimensional experiments, as reported for HOBS-NOESY,[119,121] HOBS-ROESY,[116] HOBS-TOCSY,[118] HOBS-HSQC,[118,119] HOBS-HSQMBC,[122] HOBS-inversion-recovery (IR)[121,123] and HOBS-CPMG-PROJECT,[121] with particular applications for the measurement of heteronuclear coupling constants,[122] enantiodifferentiation studies,[124] discrimination of diastereoisomers[120] and the measurement of T_1 and T_2 NMR relaxation times.[121,123] In addition, it can be also attractive for biomolecular NMR applications, as reported for the effective elimination of *residual* HH *dipolar couplings* (RDCs) contributions to line broadening when working with partially oriented proteins in anisotropic media.[119]

Comparison of ZS methods

Both the pseudo-2D and real-time ZS experiments present a set of particular advantages/drawbacks that must be compared and evaluated for their proper use, as a function of the requirements/limitations of the sample or spin systems under study (Table 1).

First, a choice between broadband or selective ZS experiment must be carried out. The main advantage of broadband ZS experiments is that all signals can be fully homodecoupled in a single-NMR experiment although effective broadband homodecoupling cannot be fulfilled for all signals when using general conditions. In contrast, although the limitation of frequency-selective ZS methods is evident because only a set of signals can be monitored per experiment, sensitivity is maximized, and each experiment can be individually optimized.

In broadband homodecoupled NMR experiments, the price for the signal simplification is a considerable penalty in sensitivity. This loss of SNR depends on the homodecoupling block and the acquisition scheme used. As was mentioned before, the low sensitivity in slice-selective methods is due to the fact that the signal only coming from a thin slice of the sample (~1–5%), and

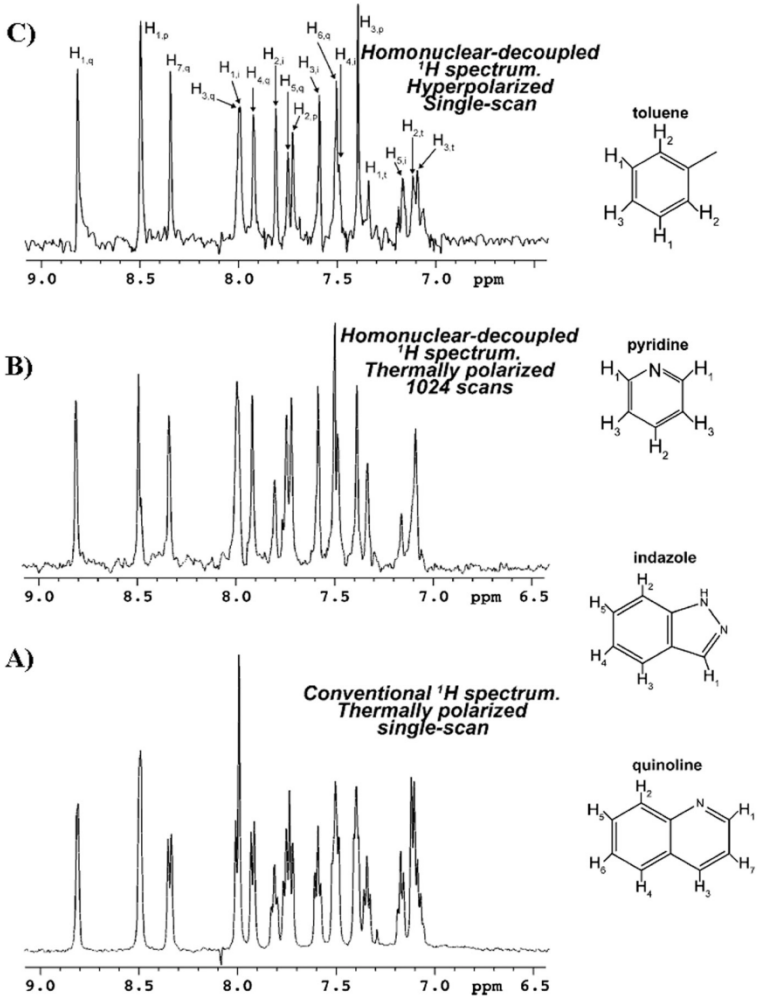

Figure 10. Application to the HyperBIRD experiment to the analysis of a mixture of heterocycle compounds. (A) Conventional ^{1}H spectrum with thermal polarization acquired with a single scan; (B) thermal polarized 1D homonuclear decoupled spectrum acquired with 1024 scans; (C) HyperBIRD spectrum after a single scan. More details can be found in the original publication. Reproduced with permission of reference.[27]

in BIRD-based experiments, it is due to the low natural abundance of ^{13}C (~1.1%). Additionally, pseudo-2D ZS experiments are more time consuming because a 2D dataset is required. When this acquisition scheme is incorporated into multidimensional experiments, the overall acquisition time can become extremely long because of the need for a 3D acquisition mode, decreasing even further the SNR per time unit. In contrast, the 1D acquisition mode of real-time ZS techniques improves the SNR per time unit although sensitivity still remains very low compared with conventional ^{1}H datasets (Fig. 11). The real-time homodecoupled HSQC experiment is the only exception of a broadband pure shift 2D experiment that does not suffers any sensitivity penalty compared with the conventional one.[20]

In terms of SNR per time unit, a single-selective HOBS method is more than one order of magnitude more sensitive than the aforementioned broadband (HOBB or pseudo-2D) ZS methods, which ensures that, for small molecules, recording series of individual selective 1D experiments can be faster and more effective than running a single-broadband experiment. As an example, the experimental SNR of each selective HOBS experiment is about 20 times higher than the equivalent HOBB experiment (Fig. 11C vs Fig. 11D). On the other hand, the theoretical SNR per time unit between the pseudo-2D and the HOBB experiments depends on $\sqrt{NE}$, where NE is the number of t_1 increments of the pesudo-2D experiment. In practice, the pseudo-2D experiment offers a better experimental behavior probably because of the narrower line widths.

In principle, pure shift NMR methods collapse J multiplet patterns irrespective of their complexity, leaving to a single peak for each chemical shift. The gain in spectral resolution can be almost of one order of magnitude, achieving a signal dispersion equivalent to those obtained in a hypothetical spectrometer of several gigahertz. For instance, chemical shift differences of ~1.5–2 Hz (~3 ppb) can be quickly distinguished in a 600-MHz spectrometer. Additionally, some differences are clearly observed when comparing the line widths of homodecoupled signals in different ZS

Table 1. Comparison of 1D ZS experiments to collect broadband homodecoupled ^{1}H NMR spectra

NMR method	Broadband *versus* band-selective	Signal selection	Parameter optimization	SNR	Acquisition mode	Line width	Implementation in nD experiments	Selective pulse	Data processing	Other features
Pseudo-2D ZS	Broadband	Spatial frequency encoding	Selective pulse and encoding gradient	1–5%	2D	Good	Requires 3D acquisition mode	Any shape and duration	Automation program[a]	Sensitivity enhancement by sequential or multiple offset excitation
Real-time 1D ZS (HOBB)	Broadband	Spatial frequency encoding	Selective pulse and encoding gradient	1–5%	1D	Medium	Ok	Pulses <10–15 ms	Conventional	Sensitivity enhancement by sequential or multiple offset excitation
Real-time 1D ZS BIRD	Broadband	^{13}C editing	Delay optimization	1%	1D	Medium	Only for $^{1}J_{CH}$ experiments, like HSQC	Not used	Conventional	Removes strong coupling effects, fails for CH_2
Real-time 1D HOBS	Band selective	Region selective	Region-selective pulse	Full sensitivity	1D	Medium	In band-selective 2D experiments	Pulses <10–15 ms	Conventional	Can be applied for single frequencies, fails for mutually coupled spins

[a]A data-processing script is available at Gareth Morris's group home page (nmr.chemistry.manchester.ac.uk).
ZS, Zangger–Sterk; HOBB, homodecoupled broadband; HOBS, homodecoupled band-selective.

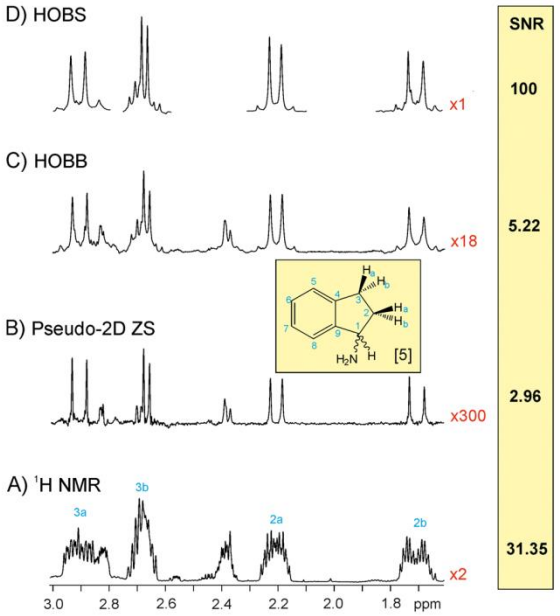

Figure 11. Relative sensitivity, signal resolution and spectral quality obtained in different ZS ^{1}H experiments at 600 MHz. Spectrum A corresponds to 50 mM (*RS*)-1-aminoindan[5] (1 : 1 proportion) in $CDCl_3$ after the addition of 4.5 equivalents of (*R*)-(−)-1-(9-anthryl)-2,2,2-trifluoroethanol (Pirkle alcohol) as chiral solvating agent. (B) Pseudo-2D ZS, (C) HOBB and (D) individual HOBS spectra for each group of signals. All four spectra were acquired within the same experimental time (~5 min) to obtain real and comparable SNR per time unit values. Spectra B–D used a 20-ms Gaussian-shaped pulse and a 2.1-G/cm encoding gradient, and a detailed description of all other acquisition and processing parameters can be found in the original publication. Reproduced with permission of reference.[124]

experiments (Fig. 11). As shown in Fig. 11B *versus* Fig. 11C and D, the pseudo-2D ZS method shows better line widths. In the pseudo-2D ZS experiment, line widths mainly depend on the number of increments used, and very good spectral resolution and excellent spectral quality are obtained collecting 16–32 increments. On the other hand, line widths in real-time HOBB and HOBS spectra are quite similar, and they are directly related with the number and duration of individual loops and the duration of the selective 180° ^{1}H pulse. As the time the FID is interrupted increases, correspondingly greater line widths are observed.

A serious challenge in all ZS experiments is the presence of strong coupling effects. It is not possible to obtain a perfect homodecoupled spectrum through ZS methods when protons are strongly coupled ($J > \Delta\delta$). When using slice selection, strong coupling effects are progressively minimized using more and more selective pulses but with a proportional decrease in sensitivity. In general, RE-BURP, rSNOB and Gaussian shapes give optimum results, and the correct choice of pulse shape and duration actually depends on the effective achievement of full homodecoupling for all signals present in the sample under study. Strong coupling effects are minimized using BIRD-based ZS experiments, but the incomplete homodecoupling for diastereotopic CH_2 groups and their decreased sensitivity must be also considered. Recently, the PSYCHE experiment has demonstrated an excellent complementarity between strong coupling effects and sensitivity. Experimentally, we have found that PSYCHE works perfectly with protons separated

by more than 50 Hz in a 600-MHz spectrometer but fails in extreme conditions, when strongly coupled signals are separated by less than 30–40 Hz. The PSYCHE approach can be implemented to improve the sensitivity in all homodecoupled experiments that will be discussed in the next sections, which were initially reported using slice selection with a selective 180° pulse.

Selectivity in slice-selective pseudo-2D ZS experiment can be enhanced as desired if the involved T_2 relaxation times allows the use of very long selective pulses. The main drawback of both HOBB and HOBS experiments is that they only accept selective pulses with a maximum duration of 10–20 ms. In general, all ZS experiments are susceptible to the presence of undesired artifacts in the form of sidebands. Practically, all real-time ZS version methods present a major number of artifacts because of the FID interruption whereas the pseudo-2D ZS method usually yields cleaner spectra where sidebands are only observed for concentrated samples.

Homodecoupled experiments and applications

All of the aforementioned ZS methodologies using BIRD or slice-selective homodecoupling have been implemented in different 1D and 2D NMR experiments (Table 2) according to the general schemes displayed in Fig. 12. A requirement for a success implementation of any ZS module is to have in-phase (IP) HH magnetization, because signals involving anti-phase (AP) components, like those found in conventional COSY or HMBC, cancel under homodecoupling conditions. The resulting pure shift spectra have a wide range of potential uses, as demonstrated for the analysis of diastereomeric[24,120,124] or complex mixtures,[105] to carry out structural elucidation studies,[6,20,22,24,25,102,104,112,113,116–119,122] to analyze diffusion[115] and molecular dynamic processes[121,123] or to measure heteronuclear coupling constants.[17,23,26,108,109,122]

Measurement of homonuclear coupling constants

A modified version of the 1D HOBB experiment has been reported to provide all J_{HH} coupling constants from a selected proton resonance. This experiment, which has been reported simultaneously by two groups,[125,126] yields a pseudo-broadband homodecoupled 1D ^{1}H spectrum where resonances coupled to the selected signal appear as doublets whereas the other remaining protons are fully homodecoupled singlets. The experiment provides information about multiple couplings analogous to that of an equivalent Gradient-encoded homonuclear SElective Refocusing Spectroscopy (G-SERF) technique[52] but in a few minutes rather than several hours. The key feature of this method is the application of an additional selective 180° ^{1}H pulse on a selected signal into the real-time homodecoupling element in order to retain specifically only those couplings from this selected proton. The main drawbacks of this technique are as follows: (i) poor selectivity because the duration of the selective 180° pulse is limited to ~10 ms, (ii) the experiment only works for well isolated resonances, (iii) there is a more pronounced presence of unwanted sideband artifacts than the original HOBB spectrum because of a major FID interruption, and (iv) the additional

Table 2. Summary of reported broadband homodecoupled 1D and 2D ^{1}H NMR experiments

NMR experiment		Homodecoupling			Acquisition mode		References
		BIRD	Slice selection	Band selection	Pseudo-2D	Real time	
1D	^{1}H NMR	✓			✓		[21], [26]
			✓		✓		[6], [24], [47], [55], [58], [105], [106], [108]
		✓				✓	[19], [27]
			✓			✓	[104]
				✓		✓	[118], [119], [120], [124]
	selTOCSY			✓		✓	[124]
	Quick-Serf		✓			✓	[125], [126]
	Inversion recovery			✓		✓	[121], [123]
	CPMG			✓		✓	[121]
2D	TOCSY		✓		✓		[112], [113], [114]
			✓			✓	[104]
				✓		✓	[118]
	DOSY		✓		✓		[105], [110], [111]
			✓			✓	[115]
	NOESY		✓		✓		[102]
				✓		✓	[119], [123]
	ROESY		✓			✓	[116]
				✓		✓	[116]
	HSQC/HSQCed		✓			✓	[117]
		✓			✓		[17], [18], [22], [23]
		✓				✓	[20], [24]
				✓		✓	[118], [119], [140]
	HSQC-TOCSY			✓		✓	[149]
	2D HSQMBC			✓		✓	[122]
			✓		✓		[109]

CPMG, Carr–Purcell–Meiboom–Gill.

180° pulse also causes more signal loss and transverse relaxation causing additional line broadening (~3 Hz), which sets the limit for the size of the couplings that could be measured. A similar pseudo-2D ZS method that improves the strong requirements on selectivity has been recently reported.[107]

Homodecoupled diffusion experiments

For the analysis of compound mixtures by NMR spectroscopy, it is important to identify and assign the different peaks belonging to each individual component. DOSY experiments are used to obtain signal separation depending on the molecular self-diffusion coefficient, which are determined by fitting the intensity decay of the NMR signal to a mono-exponential function.[127,128] However, signal overlap usually hampers a simple data analysis because the observed decays may be the result of superposition of several individual decays. In these cases, the use of more sophisticated methods, such as deconvolution, line fitting techniques or analysis of multiple-exponential decay, can be required to obtain correct values for each individual signal.

Several pure shift DOSY experiments based on the pseudo-2D ZS methodology were initially published to provide a much simplified spectrum, making the quantification of the diffusion coefficients easier and more accurate.[105,110] In principle, any diffusion pulse scheme could be adapted to the pseudo-2D ZS experiment, as represented in Fig. 12A. The resulting pure shift DOSY experiments represent a useful alternative to 3D-based DOSY experiments, which have been proposed to avoid signal overlapping and improve signal resolution. As a major drawback of these pure shift DOSY experiments is their 3D acquisition mode, requiring much longer measurement times and more elaborate data processing (Fig. 13). The pure shift DOSY experiment has been applied to the determination of the structure and solvation states of organolithium aggregates in complex solutions.[129]

Recently, an HOBB version of the popular BiPolar Longitudinal Eddy current Delay (BPLED) sequence has been also reported based on the scheme of Fig. 12B.[115] This HOBB-DOSY experiment uses the real-time acquisition, and therefore, it can be recorded and processed using the same automation protocols as for the standard DOSY experiments. The proposed method uses spatial selection, and therefore, reduced sensitivity is again the main drawback for its routine use. An equivalent sensitivity-enhanced HOBS-DOSY version that should be recorded with G_s = off has not been published, but it could be beneficial to analyze complex areas in particular cases.

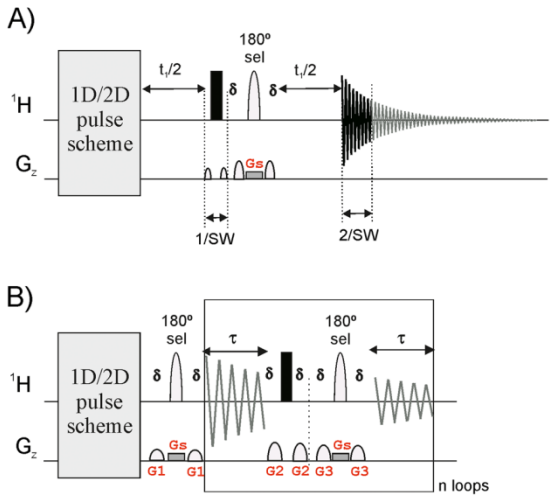

Figure 12. General pulse schemes showing the implementation of broadband homonuclear (A) pseudo-2D and (B) real-time ZS decoupling during the acquisition dimension in conventional 1D and 2D NMR experiments.

Homodecoupled T_1/T_2 relaxation experiments

The measurement of relaxation rates by NMR spectroscopy can provide important insights into the dynamics of molecules in solution. Longitudinal spin–lattice T_1 relaxation times are usually determined from the Inversion Recovery (IR) experiments[130,131] whereas transverse spin–spin T_2 relaxation times are measured from *Carr–Purcell–Meiboom–Gill* (CPMG) sequences.[132,133] One drawback of CPMG pulse trains is the presence of multiplet distortions due to J_{HH} evolution that can affect the accuracy of the measurement. An improved perfect CPMG sequence that achieves *periodic refocusing of J evolution by coherence transfer* (referred to as PROJECT) has been proposed to minimize the effects of *J* evolution during the echo periods, obtaining pure in-phase signals.[134] As mentioned previously, it has also been shown that the problem of signal overlapping can be solved through the implementation of the HOBS technique in standard IR and PROJECT experiments.[121]

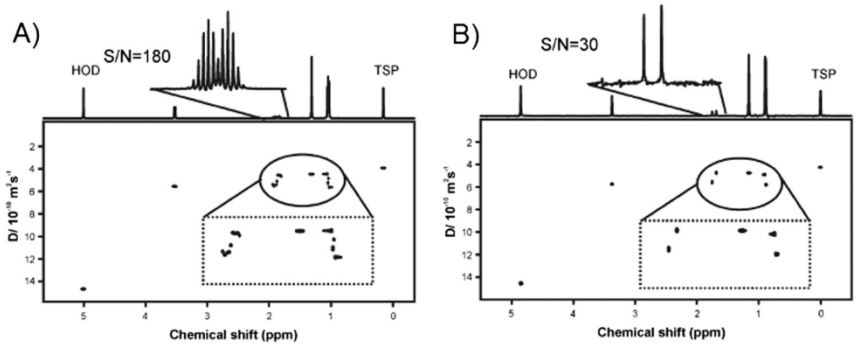

Figure 13. DOSY (A) and pure shift DOSY (B) spectra of a solution of 2-methyl-1-propanol, 2,3-dimethyl-2-butanol, and TSP in D_2O, acquired in 11 min and 2 h 10 min, respectively. Reproduced with permission of reference.[110]

Thus, T_1 and T_2 relaxation times can be accurately measured from the resulting singlet lines using conventional mono-exponential curve-fitting methods. Examples have been provided for the undecapeptide cyclosporine,[121] the small six-mer oligonucleotide d(GCCTGC) and the 16-mer d(CGACGCGTACGCGTCG)2 DNA duplex.[123] Figure 14A shows the basic scheme of the 1D HOBS-IR experiment where the conventional acquisition scheme has been replaced by an HOBS detection block. To obtain clean spectra, a selective echo element is inserted between the traditional IR block and the new acquisition block. The experimental T_1 data revealed good agreement between standard and HOBS-IR measurements (Fig. 14B vs Fig. 14C).

Figure 15A shows the pulse scheme of HOBS version of the PROJECT experiment designed to measure T_2 relaxation times or to be used as a T_2 filter. The features of the standard CPMG *versus* PROJECT are illustrated in spectra of Fig. 15C and D, and the further improvement and signal simplification achieved in the HOBS-PROJECT spectra are illustrated in Fig. 15E. Both HOBS-IR and HOBS-PROJECT experiments could be easily converted to their HOBB-IR and HOBB-PROJECT counterparts activating the encoding G_s gradient to monitor the complete ^{1}H spectrum. As noted previously, the major advantage of analyzing singlet peaks is the rapid and more accurate parameter determination using the same automatic T_1/T_2 data acquisition and processing protocols incorporated in standard NMR software packages (see exponential decay in Fig. 15F). This strategy can also be applied to other types of array experiments involving the analysis of the signal decays in severely overlapped

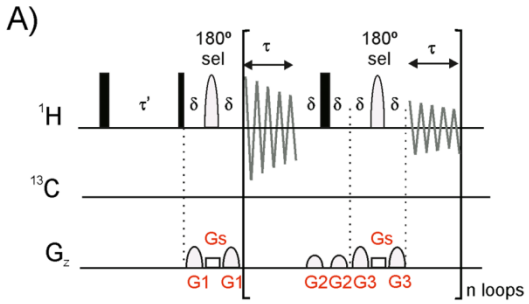

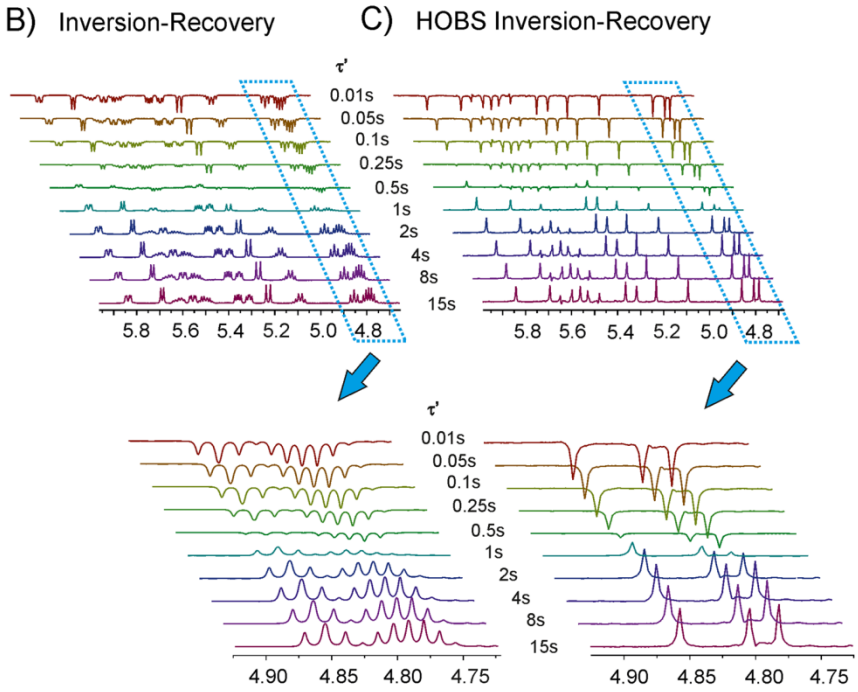

Figure 14. (A) NMR pulse scheme of the HOBB/HOBS-IR experiment designed to measure T_1 relaxation times in overlapped proton signals. 600-MHz (B) conventional and (C) HOBS IR ^{1}H NMR spectra showing the expanded area of the H_α protons corresponding to cyclosporine [3]. Homodecoupling was achieved using a 5-ms RE-BURP 180° ^{1}H pulse, $\tau = 8.9$ ms, $AQ = 569$ ms, $n = 32$ and the encoding gradient G_s switched off. Reproduced with permission of reference.[121]

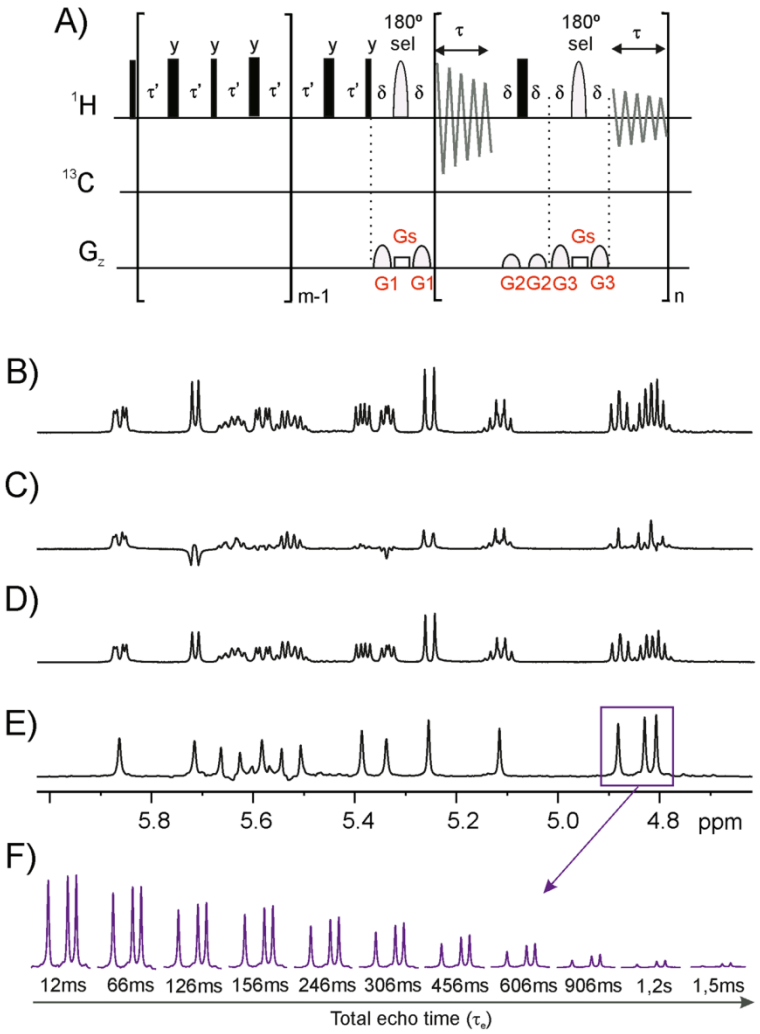

Figure 15. (A) NMR pulse scheme of the HOBB/HOBS-PROJECT experiment designed to measure T_2 relation in overlapped signals. 600-MHz (B) conventional ^{1}H, (C) standard CPMG, (D) PROJECT and (E) HOBS-PROJECT spectra of cyclosporine [3] acquired with a total echo time of $\tau_e = 156$ ms ($m = 26$ and $\tau' = 1.5$ ms) and $G_s = 0$. All spectra were collected under the same experimental conditions and are plotted at the same absolute vertical scale. (F) Signal T_2 decays for the H_5, H_8 and H_7 protons in the HOBS-PROJECT experiment. Reproduced with permission of reference.[121]

regions, such as the studies of kinetics or chemical reaction monitoring.

Homodecoupled homonuclear 2D experiments

The development of homodecoupled versions of the most popular 2D COSY, TOCSY, NOESY or ROESY experiments has been a topic of interest for many years. Homodecoupling in the indirect F1 dimension can be achieved by constant-time or BASHD methods, as discussed in Section on Classical Homodecoupling Techniques (Fig. 16B). In a complementary way, both pseudo-2D or real-time ZS homodecoupling methods can be incorporated along the acquisition dimension. The pseudo-2D ZS element can be included between the mixing time and the acquisition period (Fig. 16C), generating a pseudo-3D experiment that, in principle, would require long acquisition times. The HOBB/HOBS methods can be implemented changing continuous acquisition mode by the alternated-homodecoupling acquisition mode (Fig. 16D). Finally, real pure shift 2D experiments with broadband homodecoupling in both dimensions can be designed combining both approaches, as shown in the general schemes of Fig. 16E and F, respectively.

The 2D TOCSY experiment is a homonuclear NMR technique widely used to identify H–H correlations within networks of *J*-coupled spins. It has been reported that the resolution in the TOCSY spectrum can be improved by collapsing the in-phase multiplets to singlets for all cross-peaks, obtaining spectra where a single peak is seen for each connectivity. Homodecoupled TOCSY experiments have been proposed to simplify cross-peak appearance in the indirect F1[6] or the direct dimension using the pseudo-2D[112,113] or the real-time ZS modules,[104,118] which could be further enhanced by spectral aliasing in the indirect dimension.[135] Recently, an ultra high-resolved TOCSY experiment

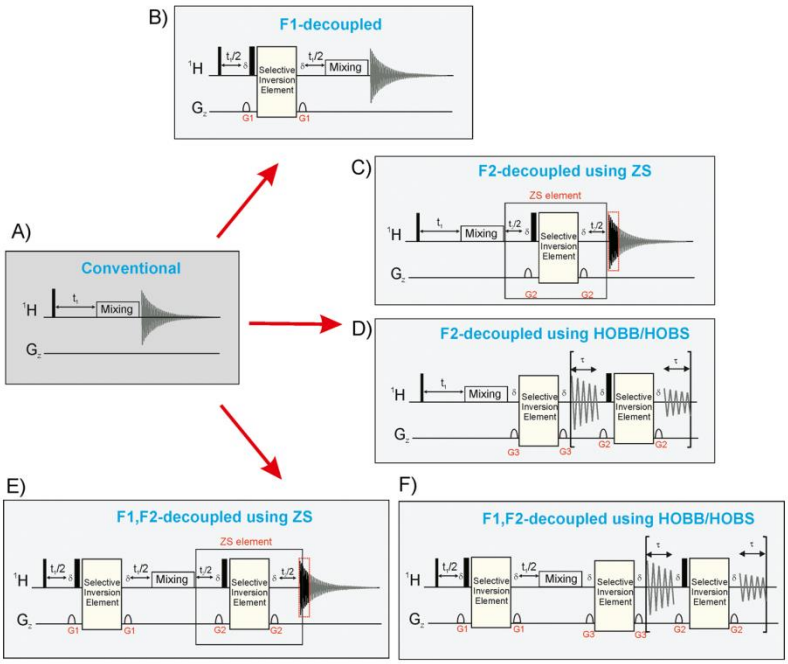

Figure 16. (B–E) General pulse schemes to obtain F1-homodecoupled, F2-homodecoupled or F1, F2-homodecoupled 2D spectra from the reference scheme of Figure A. The selective inversion element can be any building block described in Fig. 2 whereas the mixing time can be a standard TOCSY, ROESY or NOESY building block.

based on a PSYCHE scheme (Fig. 17A) affords broadband homodecoupling in the F1 dimension (Fig. 17C), and the use of covariance post-processing in the F2 dimension achieves pure shift cross-peaks in both dimensions (Fig. 17D).[112,114] This approach is an order of magnitude more sensitive than the previously published experiments.

Similar approaches have been reported to extract helpful distance restraints from simplified and well-resolved cross-peaks in broadband homodecoupled NOESY experiments based on the pseudo-2D ZS[102] and HOBS schemes.[119] This has been shown to be critical in the process of 3D structure determination of peptides, intrinsically disordered proteins[119] and nucleic acids.[123]

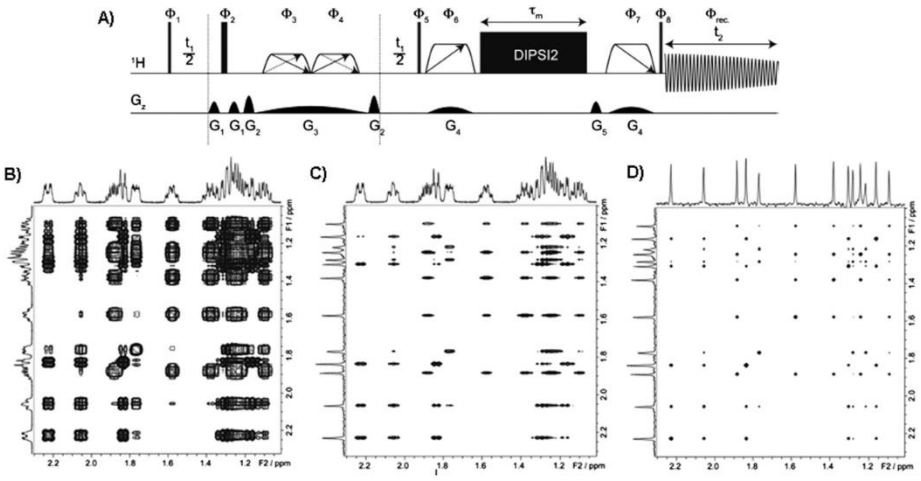

Figure 17. (A) Pulse scheme of the 2D F1-PSYCHE-TOCSY experiment; (B) expanded area of the conventional TOCSY spectrum of estradiol; (C) F1-homodecoupled PSYCHE-TOCSY spectrum acquired from sequence A; and (D) as (C) after applying covariance in the F2 dimension. Reproduced with permission of reference.[114]

Additionally, an exhaustive study comparing the performance of HOBB-ROESY *versus* HOBS-ROESY experiments has been reported for the analysis of medium-sized organic molecules (Fig. 18).[116]

Homodecoupled heteronuclear 2D experiments

The HSQC experiment is the most widely used NMR method for correlating the chemical shifts of directly bonded ^{13}C–^{1}H pairs. Conventional HSQC spectra show proton multiplet structures in the direct dimension, which can limit signal resolution when analyzing complex datasets. The pure shift methodology has been successfully implemented in HSQC experiments, as reported using the pseudo-2D ZS,[22] real-time HOBB,[117] HOBS[118] and BIRD-based[20,24] homodecoupling modules. A major breakthrough to obtain pure shift HSQC spectra of organic molecules at natural abundance is the recent development of the real-time BIRD-based HSQC experiment,[20] which does not present any additional sensitivity loss in comparison with the conventional HSQC (Fig. 19A) experiment. The resulting homodecoupled HSQC spectra show cross-peaks with collapsed multiplet J_{HH} structures for CH cross-peaks (Fig. 19D vs Fig. 19E). However, the method is not able to remove the geminal $^{2}J_{HH}$ splittings, and it is not suitable for fully ^{13}C-labeled compounds, in both cases because of the use of BIRD element. All of these advantages/inconveniences are also applicable to other related versions of the HSQC experiments, such as the reported pure shift versions of the sensitivity-improved HSQC using Preservation od Equivalent pathways (PEP) (Fig. 19B)[24] or the multiplicity-edited (ME) HSQC (Fig. 19C).[20] The performance of the pure shift HSQC and the ASAP-HMQC experiments has been compared for the rapid screening of natural products.[136] On the other hand, the pure shift HSQC has been also tested to characterize microgram samples of drug metabolites. For instance, using a 7.4-μg sample of the commercially available metabolite 3-hydroxy carbamazepine dissolved in 30 μl of deuterated solvent and a 600-MHz NMR equipped with a 1.7-mm cryogenic NMR probe, it was possible to acquire high signal-to-noise pure shift HSQC data in just over 30 min.[25] In the same study, high-quality pure shift HSQC data were recorded in slightly over 14 h for a 3-μg sample of a chromatographically isolated metabolite.

The implementation of ZS homodecoupling fails in heteronuclear correlation experiments involving anti-phase HH magnetization just prior to acquisition, like conventional HMBC/HSQMBC experiments. In addition, BIRD-based homodecoupling is not effective in heteronuclear hybrid experiments where J_{HH} is in-phase, such as HSQC-TOCSY or HSQC-NOESY, because the detected relayed ^{1}H–^{12}C magnetization is also coupled to ^{1}H–^{12}C protons. In these cases, pure shift spectra should be possible in refocused HMBC/HSQMBC, HSQC-TOCSY or HSQC-NOESY experiments applying slice selection but at expense of important sensitivity losses. On the other hand, it has been shown that pure in-phase cross-peaks with respect to J_{HH} can be obtained in refocused HSQMBC experiments using region-selective 180° ^{1}H pulses.[137] Based on this experiment, an HOBS-HSQMBC[122] experiment has been proposed to obtain band-selective pure shift long-range heteronuclear correlation spectra with a considerable enhancement in both resolution and sensitivity (Fig. 20). The major advantage of such an approach is that the selective 180° ^{1}H pulse is the same for the INEPT refocusing and homodecoupling, facilitating set-up and performance.

Measurement of heteronuclear coupling constants

It has been recognized since the early days of NMR that heteronuclear coupling constants (J_{XH}) contain very useful structural, conformational and configurational information. In the case of high-abundance nuclides ($X = {}^{19}F$, ^{31}P), the direct determination of heteronuclear couplings is often carry out through the analysis of conventional or *X*-decoupled ^{1}H multiplets, but the accurate measure of the J_{XH} can be problematic because of the simultaneous presence of large numbers of J_{HH} or because of the multiplet complexity. Several 1D and 2D pure shift experiments have been proposed to achieve simplified multiplet structures that allow the extraction of coupling values. For instance, it has been shown that J_{XH} can be directly extracted from simplified homodecoupled 1D multiplets obtained from pseudo-2D ZS spectra (Fig. 21).[108] Examples have been reported for J_{HF} and J_{HP} coupling constants, and similar results have been simultaneously reported using BIRD-based homodecoupling as a selective inversion element in the ZS experiment.[26] In Section on Efficient Measurement of Heteronuclear Coupling Constants, a simple and sensitive approach for the measurement of the sign and the

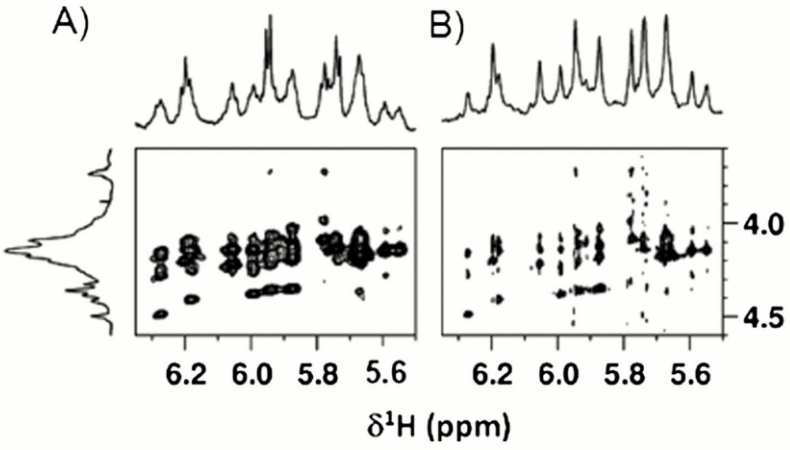

Figure 18. Expansions showing the H1′/H5 to H4′/H5′/H5″ cross-peak region of the 600-MHz (A) standard NOESY; (B) HOBS-NOESY spectra for d (CGACGCGTACGCGTCG)2 in D_2O. Reproduced with permission of reference.[123]

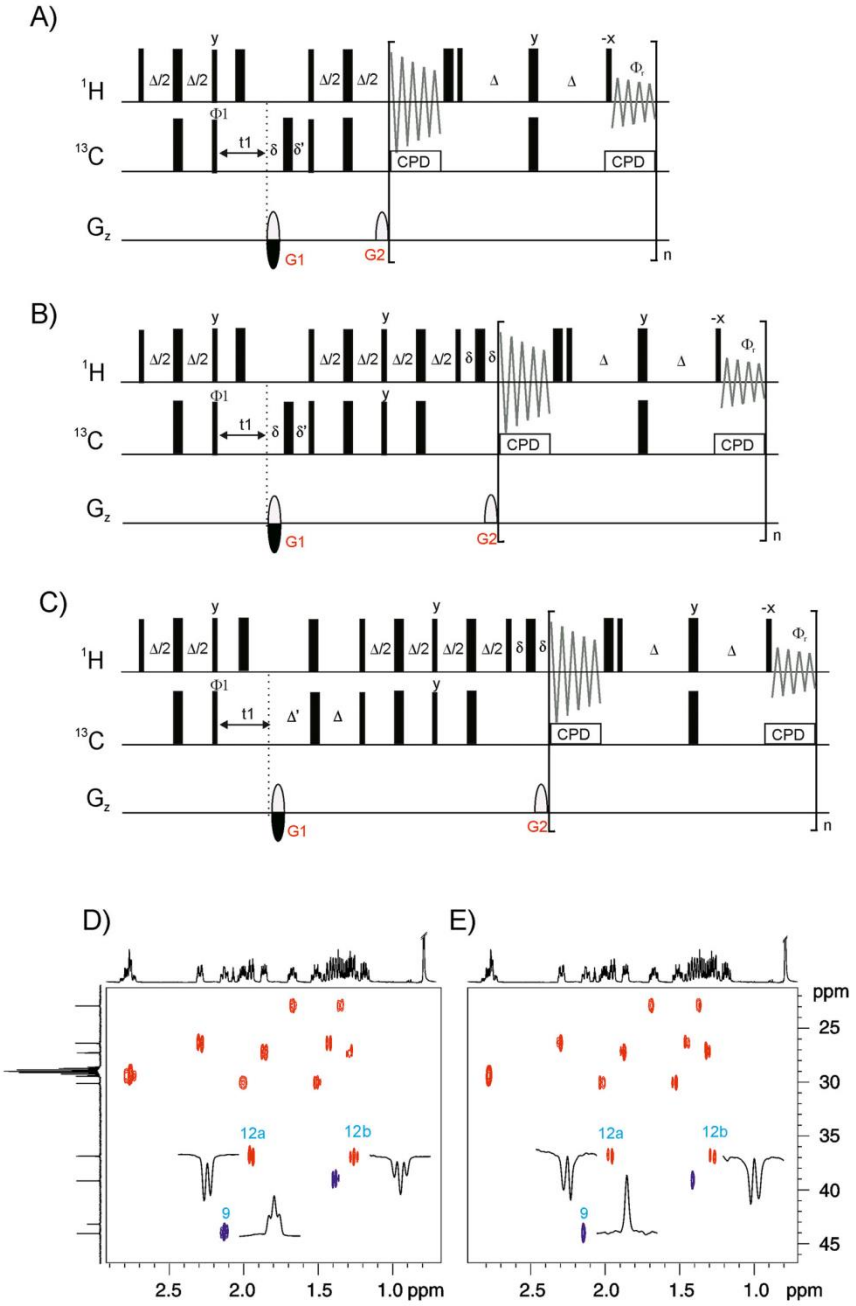

Figure 19. Basic pulse schemes of the broadband homodecoupled (A) HSQC, (B) HSQC-PEP and (C) multiplicity-edited HSQC-PEP experiments; (D and E) expanded area comparing CH and CH_2 cross-peaks in (D) conventional and (E) broadband homodecoupled multiplicity-edited HSQC-PEP spectra of estradiol [4] in $CDCl_3$.

magnitude of multiple coupling constants from high-resolved E.COSY cross-peaks in pure shift HSQC spectra is described.[138]

The measurement of one-bond scalar ($^1J_{CH}$) and residual dipolar ($^1D_{CH}$) coupling constants in isotropic and anisotropic media, respectively, can be easily carried out through F2-heteronuclear coupled HSQC-type spectra, for instance, using Clean-IP/Clean-AP (CLIP/CLAP) HSQC experiments.[139] Recently, two analog broadband homodecoupled CLIP/CLAP HSQC experiments have been simultaneously proposed, based on the implementation of the pseudo-2D ZS module (Fig. 22A).[17,23] Both approaches use the original RESET (Reducing nuclEar Spin multiplicitiEs to singuleTs)-HSQC pulse scheme as a basis,[22] where an optimum

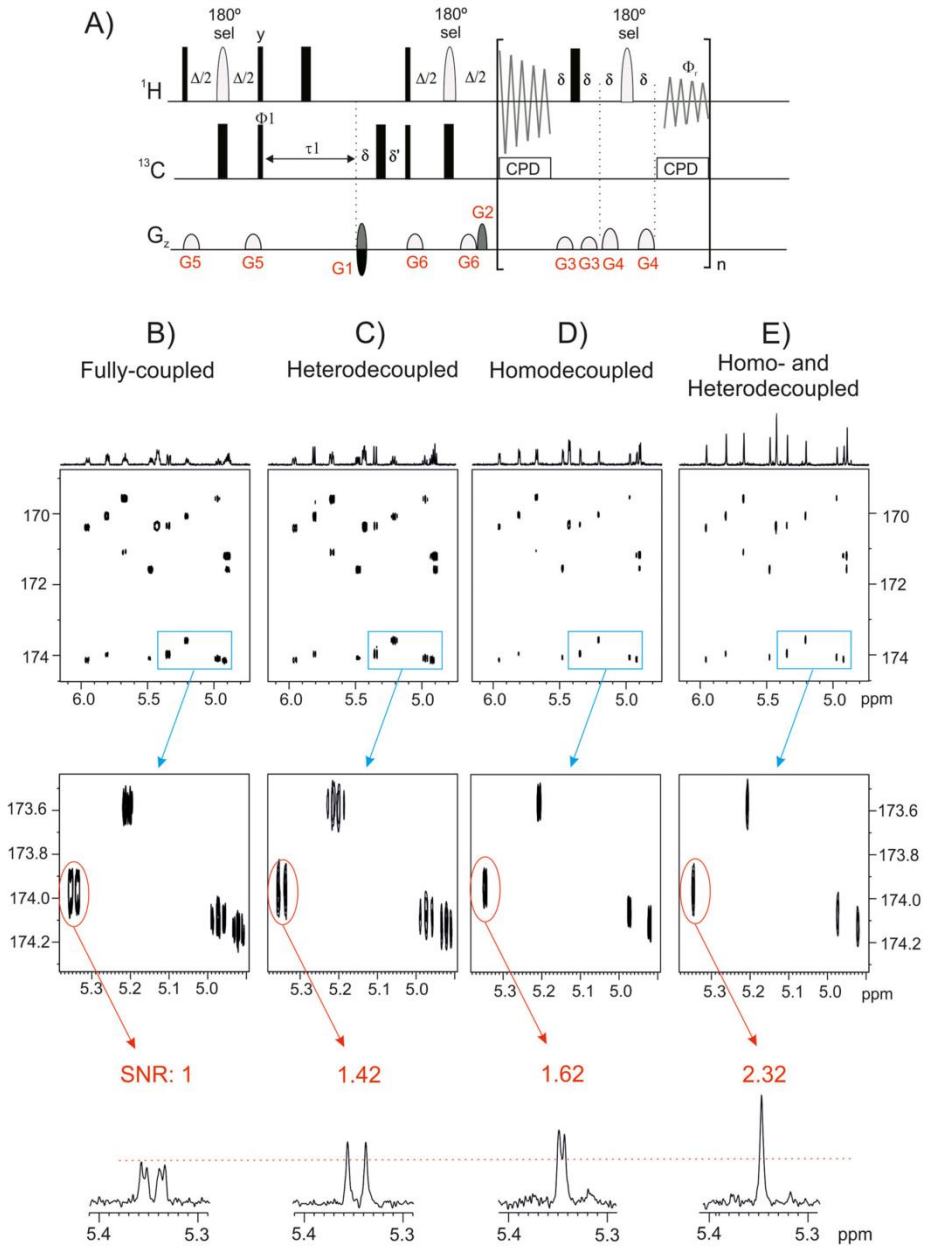

Figure 20. (A) Pulse scheme of the HOBS-HSQMBC experiment. (B–E) Resolution enhancement effects after incorporation of homonuclear or/and heteronuclear decoupling in region-selected $^{1}H\alpha-^{13}CO$ HSQMBC spectra of cyclosporine [3]: (B) 600-MHz conventional HSQMBC, (C) broadband ^{13}C-decoupled HSQMBC, (D) ^{1}H-decoupled and (E) ^{1}H and ^{13}C-decoupled HOBS-HSQMBC. The internal projection along the detected dimension is shown on top of each 2D plot, and all are plotted with the same absolute scale to compare the relative sensitivity and resolution. The experimental SNR for a selected 1D slice in each different HSQMBC spectra is shown taking the fully coupled peak (normalized value set to 1) as a reference. Reproduced with permission of reference.[122]

BIRD element allows the homonuclear decoupling while preserving heteronuclear coupling evolution. In these experiments, each homodecoupled CH cross-peak only exhibits a large doublet along the direct dimension because of $^{1}J_{CH} + {}^{1}D_{CH}$, allowing coupling constants to be extracted by measuring frequency differences between both singlets, instead of between the centers of complex multiplets (compare Fig. 22B vs Fig. 22C). These experiments lead to pure shift correlation spectra with enhanced resolution and offering interesting advantages for semi-automated peak picking or

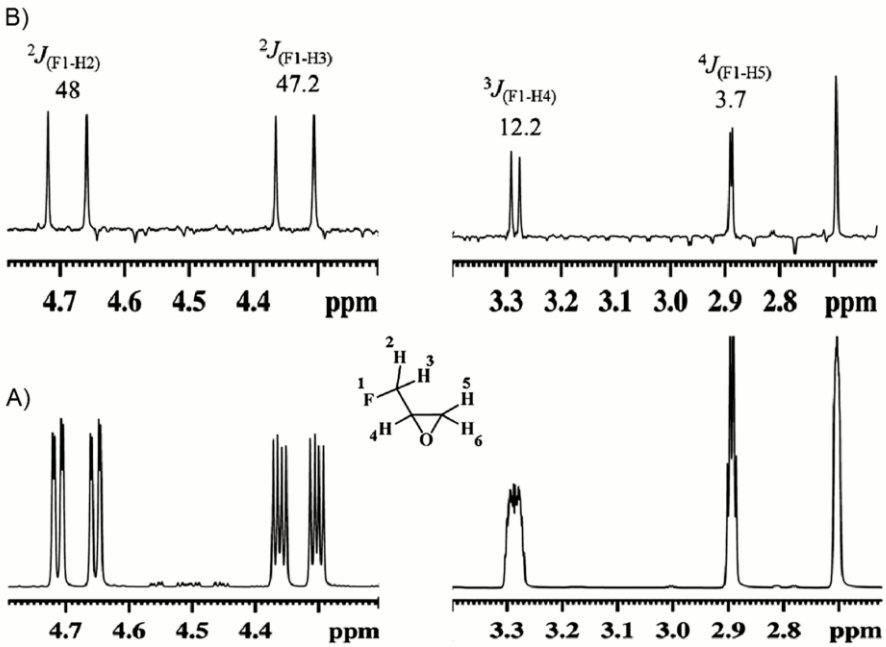

Figure 21. (A) ^{1}H NMR spectrum of the monofluorinated epiflurohydrin molecule in $CDCl_3$; (B) pseudo-2D ZS spectrum of the same molecule, depicting only $^nJ_{HF}$ couplings. Reproduced with permission of reference.[108]

automated intensity measurement. Again, the need for a 3D acquisition can limit its routine use.

Two novel but sophisticated modifications of the BIRD inversion element have been proposed to suppress the $^2J_{HH}+{}^2D_{HH}$ splitting in pseudo-3D ZS HSQC experiments: using a constant-time BIRD module[17] or a perfect-BIRD element (Fig. 23).[18] The constant-time approach necessarily limits the range of couplings accessible, while the perfect-BIRD method can accommodate a wide range of $^2J_{HH}+{}^2D_{HH}$, making perfect-BIRD particularly attractive for measurements on aligned samples. These new sequence elements provide full homonuclear broadband decoupling even in the case of diastereotopic methylene protons, but signal intensity losses can be more pronounced for aligned samples because overall sequence length becomes longer.

A ^{13}C–F2-coupled version of the sensitive HOBS-HSQMBC experiment depicted in Fig. 20A has been reported for the direct and simple measurement of small $^nJ_{CH}$ couplings.[122] The method retains the sensitivity of the original selHSQMBC experiment, and the resulting spectrum affords simplified pure in-phase doublets for all observed cross-peaks (Fig. 20C). A related multiplicity-edited approach has been reported to afford additional carbon multiplicity information by simple visual inspection of the resulting positive/negative cross-peak phases (Fig. 24A).[140] The IP pattern of the conventional selHSQMBC cross-peaks can be converted to doublets when using HOBS homodecoupling (Fig. 24C) and to singlets if additional broadband heteronuclear decoupling is applied (Fig. 24D), depending if the quantitative measurement of coupling constants or only the chemical shift assignment is of interest, respectively.

By analogy, a broadband homodecoupled version of the nonrefocused CPMG-HSQMBC experiment incorporating the pseudo-2D ZS module has been proposed to precisely measure long-range heteronuclear coupling constants from simplified anti-phase doublets. The 1D and 2D examples have been reported for the measurement of $^nJ_{PH}$, $^nJ_{SeH}$ and $^nJ_{CH}$ coupling constant in a series of compounds.[109] Long acquisition times and concentrated samples are required to achieve optimum SNR, but as mentioned in this study, sensitivity could be improved, for instance, using PSYCHE, and the determination of small *J* values from AP multiplets could be performed using multiplet fitting or by spin-state selective methods.

Ultra high-resolution NMR spectroscopy

Broadband ^{1}H homodecoupling in the acquisition F2 dimension is fully compatible with other resolution-enhanced techniques, such as spectral aliasing along the indirect F1 dimension[31,141–146] or nonuniform sampling,[147,148] opening the door to the design of ultra high-resolved 2D NMR experiments in reasonable acquisition times. A common feature of spectral aliasing is its general and very easy implementation in many routine experiments, improving the attainable resolution along the F1 dimension up to two orders of magnitude by a simple change of the ^{13}C spectral width in HSQC experiments. This approach has been recently reported in the development and application of ultra high-resolved HSQC experiments to analyze highly complex mixtures of similar isomers exhibiting near-identical ^{1}H and ^{13}C NMR spectra,[149] the determination of small chemical shift differences in enantiodifferentiation studies,[24] and for measuring the sign and the magnitude of multiple heteronuclear coupling constants from highly resolved 2D cross-peaks.[138]

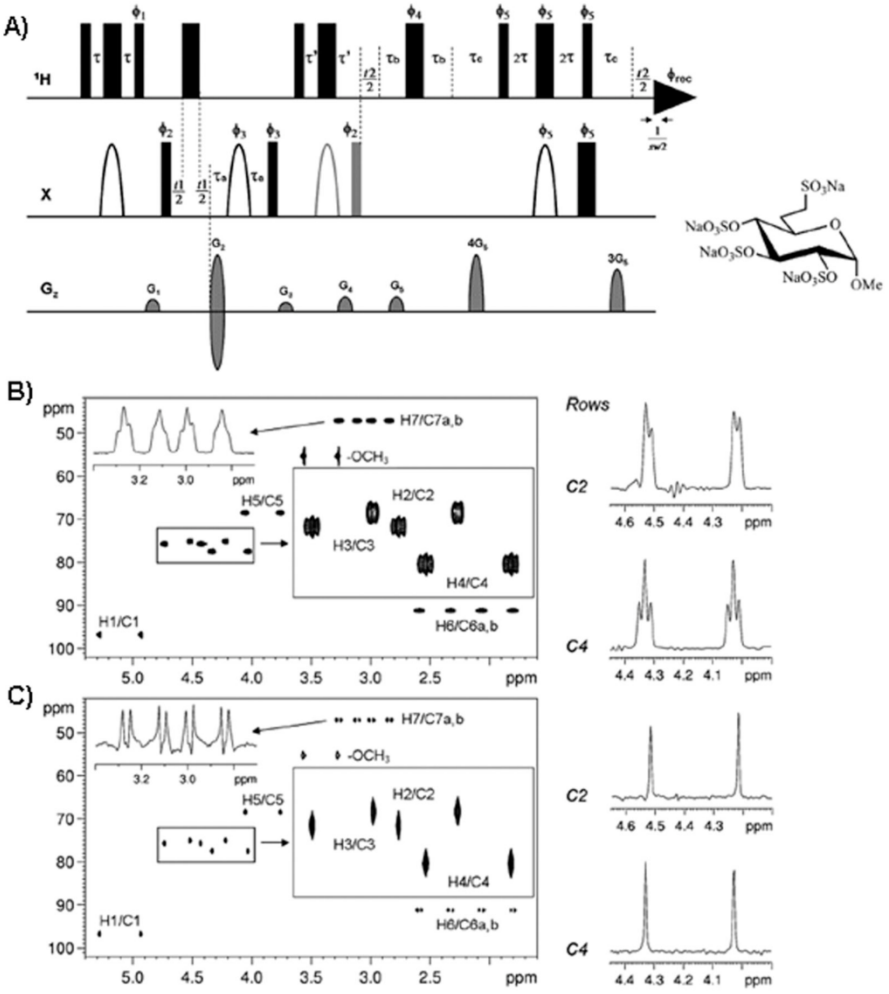

Figure 22. (A) Pulse scheme for the pseudo-3D homodecoupled CLIP/CLAP-HSQC experiment; expanded areas corresponding to the F2-coupled (B) conventional and (C) homodecoupled CLIP-HSQC spectra of tetra-sodium-(1-methyl-2,3,4-tri-O-sulfonato-6-deoxy-6-C-sulfonatomethyl-α-D-glucopyranoside dissolved in D_2O. Spectrum (C) was acquired with the pulse sequence of (A) using the same parameters as (B) and 16 FID data chunks. Reproduced with permission of reference.[23]

Analysis of near-identical ^{1}H and ^{13}C NMR spectra

Figure 25 outlines a schematic illustration showing how extremely high levels of signal dispersion can be achieved in a short range of frequencies by the simultaneous application of complementary resolution-enhanced NMR techniques. The whole ensemble of enhancements applied enables the *in situ* distinction and assignment of similar organic compounds exhibiting near-identical ^{1}H and ^{13}C NMR spectra in the same mixture.[149] Very small $\Delta\delta(^1H)$ and $\Delta\delta(^{13}C)$ have been distinguished and precisely determined, even in the presence of highly overlapped signals or severe chemical shift degeneracy in conventional 1D ^{1}H and $^{13}C\{^1H\}$ NMR spectra. Whereas $\Delta\delta(^1H)$ and $\Delta\delta(^{13}C)$ up to 3 and 17 ppb, respectively, can be established from the singlets obtained in 1D HOBS and ^{13}C NMR spectra, the high-signal dispersion achieved in spectral-aliased 2D HOBS-HSQC spectra allows an improvement in the level of detection to 1 and 5 ppb, respectively. This strategy combined with the use of HOBS versions of the HSQC-TOCSY and HSQMBC experiments has been used to unambiguously assign ^{1}H and ^{13}C chemical shifts for all peaks of different components of a complicated mixture. The proposed strategy proved to be very useful to facilitate the analysis of highly complex spectra, as found in many daily situations that exhibit high degeneracy of chemical shifts or severe signal overlap, such as the analysis of crude reactions, detection and characterization of intermediates, reaction monitoring or the analysis of complex mixtures.

Enantiodifferentiation studies

NMR has proved to be a valuable technique to determine enantiomeric purity using a great variety of auxiliary chiral sources, as, e.g. *chiral solvating agents* (CSAs). In the case of using CSAs,

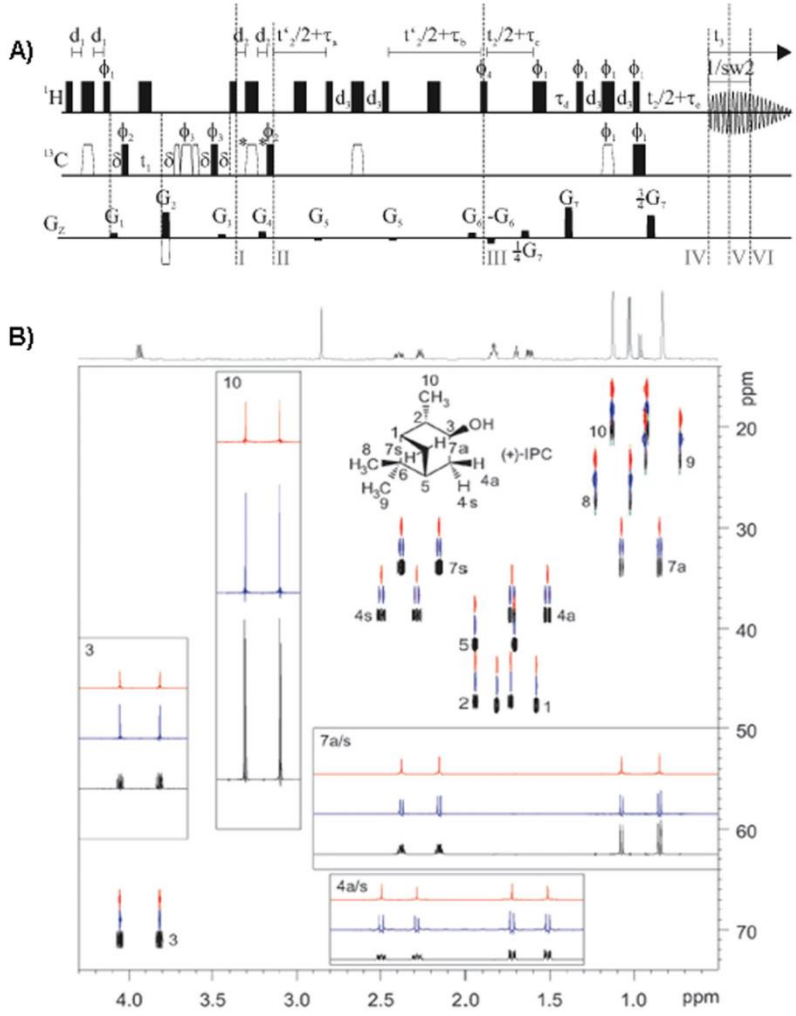

Figure 23. (A) Pulse scheme of the pseudo-3D homodecoupled CLIP-HSQC experiment incorporating a perfect BIRD inversion element. (B) F2-heterocoupled CLIP HSQC spectra without homonuclear decoupling (black) and with BIRD (blue) and with perfect BIRD (red) homonuclear decoupling during acquisition, collected for (+)-isopinocampheol in isotropic CD_2Cl_2 solution at 600-MHz proton frequency. Reproduced with permission of reference.[18]

theinitial indistinguishable mixture of enantiomers is converted into a chemical shift (δ)-resolved mixture of complementary diastereomeric complexes. As soon as there is enough chemical shift difference to achieve resolution between the signals of analogous nuclei in these diastereomeric complexes, the measure of enantiomeric purity can be carried out by direct signal integration. However, J_{HH} broadens ^{1}H NMR resonances, and accurate enantiomeric excess quantification is often hampered because of partial signal overlapping and low chemical shift. The features of homodecoupled experiments provide a great tool to avoid these overlapping problems.

Enantiodifferentiation studies involving chiral discrimination and the measurement of enantiomeric excess using some modern NMR methods, including pure shift NMR experiments, have been recently reviewed.[150] Two old classical experiments such as the conventional 1D $^{13}C\{^1H\}$ spectrum[151] or the use of the F2 projection in a 2D *J*-resolved experiments[86] offer simple set-up. An alternative method has been the distinction of different singlet lines along the indirect dimension of an F1-homodecoupled 2D spectra[152–154] or from the *z*-COSY experiment.[155]

Recently, two pure shift NMR approaches have been reported to carry out enantiodifferentiation studies using CSAs: (i) a fast determination from quickly acquired 1D HOBS spectra[124] and (ii) a 2D *spectral aliased pure shift* (SAPS) HSQC experiment.[24] In both cases, the relative sensitivity of standard 1D ^{1}H and HSQC experiments are retained and even improved because of the collapse of the signals to singlets (Fig. 26). In HOBS experiments, only the selected ^{1}H signals are studied but with full sensitivity. In practice, the experiment can be collected in a single scan, affording a powerful way to differentiate small chemical shift values into the same

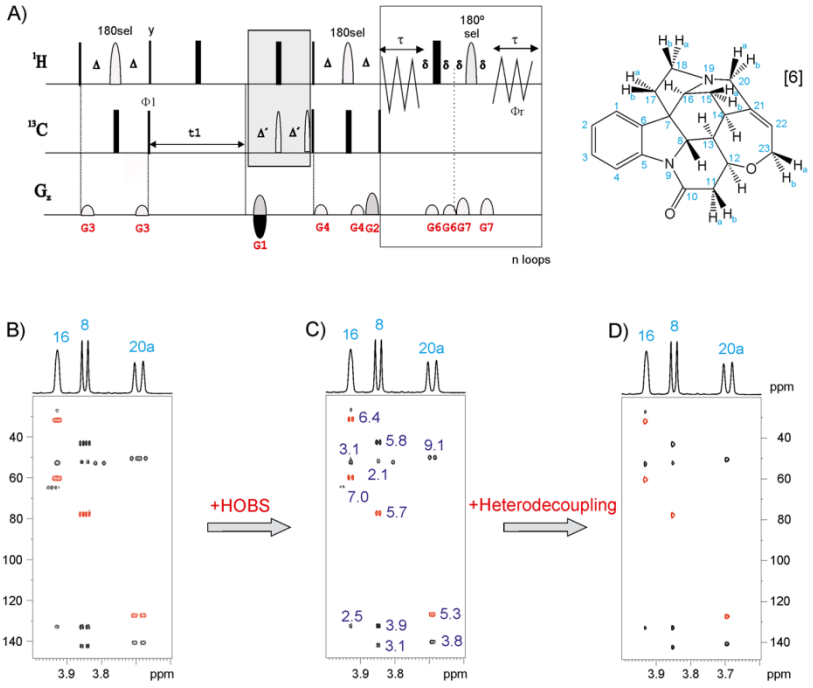

Figure 24. (A) Pulse scheme of the HOBS multiplicity-edited selHSQMBC experiment without heteronuclear decoupling during acquisition; (B) conventional ME-selHSQMBC experiment of strychnine [6] in $CDCl_3$ after selective excitation of the region around 4 ppm with a 12-ms RE-BURP 180° ^{1}H pulse; (C) HOBS-ME-selHSQMBC spectrum without ^{13}C heteronuclear decoupling showing a pure IP doublet pattern for all cross-peaks from which the magnitude of $^{n}J_{CH}$ can be measured directly; (D) as (C) but with heteronuclear decoupling during acquisition, leading to a singlets for each individual cross-peak. Black and red cross-peaks represent C/CH_2 and CH/CH_3 multiplicities, respectively. Reproduced with permission of reference.[140]

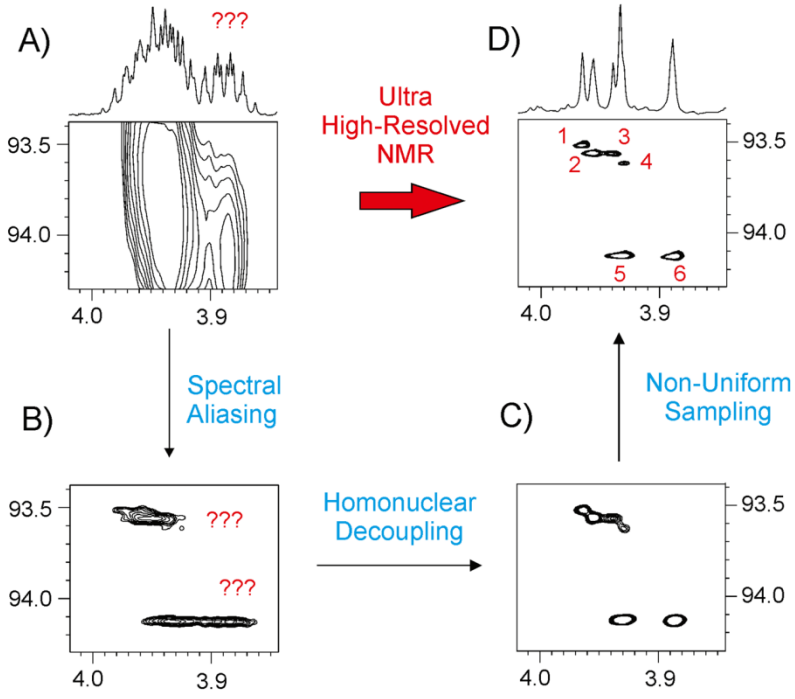

Figure 25. Schematic illustration of the resolution enhancements achieved after combining (B) spectral aliasing in the indirect dimension, (C) broadband homodecoupling in the detected dimension and (D) nonuniform sampling into a single ultra high-resolved HSQC experiment. Reproduced with permission of reference.[149]

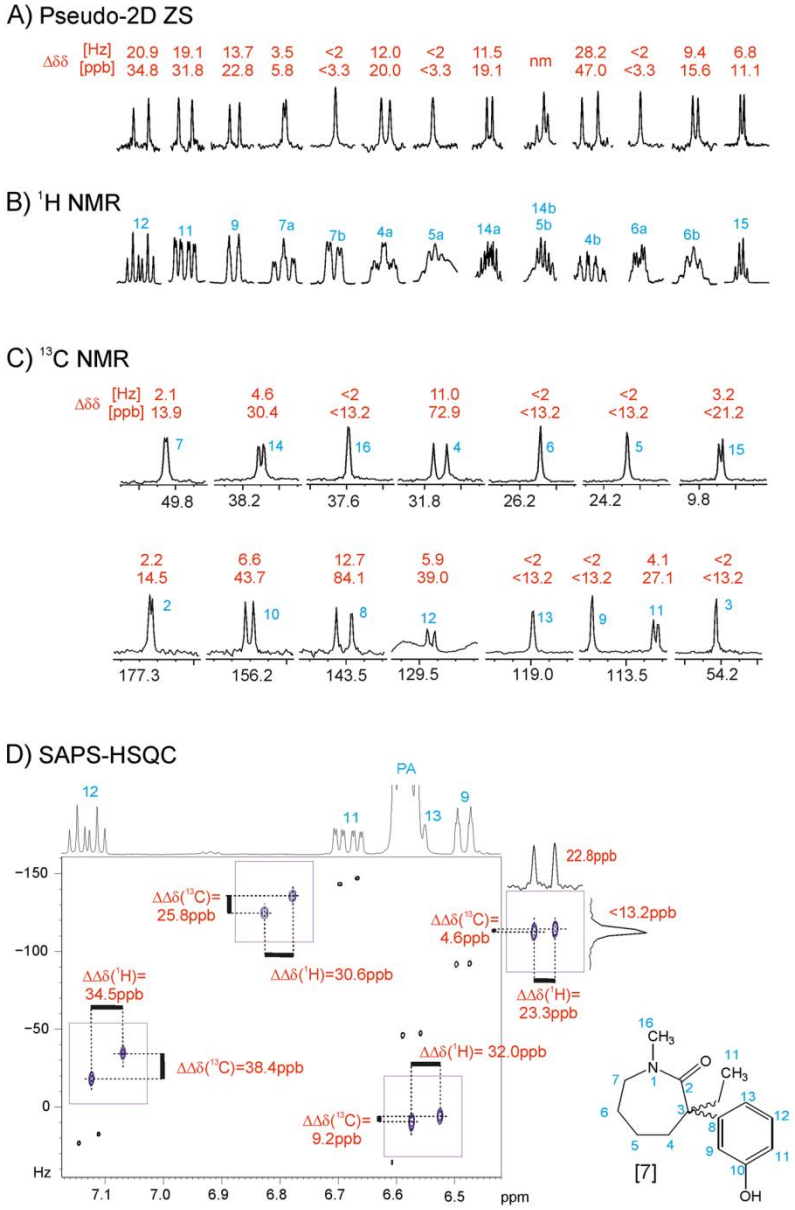

Figure 26. 600-MHz (B) conventional *versus* (A) pure shift ^{1}H multiplets; (C) ^{13}C{^{1}H} multiplets; (D) expanded aromatic area of the 2D SAPS-HSQC spectrum of racemic compound [7] complexed with 9.6 equiv. of *R*-PA in $CDCl_3$. Adapted with permission of reference.[24]

experimental time and using the same data processing as required for a conventional ^{1}H spectrum. It has been shown that the performance of the method can be improved by using multiple-frequency excitation simultaneously at different positions or appending a TOCSY transfer (1D HOBS-selTOCSY experiment) that can facilitate the analysis of signals in overcrowded areas, where conventional selective excitation could not be successfully applied. In Section on Comparison of ZS Methods, there is a comparative discussion on the results obtained from a pseudo-2D ZS, HOBB and HOBS spectra for a racemic mixture of (*RS*)-1-aminoindan complexed with Pirkle alcohol (Fig. 11). On the other hand, the combination of spectral aliasing and pure shift HSQC experiments represents an excellent routine tool for NMR enantiodifferentiation studies, yielding simultaneous ^{1}H and ^{13}C enantiodifferentiated data [$\Delta\Delta\delta(^{1}H)$ and $\Delta\Delta\delta(^{13}C)$] in short times and with high digital resolution and signal dispersion for both ^{1}H and ^{13}C nuclei. Signals that are not differentiated in conventional ^{1}H multiplets (Fig. 26A), pure shift 1D ^{1}H multiplets obtained from the pseudo-2D ZS experiment (Fig. 26B) or conventional ^{13}C peaks (Fig. 26C) can be distinguished in the SAPS-HSQC spectrum (Fig. 26D).[24] For instance, the excellent 2D dispersion of

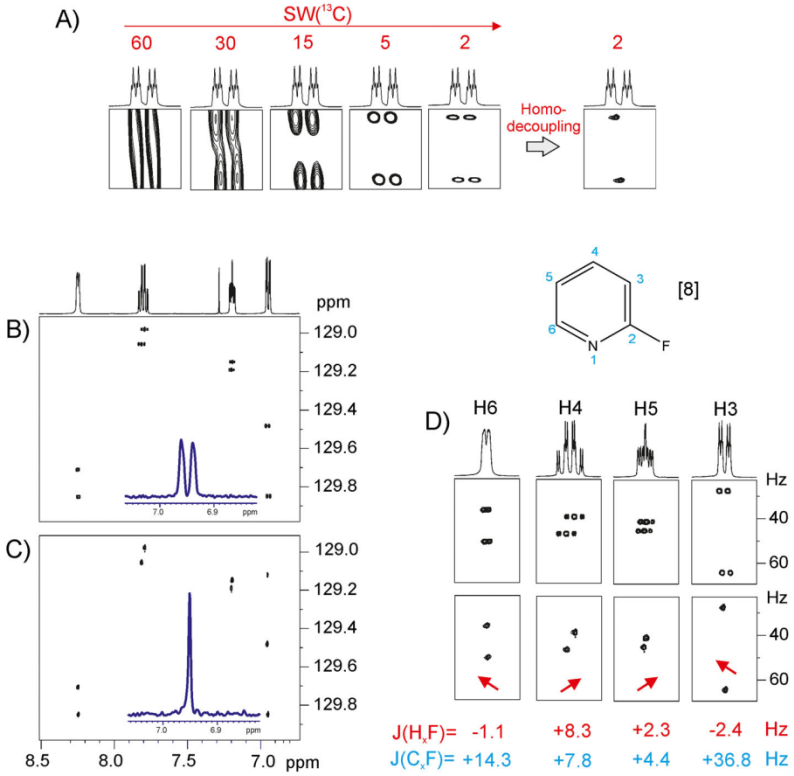

Figure 27. (A) Experimental effects on signal resolution after reducing SW(^{13}C) in HSQC experiments. In the right column, the additional benefits to add broadband ^{1}H homodecoupling along the detected F2 dimension can be appreciated. (B and C) 400-MHz 2D spectral-aliased ^{1}H-^{13}C HSQC spectrum of 2-fluoropyridine acquired with a reduced SW(^{13}C) of 2 ppm: (B) without and (C) with broadband BIRD-based ^{1}H homodecoupling in the F2 dimension. (D) Expanded cross-peaks showing the high levels of digitization and signal dispersion achieved for each experiment. Adapted from reference.[138]

the H9 protons (22.8 ppb) allows the separation of the two C9 carbons (4.6 ppb) in the SAPS-HSQC spectrum, which are indistinguishable in the 1D ^{13}C{^{1}H} spectrum.

Efficient measurement of heteronuclear coupling constants

It has been shown that the superb digital resolution achieved in SAPS-HSQC experiments allows the easy and simultaneous determination of the magnitude and the sign of J_{CX} and J_{HX} coupling constants (X = ^{19}F, ^{31}P or ^{2}H) from highly resolved E.COSY coupling patterns (Fig. 27).[138] The resulting 2D cross-peaks exhibit ultra-simplified multiplet patterns from which the measurement of the active J values is determined in a straightforward manner. As pointed out already, this general approach introduced in this study can be applicable in many experiments aimed at determining precise coupling constants along the indirect dimensions of 2D spectra.

Summary and outlook

In summary, a novel set of NMR experiments are now available for helping chemists to solve common problems encountered in their daily NMR activities. Modern pure shift NMR experiments afford simplified multiplet patterns that allow a much better analysis and interpretation of ^{1}H NMR spectra. Obtaining fully homodecoupled singlets for each proton resonance greatly minimizes the eternal problem of signal overlap. Several basic homodecoupling schemes have been evaluated, discussed and compared, and their implementation into the most standard 2D experiments has also been described. In addition, the combination with other complementary resolution-enhanced techniques tools excites the idea of ultra high-resolved NMR spectroscopy. The usefulness of these techniques have been demonstrated for a number of challenging practical applications, such as the determination of very small chemical shift differences, the analysis of highly crowded spectral regions, and the simplified and precise determination of relevant NMR parameters such as coupling constants, relaxation times or diffusion coefficients. Some challenges to improve even further the performance of these types of experiments will be of interest in the next future, such as the design of improved slice-selective methods that enhance absolute sensitivity, their robustness for a general and routine use, and the performance of perfect homodecoupling under strong coupling conditions, with a particular emphasis in the full collapse of diastereotopic CH_2 protons.

Acknowledgements

Financial support for this research provided by MINECO (project CTQ2012-32436) is gratefully acknowledged. We also thank the Servei de Ressonància Magnètica Nuclear, Universitat Autònoma de Barcelona, for allocating instrument time to this project.

References

[1] M. H. Levitt, R. Freeman, T. Frenkiel. *J. Magn. Reson.* **1982**, *47*, 328–330.
[2] A. J. Shaka, J. Keeler, T. Frenkiel, R. Freeman. *J. Magn. Reson.* **1983**, *52*, 335–338.
[3] A. J. Shaka, P. B. Barker, R. Freeman. *J. Magn. Reson.* **1985**, *64*, 547–552.
[4] E. Kupče, R. Freeman. *J. Magn. Reson.* **1995**, *115*, 273–276.
[5] R. Fu, G. Bodenhausen. *Chem. Phys. Lett.* **1995**, *245*, 415–420.
[6] K. Zangger, H. Sterk. *J. Magn. Reson.* **1997**, *489*, 486–489.
[7] N. H. Meyer, K. Zangger. *ChemPhysChem* **2014**, *15*, 49–55.
[8] R. W. Adams. *eMagRes* **2014**, *3*, 295–310.
[9] K. Zangger. *Prog. Nucl. Magn. Reson. Spectrosc.* **2015**, in press. DOI: 10.1016/j.pnmrs.2015.02.002.
[10] Y. Kown, S. Park, J. Shin, D. C. Oh. *Arch. Pharm. Res.* **2014**, *37*, 967–971.
[11] M. McCoy, L. Mueller. *J. Am. Chem. Soc.* **1992**, *114*, 2108–2112.
[12] J. Ying, F. Li, J. H. Lee, A. Bax. *J. Biomol. NMR* **2014**, *60*, 15–21.
[13] J. Farjon, W. Bermel, C. Griesinger. *J. Magn. Reson.* **2006**, *180*, 72–82.
[14] S. Paul, P. K. Madhu. *J. Indian Inst. Sci.* **2010**, *90*, 69–86.
[15] J. P. Garbow, D. P. Weitekamp, A. Pines. *Chem. Phys. Lett.* **1982**, *93*, 504–509.
[16] D. Uhrín, T. Liptaj, K. E. Kövér. *J. Magn. Reson.* **1993**, *101*, 41–46.
[17] T. Reinsperger, B. Luy. *J. Magn. Reson.* **2014**, *239*, 110–120.
[18] L. Kaltschnee, A. Kolmer, I. Timári, V. Schmidts, R. W. Adams, M. Nilsson, K. E. Kövér, G. A. Morris, C. M. Thiele. *Chem. Commun.* **2014**, *50*, 15702–15705.
[19] A. Lupulescu, G. L. Olsen, L. Frydman. *J. Magn. Reson.* **2012**, *218*, 141–146.
[20] L. Paudel, R. W. Adams, P. Király, J. A. Aguilar, M. Foroozandeh, M. J. Cliff, M. Nilsson, P. Sándor, J. P. Waltho, G. A. Morris. *Angew. Chem. Int. Ed.* **2013**, *52*, 11616–11619.
[21] J. A. Aguilar, M. Nilsson, G. A. Morris. *Angew. Chem. Int. Ed.* **2011**, *50*, 9716–9717.
[22] P. Sakhaii, B. Haase, W. Bermel. *J. Magn. Reson.* **2009**, *199*, 192–198.
[23] I. Timári, L. Kaltschnee, A. Kolmer, R. W. Adams, M. Nilsson, C. M. Thiele, G. A. Morris, K. E. Kövér. *J. Magn. Reson.* **2014**, *239*, 130–138.
[24] M. Pérez-Trujillo, L. Castañar, E. Monteagudo, L. T. Kuhn, P. Nolis, A. Virgili, R. T. Williamson, T. Parella. *Chem. Commun.* **2014**, *50*, 10214–10217.
[25] Y. Liu, M. D. Green, R. Marques, T. Pereira, R. Helmy, R. Thomas Williamson, W. Bermel, G. E. Martin. *Tetrahedron Lett.* **2014**, *55*, 5450–5453.
[26] J. A. Aguilar, G. A. Morris, A. M. Kenwright. *RSC Adv.* **2014**, *4*, 8278–8282.
[27] K. J. Donovan, L. Frydman. *Angew. Chem. Int. Ed.* **2014**, *54*, 594–598.
[28] R. Brüschweiler, C. Griesinger, O. W. Sørensen, R. R. Ernst. *J. Magn. Reson.* **1988**, *78*, 178–185.
[29] V. V. Krishnamurthy. *Magn. Reson. Chem.* **1997**, *35*, 9–12.
[30] K. Furihata, M. Tashiro. *Magn. Reson. Chem.* **2012**, *50*, 713–716.
[31] A. Cotte, M. Foroozandeh, D. Jeannerat. *Chim. Int. J. Chem.* **2012**, *66*, 764–769.
[32] W. L. Chuang, M. D. Christ, D. L. Rabenstein. *Anal. Chem.* **2001**, *73*, 2310–2316.
[33] J. Wang, D. Borchardt, D. L. Rabenstein. *Magn. Reson. Chem.* **2006**, *44*, 744–752.
[34] J. Wang, D. L. Rabenstein. *Anal. Chem.* **2007**, *79*, 6799–6803.
[35] K. Nguyen, D. L. Rabenstein. *Anal. Bioanal. Chem.* **2011**, *399*, 663–671.
[36] A. Kaerner, D. L. Rabenstein. *Magn. Reson. Chem.* **1998**, *36*, 601–607.
[37] K. Furihata, M. Tashiro. *Magn. Reson. Chem.* **2014**, *52*, 27–31.
[38] W. Kozmiński. *Pol. J. Chem.* **2000**, *1189*, 1185–1189.
[39] B. T. Martin, G. C. Chingas, O. M. McDougal. *J. Magn. Reson.* **2012**, *218*, 147–152.
[40] C. Mantel, P. A. Bayle, S. Hediger, C. Berthon, M. Bardet. *Magn. Reson. Chem.* **2010**, *48*, 600–606.
[41] P. Trigo-Mouriño, C. Merle, M. R. M. Koos, B. Luy, R. R. Gil. *Chem. Eur. J.* **2013**, *19*, 7013–7019.
[42] A. C. Pöppler, S. Frischkorn, D. Stalke, M. John. *Chemphyschem* **2013**, *14*, 3103–3107.
[43] J. Allen, K. Damodaran. *Magn. Reson. Chem.* **2015**. *53*, 200–202.
[44] T. Niklas, D. Stalke, M. John. *Chem. Commun.* **2014**, *51*, 1275–1277.
[45] B. Antalek. *Concepts Magn. Reson.* **2002**, *14*, 225–258.
[46] K. D. Park, Y. J. Lee. *Magn. Reson. Chem.* **2006**, *44*, 887–891.
[47] P. Sakhaii, B. Haase, W. Bermel, R. Kerssebaum, G. E. Wagner, K. Zangger. *J. Magn. Reson.* **2013**, *233*, 92–95.
[48] M. Vega-Vazquez, J. C. Cobas, M. Martin-Pastor. *Magn. Reson. Chem.* **2010**, *48*, 749–752.
[49] B. Sathyamoorthy, D. M. Parish, G. T. Montelione, R. Xiao, T. Szyperski. *Chemphyschem* **2014**, *15*, 1872–1879.
[50] G. E. Wagner, P. Sakhaii, W. Bermel, K. Zangger. *Chem. Commun.* **2013**, *49*, 3155–3157.
[51] N. M. Loening, M. J. Thrippleton, J. Keeler, R. G. Griffin. *J. Magn. Reson.* **2003**, *164*, 321–328.
[52] N. Giraud, L. Béguin, J. Courtieu, D. Merlet. *Angew. Chem. Int. Ed.* **2010**, *49*, 3481–3484.
[53] M. E. Di Pietro, C. Aroulanda, D. Merlet. *J. Magn. Reson.* **2013**, *234*, 101–105.
[54] S. Glanzer, E. Schrank, K. Zangger. *J. Magn. Reson.* **2013**, *232*, 1–6.
[55] L. Castañar, P. Nolis, A. Virgili, T. Parella. *Chem. Eur. J.* **2013**, *19*, 15472–15475.
[56] M. Foroozandeh, P. Giraudeau, D. Jeannerat. *Magn. Reson. Chem.* **2013**, *51*, 808–814.
[57] L. Frydman, T. Scherf, A. Lupulescu. *Proc. Natl. Acad. Sci. U. S. A.* **2002**, *99*, 15858–15862.
[58] N. Lokesh Suryaprakash. *Chem. Commun.* **2014**, *50*, 8550–8553.
[59] R. Freeman, E. Kupče. *Magn. Reson. Chem.* **2007**, *45*, 2–4.
[60] W. A. Anderson, R. Freeman. *J. Chem. Phys.* **1962**, *37*, 85–103.
[61] A. P. D. M. Espindola, R. Crouch, J. R. DeBergh, J. M. Ready, J. B. MacMillan. *J. Am. Chem. Soc.* **2009**, *131*, 15994–15995.
[62] D. Carnevale, T. F. Segawa, G. Bodenhausen. *Chem. Eur. J.* **2012**, *18*, 11573–11576.
[63] C. W. Vander Kooi, E. Kupče, E. R. P. Zuiderweg, M. Pellecchia. *J. Biomol. NMR* **1999**, *15*, 335–338.
[64] A. Hammarström, G. Otting. *J. Am. Chem. Soc.* **1994**, *116*, 8847–8848.
[65] E. Kupče, R. Freeman. *J. Magn. Reson. Ser. A* **1993**, 102, 364–369.
[66] J. P. Jesson, P. Meakin, G. Kneissel. *J. Am. Chem. Soc.* **1973**, *95*, 618–620.
[67] J. Weigelt, A. Hammarström, W. Bermel, G. Otting. *J. Magn. Reson.* **1996**, *110*, 219–224.
[68] V. D. M. Koroleva, N. Khaneja. *J. Chem. Phys.* **2012**, *137*, 094103.
[69] E. Kupče, H. Matsuo, G. Wagner. Homonuclear decoupling in proteins. in *Biological Magnetic Resonance, Volume 16: Modern Techniques in Protein NMR*, (Eds: N. R. Krishna, L. J. Berliner), **1999**, 149, 193–193.
[70] E. Kupče, G. Wagner. *J. Magn. Reson.* **1995**, *109*, 329–333.
[71] E. Kupče, G. Wagner. *J. Magn. Reson.* **1996**, *110*, 309–312.
[72] B. Vögeli, H. Kovacs, K. Pervushin. *J. Biomol. NMR* **2005**, *31*, 1–9.
[73] W. P. Aue, J. Karhan, R. R. Ernst. *J. Chem. Phys.* **1976**, *64*, 4226–4227.
[74] A. Bax, R. Freeman, G. A. Morris. *J. Magn. Reson.* **1981**, *43*, 333–338.
[75] A. J. Shaka, J. Keeler, R. Freeman. *J. Magn. Reson.* **1984**, *56*, 294–313.
[76] M. Woodley, R. Freeman. *J. Magn. Reson. Ser. A* **1994**, *109*, 103–112.
[77] M. Woodley, R. Freeman. *J. Magn. Reson. Ser. A* **1994**, *111*, 225–228.
[78] J. M. Nuzillard. *J. Magn. Reson.* **1996**, *118*, 132–135.
[79] S. Simanova, H. Sengstschmidt, R. Freeman. *J. Magn. Reson.* **1997**, *124*, 104–121.
[80] V. Mandelshtam, H. Taylor, A. J. Shaka. *J. Magn. Reson.* **1998**, *133*, 304–312.
[81] P. Mutzenhardt, F. Guenneau, D. Canet. *J. Magn. Reson.* **1999**, *141*, 312–321.
[82] M. J. Thrippleton, R. A. E. Edden, J. Keeler. *J. Magn. Reson.* **2005**, *174*, 97–109.
[83] A. J. Pell, J. Keeler. *J. Magn. Reson.* **2007**, *189*, 293–299.
[84] B. Luy. *J. Magn. Reson.* **2009**, *201*, 18–24.
[85] U. R. Prabhu, S. R. Chaudhari, N. Suryaprakash. *Chem. Phys. Lett.* **2010**, *500*, 334–341.
[86] S. R. Chaudhari, N. Suryaprakash. *Chem. Phys. Lett.* **2013**, *555*, 286–290.
[87] P. Sakhaii, B. Haase, W. Bermel. *J. Magn. Reson.* **2013**, *228*, 125–129.
[88] P. Sakhaii, W. Bermel. *J. Magn. Reson.* **2014**, *242*, 220–223.
[89] J. C. Cobas, M. Martín-Pastor. *J. Magn. Reson.* **2004**, *171*, 20–24.
[90] L. H. Lucas, W. H. Otto, C. K. Larive. *J. Magn. Reson.* **2002**, *156*, 138–145.
[91] C. Ludwig, M. R. Viant. *Phytochem. Anal.* **2010**, *21*, 22–32.
[92] A. J. Pell, R. A. E. Edden, J. Keeler. *Magn. Reson. Chem.* **2007**, *45*, 296–316.
[93] O. W. Sørensen, C. Griesinger, R. R. Ernst. *J. Am. Chem. Soc.* **1985**, *107*, 7778–7779.
[94] M. E. Girvin. *J. Magn. Reson. Ser. A* **1994**, 108, 99–102.
[95] F. J. M. van de Ven, M. E. P. Philippens. *J. Magn. Reson.* **1992**, *97*, 637–644.
[96] Y. Xia, G. Legge, K. Y. Jun, Y. Qi, H. Lee, X. Gao. *Magn. Reson. Chem.* **2005**, *43*, 372–379.

[97] M. Rance, G. Wagner, O. W. Sørensen, K. Wüthrich, R. R. Ernst. *J. Magn. Reson.* **1984**, *59*, 250–261.
[98] A. Bax, R. Freeman. *J. Magn. Reson.* **1981**, *44*, 542–561.
[99] A. G. Palmer, W. J. Fairbrother, J. Cavanagh, P. E. Wright, M. Rance. *J. Biomol. NMR* **1992**, *2*, 103–108.
[100] A. Bax, A. F. Mehlkopf, J. Smidt. *J. Magn. Reson.* **1979**, *35*, 167–169.
[101] B. T. Farmer, L. R. J. Brown. *J. Magn. Reson.* **1987**, *71*, 365–370.
[102] J. A. Aguilar, A. A. Colbourne, J. Cassani, M. Nilsson, G. A. Morris. *Angew. Chem. Int. Ed.* **2012**, *51*, 6460–6463.
[103] A. Bax. *J. Magn. Reson.* **1983**, *53*, 517–520.
[104] N. H. Meyer, K. Zangger. *Angew. Chem. Int. Ed.* **2013**, *52*, 7143–7146.
[105] J. A. Aguilar, S. Faulkner, M. Nilsson, G. A. Morris. *Angew. Chem. Int. Ed.* **2010**, *49*, 3901–3903.
[106] M. Foroozandeh, R. W. Adams, N. J. Meharry, D. Jeannerat, M. Nilsson, G. A. Morris. *Angew. Chem. Int. Ed.* **2014**, *53*, 6990–6992.
[107] S.R. Chaudhari, N. Suryaprakash. *ChemPhysChem* **2015**, *16*, 1079–1082.
[108] S. R. Chaudhari, N. Suryaprakash. *RSC Adv.* **2014**, *4*, 15018–15021.
[109] I. Timári, T. Z. Illyés, R. W. Adams, M. Nilsson, L. Szilágyi, G. A. Morris, K. E. Kövér. *Chem. Eur. J.* **2015**, *21*, 3472–3479.
[110] M. Nilsson, G. A. Morris. *Chem. Commun.* **2007**, 933–935.
[111] S. Islam, J. A. Aguilar, M. W. Powner, M. Nilsson, G. A. Morris, J. D. Sutherland. *Chem. Eur. J.* **2013**, *19*, 4586–4595.
[112] G. A. Morris, J. A. Aguilar, R. Evans, S. Haiber, M. Nilsson. *J. Am. Chem. Soc.* **2010**, *132*, 12770–12772.
[113] J. J. Koivisto. *Chem. Commun.* **2013**, *49*, 96–98.
[114] M. Foroozandeh, R. W. Adams, M. Nilsson, G. A. Morris. *J. Am. Chem. Soc.* **2014**, *136*, 11867–11869.
[115] S. Glanzer, K. Zangger. *Chem. Eur. J.* **2014**, *20*, 11171–11175.
[116] V. M. R. Kakita, J. Bharatam. *Magn. Reson. Chem.* **2014**, *52*, 389–394.
[117] N. H. Meyer, K. Zangger. *Chem. Commun.* **2014**, *50*, 1488–1490.
[118] L. Castañar, P. Nolis, A. Virgili, T. Parella. *Chem. Eur. J.* **2013**, *19*, 17283–17286.
[119] J. Ying, J. Roche, A. Bax. *J. Magn. Reson.* **2014**, *241*, 97–102.
[120] R. W. Adams, L. Byrne, P. Király, M. Foroozandeh, L. Paudel, M. Nilsson, J. Clayden, G. A. Morris. *Chem. Commun.* **2014**, *50*, 2512–2514.
[121] L. Castañar, P. Nolis, A. Virgili, T. Parella. *J. Magn. Reson.* **2014**, *244*, 30–35.
[122] L. Castañar, J. Saurí, P. Nolis, A. Virgili, T. Parella. *J. Magn. Reson.* **2014**, *238*, 63–69.
[123] J. M. McKenna, J. A. Parkinson. *Magn. Reson. Chem.* **2015**, *53*, 249–255.
[124] L. Castañar, M. Pérez-Trujillo, P. Nolis, E. Monteagudo, A. Virgili, T. Parella. *Chemphyschem* **2014**, *15*, 854–857.
[125] N. Gubensäk, W. M. F. Fabian, K. Zangger. *Chem. Commun.* **2014**, *50*, 12254–12257.
[126] N. Lokesh, S. R. Chaudhari, N. Suryaprakash. *Chem. Commun.* **2014**, *50*, 15597–15600.
[127] C. S. Johnson Jr. *Prog. Nucl. Magn. Reson. Spectrosc.* **1999**, *34*, 203–256.
[128] Y. Cohen, L. Avram, L. Frish. *Angew. Chem. Int. Ed.* **2005**, *44*, 520–554.
[129] G. Hamdoun, M. Sebban, E. Cossoul, A. Harrison-Marchand, J. Maddaluno, H. Oulyadi. *Chem. Commun.* **2014**, *50*, 4073–4075.
[130] P. B. Kingsley. *Concepts Magn. Reson.* **1999**, *11*, 29–49.
[131] P. B. Kingsley. *Concepts Magn. Reson.* **1999**, *11*, 243–276.
[132] H. Y. Carr, E. M. Purcell. *Phys. Rev.* **1954**, *274*, 630–638.
[133] S. Meiboom, D. Gill. *Rev. Sci. Instrum.* **1958**, *29*, 688–691.
[134] J. A. Aguilar, M. Nilsson, G. Bodenhausen, G. A. Morris. *Chem. Commun.* **2012**, *48*, 811–813.
[135] A. Cotte, M. Foroozandeh, D. Jeannerat. *Chimia* **2012**, *66*, 764–769.
[136] W. Reynolds, R. Breton, D. Burns. *Planta Med.* **2014**, *80*, IL26.
[137] S. Gil, J. F. Espinosa, T. Parella. *J. Magn. Reson.* **2010**, *207*, 312–321.
[138] N. Marcó, A. Fredi, T. Parella. *Chem. Commun.* **2015**, *51*, 3262–3265.
[139] A. Enthart, J. C. Freudenberger, J. Furrer, H. Kessler, B. Luy. *J. Magn. Reson.* **2008**, *192*, 314–322.
[140] J. Saurí, E. Sistaré, R. T. Williamson, G. E. Martin, T. Parella. *J. Magn. Reson.* **2015**, *252*, 170–175.
[141] D. Jeannerat. *Magn. Reson. Chem.* **2003**, *41*, 3–17.
[142] I. Baskyr, T. Brand, M. Findeisen, S. Berger. *Angew. Chem. Int. Ed.* **2006**, *45*, 7821–7824.
[143] D. Jeannerat. *J. Magn. Reson.* **2007**, *186*, 112–122.
[144] B. Vitorge, S. Bieri, M. Humam, P. Christen, K. Hostettmann, O. Muñoz, S. Loss, D. Jeannerat. *Chem. Commun.* **2009**, 950–952.
[145] G. B. B. Njock, D. E. Pegnyem, T. A. Bartholomeusz, P. Christen, B. Vitorge, J. M. Nuzillard, R. Shivapurkar, M. Foroozandeh, D. Jeannerat. *Chimia* **2010**, *64*, 235–240.
[146] M. Foroozandeh, D. Jeannerat. *ChemPhysChem* **2010**, *11*, 2503–2505.
[147] J. C. Hoch, M. W. Maciejewski, M. Mobli, A. D. Schuyler, A. S. Stern. *Acc. Chem. Res.* **2014**, *47*, 708–717.
[148] M. Mobli, J. C. Hoch. *Prog. Nucl. Magn. Reson. Spectrosc.* **2014**, *83*, 21–41.
[149] L. Castañar, R. Roldán, P. Clapés, A. Virgili, T. Parella. *Chem. Eur. J.* **2015**, in press, DOI: 10.1002/chem.201500521.
[150] S. R. Chaudhari, S. N. Suryaprakash. *J. Indian Inst. Sci.* **2014**, *94*, 485–516.
[151] M. Pérez-Trujillo, E. Monteagudo, T. Parella. *Anal. Chem.* **2013**, *85*, 10887–10894.
[152] N. Lokesh, S. R. Chaudhari, N. Suryaprakash. *Org. Biomol. Chem.* **2014**, *12*, 993–997.
[153] N. Nath, D. Kumari, N. Suryaprakash. *Chem. Phys. Lett.* **2011**, *508*, 149–154.
[154] N. Giraud, M. Joos, J. Courtieu, D. Merlet. *Magn. Reson. Chem.* **2009**, *47*, 300–306.
[155] U. R. Prabhu, N. Suryaprakash. *J. Magn. Reson.* **2010**, *202*, 217–222.

PULSE PROGRAMS
AND DATA SET EXAMPLES

In the following link are available all the Data Set Examples and the corresponding Pulse Program Code for Bruker of each Publication presented in this doctoral thesis.

http://sermn.uab.cat/2015/05/lauracastanar-phdthesis/